

Self-Condensing Ring-Opening Metathesis Polymerization

Hanan Nasser Almuzaini

Dissertation submitted to the faculty of the Virginia Polytechnic Institute and State  
University in partial fulfillment of the requirements for the degree of

Doctor of Philosophy

in

Chemistry

Michael D. Schulz, Chair

Richard D. Gandour

Paul A. Deck

Alan R. Esker

April 26<sup>th</sup>, 2023

Blacksburg, VA, USA

Keywords: Latent olefin metathesis catalysts, catalyst activation, ring-opening metathesis  
polymerization, hyperbranched polymer synthesis

# Self-Condensing Ring-Opening Metathesis Polymerization

Hanan Nasser Almuzaini

## ABSTRACT

Ring-opening metathesis polymerization (ROMP) is a great tool for synthesizing polyolefin materials with different topologies, including hyperbranched polymers—polymers with high degrees of branching and many end groups. However, hyperbranched polymer synthesis via ROMP is challenging due to multifunctional-monomer or multi-polymerization requirements. To simplify the synthesis of hyperbranched ROMP polymers, we developed a new synthetic approach: *Self-condensing ROMP*.

The self-condensing ROMP approach involves a ROMP initiator modification to attach a ROMP-polymerizable group (a ROMP monomer), producing a ROMP “*inimer*” (initiator + monomer). The ROMP inimer initiates the polymerization and becomes a branching unit in the polymer structure, resulting in single-step hyperbranched polymer synthesis. The key challenge is controlling of this approach the ROMP initiator reactivity to avoid initiating polymerization during the ROMP inimer synthesis.

Well-defined ruthenium-based olefin metathesis catalysts are common ROMP initiators due to their high stability, reactivity, and functional group tolerance. Thus, we studied the olefin metathesis catalyst activation temperature to enable ROMP initiator-monomer coupling. Based on the catalyst activity, we designed and synthesized a series of ROMP inimers. Then, we synthesized hyperbranched polymers via self-condensing ROMP. The characterization of hyperbranched polymers indicated the effect of branching density on the physical properties of the polymer. This approach introduced a new class of olefin metathesis complexes, ROMP inimers, containing both the initiator and propagating

center. This approach provides a way to synthesize hyperbranched polymers from any known ROMP monomers in a single step.

This dissertation also includes the synthesis and characterization of a bimetallic Ru complex that could directly synthesize cyclic polyolefin. We also include the synthesis and characterization of copper-ruthenium bimetallic olefin metathesis catalysts.

# Self-Condensing Ring-Opening Metathesis Polymerization

Hanan Nasser Almuzaini

## GENERAL AUDIENCE ABSTRACT

Hyperbranched polymers are a class of polymers having highly branching structures and functional end-groups, and presenting distinct physical and chemical properties compared with linear polymers. Hyperbranched polymers have been used for many applications including processing additives, cross-linkers, compatibilizers, and catalyst supports. Well-defined ruthenium-based olefin metathesis catalysts enable the synthesis of materials with different topologies, functionalities, and chemical and physical properties via ring-opening metathesis polymerization (ROMP). Ligand modifications on ruthenium catalysts have been applied to improve the catalyst stability and reactivity. However, this dissertation modifies olefin metathesis catalysts to synthesize hyperbranched polymers in a single step.

This dissertation illustrates catalyst functionalization with a ROMP monomer moiety to synthesize a ROMP inimer (inimer= initiator + monomer). The ROMP initiator—olefin metathesis catalyst—and ROMP monomer coupling produces an “*inimer*”. The inimer can undergo self-condensing ROMP with a ROMP monomer addition to synthesize hyperbranched polymers. This approach introduced a new class of olefin metathesis complexes containing both the initiator and propagating center. This approach also provides a way to synthesize hyperbranched polymers from any known ROMP monomers in a single step.

## ACKNOWLEDGMENTS

I am very grateful to my advisor Dr. Michael Schulz for his patience, invaluable insights and ideas, and support. Without his guidance, this work would not have been accomplished. I would also like to thank my committee members: Profs. Rich Gandour, Paul Deck, and Alan Esker for their guidance, insightful comments, and recommendations. I thank Dr. Carla Slebodnick for her work on X-ray crystallography. She characterized more than 25 olefin metathesis complexes and her work is presented in each chapter of this dissertation. I really appreciate her work and patience in collecting the data.

I would like to thank the following people for helping with this dissertation: Dr. Murthy Shanaiah and Ken Knott for their support in the NMR studies, Dr. Rituraj Borgohain and Dr. Patrick Finley for their support in the DSC activation temperature studies, Dr. Robert Moore and Dr. John Matson and their group members for their support in material characterization.

I am grateful to have the pleasure of working with Schulz research group alumni and current members, particularly Dr. Brady Hall, Dr. Ryan Archer, Ophelia Wadsworth, Tiffany Thompson, Rachel Bianculli, Meagan Mazza, Jon Mase, Nuren Iftekhar, Connor Gallagher, Zhen Shi, Gillian Su, and Amira Mohamed, and all our undergraduate research assistants, especially Grace Dinges who worked with me.

I would also like to give special thanks to my husband Abdulmohsen, and my son Badr for their continuous support. Many thanks to my greatest mom and dad, your prayer for me was what sustained me this far. Special thanks to my sisters (Eman, Ashwaq,

Rawan, and Goot), and brothers (Saad and Moad) for being close to me. I would also like to thank my friends here at Virginia Tech and elsewhere for their friendship and support.

I would like to extend my gratitude to the Saudi Arabia government for the full 5 years scholarship. I also express my thanks to the Saudi Arabian Cultural Mission (SACM) in the USA which facilitated the funding. Finally, I would like to thank everyone who supported me somehow in my academic years. It would be impossible to mention all of them here, but I am very grateful for their support.

## TABLE OF CONTENTS

<b>ABSTRACT</b> .....	<b>ii</b>
<b>GENERAL AUDIENCE ABSTRACT</b> .....	<b>iv</b>
<b>ACKNOWLEDGMENTS</b> .....	<b>v</b>
<b>TABLE OF CONTENTS</b> .....	<b>vii</b>
<i>Chapter 1. Literature Review</i> .....	<i>1</i>
<b>1.1. Ring-Opening Metathesis Polymerization</b> .....	<b>1</b>
<b>1.2. Development of Latent Olefin Metathesis Catalysts</b> .....	<b>2</b>
<b>1.3. Hyperbranched ROMP Polymers</b> .....	<b>11</b>
<b>1.4. Self-Condensing Polymerization</b> .....	<b>14</b>
<b>1.5. Current Approach: Self-Condensing Ring-Opening Metathesis Polymerization</b> .....	<b>18</b>
<b>1.6. Study Objectives</b> .....	<b>21</b>
<b>1.7. Synthesis of Bimetallic Olefin Metathesis Catalysts</b> .....	<b>24</b>
<b>1.8. References</b> .....	<b>26</b>
<i>Chapter 2. Monomer Identity Effects on Latent Olefin Metathesis Catalyst Activation</i>	
<i>Temperature</i> .....	<i>31</i>
<b>2.1. Abstract</b> .....	<b>31</b>
<b>2.2. Introduction</b> .....	<b>32</b>
<b>2.3. Results and Discussion</b> .....	<b>34</b>
<b>2.4. Conclusions</b> .....	<b>43</b>
<b>2.5. References</b> .....	<b>44</b>
<b>2.6. EXPERIMENTAL SECTION</b> .....	<b>46</b>
<i>Chapter 3. Studies on Electronic Effects in Imine Chelated Ruthenium Olefin</i>	
<i>Metathesis Catalysts</i> .....	<i>81</i>

3.1. Abstract.....	81
3.2. Introduction .....	82
3.3. Results and Discussion.....	82
3.4. Conclusions and Future Work.....	91
3.5. References .....	92
3.6. Experimental Section .....	93
<i>Chapter 4. Imine-Chelated Ruthenium Olefin Metathesis Inimer .....</i>	<i>181</i>
4.1. Abstract.....	181
4.2. Introduction .....	181
4.3. Results and Discussion.....	183
4.4. Conclusion.....	193
4.5. References .....	194
4.6. Experimental Section .....	196
<i>Chapter 5. Synthesis of Azo and Imine Ring-Opening Metathesis Polymerization Inimers.....</i>	<i>240</i>
5.1. Abstract.....	240
5.2. Introduction .....	241
5.3. Results and Discussions .....	244
5.4. Conclusion.....	260
5.5. References .....	262
5.6. Experimental Section .....	264
<i>Chapter 6. Synthesis and Characterization of Bimetallic Olefin Metathesis Catalysts .....</i>	<i>358</i>
6.1. Abstract.....	358
6.2. Introduction .....	359

<b>6.3. Results and Discussion.....</b>	<b>363</b>
<b>6.4. Conclusions and Future Work.....</b>	<b>369</b>
<b>6.5. References.....</b>	<b>370</b>
<b>6.6. Experimental Section.....</b>	<b>372</b>
<b><i>Chapter 7. Synthesis and Characterization of Copper-Ruthenium Olefin Metathesis</i></b>	
<b><i>Catalysts.....</i></b>	<b><i>416</i></b>
<b>7.1. Abstract.....</b>	<b>416</b>
<b>7.2. Introduction.....</b>	<b>417</b>
<b>7.3. Results and Dissections.....</b>	<b>419</b>
<b>7.4. Conclusions and Future Work.....</b>	<b>424</b>
<b>7.5. References.....</b>	<b>425</b>
<b>7.6. EXPERIMENTAL SECTION.....</b>	<b>426</b>
<b><i>Chapter 8. Summary and Future Outlook.....</i></b>	<b><i>468</i></b>

# Self-Condensing Ring-Opening Metathesis Polymerization

## Chapter 1. Literature Review

### 1.1. Ring-Opening Metathesis Polymerization

Ring-opening metathesis polymerization (ROMP) is a subclass of olefin metathesis involving breaking and reforming the double bonds of an unsaturated strained cyclic monomer.<sup>1</sup> Well-defined ruthenium-based olefin metathesis catalysts are the most common ROMP initiators due to their functional group tolerance, and oxygen and moisture stability.<sup>2</sup> Polymerization via traditional ROMP involves olefin metathesis catalyst activation to ring-open a ROMP monomer (**Figure 1.1**).<sup>3-5</sup> The polymers grow with the ruthenium center attached on one side of the polymer and the benzylidene ligand attached to the other side. Polymers are terminated with vinyl ether addition to release the deactivated metal metathesis catalyst (**Figure 1.1**).

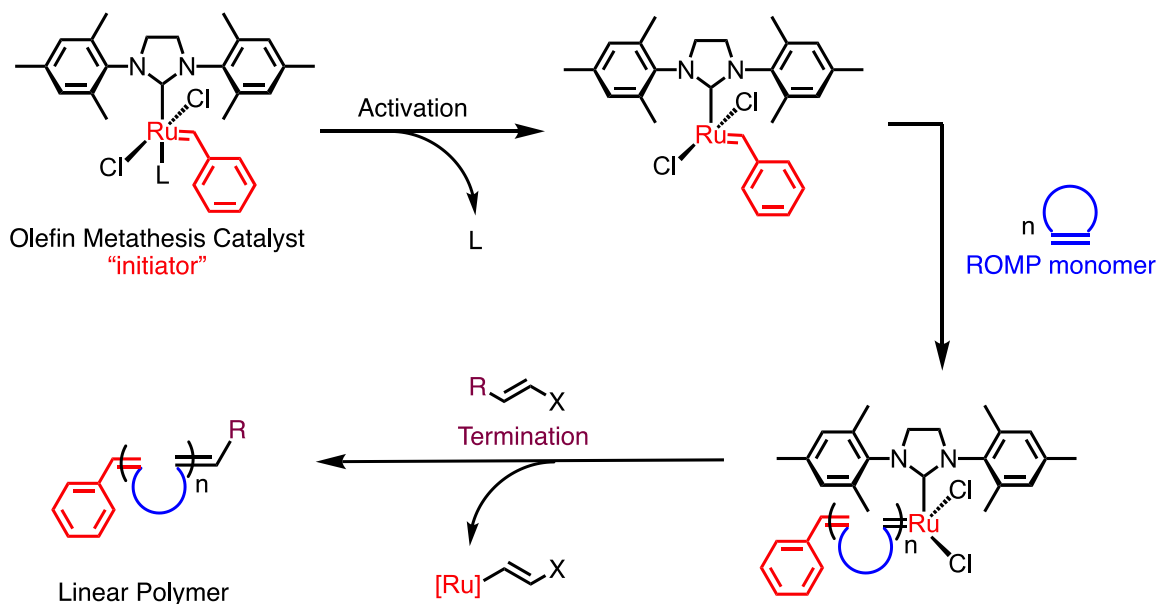


**Figure 1.1. Traditional ROMP is catalyzed by ruthenium-based olefin metathesis catalysts.**

The development of well-defined ruthenium-based olefin metathesis catalysts enables the synthesis of materials with different topologies, functionalities, and chemical and physical properties.<sup>2</sup> However, olefin metathesis catalyst modification is still required to control catalyst activity and stability. Ligand modification allowed the synthesis of highly stable and catalysts unreactive at room temperature, known as *latent* olefin metathesis catalysts.<sup>2</sup>

## 1.2. Development of Latent Olefin Metathesis Catalysts

Latent olefin metathesis catalysts are pre-catalysts with negligible activity at a given temperature, usually room temperature, and significant reactivity when suitable stimuli are applied.<sup>6</sup> Many latent olefin metathesis catalysts were developed based on the Grubbs second-generation catalyst (G2) (**Figure 1.2**).<sup>7-19</sup> These latent catalysts have an alkylidene ligand stabilizing the catalyst by ligand chelation (**Figure 1.2**). Using an unreactive catalyst at room temperature allows the monomer to be mixed with the catalyst before starting the polymerization, which gives the formulation enough time to handle without unwanted polymerization.<sup>20</sup> Latent olefin metathesis catalysts have longer shelf lives than more active catalysts.<sup>21</sup> The ability to control the catalyst reactivity enables the development of smart reaction systems, where multiple reaction components can be selectively activated at specific times in the presence of other components.<sup>21</sup> Furthermore, latent olefin metathesis catalysts have been used to study the mechanism of metathesis reactions.<sup>22</sup>

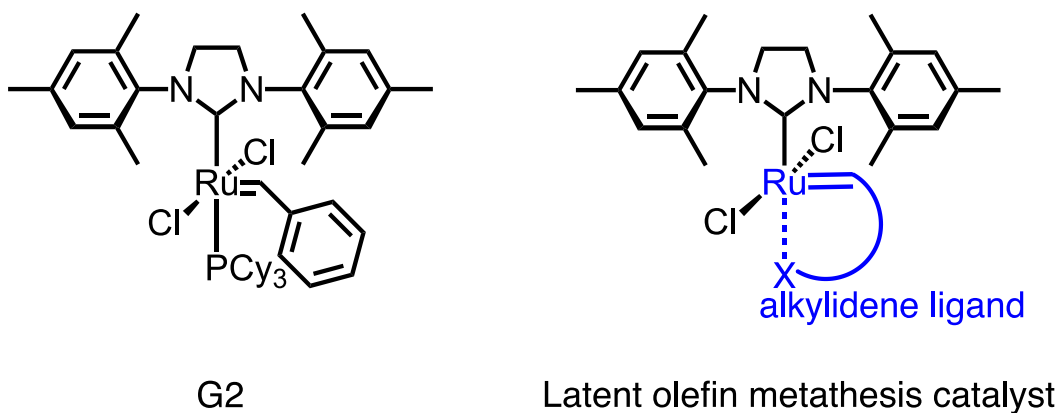


**Figure 1.2. Grubbs second generation catalyst and a latent catalyst chelating alkylidene ligand.**

Development of latent olefin metathesis catalysts has given rise to catalysts that are inactive at room temperature in the presence of ROMP monomers and other olefins, but that can be activated by physical factors such as elevated temperature, mechanical force, or light.<sup>23,24</sup> For example, catalyst **[Ru] 1** (**Figure 1.3**) is a sulfur-chelated ruthenium latent olefin metathesis catalyst showing stability at room temperature, but was activated upon heating or light.<sup>25, 26</sup> Latent olefin metathesis catalysts can also be activated by chemical addition. HCl, TMSCl<sup>20</sup>, and Cu(I) salts<sup>27</sup> are commonly used as chemically effective activation approaches.<sup>25, 28</sup> For example, catalyst **[Ru] 2** (**Figure 1.3**) is a latent catalyst that was activated by HCl addition.<sup>26</sup> Even though chemical activation requires adding a reagent, which could contaminate the final product, an excellent interconversion between the inactive and active forms can be achieved.<sup>6</sup>

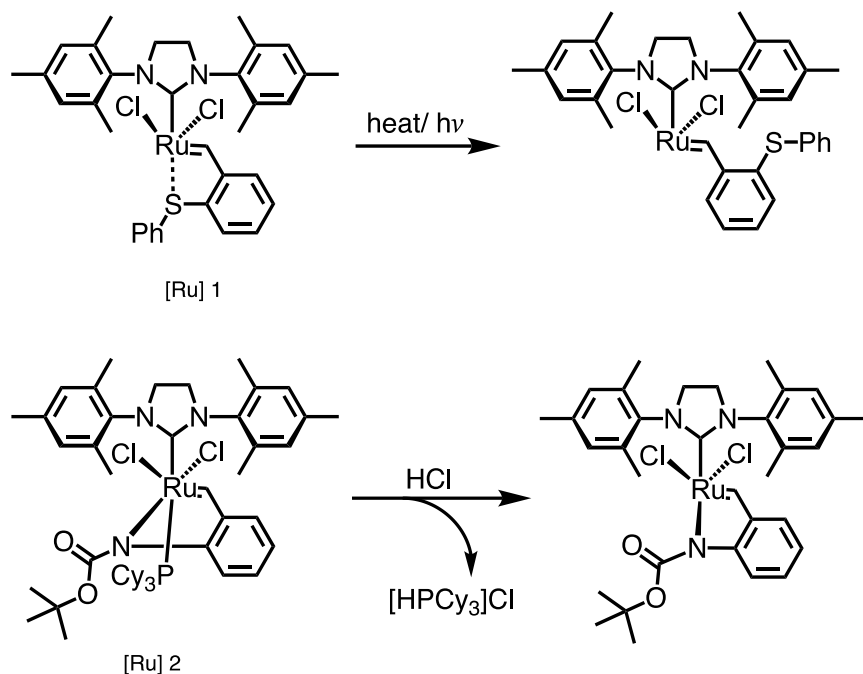


**Figure 1.3. Latent olefin metathesis catalysts activation examples.**

The latency of olefin metathesis catalysts can be controlled by varying chelated heteroatoms,<sup>10, 15, 29</sup> steric and electronic properties of the ligands,<sup>6, 15, 30</sup> or chelate ring size.<sup>9</sup> For example, well-defined Hoveyda–Grubbs second-generation catalyst **[Ru] 3** (**Figure 1.4**) showed reactivity in olefin metathesis reactions at or below room temperature due to the ether chelation, which is not strong enough to render **[Ru] 3** latent.<sup>31,10</sup> Grela and co-workers synthesized **[Ru] 4** to study the effect of adding diethylamino as an electron-donating group to the benzylidene ligand. **[Ru] 4** showed practically no activity at room temperature in olefin metathesis but was activated by acid addition or heat.<sup>17</sup>



91% conversion using a latent catalyst **[Ru] 7** with phenyl substituted group under the previous reaction conditions.<sup>15</sup>

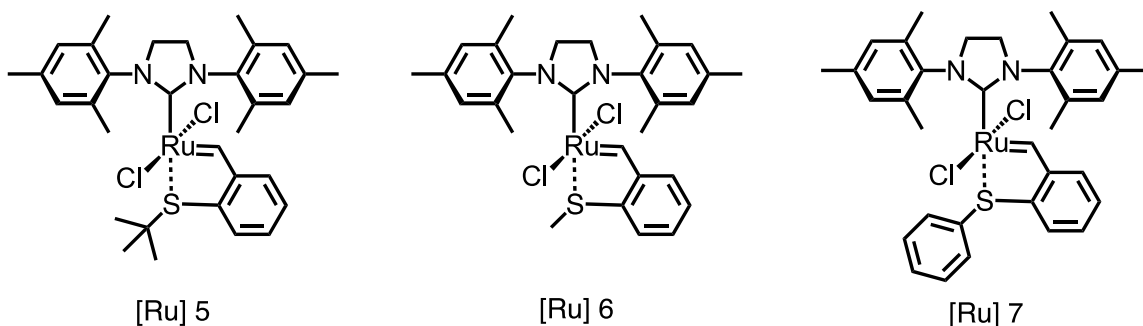


**Figure 1.5. Sulfur-chelated olefin metathesis catalysts.**

Other sulfur-chelated ruthenium catalysts (**Figure 1.6**) were synthesized to study the polymerization of active ROMP monomers: dicyclopentadiene and unsubstituted norbornene.<sup>6</sup> These monomers can be polymerized at room temperature with sulfur-chelated olefin metathesis catalysts due to the monomer high reactivity.<sup>6</sup> To increase the latency of sulfur-chelated olefin metathesis catalysts, the interaction between the Ru atom and the ligand should increase. To achieve stronger interaction, the activity of a three-point chelate catalyst having two heteroatoms that can interact with Ru was studied. The first attempt was synthesizing sulfur-oxygen complex **[Ru] 8** with a  $(\text{CH}_2)_2\text{OCH}_3$  group. The latency of the sulfur-oxygen complex is not affected by the presence of two heteroatoms because the oxygen was unable to interact with the Ru atom.<sup>6</sup> That observation was explained by the insignificant shift of the  $\text{O-CH}_3$   $^{13}\text{C}$  NMR signal in the spectrum of the free ligand and catalyst complex, indicating that the interaction occurs only between the Ru and sulfur atom.<sup>6</sup> As a result, this catalyst has a bidentate chelate complex. To show that a bidentate chelate complex does not increase the latency of the olefin metathesis

catalyst, the polymerization of dicyclopentadiene was studied using this catalyst. After 2 h at room temperature, the polymerization reached 40% conversion of the monomer.<sup>6</sup>

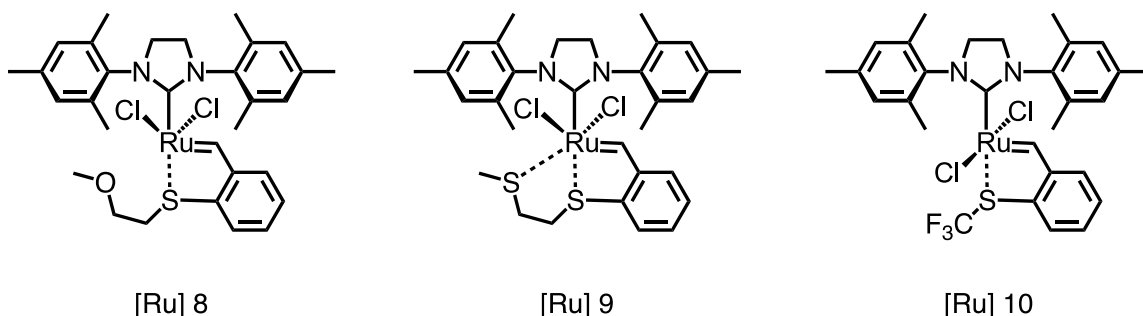


**Figure 1.6. Bidentate and tridentate chelate complexes.**

Another attempt was to synthesize a sulfur-sulfur complex **[Ru] 9** with a  $(\text{CH}_2)_2\text{SCH}_3$  group (**Figure 1.6**). This complex showed higher catalyst latency compared with the sulfur–oxygen complex. This catalyst has a second interaction between the sulfur of the thioether group and the Ru atom, forming a tridentate chelate complex.<sup>6</sup> The sulfur binding to the Ru atom was supported by the significant  $^{13}\text{C}$  NMR S- $\text{CH}_3$  signal shift from 15.4 ppm in the free ligand to 40.6 ppm in the catalyst. The conversion of the dicyclopentadiene monomer was less than 1% after 2 h at room temperature.<sup>6</sup> Upon increasing the temperature to 80 °C for one hour, the conversion of the ROMP monomer increased to 36%.<sup>6</sup> The downside of the higher latency of the sulfur–sulfur complex is that polymerization takes a longer time to achieve higher conversion; only a 46% conversion was achieved after 3 h of polymerizing dicyclopentadiene at 80 °C. Furthermore, decomposition may occur at higher temperatures, causing a decrease in the conversion; a 37% conversion was achieved at 110 °C under the previous conditions.<sup>6</sup>

The effect of adding a strong electron withdrawing group was studied by synthesizing a sulfur-chelated ruthenium catalyst **[Ru] 10** having a  $\text{CF}_3$  (**Figure 1.6**). This

complex displayed higher stability at room temperature and increased activity when activated, due to the weak S–Ru bond resulting from the electron-withdrawing CF<sub>3</sub> substituted group.<sup>6</sup> With this catalyst, less than 1% conversion was achieved after 24 h of reaction with diethyl diallylmalonate at 27 °C. At 80 °C, 75% conversion was achieved after only 1 hour. Furthermore, a higher conversion was accomplished when this catalyst was activated by UV light instead of thermal activation. In this case, the conversion increased to 86% and the polymerization was done in 2 h at room temperature.<sup>6</sup>

Additionally, an azo-based chelating ruthenium olefin metathesis catalyst has been synthesized (**Figure 1.7**).<sup>32</sup> This catalyst was thermally stable and activated by UV light due to a fast  $\pi$ - $\pi^*$  transition in the N–N=N moiety.<sup>32</sup> The synthesis of this catalyst generates two isomers in a 100:3 ratio (**Figure 1.7**). The major isomer is the result of the interaction between the Ru atom and aryl nitrogen atom to generate a five-member ring that is resonance stabilized. However, a minor resonance contributor has an interaction between the Ru and the other N atom forming a six-member ring. This isomer has lower ring strain, but cannot be stabilized by any resonance form.<sup>32</sup>

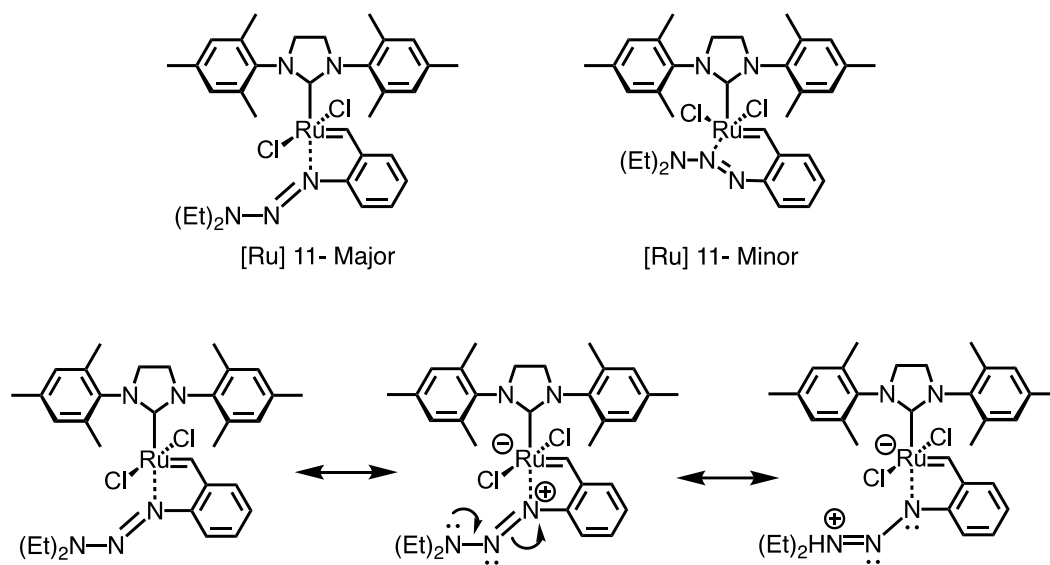


**Figure 1.7. Two isomers and resonance structures of the azo-based chelating ruthenium olefin metathesis catalyst.**

The latency of the azo-based chelating ruthenium olefin metathesis catalyst was demonstrated by mixing the catalyst with ROMP monomers: *cis*-cyclooctene and dicyclopentadiene. No reaction was observed at room temperature, or when the reaction mixture was heated to 50 °C for 24 h.<sup>32</sup> However, more than 95 % conversion of *cis*-cyclooctene and 81 % conversion of dicyclopentadiene were observed when the reaction mixture was exposed to UV light at room temperature for 2 h.<sup>32</sup>

The latent *N*-chelating azo benzene ruthenium metathesis catalyst [**Ru**] **12** (Figure 1.8) was synthesized to study the catalyst activation by either temperature or UV light.<sup>29</sup> Two isomers with different chelate ring sizes were isolated. The six-member chelating ring, in this case, is more stable than the five-member chelating ring. This observation was explained by the length of the Ru-N bond: a shorter bond is formed with a six-member ring, resulting in greater interaction between the Ru and nitrogen atom.<sup>29</sup> This catalyst displays high stability at room temperature in both solid- and solution-state but can be

activated by both thermal or UV light to promote ROMP and ring-closing metathesis of two different monomers (**Figure 1.9**).<sup>29</sup>

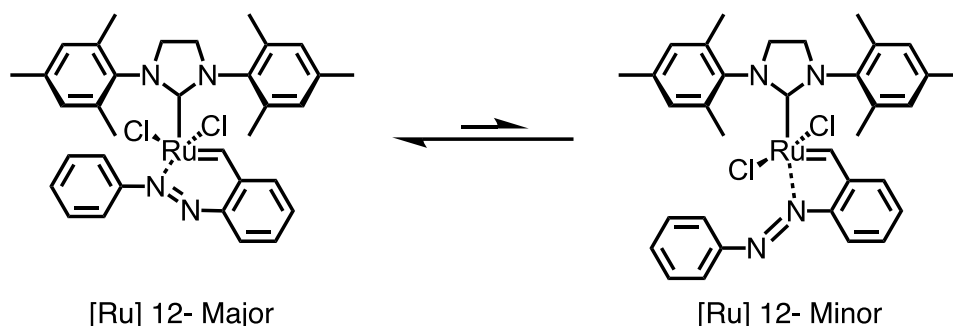


**Figure 1.8. Two isomers of the latent N-chelating azo benzene ruthenium metathesis catalyst.**

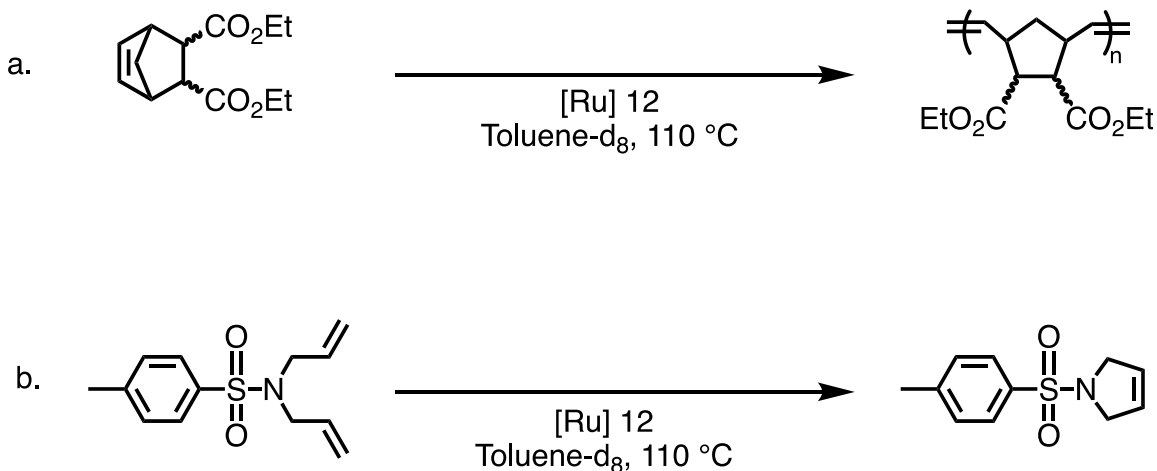


**Figure 1.9. The latent N-chelating azo benzene ruthenium olefin metathesis catalyst reactions tested: a. ROMP and b. Ring-closing olefin metathesis.**

The effect of chelating ring size was studied by synthesizing two imine-chelated ruthenium catalysts: **[Ru] 13** with a five-member chelating imine ring and **[Ru] 14** with a six-member chelating imine ring (**Figure 1.10**).<sup>9</sup> The latency of **[Ru] 13** is lower than the latency of **[Ru] 14**. This result was explained by measuring catalyst activation temperature

by differential scanning calorimetry (DSC). **[Ru] 13** and **14** were activated at 48 and 55 °C respectively. Also, **[Ru] 13** showed higher reactivity in ROMP compared to **[Ru] 14**.<sup>9</sup>

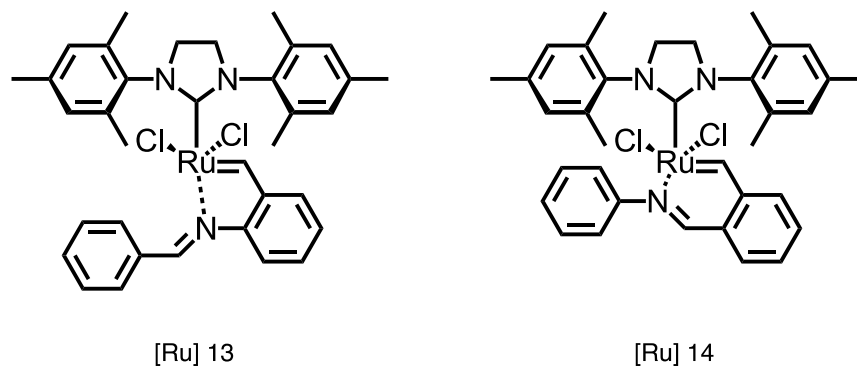


**Figure 1.10. Catalysts with imine chelation.**

### 1.3. Hyperbranched ROMP Polymers

Ligand modifications on ruthenium catalysts have been applied to improve the catalyst stability and reactivity.<sup>33-40</sup> However, ligand modifications have not been explored in the application of synthesizing hyperbranched polymers—irregular branching with a high number of end functional groups—via ROMP. Hyperbranched ROMP polymer synthesis is challenging due to the requirement of multi-functional ROMP monomers or multi-polymerization approaches.

Hyperbranched polymers display different chemical and physical properties relative to their linear counterparts.<sup>41, 42</sup> Hyperbranched polymers have a lower viscosity, higher solubility, and lower chain entanglement compared to their linear analogues. Hyperbranched polymers are polydisperse and often synthesized in a single step.<sup>43</sup> Hyperbranched polymers have been used for many applications including processing additives, cross-linkers, compatibilizers, and catalyst supports.<sup>42-45</sup>

ROMP has been used to synthesize hyperbranched polymers by using multifunctional ROMP monomers or a combination of two synthetic approaches. For example, dicyclopentadiene was a multifunctional ROMP monomer that can be polymerized in the presence of monoterpenes, d-limonene, limonene oxide, and  $\beta$ -pinene to produce hyperbranched polymers (**Figure 1.11**).<sup>46</sup> Chain transfer occurs during ROMP when a monoterpene alkene reacts with the olefin metathesis initiator. The degree of branching (DB) in this polymerization depends on the polymerization time, initiator loading, and choice of monoterpene.<sup>46</sup> Hyperbranched polymers were also synthesized using a “*termimer*”—a single molecule that combines a functionalized *cis*-vinyl ether end-capping reagent and a ROMP monomer (**Figure 1.12**).<sup>47</sup> The terminator allows the combination of two propagating ROMP chains into one branched structure.<sup>47</sup>

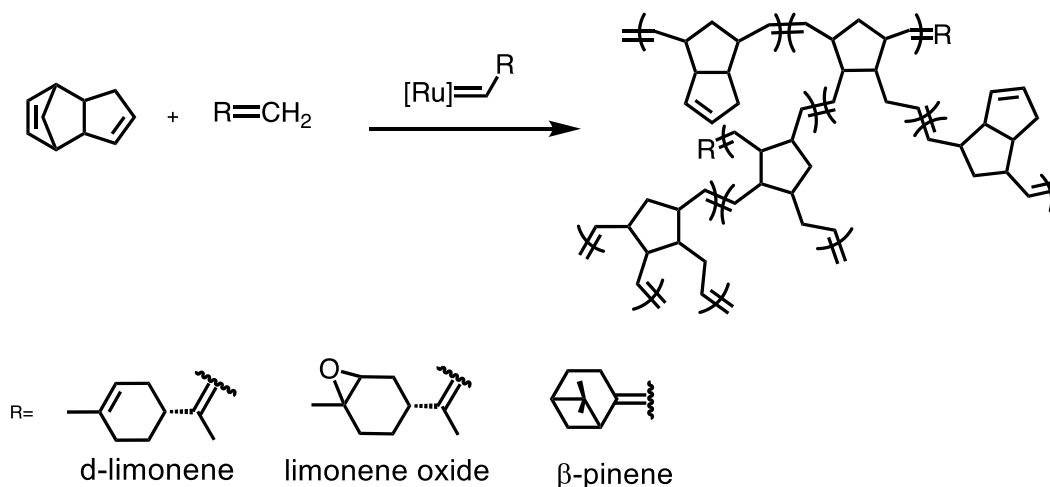


**Figure 1.11. Hyperbranched polymer synthesis with multifunction ROMP monomer.**

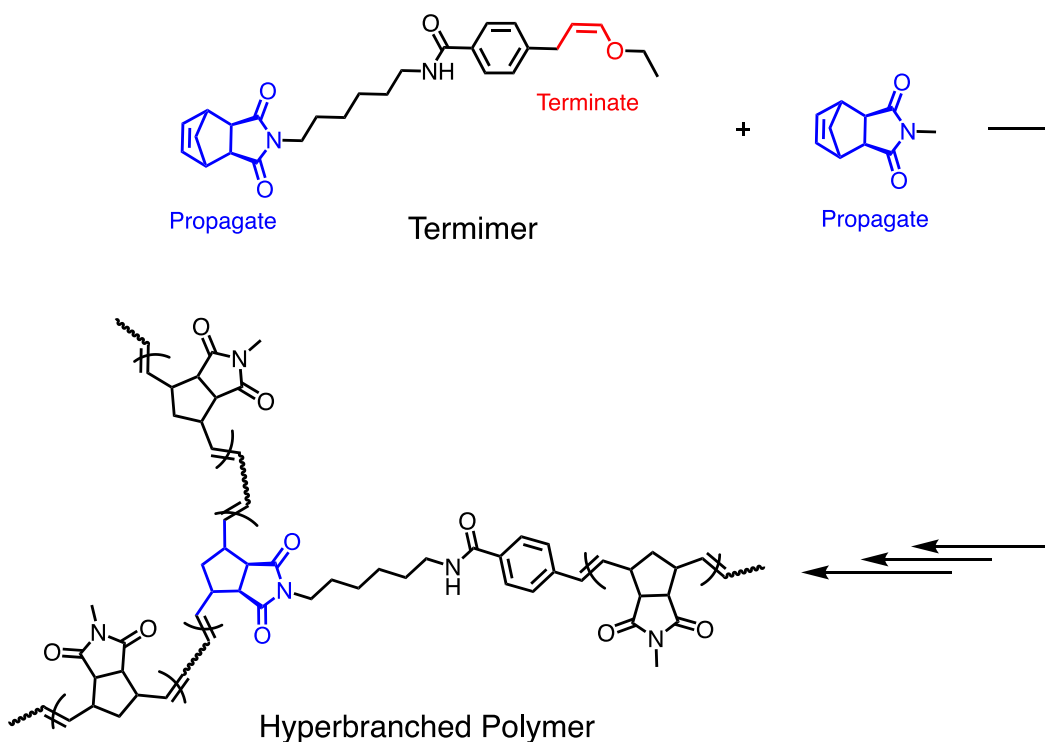


**Figure 1.12. Hyperbranched polymer synthesis using a termimer.**

Additionally, the combination of two polymerization mechanisms was applied to prepare hyperbranched polymers via ROMP. For example, hyperbranched polymers were prepared by combining ring-opening metathesis and cross-metathesis with a single monomer and reaction: a cyclic olefin for the ring-opening metathesis and the terminal olefin for cross-metathesis (**Figure 1.13**).<sup>48</sup> Tandem ROMP and acyclic diene metathesis (ADMET) polymerization were also studied as a route to synthesize hyperbranched polymers.<sup>49-51</sup> Furthermore, ROMP has been used to synthesize AB<sub>n</sub>-type macromonomers for long-chain branched ROMP polymers.<sup>52</sup> While successful, these approaches have inherent disadvantages ranging from requiring multiple reactions to form the final hyperbranched structure, to needing specialized monomers.

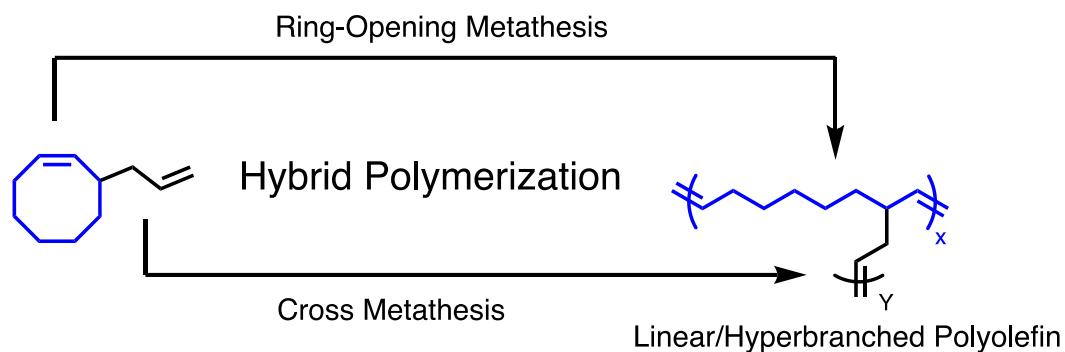


**Figure 1.13. Hyperbranched polymers were prepared by combining ring-opening metathesis and cross-metathesis.**

#### 1.4. Self-Condensing Polymerization

To simplify the synthesis of hyperbranched ROMP polymers, we are introducing a novel approach: *self-condensing ring-opening metathesis polymerization*. Self-condensing polymerization has already been applied to other polymerization approaches. A single molecule containing both an initiator and a monomer, an *inimer*, is required to enable self-condensing polymerization. The hyperbranched polymers are synthesized in a single step without the need for multi-functional monomers or multi-polymerization approaches.

Self-condensing vinyl polymerization (SCVP) was introduced in 1995 by Fréchet and coworkers to incorporate more chain-growth character into the mechanism of hyperbranched polymer synthesis.<sup>53</sup> Self-condensing polymerization requires a single molecule containing both an initiator and monomer moiety, an *inimer* (**Figure 1.14**). By combining a polymerizable group, “a monomer”, and an initiator into one chemical entity, hyperbranched polymers are synthesized in a single step in a controlled manner.<sup>53, 54</sup> The polymerization starts with inimer activation to form a radical, cation, or carbanion, which goes on to react with a vinyl group on the monomer to form a covalent bond with a new

active site on the  $\alpha$ -carbon of the double bond (**Figure 1.14**). Controlled radical polymerization systems are preferred to avoid gelation, which minimizes radical–radical coupling.<sup>55</sup> Another advantage of SCVP is the variety of vinyl monomers that can be used.

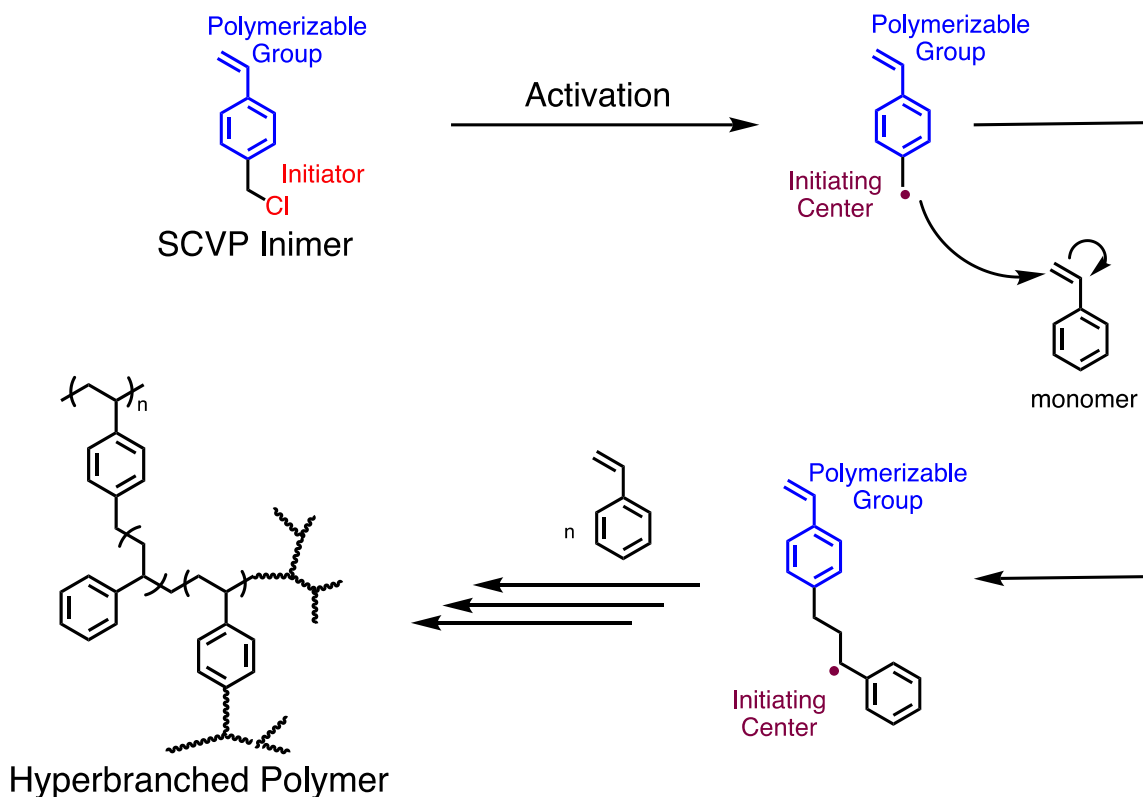


**Figure 1.14. Hyperbranched polymer synthesis via SCVP.**

The SCVP concept was later expanded to ring-opening polymerization (ROP), self-condensing ring-opening polymerization (SCROP). Hyperbranched polyesters were prepared from the self-condensing cyclic ester polymerization of bis(hydroxymethyl)-substituted  $\epsilon$ -caprolactone (**Figure 1.15**).<sup>56, 57</sup> The single molecule, i.e., SCROP inimer, contains both the alcohol group acting as an initiator and caprolactone acting as a monomer. The polymerization starts with inimer activation catalyzed by stannous octoate at 110 °C. The active inimer reacts with another inimer to form a dimer, which still has both an

initiating center and a polymerizable group. The dimer can activate to react with other inimers or dimers to build the hyperbranched structure.<sup>57</sup> As a result, the synthesis of hyperbranched polymers via SCROP can proceed entirely through one type of reactive molecule.<sup>57</sup>

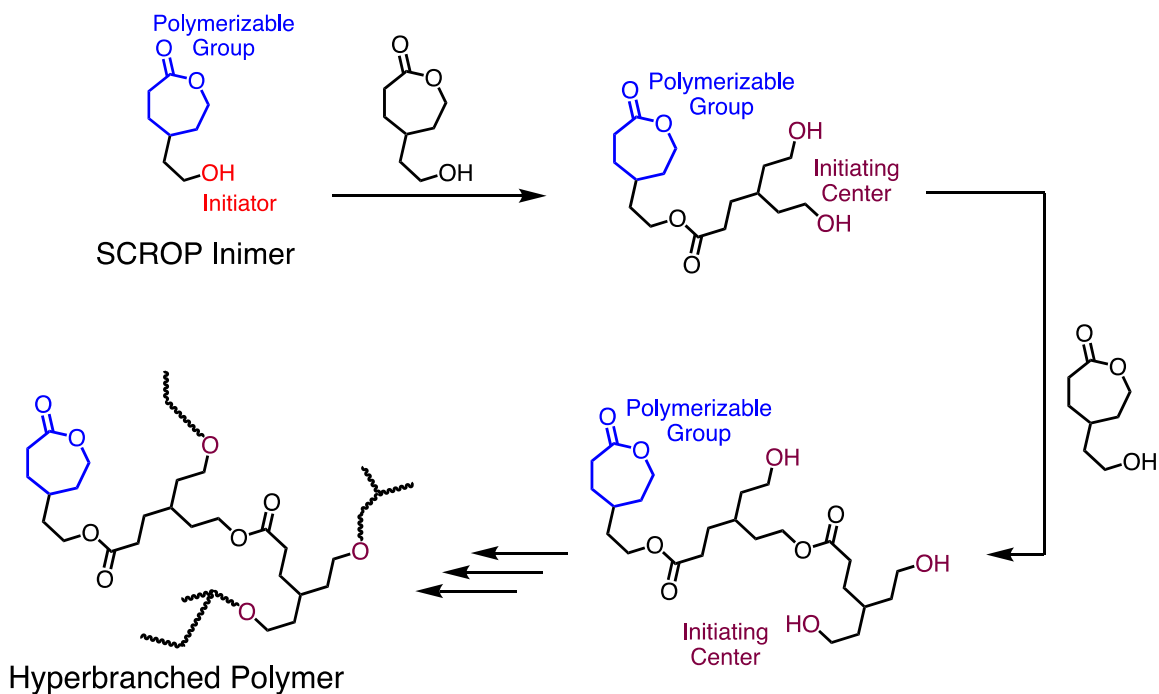


**Figure 1.15. Synthesis of hyperbranched polymers via SCROP.**

Similarly, a hyperbranched polyphosphate was synthesized by using a hydroxyl-functionalized cyclic phosphate inimer, 2-(2-hydroxyethoxy)ethoxy-2-oxo-1,3,2-dioxaphospholane (HEEP) (**Figure 1.16**).<sup>58</sup> The polymerization involves an activation step of the SCROP inimer. Then, the inimer can react with another inimer to form the hyperbranched polymer.<sup>58</sup> These polymerizations were performed without any catalyst, resulting in a highly pure polymer. These two examples of SCROP polymers have a great number of terminal hydroxyl groups, thus enabling further modification and functionalization.<sup>58</sup> The self-condensing concept was also expanded to include a radical

chain transfer agent (CTA)-monomer molecules and radical addition–fragmentation chain transfer (RAFT) polymerization.<sup>59</sup> Despite the considerable utility of this approach, this concept has not been applied to olefin metathesis polymerization, which we aim to do in this study.

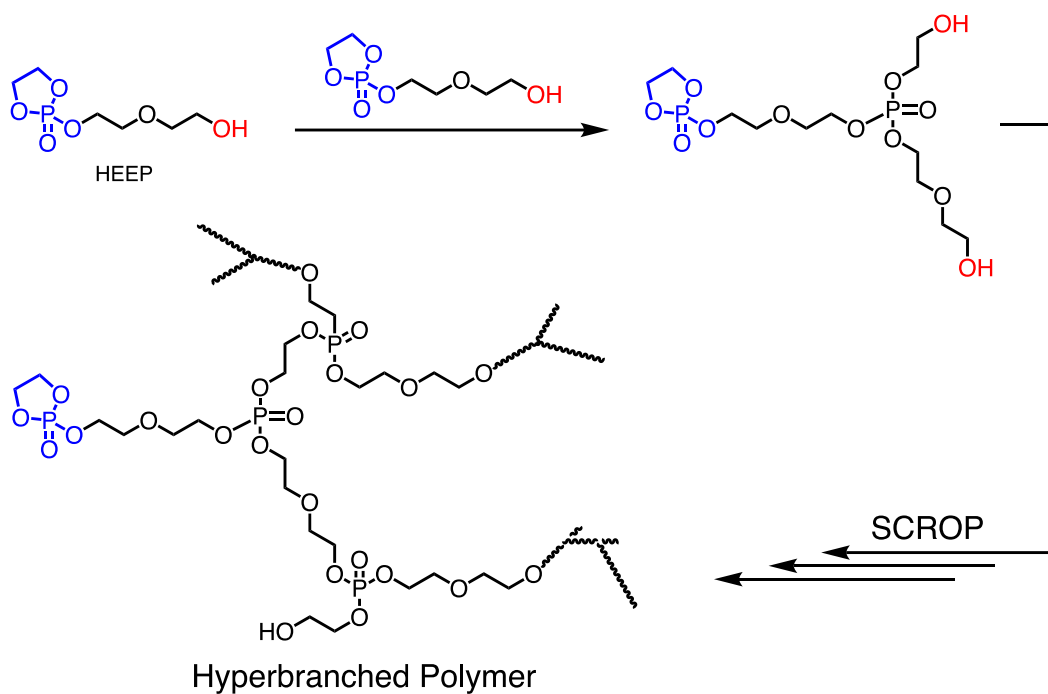


**Figure 1.16. Hyperbranched polyphosphate synthesis via SCROP.**

## 1.5. Current Approach: Self-Condensing Ring-Opening Metathesis Polymerization

### Overview

Self-condensing polymerization simplifies the synthesis of hyperbranched polymers by producing the hyperbranched structure in a single step. ROMP is a synthetic tool to prepare polymers with olefins in the polymer backbones. Similar to the SCVP and SCROP, the self-condensing ROMP approach requires the synthesis of an olefin metathesis inimer, i.e., a ROMP monomer attached to an olefin metathesis catalyst (the initiator) (**Figure 1. 17**). The key advance required to synthesize a ROMP inimer is an approach to attaching a ROMP monomer to the catalyst itself without initiating polymerization.

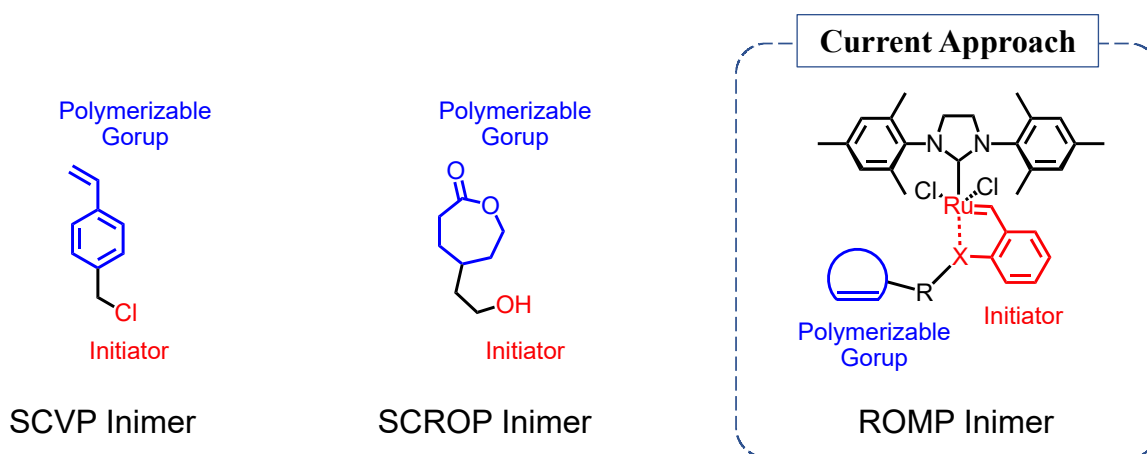


**Figure 1.17. Example of SCVP and SCROP inimer, and current approach: self-condensing ROMP inimer.**

Ruthenium-based olefin metathesis catalysts are active at or below room temperature. Controlling olefin metathesis catalyst activity is critical to prevent initiated polymerization during the inimer synthesis. Latent catalysts with chelating benzylidene ligands showed stability at room temperature. Thus, to synthesize a ROMP inimer, a latent olefin metathesis catalyst having a functional group can be coupled to a ROMP monomer

at a temperature below the catalyst activation temperature must be used (**Figure 1.18**). Then, the ROMP inimer can undergo self-condensing ROMP with ROMP monomer addition to prepare hyperbranched polymers. The ROMP inimer becomes a branching unit and the monomer addition forms the linear segment (**Figure 1.18**).

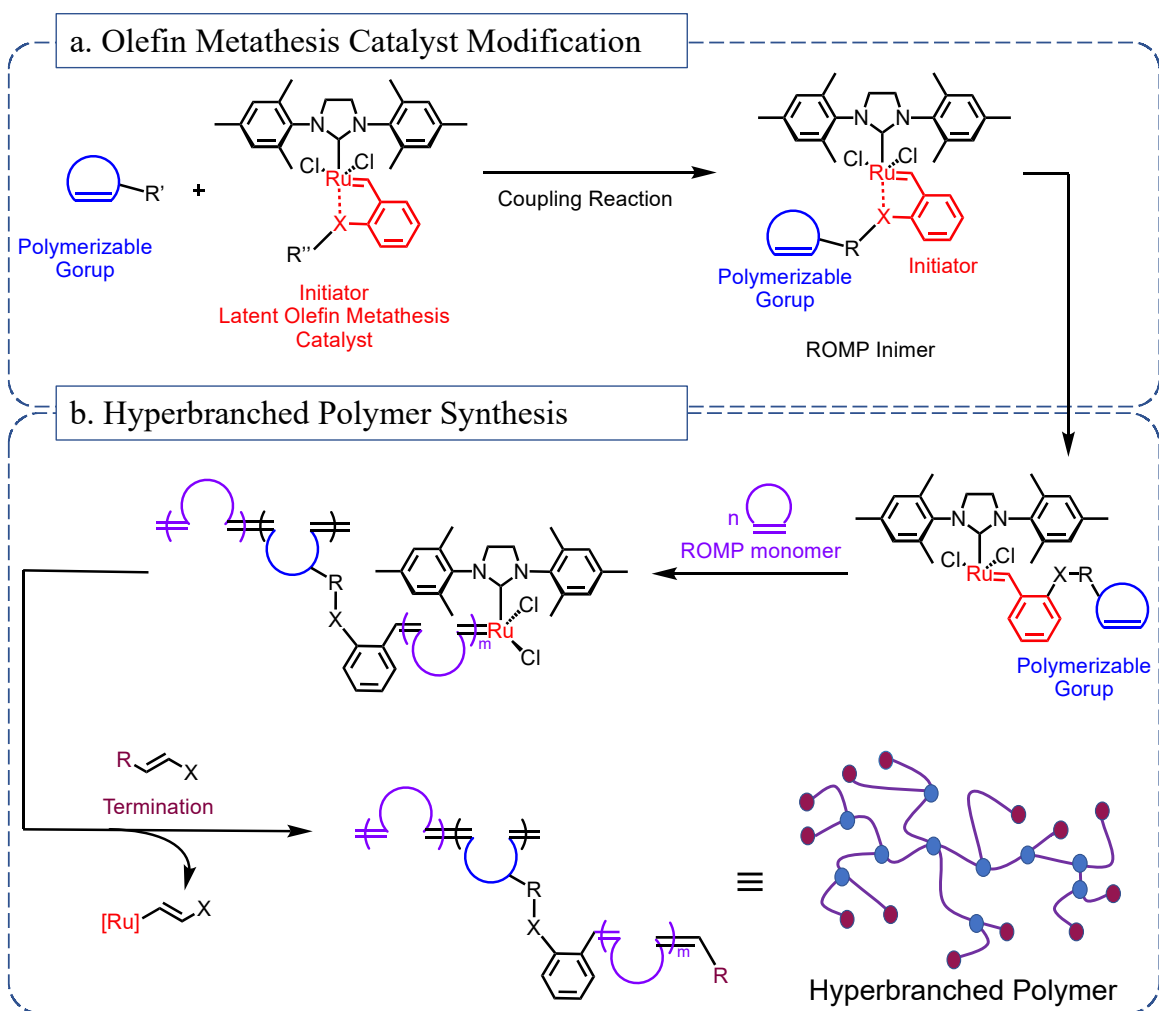


**Figure 1.18. Current approach: Hyperbranched polymer synthesis via self-condensing ROMP.**

The ROMP inimer should be stable at room temperature but activated upon heating to initiate the polymerization. However, latent olefin metathesis catalysts often show a slow initiation rate due to the strong chelation. Ligand modification around the ruthenium center

can increase the catalyst initiation rate. As a result, designing an effective ROMP inimer requires a catalyst having high stability in the monomer coupling reaction and high reactivity in self-condensing ROMP. Studying the stability and reactivity of latent olefin metathesis catalysts with different ligands will assist in designing effective ROMP inimers.

Controlling the hyperbranched polymer degree of branching is critical as the branching density affects the polymer properties. With the self-condensing approach, the degree of branching can be controlled by adjusting the monomer-to-inimer ratio. As each inimer becomes a branch point in the final polymer, increasing the inimer molar ratio produces hyperbranched polymers with a higher degree of branching. Increasing the monomer molar ratio will produce longer linear segments and fewer dendric units, resulting in decreased degree of branching. Polymer branching density can also be affected by the inimer activity. ROMP inimers with high initiation rates will form branching units, increasing the branching density (**Figure 1. 19**). However, polymerization with ROMP inimers that have a low initiation rate will produce more linear segments because a major amount of the inimer will remain inactive during the polymerization. Consequently, controlling ROMP inimer activity is important to initiate the polymerization and form more branching units.

The main advantages of the self-condensing ROMP are the ability to use a single monomer and control the degree of branching by tuning the catalyst-to-monomer ratio. In this approach, only ROMP occurs, resulting in a hyperbranched architecture in a single step. Additionally, this approach will be compatible with already-established ROMP monomers, enabling direct comparisons with linear and bottlebrush polymers reported in the literature.

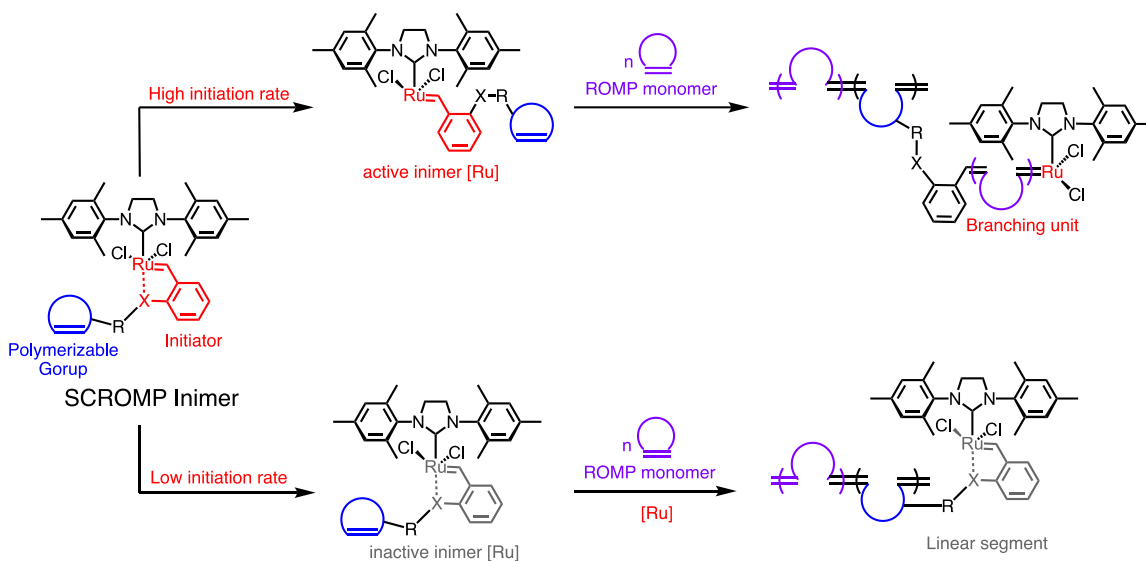


**Figure 1.19. ROMP inimer activity effects on the polymer final structure.**

## 1.6. Study Objectives

### **Objective 1: Synthesis of latent olefin metathesis catalysts with controlling catalyst stability and activity**

We hypothesized that latent olefin metathesis catalysts would enable the ROMP monomer coupling reaction to produce a ROMP inimer and avoid initiating polymerization prematurely. However, the inimer should have a higher reactivity upon activation to initiate self-condensing polymerization and form the branching polymer structure. Therefore, we aimed to synthesize a series of modified benzylidene ligands having different heteroatoms and functional groups (**Figure 1.20.a**). Then, different latent olefin metathesis catalysts will be synthesized using the modified benzylidene ligands (**Figure 1.20.b**). We aimed to characterize the synthesized catalysts to confirm their structure and activity using NMR spectroscopy and X-ray diffraction (**Figure 1.20.c**). We hypothesized that these catalysts would have different reactivity based on their geometry, heteroatom chelation, electron density, and ring-size chelation. We aimed to measure the activation temperature of the

modified latent olefin metathesis catalysts in ROMP using different ROMP monomers (**Figure 1.20.d**). Based on the DSC measurements, further modified benzylidene ligands can be designed (**Figure 1.20.a**).

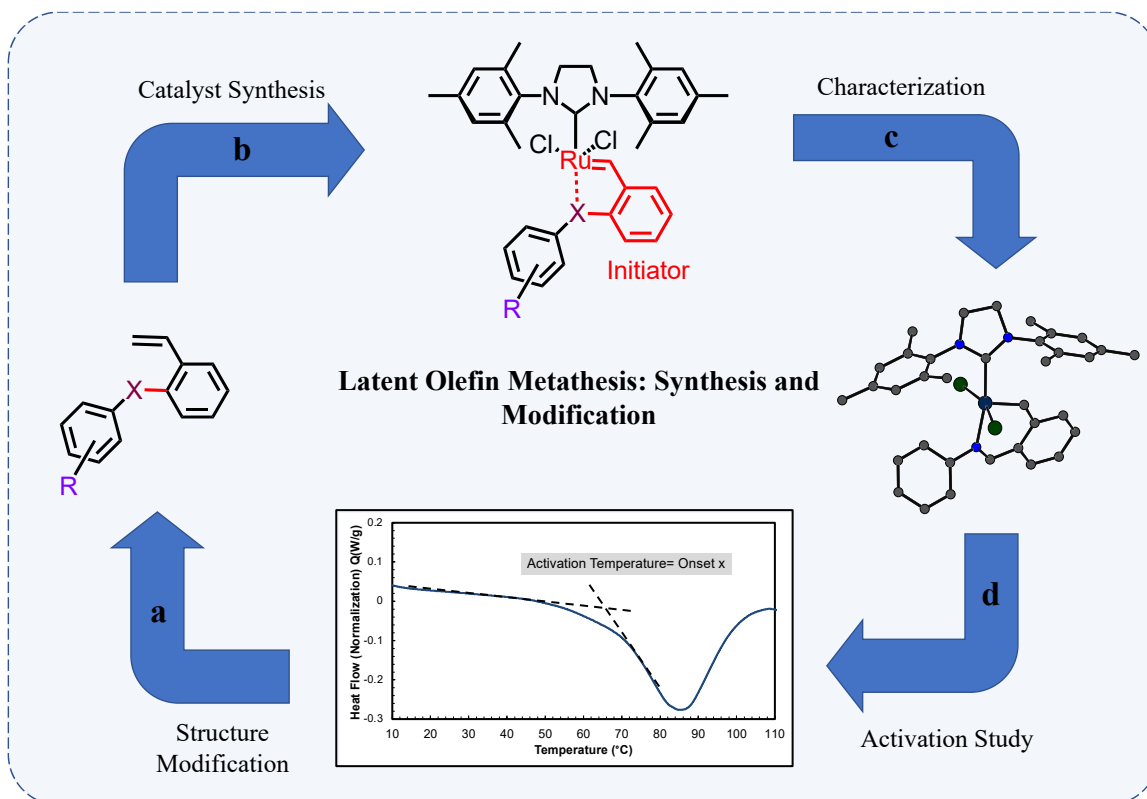


**Figure 1.20. Objective 1. Design and synthesize latent olefin metathesis catalysts.**

**Objective 2: Synthesize effective ROMP inimers and hyperbranched polymers:**

We aimed to synthesize a series of ROMP inimers having different chelating ligands and monomer moieties (**Figure 1.21.a**). Varying the chelating ligand will control the inimer activity and stability while varying the ROMP moieties will control the final structure and properties of the hyperbranched polymer. Then, we aimed to synthesize a series of hyperbranched polymers with different ROMP monomers and degrees of branching (**Figure 1.21.b**). We hypothesized that the polymer degree of branching can be

controlled with varying monomer-to-inimer ratios. As each inimer becomes a branch point in the final polymer, increasing the inimer molar ratio produces hyperbranched polymers having a higher degree of branching. Increasing the monomer ratio will lengthen the linear segments and produce fewer dendric units, resulting in decreased DB. Polymer branching density may also be affected by the inimer activity. Inimers having a higher initiation rate will form branching units while inimers with a lower initiation rate will form hyperbranched polymers with longer linear segments.

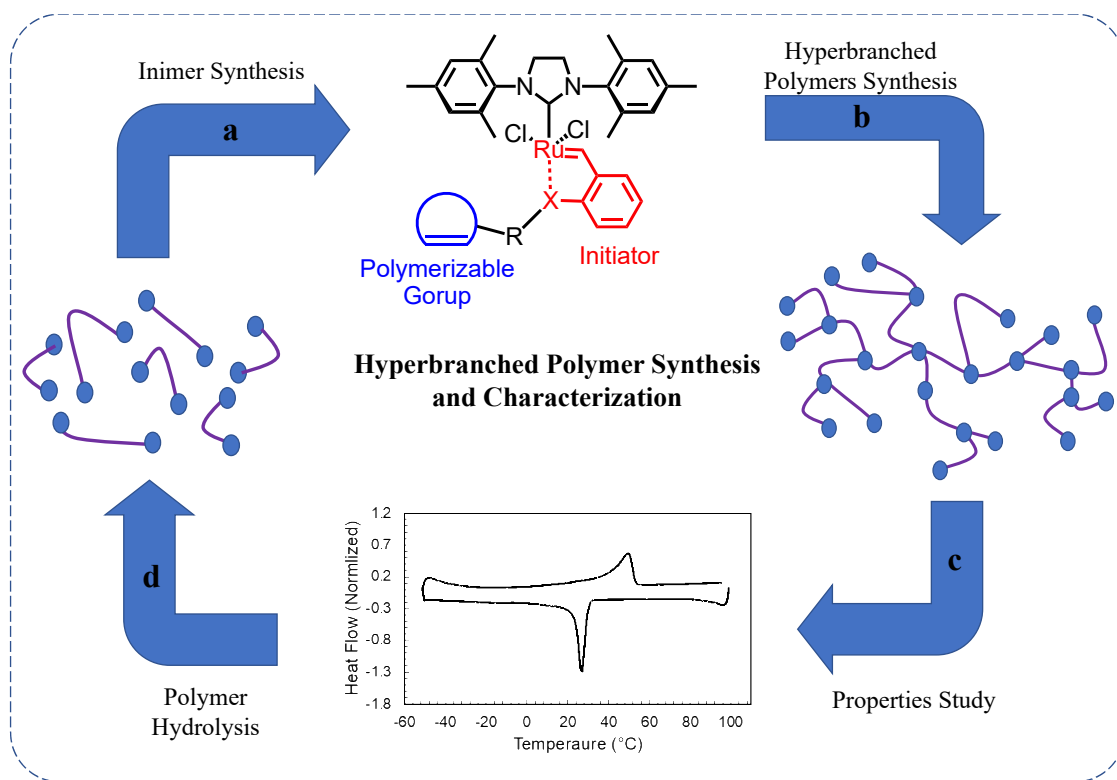


**Figure 1.21. Objective 2. synthesis of effective ROMP inimer and hyperbranched polymers.**

We aimed to study polymer physical properties and compare them to linear analogs to estimate the effect of the polymer branching density. We hypothesized that the branching structure will lower the melting, glass transition, and degradation temperatures compared

to linear polymers. Therefore, we aimed to synthesize linear polymers with number average molecular weight ( $M_n$ ) similar to the hyperbranched polymers'  $M_n$  and measure each polymer's physical properties using thermogravimetric analysis (TGA) and differential scanning calorimetry (DSC) (**Figure 1.21.c**).

Self-condensing ROMP requires an initiator–monomer coupling reaction to form a linkage between the initiation and propagating center. This linkage will remain in the polymer branching units, enabling chemical branch point degradation. Degradation of the hyperbranched polymer releases linear segments. Hydrolytic degradability is a key difference between the hyperbranched polymers and the analogous linear ROMP polymers. Hydrolysis can be done using basic or acidic conditions depending on the linkage type (**Figure 1.21.d**). Size-exclusion chromatography SEC can be used to measure the difference in  $M_n$  before and after hydrolysis.

### 1.7. Synthesis of Bimetallic Olefin Metathesis Catalysts

Although a few examples of bimetallic complexes were developed in recent years, this class of catalysts showed interesting geometry, reactivity, and stability.<sup>60, 61</sup> Here, we developed two bimetallic catalyst synthetic approaches: The first approach is a homo bimetallic ruthenium-based olefin metathesis catalyst that was developed based on benzylidene ligand modification (**Figure 1.22.a**). The second approach is a hetero bimetallic copper-ruthenium olefin metathesis catalyst that was developed based on the addition of copper (I) salts (**Figure 1.22.b**). Both approaches produce catalysts with different catalyst geometry compared with monometallic complexes. The two approaches may open the way to synthesizing bimetallic complexes with different functionality and properties.

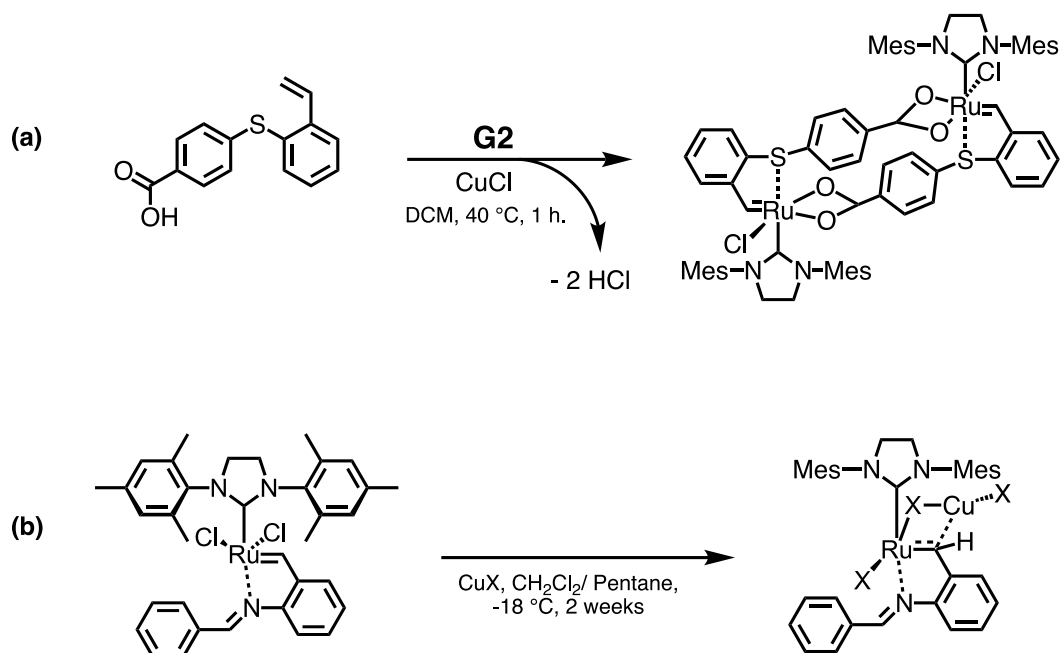


**Figure 1.22. Synthesis of bimetallic catalysts.**

In conclusion, this dissertation includes olefin metathesis catalysts development which enables ROMP inimers and novel complex synthesis. We studied olefin metathesis catalyst activation temperature as a function of monomer and catalyst identity and ligand electronic density. We developed a ROMP inimer synthetic approach and we explored the self-condensing ROMP capability in synthesizing hyperbranched polymers. We also developed synthetic approaches to prepare novel bimetallic complexes.

## 1.8. References

- (1) Bielawski, C. W.; Grubbs, R. H. Living ring-opening metathesis polymerization. *Prog. Polym. Sci.* **2007**, *32* (1), 1-29. DOI: <https://doi.org/10.1016/j.progpolymsci.2006.08.006>.
- (2) Bano, T.; Zahoor, A. F.; Rasool, N.; Irfan, M.; Mansha, A. Recent trends in Grubbs catalysis toward the synthesis of natural products: a review. *J. Iran. Chem. Soc.* **2022**, *19* (6), 2131-2170. DOI: 10.1007/s13738-021-02463-x.
- (3) Lee, H.-K.; Bang, K.-T.; Hess, A.; Grubbs, R. H.; Choi, T.-L. Multiple Olefin Metathesis Polymerization That Combines All Three Olefin Metathesis Transformations: Ring-Opening, Ring-Closing, and Cross Metathesis. *J. Am. Chem. Soc.* **2015**, *137* (29), 9262-9265. DOI: 10.1021/jacs.5b06033.
- (4) Park, H.; Kang, E.-H.; Müller, L.; Choi, T.-L. Versatile Tandem Ring-Opening/Ring-Closing Metathesis Polymerization: Strategies for Successful Polymerization of Challenging Monomers and Their Mechanistic Studies. *J. Am. Chem. Soc.* **2016**, *138* (7), 2244-2251. DOI: 10.1021/jacs.5b12223.
- (5) Lee, H.-K.; Lee, J.; Kockelmann, J.; Herrmann, T.; Sarif, M.; Choi, T.-L. Superior Cascade Ring-Opening/Ring-Closing Metathesis Polymerization and Multiple Olefin Metathesis Polymerization: Enhancing the Driving Force for Successful Polymerization of Challenging Monomers. *J. Am. Chem. Soc.* **2018**, *140* (33), 10536-10545. DOI: 10.1021/jacs.8b05613.
- (6) Ginzburg, Y.; Anaby, A.; Vidavsky, Y.; Diesendruck, C. E.; Ben-Asuly, A.; Goldberg, I.; Lemcoff, N. G. Widening the Latency Gap in Chelated Ruthenium Olefin Metathesis Catalysts. *Organometallics* **2011**, *30* (12), 3430-3437. DOI: 10.1021/om200323c.
- (7) van der Schaaf, P. A.; Kolly, R.; Kirner, H.-J.; Rime, F.; Mühlebach, A.; Hafner, A. Synthesis and reactivity of novel ruthenium carbene catalysts. X-ray structures of [RuCl<sub>2</sub>( $\cdot$ CHSC<sub>6</sub>H<sub>5</sub>)(PiPr<sub>3</sub>)<sub>2</sub>] and [RuCl<sub>2</sub>(CHCH<sub>2</sub>CH<sub>2</sub>-C,N-2-C<sub>5</sub>H<sub>4</sub>N)(PiPr<sub>3</sub>)]. *Journal of Organometallic Chemistry* **2000**, *606* (1), 65-74. DOI: [https://doi.org/10.1016/S0022-328X\(00\)00289-8](https://doi.org/10.1016/S0022-328X(00)00289-8).
- (8) Ung, T.; Hejl, A.; Grubbs, R. H.; Schrodi, Y. Latent Ruthenium Olefin Metathesis Catalysts That Contain an N-Heterocyclic Carbene Ligand. *Organometallics* **2004**, *23* (23), 5399-5401. DOI: 10.1021/om0493210.
- (9) Slugovc, C.; Burtscher, D.; Stelzer, F.; Mereiter, K. Thermally Switchable Olefin Metathesis Initiators Bearing Chelating Carbenes: Influence of the Chelate's Ring Size. *Organometallics* **2005**, *24* (10), 2255-2258. DOI: 10.1021/om050141f.
- (10) Hejl, A.; Day, M. W.; Grubbs, R. H. Latent Olefin Metathesis Catalysts Featuring Chelating Alkylidenes. *Organometallics* **2006**, *25* (26), 6149-6154. DOI: 10.1021/om060620u.
- (11) Benitez, D.; Goddard, W. A. The Isomerization Equilibrium between Cis and Trans Chloride Ruthenium Olefin Metathesis Catalysts from Quantum Mechanics Calculations. *J. Am. Chem. Soc.* **2005**, *127* (35), 12218-12219. DOI: 10.1021/ja051796a.
- (12) Barbasiewicz, M.; Szadkowska, A.; Bujok, R.; Grela, K. Structure and Activity Peculiarities of Ruthenium Quinoline and Quinoxaline Complexes: Novel Metathesis Catalysts. *Organometallics* **2006**, *25* (15), 3599-3604. DOI: 10.1021/om060091u.

- (13) Gstrein, X.; Burtscher, D.; Szadkowska, A.; Barbasiewicz, M.; Stelzer, F.; Grela, K.; Slugovc, C. Ruthenium quinoline and quinoxaline complexes: Thermally triggered initiators for ring opening metathesis polymerization. *J. Polym. Sci. Pol. Chem.* **2007**, *45* (15), 3494-3500. DOI: 10.1002/pola.22083 (accessed 2019/03/15).
- (14) Ben-Asuly, A.; Tzur, E.; Diesendruck, C. E.; Sigalov, M.; Goldberg, I.; Lemcoff, N. G. A Thermally Switchable Latent Ruthenium Olefin Metathesis Catalyst. *Organometallics* **2008**, *27* (5), 811-813. DOI: 10.1021/om701180z.
- (15) Kost, T.; Sigalov, M.; Goldberg, I.; Ben-Asuly, A.; Lemcoff, N. G. Latent sulfur chelated ruthenium catalysts: Steric acceleration effects on olefin metathesis. *J. Organomet. Chem.* **2008**, *693* (12), 2200-2203. DOI: <https://doi.org/10.1016/j.jorganchem.2008.03.028>.
- (16) Lexer, C.; Burtscher, D.; Perner, B.; Tzur, E.; Lemcoff, N. G.; Slugovc, C. Olefin metathesis catalyst bearing a chelating phosphine ligand. *Journal of Organometallic Chemistry* **2011**, *696* (11), 2466-2470. DOI: <https://doi.org/10.1016/j.jorganchem.2011.03.005>.
- (17) Gułajski, Ł.; Michrowska, A.; Bujok, R.; Grela, K. New tunable catalysts for olefin metathesis: Controlling the initiation through electronic factors. *J. Mol. Catal. A Chem.* **2006**, *254* (1), 118-123. DOI: <https://doi.org/10.1016/j.molcata.2005.12.049>.
- (18) Gawin, R.; Makal, A.; Woźniak, K.; Mauduit, M.; Grela, K. A Dormant Ruthenium Catalyst Bearing a Chelating Carboxylate Ligand: In Situ Activation and Application in Metathesis Reactions. *Angew. Chem. Int. Ed.* **2007**, *46* (38), 7206-7209. DOI: 10.1002/anie.200701302 (accessed 2019/03/15).
- (19) Żukowska, K.; Szadkowska, A.; Pazio, A. E.; Woźniak, K.; Grela, K. Thermal Switchability of N-Chelating Hoveyda-type Catalyst Containing a Secondary Amine Ligand. *Organometallics* **2012**, *31* (1), 462-469. DOI: 10.1021/om2011062.
- (20) Kozłowska, A.; Dranka, M.; Zachara, J.; Pump, E.; Slugovc, C.; Skowerski, K.; Grela, K. Chelating Ruthenium Phenolate Complexes: Synthesis, General Catalytic Activity, and Applications in Olefin Metathesis Polymerization. *Chem. Eur. J.* **2014**, *20* (43), 14120-14125. DOI: 10.1002/chem.201403580.
- (21) Diesendruck, C. E.; Iliashevsky, O.; Ben-Asuly, A.; Goldberg, I.; Lemcoff, N. G. Latent and Switchable Olefin Metathesis Catalysts. *Macromol. Symp.* **2010**, *293* (1), 33-38. DOI: 10.1002/masy.200900036.
- (22) Vidavsky, Y.; Anaby, A.; Lemcoff, N. G. Chelating alkylidene ligands as pacifiers for ruthenium catalysed olefin metathesis. *Dalton Trans.* **2012**, *41* (1), 32-43, 10.1039/C1DT11404B. DOI: 10.1039/C1DT11404B.
- (23) Teator, A. J.; Bielawski, C. W. Remote control grubbs catalysts that modulate ring-opening metathesis polymerizations. *J. Polym. Sci. Pol. Chem.* **2017**, *55* (18), 2949-2960. DOI: 10.1002/pola.28665 (accessed 2019/03/15).
- (24) Monsaert, S.; Lozano Vila, A.; Drozdak, R.; Van Der Voort, P.; Verpoort, F. Latent olefin metathesis catalysts. *Chem. Soc. Rev.* **2009**, *38* (12), 3360-3372, 10.1039/B902345N. DOI: 10.1039/B902345N.
- (25) Gawin, R.; Makal, A.; Woźniak, K.; Mauduit, M.; Grela, K. A Dormant Ruthenium Catalyst Bearing a Chelating Carboxylate Ligand: In Situ Activation and Application in Metathesis Reactions. *Angew.* **2007**, *46* (38), 7206-7209. DOI: 10.1002/anie.200701302.
- (26) Samec, J. S. M.; Keitz, B. K.; Grubbs, R. H. Latent ruthenium olefin metathesis catalysts featuring a phosphine or an N-heterocyclic carbene ligand. *J. Organomet.*

- Chem.* **2010**, 695 (14), 1831-1837. DOI: <https://doi.org/10.1016/j.jorganchem.2010.04.017>.
- (27) Voigtritter, K.; Ghorai, S.; Lipshutz, B. H. Rate Enhanced Olefin Cross-Metathesis Reactions: The Copper Iodide Effect. *J. Org. Chem.* **2011**, 76 (11), 4697-4702. DOI: 10.1021/jo200360s.
- (28) Malinowska, M.; Kozłowska, M.; Hryniewicka, A.; Morzycki, J. W. New olefin metathesis catalyst bearing N-mesitylimidazole and nitrate ligands – Synthesis, activity, and performance in aqueous media. *J. Organomet. Chem.* **2019**, 896, 154-161. DOI: <https://doi.org/10.1016/j.jorganchem.2019.06.018>.
- (29) Sashuk, V.; Danylyuk, O. A Thermo- and Photo-Switchable Ruthenium Initiator For Olefin Metathesis. *Chem.: Eur. J.* **2016**, (19), 6528, Report. DOI: 10.1002/chem.201600776 From EBSCOhost edsgao.
- (30) Duan, Y.; Wang, T.; Xie, Q.; Yu, X.; Guo, W.; Wang, J.; Liu, G. Highly efficient nitrogen chelated ruthenium carbene metathesis catalysts. *Dalton Trans.* **2016**, 45 (48), 19441-19448, 10.1039/C6DT03899A. DOI: 10.1039/C6DT03899A.
- (31) Garber, S. B.; Kingsbury, J. S.; Gray, B. L.; Hoveyda, A. H. Efficient and Recyclable Monomeric and Dendritic Ru-Based Metathesis Catalysts. *J. Am. Chem. Soc.* **2000**, 122 (34), 8168-8179. DOI: 10.1021/ja001179g.
- (32) Wang, D.; Unold, J.; Bubrin, M.; Elser, I.; Frey, W.; Kaim, W.; Xu, G.; Buchmeiser, M. R. Ruthenium–Triazene Complexes as Latent Catalysts for UV-Induced ROMP. *Eur. J. Inorg. Chem.* **2013**, 2013 (31), 5462-5468. DOI: 10.1002/ejic.201301048.
- (33) Diesendruck, C. E.; Tzur, E.; Lemcoff, N. G. The Versatile Alkylidene Moiety in Ruthenium Olefin Metathesis Catalysts. *Eur. J. Inorg. Chem.* **2009**, 2009 (28), 4185-4203. DOI: 10.1002/ejic.200900526.
- (34) Grela, K.; Harutyunyan, S.; Michrowska, A. A Highly Efficient Ruthenium Catalyst for Metathesis Reactions. *Angew. Chem. Int. Ed. Engl.* **2002**, 41 (21), 4038-4040. DOI: 10.1002/1521-3773(20021104)41:21<4038::AID-ANIE4038>3.0.CO;2-0.
- (35) Moore, C.; Bark, B.; Szymczak, N. Simple Ligand Modifications with Pendent OH Groups Dramatically Impact the Activity and Selectivity of Ruthenium Catalysts for Transfer Hydrogenation: The Importance of Alkali Metals. *ACS Catalysis* **2016**, 6, 1981-1990. DOI: 10.1021/acscatal.6b00229.
- (36) Hong, S. H.; Grubbs, R. H. Highly Active Water-Soluble Olefin Metathesis Catalyst. *J. Polym. Sci.* **2006**, 128 (11), 3508-3509. DOI: 10.1021/ja058451c.
- (37) Hongfa, C.; Tian, J.; Bazzi, H. S.; Bergbreiter, D. E. Heptane-Soluble Ring-Closing Metathesis Catalysts. *Org Lett.* **2007**, 9 (17), 3259-3261. DOI: 10.1021/ol071210k.
- (38) Kingsbury, J. S.; Garber, S. B.; Giftos, J. M.; Gray, B. L.; Okamoto, M. M.; Farrer, R. A.; Fourkas, J. T.; Hoveyda, A. H. Immobilization of Olefin Metathesis Catalysts on Monolithic Sol–Gel: Practical, Efficient, and Easily Recyclable Catalysts for Organic and Combinatorial Synthesis. *Angew. Chem. Int. Ed. Engl.* **2001**, 40 (22), 4251-4256. DOI: 10.1002/1521-3773(20011119)40:22<4251::AID-ANIE4251>3.0.CO;2-L.
- (39) Connon, S. J.; Blechert, S. A solid-Supported phosphine-Free ruthenium alkylidene for olefin metathesis in methanol and water. *Bioorg. Med. Chem. Lett.* **2002**, 12 (14), 1873-1876. DOI: [https://doi.org/10.1016/S0960-894X\(02\)00260-3](https://doi.org/10.1016/S0960-894X(02)00260-3).
- (40) Gatard, S.; Nlate, S.; Cloutet, E.; Bravic, G.; Blais, J.-C.; Astruc, D. Dendritic Stars by Ring-Opening-Metathesis Polymerization from Ruthenium–Carbene Initiators. *Angew.* **2003**, 42 (4), 452-456. DOI: 10.1002/anie.200390137.

- (41) Frey, H.; Hölter, D. Degree of branching in hyperbranched polymers. 3 Copolymerization of AB<sub>m</sub>-monomers with AB and AB<sub>n</sub>-monomers. *Acta Polymerica* **1999**, *50* (2-3), 67-76. DOI: 10.1002/(SICI)1521-4044(19990201)50:2/3<67::AID-APOL67>3.0.CO;2-W (accessed 2019/03/15).
- (42) Alfurhood, J. A.; Bachler, P. R.; Sumerlin, B. S. Hyperbranched polymers via RAFT self-condensing vinyl polymerization. *Polym. Chem.* **2016**, *7* (20), 3361-3369, 10.1039/C6PY00571C. DOI: 10.1039/C6PY00571C.
- (43) Zheng, Y.; Li, S.; Weng, Z.; Gao, C. Hyperbranched polymers: advances from synthesis to applications. *Chem. Soc. Rev.* **2015**, *44* (12), 4091-4130, 10.1039/C4CS00528G. DOI: 10.1039/C4CS00528G.
- (44) Yan, D.; Gao, C.; Frey, H. *Hyperbranched polymers: synthesis, properties, and applications*; John Wiley & Sons, 2011.
- (45) Voit, B. New developments in hyperbranched polymers. *J. Polym. Sci. Pol. Chem.* **2000**, *38* (14), 2505-2525. DOI: 10.1002/1099-0518(20000715)38:14<2505::AID-POLA10>3.0.CO;2-8 (accessed 2019/03/15).
- (46) Mathers, R. T.; Damodaran, K.; Rendos, M. G.; Lavrich, M. S. Functional Hyperbranched Polymers Using Ring-Opening Metathesis Polymerization of Dicyclopentadiene with Monoterpenes. *Macromolecules* **2009**, *42* (5), 1512-1518. DOI: 10.1021/ma802441t.
- (47) Hanik, N.; Kilbinger, A. F. M. Branched Polymers via ROMP of Termimers. *Macromol. Rapid Commun.* **2016**, *37* (6), 532-538. DOI: 10.1002/marc.201500628.
- (48) Ren, N.; Zhu, X. Hybrid Polymerization of Ring-Opening Metathesis and Cross-Metathesis for Polyolefins with Tunable Architectures. *Macromolecules* **2018**, *51* (23), 9555-9561. DOI: 10.1021/acs.macromol.8b02135.
- (49) Ding, L.; Xie, M.; Yang, D.; Song, C. Efficient Synthesis of Long-Chain Highly Branched Polymers via One-Pot Tandem Ring-Opening Metathesis Polymerization and Acyclic Diene Metathesis Polymerization. *Macromolecules* **2010**, *43* (24), 10336-10342. DOI: 10.1021/ma1020903 (accessed 2014/05/09).
- (50) Ding, L.; Yang, G.; Xie, M.; Gao, D.; Yu, J.; Zhang, Y. More insight into tandem ROMP and ADMET polymerization for yielding reactive long-chain highly branched polymers and their transformation to functional polymer nanoparticles. *Polymer* **2012**, *53* (2), 333-341. DOI: <http://dx.doi.org/10.1016/j.polymer.2011.12.022>.
- (51) Ding, L.; Lin, L.; Wang, C.; Qiu, J.; Zhu, Z. Facile synthesis of linear-hyperbranched polyphosphoesters via one-pot tandem ROMP and ADMET polymerization and their transformation to architecturally defined nanoparticles. *J. Polym. Sci.* **2015**, *53* (8), 964-972. DOI: 10.1002/pola.27524.
- (52) Hilf, S.; Wurm, F.; Kilbinger, A. F. M. Long-chain branched ROMP polymers. *J. Polym. Sci.* **2009**, *47* (24), 6932-6940. DOI: 10.1002/pola.23733.
- (53) Fréchet, J. M. J.; Henmi, M.; Gitsov, I.; Aoshima, S.; Leduc, M. R.; Grubbs, R. B. Self-Condensing Vinyl Polymerization: An Approach to Dendritic Materials. *Science* **1995**, *269* (5227), 1080, 10.1126/science.269.5227.1080.
- (54) Gaynor, S. G.; Edelman, S.; Matyjaszewski, K. Synthesis of Branched and Hyperbranched Polystyrenes. *Macromolecules* **1996**, *29* (3), 1079-1081. DOI: 10.1021/ma9513877.

- (55) In-Yup, J.; Hyuk-Jun, N.; Jong-Beom, B. Hyperbranched Macromolecules: From Synthesis to Applications. *Molecules* **2018**, *23* (3), 657, Article. DOI: 10.3390/molecules23030657 .
- (56) Trollsås, M.; Löwenhielm, P.; Lee, V. Y.; Möller, M.; Miller, R. D.; Hedrick, J. L. New Approach to Hyperbranched Polyesters: Self-Condensing Cyclic Ester Polymerization of Bis(hydroxymethyl)-Substituted  $\epsilon$ -Caprolactone. *Macromolecules* **1999**, *32* (26), 9062-9066. DOI: 10.1021/ma991039v.
- (57) Liu, M.; Vladimirov, N.; Fréchet, J. M. J. A New Approach to Hyperbranched Polymers by Ring-Opening Polymerization of an AB Monomer: 4-(2-Hydroxyethyl)- $\epsilon$ -caprolactone. *Macromolecules* **1999**, *32* (20), 6881-6884. DOI: 10.1021/ma990785x.
- (58) Liu, J.; Huang, W.; Zhou, Y.; Yan, D. Synthesis of Hyperbranched Polyphosphates by Self-Condensing Ring-Opening Polymerization of HEEP without Catalyst. *Macromolecules* **2009**, *42* (13), 4394-4399. DOI: 10.1021/ma900798h.
- (59) Han, J.; Li, S.; Tang, A.; Gao, C. Water-Soluble and Clickable Segmented Hyperbranched Polymers for Multifunctionalization and Novel Architecture Construction. *Macromolecules* **2012**, *45* (12), 4966-4977. DOI: 10.1021/ma300718d.
- (60) Dias, E. L.; Grubbs, R. H. Synthesis and Investigation of Homo- and Heterobimetallic Ruthenium Olefin Metathesis Catalysts Exhibiting Increased Activities. *Organometallics* **1998**, *17* (13), 2758-2767. DOI: 10.1021/om9708788.
- (61) Grudzień, K.; Malinska, M.; Barbasiewicz, M. Synthesis and Properties of Bimetallic Hoveyda–Grubbs Metathesis Catalysts. *Organometallics* **2012**, *31* (9), 3636-3646. DOI: 10.1021/om3001372.

## Chapter 2. Monomer Identity Effects on Latent Olefin Metathesis Catalyst

### Activation Temperature

Hanan N. Almuzaini,<sup>a,b</sup> Carla Slebodnick,<sup>a</sup> Michael D. Schulz<sup>a,b</sup>

<sup>a</sup> Department of Chemistry, Virginia Polytechnic Institute and State University,  
Blacksburg, VA 24061

<sup>b</sup> Macromolecules Innovation Institute, Virginia Polytechnic Institute and State  
University, Blacksburg, VA 24061

#### 2.1. Abstract

Latent olefin metathesis catalysts are pre-catalysts that exhibit negligible activity at room temperature in the presence of olefins. However, these catalysts can be activated by external stimuli. This property enables olefin–catalyst mixtures to be prepared, stored, and handled as homogenous solutions before a reaction occurs. The effects of several parameters on catalyst activity such as steric, electronic, and chelation effects, have been previously studied. However, the effect of monomer identity has not been previously explored. This work measured the activation temperature of five ruthenium-based latent olefin metathesis catalysts. These catalysts have either a benzylidene or an indenylidene ligand, a five- or six-member chelating ring, and sulfur, nitrogen, or phosphorous chelation. We studied the reactivity of these catalysts by polymerizing a series of ROMP monomers and monitoring catalyst activation temperature by differential scanning calorimetry (DSC). The measurements show that the monomer identity significantly affects catalyst reactivity. The activation temperatures ranged from the monomer melting point to 115 °C and varied by both catalyst and monomer identity. Generally, olefin metathesis catalysts are activated

at a lower temperature when polymerizing monomers that have both lower melting temperatures and higher activity.

## 2.2. Introduction

The development of effective olefin metathesis catalysts has enabled the preparation of precision polyolefins,<sup>1-5</sup> advanced polymer architectures,<sup>6</sup> and functional materials.<sup>7</sup> Ruthenium-based olefin metathesis catalysts in particular are widely used due to their relative stability, high activity, fast initiation, and ease of use.<sup>8</sup> However, for some purposes, catalysts with negligible room-temperature activity and high thermal stability are desirable. For example, ring-opening metathesis polymerization (ROMP) often requires mixing monomer and catalyst to prepare homogenous solutions before polymerization occurs. Unfortunately, olefin metathesis catalysts can be activated at or below room temperature,<sup>8</sup> making it challenging to prepare, store, and handle monomer-catalyst mixtures.

Therefore, latent olefin metathesis catalysts—pre-catalysts presenting negligible activity at a given temperature (usually room temperature) and significant reactivity when suitable stimuli are applied—have long been explored, particularly in the context of ROMP.<sup>9-13</sup> The high thermal stability of these latent catalysts enables the preparation, storage, and handling of monomer-catalyst mixtures. Because controlling the activation temperature is critical to effectively initiate polymerization, several modified catalysts have been developed by varying the steric and electronic properties of the ligands,<sup>12, 14, 15</sup> or varying the chelate ring size.<sup>13</sup> However, the effect of monomer identity on catalyst activation temperature is underexplored.

ROMP monomers have different reactivities, stereochemistry, and substituents. While several studies have explored the effect of monomer stereochemistry (*exo* vs *endo*) and substituents on the rate of polymerization,<sup>16-19</sup> the influence of the monomer identity on catalyst activation has not been investigated. In this study, we report a series of ROMP monomer polymerizations to identify how monomer identity affects the activation temperature of five latent olefin metathesis catalysts commonly used in ROMP and other olefin metathesis reactions (**[Ru]1-5, Figure 2.1**).

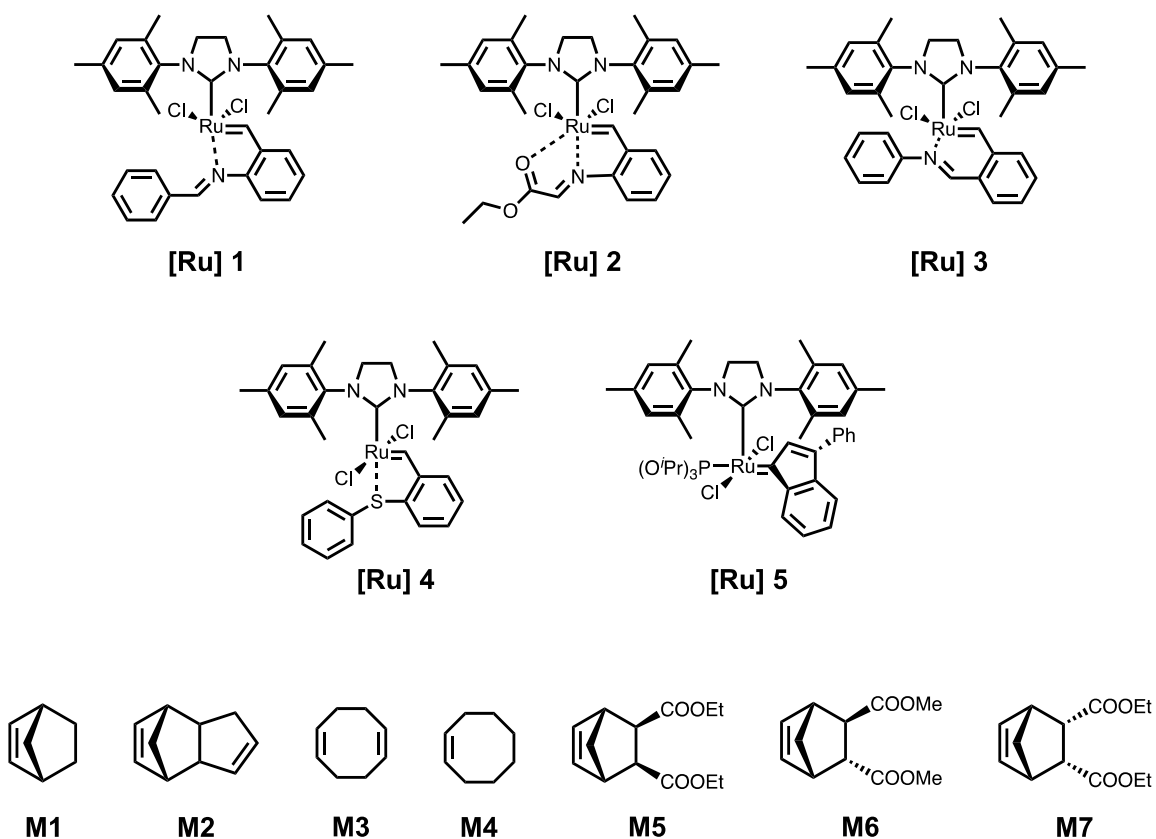


**Figure 2.1. Catalysts and monomers used in this study.**

This study includes catalysts with a benzylidene **[Ru]1-4** or an indenylidene ligand **[Ru]5**, catalysts with sulfur **[Ru]1**, nitrogen **[Ru]2-4**, and phosphorous **[Ru]5** chelation, and a five- or six-member chelating ring **[Ru]2** and **3**. The reactivity of these catalysts has

been previously studied in different metathesis reactions, and they all exhibited thermal stability and negligible room temperature activity, with each activated at different temperatures.<sup>12-14, 20</sup> In this study, we aimed to investigate the activation of these catalysts in polymerizing seven ROMP monomers. Several parameters were considered in selecting the ROMP monomers (**Figure 2.1**), including ring strain energy, melting temperature, and stereochemistry.

### 2.3. Results and Discussion

#### Synthesis and structural characterization of latent olefin metathesis catalysts

**[Ru] 1**, **3**, and **4** were synthesized by using literature procedures (**Figure 2.2**). Complexes **[Ru] 2** and **5** were obtained from Strem and Sigma Aldrich, respectively, and were used without purification.<sup>12, 13</sup> The synthesis of **[Ru] 1**, **3**, and **4** was confirmed by <sup>1</sup>H NMR spectroscopy and single-crystal X-ray diffraction (**Figure 2.3** and the experimental section). NMR and crystal analysis confirmed the synthesis of the trans **[Ru] 1** and **3** isomers, and the *cis* **[Ru] 4** isomer, as reported previously.<sup>12, 13</sup> **[Ru] 1**, and **3** showed similar bond lengths but different angles around the Ru atom. **[Ru] 3** has a wider C11-Ru1-Cl2 angle (162.36(2)°) compared to **[Ru] 1**(152.53(4) °), while **[Ru] 1** has a wider C1-Ru1-N3 angle (174.84(15)°) compared to **[Ru] 3** (169.78(9)°). These differences in bond angles are presumably due to the difference in chelating ring size. **[Ru] 4** showed different bond angles due to the formation of the *cis* isomer. An obvious difference between these complexes is the bond length between the Ru center and the chelating atom. **[Ru] 4** showed the longest Ru-chelation atom bond length 2.3386(3) Å, while **[Ru] 3** has the shortest bond length 2.0968(19) Å and **[Ru] 1** has 2.174(4) Å.

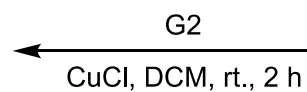
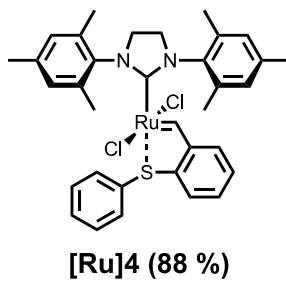
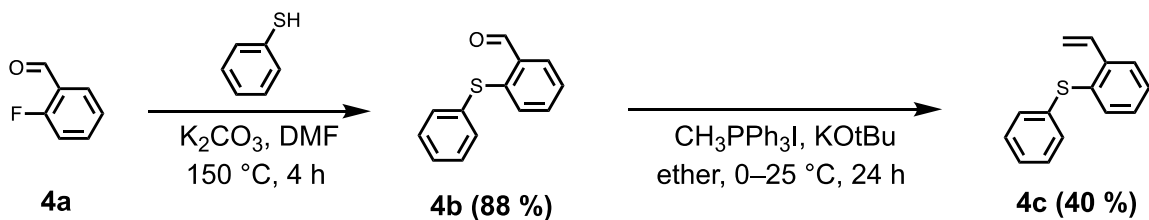
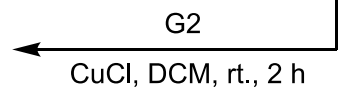
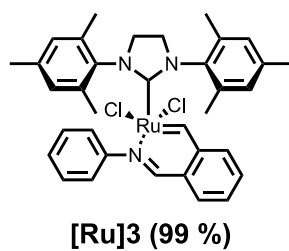
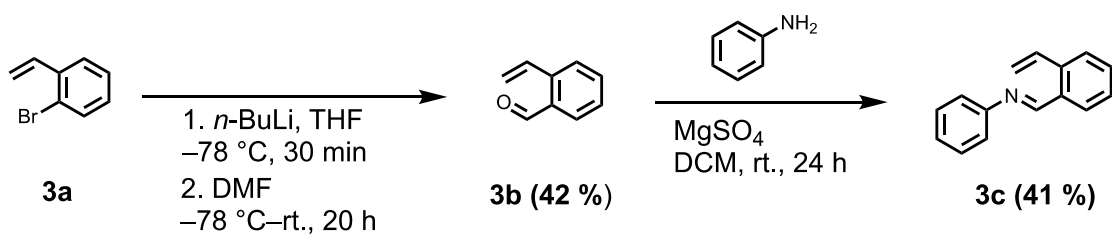
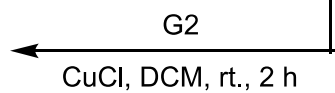
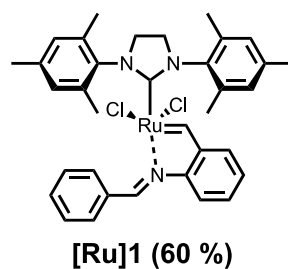
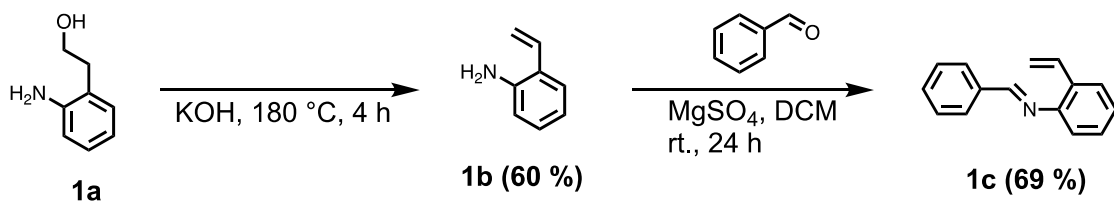


Figure 2.2. Synthesis of olefin metathesis catalysts [Ru] 1, [Ru] 3, and [Ru] 4.

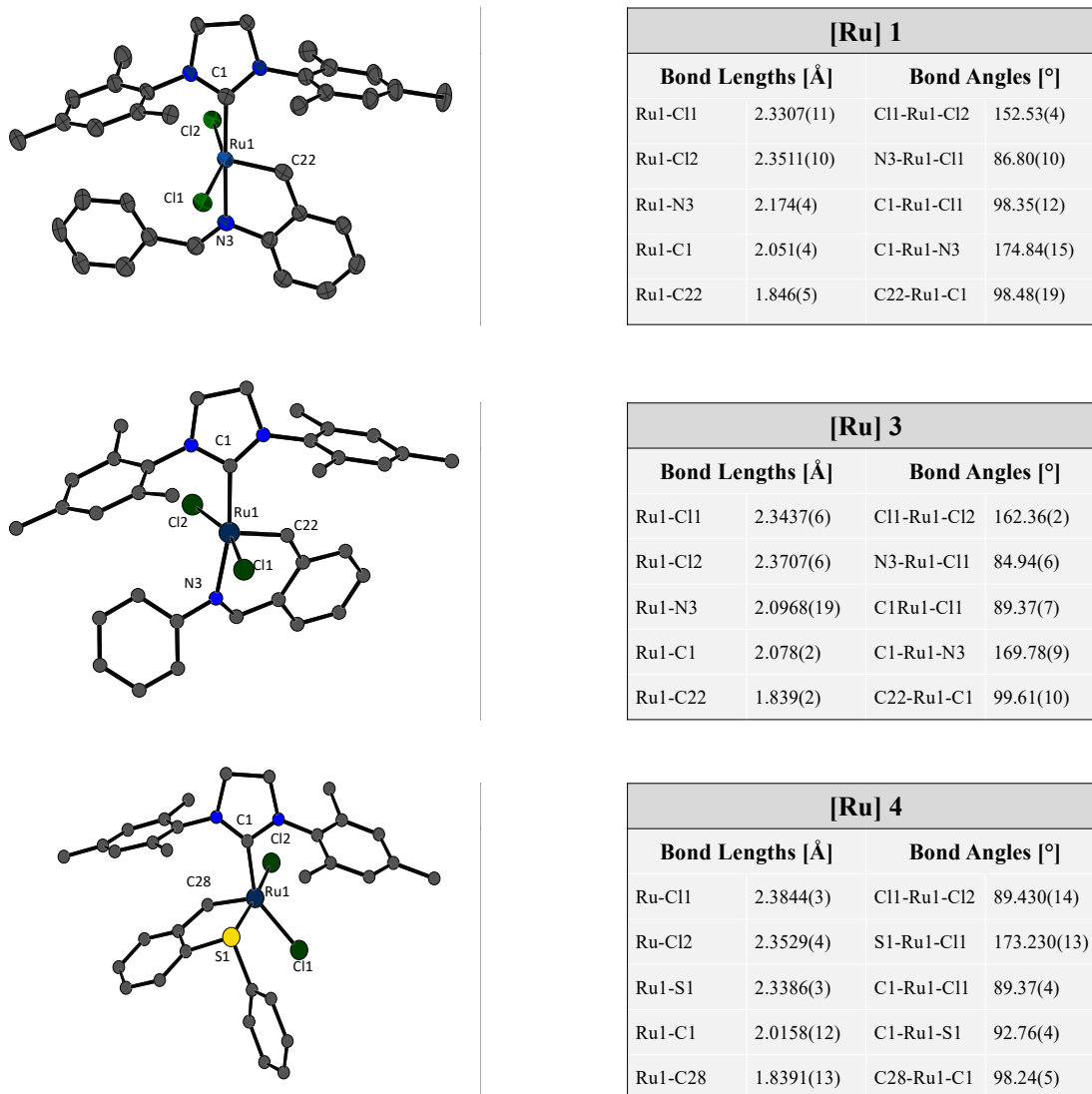
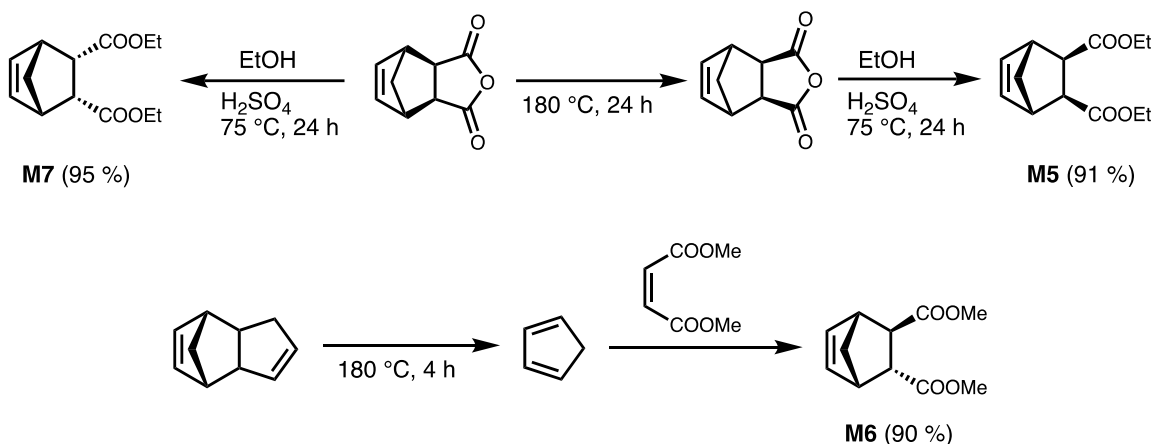


Figure 2.3. Crystal structures confirmed the synthesis of [Ru] 1, [Ru] 3, and [Ru] 4.

### Synthesis of ROMP monomers

M1–4 monomers are commercially available and were used without further purification. M5–7 monomers were synthesized following literature procedures (Figure 2.4).<sup>17, 21</sup> The monomer melting temperature was determined by DSC with a ramp rate of 3 °C/min between –70 to 60 °C. The DSC measurement showed an endothermic peak

indicating the monomer melting point as listed in **Table 2.1**. **M7** is liquid at room temperature and its DSC thermogram did not show a peak even near  $-70\text{ }^{\circ}\text{C}$ , indicating a melting temperature below  $-70\text{ }^{\circ}\text{C}$ .



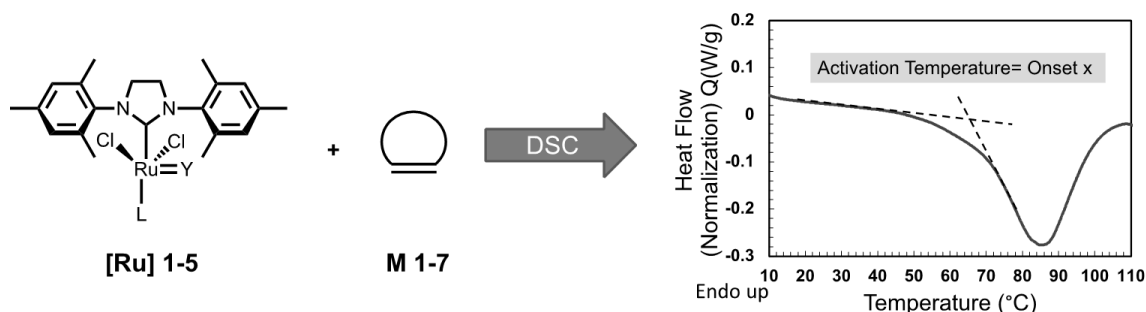
**Figure 2.4. Synthesis of ROMP monomers.**

### Catalytic activity

The activity of **[Ru] 1–5** was evaluated in ROMP of a series of commercially available and synthesized ROMP monomers (**Table 2.1**). In all cases, ROMP reactions were conducted in a DSC pan. A mixture of each catalyst (1 equiv.) with each monomer (10 equiv.) was prepared in a high-volume DSC pan. The activation temperature was measured by DSC, which detects the large exothermic peak associated with the polymerization (**Figure 2.5**). **Table 1** shows duplicate activation temperature measurements, which revealed minor variations ( $0\text{--}5\text{ }^{\circ}\text{C}$ ) between the first and second trials.

The DSC measurements showed variable activation temperatures for these catalysts throughout the series, which were affected by both the catalyst and monomer identity. Complex **[Ru] 1** showed the lowest activation temperatures, which was attributed to the

influence of the ring size of the chelate. **[Ru] 2** was activated at a higher temperature compared to **[Ru] 1** in polymerizing monomers **M2**, **M5**, and **M6**. A crystal structure analysis conducted in a previous study showed 3-point chelation with an octahedral structure for **[Ru] 2**.<sup>14</sup> This catalyst has both O-Ru and N-Ru chelation,<sup>14</sup> which stabilized **[Ru] 2** and increased the catalyst activation temperature. However, we observed the opposite trend with diester-functionalized monomers. **[Ru] 2** was activated at lower temperatures compared to **[Ru] 1** in polymerizing **M5**, **M6**, and **M7**.

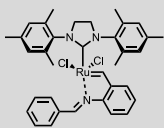
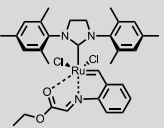
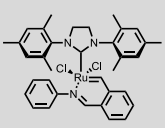
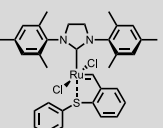
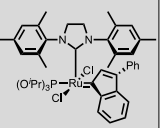


**Figure 2.5. DSC measurement of catalyst's activation temperature.**

**[Ru] 3** showed similar activation temperatures in polymerizing **M1** and **M2** compared with **[Ru] 1**. However, the **[Ru] 3** activation temperature was higher when polymerizing **M3** to **M7**. DSC results revealed the influence of chelating ring size on the catalyst activity. **[Ru] 3** has a six-member chelating ring that stabilized the catalyst and formed a shorter Ru1-N3 bond length of 2.0968(19) Å (**Figure 2.3**). However, **[Ru] 1** had a five-member chelating ring with a longer Ru1-N3 bond length of 2.174(4) Å. The Ru-N bond strength in **[Ru] 1** was presumably weaker, which decreased the complex activation temperature. The chelating ring size effect was not obvious in polymerizing **M1** and **M2**, perhaps due to those monomers having higher reactivity. However, the ring chelating size

effect became more pronounced when monomers were polymerized with lower reactivity such as **M4**, or with a stereochemistry effect such as **M5-7**.

**Table 2.1. DSC measurements of catalyst activation temperatures.**

Catalyst						
Monomer		[Ru]1	[Ru]2	[Ru]3	[Ru]4	[Ru]5
Identity	Melting point (°C)	Activation Temperature (°C)				
 <b>M1</b>	44- 47	48/ 48	53/ 51	48/ 50	49/ 50	70/ 72
 <b>M2</b>	32	39/36	51/ 47	34/ 34	55/ 60	91/ 87
 <b>M3</b>	-69	43/ 41	42/ 41	46/ 51	41/ 45	85/ 82
 <b>M4</b>	-18	66/ 62	115/ 116	73/ 75	114/ 114	79/ 83
 <b>M5</b>	8	52/ 53	50/ 50	77/ 81	77/ 77	79/ 79
 <b>M6</b>	33	67/ 65	38/ 40	91/ 94	78/ 78	90/ 85
 <b>M7</b>	Below -70	88/ 86	68/ 72	101/ 105	105/ 98	97/ 95

**[Ru]4** also features a five-member chelate ring, but with a longer Ru–S bond (2.3386(3) Å) compared to **[Ru] 1**. **[Ru] 4** had activation temperatures ranging between

41–114 °C. Interestingly, **[Ru]4** was activated at higher temperatures compared to **[Ru] 1** in polymerizing **M2**, 4-7. For example, **[Ru] 4** was activated at 114 °C, a 52 °C difference compared to the polymerization of **M4** with **[Ru] 1**. The DSC results illustrated the effect of the less active *cis* conformation and sulfur chelation, which strengthened the ligation to ruthenium.<sup>12</sup> The effect of sulfur chelation was similar to the effect of 3-point chelation and increased the activation temperature when the less active ROMP monomer **M4** (112–116 °C) was polymerized. However, the **[Ru] 4** activation temperature increased with a stereochemistry effect (**M5–7**) were polymerized compared to unfunctionalized monomers.

Among the series, **[Ru] 5** had the highest activation temperatures, and ranged between 70 and 97 °C. The differences in the activation temperatures among the monomer series with this catalyst were between 6 and 19 °C, which was much less than the other catalysts: **[Ru] 1**, **[Ru] 2**, **[Ru] 3**, and **[Ru] 4**, showed differences of 52, 75, 71, and 73 °C, respectively, between the lowest and the highest activation temperatures. The DSC measurements showed that the higher activation temperature correlated with the replacement of the benzylidene with an indenylidene, which led to a more stable pre-catalyst.<sup>20</sup> However, the **[Ru] 5** activation temperature was not highly affected by the monomer identity compared with other catalysts.

### **Effect of monomer identity on the catalytic behavior**

These results demonstrated that both catalyst and monomer identity affected the catalyst activation temperature. Monomers with different reactivity were included: **M1–M4** strain energy = 27, 26, 13, and 7.4 kcal/mol respectively.<sup>22</sup> Activation temperatures of

[Ru] 1-4 in polymerizing M1 were similar, and ranged from 48 to 51 °C. The melting temperature of M1 (44 – 47 °C) prevented activation below 47 °C in the DSC measurements, which were done without a solvent. However, the activation temperature of [Ru] 5 was higher, and ranged from 70 to 72 °C, almost 24 °C higher than the other catalysts, which confirmed that catalyst identity also affected activation temperature.

M2 has ring strain energy similar to M1 (27 and 26 kcal/mol, respectively). However, the activation temperatures for polymerizing M2 ranged between 34 to 91 °C. The lower activation temperature of [Ru] 1 and [Ru]3 for the polymerization of M2 compared to M1 was likely due to the lower melting temperature of M2 (32 °C). The activation temperatures of catalysts in polymerizing M2 were affected by the 3-point chelation ([Ru] 2) and sulfur chelation ([Ru] 4), and resulted in an increased activation temperature of 46/46 and 55/60 °C, respectively. However, the effect of the ring size chelation was not apparent for the polymerization of M2, with only a 5 – 6 °C difference between [Ru] 1 and [Ru] 3. Similar to M1, the activation temperature for the polymerization M2 with [Ru] 5 was much higher (91/ 87 °C) than the other four complexes, and indicated the larger effect of the indenylidene ligand.

The activation temperatures of the catalysts to polymerize M3 ranged between 41 and 85 °C. However, the ring size chelation, the 3-point chelation, and the sulfur chelation did not significantly affect the activation temperature of the catalysts for the polymerization of M3. [Ru] 1, [Ru] 1, [Ru] 3, and [Ru] 4 were all activated at similar temperatures for the polymerization of M3, and indicated that these catalysts behaved differently for the

polymerization of different monomers. Similar to the other monomers, higher activation temperatures were observed when **M3** was polymerized with **[Ru] 5**.

DSC measurements revealed highly varied activation temperatures in polymerizing **M4**. The effect of 3-point chelation and S-chelation (and *cis* conformation) were much higher than the effect of chelate ring size for this monomer, and **[Ru]2** and **[Ru]4** had the highest activation temperatures of the entire series of monomers and catalysts when **M4** was polymerized. However, the activation temperature of **[Ru] 5**, in this case, was lower than **[Ru] 2** and **[Ru] 4** and indicated that the indenylidene catalyst was much less sensitive to monomer variations since activation occurred around the same temperature for most monomers.

#### **Effect of monomer stereochemistry**

For exploration of the effect of monomer stereochemistry (*exo* vs *endo*), we synthesized three functionalized monomers, **M5-7**. Overall, the use of a 3-point chelation catalyst **[Ru] 2** decreased the activation temperature when these monomers were polymerized, compared to the other catalysts studied. In addition, the activation temperatures of the five catalysts increased by 2–33 °C in the presence of two *exo* ester substitutions (**M5**) compared to unfunctionalized norbornene (**M1**). However, the difference in activation temperature became even higher with the introduction of one *endo* ester substitution **M6**, with the difference in the activation temperature for the polymerization of **M1** and **M6** which ranged between 17 and 43 °C. In the case of the polymerization of **M7**, which had two *endo* esters, all five catalysts were activated at higher temperatures. These results highlighted the effect of monomer substituents and

stereochemistry on the activation temperature of these types of ester-substituted monomers. These findings were consistent with the effect of stereochemistry on the rate of polymerization, as reported by Guironnet and coworkers, and indicated that monomer stereochemistry affected both catalyst activation temperature and the rate of polymerization.<sup>16</sup>

## **2.4. Conclusions**

In this study, we illustrated the effect of both catalyst structure and monomer identity on the activation temperature of latent olefin metathesis catalysts. We measured the activation temperature of five ROMP catalysts for a series of monomers by DSC. We found that the activation temperature was affected by the catalyst ligands, atom chelation, and ring size, as well as the monomer reactivity, stereochemistry, and melting point. The activation temperature of these catalysts ranged from the monomer melting point up to 115 °C. The catalysts were activated at a lower temperature when polymerizing monomers with both high strain energy and lower melting point. The monomer stereochemistry also affected the catalyst activation temperature. These results provided additional insights into the activation conditions of latent olefin metathesis catalysts and were valuable in the design and synthesis of new polymers and materials. The results obtained from this work will guide the selection of optimal conditions for initiating olefin metathesis catalysts and synthesizing polymers by ROMP.

## 2.5. References

- (1) Schulz, M. D.; Wagener, K. B. Precision Polymers through ADMET Polymerization. *Macromol. Chem. Phys.* **2014**, *215* (20), 1936-1945. DOI: 10.1002/macp.201400268.
- (2) Schulz, M. D.; Wagener, K. B. ADMET Polymerization. In *Handbook of Metathesis*, Wiley-VCH Verlag GmbH & Co. KGaA, 2015; pp 313-355.
- (3) Caire da Silva, L.; Rojas, G.; Schulz, M. D.; Wagener, K. B. Acyclic diene metathesis polymerization: History, methods and applications. *Prog. Polym. Sci.* **2017**, *69*, 79-107. DOI: <https://doi.org/10.1016/j.progpolymsci.2016.12.001>.
- (4) Atallah, P.; Wagener, K. B.; Schulz, M. D. ADMET: The Future Revealed. *Macromolecules* **2013**, *46* (12), 4735-4741. DOI: 10.1021/ma400067b (accessed 2014/05/09).
- (5) Pribyl, J.; Wagener, K. B.; Rojas, G. ADMET polymers: synthesis, structure elucidation, and function. *Mater. Chem. Front.* **2021**, *5* (1), 14-43, 10.1039/D0QM00273A. DOI: 10.1039/D0QM00273A.
- (6) Sheiko, S. S.; Sumerlin, B. S.; Matyjaszewski, K. Cylindrical molecular brushes: Synthesis, characterization, and properties. *Prog. Polym. Sci.* **2008**, *33* (7), 759-785. DOI: <https://doi.org/10.1016/j.progpolymsci.2008.05.001>.
- (7) Sutthasupa, S.; Shiotsuki, M.; Sanda, F. Recent advances in ring-opening metathesis polymerization, and application to synthesis of functional materials. *Polym J* **2010**, *42* (12), 905-915.
- (8) Ogba, O. M.; Warner, N. C.; O'Leary, D. J.; Grubbs, R. H. Recent advances in ruthenium-based olefin metathesis. *Chem. Soc. Rev.* **2018**, *47* (12), 4510-4544, 10.1039/C8CS00027A. DOI: 10.1039/C8CS00027A.
- (9) Monsaert, S.; Lozano Vila, A.; Drozdak, R.; Van Der Voort, P.; Verpoort, F. Latent olefin metathesis catalysts. *Chem. Soc. Rev.* **2009**, *38* (12), 3360-3372, 10.1039/B902345N. DOI: 10.1039/B902345N.
- (10) Diesendruck, C. E.; Iliashevsky, O.; Ben-Asuly, A.; Goldberg, I.; Lemcoff, N. G. Latent and Switchable Olefin Metathesis Catalysts. *Macromolecular Symposia* **2010**, *293* (1), 33-38. DOI: 10.1002/masy.200900036.
- (11) Teator, A. J.; Bielawski, C. W. Remote control grubbs catalysts that modulate ring-opening metathesis polymerizations. *Journal of Polymer Science Part A: Polymer Chemistry* **2017**, *55* (18), 2949-2960. DOI: 10.1002/pola.28665 (accessed 2019/03/15).
- (12) Kost, T.; Sigalov, M.; Goldberg, I.; Ben-Asuly, A.; Lemcoff, N. G. Latent sulfur chelated ruthenium catalysts: Steric acceleration effects on olefin metathesis. *J. Organomet. Chem.* **2008**, *693* (12), 2200-2203. DOI: <https://doi.org/10.1016/j.jorganchem.2008.03.028>.
- (13) Slugovc, C.; Burtscher, D.; Stelzer, F.; Mereiter, K. Thermally Switchable Olefin Metathesis Initiators Bearing Chelating Carbenes: Influence of the Chelate's Ring Size. *Organometallics* **2005**, *24* (10), 2255-2258. DOI: 10.1021/om050141f.
- (14) Duan, Y.; Wang, T.; Xie, Q.; Yu, X.; Guo, W.; Wang, J.; Liu, G. Highly efficient nitrogen chelated ruthenium carbene metathesis catalysts. *Dalton Trans.* **2016**, *45* (48), 19441-19448, 10.1039/C6DT03899A. DOI: 10.1039/C6DT03899A.
- (15) Ginzburg, Y.; Anaby, A.; Vidavsky, Y.; Diesendruck, C. E.; Ben-Asuly, A.; Goldberg, I.; Lemcoff, N. G. Widening the Latency Gap in Chelated Ruthenium Olefin

- Metathesis Catalysts. *Organometallics* **2011**, *30* (12), 3430-3437. DOI: 10.1021/om200323c.
- (16) Hyatt, M. G.; Walsh, D. J.; Lord, R. L.; Andino Martinez, J. G.; Guironnet, D. Mechanistic and Kinetic Studies of the Ring Opening Metathesis Polymerization of Norbornenyl Monomers by a Grubbs Third Generation Catalyst. *J. Am. Chem. Soc.* **2019**, *141* (44), 17918-17925. DOI: 10.1021/jacs.9b09752.
- (17) Chang, A. B.; Lin, T.-P.; Thompson, N. B.; Luo, S.-X.; Liberman-Martin, A. L.; Chen, H.-Y.; Lee, B.; Grubbs, R. H. Design, Synthesis, and Self-Assembly of Polymers with Tailored Graft Distributions. *J. Am. Chem. Soc.* **2017**, *139* (48), 17683-17693. DOI: 10.1021/jacs.7b10525.
- (18) Radzinski, S. C.; Foster, J. C.; Chapleski, R. C.; Troya, D.; Matson, J. B. Bottlebrush Polymer Synthesis by Ring-Opening Metathesis Polymerization: The Significance of the Anchor Group. *J. Am. Chem. Soc.* **2016**, *138* (22), 6998-7004. DOI: 10.1021/jacs.5b13317.
- (19) Robertson, I. D.; Pruitt, E. L.; Moore, J. S. Frontal Ring-Opening Metathesis Polymerization of Exo-Dicyclopentadiene for Low Catalyst Loadings. *ACS Macro Lett.* **2016**, *5* (5), 593-596. DOI: 10.1021/acsmacrolett.6b00227.
- (20) Bantreil, X.; Schmid, T. E.; Randall, R. A. M.; Slawin, A. M. Z.; Cazin, C. S. J. Mixed N-heterocyclic carbene/phosphite ruthenium complexes: towards a new generation of olefin metathesis catalysts. *Chem. Commun.* **2010**, *46* (38), 7115-7117, 10.1039/C0CC02448A. DOI: 10.1039/C0CC02448A.
- (21) Niwayama, S.; Cho, H.; Zabet-Moghaddam, M.; Whittlesey, B. R. Remote Exo/Endo Selectivity in Selective Monohydrolysis of Dialkyl Bicyclo[2.2.1]heptane-2,3-dicarboxylate Derivatives. *J. Org. Chem.* **2010**, *75* (11), 3775-3780. DOI: 10.1021/jo100564e.
- (22) Schleyer, P. v. R.; Williams, J. E.; Blanchard, K. R. Evaluation of strain in hydrocarbons. The strain in adamantane and its origin. *J. Am. Chem. Soc.* **1970**, *92* (8), 2377-2386. DOI: 10.1021/ja00711a030.

## 2.6. EXPERIMENTAL SECTION

### General methods

All reactions were performed using oven-dried glassware equipped with a magnetic stir bar under an air atmosphere unless otherwise noted. 2-Bromostyrene and 2-aminophenethyl alcohol were purchased from AmBeed. 2-Fluorbenzaldehyde, thiophenol, methyltriphenylphosphonium iodide, and aniline were purchased from Oakwood. G2 was donated from Materia and purchased from AmBeed. **[Ru]4** and **5** were obtained from Strem and Sigma Aldrich, respectively. Deuterated solvents were obtained from Cambridge Isotope Laboratories. Unless otherwise stated, all other reagents were purchased at the highest commercial quality and used without further purification.

### Measurements

$^1\text{H}$  NMR and  $^{13}\text{C}$  NMR data were collected in  $\text{CDCl}_3$  or  $\text{CD}_2\text{Cl}_2$  at 25 °C unless otherwise noted using an Agilent U4-DD2 400 MHz, or a Bruker Advance II 500 MHz NMR instrument. Chemical shifts were reported in ppm and referenced to the  $\text{CHCl}_3$  singlet at 7.26 ppm, TMS singlet at 0 ppm, or  $\text{CD}_2\text{Cl}_2$  triplet at 5.32 ppm for  $^1\text{H}$  NMR.  $^{13}\text{C}$  NMR spectra were referenced to the center peak of the  $\text{CDCl}_3$  triplet at 77.00 ppm, or  $\text{CD}_2\text{Cl}_2$  at 54.00 ppm. The following abbreviations (or combinations thereof) were used to explain the multiplicities: s = singlet, d = doublet, t = triplet, q = quartet, m = multiplet, br = broad, and \* for the residual deuterated solvent peak.

Catalyst activation temperature was determined using DSC with a DSC Q2500 from TA instruments equipped with an autosampler. Sample masses ranging from 6-10 mg were crimped in a high-volume pan and lid and then loaded into the cell alongside a reference pan. The method incorporated equilibration at 25 °C and the samples were heated from 25

°C to 150 °C at a rate of 3 °C/ min. The activation temperature was determined as the onset point of the slope from the baseline of an exothermic transition.

### **General procedure for the synthesis of benzylidene ligands (1c, 3c, 4c)**

**2-Vinylaniline (1b):** To a 100 mL round-bottom flask equipped with a stir bar, short path distillation head, and tared receiving flask was added 2-aminophenethyl alcohol (**1a**) (1 equiv., 5.0 g) and potassium hydroxide (1 equiv., 2.04 g). The mixture was heated to 180 °C. With continued heating and applied vacuum for 4 h, the clear product distilled over (83 – 90 °C) to the tared receiving flask (Yield 2.60 g, 60 %).

<sup>1</sup>H NMR (400 MHz, CDCl<sub>3</sub>): δ 7.30 (d, *J* = 7.6 Hz, 1H), 7.10 (t, *J* = 6.8 Hz, 1H), 6.85 – 6.73 (m, 2H), 6.69 (d, *J* = 7.7 Hz, 1H), 5.64 (d, *J* = 17.2 Hz, 1H), 5.33 (d, *J* = 11.0 Hz, 1H), 3.76 (s, 2H).

<sup>13</sup>C NMR (101 MHz, CDCl<sub>3</sub>): δ 143.8, 132.9, 128.9, 127.5, 124.2, 119.1, 116.2, 115.8.

**(E)-1-phenyl-N-(2-vinylphenyl) methanimine (1c):** A round bottom flask was charged with **1b** (1 equiv., 0.30 g), benzaldehyde (1 equiv., 0.33 g), MgSO<sub>4</sub> (1g/1.0 mmol aldehyde, 2.80 g) and DCM (30 mL). The reaction mixture was stirred at room temperature under N<sub>2</sub> for 24 h after which the mixture was filtered and concentrated under reduced pressure. The crude product was used (as is) (Yield 0.40 g, 69 %).

<sup>1</sup>H NMR (400 MHz, CDCl<sub>3</sub>) δ 8.81 (s, 1H), 8.11 (dd, *J* = 7.4, 1.0 Hz, 1H), 7.48 – 7.38 (m, 4H), 7.37 – 7.29 (m, 1H), 7.24 – 7.15 (m, 3H), 6.76 – 6.62 (m, 1H), 5.68 (d, *J* = 17.3 Hz, 1H), 5.47 (dd, *J* = 11.0, 0.7 Hz, 1H).

$^{13}\text{C}$  NMR (101 MHz,  $\text{CDCl}_3$ )  $\delta$  192.4, 158.9, 152.4, 139.2, 133.8, 133, 131, 129.3, 129.2, 127.98, 127.96, 127.1, 125.9, 120.9, 118.55, 118.52, 115.1.

**2-Vinylbenzaldehyde (3b):** *N*-BuLi in 1 M hexane (1.1 equiv., 0.77 g) was added to a solution of 2-bromostyrene (**3a**) (1 equiv., 2.00 g) in 50 mL of THF at  $-78\text{ }^\circ\text{C}$  and stirred for 30 min. Then, DMF (1.5 equiv., 1 mL) was added dropwise. The reaction mixture was stirred for 20 h while the temperature was increased to room temperature. The organic layer was washed with brine, dried over  $\text{MgSO}_4$ , and filtered. The crude product was purified by column chromatography (hexane-acetone 9:1) to produce the pure product as a clear liquid (Yield 600 mg, 42 %).

$^1\text{H}$  NMR (400 MHz,  $\text{CDCl}_3$ )  $\delta$  10.30 (s, 1H), 7.86 – 7.81 (m, 1H), 7.58 (t,  $J = 1.7$  Hz, 2H), 7.57 – 7.49 (m, 1H), 7.48 – 7.40 (m, 1H), 5.70 (dd,  $J = 17.4, 1.2$  Hz, 1H), 5.52 (dd,  $J = 11.0, 1.2$  Hz, 1H).

$^{13}\text{C}$  NMR (101 MHz,  $\text{CDCl}_3$ )  $\delta$  192.6, 140.6, 133.9, 133.5, 133, 131.4, 128.1, 127.6, 119.6.

**(*E*)-*N*-(2-vinylbenzylidene)aniline (3c):** A round bottom flask was charged with **3b** (1 equiv., 0.30 g), aniline (1.1 equiv., 0.37 g),  $\text{MgSO}_4$  (1g/1.0 mmol aldehyde, 2.80 g) and DCM (30 mL). The reaction mixture was stirred at room temperature under  $\text{N}_2$  for 24 h after which the mixture was filtered and concentrated under reduced pressure. The crude product was used (as is) (Yield 0.24 g, 41%).

$^1\text{H}$  NMR (400 MHz,  $\text{CDCl}_3$ )  $\delta$  8.80 (s, 1H), 8.10 (dd,  $J = 7.7, 0.7$  Hz, 1H), 7.48 – 7.13 (m, 8H), 6.68 (dd,  $J = 8.5, 1.1$  Hz, 1H), 5.46 (dd,  $J = 11.0, 0.7$  Hz, 1H), 3.63 (s, 1H).

$^{13}\text{C}$  NMR (101 MHz,  $\text{CDCl}_3$ )  $\delta$  158.9, 152.4, 139.2, 133.8, 133.1, 131.1, 129.3, 129.1, 127.98, 127.96, 127.1, 125.9, 120.9, 118.55, 118.52, 115.1.

**2-(phenylthiol) benzaldehyde (4b):** 2-Fluorbenzaldehyde (**4a**) (1 equiv., 5.00 g) was added to potassium carbonate (2.1 equiv., 11.70 g), and thiophenol (1 equiv., 4.44 g) in 40 mL DMF. The mixture was stirred at 150 °C for 4 h under an N<sub>2</sub> atmosphere. After cooling, the mixture was poured into 50 mL DI water and extracted with DCM (3×50 mL). The extracts were dried over MgSO<sub>4</sub>, and the solvent was removed under reduced pressure. The crude product was used without any further purification (Yield 7.6 g, 88 %).

<sup>1</sup>H NMR (400 MHz, CDCl<sub>3</sub>, ppm): δ 10.37 (s, 1H), 7.89 – 7.82 (m, 1H), 7.43 – 7.30 (m, 7H), 7.08 (dd, J = 7.9, 1.2 Hz, 1H).

**2-(phenylthiol)-styrene (4c):** Methyltriphenylphosphonium iodide (1.4 equiv., 20.07 g) was dissolved in 50 mL of diethyl ether. Potassium *tert*-butoxide (1.5 equiv., 6.00 g) was added in one portion at 0 °C. After stirring for 20 min under N<sub>2</sub> atmosphere, **4b** (1 equiv., 7.6 g) in 15 mL of diethyl ether was added dropwise at 0 °C and the reaction mixture was warmed to room temperature and stirred overnight. The mixture was poured into 50 mL DI water and extracted with ether (3×30 mL). The extract was dried over MgSO<sub>4</sub>, and the solvent was removed under reduced pressure. The crude product was further purified by chromatography on silica gel (hexane-acetone gradient 9:1 to 7:3) to yield **4c** as a colorless oil (Yield 3.05 g, 40 %).

<sup>1</sup>H NMR (400 MHz, CDCl<sub>3</sub>) δ 7.65–7.57 (m, 1H), 7.42–7.08 (m, 9H), 5.70 (dd, J = 17.4, 1.2 Hz, 1H), 5.29 (dd, J = 11.0, 1.3 Hz, 1H).

<sup>13</sup>C NMR (101 MHz, CDCl<sub>3</sub>) δ 139.8, 136.5, 134.6, 133.9, 132.8, 129.4, 129.1, 128.5, 128.3, 126.3, 126.2, 116.2.

### Synthesis of catalysts [Ru] 1-3

A round bottom flask was charged with 1 equiv. of G2 and 1 equiv. of CuCl(I), and 1.2 equiv. of benzylidene ligand. DCM was added to the reaction flask under N<sub>2</sub> atmosphere. The reaction mixture was stirred at room temperature for 2 h. The solvent was evaporated, and the crude product was purified by column chromatography. **[Ru]1** (Yield 60 %) <sup>1</sup>H NMR (400 MHz, CDCl<sub>3</sub>): δ 17.02 (s, 1H), 9.32 (s, 1H), 7.92–7.89 (m, 2H), 7.53 (d, J = 22.2 Hz, 2H), 7.40 (d, J = 8.1 Hz, 1H), 7.23–7.17 (m, 3H), 7.09 (s, 4H), 6.90 (dd, J = 7.6, 1.4 Hz, 1H), 4.02 (s, 4H), 2.46 (s, 18H). **[Ru]3** (Yield 99 %) <sup>1</sup>H NMR (400 MHz, CDCl<sub>3</sub>): δ 18.72 (s, 1H), 8.67 (s, 1H), 7.86–6.98 (m, 13H), 6.83 (d, J = 7.8 Hz, 1H), 4.10 (s, 4H), 2.49 (d, J = 18.9 Hz, 18H). **[Ru]4** (Yield 88 %) <sup>1</sup>H NMR (400 MHz, CDCl<sub>3</sub>): δ 17.15 (s, 1H), 7.56–6.71 (m, 12H), 6.04 (s, 1H), 4.34–3.87 (m, 4H), 2.76–2.08 (m, 18H).

### Synthesis of M5-7

Monomers were synthesized following a literature procedure and characterized by <sup>1</sup>H NMR.<sup>1,2</sup> **M5** (Yield 91 %) <sup>1</sup>H NMR (400 MHz, CDCl<sub>3</sub>): δ 6.19 (s, 2H), 4.08 (dd, J = 11.0, 7.2 Hz, 4H), 3.09–3.03 (m, 2H), 2.58 (d, J = 1.9 Hz, 2H), 2.14–2.10 (m, 1H), 1.47 (dt, J = 9.0, 1.8 Hz, 1H), 1.23 (t, J = 7.1 Hz, 6H). **M6** (Yield 90 %) <sup>1</sup>H NMR (400 MHz, CDCl<sub>3</sub>): δ 6.33–6.24 (m, 1H), 6.17–5.99 (m, 1H), 3.71 (d, J = 3.1 Hz, 3H), 3.64 (d, J = 3.1 Hz, 3H), 3.43 – 3.33 (m, 1H), 3.28–3.24 (m, 1H), 3.12 (dtd, J = 3.2, 1.6, 0.8 Hz, 1H), 2.68 (ddd, J = 2.9, 1.6, 0.9 Hz, 1H), 1.63–1.60 (m, 1H), 1.48–1.44 (m, 1H). **M7** (Yield 95 %) <sup>1</sup>H NMR (400 MHz, CDCl<sub>3</sub>): δ 6.23 (s, 2H), 4.04 (dq, J = 11.0, 5.4, 2.5, 1.6 Hz, 4H), 3.29–3.20 (m, 2H), 3.16–3.11 (m, 2H), 1.46–1.42 (m, 1H), 1.30 (dt, J = 8.5, 1.6 Hz, 1H), 1.22–1.17 (m, 6H).

Figure 2.6.1. DSC traces of [Ru] 1 activation temperature in ROMP

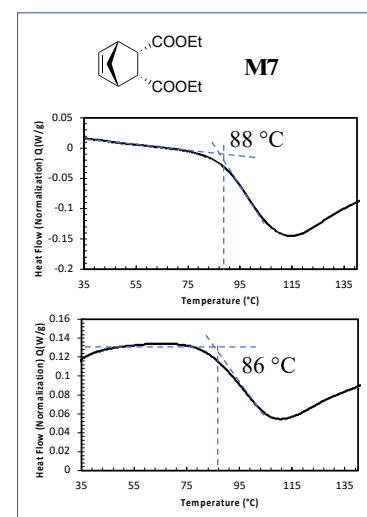
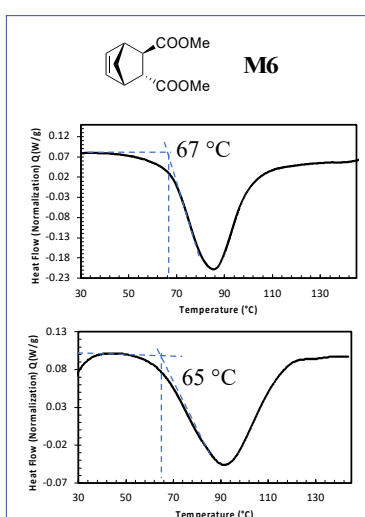
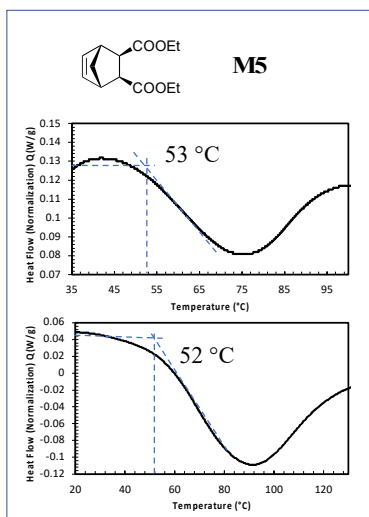
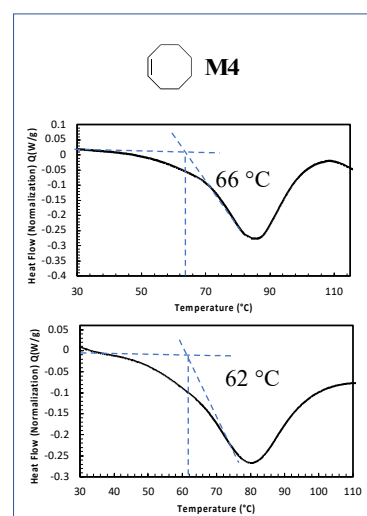
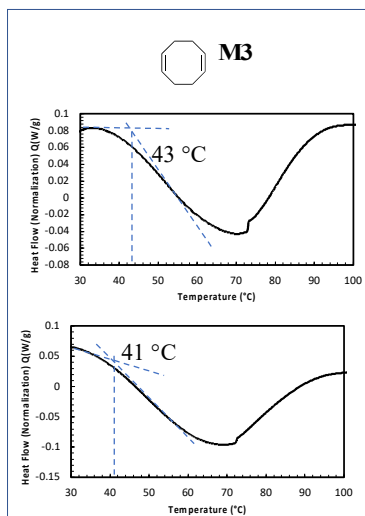
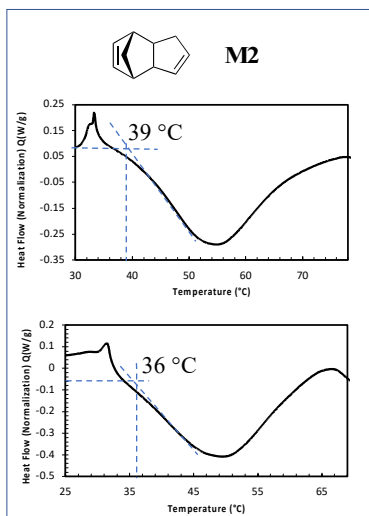
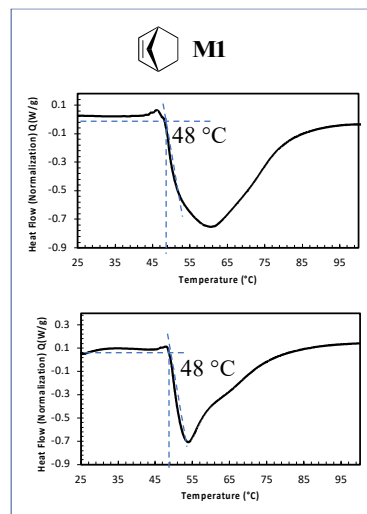
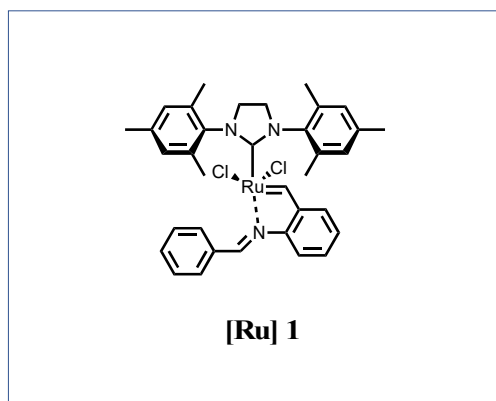


Figure 2.6.2. DSC traces of [Ru] 2 activation temperature in ROMP

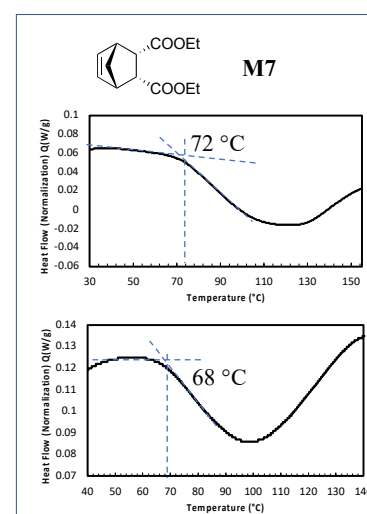
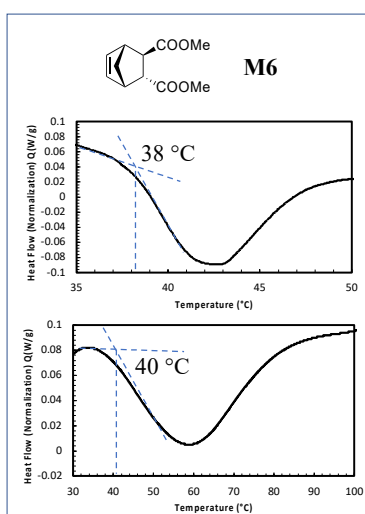
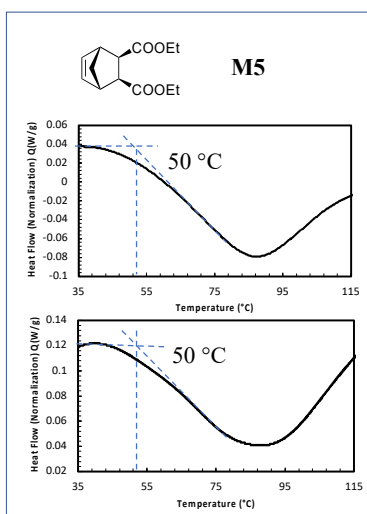
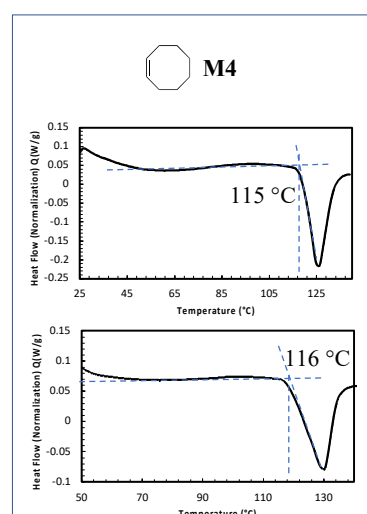
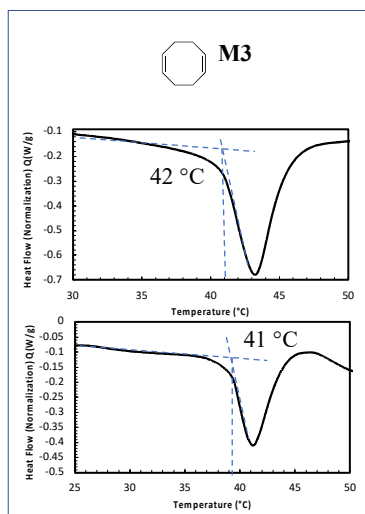
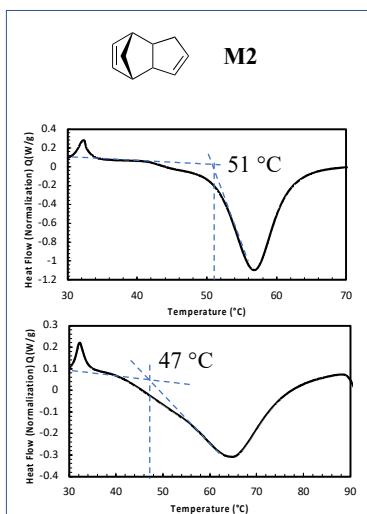
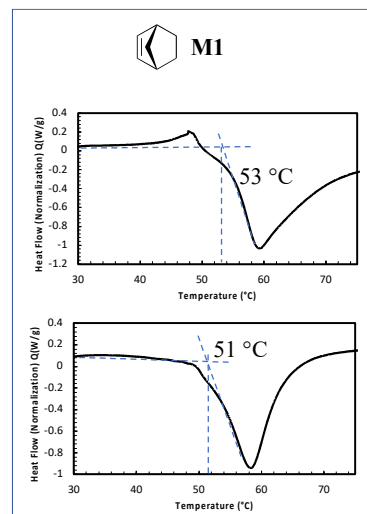
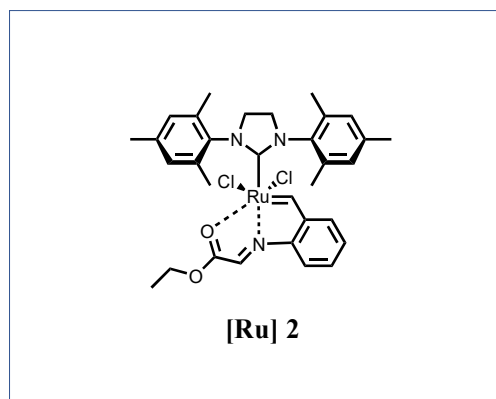


Figure 2.6.3. DSC traces of [Ru] 3 activation temperature in ROMP

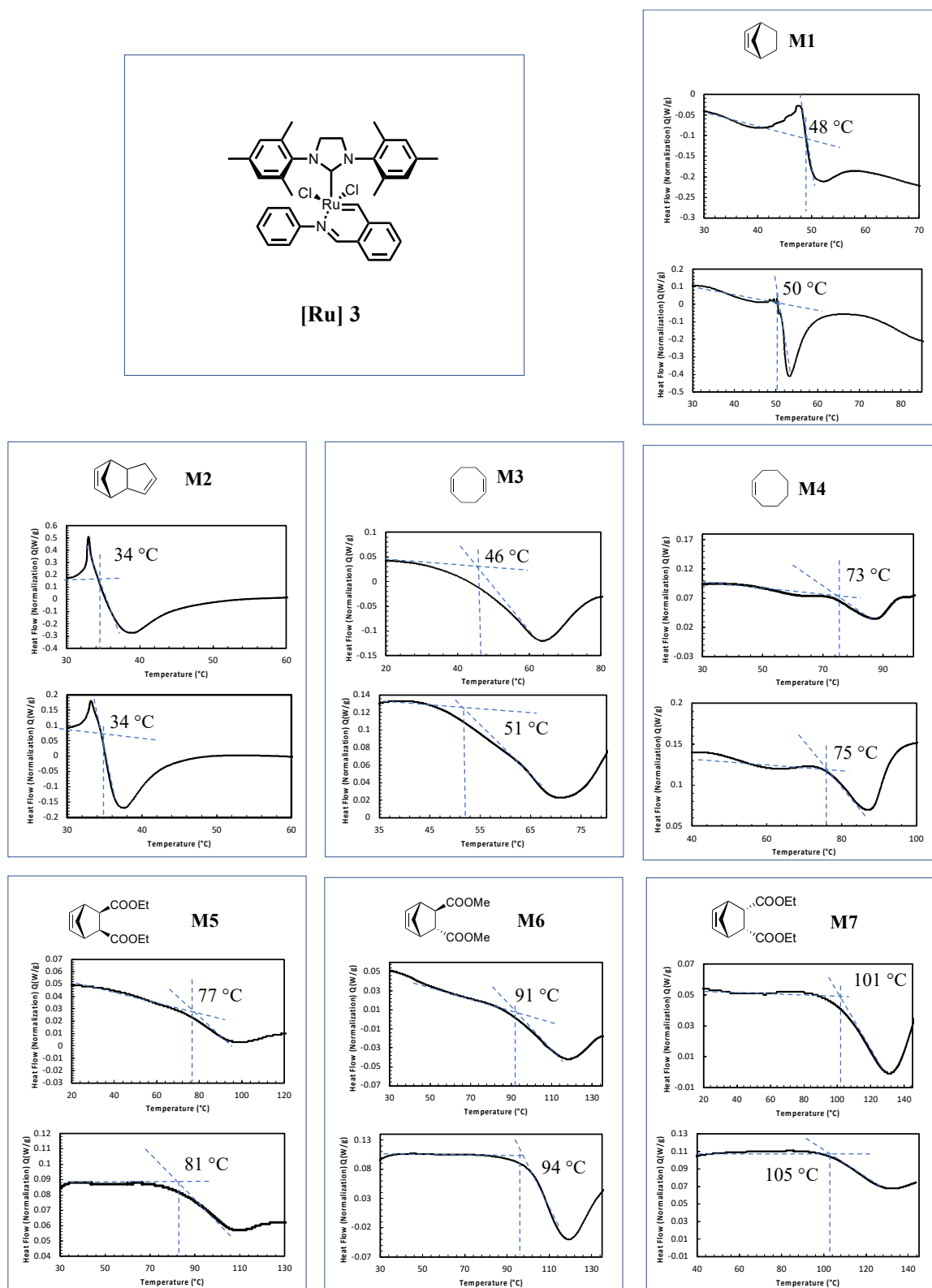


Figure 2.6.4. DSC traces of [Ru] 4 activation temperature in ROMP

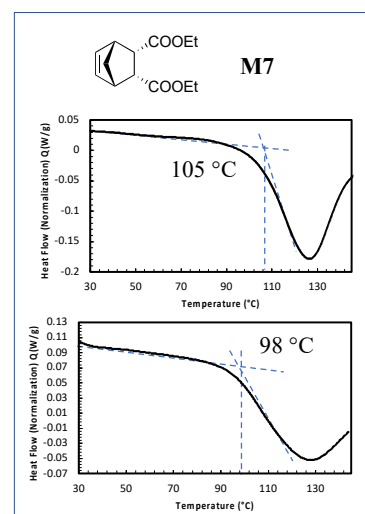
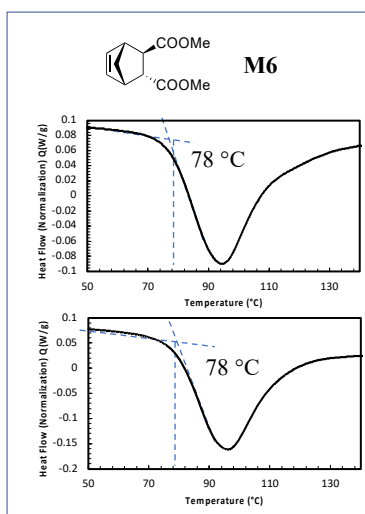
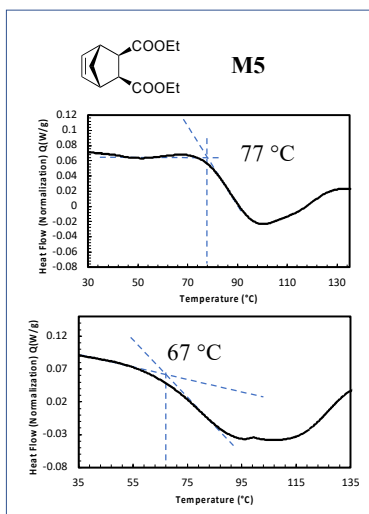
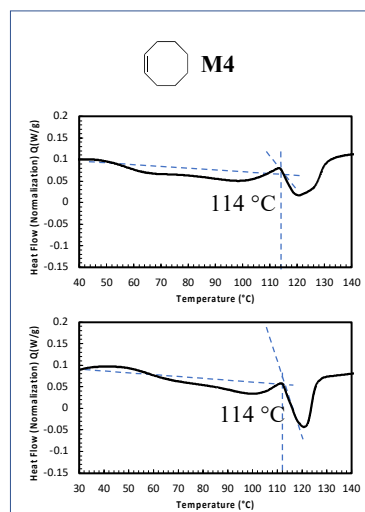
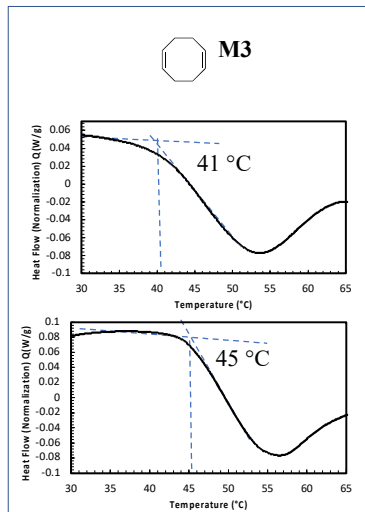
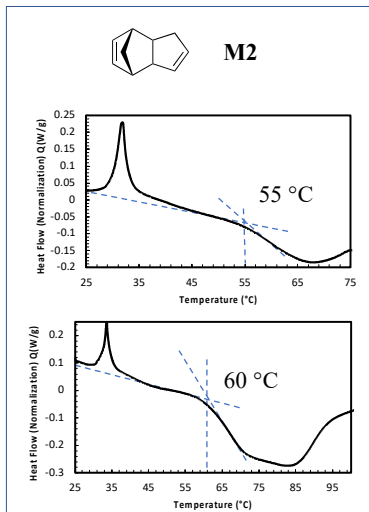
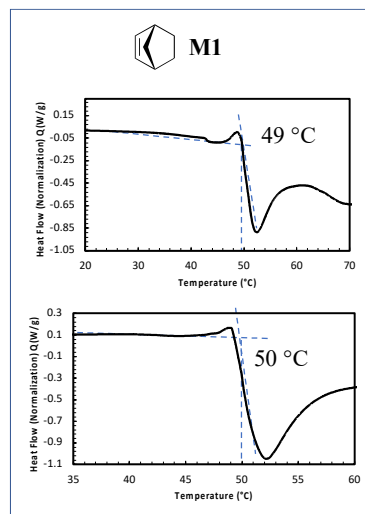
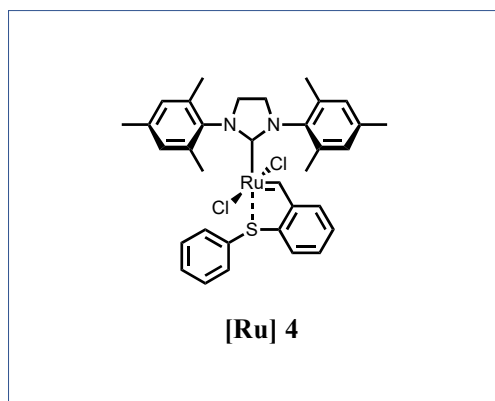


Figure 2.6.5. DSC traces of [Ru] 5 activation temperature in ROMP

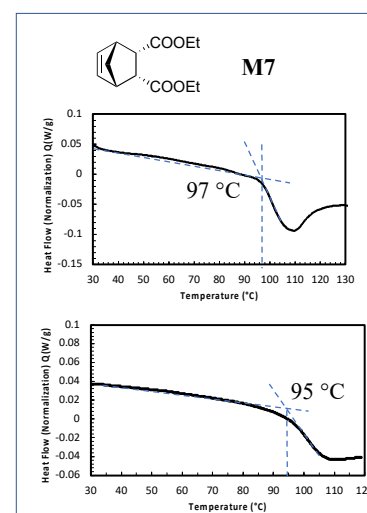
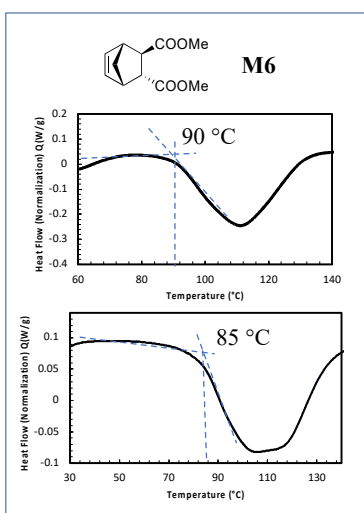
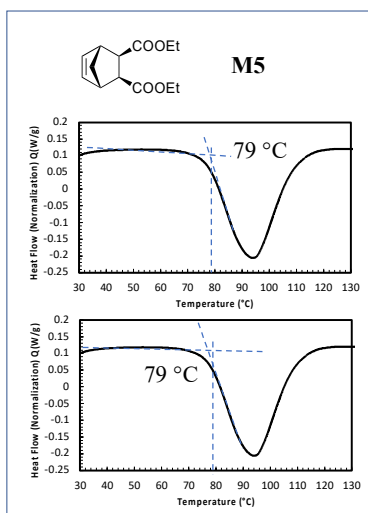
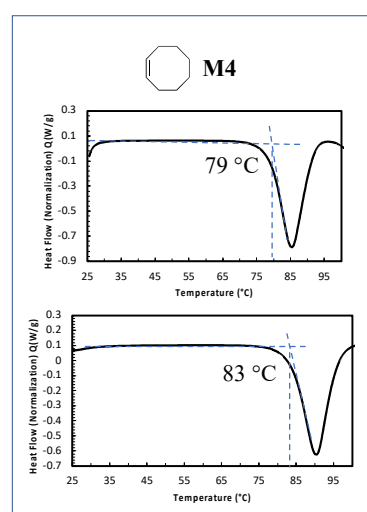
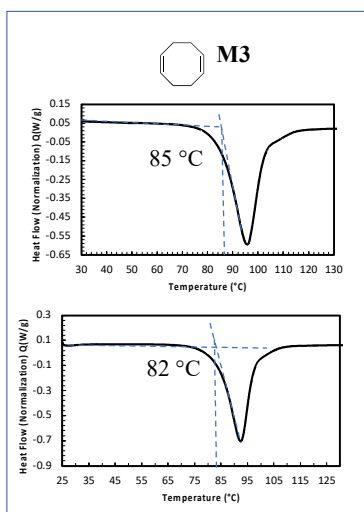
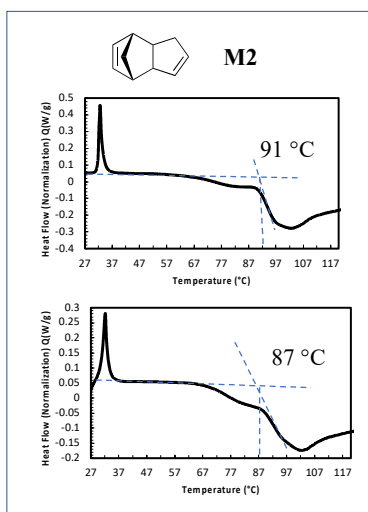
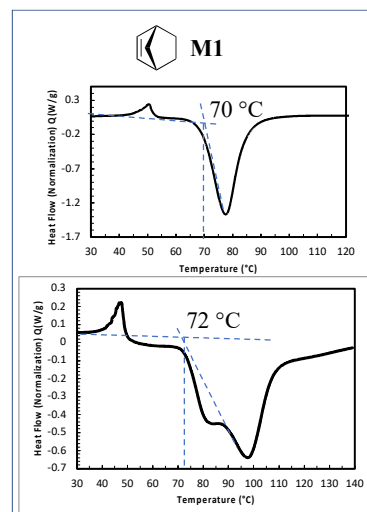
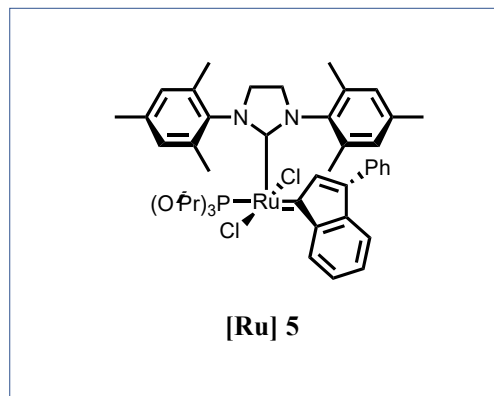


Figure 2.6.6. DSC traces of monomers' melting temperature

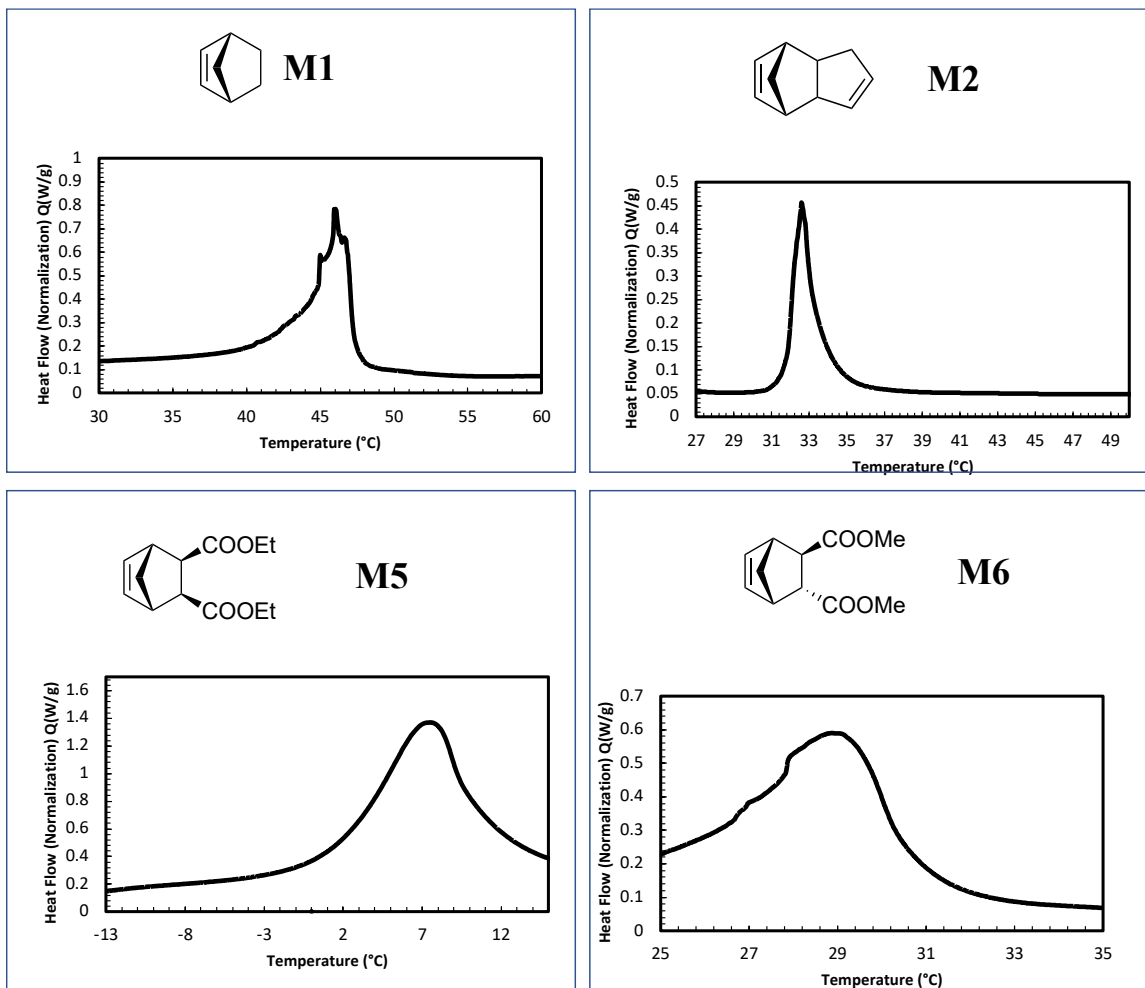
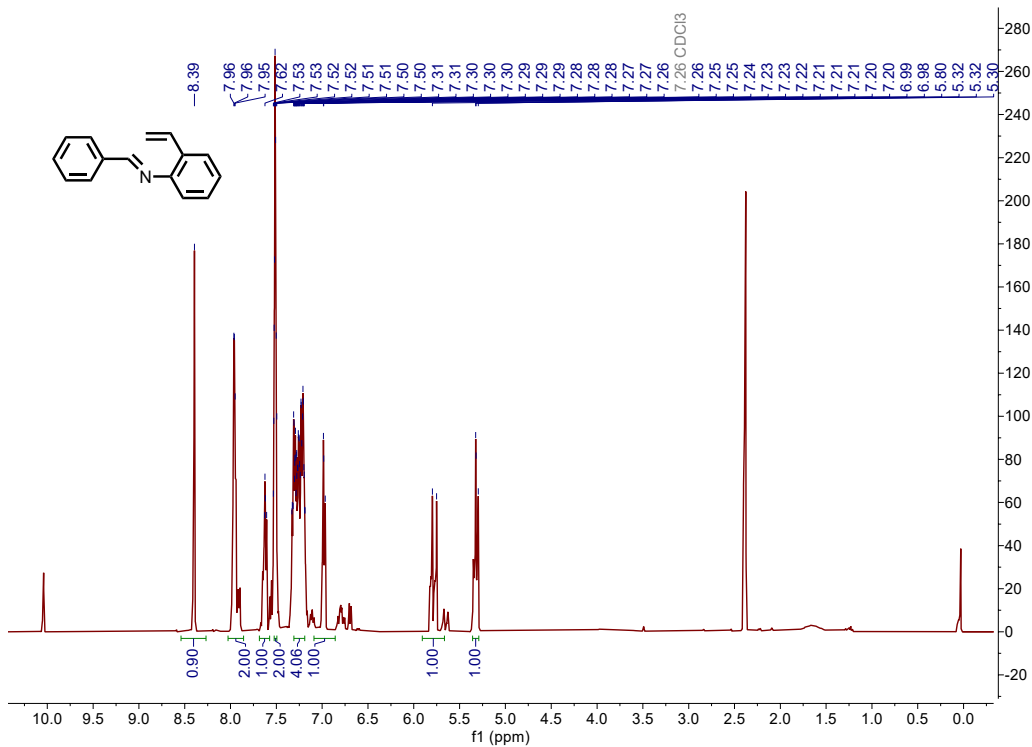
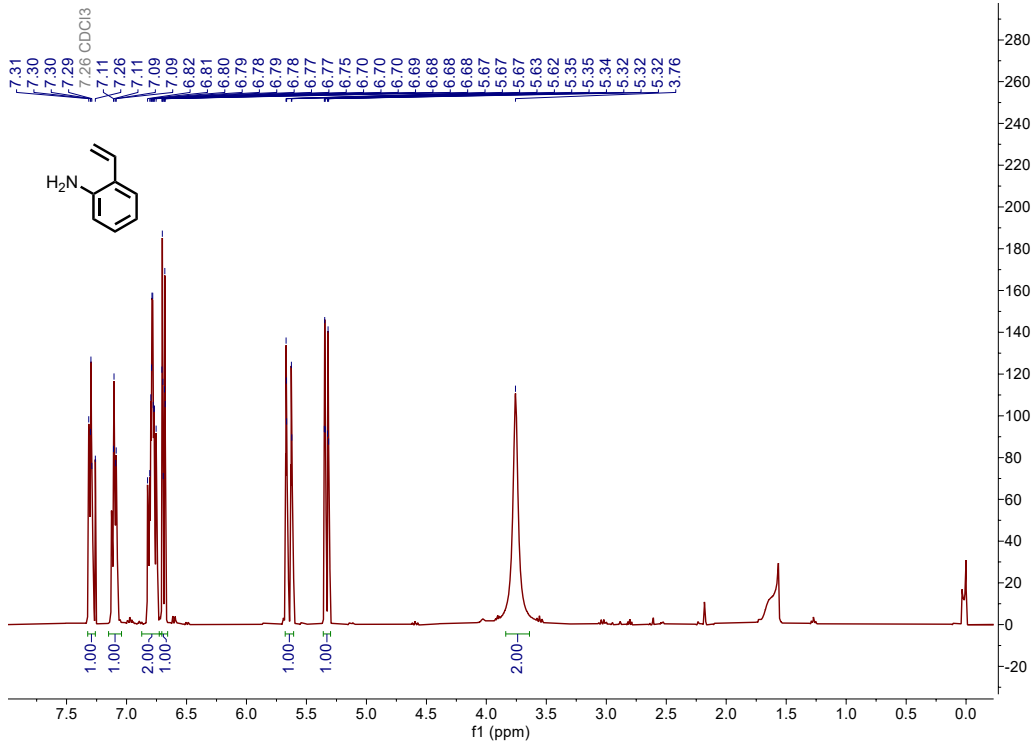
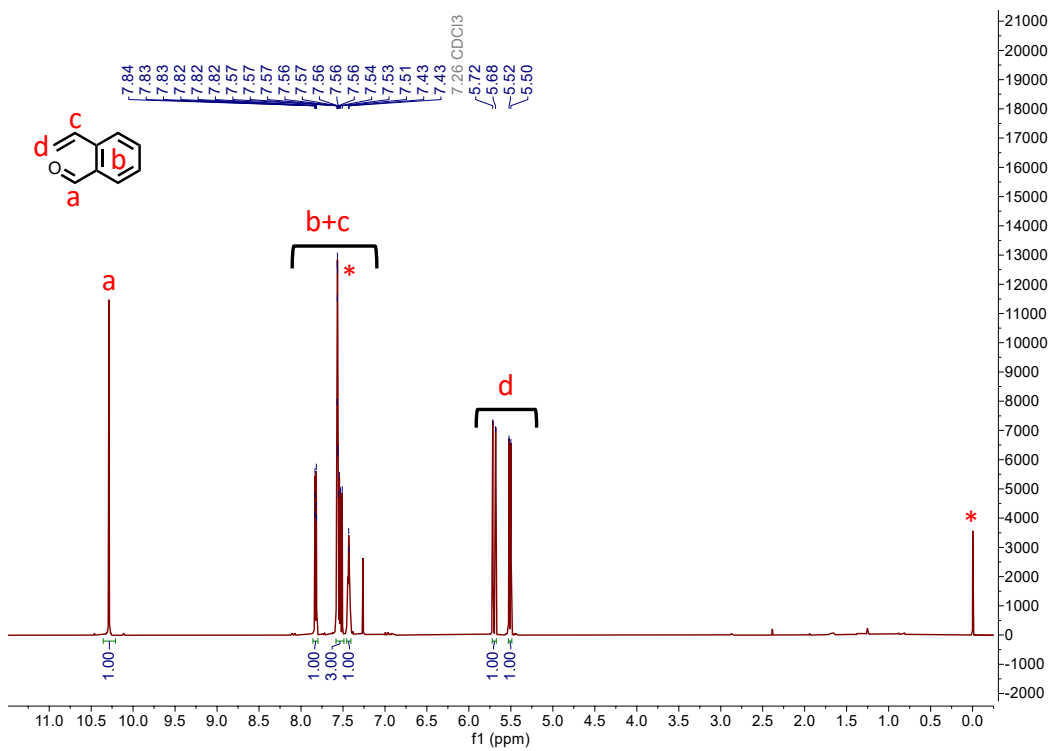
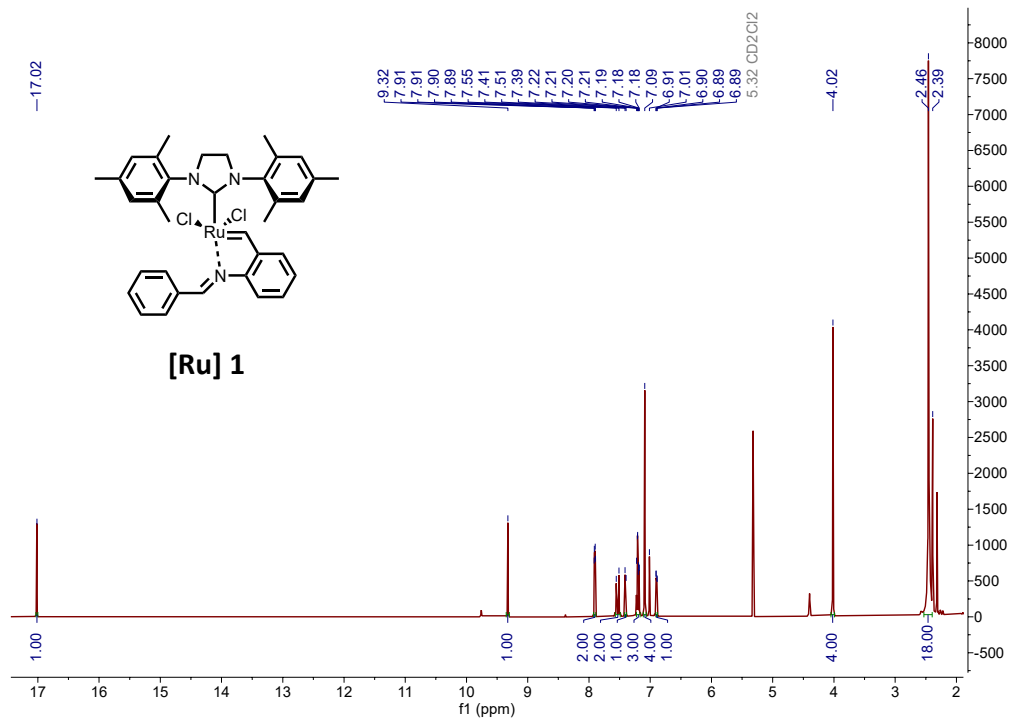
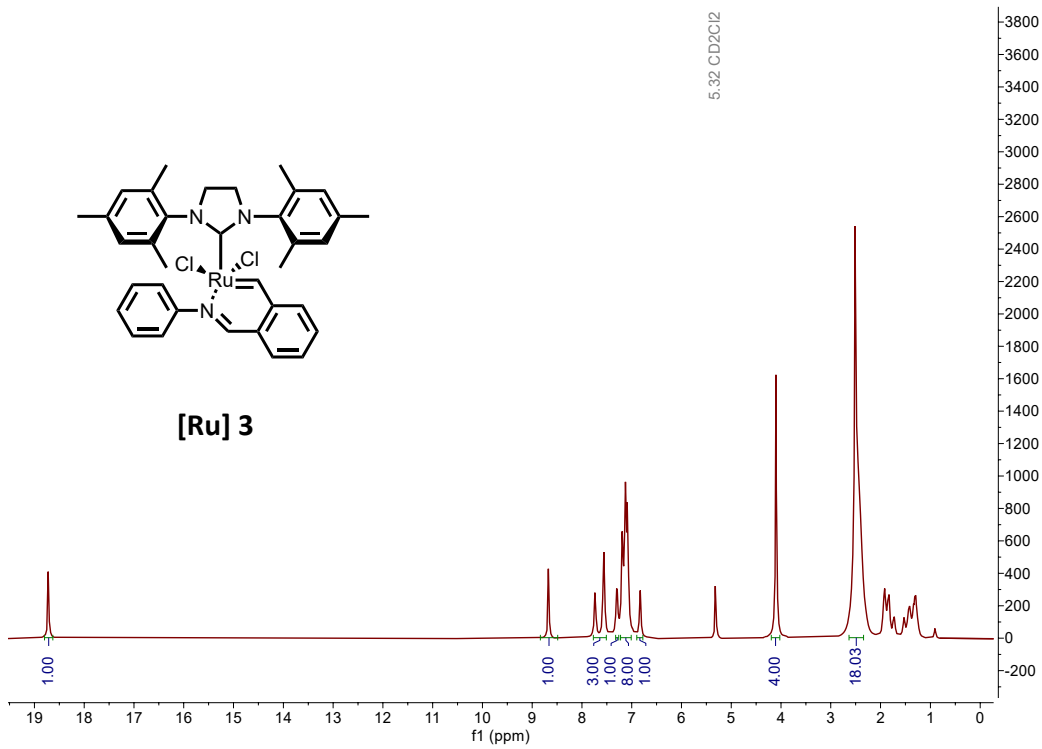
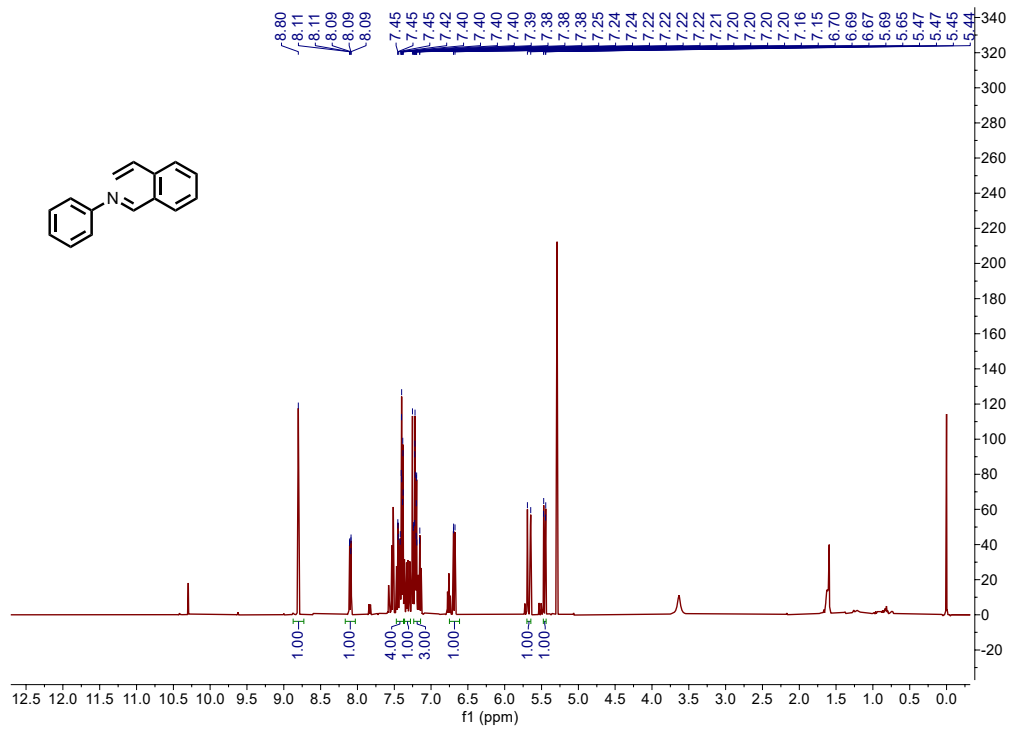
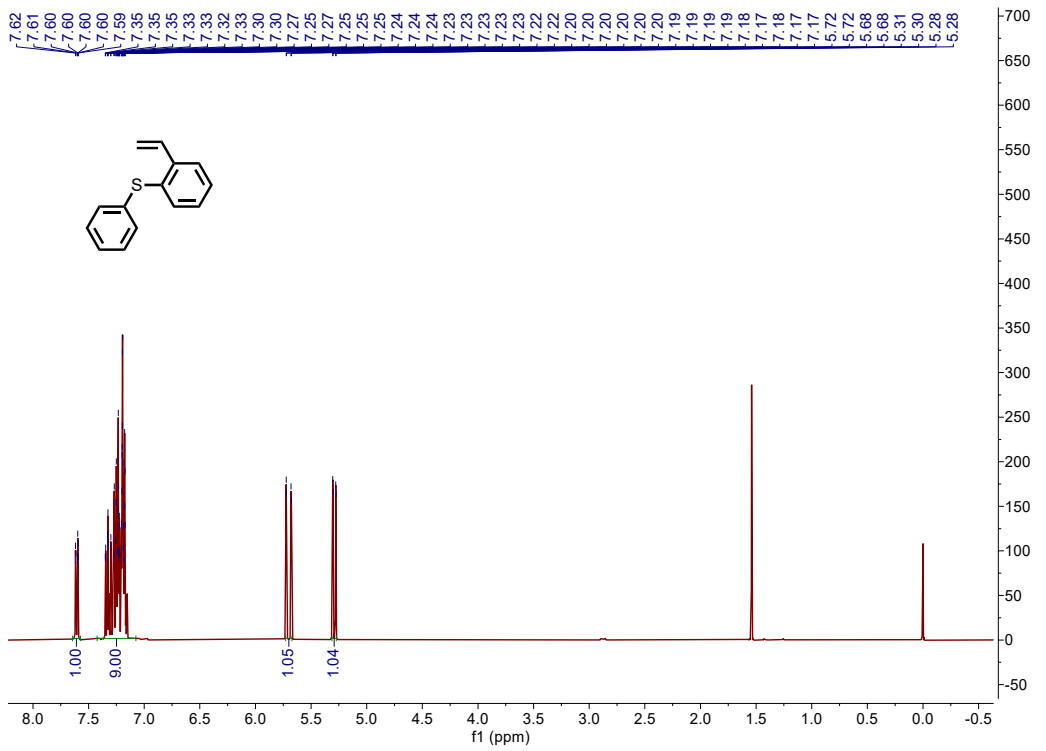
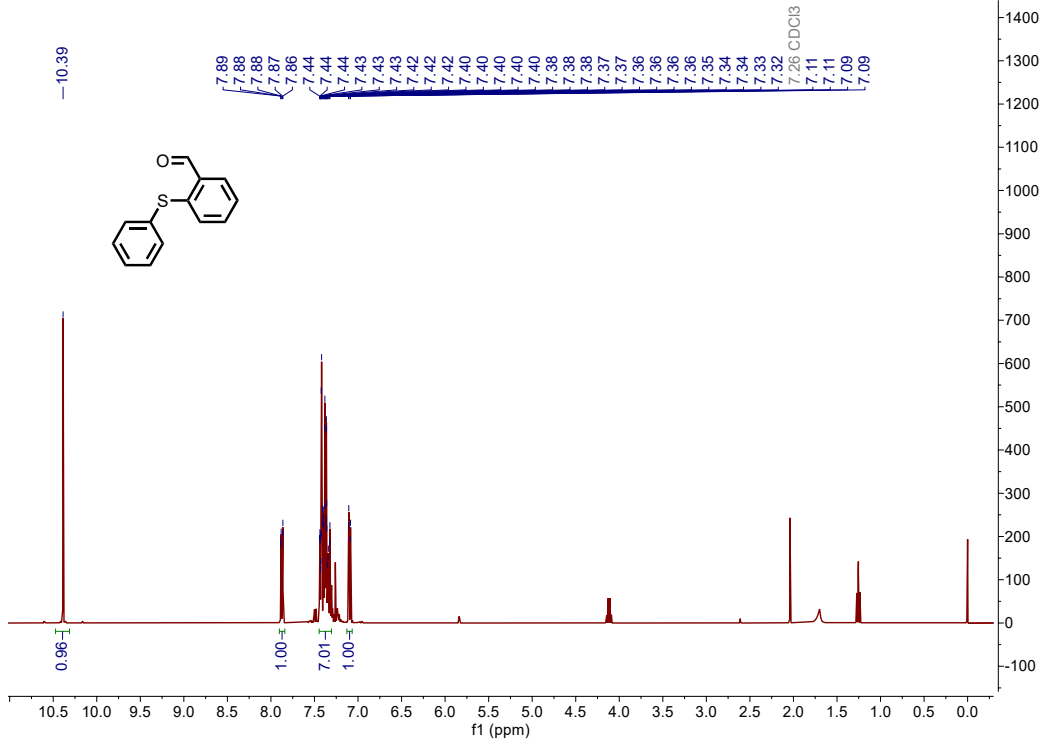


Figure 2.6.7. NMR characterization



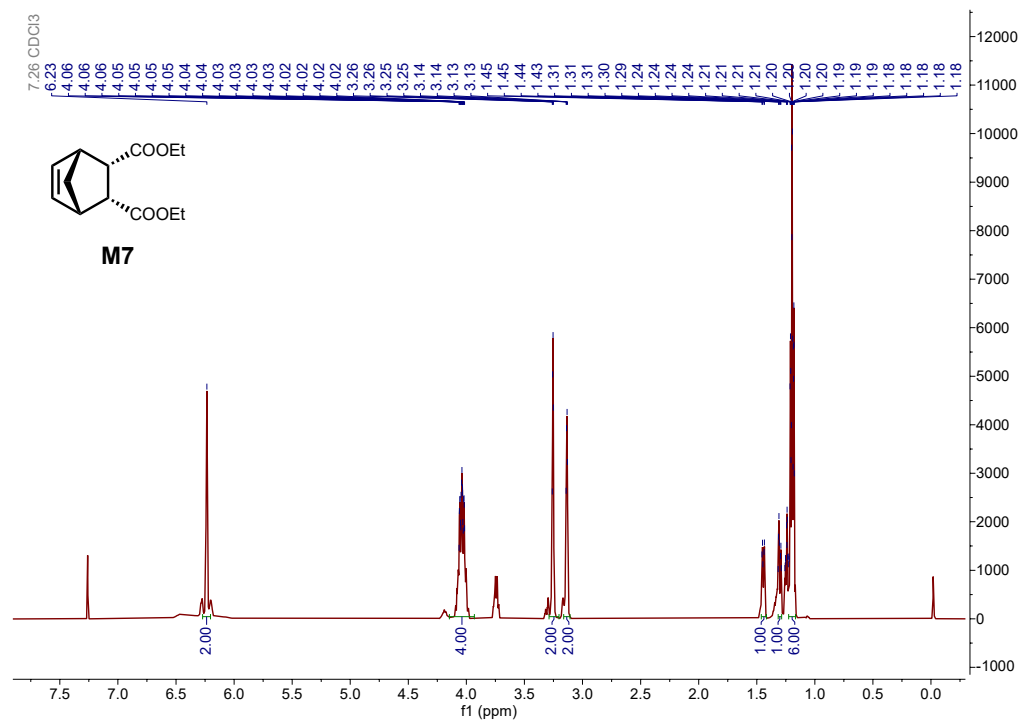






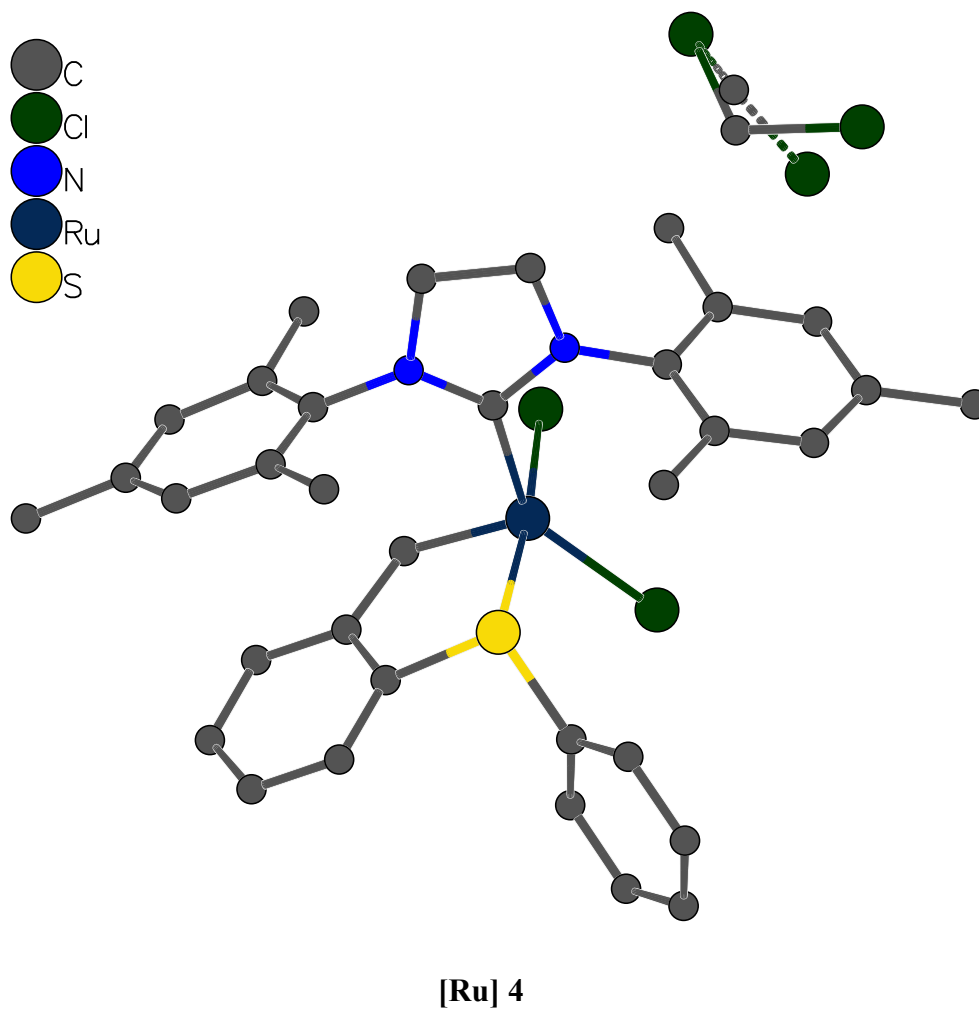






## Catalyst Crystal Structure

**Acknowledgements:** We thank the support of the National Science Foundation under CHE-1726077 for crystallography experiments.



## Experimental

A brown prism (0.11 x 0.23 x 0.26 mm<sup>3</sup>) was centered on the goniometer of a Rigaku Oxford Diffraction Synergy-S diffractometer equipped with a HyPix6000HE detector and operating with MoK $\alpha$  radiation. The data collection routine, unit cell

refinement, and data processing were carried out with the program CrysAlisPro.<sup>1</sup> The Laue symmetry and systematic absences were consistent with the monoclinic space group  $P2_1/c$ . The structure was solved using SHELXT<sup>2</sup> and refined using SHELXL<sup>3</sup> via Olex2.<sup>4</sup> The final refinement model involved anisotropic displacement parameters for non-hydrogen atoms and a riding model for all hydrogen atoms. A  $\text{CH}_2\text{Cl}_2$  solvate was modeled with 2-position disorder with relative occupancies that refined to 0.708(3) and 0.292(3); the bond lengths and ellipsoids were restrained DFIX and SIMU, respectively. In addition, anisotropic displacement parameters on a phenyl ring and a mesityl ring were elongated and somewhat irregular in shape; these are attributed to dynamic disorder at the data collection temperature of 200 K. Just below 200 K, the crystals undergo a phase transition and crack into many pieces. The phase transition likely results from the dynamic groups freezing into position. Olex2<sup>5</sup> was used for molecular graphics generation.

**Table 2.6.1. Crystal data and structure refinement for cs2903 [Ru] 4.**

Identification code	HA-2-75
Empirical formula	$\text{C}_{34}\text{H}_{36}\text{Cl}_2\text{N}_2\text{RuS} \cdot \text{CH}_2\text{Cl}_2$

- 
- (1) CrysAlisPro Software System, v1.171.41.105a, Rigaku Oxford Diffraction, **2021**, Rigaku Corporation, Oxford, UK.
  - (2) Sheldrick, G. M. "SHELXT – Integrated space-group and crystal structure determination." *Acta Cryst.* **2015**, *A71*, 3–8.
  - (3) Sheldrick, G. M. "Crystal structure refinement with SHELXL." *Acta Cryst.* **2015**, *C71*, 3–8.
  - (4) Dolomanov, O.V.; Bourhis, L. J.; Gildea, R. J.; Howard, J. A. K.; Puschmann, H. *J. Appl. Cryst.* **2009**, *42*, 339–341.
  - (5) Dolomanov, O.V.; Bourhis, L. J.; Gildea, R. J.; Howard, J. A. K.; Puschmann, H. *J. Appl. Cryst.* **2009**, *42*, 339–341.

Formula weight	761.60
Temperature/K	200.00(15)
Crystal system	monoclinic
Space group	P2 <sub>1</sub> /c
a/Å	8.08610(10)
b/Å	18.3296(3)
c/Å	24.0578(3)
α/°	90
β/°	98.9570(10)
γ/°	90
Volume/Å <sup>3</sup>	3522.24(9)
Z	4
ρ <sub>calc</sub> /cm <sup>3</sup>	1.436
μ/mm <sup>-1</sup>	0.835
F(000)	1560.0
Crystal size/mm <sup>3</sup>	0.26 × 0.23 × 0.11
Radiation	Mo Kα (λ = 0.71073)
2θ range for data collection/°	5.564 to 76.65
Index ranges	-13 ≤ h ≤ 13, -31 ≤ k ≤ 30, -40 ≤ l ≤ 40
Reflections collected	109895
Independent reflections	18426 [R <sub>int</sub> = 0.0314, R <sub>sigma</sub> = 0.0245]
Data/restraints/parameters	18426/52/413
Goodness-of-fit on F <sup>2</sup>	1.054
Final R indexes [I ≥ 2σ (I)]	R <sub>1</sub> = 0.0365, wR <sub>2</sub> = 0.0970
Final R indexes [all data]	R <sub>1</sub> = 0.0522, wR <sub>2</sub> = 0.1029
Largest diff. peak/hole / e Å <sup>-3</sup>	1.13/-0.85

**Table 2.6.2. Bond Lengths for cs2903 [Ru] 4.**

Atom	Atom	Length/Å	Atom	Atom	Length/Å
Ru1	C11	2.3844 (3)	C14	C15	1.385 (3)
Ru1	C12	2.3529 (4)	C14	C19	1.505 (3)
Ru1	S1	2.3386 (3)	C15	C16	1.389 (3)
Ru1	C1	2.0158 (12)	C16	C17	1.377 (3)
Ru1	C28	1.8391 (13)	C16	C20	1.513 (3)
S1	C22	1.7806 (15)	C17	C18	1.385 (2)
S1	C29	1.7857 (15)	C18	C21	1.503 (2)
N1	C1	1.3395 (16)	C22	C23	1.388 (2)
N1	C2	1.4744 (18)	C22	C27	1.390 (2)
N1	C4	1.4257 (18)	C23	C24	1.386 (3)
N2	C1	1.3378 (17)	C24	C25	1.379 (3)
N2	C3	1.4774 (18)	C25	C26	1.389 (2)
N2	C13	1.4311 (19)	C26	C27	1.403 (2)

**Table 2.6.2. Bond Lengths for cs2903 [Ru] 4.**

Atom	Atom	Length/Å	Atom	Atom	Length/Å
C2	C3	1.502 (3)	C27	C28	1.4570 (19)
C4	C5	1.397 (2)	C29	C30	1.371 (2)
C4	C9	1.398 (2)	C29	C34	1.388 (2)
C5	C6	1.393 (2)	C30	C31	1.393 (3)
C5	C10	1.503 (2)	C31	C32	1.362 (3)
C6	C7	1.380 (2)	C32	C33	1.373 (3)
C7	C8	1.389 (2)	C33	C34	1.386 (2)
C7	C11	1.499 (2)	Cl3	C35A	1.775 (6)
C8	C9	1.395 (2)	Cl3	C35B	1.673 (16)
C9	C12	1.506 (2)	C35A	Cl4A	1.760 (7)
C13	C14	1.393 (2)	C35B	Cl4B	1.787 (15)
C13	C18	1.398 (2)			

**Table 2.6.3. Bond Angles for cs2903 [Ru] 4.**

Atom	Atom	Atom	Angle/°	Atom	Atom	Atom	Angle/°
Cl2	Ru1	Cl1	89.430 (14)	C8	C9	C12	120.35 (15)
S1	Ru1	Cl1	173.230 (13)	C14	C13	N2	118.98 (14)
S1	Ru1	Cl2	92.533 (14)	C14	C13	C18	121.22 (14)
C1	Ru1	Cl1	89.37 (4)	C18	C13	N2	119.51 (14)
C1	Ru1	Cl2	144.63 (4)	C13	C14	C19	122.10 (17)
C1	Ru1	S1	92.76 (4)	C15	C14	C13	118.12 (17)
C28	Ru1	Cl1	89.82 (4)	C15	C14	C19	119.73 (17)
C28	Ru1	Cl2	117.11 (4)	C14	C15	C16	122.10 (19)
C28	Ru1	S1	83.52 (4)	C15	C16	C20	120.3 (2)
C28	Ru1	C1	98.24 (5)	C17	C16	C15	118.06 (19)
C22	S1	Ru1	99.36 (5)	C17	C16	C20	121.6 (2)
C22	S1	C29	100.61 (7)	C16	C17	C18	122.33 (18)
C29	S1	Ru1	117.07 (5)	C13	C18	C21	122.51 (15)
C1	N1	C2	112.38 (12)	C17	C18	C13	118.04 (16)
C1	N1	C4	127.90 (11)	C17	C18	C21	119.37 (15)
C4	N1	C2	119.59 (12)	C23	C22	S1	123.76 (14)
C1	N2	C3	113.08 (12)	C23	C22	C27	122.23 (15)
C1	N2	C13	126.01 (11)	C27	C22	S1	114.00 (10)
C13	N2	C3	120.48 (12)	C24	C23	C22	117.97 (19)
N1	C1	Ru1	133.67 (10)	C25	C24	C23	121.32 (17)
N2	C1	Ru1	118.14 (9)	C24	C25	C26	120.33 (17)
N2	C1	N1	108.16 (11)	C25	C26	C27	119.62 (17)
N1	C2	C3	103.43 (12)	C22	C27	C26	118.50 (14)
N2	C3	C2	102.34 (11)	C22	C27	C28	117.39 (13)
C5	C4	N1	119.73 (13)	C26	C27	C28	124.04 (15)
C5	C4	C9	121.63 (13)	C27	C28	Ru1	124.88 (11)
C9	C4	N1	118.51 (13)	C30	C29	S1	117.62 (12)

**Table 2.6.3. Bond Angles for cs2903 [Ru] 4.**

Atom	Atom	Atom	Angle/°	Atom	Atom	Atom	Angle/°
C4	C5	C10	121.77 (14)	C30	C29	C34	120.25 (15)
C6	C5	C4	117.92 (14)	C34	C29	S1	122.11 (13)
C6	C5	C10	120.30 (14)	C29	C30	C31	119.55 (18)
C7	C6	C5	121.95 (15)	C32	C31	C30	120.6 (2)
C6	C7	C8	118.79 (15)	C31	C32	C33	119.68 (18)
C6	C7	C11	120.51 (17)	C32	C33	C34	120.83 (17)
C8	C7	C11	120.70 (17)	C33	C34	C29	119.05 (17)
C7	C8	C9	121.54 (15)	Cl4A	C35A	Cl3	114.4 (3)
C4	C9	C12	121.65 (15)	Cl3	C35B	Cl4B	94.6 (8)
C8	C9	C4	118.00 (14)				

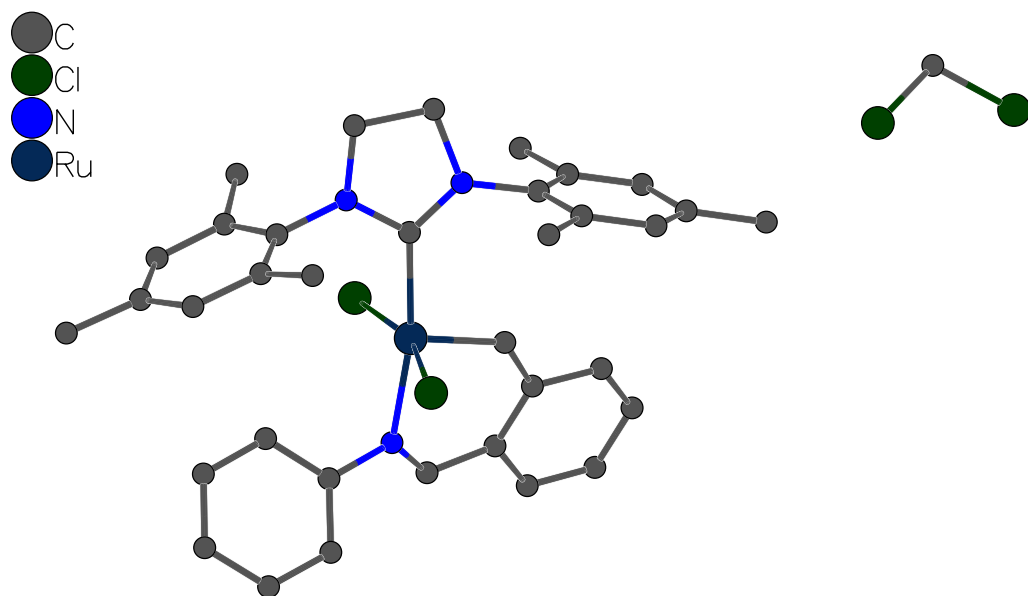
**Table 2.6.4. Torsion Angles for cs2903 [Ru] 4.**

A	B	C	D	Angle/°	A	B	C	D	Angle/°
Ru1	S1	C22	C23	172.84 (13)	C5	C6	C7	C11	-179.92 (16)
Ru1	S1	C22	C27	-8.16 (10)	C6	C7	C8	C9	-2.3 (2)
Ru1	S1	C29	C30	119.35 (16)	C7	C8	C9	C4	0.9 (2)
Ru1	S1	C29	C34	-62.14 (15)	C7	C8	C9	C12	-178.71 (14)
Cl1	Ru1	C28	C27	171.56 (10)	C9	C4	C5	C6	-4.98 (19)
Cl2	Ru1	C28	C27	82.30 (11)	C9	C4	C5	C10	173.81 (13)
S1	Ru1	C28	C27	-7.23 (10)	C10	C5	C6	C7	-175.25 (14)
S1	C22	C23	C24	179.79 (13)	C11	C7	C8	C9	177.61 (16)
S1	C22	C27	C26	-178.31 (10)	C13	N2	C1	Ru1	-7.38 (19)
S1	C22	C27	C28	4.60 (15)	C13	N2	C1	N1	174.39 (13)
S1	C29	C30	C31	178.8 (2)	C13	N2	C3	C2	-179.03 (15)
S1	C29	C34	C33	-177.61 (14)	C13	C14	C15	C16	-0.7 (4)
N1	C2	C3	N2	7.33 (18)	C14	C13	C18	C17	-4.2 (3)
N1	C4	C5	C6	179.24 (12)	C14	C13	C18	C21	172.34 (16)
N1	C4	C5	C10	-1.97 (19)	C14	C15	C16	C17	-1.6 (5)
N1	C4	C9	C8	178.63 (12)	C14	C15	C16	C20	179.3 (3)
N1	C4	C9	C12	-1.74 (19)	C15	C16	C17	C18	1.0 (5)
N2	C13	C14	C15	177.41 (19)	C16	C17	C18	C13	1.8 (3)
N2	C13	C14	C19	0.1 (3)	C16	C17	C18	C21	-174.8 (2)
N2	C13	C18	C17	-177.92 (16)	C18	C13	C14	C15	3.7 (3)
N2	C13	C18	C21	-1.4 (2)	C18	C13	C14	C19	-173.70 (17)
C1	Ru1	C28	C27	-99.10 (11)	C19	C14	C15	C16	176.7 (3)
C1	N1	C2	C3	-7.1 (2)	C20	C16	C17	C18	-179.9 (3)
C1	N1	C4	C5	-84.61 (18)	C22	S1	C29	C30	-134.29 (17)
C1	N1	C4	C9	99.47 (17)	C22	S1	C29	C34	44.22 (15)
C1	N2	C3	C2	-6.16 (18)	C22	C23	C24	C25	-1.7 (3)
C1	N2	C13	C14	107.38 (18)	C22	C27	C28	Ru1	3.55 (16)

**Table 2.6.4. Torsion Angles for cs2903 [Ru] 4.**

A	B	C	D	Angle/°	A	B	C	D	Angle/°
C1	N2	C13	C18	-78.8 (2)	C23	C22	C27	C26	0.7 (2)
C2	N1	C1	Ru1	-174.47 (13)	C23	C22	C27	C28	-176.38 (13)
C2	N1	C1	N2	3.38 (18)	C23	C24	C25	C26	0.9 (3)
C2	N1	C4	C5	91.00 (17)	C24	C25	C26	C27	0.7 (3)
C2	N1	C4	C9	-84.91 (18)	C25	C26	C27	C22	-1.5 (2)
C3	N2	C1	Ru1	-179.79 (10)	C25	C26	C27	C28	175.40 (14)
C3	N2	C1	N1	1.98 (17)	C26	C27	C28	Ru1	-173.37 (11)
C3	N2	C13	C14	-80.7 (2)	C27	C22	C23	C24	0.9 (2)
C3	N2	C13	C18	93.13 (18)	C29	S1	C22	C23	52.83 (14)
C4	N1	C1	Ru1	1.4 (2)	C29	S1	C22	C27	-128.16 (11)
C4	N1	C1	N2	179.26 (13)	C29	C30	C31	C32	-0.9 (5)
C4	N1	C2	C3	176.69 (14)	C30	C29	C34	C33	0.9 (3)
C4	C5	C6	C7	3.6 (2)	C30	C31	C32	C33	0.4 (4)
C5	C4	C9	C8	2.80 (19)	C31	C32	C33	C34	0.7 (4)
C5	C4	C9	C12	-177.57 (13)	C32	C33	C34	C29	-1.4 (3)
C5	C6	C7	C8	0.0 (2)	C34	C29	C30	C31	0.3 (4)

This report has been created with Olex2, compiled on 2022.04.07 svn.rea3783a0 for OlexSys. Please [let us know](#) if there are any errors or if you would like to have additional features.



[Ru] 3

## Experimental

A yellow-brown crystal ( $0.03 \times 0.10 \times 0.12 \text{ mm}^3$ ) was cut from a cluster of intergrown crystals and centered on the goniometer of a Rigaku Oxford Diffraction Synergy-S diffractometer equipped with a HyPix6000HE detector and operating with  $\text{CuK}\alpha$  radiation. The data collection routine, unit cell refinement, and data processing were carried out with the program CrysAlisPro.<sup>6</sup> The Laue symmetry and systematic absences were consistent with the monoclinic space group  $P2_1/c$ . The structure was solved using

---

(6) CrysAlisPro Software System, v1.171.41.105a, Rigaku Oxford Diffraction, 2021, Rigaku Corporation, Oxford, UK.

SHELXT<sup>7</sup> and refined using SHELXL<sup>8</sup> via Olex2.<sup>9</sup> The final refinement model involved anisotropic displacement parameters for non-hydrogen atoms and a riding model for all hydrogen atoms. Olex2<sup>10</sup> was used for molecular graphics generation.

**Table 2.6.5. Crystal data and structure refinement for cs2849 [Ru] 3.**

Identification code	cs2849
Empirical formula	C <sub>36</sub> H <sub>39</sub> Cl <sub>4</sub> N <sub>3</sub> Ru
Formula weight	756.57
Temperature/K	100.00(10)
Crystal system	monoclinic
Space group	<i>P</i> 2 <sub>1</sub> / <i>c</i>
<i>a</i> /Å	18.8082(2)
<i>b</i> /Å	10.19550(10)
<i>c</i> /Å	19.3233(2)
$\alpha$ /°	90
$\beta$ /°	112.8670(10)
$\gamma$ /°	90
Volume/Å <sup>3</sup>	3414.20(6)
<i>Z</i>	4
$\rho_{\text{calc}}$ /cm <sup>3</sup>	1.472
$\mu$ /mm <sup>-1</sup>	6.823
<i>F</i> (000)	1552.0
Crystal size/mm <sup>3</sup>	0.12 × 0.096 × 0.03
Radiation	Cu K $\alpha$ ( $\lambda$ = 1.54184)
2 $\Theta$ range for data collection/°	5.1 to 154.662
Index ranges	-23 ≤ <i>h</i> ≤ 23, -12 ≤ <i>k</i> ≤ 12, -24 ≤ <i>l</i> ≤ 24
Reflections collected	79800
Independent reflections	7233 [ <i>R</i> <sub>int</sub> = 0.0562, <i>R</i> <sub>sigma</sub> = 0.0231]
Data/restraints/parameters	7233/0/403
Goodness-of-fit on <i>F</i> <sup>2</sup>	1.066

(7) Sheldrick, G. M. "SHELXT – Integrated space-group and crystal structure determination." *Acta Cryst.* **2015**, *A71*, 3–8.

(8) Sheldrick, G. M. "Crystal structure refinement with SHELXL." *Acta Cryst.* **2015**, *C71*, 3–8.

(9) Dolomanov, O.V.; Bourhis, L. J.; Gildea, R. J.; Howard, J. A. K.; Puschmann, H. *J. Appl. Cryst.* **2009**, *42*, 339–341.

(10) Dolomanov, O.V.; Bourhis, L. J.; Gildea, R. J.; Howard, J. A. K.; Puschmann, H. *J. Appl. Cryst.* **2009**, *42*, 339–341.

Final R indexes [ $I \geq 2\sigma(I)$ ]  $R_1 = 0.0411$ ,  $wR_2 = 0.1137$   
 Final R indexes [all data]  $R_1 = 0.0424$ ,  $wR_2 = 0.1150$   
 Largest diff. peak/hole /  $e \text{ \AA}^{-3}$  0.87/-1.65

**Table 2.6.6 Bond Lengths for cs2849 [Ru] 3.**

Atom	Atom	Length/Å	Atom	Atom	Length/Å
Ru1	C11	2.3437 (6)	C13	C18	1.394 (3)
Ru1	C12	2.3707 (6)	C14	C15	1.399 (4)
Ru1	N3	2.0968 (19)	C14	C19	1.503 (4)
Ru1	C1	2.078 (2)	C15	C16	1.392 (4)
Ru1	C22	1.839 (2)	C16	C17	1.391 (4)
N1	C1	1.341 (3)	C16	C20	1.506 (4)
N1	C2	1.477 (3)	C17	C18	1.394 (3)
N1	C4	1.434 (3)	C18	C21	1.507 (3)
N2	C1	1.342 (3)	C22	C23	1.449 (3)
N2	C3	1.481 (3)	C23	C24	1.408 (3)
N2	C13	1.431 (3)	C23	C28	1.416 (3)
N3	C29	1.283 (3)	C24	C25	1.385 (3)
N3	C30	1.431 (3)	C25	C26	1.400 (4)
C2	C3	1.528 (4)	C26	C27	1.380 (4)
C4	C5	1.399 (4)	C27	C28	1.399 (3)
C4	C9	1.399 (4)	C28	C29	1.453 (3)
C5	C6	1.397 (4)	C30	C31	1.391 (4)
C5	C10	1.511 (4)	C30	C35	1.392 (4)
C6	C7	1.389 (5)	C31	C32	1.391 (4)
C7	C8	1.386 (5)	C32	C33	1.388 (4)
C7	C11	1.508 (4)	C33	C34	1.386 (4)
C8	C9	1.391 (4)	C34	C35	1.396 (4)
C9	C12	1.512 (4)	C13	C36	1.757 (4)
C13	C14	1.401 (3)	C14	C36	1.770 (4)

**Table 2.6.7. Bond Angles for cs2849 [Ru] 3.**

Atom	Atom	Atom	Angle/°	Atom	Atom	Atom	Angle/°
C11	Ru1	C12	162.36 (2)	C8	C9	C12	120.0 (3)
N3	Ru1	C11	84.94 (6)	C14	C13	N2	118.5 (2)
N3	Ru1	C12	87.68 (6)	C18	C13	N2	119.5 (2)
C1	Ru1	C11	89.37 (7)	C18	C13	C14	122.0 (2)
C1	Ru1	C12	95.35 (6)	C13	C14	C19	121.1 (2)
C1	Ru1	N3	169.78 (9)	C15	C14	C13	118.2 (2)
C22	Ru1	C11	98.25 (8)	C15	C14	C19	120.6 (2)
C22	Ru1	C12	97.70 (8)	C16	C15	C14	120.8 (2)
C22	Ru1	N3	89.62 (9)	C15	C16	C20	120.5 (2)
C22	Ru1	C1	99.61 (10)	C17	C16	C15	119.4 (2)
C1	N1	C2	113.8 (2)	C17	C16	C20	120.1 (2)

**Table 2.6.7. Bond Angles for cs2849 [Ru] 3.**

Atom	Atom	Atom	Angle/°	Atom	Atom	Atom	Angle/°
C1	N1	C4	126.4(2)	C16	C17	C18	121.5(2)
C4	N1	C2	118.2(2)	C13	C18	C21	121.4(2)
C1	N2	C3	113.4(2)	C17	C18	C13	118.0(2)
C1	N2	C13	127.7(2)	C17	C18	C21	120.6(2)
C13	N2	C3	118.40(19)	C23	C22	Ru1	127.44(17)
C29	N3	Ru1	125.94(17)	C24	C23	C22	117.9(2)
C29	N3	C30	118.2(2)	C24	C23	C28	118.0(2)
C30	N3	Ru1	115.41(15)	C28	C23	C22	124.1(2)
N1	C1	Ru1	120.19(17)	C25	C24	C23	121.6(2)
N1	C1	N2	106.9(2)	C24	C25	C26	119.9(2)
N2	C1	Ru1	132.75(18)	C27	C26	C25	119.4(2)
N1	C2	C3	101.5(2)	C26	C27	C28	121.5(2)
N2	C3	C2	101.6(2)	C23	C28	C29	122.2(2)
C5	C4	N1	119.2(2)	C27	C28	C23	119.5(2)
C5	C4	C9	121.3(2)	C27	C28	C29	117.9(2)
C9	C4	N1	119.3(2)	N3	C29	C28	124.6(2)
C4	C5	C10	122.4(2)	C31	C30	N3	120.6(2)
C6	C5	C4	118.1(3)	C31	C30	C35	120.3(2)
C6	C5	C10	119.4(3)	C35	C30	N3	119.1(2)
C7	C6	C5	121.9(3)	C30	C31	C32	119.8(3)
C6	C7	C11	121.2(3)	C33	C32	C31	120.3(3)
C8	C7	C6	118.2(3)	C34	C33	C32	119.7(2)
C8	C7	C11	120.6(3)	C33	C34	C35	120.6(3)
C7	C8	C9	122.2(3)	C30	C35	C34	119.2(3)
C4	C9	C12	121.7(2)	C13	C36	C14	110.77(19)
C8	C9	C4	118.1(3)				

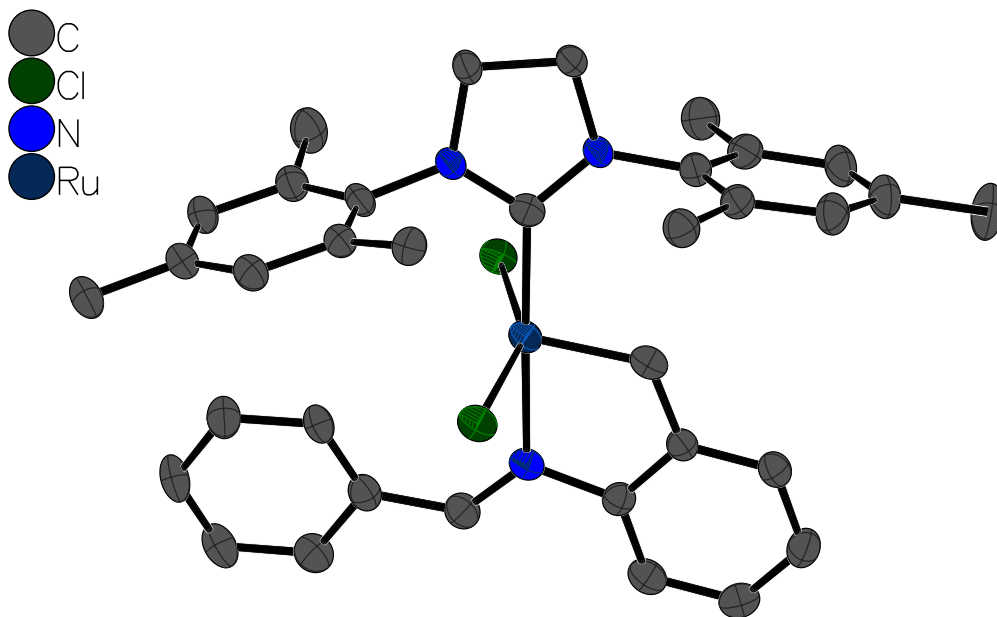
**Table 2.6.8. Torsion Angles for cs2849 [Ru] 3.**

A	B	C	D	Angle/°	A	B	C	D	Angle/°
Ru1	N3	C29	C28	13.3(3)	C7	C8	C9	C4	-2.4(4)
Ru1	N3	C30	C31	-139.88(19)	C7	C8	C9	C12	172.8(3)
Ru1	N3	C30	C35	39.7(3)	C9	C4	C5	C6	-4.6(4)
Ru1	C22	C23	C24	164.97(19)	C9	C4	C5	C10	171.8(2)
Ru1	C22	C23	C28	-16.1(4)	C10	C5	C6	C7	-174.5(3)
C11	Ru1	C22	C23	-60.2(2)	C11	C7	C8	C9	-177.2(3)
C12	Ru1	C22	C23	112.3(2)	C13	N2	C1	Ru1	-2.5(4)
N1	C2	C3	N2	-15.6(3)	C13	N2	C1	N1	-178.1(2)
N1	C4	C5	C6	-179.3(2)	C13	N2	C3	C2	-172.9(2)
N1	C4	C5	C10	-3.0(4)	C13	C14	C15	C16	0.4(4)
N1	C4	C9	C8	179.5(2)	C14	C13	C18	C17	1.3(3)
N1	C4	C9	C12	4.5(4)	C14	C13	C18	C21	179.5(2)
N2	C13	C14	C15	178.3(2)	C14	C15	C16	C17	1.3(4)

**Table 2.6.8. Torsion Angles for cs2849 [Ru] 3.**

A	B	C	D	Angle/°	A	B	C	D	Angle/°
N2	C13	C14	C19	1.0 (3)	C14	C15	C16	C20	-179.7 (2)
N2	C13	C18	C17	-178.8 (2)	C15	C16	C17	C18	-1.8 (4)
N2	C13	C18	C21	-0.5 (3)	C16	C17	C18	C13	0.6 (4)
N3	Ru1	C22	C23	24.6 (2)	C16	C17	C18	C21	-177.7 (2)
N3	C30	C31	C32	-178.9 (2)	C18	C13	C14	C15	-1.8 (4)
N3	C30	C35	C34	178.3 (2)	C18	C13	C14	C19	-179.1 (2)
C1	Ru1	C22	C23	-150.9 (2)	C19	C14	C15	C16	177.8 (2)
C1	N1	C2	C3	14.0 (3)	C20	C16	C17	C18	179.1 (2)
C1	N1	C4	C5	-107.8 (3)	C22	C23	C24	C25	179.5 (2)
C1	N1	C4	C9	77.3 (3)	C22	C23	C28	C27	-178.6 (2)
C1	N2	C3	C2	14.6 (3)	C22	C23	C28	C29	-5.0 (4)
C1	N2	C13	C14	-89.9 (3)	C23	C24	C25	C26	-1.0 (4)
C1	N2	C13	C18	90.2 (3)	C23	C28	C29	N3	5.1 (4)
C2	N1	C1	Ru1	178.31 (17)	C24	C23	C28	C27	0.3 (3)
C2	N1	C1	N2	-5.5 (3)	C24	C23	C28	C29	173.9 (2)
C2	N1	C4	C5	87.6 (3)	C24	C25	C26	C27	0.6 (4)
C2	N1	C4	C9	-87.2 (3)	C25	C26	C27	C28	0.2 (4)
C3	N2	C1	Ru1	169.19 (19)	C26	C27	C28	C23	-0.7 (4)
C3	N2	C1	N1	-6.4 (3)	C26	C27	C28	C29	-174.6 (2)
C3	N2	C13	C14	98.8 (3)	C27	C28	C29	N3	178.8 (2)
C3	N2	C13	C18	-81.2 (3)	C28	C23	C24	C25	0.5 (4)
C4	N1	C1	Ru1	13.2 (3)	C29	N3	C30	C31	47.4 (3)
C4	N1	C1	N2	-170.6 (2)	C29	N3	C30	C35	-133.1 (2)
C4	N1	C2	C3	-179.5 (2)	C30	N3	C29	C28	-174.7 (2)
C4	C5	C6	C7	1.9 (4)	C30	C31	C32	C33	0.2 (4)
C5	C4	C9	C8	4.8 (4)	C31	C30	C35	C34	-2.1 (4)
C5	C4	C9	C12	-170.3 (2)	C31	C32	C33	C34	-1.3 (4)
C5	C6	C7	C8	0.4 (4)	C32	C33	C34	C35	0.7 (4)
C5	C6	C7	C11	177.4 (3)	C33	C34	C35	C30	1.0 (4)
C6	C7	C8	C9	-0.2 (4)	C35	C30	C31	C32	1.5 (4)

This report has been created with Olex2, compiled on 2022.04.07 svn.rea3783a0 for OlexSys. Please [let us know](#) if there are any errors or if you would like to have additional features.



**[Ru] 1**

## Experimental

A brownish-yellow plate (0.03 x 0.09 x 0.12 mm<sup>3</sup>) was centered on the goniometer of a Rigaku Oxford Diffraction Synergy-S diffractometer equipped with a HyPix6000HE detector and operating with CuK $\alpha$  radiation. The data collection routine, unit cell refinement, and data processing were carried out with the program CrysAlisPro.<sup>11</sup> The Laue symmetry and systematic absences were consistent with the monoclinic space group *I2/a*. The structure was solved using SHELXT<sup>12</sup> and refined using SHELXL<sup>13</sup> via Olex2.<sup>14</sup>

---

(11) CrysAlisPro Software System, v1.171.42.xx, Rigaku Oxford Diffraction, **2022**, Rigaku Corporation, Oxford, UK.

(12) Sheldrick, G. M. "SHELXT – Integrated space-group and crystal structure determination." *Acta Cryst.* **2015**, *A71*, 3–8.

(13) Sheldrick, G. M. "Crystal structure refinement with SHELXL." *Acta Cryst.* **2015**, *C71*, 3–8.

(14) Dolomanov, O.V.; Bourhis, L. J.; Gildea, R. J.; Howard, J. A. K.; Puschmann, H. *J. Appl. Cryst.* **2009**, *42*, 339–341.

The final refinement model involved anisotropic displacement parameters for non-hydrogen atoms and a riding model for all hydrogen atoms. The difference electron density map from the final structure model suggested there is a small amount of whole molecule disorder and showed a relatively large difference peak of 3.3 e-/Å<sup>3</sup> where Ru would reside. Refinement of the Ru as disordered suggest the minor conformation of the molecule amounts to ~5% occupancy. With such a low occupancy, only the major conformation was used in the structure model. Olex2<sup>15</sup> was used for molecular graphics generation.

**Table 2.6.9. Crystal data and structure refinement for cs2925 [Ru] 1.**

Identification code	cs2925
Empirical formula	C <sub>35</sub> H <sub>37</sub> Cl <sub>2</sub> N <sub>3</sub> Ru
Formula weight	671.64
Temperature/K	99.98(10)
Crystal system	monoclinic
Space group	<i>I</i> 2/a
a/Å	23.2621(3)
b/Å	10.15680(10)
c/Å	27.3417(4)
α/°	90
β/°	100.7970(10)
γ/°	90
Volume/Å <sup>3</sup>	6345.62(14)
Z	8
ρ <sub>calc</sub> /cm <sup>3</sup>	1.406
μ/mm <sup>-1</sup>	5.758
F(000)	2768.0
Crystal size/mm <sup>3</sup>	0.12 × 0.09 × 0.03
Radiation	Cu Kα (λ = 1.54184)
2θ range for data collection/°	7.738 to 154.558
Index ranges	-29 ≤ h ≤ 29, -12 ≤ k ≤ 12, -34 ≤ l ≤ 34
Reflections collected	54791
Independent reflections	6639 [R <sub>int</sub> = 0.0609, R <sub>sigma</sub> = 0.0326]
Data/restraints/parameters	6639/0/376

---

(15) Dolomanov, O.V.; Bourhis, L. J.; Gildea, R. J.; Howard, J. A. K.; Puschmann, H. *J. Appl. Cryst.* **2009**, *42*, 339–341.

Goodness-of-fit on $F^2$	1.033
Final R indexes [ $I \geq 2\sigma(I)$ ]	$R_1 = 0.0581$ , $wR_2 = 0.1374$
Final R indexes [all data]	$R_1 = 0.0620$ , $wR_2 = 0.1400$
Largest diff. peak/hole / $e \text{ \AA}^{-3}$	3.31/-1.74

**Table 2.6.10. Bond Lengths for cs2925 [Ru] 1.**

Atom	Atom	Length/Å	Atom	Atom	Length/Å
Ru1	C11	2.3307 (11)	C13	C14	1.402 (6)
Ru1	C12	2.3511 (10)	C13	C18	1.396 (6)
Ru1	N3	2.174 (4)	C14	C15	1.399 (6)
Ru1	C1	2.051 (4)	C14	C19	1.498 (6)
Ru1	C22	1.846 (5)	C15	C16	1.385 (7)
N1	C1	1.345 (5)	C16	C17	1.386 (7)
N1	C2	1.476 (5)	C16	C20	1.518 (6)
N1	C4	1.447 (5)	C17	C18	1.408 (6)
N2	C1	1.349 (6)	C18	C21	1.507 (7)
N2	C3	1.473 (5)	C22	C23	1.450 (6)
N2	C13	1.441 (5)	C23	C24	1.401 (6)
N3	C28	1.442 (5)	C23	C28	1.396 (6)
N3	C29	1.286 (6)	C24	C25	1.390 (7)
C2	C3	1.526 (5)	C25	C26	1.398 (7)
C4	C5	1.398 (7)	C26	C27	1.387 (7)
C4	C9	1.398 (6)	C27	C28	1.387 (6)
C5	C6	1.400 (6)	C29	C30	1.450 (6)
C5	C10	1.504 (6)	C30	C31	1.398 (7)
C6	C7	1.382 (7)	C30	C35	1.397 (6)
C7	C8	1.391 (8)	C31	C32	1.392 (6)
C7	C11	1.514 (7)	C32	C33	1.391 (7)
C8	C9	1.408 (6)	C33	C34	1.377 (8)
C9	C12	1.502 (7)	C34	C35	1.377 (7)

**Table 2.6.11. Bond Angles for cs2925 [Ru] 1.**

Atom	Atom	Atom	Angle/°	Atom	Atom	Atom	Angle/°
C11	Ru1	C12	152.53 (4)	C4	C9	C12	122.5 (4)
N3	Ru1	C11	86.80 (10)	C8	C9	C12	120.1 (4)
N3	Ru1	C12	89.16 (10)	C14	C13	N2	118.0 (4)
C1	Ru1	C11	98.35 (12)	C18	C13	N2	119.6 (4)
C1	Ru1	C12	86.13 (12)	C18	C13	C14	121.8 (4)
C1	Ru1	N3	174.84 (15)	C13	C14	C19	122.2 (4)
C22	Ru1	C11	98.12 (14)	C15	C14	C13	117.8 (4)
C22	Ru1	C12	108.06 (14)	C15	C14	C19	119.9 (4)
C22	Ru1	N3	80.99 (17)	C16	C15	C14	121.9 (4)

**Table 2.6.11. Bond Angles for cs2925 [Ru] 1.**

Atom	Atom	Atom	Angle/°	Atom	Atom	Atom	Angle/°
C22	Ru1	C1	98.48(19)	C15	C16	C17	118.7(4)
C1	N1	C2	113.5(3)	C15	C16	C20	120.8(5)
C1	N1	C4	129.9(4)	C17	C16	C20	120.5(4)
C4	N1	C2	115.3(3)	C16	C17	C18	121.8(4)
C1	N2	C3	114.1(3)	C13	C18	C17	117.7(4)
C1	N2	C13	127.6(4)	C13	C18	C21	123.1(4)
C13	N2	C3	117.7(3)	C17	C18	C21	119.2(4)
C28	N3	Ru1	110.5(3)	C23	C22	Ru1	118.2(3)
C29	N3	Ru1	132.1(3)	C24	C23	C22	121.9(4)
C29	N3	C28	117.4(4)	C28	C23	C22	117.8(4)
N1	C1	Ru1	128.3(3)	C28	C23	C24	120.3(4)
N1	C1	N2	107.1(4)	C25	C24	C23	119.5(4)
N2	C1	Ru1	123.4(3)	C24	C25	C26	119.4(4)
N1	C2	C3	102.9(3)	C27	C26	C25	121.3(4)
N2	C3	C2	102.2(3)	C26	C27	C28	119.1(4)
C5	C4	N1	118.1(4)	C23	C28	N3	112.4(4)
C9	C4	N1	119.7(4)	C27	C28	N3	127.3(4)
C9	C4	C5	122.2(4)	C27	C28	C23	120.3(4)
C4	C5	C6	117.8(4)	N3	C29	C30	128.2(4)
C4	C5	C10	121.0(4)	C31	C30	C29	127.3(4)
C6	C5	C10	121.1(4)	C35	C30	C29	113.9(4)
C7	C6	C5	122.3(5)	C35	C30	C31	118.8(4)
C6	C7	C8	118.3(4)	C32	C31	C30	119.7(4)
C6	C7	C11	121.4(5)	C33	C32	C31	120.2(5)
C8	C7	C11	120.4(5)	C34	C33	C32	120.2(4)
C7	C8	C9	122.1(4)	C35	C34	C33	119.8(4)
C4	C9	C8	117.4(4)	C34	C35	C30	121.3(5)

**Table 2.6.12. Torsion Angles for cs2925 [Ru] 1.**

A	B	C	D	Angle/°	A	B	C	D	Angle/°
Ru1	N3	C28	C23	2.8(4)	C7	C8	C9	C4	-0.4(7)
Ru1	N3	C28	C27	-177.2(4)	C7	C8	C9	C12	-179.8(5)
Ru1	N3	C29	C30	-2.9(7)	C9	C4	C5	C6	1.3(7)
Ru1	C22	C23	C24	179.9(3)	C9	C4	C5	C10	-174.9(4)
Ru1	C22	C23	C28	1.0(5)	C10	C5	C6	C7	175.1(5)
C11	Ru1	C22	C23	86.0(3)	C11	C7	C8	C9	179.8(5)
C12	Ru1	C22	C23	-85.6(3)	C13	N2	C1	Ru1	21.2(6)
N1	C2	C3	N2	4.4(4)	C13	N2	C1	N1	-170.3(4)
N1	C4	C5	C6	-176.5(4)	C13	N2	C3	C2	168.4(4)

**Table 2.6.12. Torsion Angles for cs2925 [Ru] 1.**

A	B	C	D	Angle/°	A	B	C	D	Angle/°
N1	C4	C5	C10	7.3 (6)	C13	C14	C15	C16	-2.7 (7)
N1	C4	C9	C8	177.1 (4)	C14	C13	C18	C17	-3.8 (7)
N1	C4	C9	C12	-3.4 (7)	C14	C13	C18	C21	173.0 (5)
N2	C13	C14	C15	177.3 (4)	C14	C15	C16	C17	-1.6 (7)
N2	C13	C14	C19	1.1 (7)	C14	C15	C16	C20	179.2 (5)
N2	C13	C18	C17	-175.6 (4)	C15	C16	C17	C18	3.3 (7)
N2	C13	C18	C21	1.3 (7)	C16	C17	C18	C13	-0.7 (7)
N3	Ru1	C22	C23	0.6 (3)	C16	C17	C18	C21	-177.7 (5)
N3	C29	C30	C31	-5.6 (8)	C18	C13	C14	C15	5.5 (7)
N3	C29	C30	C35	175.5 (5)	C18	C13	C14	C19	-170.8 (4)
C1	Ru1	C22	C23	-174.2 (3)	C19	C14	C15	C16	173.6 (4)
C1	N1	C2	C3	-4.9 (5)	C20	C16	C17	C18	-177.4 (5)
C1	N1	C4	C5	-81.8 (6)	C22	C23	C24	C25	-178.4 (4)
C1	N1	C4	C9	100.4 (6)	C22	C23	C28	N3	-2.6 (6)
C1	N2	C3	C2	-3.0 (5)	C22	C23	C28	C27	177.4 (4)
C1	N2	C13	C14	80.8 (6)	C23	C24	C25	C26	0.7 (7)
C1	N2	C13	C18	-107.2 (5)	C24	C23	C28	N3	178.5 (4)
C2	N1	C1	Ru1	171.0 (3)	C24	C23	C28	C27	-1.5 (6)
C2	N1	C1	N2	3.2 (5)	C24	C25	C26	C27	-0.9 (7)
C2	N1	C4	C5	84.3 (5)	C25	C26	C27	C28	-0.1 (7)
C2	N1	C4	C9	-93.5 (5)	C26	C27	C28	N3	-178.7 (4)
C3	N2	C1	Ru1	-168.4 (3)	C26	C27	C28	C23	1.3 (7)
C3	N2	C1	N1	0.1 (5)	C28	N3	C29	C30	177.9 (4)
C3	N2	C13	C14	-89.2 (5)	C28	C23	C24	C25	0.5 (6)
C3	N2	C13	C18	82.8 (5)	C29	N3	C28	C23	-177.8 (4)
C4	N1	C1	Ru1	-22.8 (7)	C29	N3	C28	C27	2.2 (6)
C4	N1	C1	N2	169.5 (4)	C29	C30	C31	C32	-178.6 (5)
C4	N1	C2	C3	-173.3 (4)	C29	C30	C35	C34	179.4 (4)
C4	C5	C6	C7	-1.1 (7)	C30	C31	C32	C33	-0.6 (7)
C5	C4	C9	C8	-0.6 (7)	C31	C30	C35	C34	0.4 (7)
C5	C4	C9	C12	178.8 (4)	C31	C32	C33	C34	0.1 (8)
C5	C6	C7	C8	0.2 (8)	C32	C33	C34	C35	0.6 (8)
C5	C6	C7	C11	-179.1 (5)	C33	C34	C35	C30	-0.9 (8)
C6	C7	C8	C9	0.6 (8)	C35	C30	C31	C32	0.3 (7)

This report has been created with Olex2, compiled on 2022.04.07 svn.rca3783a0 for OlexSys. Please [let us know](#) if there are any errors or if you would like to have additional features.

## Experimental Section References

(1) Niwayama, S.; Cho, H.; Zabet-Moghaddam, M.; Whittlesey, B. R. Remote Exo/Endo Selectivity in Selective Monohydrolysis of Dialkyl Bicyclo[2.2.1]heptane-2,3-dicarboxylate Derivatives. *J. Org. Chem.* **2010**, *75* (11), 3775-3780. DOI: 10.1021/jo100564e.

(2) Chang, A. B.; Lin, T.-P.; Thompson, N. B.; Luo, S.-X.; Liberman-Martin, A. L.; Chen, H.-Y.; Lee, B.; Grubbs, R. H. Design, Synthesis, and Self-Assembly of Polymers with Tailored Graft Distributions. *J. Am. Chem. Soc.* **2017**, *139* (48), 17683-17693. DOI: 10.1021/jacs.7b10525.

## Chapter 3. Studies on Electronic Effects in Imine Chelated Ruthenium Olefin

### Metathesis Catalysts

Hanan N. Almuzaini,<sup>a,b</sup> Carla Slebodnick,<sup>a</sup> Michael D. Schulz<sup>a,b</sup>

<sup>a</sup> Department of Chemistry, Virginia Polytechnic Institute and State University,  
Blacksburg, VA 24061

<sup>b</sup> Macromolecules Innovation Institute, Virginia Polytechnic Institute and State  
University, Blacksburg, VA 24061

#### 3.1. Abstract

Olefin metathesis is an important tool in forming carbon-carbon double bonds, enabled by the development of well-defined olefin metathesis catalysts. Here, our aim is to study the effect of electron-withdrawing and electron-donating substituents on imine-chelated ruthenium catalyst activation temperature. We synthesized a series of novel imine-chelated ruthenium complexes having different substitutions to evaluate the electronic effect. The catalyst structures were determined by <sup>1</sup>H NMR spectroscopy and single-crystal X-ray diffraction, and analyzed to find correlations between the catalyst structural features and activity. Differential scanning calorimetry was used to measure the catalysts' activation temperature in polymerizing a series of ROMP monomers. Although these complexes showed similar structural characteristics, the activation temperatures of these complexes in polymerizing ROMP monomers are different. The complexes were activated at different temperatures ranging from 36 to 100 °C, indicating the dependence of catalyst activity on both the catalyst and monomer identity.

### 3.2. Introduction

Olefin metathesis, which involves carbon–carbon double bond breaking and reforming, is an elegant method to prepare natural and synthetic products and polymers.<sup>1</sup> Ruthenium-based olefin metathesis catalysts are widely used in olefin metathesis due to their high stability, easy accessibility, and functional group compatibility.<sup>1</sup> Previous studies developed catalysts with activities ranging from highly reactive at room temperature to latent (no activity at room temperature).<sup>1</sup> For example, the Hoveyda–Grubbs second-generation catalyst can be activated at or below room temperature in the presence of an olefin.<sup>2,3</sup> However, functionalizing the Hoveyda–Grubbs catalyst with a diethylamino moiety as an electron-donating group on the benzylidene ligand enhanced the catalyst stability at room temperature.<sup>4</sup> The effect of a strong electron-withdrawing group such as CF<sub>3</sub> was studied on a sulfur-chelated ruthenium catalyst. This complex displayed higher stability at room temperature and increased activity when activated, due to the weakened S–Ru bond resulting from the electron-withdrawing CF<sub>3</sub> substituted group.<sup>5</sup>

Examples of imine-chelated ruthenium olefin metathesis catalysts showed higher stability at room temperature and activation with external stimuli.<sup>6, 7</sup> However, these catalysts showed a low initiation rate upon activation due to the strong chelation of the imine.<sup>3, 6, 7</sup> Here, our aim is to control the imine-chelated ruthenium catalyst activation temperature by varying the electronic density in the chelating benzylidene ligand by installing both electron-donating and electron-withdrawing groups.

### 3.3. Results and Discussion

We aimed to examine the electronic effects in the phenyl–benzylidene ligand of complexes [Ru] 1-9 on the activation temperature of the catalysts. The design of catalysts

[Ru] 1-3 was based on the idea that increasing the electron density in the benzylidene ligand could increase the catalyst latency. Conversely, the design of [Ru] 5-9 was based on decreasing the electron density and thereby increasing the catalyst activity. Variations in structural parameters, Ru–N bond strength, and catalyst activation temperature were examined as a function of the Hammett constant ( $\sigma_{p,m}$ ).

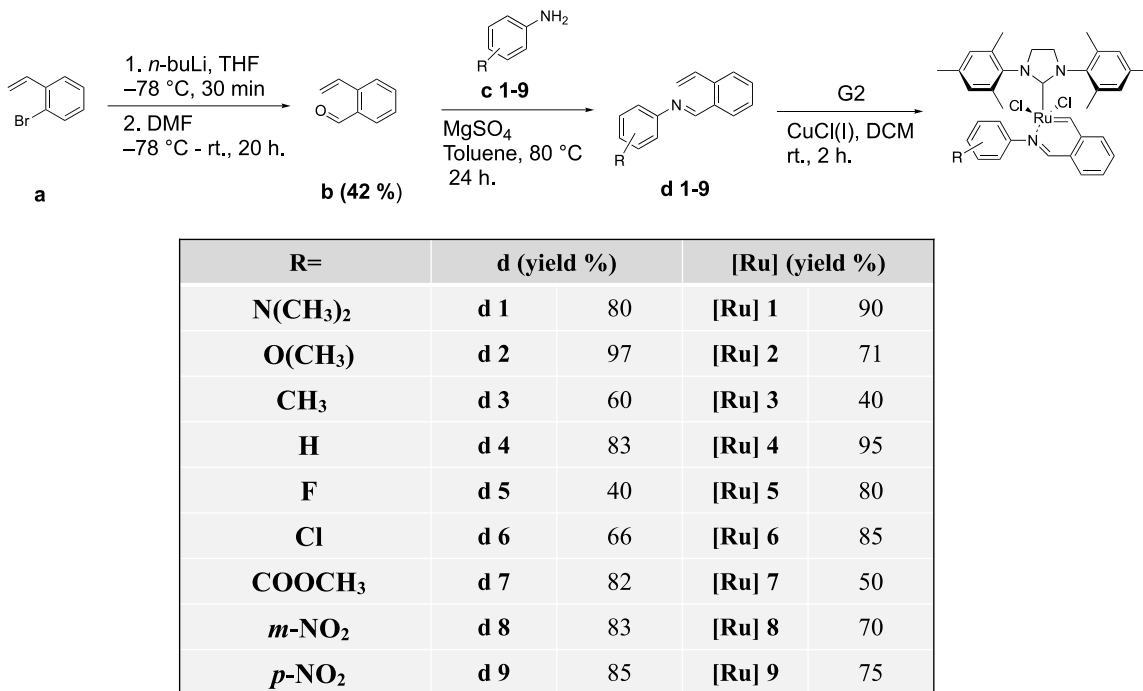
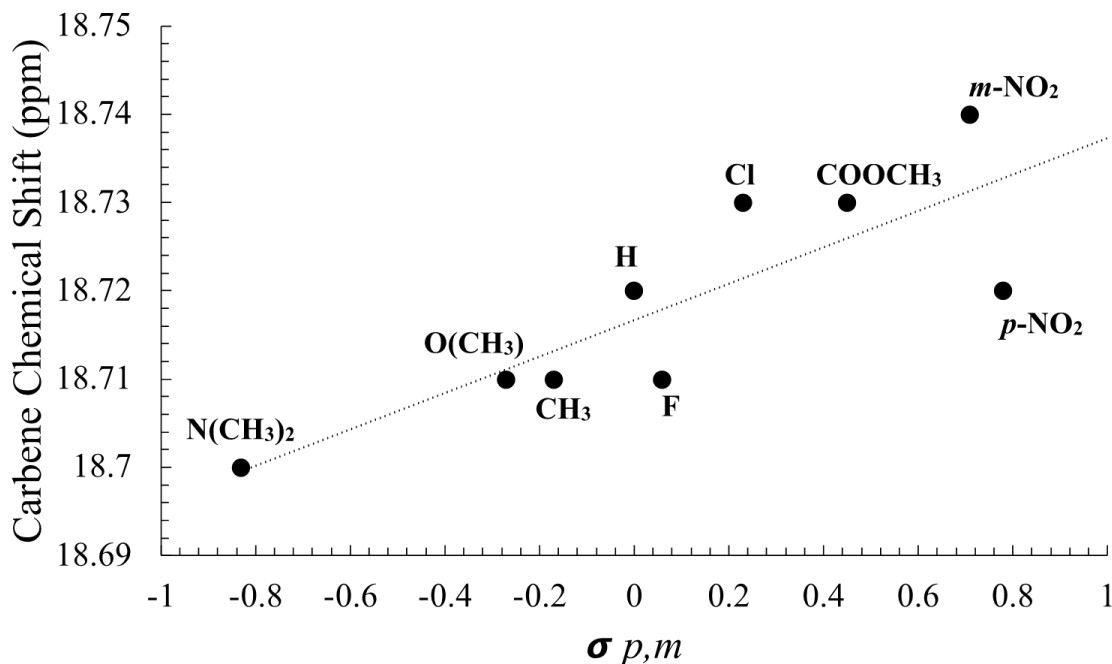


Figure 3.1. Synthesis of olefin metathesis catalysts: [Ru] 1-9.

The benzylidene ligands **d 1-9** were synthesized following the synthetic procedure presented in **Figure 3.1**. Then, ligands underwent a carbene exchange reaction with Grubbs second-generation catalysts (**G2**) with Cu(I)Cl addition to produce catalysts **[Ru] 1-9**. These catalysts are stable and easy to isolate from the reaction mixture. The synthesis of **[Ru] 1-9** was confirmed by <sup>1</sup>H NMR spectroscopy and X-ray crystallography. <sup>1</sup>H NMR spectroscopy showed insignificant differences in the chemical shift of the carbene, imine, and NHC ligand peaks of the catalysts. Plotting carbene chemical shift (ppm) versus  $\sigma_{p,m}$

showed only a 0.04 ppm difference among the series, which suggests that the electron density did not affect the catalyst structure at the carbene ( **Figure 3.2**).



**Figure 3.2.** Carbene  $^1H$  NMR chemical shifts vs.  $\sigma_{p,m}$  for the catalysts.

The crystal analysis also showed similar bond lengths and angles for all the catalysts (Figures 3.3 and 4). For example, the N–Ru bond length is in the range of 2.0797–2.116 Å with a difference of only 0.0393 Å (**Figure 3.3**). This result suggests that the differences in electronic density did not significantly affect the catalyst structures, and consequently, these complexes would show similar reactivity. However, the activation temperature—the temperature at which a polymerization or reaction is initiated under specific conditions—varied among the catalysts in this series when polymerizing ring-opening metathesis polymerization (ROMP) monomers.

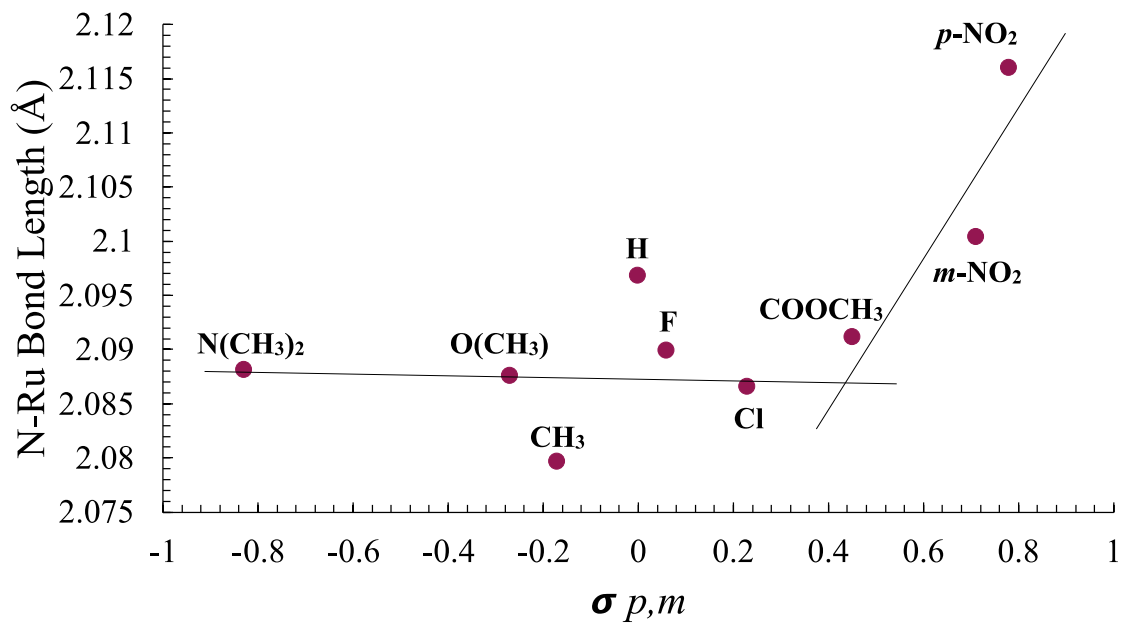


Figure 3.3. N-Ru bond length vs.  $\sigma_{p,m}$  of the catalysts.

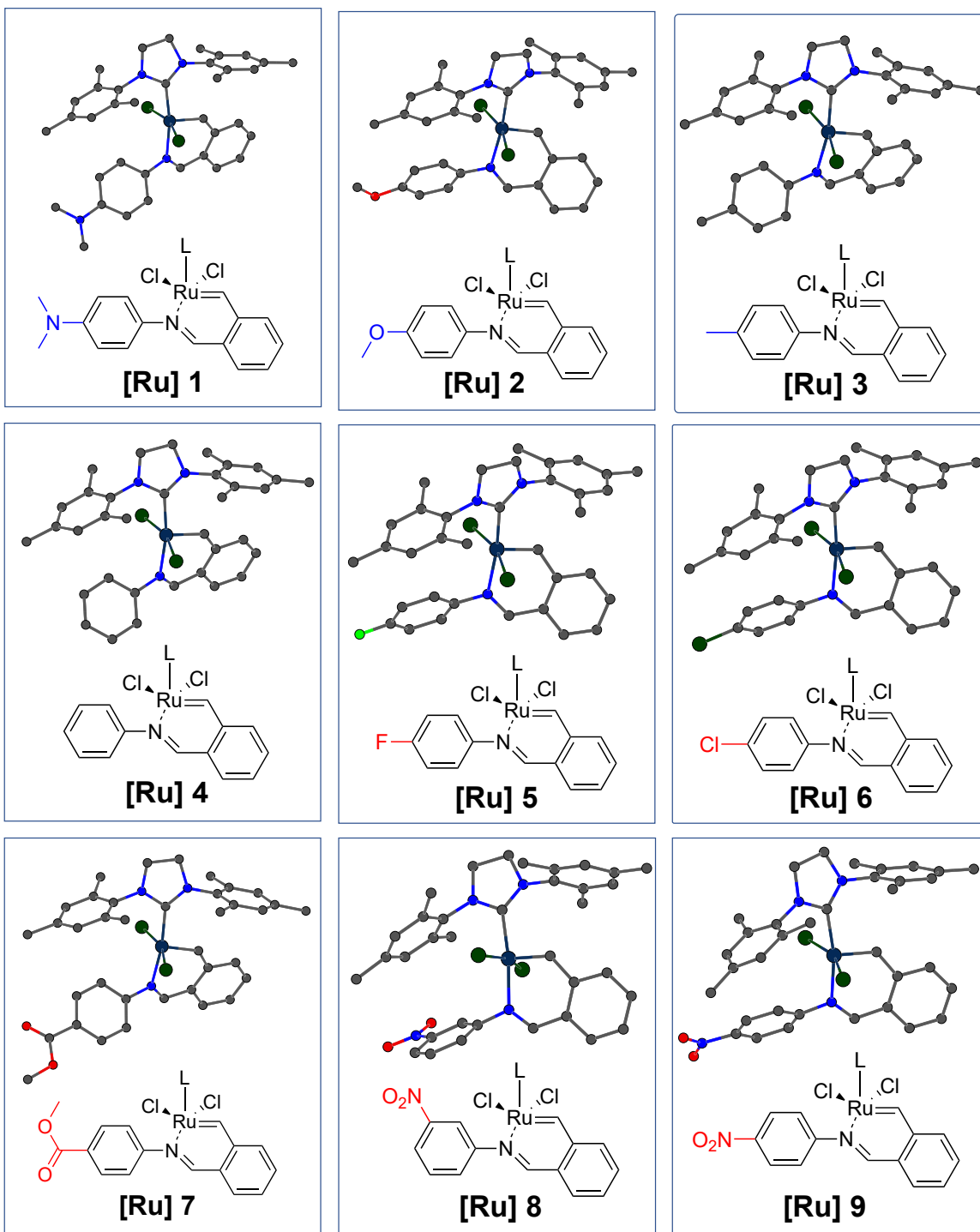
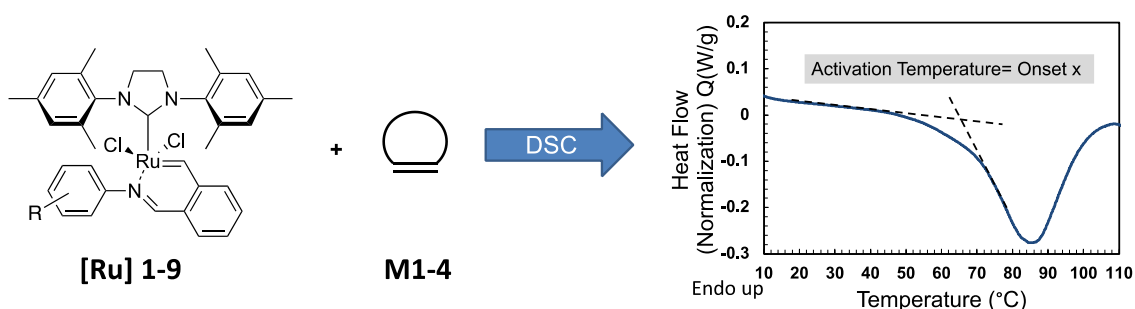


Figure 3.4. Catalyst crystal structures. (L stands for N-heterocyclic carbene)

The activation temperature of **[Ru] 1-9** was evaluated in ROMP of norbornene (**M1**), cyclooctadiene (**M2**), cyclooctene (**M3**), and *exo*-diester functionalized norbornene (**M4**). In all cases, ROMP reactions were conducted in a differential scanning calorimetry (DSC) pan. A mixture of each catalyst (1 equiv.) with each monomer (10 equiv.) was prepared in a high-volume DSC pan. DSC detects the activation temperature of the catalysts as a large exothermic peak associated with activation temperature (**Figure 3.5**). We reported the activation temperature of the catalysts using the onset point.



**Figure 3.5. DSC measurement of the activation temperature of a catalyst.**

Plotting the activation temperature of the catalysts for the polymerization of **M1** versus  $\sigma_{p,m}$  showed a range of activation temperature between 51 and 87 °C. Lower activation temperatures (51, 52, and 56 °C) were associated with **[Ru] 1**, **[Ru] 4**, and **[Ru] 8** ( $R = N(CH_3)_2$ , H, and *m*-NO<sub>2</sub>, respectively) for the polymerization of **M1**. However, the highest activation temperature (87 °C) was associated with **[Ru] 3** and **[Ru] 5** having CH<sub>3</sub> and F respectively. The general trend is that activation temperature increases with increasing  $\sigma_{p,m}$  up to a midpoint, after which activation temperature decreases. The conspicuous outlier to this trend, however, is the unfunctionalized **[Ru] 1**, which had one of the lower activation temperatures when polymerization **M1**. The activation temperature increases again with the *p*-NO<sub>2</sub> functionalization. Interestingly, unfunctionalized **[Ru] 1**

showed a lower activation temperature compared to the other catalysts having an electronegative group such as [Ru] 5 and 6 having a halide, or a strong electron-withdrawing group such as [Ru] 8 and 9 having a nitro group.

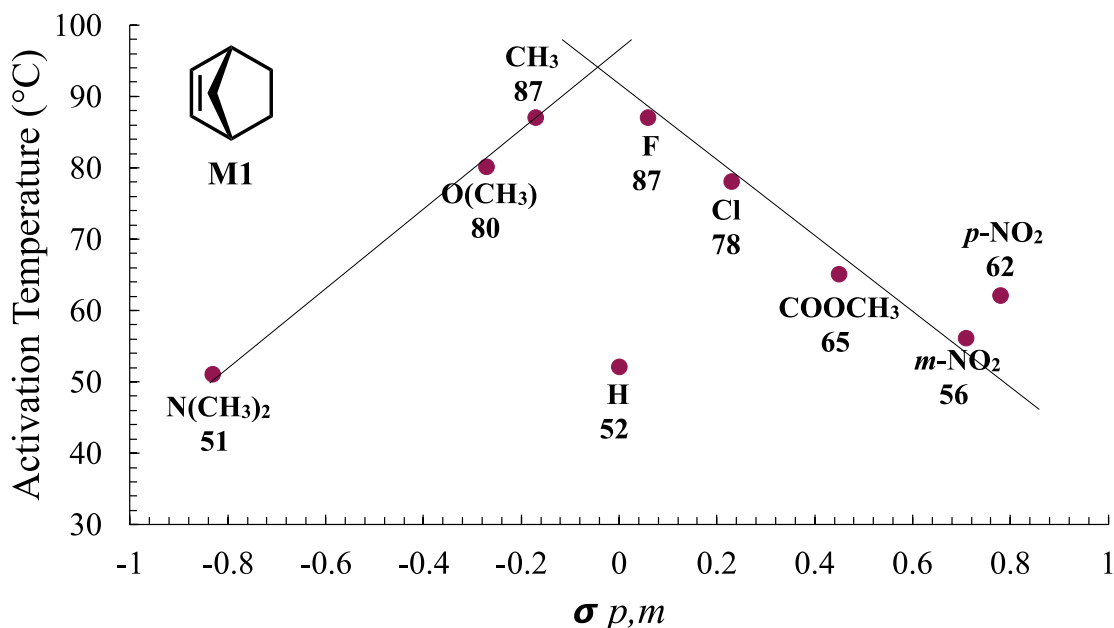


**Figure 3.6.** Activation temperature of [Ru] 1-9 for the polymerization of M1 vs  $\sigma_{p,m}$ .

Next, we measured the activation temperature of the catalysts for the polymerization of cyclooctadiene (M2). The activation temperature ranged from 40 to 100 °C. However, we observed no correlation between the catalysts' activation temperature and  $\sigma_{p,m}$  (Figure 3.7). [Ru] 1 activation temperature was 90 °C with the electron donor group, N(CH<sub>3</sub>)<sub>2</sub>, and decreased to 40 °C as the electronic density decreased with the introduction of nitro electron-withdrawing groups in the meta position. [Ru] 2, 3, 6, 7 mainly followed the decreasing activation temperature trend. However, [Ru] 5 (R= F) and [Ru] 9 (R= *m*-NO<sub>2</sub>) did not follow the trend and had higher activation temperatures: 100 and 93 °C respectively.

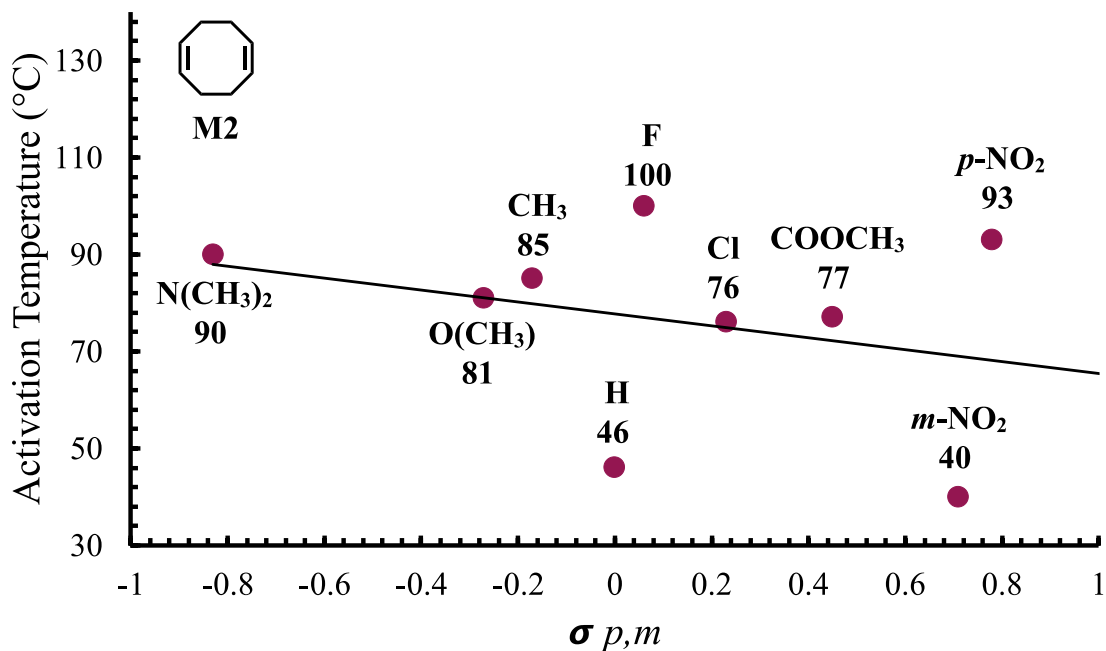


**Figure 3.7.** Activation temperature of [Ru] 1-9 for the polymerization of M2 vs  $\sigma_{p,m}$ .

To further investigate the effect of electronic density on the activation temperature of the catalysts, we measured the activation temperature of these catalysts [Ru] 1-9 in polymerizing M3. The activation temperatures varied among the series, ranging from 41 to 96 °C. The lowest activation temperature, in this case, corresponded to [Ru] 3 having a CH<sub>3</sub> group. We did duplicate measurements to assess the [Ru] 3 activation temperature in polymerizing M3, but the result was invariable. The activation temperature showed unclear correlation with  $\sigma_{p,m}$ . Even though the activation temperature of [Ru] 1 was higher than [Ru] 9, higher activation temperature was indicated with [Ru] 5 and [Ru] 7, R= F, and COOCH<sub>3</sub> respectively compared with [Ru] 4, [Ru] 6. Additionally, [Ru] 8 showed a lower activation temperature compared to [Ru] 9 with a 23 °C difference.

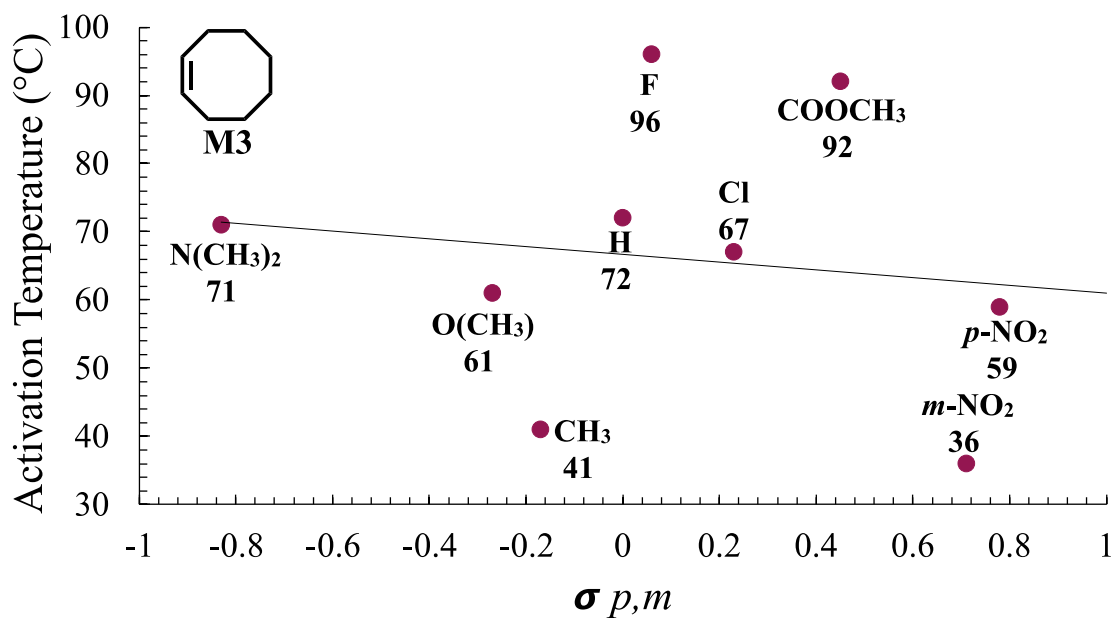


**Figure 3.8.** Activation temperature of [Ru] 1-9 for the polymerization of M3 vs  $\sigma_{p,m}$ .

We also studied the activation temperature of the catalysts for the polymerization M4. The activation temperature ranged between 72 and 93 °C. [Ru] 1 showed a lower activation temperature (72 °C) compared to [Ru] 8 and [Ru] 9 (90 and 83 °C, respectively). Similar to the result for polymerization M1 and M2, unfunctionalized catalyst, [Ru] 4, showed a lower activation temperature of 73 °C compared with other functionalized catalysts.

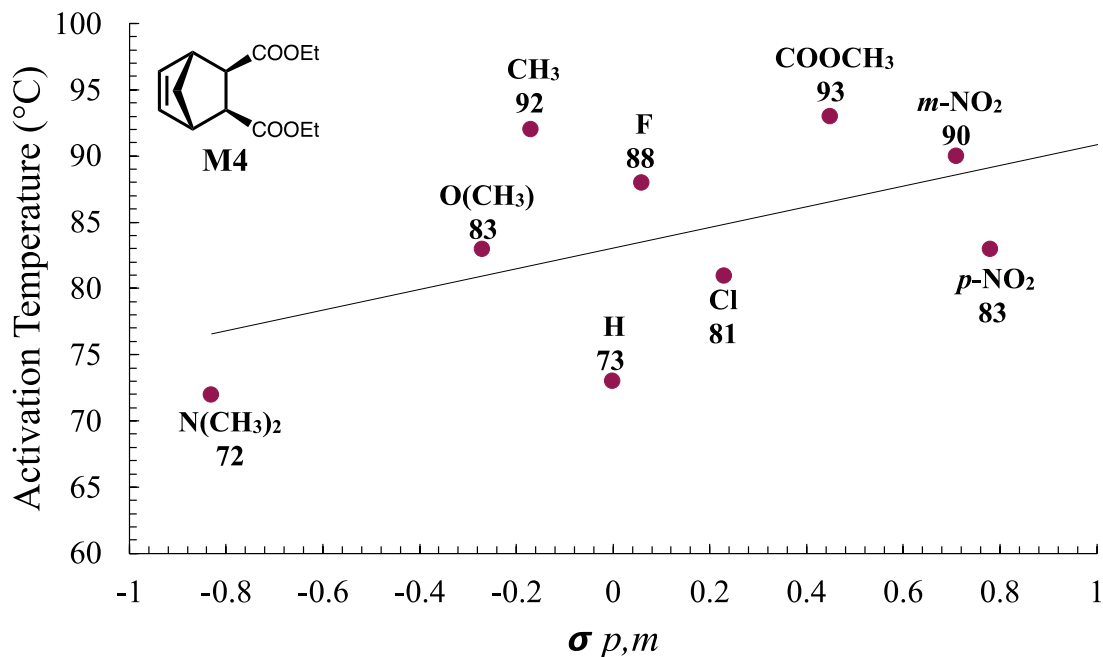


**Figure 3.9.** Activation temperature of [Ru] 1-9 for the polymerization M4 vs  $\sigma_{p,m}$ .

### 3.4. Conclusions and Future Work

Varied electronic density on the imine chelated ruthenium olefin metathesis catalyst [Ru] 1-9 benzylidene ligand did not significantly affect the <sup>1</sup>H NMR spectroscopy or crystal analysis of the catalysts but affected the activation temperatures. We did not observe a clear trend in the activation temperature of the catalysts for the polymerization of four different ROMP monomers. Each activation temperature varied based on the monomer and catalyst identity. In general, the unfunctionalized catalyst [Ru] 1 mostly showed lower activation temperatures compared to other functionalized catalysts. We did duplicate measurements for the results that obviously did not follow a certain trend. However, the results were consistent across multiple measurements.

For future work, we will investigate the behavior of the catalysts in solution to assess their activation temperature, and initiation and polymerization rate to better understand the effect of the electronic density on reactivity.

### 3.5. References

- (1) Bano, T.; Zahoor, A. F.; Rasool, N.; Irfan, M.; Mansha, A. Recent trends in Grubbs catalysis toward the synthesis of natural products: a review. *J. Iran. Chem. Soc.* **2022**, *19* (6), 2131-2170. DOI: 10.1007/s13738-021-02463-x.
- (2) Garber, S. B.; Kingsbury, J. S.; Gray, B. L.; Hoveyda, A. H. Efficient and Recyclable Monomeric and Dendritic Ru-Based Metathesis Catalysts. *J. Am. Chem. Soc.* **2000**, *122* (34), 8168-8179. DOI: 10.1021/ja001179g.
- (3) Hejl, A.; Day, M. W.; Grubbs, R. H. Latent Olefin Metathesis Catalysts Featuring Chelating Alkylidenes. *Organometallics* **2006**, *25* (26), 6149-6154. DOI: 10.1021/om060620u.
- (4) Gułajski, Ł.; Michrowska, A.; Bujok, R.; Grela, K. New tunable catalysts for olefin metathesis: Controlling the initiation through electronic factors. *J. Mol. Catal. A Chem.* **2006**, *254* (1), 118-123. DOI: <https://doi.org/10.1016/j.molcata.2005.12.049>.
- (5) Ginzburg, Y.; Anaby, A.; Vidavsky, Y.; Diesendruck, C. E.; Ben-Asuly, A.; Goldberg, I.; Lemcoff, N. G. Widening the Latency Gap in Chelated Ruthenium Olefin Metathesis Catalysts. *Organometallics* **2011**, *30* (12), 3430-3437. DOI: 10.1021/om200323c.
- (6) Duan, Y.; Wang, T.; Xie, Q.; Yu, X.; Guo, W.; Wang, J.; Liu, G. Highly efficient nitrogen chelated ruthenium carbene metathesis catalysts. *Dalton Trans.* **2016**, *45* (48), 19441-19448, 10.1039/C6DT03899A. DOI: 10.1039/C6DT03899A.
- (7) Slugovc, C.; Burtscher, D.; Stelzer, F.; Mereiter, K. Thermally Switchable Olefin Metathesis Initiators Bearing Chelating Carbenes: Influence of the Chelate's Ring Size. *Organometallics* **2005**, *24* (10), 2255-2258. DOI: 10.1021/om050141f.

### 3.6. Experimental Section

#### General methods

All reactions were performed using oven-dried glassware equipped with a magnetic stir bar under an air atmosphere unless otherwise noted. 2-Bromostyrene was purchased from AmBeed. 4-Fluoroaniline, 4-chloroaniline, 3-nitroaniline, aniline, 4-nitroaniline, and N,N-Dimethylethylenediamine were obtained from Oakwood. The Grubbs second-generation catalyst (G2) was donated from Materia and purchased from AmBeed. Deuterated solvents were obtained from Cambridge Isotope Laboratories. Unless otherwise stated, all other reagents were purchased at the highest commercial quality and used without further purification.

#### Measurements

$^1\text{H}$  NMR and  $^{13}\text{C}$  NMR data were collected at 25 °C in  $\text{CDCl}_3$  or  $\text{CD}_2\text{Cl}_2$  unless otherwise noted using an Agilent U4-DD2 400 MHz, or Bruker Advance II 500 MHz NMR instrument. Chemical shifts were reported in ppm and referenced to the  $\text{CHCl}_3$  singlet at 7.26 ppm, TMS singlet at 0 ppm, or  $\text{CD}_2\text{Cl}_2$  triplet at 5.32 ppm for  $^1\text{H}$  NMR.  $^{13}\text{C}$  NMR spectra were referenced to the center peak of the  $\text{CDCl}_3$  triplet at 77.00 ppm, or  $\text{CD}_2\text{Cl}_2$  at 54.00 ppm. The following abbreviations (or combinations thereof) were used to explain the multiplicities: s = singlet, d = doublet, t = triplet, q = quartet, m = multiplet, br = broad, and \* for the deuterated solvent peak.

Catalyst activation temperature was determined using differential scanning calorimetry (DSC) with a DSC Q2500 from TA instruments equipped with an autosampler. Sample masses ranging from 6-10 mg were crimped in a high-volume pan and lid and then loaded into the cell alongside a reference pan. The method incorporated equilibration at 25

°C for 3 min and the samples were heated from 25 °C to 150 °C at a rate of 3 °C/ min. The activation temperature was determined as the onset point of the slope from the baseline of an exothermic transition.

**2-Vinylbenzaldehyde (b):** N-BuLi in 1 M hexane (1.1 equiv., 0.77 g) was added to a solution of 2-bromostyrene (**a**) (1 equiv., 2.00 g) in 50 mL of dry THF at -78 °C and stirred for 30 min. Then, DMF (1.5 equiv., 1 mL) was added dropwise. The reaction mixture was stirred for 20 h while the temperature was increased to room temperature. The organic layer was washed with brine, dried over MgSO<sub>4</sub>, and filtered. The crude product was purified by column chromatography (hexane-acetone 9:1) to produce the pure product as a clear liquid (Yield 600 mg, 42 %).

<sup>1</sup>H NMR (400 MHz, CDCl<sub>3</sub>-d) δ 10.30 (s, 1H), 7.86 – 7.81 (m, 1H), 7.58 (t, J = 1.7 Hz, 2H), 7.57 – 7.49 (m, 1H), 7.48 – 7.40 (m, 1H), 5.70 (dd, J = 17.4, 1.2 Hz, 1H), 5.52 (dd, J = 11.0, 1.2 Hz, 1H).

<sup>13</sup>C NMR (101 MHz, CDCl<sub>3</sub>) δ 192, 140, 134, 133, 133.03, 131, 128, 127, 119.

**Benzylidene ligand d 1-9:** A round bottom flask was charged with **b** (1 equiv.), aniline derivatives (1 equiv.), and MgSO<sub>4</sub> (1g/1.0 mmol aldehyde) in toluene. The reaction mixture was stirred at 80 °C under N<sub>2</sub> for 24 h. Then the mixture was filtered and concentrated under reduced pressure. The crude product was used (as is).

**d 1** (Yield 80 %). <sup>1</sup>H NMR (400 MHz, CDCl<sub>3</sub>) δ 8.85 (s, 1H), 8.08 (dd, J = 7.5, 1.8 Hz, 1H), 7.52 – 7.48 (m, 1H), 7.42 – 7.28 (m, 3H), 7.27 – 7.24 (m, 3H), 6.76 (d, J = 9.0 Hz, 2H), 5.66 (dd, J = 17.4, 1.3 Hz, 1H), 5.43 (dd, J = 11.0, 1.3 Hz, 1H), 2.99 (s, 6H).

$^{13}\text{C}$  NMR (101 MHz,  $\text{CDCl}_3$ )  $\delta$  154, 141, 138, 134, 130, 127.8, 127.5, 126, 122, 117, 112, 41.

**d 2** (Yield 97 %).  $^1\text{H}$  NMR (400 MHz,  $\text{CDCl}_3$ )  $\delta$  8.83 (s, 1H), 8.09 (d,  $J = 7.7$  Hz, 1H), 7.68 – 7.06 (m, 10H), 5.67 (d,  $J = 17.3$  Hz, 1H), 5.46 (dd,  $J = 11.0, 1.3$  Hz, 1H), 3.84 (s, 3H).

$^{13}\text{C}$  NMR (101 MHz,  $\text{CDCl}_3$ )  $\delta$  158, 156, 145, 138, 133.9, 133.3, 130, 129, 128, 127.9, 127.7, 127.0, 122, 118, 114, 55.

**d 3** (Yield 41%).  $^1\text{H}$  NMR (400 MHz,  $\text{CDCl}_3$ )  $\delta$  8.82 (d,  $J = 2.3$  Hz, 1H), 8.10 (d,  $J = 7.8$  Hz, 1H), 7.60 – 7.11 (m, 12H), 5.67 (d,  $J = 17.3$  Hz, 1H), 5.46 (d,  $J = 10.7$  Hz, 1H), 2.39 (d,  $J = 2.0$  Hz, 3H).

$^{13}\text{C}$  NMR (101 MHz,  $\text{CDCl}_3$ )  $\delta$  158, 149, 139, 135, 133.8, 133.2, 130, 129.8, 129.7, 127.9, 127.8, 127, 120, 118, 21.

**d 4** (Yield 41%).  $^1\text{H}$  NMR (400 MHz,  $\text{CDCl}_3$ )  $\delta$  8.80 (s, 1H), 8.10 (dd,  $J = 7.7, 0.7$  Hz, 1H), 7.48 – 7.13 (m, 8H), 6.68 (dd,  $J = 8.5, 1.1$  Hz, 1H), 5.46 (dd,  $J = 11.0, 0.7$  Hz, 1H), 3.63 (s, 1H).

$^{13}\text{C}$  NMR (101 MHz,  $\text{CDCl}_3$ )  $\delta$  158, 152, 139, 133.8, 133.1, 131, 129.3, 129.1, 127.98, 127.96, 127.07, 125, 120, 118.55, 118.52, 115.

**d 5** (Yield 40 %).  $^1\text{H}$  NMR (400 MHz,  $\text{CDCl}_3$ )  $\delta$  8.79 (s, 1H), 8.09 (dd,  $J = 7.7, 1.5$  Hz, 1H), 7.64 – 7.02 (m, 11H), 5.68 (dd,  $J = 17.4, 1.3$  Hz, 1H), 5.48 (dd,  $J = 11.0, 1.3$  Hz, 1H).

$^{13}\text{C}$  NMR (101 MHz,  $\text{CDCl}_3$ )  $\delta$  162, 160, 158.62, 158.60, 139, 133, 132, 131, 129, 128, 127.99, 127.95, 127.13, 125, 122.42, 122.34, 118, 115.98, 115.95, 115.76, 115.73.

**d 6** (Yield 66 %).  $^1\text{H}$  NMR (400 MHz,  $\text{CDCl}_3$ )  $\delta$  8.78 (s, 1H), 8.08 (dd,  $J = 7.8, 1.5$  Hz, 1H), 7.55 – 7.29 (m, 7H), 7.17 – 7.13 (m, 2H), 5.67 (dd,  $J = 17.3, 1.3$  Hz, 1H), 5.47 (dd,  $J = 11.0, 1.2$  Hz, 1H).

$^{13}\text{C}$  NMR (101 MHz,  $\text{CDCl}_3$ )  $\delta$  159, 150, 139, 133, 132, 131.5, 131.3, 129.23, 129.1, 128, 127.9, 127.2, 122, 118, 116.

**d 7** (Yield 82 %).  $^1\text{H}$  NMR (400 MHz,  $\text{CDCl}_3$ )  $\delta$  8.76 (s, 1H), 8.06 (d,  $J = 8.8$  Hz, 2H), 7.83 (d,  $J = 4.7$  Hz, 2H), 7.48 – 7.45 (m, 1H), 7.18 (d,  $J = 8.8$  Hz, 2H), 6.62 – 6.60 (m, 2H), 5.69 – 5.63 (m, 1H), 5.46 (dd,  $J = 11.0, 1.2$  Hz, 1H), 3.90 (s, 3H).

$^{13}\text{C}$  NMR (101 MHz,  $\text{CDCl}_3$ )  $\delta$  192, 133, 131.59, 131.56, 131.21, 130, 127.91, 127.44, 127.21, 120, 119, 113.

**d 9** (Yield 85 %).  $^1\text{H}$  NMR (400 MHz,  $\text{CDCl}_3$ )  $\delta$  8.76 (t,  $J = 0.5$  Hz, 1H), 8.30 – 8.25 (m, 2H), 8.07 (d,  $J = 9.1$  Hz, 2H), 7.41 (d,  $J = 1.7$  Hz, 2H), 7.32 (dd,  $J = 17.4, 11.0$  Hz, 1H), 7.25 – 7.20 (m, 2H), 6.62 (d,  $J = 9.1$  Hz, 1H), 5.68 (dd,  $J = 17.3, 1.2$  Hz, 1H), 5.50 (dd,  $J = 11.0, 1.2$  Hz, 1H).

### Synthesis of catalysts [Ru]1-9

A round bottom flask was charged with 1 equiv. of G2 and 1 equiv. of  $\text{CuCl(I)}$ , and 1.2 equiv. of benzylidene ligand (d 1-9). DCM was added to the reaction flask under  $\text{N}_2$ . The reaction mixture was stirred at rt for 2 h. The solvent was evaporated, and the crude product was purified by column chromatography.

**[Ru] 1** (Yield 90 %)  $^1\text{H}$  NMR (500 MHz,  $\text{CD}_2\text{Cl}_2$ )  $\delta$  18.70 (s, 1H), 8.65 (s, 1H), 7.74 – 7.69 (m, 1H), 7.56 – 7.53 (m, 1H), 7.48 (td,  $J = 7.5, 1.3$  Hz, 1H), 7.15 (d,  $J = 1.1$  Hz, 4H), 6.97 (d,  $J = 8.9$  Hz, 2H), 6.76 (ddd,  $J = 7.8, 1.4, 0.7$  Hz, 1H), 6.46 (d,  $J = 9.0$  Hz, 2H), 4.11 (s, 4H), 3.00 (s, 6H), 2.52 (s, 18H).

$^{13}\text{C}$  NMR (126 MHz,  $\text{CD}_2\text{Cl}_2$ )  $\delta$  310, 214, 206, 162, 150, 142, 140, 138, 134, 132, 129, 128, 126, 122.5, 122.2, 112, 40, 30.

**[Ru] 2** (Yield 71 %)  $^1\text{H}$  NMR (500 MHz,  $\text{CD}_2\text{Cl}_2$ )  $\delta$  18.72 (s, 1H), 8.65 (s, 1H), 7.74 (d,  $J = 1.3$  Hz, 1H), 7.61 – 7.49 (m, 2H), 7.14 (s, 4H), 7.08 – 6.98 (m, 2H), 6.84 – 6.77 (m, 1H), 6.74 – 6.66 (m, 2H), 4.11 (s, 4H), 3.84 (s, 3H), 2.52 (s, 18H).

$^{13}\text{C}$  NMR (126 MHz,  $\text{CD}_2\text{Cl}_2$ )  $\delta$  310.44, 310.37, 213, 165, 159, 144, 142, 138, 135.1, 133.5, 129, 128, 126, 122.9, 122.3, 114, 55, 21.

**[Ru] 3** (Yield 40 %)  $^1\text{H}$  NMR (500 MHz,  $\text{CD}_2\text{Cl}_2$ )  $\delta$  18.71 (s, 1H), 8.66 (s, 1H), 7.73 (td,  $J = 7.5, 1.3$  Hz, 1H), 7.54 (ddt,  $J = 13.5, 7.5, 1.3$  Hz, 2H), 7.12 (s, 4H), 6.98 (d,  $J = 1.2$  Hz, 4H), 6.80 (dd,  $J = 7.7, 1.1$  Hz, 1H), 4.10 (s, 4H), 2.43 (d,  $J = 57.9$  Hz, 18H), 2.35 (s, 3H).

$^{13}\text{C}$  NMR (126 MHz,  $\text{CD}_2\text{Cl}_2$ )  $\delta$  310, 213, 166, 148, 142, 138, 137, 135, 133, 129.65, 129.61, 129.57, 128, 126.36, 126.35, 122, 121, 30, 21, 20.

**[Ru] 4** (Yield 95 %)  $^1\text{H}$  NMR (500 MHz,  $\text{CD}_2\text{Cl}_2$ )  $\delta$  18.72 (s, 1H), 8.67 (s, 1H), 7.86 – 6.98 (m, 13H), 6.83 (d,  $J = 7.8$  Hz, 1H), 4.10 (s, 4H), 2.49 (d,  $J = 18.9$  Hz, 18H).

**[Ru] 5** (Yield 80 %)  $^1\text{H}$  NMR (500 MHz,  $\text{CD}_2\text{Cl}_2$ )  $\delta$  18.73 (s, 1H), 8.64 (s, 1H), 7.75 (d,  $J = 1.2$  Hz, 1H), 7.65 – 7.46 (m, 2H), 7.21 – 6.99 (m, 8H), 6.83 (dd,  $J = 7.6, 0.9$  Hz, 1H), 4.11 (d,  $J = 1.0$  Hz, 4H), 2.52 (s, 18H).

$^{13}\text{C}$  NMR (151 MHz,  $\text{CD}_2\text{Cl}_2$ )  $\delta$  310.38, 310.35, 213, 168, 150, 142, 135, 134, 133, 130, 128.97, 128.71, 126, 123, 123, 21.

**[Ru] 6** (Yield 85 %)  $^1\text{H}$  NMR (500 MHz,  $\text{CD}_2\text{Cl}_2$ )  $\delta$  18.69 (s, 1H), 8.63 (s, 1H), 7.75 (dd,  $J = 7.5, 1.2$  Hz, 1H), 7.57 (dt,  $J = 7.6, 1.5$  Hz, 2H), 7.09 (dtd,  $J = 8.9, 4.7, 2.5$  Hz, 6H), 6.90 – 6.81 (m, 3H), 4.11 (s, 4H), 2.49 (s, 18H).

$^{13}\text{C}$  NMR (126 MHz,  $\text{CD}_2\text{Cl}_2$ )  $\delta$  310, 213, 168, 163, 161, 147.44, 147.42, 142, 138, 135, 134, 129, 128, 126, 123.74, 123.67, 122, 115.66, 115.48, 21.

**[Ru] 7** (Yield 50 %)  $^1\text{H}$  NMR (500 MHz,  $\text{CD}_2\text{Cl}_2$ )  $\delta$  18.71 (s, 1H), 8.64 (s, 1H), 7.76 (d,  $J = 1.3$  Hz, 1H), 7.60 – 7.54 (m, 2H), 7.19 – 7.04 (m, 6H), 6.87 (t,  $J = 8.7$  Hz, 2H), 6.84 – 6.82 (m, 1H), 4.12 (s, 4H), 2.46 (d,  $J = 33.0$  Hz, 18H).

$^{13}\text{C}$  NMR (126 MHz,  $\text{CD}_2\text{Cl}_2$ )  $\delta$  310.39, 310.31, 213, 168, 163, 161, 147.45, 147.43, 142, 139, 135, 134, 129, 128, 126, 123.74, 123.67, 122, 115.66, 115.48.

**[Ru] 8** (Yield 70 %)  $^1\text{H}$  NMR (600 MHz,  $\text{CD}_2\text{Cl}_2$ )  $\delta$  18.74 (s, 1H), 8.69 (s, 1H), 8.13 (ddd,  $J = 8.2, 2.2, 1.0$  Hz, 1H), 8.00 (t,  $J = 2.2$  Hz, 1H), 7.80 (td,  $J = 7.5, 1.2$  Hz, 1H), 7.64 – 7.60 (m, 2H), 7.53 (ddd,  $J = 7.9, 2.1, 1.0$  Hz, 1H), 7.32 (t,  $J = 8.1$  Hz, 1H), 7.14 – 6.93 (m, 4H), 6.87 – 6.82 (m, 1H), 4.11 (s, 4H), 2.42 (s, 18H).

$^{13}\text{C}$  NMR (151 MHz,  $\text{CD}_2\text{Cl}_2$ )  $\delta$  212, 170, 151, 148, 141, 138, 136, 135, 129.63, 129.61, 129.49, 128, 125, 123, 121, 116, 21.

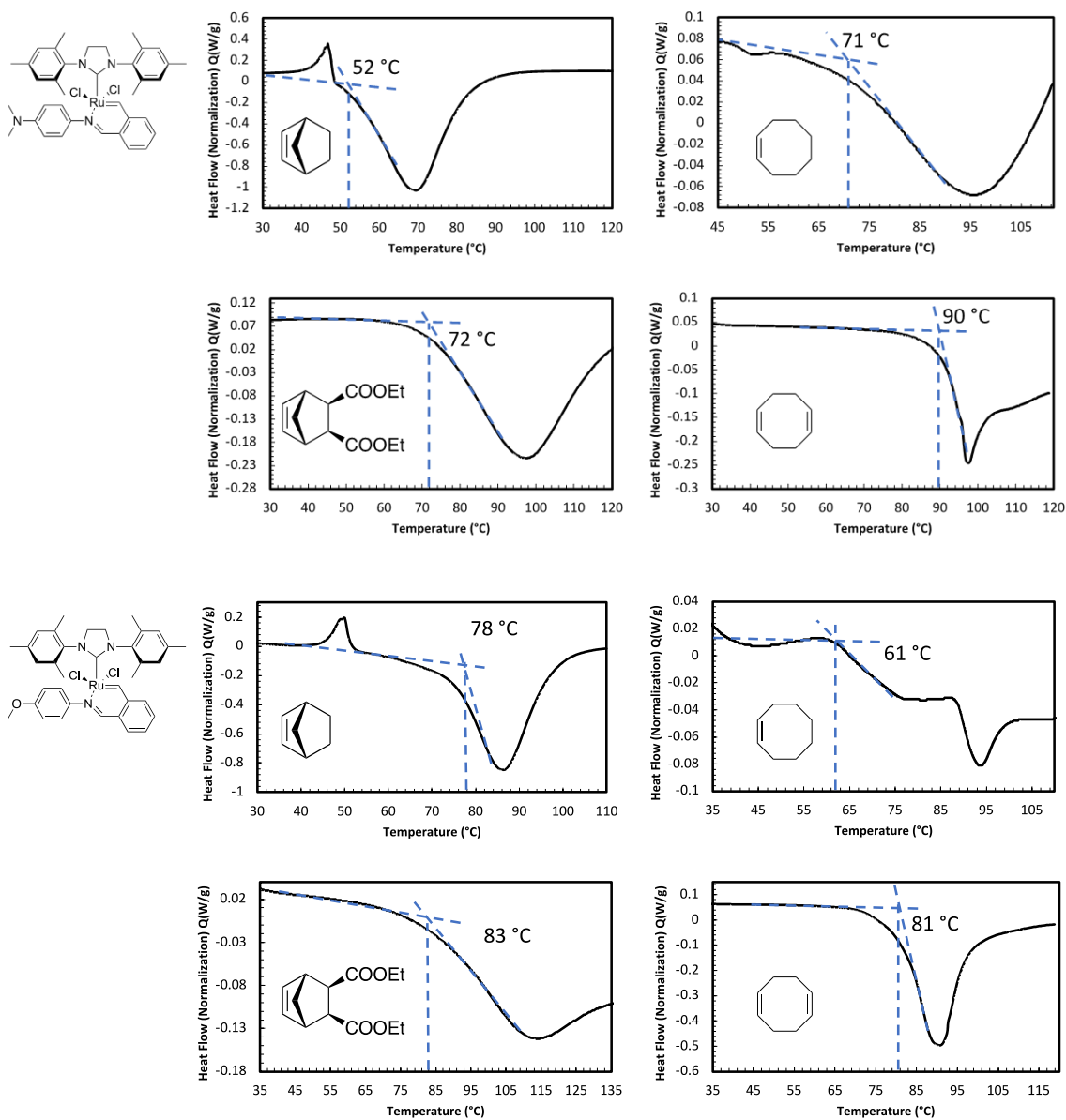
**[Ru] 9** (Yield 75 %)  $^1\text{H}$  NMR (400 MHz,  $\text{CD}_2\text{Cl}_2$ )  $\delta$  18.72 (s, 1H), 8.69 (s, 1H), 8.08 – 7.97 (m, 2H), 7.79 (td,  $J = 7.5, 1.3$  Hz, 1H), 7.65 – 7.60 (m, 2H), 7.28 – 7.24 (m, 2H), 7.10 (s, 4H), 6.85 (ddq,  $J = 7.6, 1.2, 0.6$  Hz, 1H), 4.12 (s, 4H), 2.47 (d,  $J = 30.5$  Hz, 18H).

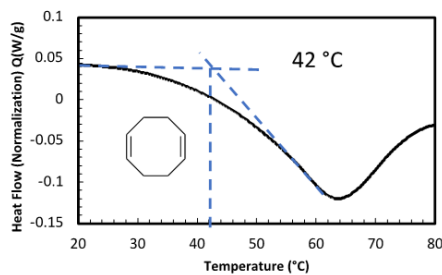
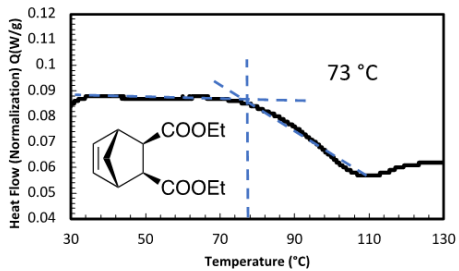
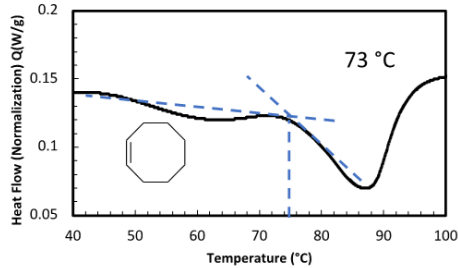
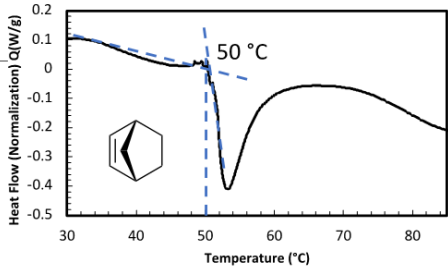
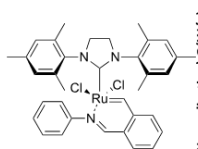
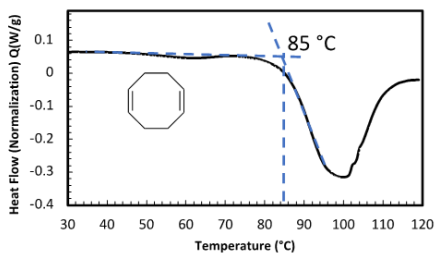
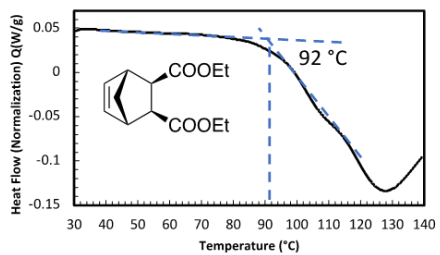
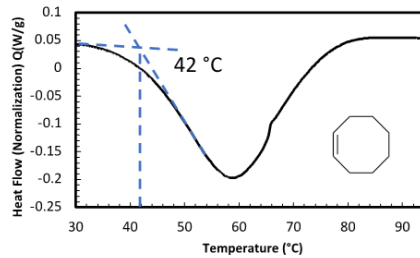
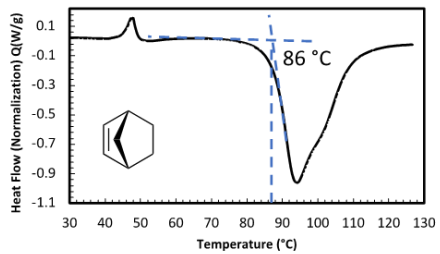
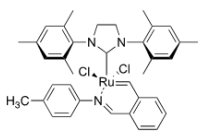
$^{13}\text{C}$  NMR (101 MHz,  $\text{CD}_2\text{Cl}_2$ )  $\delta$  214, 172, 158, 148, 144, 141, 138, 137.00, 131, 131, 128.16, 128.03, 127, 126, 125, 125, 115, 33, 28, 23.

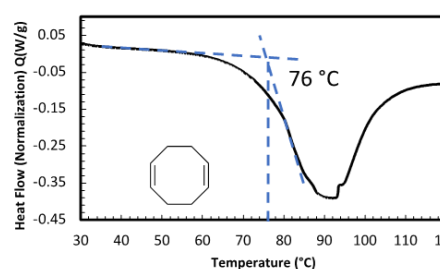
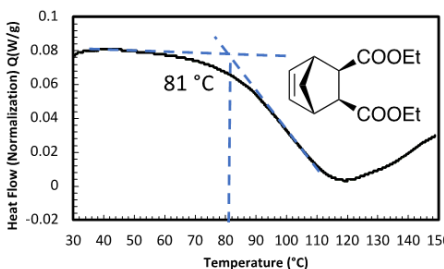
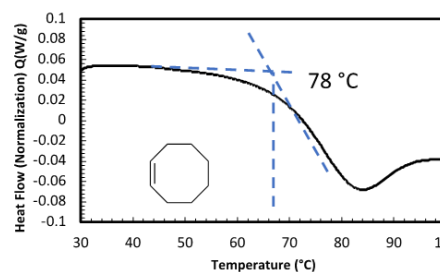
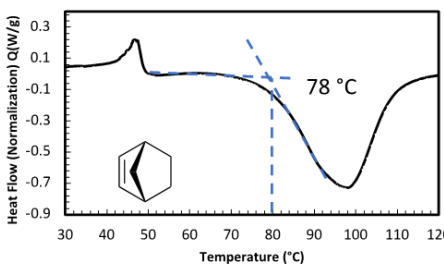
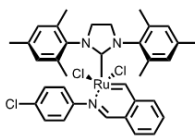
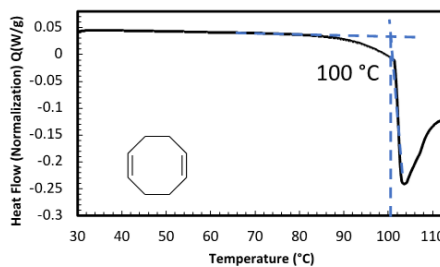
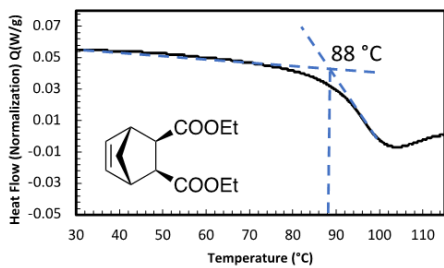
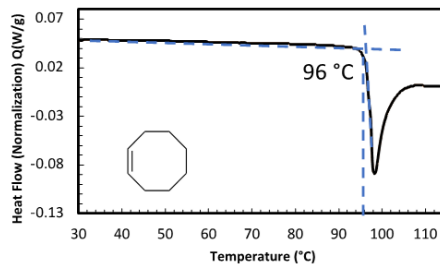
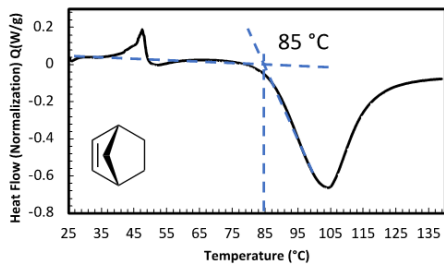
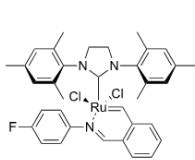
#### **Synthesis of ROMP monomer M4**

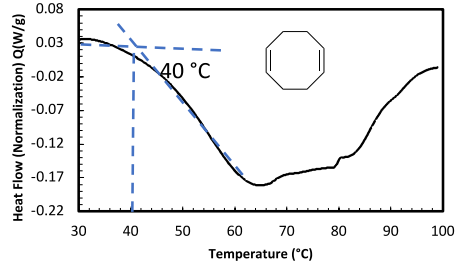
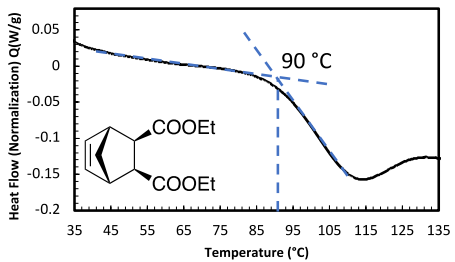
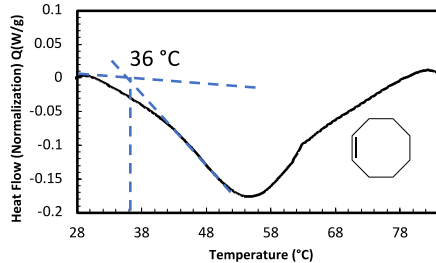
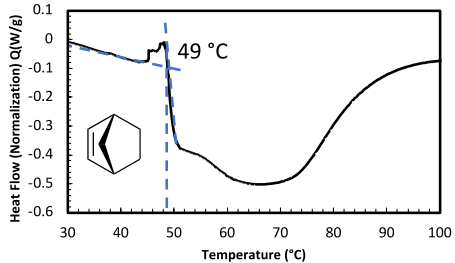
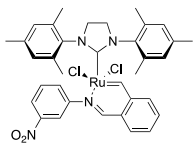
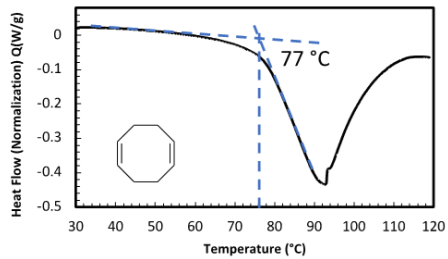
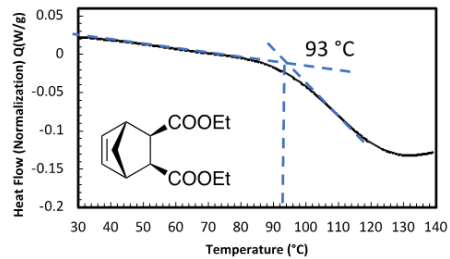
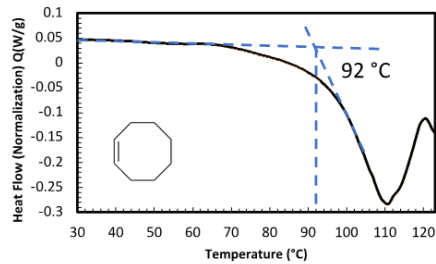
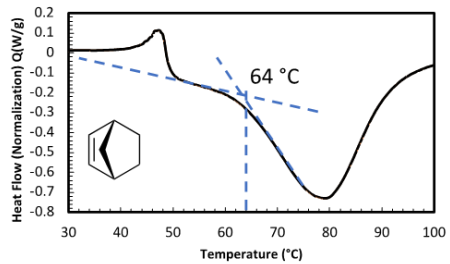
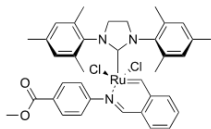
**M4** was synthesized following a literature procedure and characterized by  $^1\text{H}$  NMR.<sup>1,2</sup> **M4** (Yield 91 %)  $^1\text{H}$  NMR (400 MHz,  $\text{CDCl}_3$ ):  $\delta$  6.19 (s, 2H), 4.08 (dd,  $J = 11.0, 7.2$  Hz, 4H), 3.09 – 3.03 (m, 2H), 2.58 (d,  $J = 1.9$  Hz, 2H), 2.14 – 2.10 (m, 1H), 1.47 (dt,  $J = 9.0, 1.8$  Hz, 1H), 1.23 (t,  $J = 7.1$  Hz, 6H).

Figure 3.6.1. DSC activation temperature traces









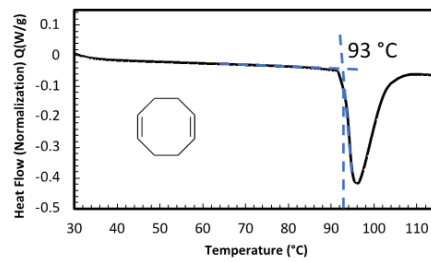
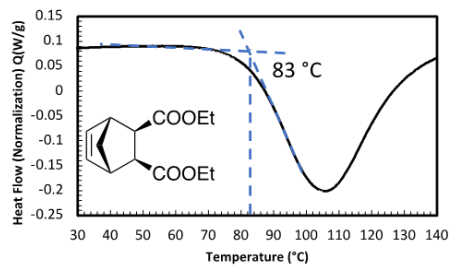
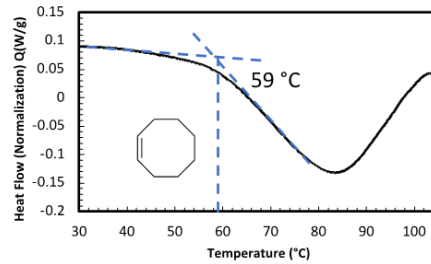
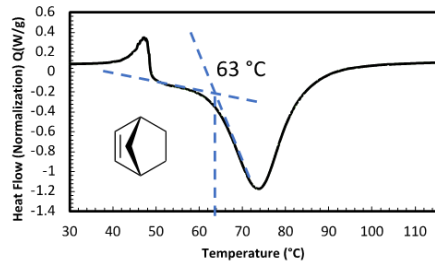
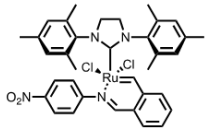
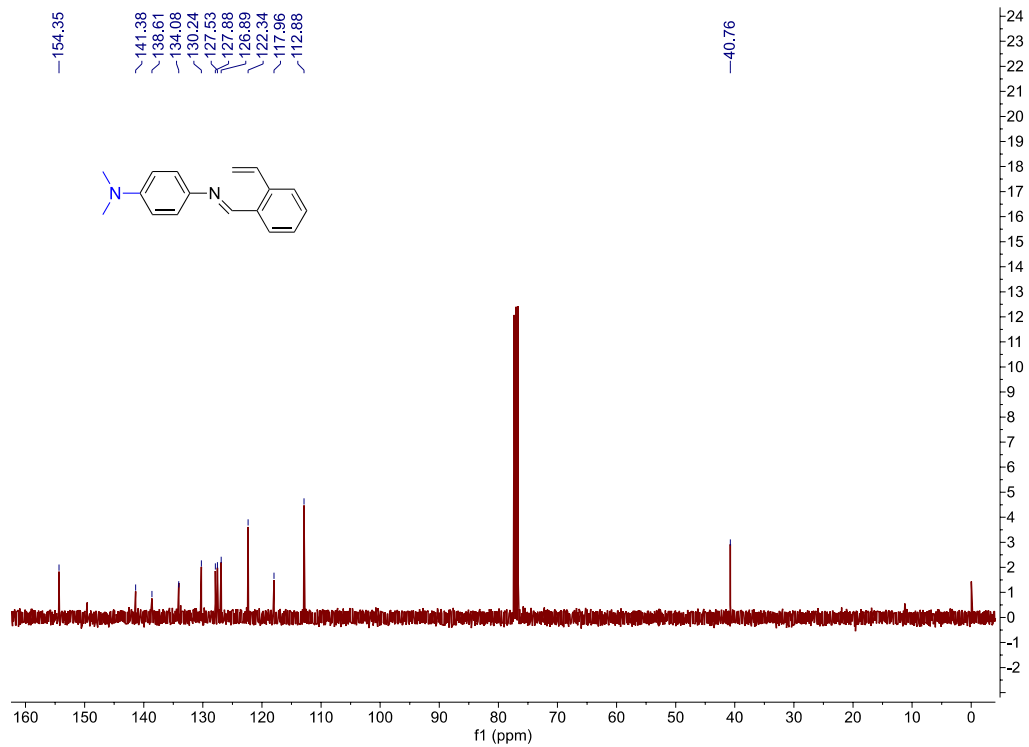
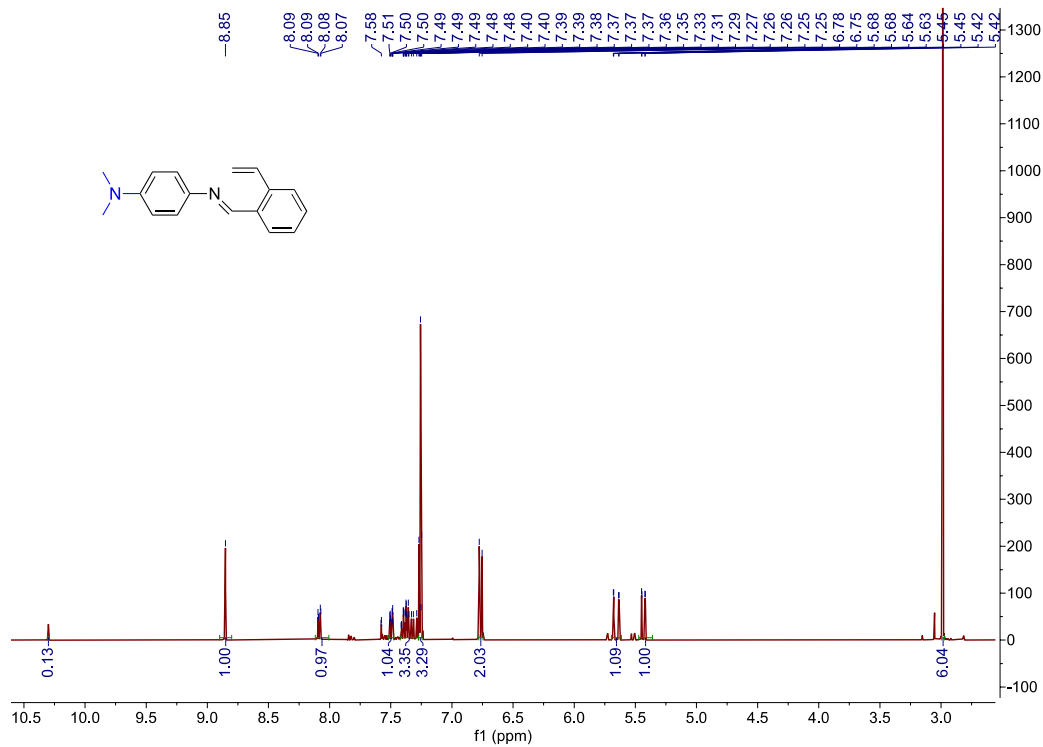
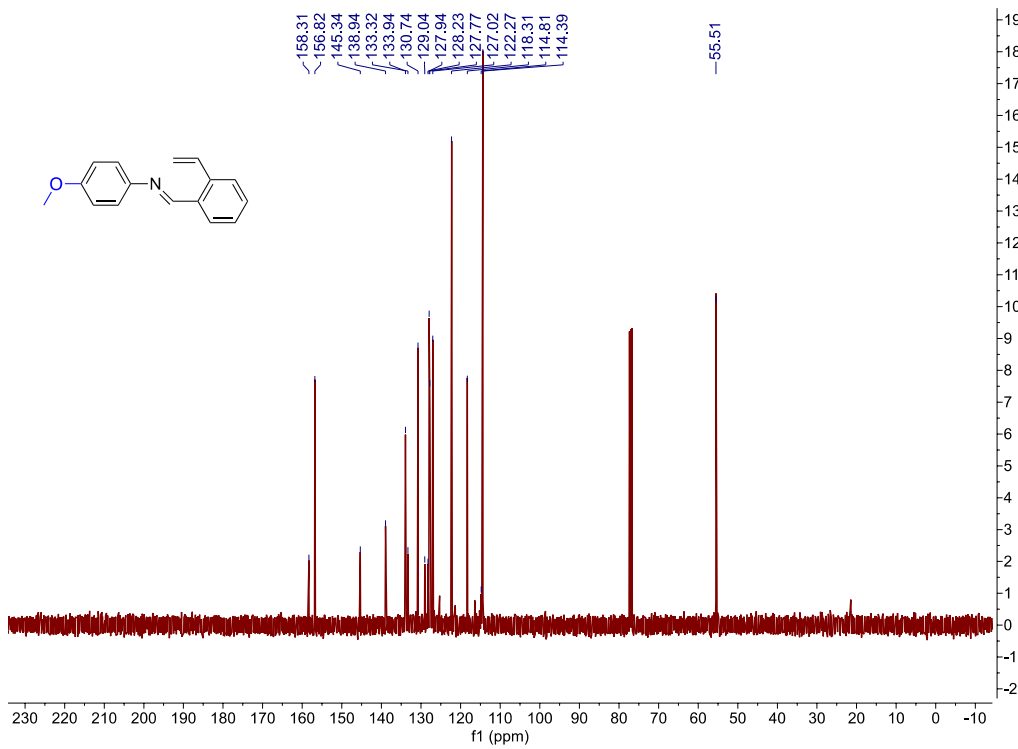
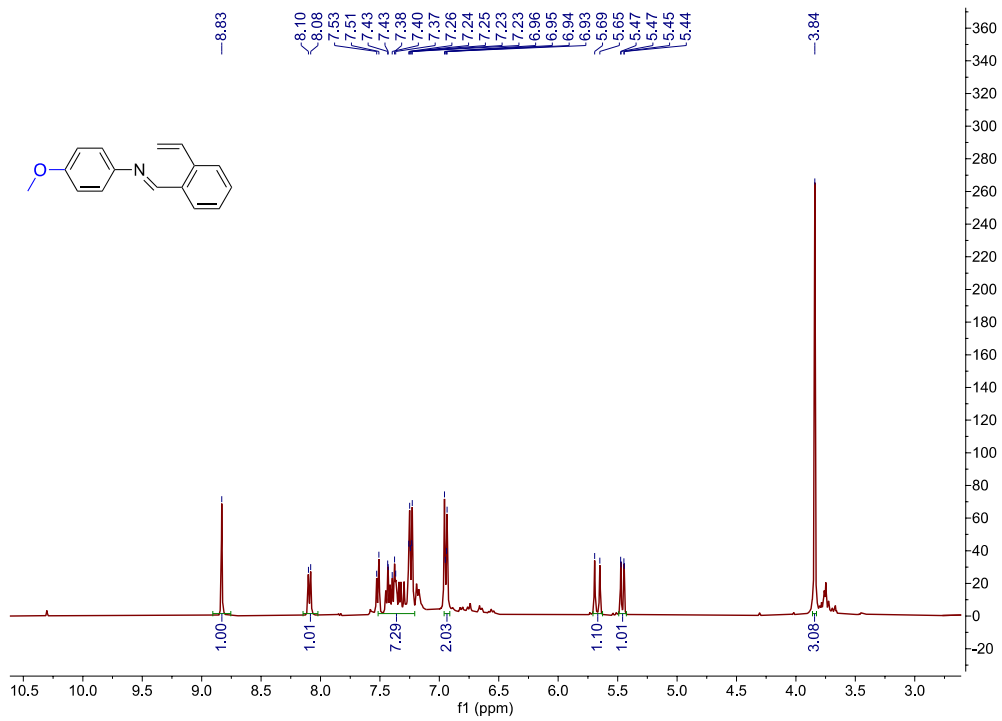
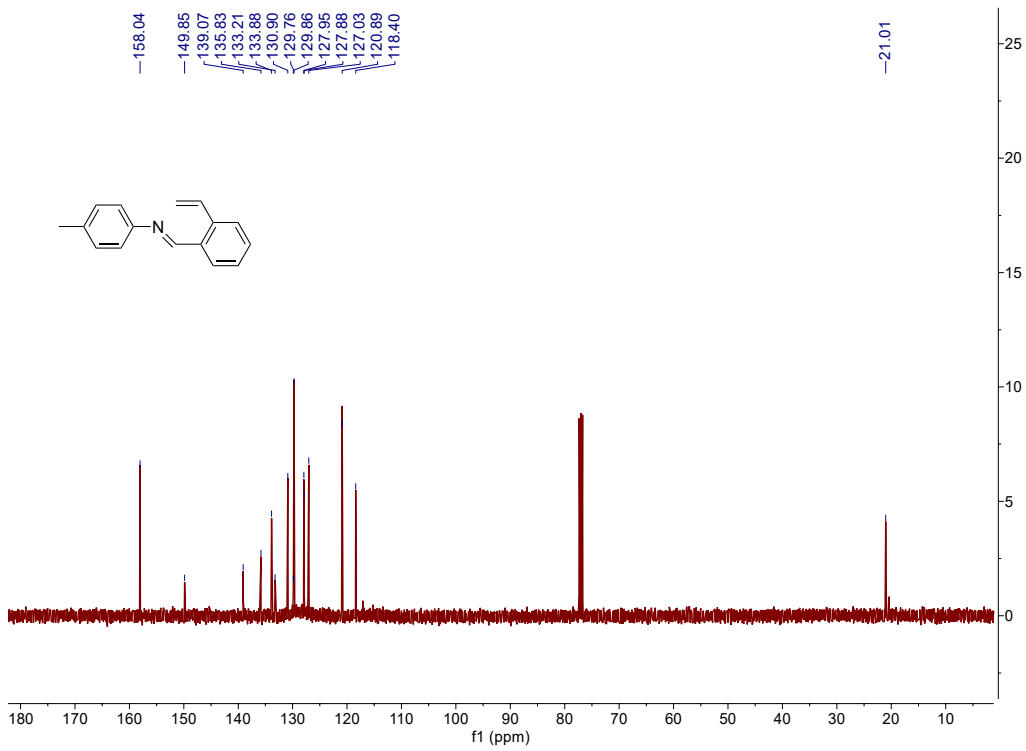
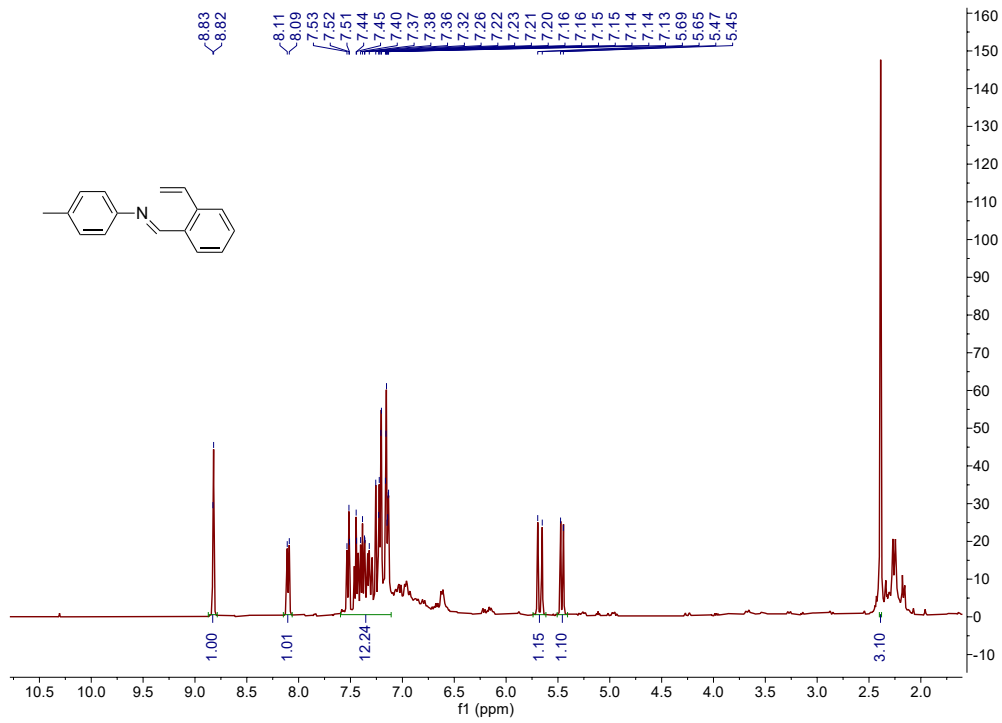
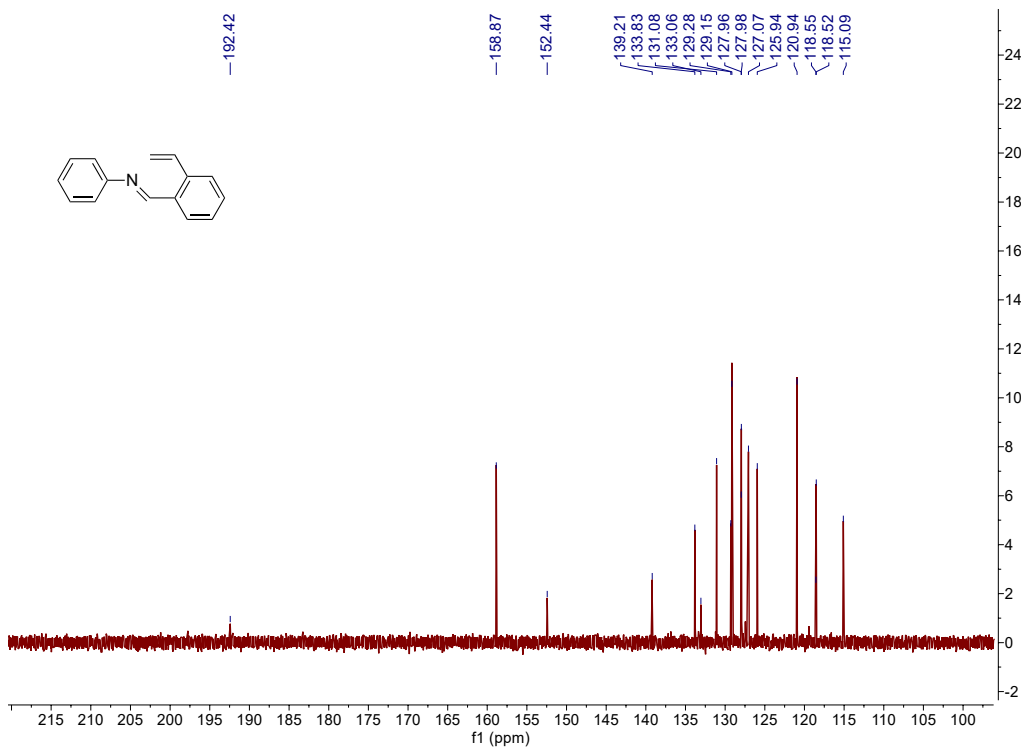
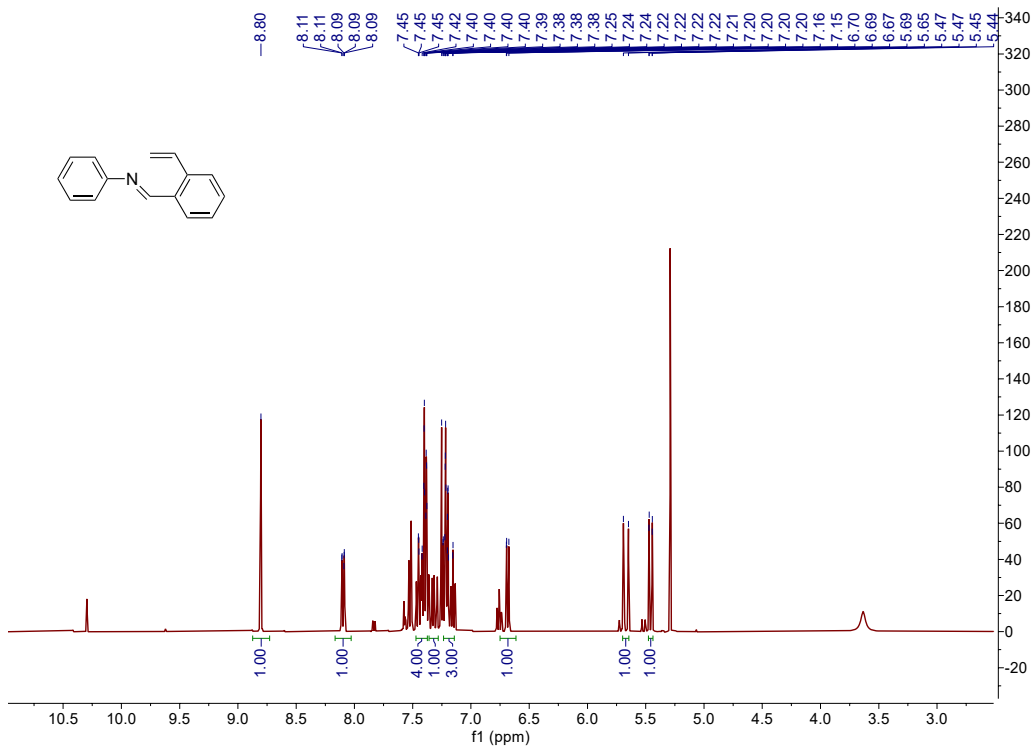


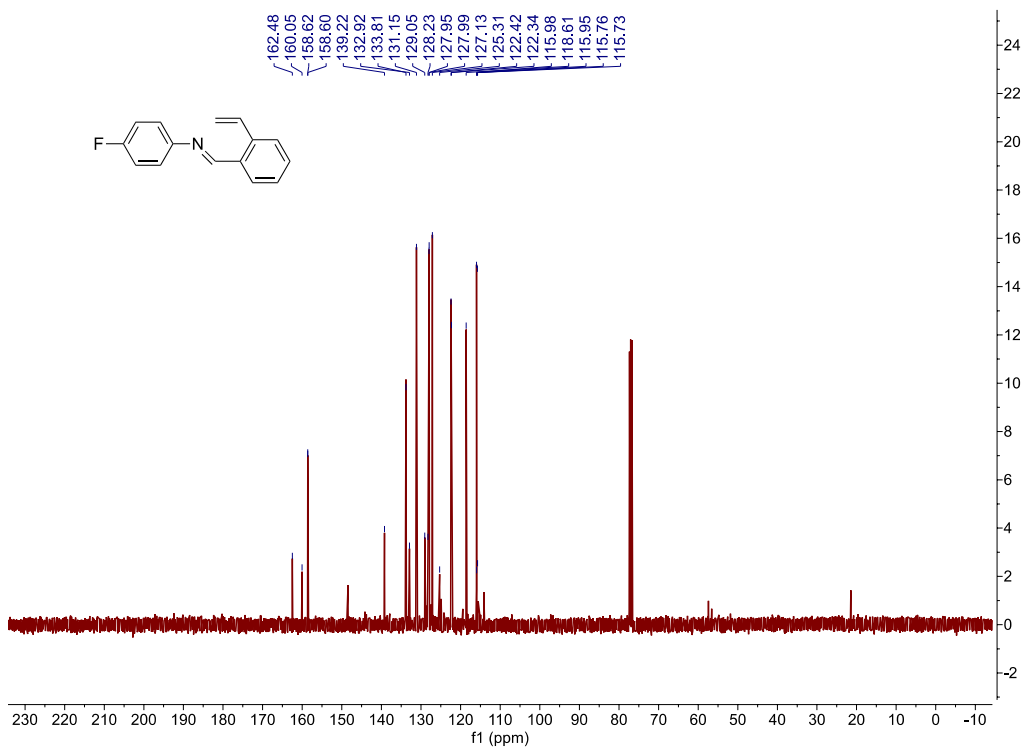
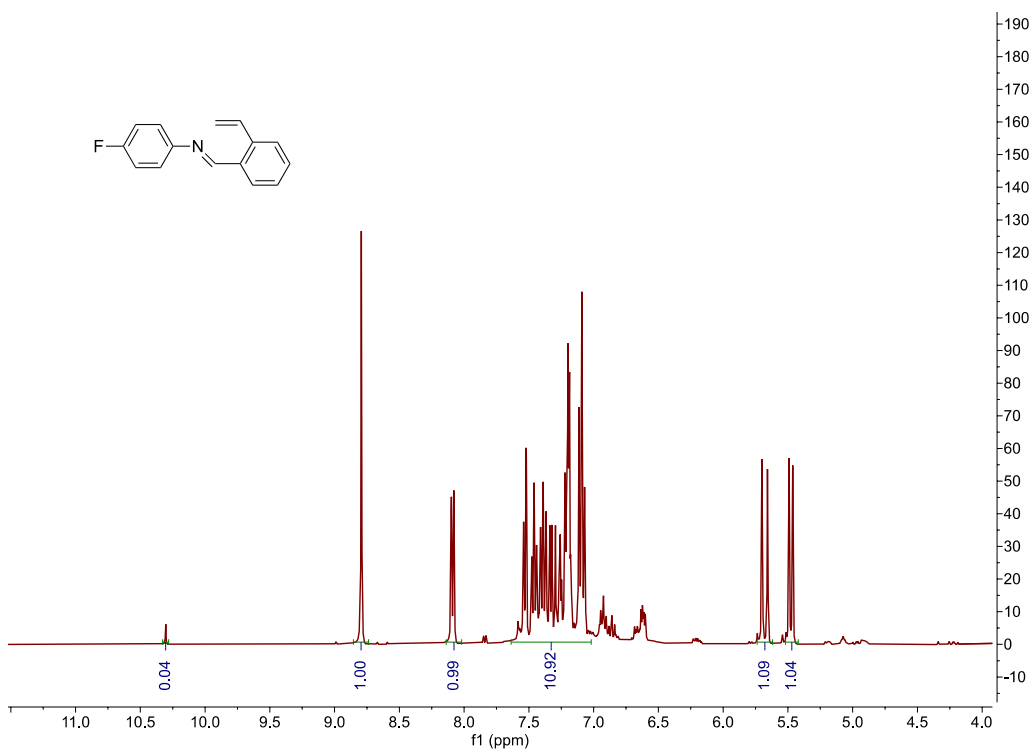
Figure 3.6.2. NMR characterization

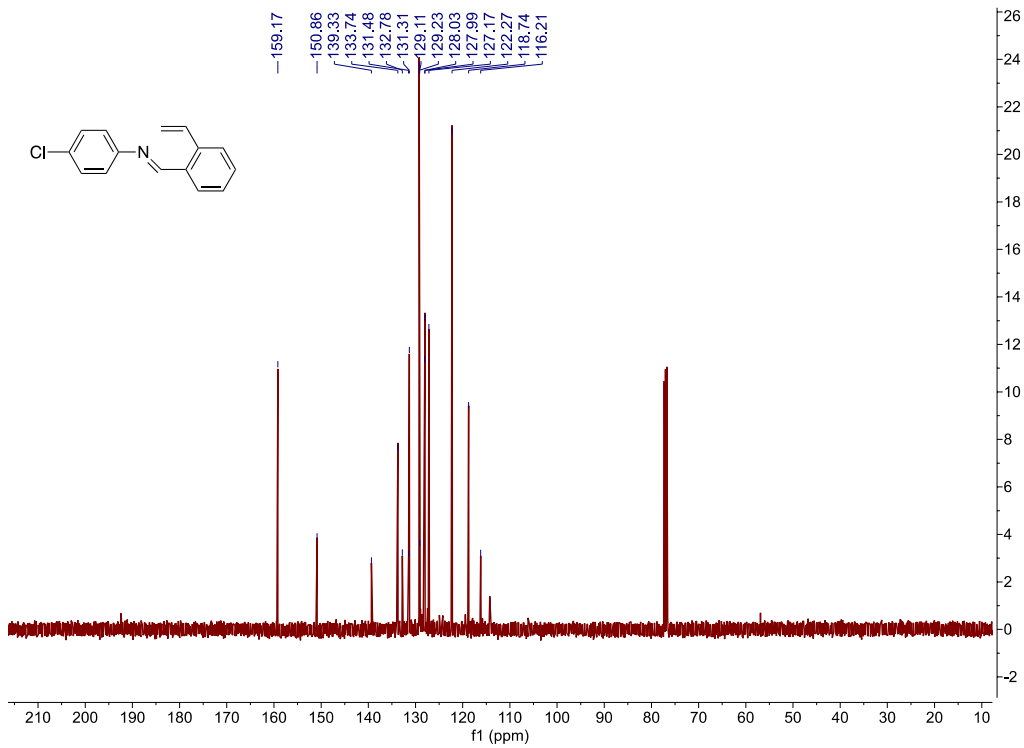
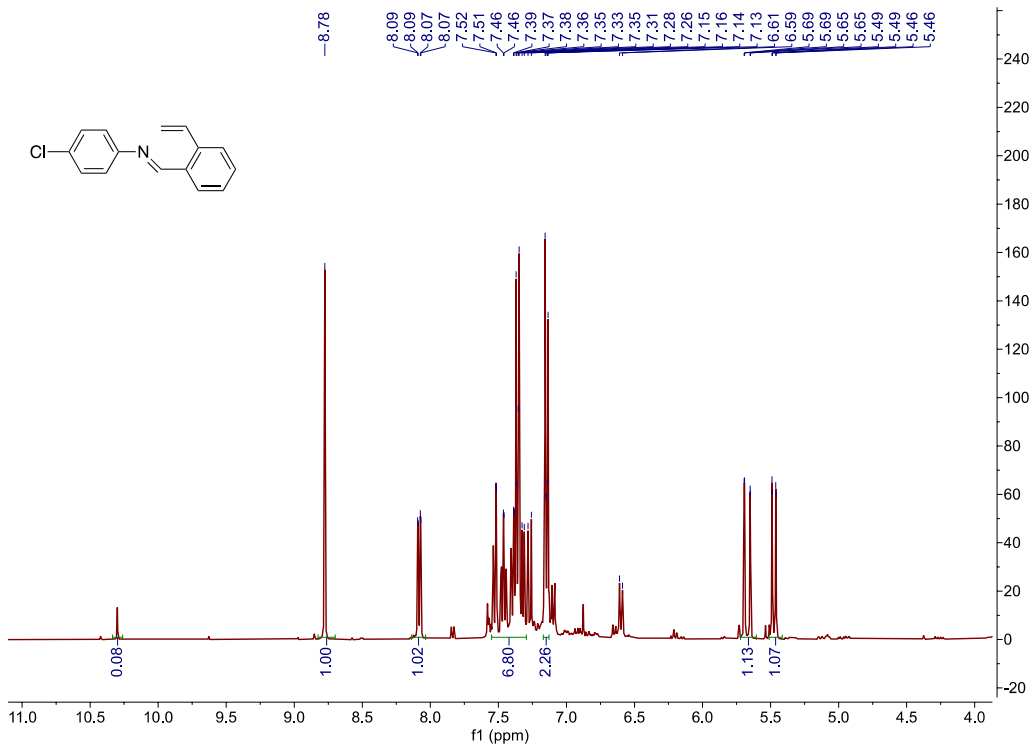


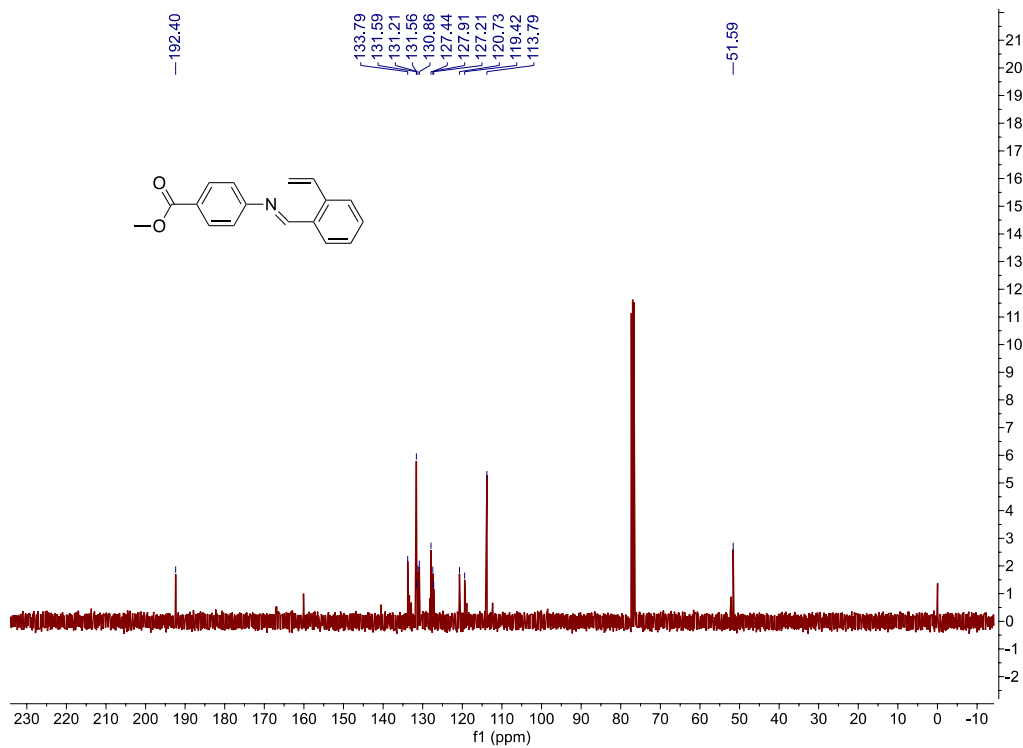
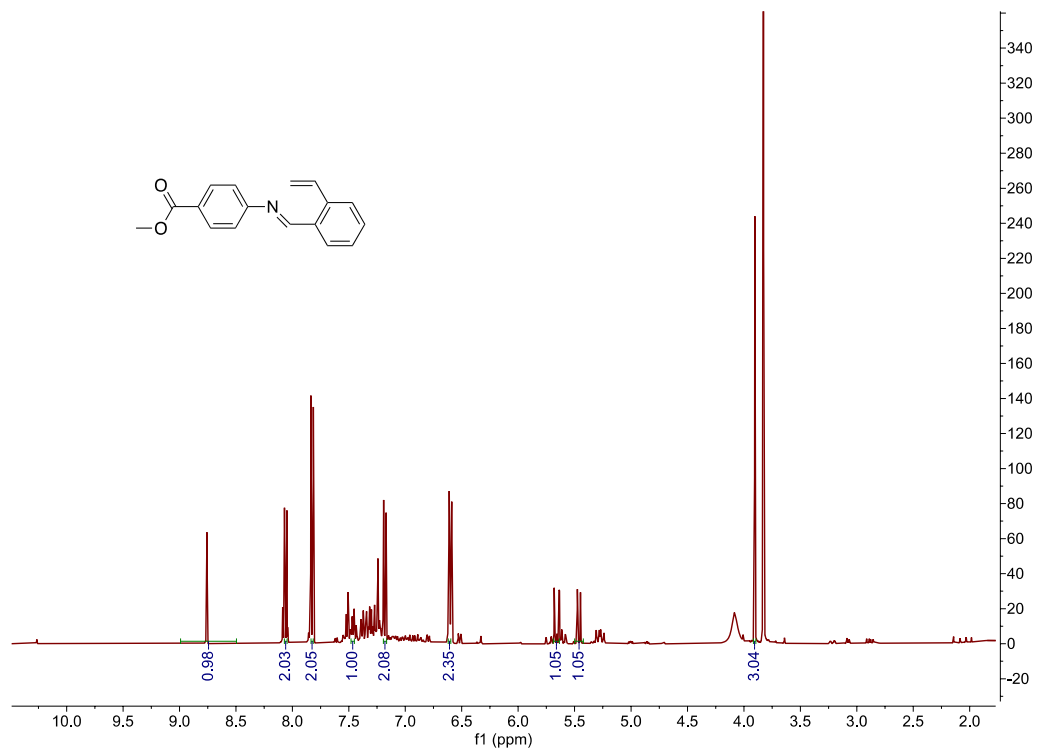


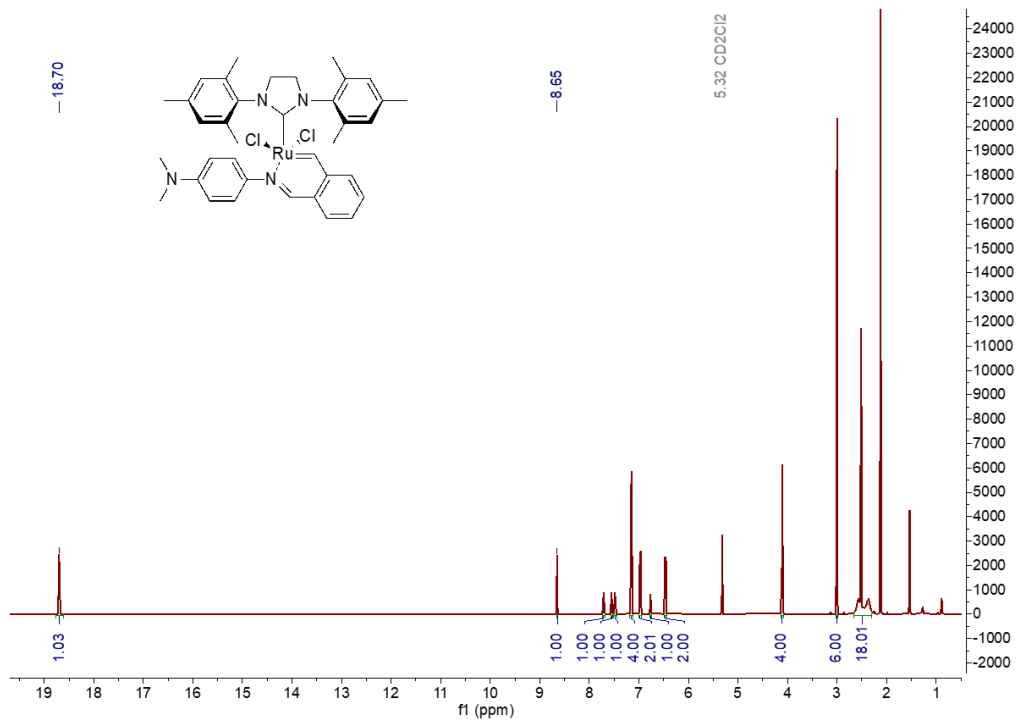
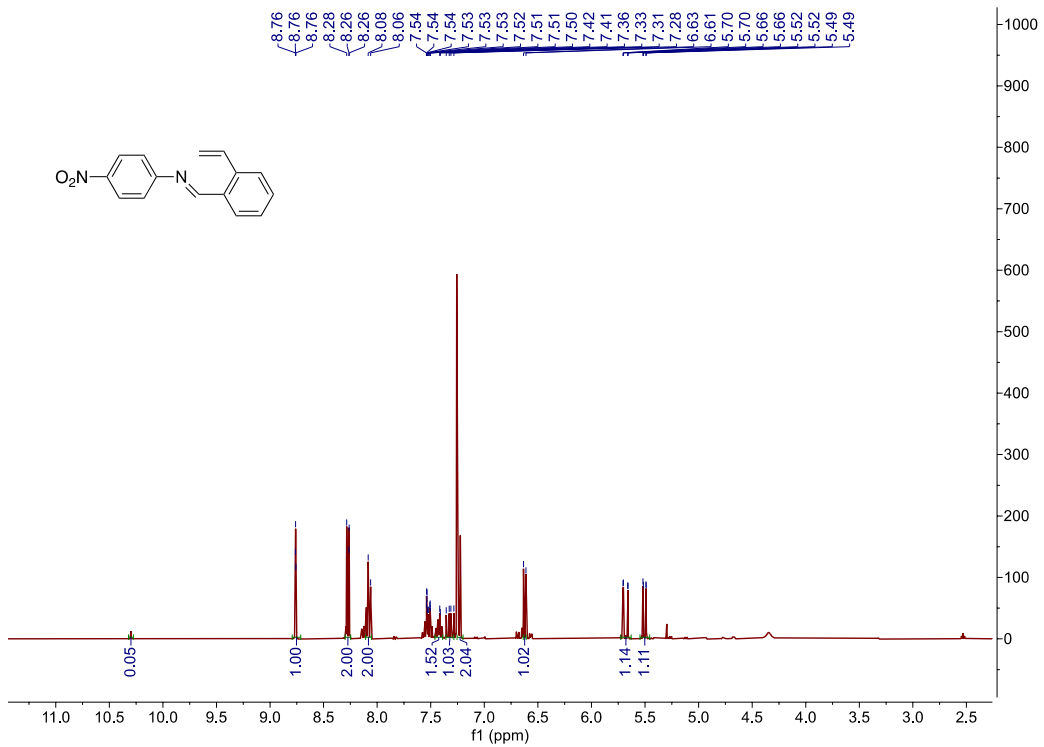


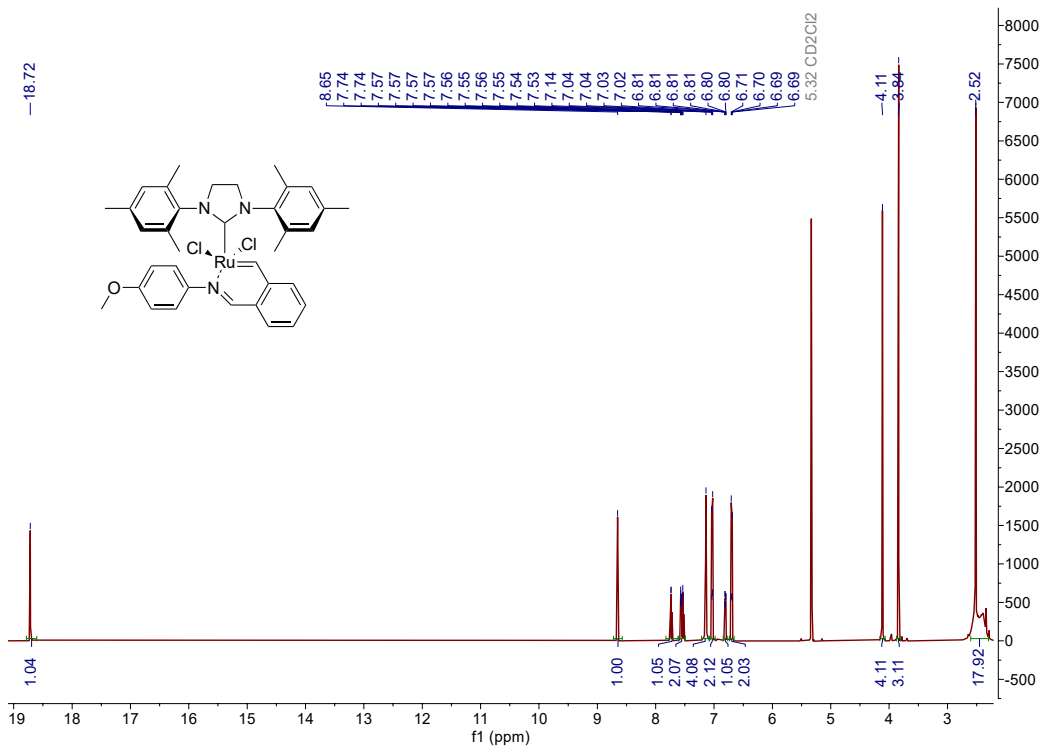
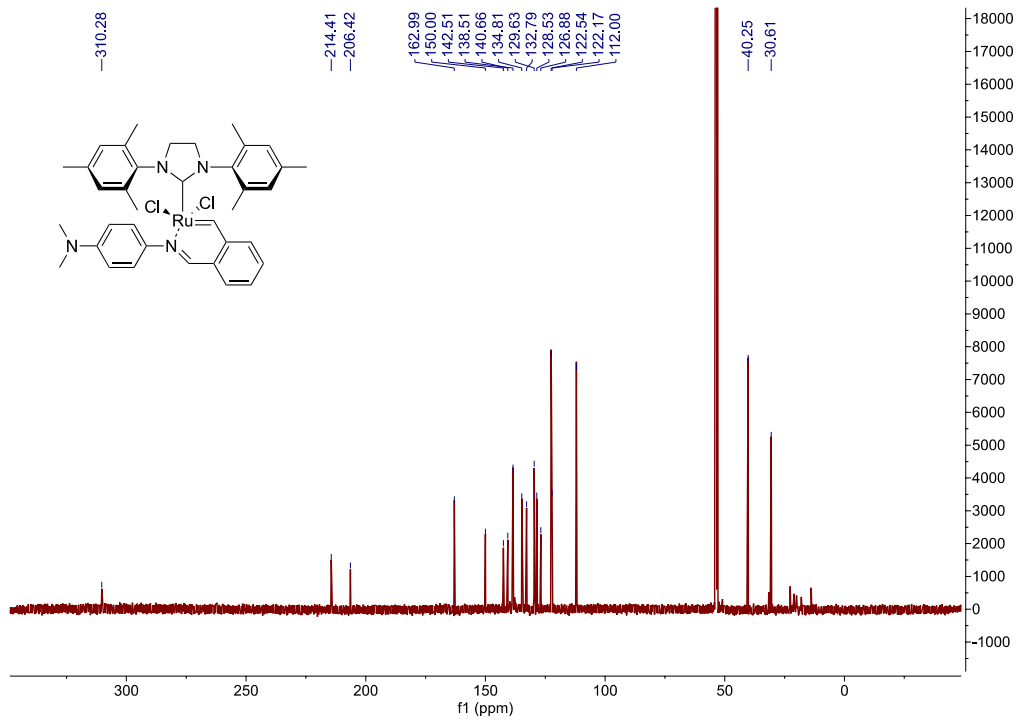




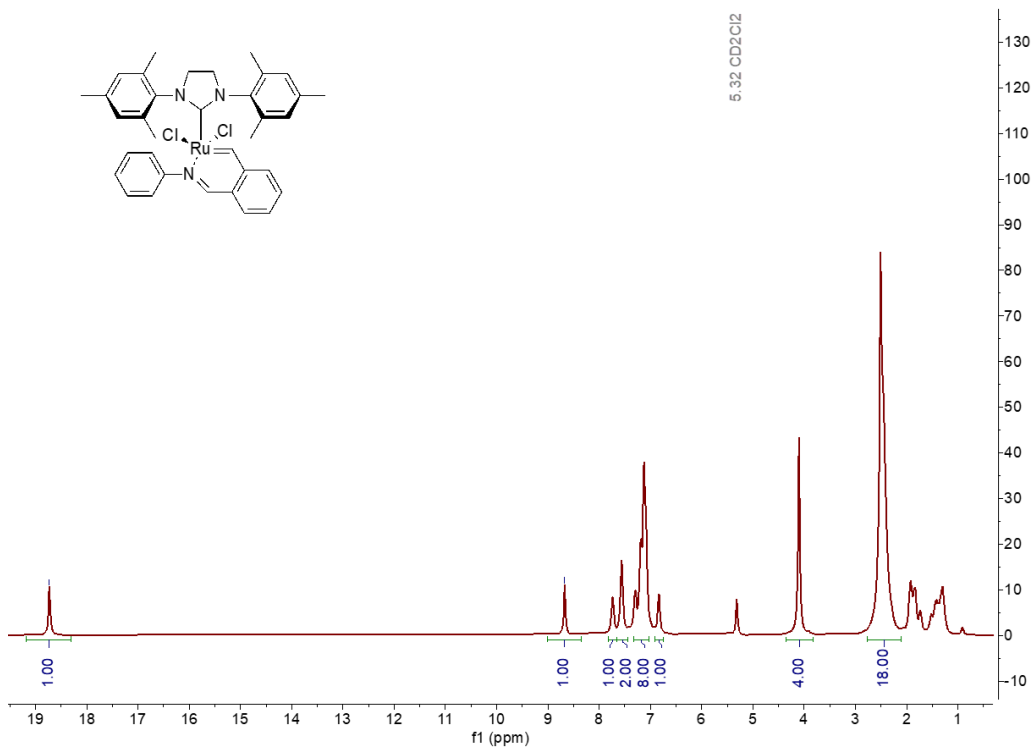
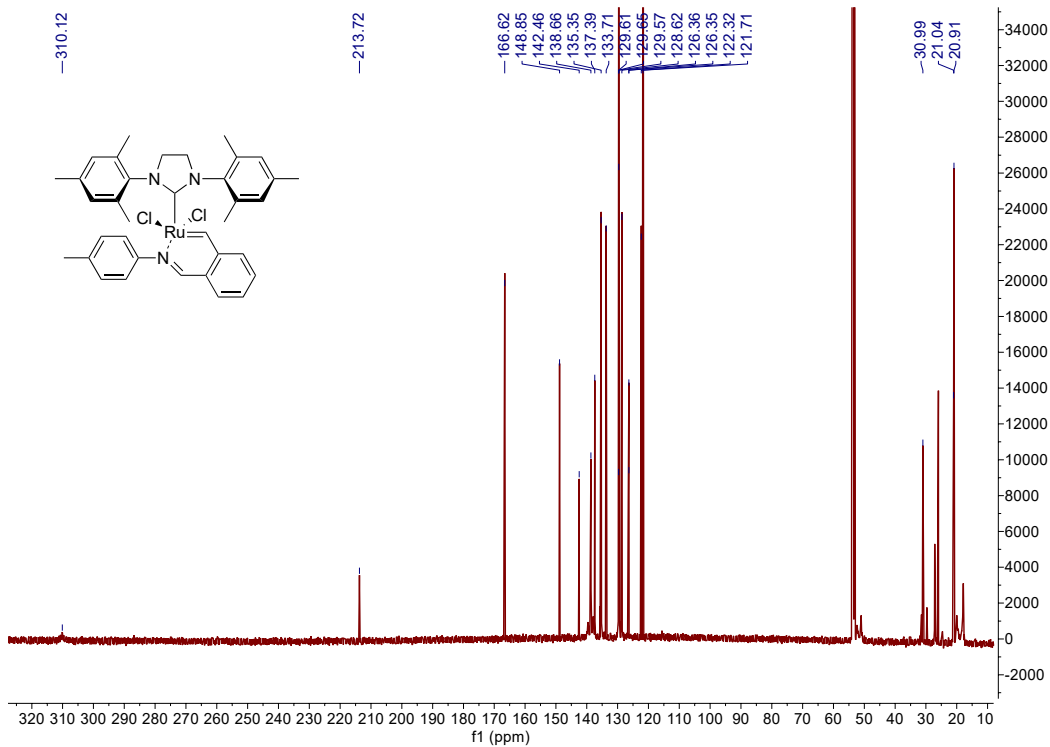


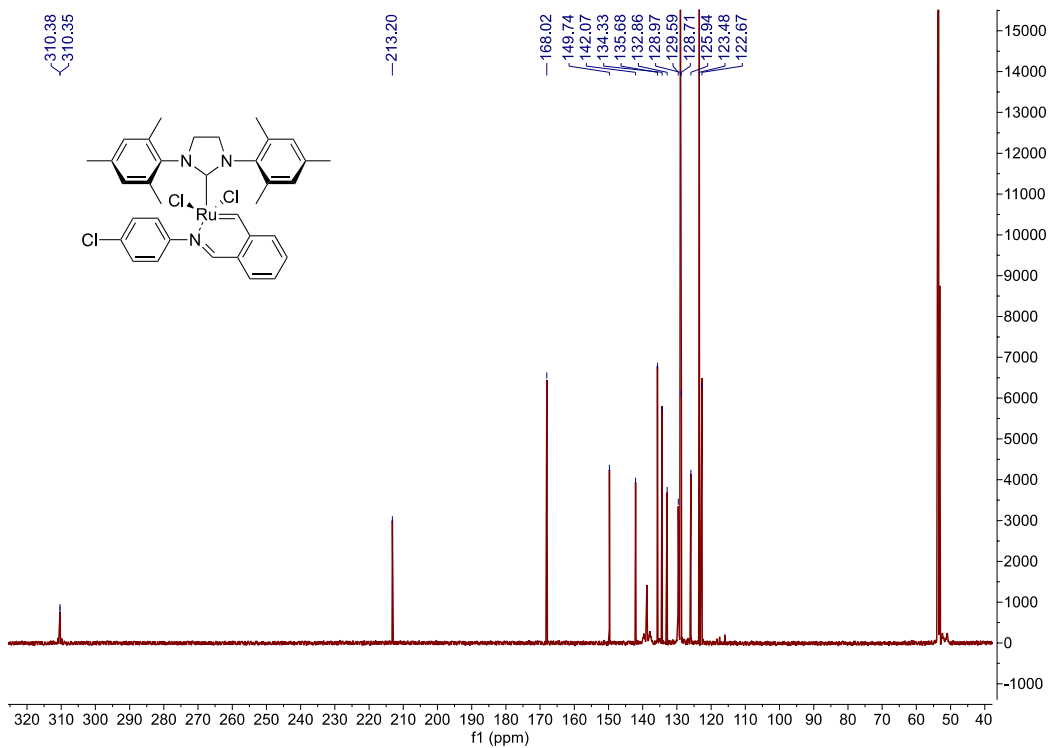
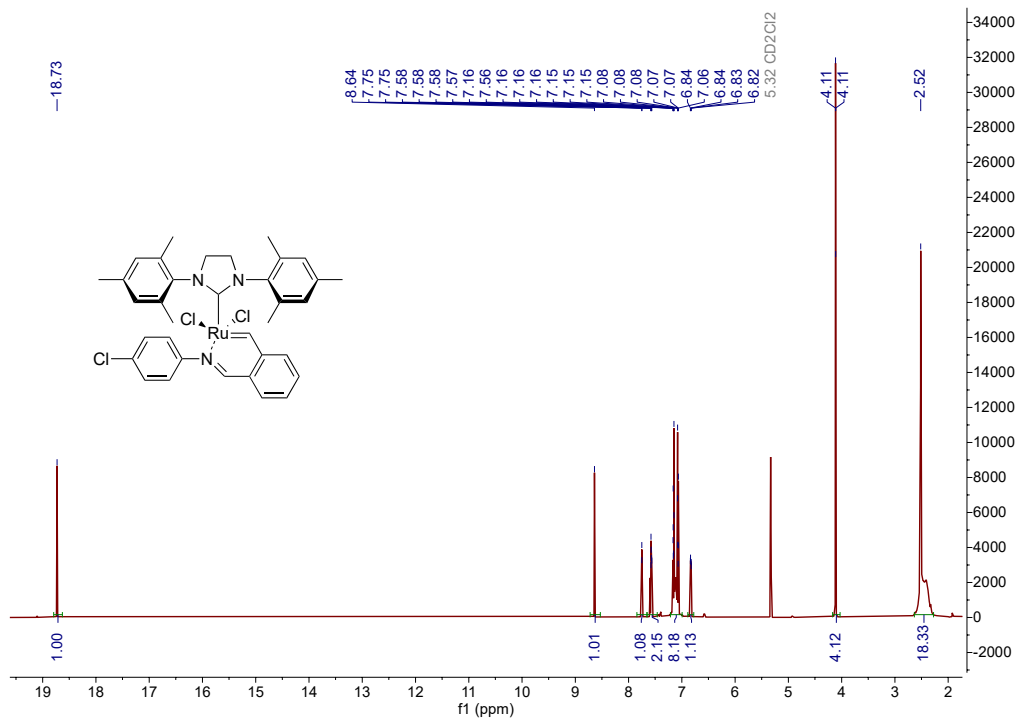


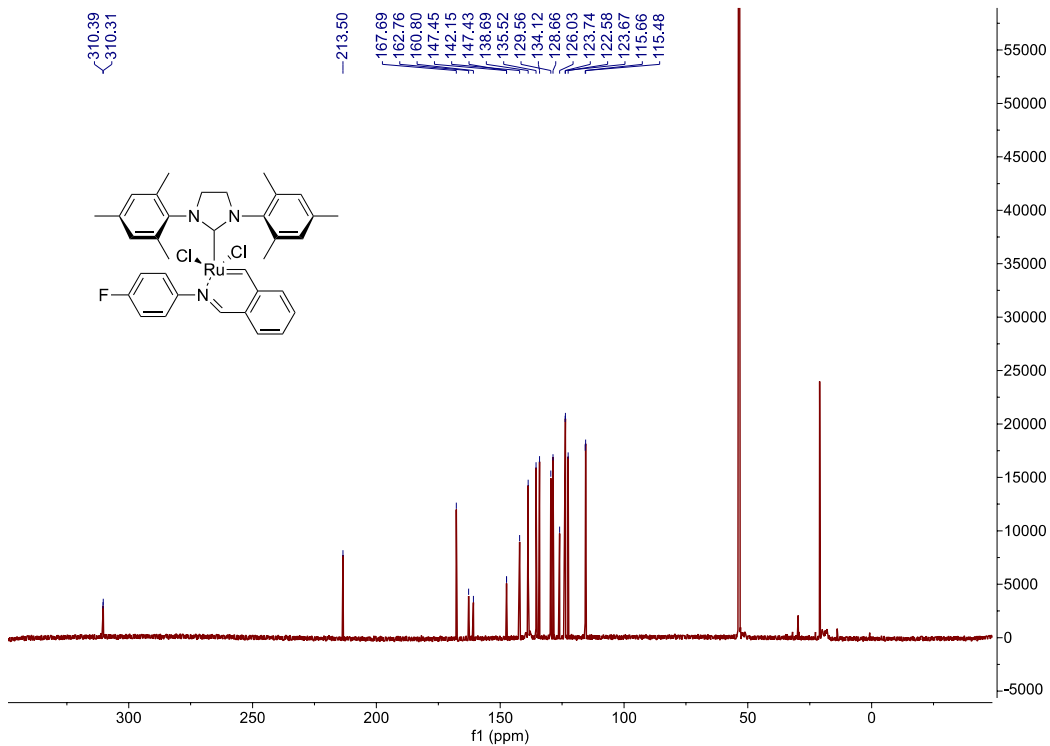
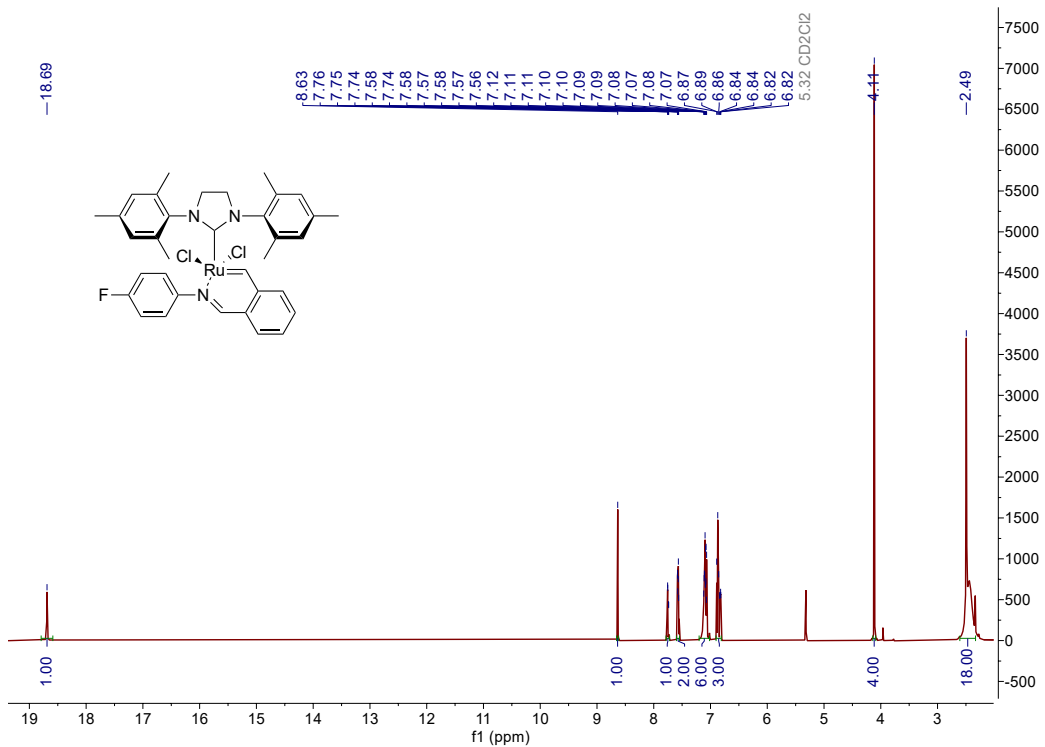


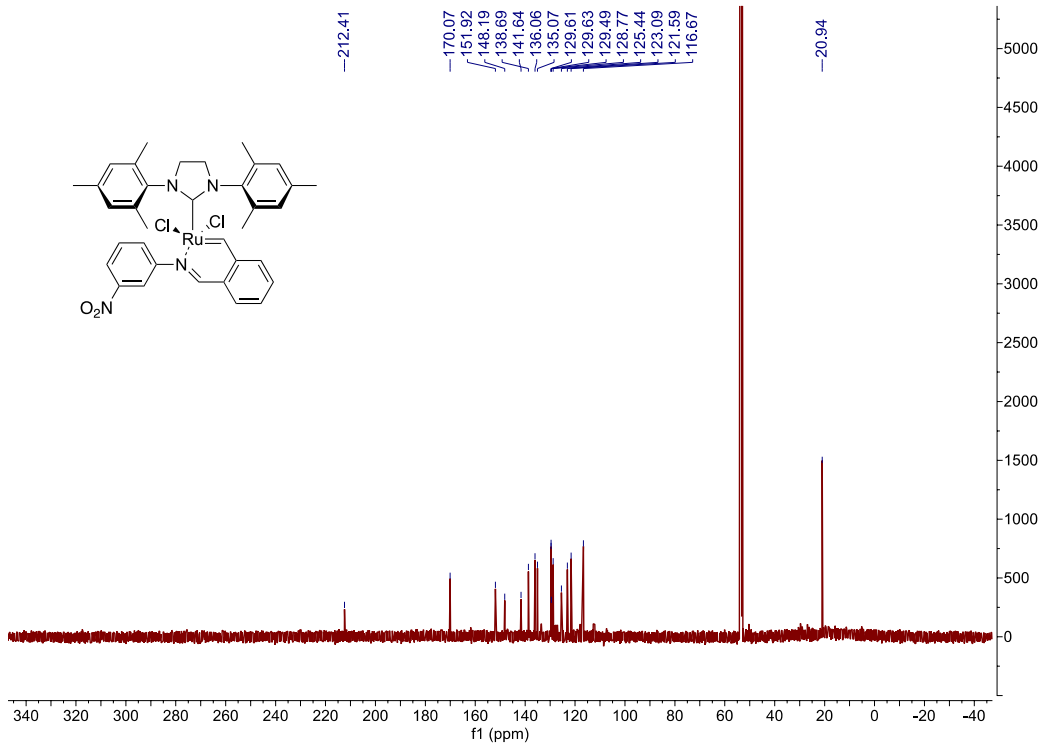
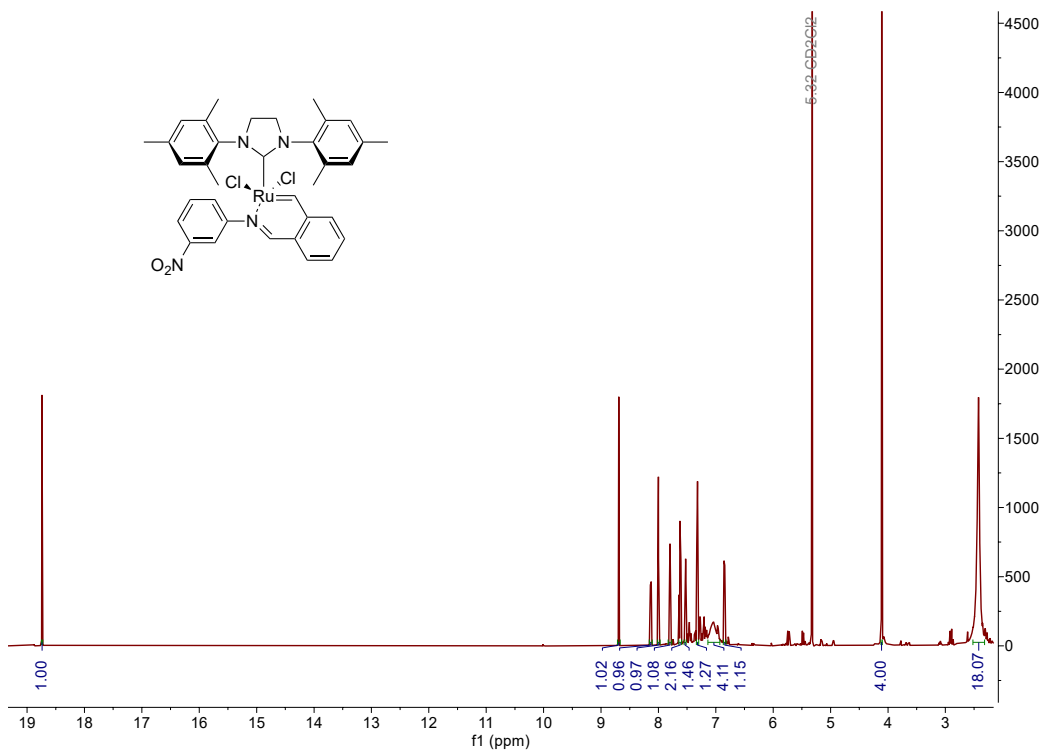


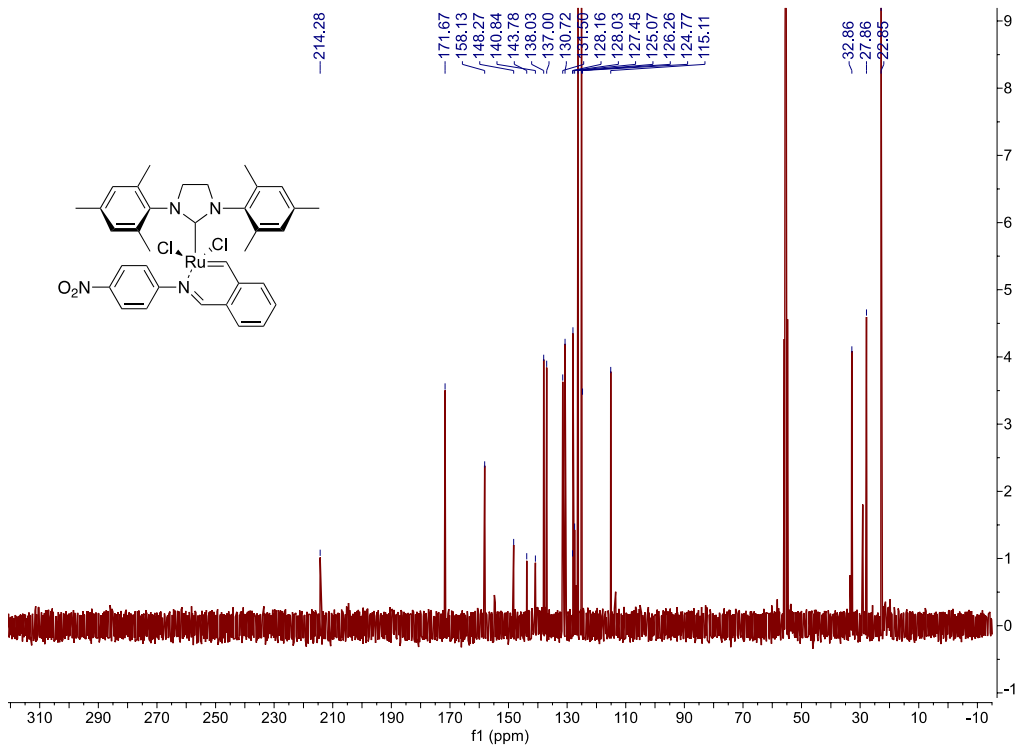
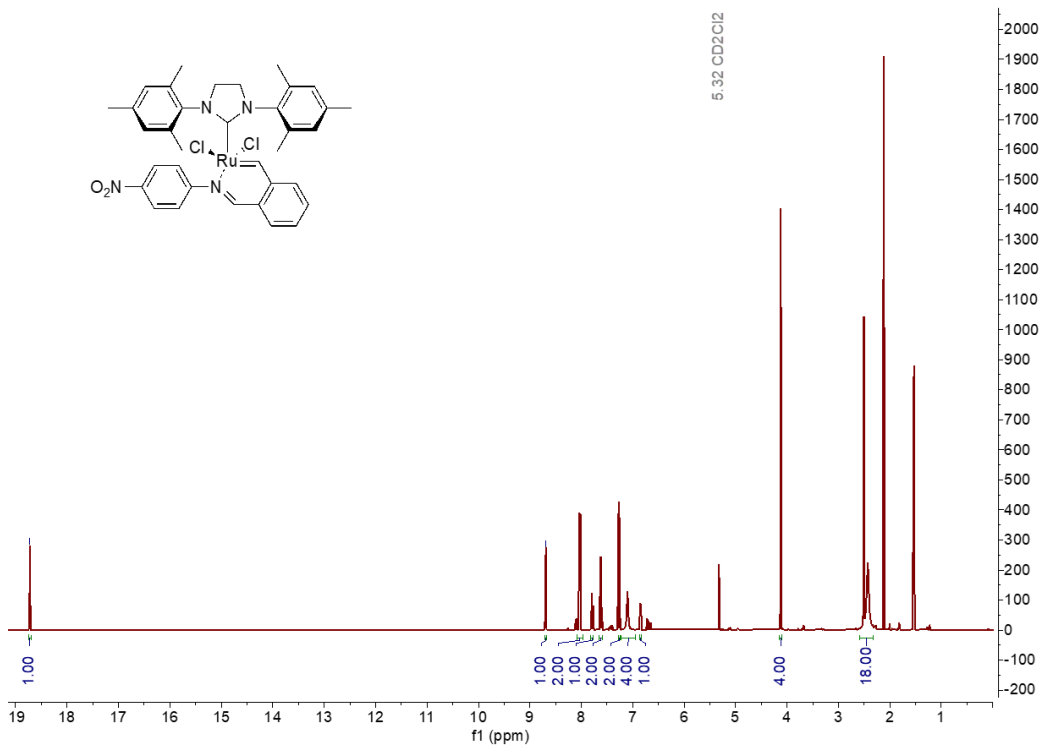












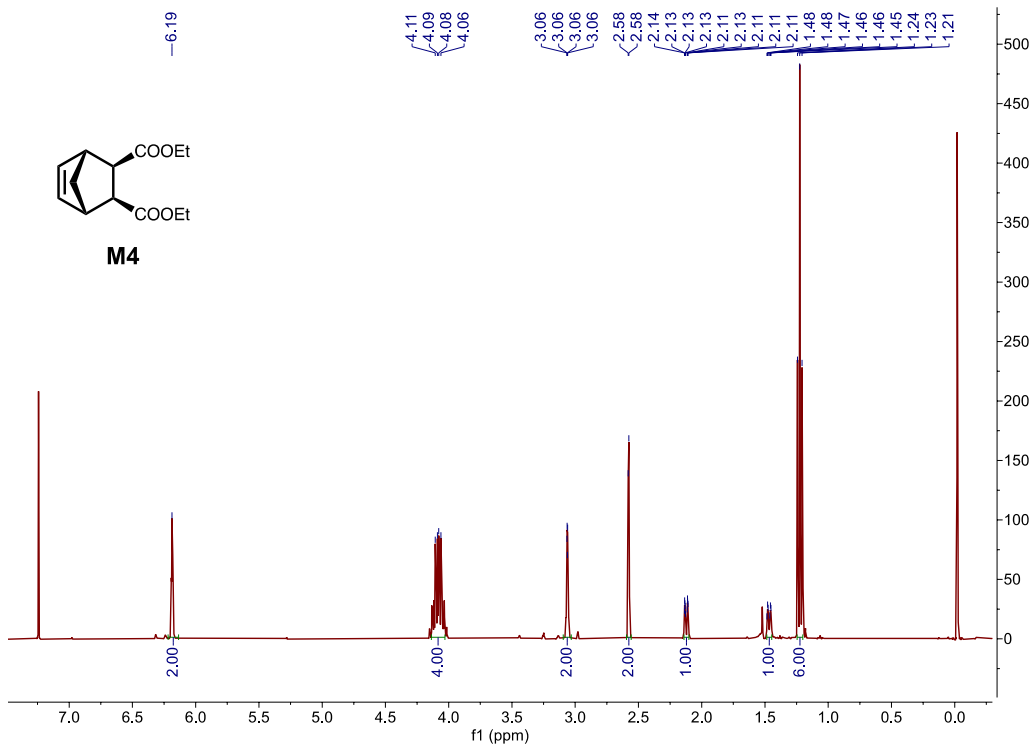
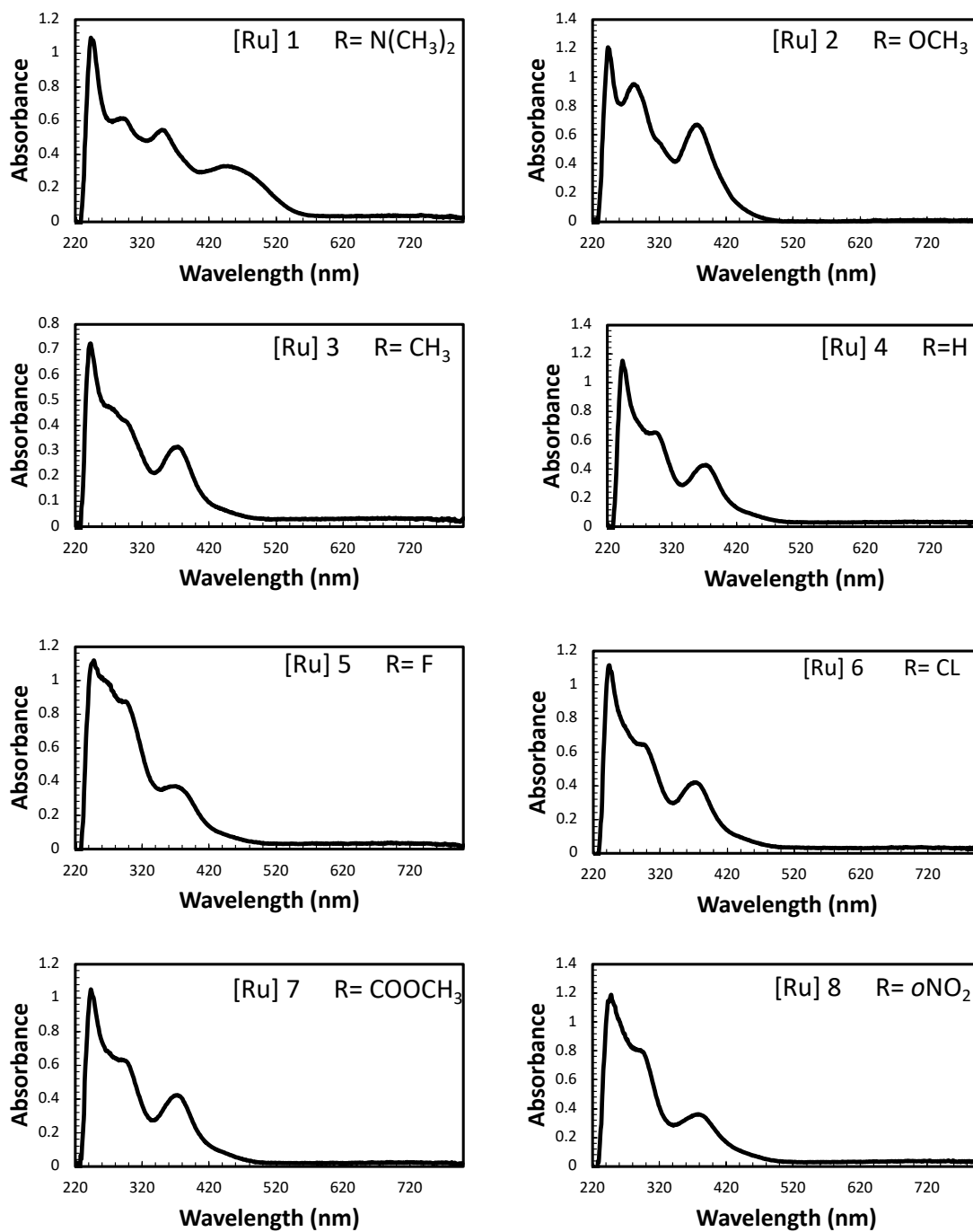
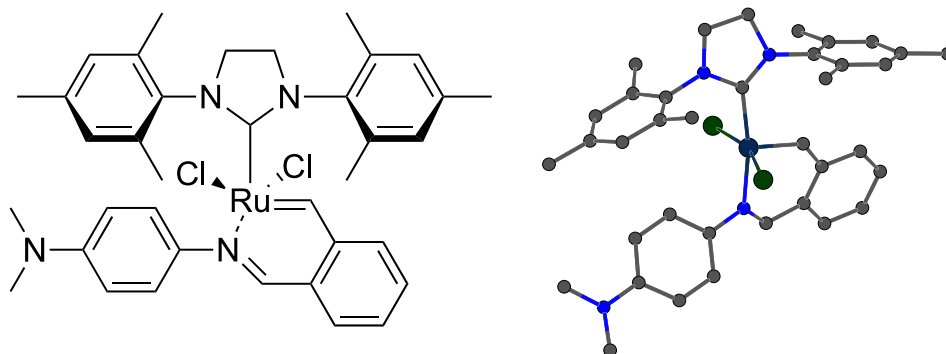


Figure 3.6.3. UV-vis spectra of [Ru] 1-8



## Catalyst Crystal Structure

**Acknowledgements:** We thank the support of the National Science Foundation under CHE-1726077 for crystallography experiments.



[Ru] 1

## Experimental

A blue-green plate (0.05 x 0.44 x 0.49 mm<sup>3</sup>) was centered on the goniometer of a Rigaku Oxford Diffraction Synergy-S diffractometer equipped with a HyPix6000HE detector and operating with MoK $\alpha$  radiation. The data collection routine, unit cell refinement, and data processing were carried out with the program CrysAlisPro.<sup>16</sup> The Laue symmetry and systematic absences were consistent with the monoclinic space group  $P2_1/c$ . The structure was solved using SHELXT<sup>17</sup> and refined using SHELXL<sup>18</sup> via Olex2.<sup>19</sup> The final refinement model involved anisotropic displacement parameters for

---

(16) CrysAlisPro Software System, v1.171.41.105a, Rigaku Oxford Diffraction, 2021, Rigaku Corporation, Oxford, UK.

(17) Sheldrick, G. M. "SHELXT – Integrated space-group and crystal structure determination." *Acta Cryst.* **2015**, *A71*, 3–8.

(18) Sheldrick, G. M. "Crystal structure refinement with SHELXL." *Acta Cryst.* **2015**, *C71*, 3–8.

(19) Dolomanov, O.V.; Bourhis, L. J.; Gildea, R. J.; Howard, J. A. K.; Puschmann, H. *J. Appl. Cryst.* **2009**, *42*, 339–341.

non-hydrogen atoms and a riding model for all hydrogen atoms. Two CH<sub>2</sub>Cl<sub>2</sub> molecules were refined with 2-position disorder models. The relative occupancies of the disordered molecules refined to 0.903(3)/0.097(3) and 0.964(2)/0.036(2). Olex2<sup>20</sup> AND/OR was used for molecular graphics generation.

**Table 3.6.1. Crystal data and structure refinement for cs2841 [Ru] 1.**

Identification code	cs2841
Empirical formula	C <sub>39</sub> H <sub>46</sub> Cl <sub>6</sub> N <sub>4</sub> Ru
Formula weight	884.57
Temperature/K	100.00(12)
Crystal system	monoclinic
Space group	P2 <sub>1</sub> /c
a/Å	20.1137(2)
b/Å	10.04740(10)
c/Å	19.5990(2)
α/°	90
β/°	91.5380(10)
γ/°	90
Volume/Å <sup>3</sup>	3959.34(7)
Z	4
ρ <sub>calc</sub> /g/cm <sup>3</sup>	1.484
μ/mm <sup>-1</sup>	0.835
F(000)	1816.0
Crystal size/mm <sup>3</sup>	0.49 × 0.44 × 0.05
Radiation	Mo Kα (λ = 0.71073)
2θ range for data collection/°	5.01 to 76.55
Index ranges	-34 ≤ h ≤ 33, -17 ≤ k ≤ 17, -32 ≤ l ≤ 33
Reflections collected	133458
Independent reflections	20948 [R <sub>int</sub> = 0.0411, R <sub>sigma</sub> = 0.0284]
Data/restraints/parameters	20948/0/473
Goodness-of-fit on F <sup>2</sup>	1.041
Final R indexes [I ≥ 2σ (I)]	R <sub>1</sub> = 0.0305, wR <sub>2</sub> = 0.0758
Final R indexes [all data]	R <sub>1</sub> = 0.0405, wR <sub>2</sub> = 0.0791

(20) Dolomanov, O.V.; Bourhis, L. J.; Gildea, R. J.; Howard, J. A. K.; Puschmann, H. *J. Appl. Cryst.* **2009**, *42*, 339–341.

Largest diff. peak/hole / e Å<sup>-3</sup> 0.84/-0.94

**Table 3.6.2. Bond Lengths for cs2841 [Ru] 1.**

Atom	Atom	Length/Å	Atom	Atom	Length/Å
Ru1	C11	2.3691(2)	C14	C19	1.5049(18)
Ru1	C12	2.3424(2)	C15	C16	1.383(2)
Ru1	N3	2.0881(8)	C16	C17	1.387(2)
Ru1	C1	2.0667(10)	C16	C20	1.5119(19)
Ru1	C22	1.8346(10)	C17	C18	1.3982(18)
N1	C1	1.3474(13)	C18	C21	1.4987(19)
N1	C2	1.4778(14)	C22	C23	1.4509(13)
N1	C4	1.4280(13)	C23	C24	1.4031(14)
N2	C1	1.3563(13)	C23	C28	1.4147(14)
N2	C3	1.4707(14)	C24	C25	1.3906(14)
N2	C13	1.4298(14)	C25	C26	1.3908(16)
N3	C29	1.2903(12)	C26	C27	1.3858(15)
N3	C30	1.4252(13)	C27	C28	1.4030(13)
N4	C33	1.3827(14)	C28	C29	1.4473(14)
N4	C36	1.4528(17)	C30	C31	1.3921(14)
N4	C37	1.4528(17)	C30	C35	1.3948(14)
C2	C3	1.5196(16)	C31	C32	1.3891(15)
C4	C5	1.3974(14)	C32	C33	1.4056(16)
C4	C9	1.3998(14)	C33	C34	1.4077(16)
C5	C6	1.3939(15)	C34	C35	1.3869(15)
C5	C10	1.4989(15)	Cl3A	C38	1.7621(13)
C6	C7	1.3946(15)	Cl4A	C38	1.7624(15)
C7	C8	1.3918(15)	C38	Cl4B	1.566(13)
C7	C11	1.5049(15)	C38	Cl3B	1.813(11)
C8	C9	1.3927(15)	Cl5A	C39	1.7512(17)
C9	C12	1.5015(15)	Cl6A	C39	1.7662(17)
C13	C14	1.4047(16)	C39	Cl6B	1.692(7)
C13	C18	1.4018(16)	C39	Cl5B	1.889(7)
C14	C15	1.3915(17)			

**Table 3.6.3. Bond Angles for cs2841 [Ru] 1.**

Atom	Atom	Atom	Angle/°	Atom	Atom	Atom	Angle/°
C12	Ru1	C11	161.480(10)	C14	C13	N2	119.34(10)
N3	Ru1	C11	88.17(2)	C18	C13	N2	119.19(10)
N3	Ru1	C12	84.91(2)	C18	C13	C14	120.92(10)
C1	Ru1	C11	94.68(3)	C13	C14	C19	121.54(11)
C1	Ru1	C12	89.52(3)	C15	C14	C13	118.45(11)
C1	Ru1	N3	170.19(4)	C15	C14	C19	119.78(12)
C22	Ru1	C11	98.69(3)	C16	C15	C14	121.78(12)
C22	Ru1	C12	98.42(3)	C15	C16	C17	118.67(12)
C22	Ru1	N3	89.63(4)	C15	C16	C20	120.44(15)
C22	Ru1	C1	99.19(4)	C17	C16	C20	120.84(15)
C1	N1	C2	113.18(9)	C16	C17	C18	121.95(12)
C1	N1	C4	128.02(8)	C13	C18	C21	122.20(11)
C4	N1	C2	118.55(8)	C17	C18	C13	117.96(12)
C1	N2	C3	113.57(9)	C17	C18	C21	119.73(12)
C1	N2	C13	126.99(9)	C23	C22	Ru1	127.74(8)
C13	N2	C3	118.13(8)	C24	C23	C22	118.05(9)
C29	N3	Ru1	126.35(7)	C24	C23	C28	118.20(9)
C29	N3	C30	117.61(8)	C28	C23	C22	123.74(9)
C30	N3	Ru1	115.61(6)	C25	C24	C23	121.50(10)
C33	N4	C36	119.00(10)	C24	C25	C26	119.88(10)
C33	N4	C37	119.19(11)	C27	C26	C25	119.77(9)
C37	N4	C36	116.85(10)	C26	C27	C28	120.99(10)
N1	C1	Ru1	132.94(7)	C23	C28	C29	122.61(9)
N1	C1	N2	106.37(8)	C27	C28	C23	119.65(9)
N2	C1	Ru1	120.46(7)	C27	C28	C29	117.56(9)
N1	C2	C3	101.93(9)	N3	C29	C28	124.28(9)
N2	C3	C2	101.63(8)	C31	C30	N3	121.65(9)
C5	C4	N1	118.77(9)	C31	C30	C35	118.61(9)
C5	C4	C9	121.67(9)	C35	C30	N3	119.74(9)
C9	C4	N1	119.55(9)	C32	C31	C30	120.81(10)
C4	C5	C10	120.76(10)	C31	C32	C33	121.15(10)
C6	C5	C4	118.49(9)	N4	C33	C32	121.10(10)
C6	C5	C10	120.70(10)	N4	C33	C34	121.68(10)
C5	C6	C7	121.13(10)	C32	C33	C34	117.21(10)
C6	C7	C11	120.34(10)	C35	C34	C33	121.30(10)

**Table 3.6.3. Bond Angles for cs2841 [Ru] 1.**

Atom	Atom	Atom	Angle/°	Atom	Atom	Atom	Angle/°
C8	C7	C6	118.98(10)	C34	C35	C30	120.66(10)
C8	C7	C11	120.68(10)	Cl3A	C38	Cl4A	112.25(7)
C7	C8	C9	121.60(9)	Cl4B	C38	Cl3B	117.5(7)
C4	C9	C12	121.37(9)	Cl5A	C39	Cl6A	111.74(9)
C8	C9	C4	118.10(9)	Cl6B	C39	Cl5B	109.7(3)
C8	C9	C12	120.48(9)				

**Table 3.6.4. Torsion Angles for cs2841 [Ru] 1.**

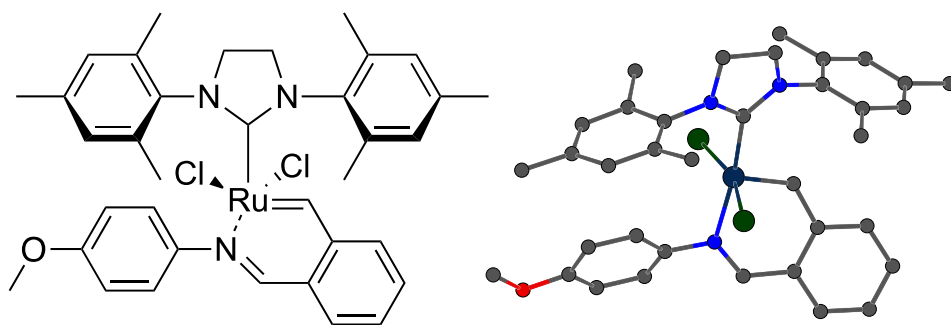
A	B	C	D	Angle/°	A	B	C	D	Angle/°
Ru1	N3	C29	C28	12.46(14)	C9	C4	C5	C6	-1.61(15)
Ru1	N3	C30	C31	-139.67(8)	C9	C4	C5	C10	-178.93(10)
Ru1	N3	C30	C35	39.52(11)	C10	C5	C6	C7	177.45(10)
Ru1	C22	C23	C24	164.30(8)	C11	C7	C8	C9	178.82(10)
Ru1	C22	C23	C28	-16.76(14)	C13	N2	C1	Ru1	12.55(15)
Cl1	Ru1	C22	C23	112.35(9)	C13	N2	C1	N1	-172.22(10)
Cl2	Ru1	C22	C23	-60.54(9)	C13	N2	C3	C2	-177.05(10)
N1	C2	C3	N2	-17.10(12)	C13	C14	C15	C16	-2.65(17)
N1	C4	C5	C6	179.78(9)	C14	C13	C18	C17	-5.49(16)
N1	C4	C5	C10	2.46(15)	C14	C13	C18	C21	170.65(11)
N1	C4	C9	C8	-179.90(9)	C14	C15	C16	C17	-1.08(19)
N1	C4	C9	C12	-2.29(15)	C14	C15	C16	C20	-178.44(12)
N2	C13	C14	C15	177.47(10)	C15	C16	C17	C18	1.59(19)
N2	C13	C14	C19	2.94(15)	C16	C17	C18	C13	1.65(18)
N2	C13	C18	C17	-176.97(10)	C16	C17	C18	C21	-174.59(12)
N2	C13	C18	C21	-0.82(16)	C18	C13	C14	C15	6.00(16)
N3	Ru1	C22	C23	24.26(9)	C18	C13	C14	C19	-168.52(11)
N3	C30	C31	C32	-177.33(10)	C19	C14	C15	C16	171.97(11)
N3	C30	C35	C34	176.49(9)	C20	C16	C17	C18	178.95(12)
N4	C33	C34	C35	-174.79(10)	C22	C23	C24	C25	179.40(9)
C1	Ru1	C22	C23	-151.42(9)	C22	C23	C28	C27	-178.78(9)
C1	N1	C2	C3	16.03(13)	C22	C23	C28	C29	-3.75(15)
C1	N1	C4	C5	-89.22(13)	C23	C24	C25	C26	-0.74(15)
C1	N1	C4	C9	92.14(13)	C23	C28	C29	N3	4.68(16)
C1	N2	C3	C2	15.07(14)	C24	C23	C28	C27	0.17(14)
C1	N2	C13	C14	81.24(14)	C24	C23	C28	C29	175.20(9)

**Table 3.6.4. Torsion Angles for cs2841 [Ru] 1.**

A	B	C	D	Angle/°	A	B	C	D	Angle/°
C1	N2	C13	C18	-107.15(13)	C24	C25	C26	C27	0.51(16)
C2	N1	C1	Ru1	167.23(9)	C25	C26	C27	C28	0.05(16)
C2	N1	C1	N2	-7.16(12)	C26	C27	C28	C23	-0.39(15)
C2	N1	C4	C5	96.95(12)	C26	C27	C28	C29	-175.67(9)
C2	N1	C4	C9	-81.68(13)	C27	C28	C29	N3	179.81(10)
C3	N2	C1	Ru1	179.14(8)	C28	C23	C24	C25	0.39(14)
C3	N2	C1	N1	-5.62(13)	C29	N3	C30	C31	47.38(14)
C3	N2	C13	C14	-84.82(13)	C29	N3	C30	C35	-133.44(10)
C3	N2	C13	C18	86.80(13)	C30	N3	C29	C28	-175.43(9)
C4	N1	C1	Ru1	-6.87(17)	C30	C31	C32	C33	1.11(17)
C4	N1	C1	N2	178.74(10)	C31	C30	C35	C34	-4.30(15)
C4	N1	C2	C3	-169.26(10)	C31	C32	C33	N4	173.97(11)
C4	C5	C6	C7	0.13(15)	C31	C32	C33	C34	-4.75(16)
C5	C4	C9	C8	1.50(15)	C32	C33	C34	C35	3.93(16)
C5	C4	C9	C12	179.11(10)	C33	C34	C35	C30	0.56(16)
C5	C6	C7	C8	1.41(16)	C35	C30	C31	C32	3.48(15)
C5	C6	C7	C11	-178.93(10)	C36	N4	C33	C32	169.17(11)
C6	C7	C8	C9	-1.53(15)	C36	N4	C33	C34	-12.16(17)
C7	C8	C9	C4	0.10(15)	C37	N4	C33	C32	14.86(17)

This report has been created with Olex2, compiled on 2022.04.07 svn.rca3783a0 for OlexSys.

Please [let us know](#) if there are any errors or if you would like to have additional features.

**[Ru] 2**

## Experimental

A blue plate (0.05 x 0.17 x 0.18 mm<sup>3</sup>) was centered on the goniometer of a Rigaku Oxford Diffraction Synergy-S diffractometer equipped with a HyPix6000HE detector and operating with MoK $\alpha$  radiation. The data collection routine, unit cell refinement, and data processing were carried out with the program CrysAlisPro.<sup>21</sup> The Laue symmetry and systematic absences were consistent with the monoclinic space group  $P2_1/c$ . The structure was solved using SHELXT<sup>22</sup> and refined using SHELXL<sup>23</sup> via Olex2.<sup>24</sup> The final refinement model involved anisotropic displacement parameters for non-hydrogen atoms and a riding model for all hydrogen atoms. Olex2<sup>25</sup> was used for molecular graphics generation.

**Table 3.6.5. Crystal data and structure refinement for cs2919 [Ru] 2.**

Identification code	HA-2-85
Empirical formula	C <sub>37</sub> H <sub>41</sub> Cl <sub>4</sub> N <sub>3</sub> ORu
Formula weight	786.60
Temperature/K	99.98(13)
Crystal system	monoclinic
Space group	$P2_1/c$
a/Å	19.1063(2)
b/Å	10.00920(10)
c/Å	19.5128(2)
$\alpha$ /°	90
$\beta$ /°	111.1390(10)
$\gamma$ /°	90
Volume/Å <sup>3</sup>	3480.50(7)
Z	4
$\rho_{\text{calc}}/\text{cm}^3$	1.501

(21) CrysAlisPro Software System, v1.171.42.xx, Rigaku Oxford Diffraction, 2022, Rigaku Corporation, Oxford, UK.

(22) Sheldrick, G. M. "SHELXT – Integrated space-group and crystal structure determination." *Acta Cryst.* **2015**, *A71*, 3–8.

(23) Sheldrick, G. M. "Crystal structure refinement with SHELXL." *Acta Cryst.* **2015**, *C71*, 3–8.

(24) Dolomanov, O.V.; Bourhis, L. J.; Gildea, R. J.; Howard, J. A. K.; Puschmann, H. *J. Appl. Cryst.* **2009**, *42*, 339–341.

(25) Dolomanov, O.V.; Bourhis, L. J.; Gildea, R. J.; Howard, J. A. K.; Puschmann, H. *J. Appl. Cryst.* **2009**, *42*, 339–341.

$\mu/\text{mm}^{-1}$	0.792
F(000)	1616.0
Crystal size/ $\text{mm}^3$	$0.18 \times 0.17 \times 0.05$
Radiation	Mo K $\alpha$ ( $\lambda = 0.71073$ )
2 $\Theta$ range for data collection/ $^\circ$	5.116 to 76.702
Index ranges	$-32 \leq h \leq 32, -17 \leq k \leq 17, -32 \leq l \leq 34$
Reflections collected	175314
Independent reflections	18516 [ $R_{\text{int}} = 0.0355, R_{\text{sigma}} = 0.0174$ ]
Data/restraints/parameters	18516/0/422
Goodness-of-fit on $F^2$	1.040
Final R indexes [ $I \geq 2\sigma(I)$ ]	$R_1 = 0.0236, wR_2 = 0.0609$
Final R indexes [all data]	$R_1 = 0.0276, wR_2 = 0.0622$
Largest diff. peak/hole / $e \text{ \AA}^{-3}$	1.29/-1.12

**Table 3.6.6. Bond Lengths for cs2919 [Ru] 2.**

Atom	Atom	Length/Å	Atom	Atom	Length/Å
Ru1	C11	2.3762(2)	C13	C14	1.3972(11)
Ru1	C12	2.3461(2)	C13	C18	1.4003(10)
Ru1	N3	2.0876(7)	C14	C15	1.3978(11)
Ru1	C1	2.0651(7)	C14	C19	1.5033(11)
Ru1	C22	1.8324(7)	C15	C16	1.3945(12)
O1	C33	1.3650(10)	C16	C17	1.3947(11)
O1	C36	1.4245(12)	C16	C20	1.5028(11)
N1	C1	1.3563(10)	C17	C18	1.3958(11)
N1	C2	1.4707(10)	C18	C21	1.4993(11)
N1	C4	1.4305(10)	C22	C23	1.4525(11)
N2	C1	1.3480(10)	C23	C24	1.4068(11)
N2	C3	1.4737(10)	C23	C28	1.4149(11)
N2	C13	1.4280(10)	C24	C25	1.3900(11)
N3	C29	1.2920(10)	C25	C26	1.3949(13)
N3	C30	1.4270(10)	C26	C27	1.3892(12)
C2	C3	1.5190(11)	C27	C28	1.4019(11)
C4	C5	1.4048(12)	C28	C29	1.4489(11)
C4	C9	1.4039(11)	C30	C31	1.3980(11)
C5	C6	1.3971(12)	C30	C35	1.3931(11)
C5	C10	1.5048(13)	C31	C32	1.3876(12)
C6	C7	1.3959(14)	C32	C33	1.3947(12)
C7	C8	1.3890(14)	C33	C34	1.3955(12)
C7	C11	1.5095(13)	C34	C35	1.3932(11)
C8	C9	1.3975(12)	C13	C37	1.7632(12)
C9	C12	1.5039(13)	C14	C37	1.7643(11)

**Table 3.6.7. Bond Angles for cs2919 [Ru] 2.**

Atom	Atom	Atom	Angle/°	Atom	Atom	Atom	Angle/°
C12	Ru1	C11	162.172(8)	C8	C9	C12	119.02(8)
N3	Ru1	C11	88.246(19)	C14	C13	N2	118.55(7)
N3	Ru1	C12	84.720(19)	C14	C13	C18	121.98(7)
C1	Ru1	C11	95.64(2)	C18	C13	N2	119.45(7)
C1	Ru1	C12	88.74(2)	C13	C14	C15	118.24(7)
C1	Ru1	N3	169.52(3)	C13	C14	C19	120.89(7)
C22	Ru1	C11	98.07(3)	C15	C14	C19	120.83(7)
C22	Ru1	C12	98.27(3)	C16	C15	C14	121.17(7)
C22	Ru1	N3	89.87(3)	C15	C16	C17	119.13(7)
C22	Ru1	C1	99.19(3)	C15	C16	C20	120.90(8)
C33	O1	C36	116.78(7)	C17	C16	C20	119.97(7)
C1	N1	C2	113.25(6)	C16	C17	C18	121.39(7)
C1	N1	C4	126.76(6)	C13	C18	C21	121.41(7)
C4	N1	C2	118.70(6)	C17	C18	C13	118.04(7)
C1	N2	C3	113.11(6)	C17	C18	C21	120.52(7)
C1	N2	C13	127.70(6)	C23	C22	Ru1	127.44(6)
C13	N2	C3	118.78(6)	C24	C23	C22	117.98(7)
C29	N3	Ru1	125.95(5)	C24	C23	C28	118.21(7)
C29	N3	C30	117.83(7)	C28	C23	C22	123.79(7)
C30	N3	Ru1	115.43(5)	C25	C24	C23	121.49(8)
N1	C1	Ru1	120.54(5)	C24	C25	C26	119.94(7)
N2	C1	Ru1	132.85(5)	C27	C26	C25	119.54(7)
N2	C1	N1	106.36(6)	C26	C27	C28	121.16(8)
N1	C2	C3	101.54(6)	C23	C28	C29	122.67(7)
N2	C3	C2	101.75(6)	C27	C28	C23	119.65(7)
C5	C4	N1	118.91(7)	C27	C28	C29	117.49(7)
C9	C4	N1	119.47(7)	N3	C29	C28	124.24(7)
C9	C4	C5	121.16(7)	C31	C30	N3	121.58(7)
C4	C5	C10	122.24(8)	C35	C30	N3	119.07(7)
C6	C5	C4	118.10(8)	C35	C30	C31	119.35(7)
C6	C5	C10	119.56(8)	C32	C31	C30	120.27(7)
C7	C6	C5	122.02(8)	C31	C32	C33	120.03(7)
C6	C7	C11	121.12(10)	O1	C33	C32	115.73(7)
C8	C7	C6	118.24(8)	O1	C33	C34	124.29(8)
C8	C7	C11	120.58(10)	C32	C33	C34	119.97(7)

**Table 3.6.7. Bond Angles for cs2919 [Ru] 2.**

<b>Atom</b>	<b>Atom</b>	<b>Atom</b>	<b>Angle/°</b>	<b>Atom</b>	<b>Atom</b>	<b>Atom</b>	<b>Angle/°</b>
C7	C8	C9	122.05(8)	C35	C34	C33	119.60(8)
C4	C9	C12	122.50(7)	C30	C35	C34	120.53(7)
C8	C9	C4	118.24(8)	C13	C37	C14	110.88(6)

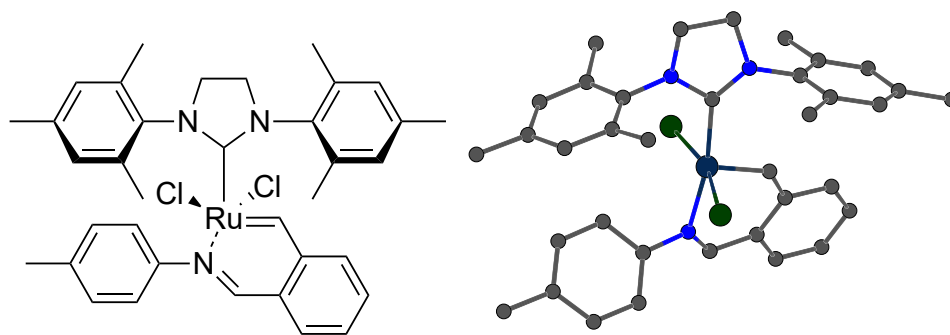
**Table 3.6.8. Torsion Angles for cs2919 [Ru] 2.**

A	B	C	D	Angle/°	A	B	C	D	Angle/°
Ru1	N3	C29	C28	-13.97(11)	C7	C8	C9	C12	-172.28(8)
Ru1	N3	C30	C31	144.91(6)	C9	C4	C5	C6	4.90(12)
Ru1	N3	C30	C35	-35.23(9)	C9	C4	C5	C10	-171.53(8)
Ru1	C22	C23	C24	-164.46(6)	C10	C5	C6	C7	174.20(9)
Ru1	C22	C23	C28	16.77(11)	C11	C7	C8	C9	177.53(9)
C11	Ru1	C22	C23	-112.96(7)	C13	N2	C1	Ru1	5.99(12)
C12	Ru1	C22	C23	59.89(7)	C13	N2	C1	N1	-179.91(7)
O1	C33	C34	C35	175.65(8)	C13	N2	C3	C2	169.39(7)
N1	C2	C3	N2	18.75(9)	C13	C14	C15	C16	-0.27(12)
N1	C4	C5	C6	177.06(7)	C14	C13	C18	C17	-1.72(11)
N1	C4	C5	C10	0.63(12)	C14	C13	C18	C21	-179.89(7)
N1	C4	C9	C8	-176.98(7)	C14	C15	C16	C17	-1.51(12)
N1	C4	C9	C12	-2.67(12)	C14	C15	C16	C20	179.30(8)
N2	C13	C14	C15	-179.40(7)	C15	C16	C17	C18	1.72(12)
N2	C13	C14	C19	-1.71(11)	C16	C17	C18	C13	-0.14(11)
N2	C13	C18	C17	179.61(7)	C16	C17	C18	C21	178.05(7)
N2	C13	C18	C21	1.44(11)	C18	C13	C14	C15	1.92(11)
N3	Ru1	C22	C23	-24.75(7)	C18	C13	C14	C19	179.60(7)
N3	C30	C31	C32	175.94(7)	C19	C14	C15	C16	-177.96(8)
N3	C30	C35	C34	-175.66(7)	C20	C16	C17	C18	-179.08(7)
C1	Ru1	C22	C23	149.95(7)	C22	C23	C24	C25	-179.47(7)
C1	N1	C2	C3	-16.59(9)	C22	C23	C28	C27	178.74(7)
C1	N1	C4	C5	109.21(9)	C22	C23	C28	C29	3.76(12)
C1	N1	C4	C9	-78.49(10)	C23	C24	C25	C26	0.85(12)
C1	N2	C3	C2	-17.45(9)	C23	C28	C29	N3	-3.86(12)
C1	N2	C13	C14	89.10(10)	C24	C23	C28	C27	-0.04(11)
C1	N2	C13	C18	-92.19(10)	C24	C23	C28	C29	-175.02(7)
C2	N1	C1	Ru1	-178.70(6)	C24	C25	C26	C27	-0.39(12)
C2	N1	C1	N2	6.32(9)	C25	C26	C27	C28	-0.27(12)
C2	N1	C4	C5	-84.69(10)	C26	C27	C28	C23	0.48(12)
C2	N1	C4	C9	87.61(10)	C26	C27	C28	C29	175.72(7)
C3	N2	C1	Ru1	-166.43(6)	C27	C28	C29	N3	-178.95(8)
C3	N2	C1	N1	7.67(9)	C28	C23	C24	C25	-0.63(11)
C3	N2	C13	C14	-98.86(9)	C29	N3	C30	C31	-44.69(11)
C3	N2	C13	C18	79.86(9)	C29	N3	C30	C35	135.17(8)

**Table 3.6.8. Torsion Angles for cs2919 [Ru] 2.**

A	B	C	D	Angle/°	A	B	C	D	Angle/°
C4	N1	C1	Ru1	-11.96(11)	C30	N3	C29	C28	176.76(7)
C4	N1	C1	N2	173.06(7)	C30	C31	C32	C33	-0.28(12)
C4	N1	C2	C3	175.50(7)	C31	C30	C35	C34	4.21(12)
C4	C5	C6	C7	-2.33(13)	C31	C32	C33	O1	-175.39(8)
C5	C4	C9	C8	-4.86(12)	C31	C32	C33	C34	4.23(12)
C5	C4	C9	C12	169.45(8)	C32	C33	C34	C35	-3.95(12)
C5	C6	C7	C8	-0.19(14)	C33	C34	C35	C30	-0.29(13)
C5	C6	C7	C11	-177.46(9)	C35	C30	C31	C32	-3.92(12)
C6	C7	C8	C9	0.24(14)	C36	O1	C33	C32	-176.85(8)
C7	C8	C9	C4	2.24(13)	C36	O1	C33	C34	3.55(12)

This report has been created with Olex2, compiled on 2022.04.07 svn.rca3783a0 for OlexSys. Please [let us know](#) if there are any errors or if you would like to have additional features.

**[Ru] 3**

## Experimental

A yellow-brown plate (mm<sup>3</sup>) was centered on the goniometer of a Rigaku Oxford Diffraction Synergy-S diffractometer equipped with a HyPix6000HE detector and operating with MoK $\alpha$  radiation. The data collection routine, unit cell refinement, and data

processing were carried out with the program CrysAlisPro.<sup>26</sup> The Laue symmetry and systematic absences were consistent with the monoclinic space group  $P2_1/c$ . The structure was solved using SHELXT<sup>27</sup> and refined using SHELXL<sup>28</sup> via Olex2.<sup>29</sup> A 2-position disorder model was used for the CH<sub>2</sub>Cl<sub>2</sub> molecule with relative occupancies that refined to 0.650(13) and 0.350(13); the SIMU instruction was used on the molecule to help maintain more chemically reasonable anisotropic displacement ellipsoids. The final refinement model involved anisotropic displacement parameters for non-hydrogen atoms and a riding model for all hydrogen atoms. Olex2<sup>30</sup> was used for molecular graphics generation.

**Table 3.6.9. Crystal data and structure refinement for cs2913 [Ru] 3.**

Identification code	HA-2-79
Empirical formula	C <sub>37</sub> H <sub>41</sub> Cl <sub>4</sub> N <sub>3</sub> Ru
Formula weight	770.60
Temperature/K	100.00(10)
Crystal system	monoclinic
Space group	$P2_1/c$
a/Å	19.2099(2)
b/Å	10.04940(10)
c/Å	19.5617(2)
$\alpha/^\circ$	90
$\beta/^\circ$	111.9240(10)
$\gamma/^\circ$	90
Volume/Å <sup>3</sup>	3503.24(7)
Z	4
$\rho_{\text{calc}}/\text{cm}^3$	1.461
$\mu/\text{mm}^{-1}$	0.783

(26) CrysAlisPro Software System, v1.171.41.105a, Rigaku Oxford Diffraction, **2021**, Rigaku Corporation, Oxford, UK.

(27) Sheldrick, G. M. "SHELXT – Integrated space-group and crystal structure determination." *Acta Cryst.* **2015**, *A71*, 3–8.

(28) Sheldrick, G. M. "Crystal structure refinement with SHELXL." *Acta Cryst.* **2015**, *C71*, 3–8.

(29) Dolomanov, O.V.; Bourhis, L. J.; Gildea, R. J.; Howard, J. A. K.; Puschmann, H. *J. Appl. Cryst.* **2009**, *42*, 339–341.

(30) Dolomanov, O.V.; Bourhis, L. J.; Gildea, R. J.; Howard, J. A. K.; Puschmann, H. *J. Appl. Cryst.* **2009**, *42*, 339–341.

F(000)	1584.0
Crystal size/mm <sup>3</sup>	0.29 × 0.15 × 0.04
Radiation	Mo K $\alpha$ ( $\lambda$ = 0.71073)
2 $\theta$ range for data collection/ $^{\circ}$	5.526 to 76.55
Index ranges	-32 $\leq$ h $\leq$ 32, -17 $\leq$ k $\leq$ 17, -32 $\leq$ l $\leq$ 32
Reflections collected	174331
Independent reflections	18642 [R <sub>int</sub> = 0.0367, R <sub>sigma</sub> = 0.0201]
Data/restraints/parameters	18642/66/441
Goodness-of-fit on F <sup>2</sup>	1.026
Final R indexes [I $\geq$ 2 $\sigma$ (I)]	R <sub>1</sub> = 0.0238, wR <sub>2</sub> = 0.0594
Final R indexes [all data]	R <sub>1</sub> = 0.0313, wR <sub>2</sub> = 0.0617
Largest diff. peak/hole / e $\text{\AA}^{-3}$	0.68/-0.50

**Table 3.6.10 Bond Lengths for cs2913 [Ru] 3.**

Atom	Atom	Length/ $\text{\AA}$	Atom	Atom	Length/ $\text{\AA}$
Ru1	C11	2.34845(19)	C14	C19	1.5046(12)
Ru1	C12	2.37853(19)	C15	C16	1.3931(12)
Ru1	N3	2.0797(7)	C16	C17	1.3950(11)
Ru1	C1	2.0616(7)	C16	C20	1.5029(12)
Ru1	C22	1.8330(8)	C17	C18	1.3949(11)
N1	C1	1.3546(10)	C18	C21	1.4995(11)
N1	C2	1.4692(11)	C22	C23	1.4516(11)
N1	C4	1.4309(11)	C23	C24	1.4052(11)
N2	C1	1.3433(10)	C23	C28	1.4166(11)
N2	C3	1.4751(11)	C24	C25	1.3892(11)
N2	C13	1.4301(10)	C25	C26	1.3933(13)
N3	C29	1.2882(10)	C26	C27	1.3877(13)
N3	C30	1.4294(11)	C27	C28	1.4001(11)
C2	C3	1.5215(13)	C28	C29	1.4484(11)
C4	C5	1.4023(12)	C30	C31	1.3917(12)
C4	C9	1.4028(13)	C30	C35	1.3930(12)
C5	C6	1.3987(13)	C31	C32	1.3948(13)
C5	C10	1.5022(14)	C32	C33	1.3886(15)
C6	C7	1.3834(16)	C33	C34	1.3921(14)
C7	C8	1.3890(16)	C33	C36	1.5058(13)
C7	C11	1.5111(14)	C34	C35	1.3879(12)
C8	C9	1.3974(13)	Cl3A	C37A	1.731(9)

**Table 3.6.10 Bond Lengths for cs2913 [Ru] 3.**

Atom	Atom	Length/Å	Atom	Atom	Length/Å
C9	C12	1.5030(14)	C14A	C37A	1.787(9)
C13	C14	1.3958(11)	C13B	C37B	1.808(18)
C13	C18	1.3989(11)	C14B	C37B	1.691(17)
C14	C15	1.3949(12)			

**Table 3.6.11. Bond Angles for cs2913 [Ru] 3.**

Atom	Atom	Atom	Angle/°	Atom	Atom	Atom	Angle/°
C11	Ru1	C12	163.696(8)	C14	C13	N2	118.49(7)
N3	Ru1	C11	85.652(19)	C14	C13	C18	122.02(7)
N3	Ru1	C12	87.47(2)	C18	C13	N2	119.49(7)
C1	Ru1	C11	88.60(2)	C13	C14	C19	120.80(8)
C1	Ru1	C12	95.73(2)	C15	C14	C13	118.25(7)
C1	Ru1	N3	169.46(3)	C15	C14	C19	120.89(8)
C22	Ru1	C11	97.66(3)	C16	C15	C14	121.30(7)
C22	Ru1	C12	97.08(2)	C15	C16	C17	118.97(7)
C22	Ru1	N3	89.79(3)	C15	C16	C20	120.88(8)
C22	Ru1	C1	99.74(3)	C17	C16	C20	120.15(8)
C1	N1	C2	113.59(7)	C18	C17	C16	121.47(7)
C1	N1	C4	126.36(7)	C13	C18	C21	121.58(7)
C4	N1	C2	118.86(7)	C17	C18	C13	117.98(7)
C1	N2	C3	113.35(7)	C17	C18	C21	120.39(7)
C1	N2	C13	127.42(7)	C23	C22	Ru1	127.38(6)
C13	N2	C3	118.84(6)	C24	C23	C22	117.81(7)
C29	N3	Ru1	127.17(6)	C24	C23	C28	118.11(7)
C29	N3	C30	118.71(7)	C28	C23	C22	124.07(7)
C30	N3	Ru1	113.65(5)	C25	C24	C23	121.55(8)
N1	C1	Ru1	119.99(5)	C24	C25	C26	119.92(8)
N2	C1	Ru1	133.29(6)	C27	C26	C25	119.61(8)
N2	C1	N1	106.51(6)	C26	C27	C28	121.14(8)
N1	C2	C3	101.63(7)	C23	C28	C29	122.50(7)
N2	C3	C2	101.98(7)	C27	C28	C23	119.67(7)
C5	C4	N1	119.35(8)	C27	C28	C29	117.68(7)
C5	C4	C9	121.40(8)	N3	C29	C28	123.83(7)

**Table 3.6.11. Bond Angles for cs2913 [Ru] 3.**

<b>Atom</b>	<b>Atom</b>	<b>Atom</b>	<b>Angle/°</b>	<b>Atom</b>	<b>Atom</b>	<b>Atom</b>	<b>Angle/°</b>
C9	C4	N1	118.90(8)	C31	C30	N3	121.55(8)
C4	C5	C10	122.39(8)	C31	C30	C35	119.80(8)
C6	C5	C4	118.00(9)	C35	C30	N3	118.63(7)
C6	C5	C10	119.37(9)	C30	C31	C32	119.59(9)
C7	C6	C5	121.98(9)	C33	C32	C31	121.24(9)
C6	C7	C8	118.56(9)	C32	C33	C34	118.26(8)
C6	C7	C11	120.39(11)	C32	C33	C36	122.01(9)
C8	C7	C11	121.02(11)	C34	C33	C36	119.72(10)
C7	C8	C9	122.04(10)	C35	C34	C33	121.40(9)
C4	C9	C12	122.34(8)	C34	C35	C30	119.63(8)
C8	C9	C4	117.86(9)	Cl3A	C37A	Cl4A	111.1(5)
C8	C9	C12	119.74(9)	Cl4B	C37B	Cl3B	111.3(10)

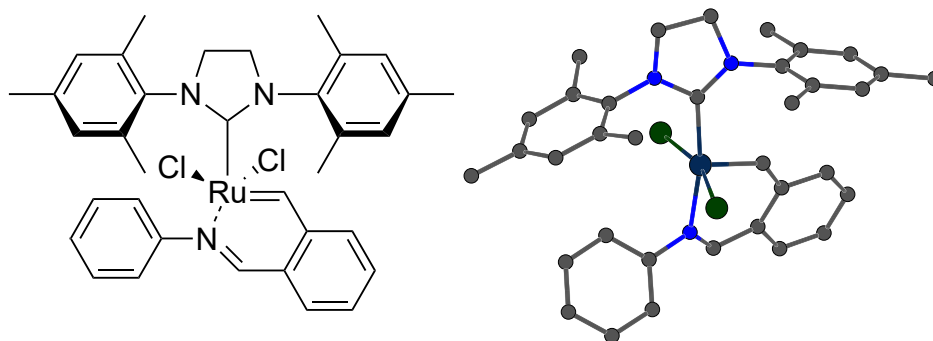
**Table 3.6.12 Torsion Angles for cs2913 [Ru] 3.**

A	B	C	D	Angle/°	A	B	C	D	Angle/°
Ru1	N3	C29	C28	11.12(11)	C7	C8	C9	C12	-174.90(10)
Ru1	N3	C30	C31	-134.39(7)	C9	C4	C5	C6	4.67(13)
Ru1	N3	C30	C35	44.29(9)	C9	C4	C5	C10	-169.70(8)
Ru1	C22	C23	C24	164.25(6)	C10	C5	C6	C7	172.06(9)
Ru1	C22	C23	C28	-17.34(11)	C11	C7	C8	C9	177.64(10)
C11	Ru1	C22	C23	-61.82(7)	C13	N2	C1	Ru1	-4.58(13)
C12	Ru1	C22	C23	111.19(7)	C13	N2	C1	N1	-179.20(8)
N1	C2	C3	N2	-16.08(10)	C13	N2	C3	C2	-171.69(8)
N1	C4	C5	C6	177.81(8)	C13	C14	C15	C16	-0.31(12)
N1	C4	C5	C10	3.44(13)	C14	C13	C18	C17	0.96(11)
N1	C4	C9	C8	-177.75(8)	C14	C13	C18	C21	178.40(7)
N1	C4	C9	C12	-0.62(13)	C14	C15	C16	C17	1.30(12)
N2	C13	C14	C15	179.76(7)	C14	C15	C16	C20	-178.97(8)
N2	C13	C14	C19	2.44(11)	C15	C16	C17	C18	-1.18(12)
N2	C13	C18	C17	-179.65(7)	C16	C17	C18	C13	0.07(11)
N2	C13	C18	C21	-2.21(11)	C16	C17	C18	C21	-177.40(8)
N3	Ru1	C22	C23	23.76(7)	C18	C13	C14	C15	-0.85(11)
N3	C30	C31	C32	-179.21(8)	C18	C13	C14	C19	-178.16(8)
N3	C30	C35	C34	178.39(8)	C19	C14	C15	C16	177.00(8)
C1	Ru1	C22	C23	-151.72(7)	C20	C16	C17	C18	179.10(8)
C1	N1	C2	C3	14.31(11)	C22	C23	C24	C25	178.99(7)
C1	N1	C4	C5	77.76(11)	C22	C23	C28	C27	-178.19(7)
C1	N1	C4	C9	-108.93(10)	C22	C23	C28	C29	-2.68(12)
C1	N2	C3	C2	14.94(11)	C23	C24	C25	C26	-0.89(12)
C1	N2	C13	C14	-90.43(10)	C23	C28	C29	N3	4.76(12)
C1	N2	C13	C18	90.16(10)	C24	C23	C28	C27	0.21(11)
C2	N1	C1	Ru1	178.98(6)	C24	C23	C28	C29	175.73(7)
C2	N1	C1	N2	-5.54(10)	C24	C25	C26	C27	0.58(12)
C2	N1	C4	C5	-88.98(10)	C25	C26	C27	C28	0.11(12)
C2	N1	C4	C9	84.33(11)	C26	C27	C28	C23	-0.51(12)
C3	N2	C1	Ru1	168.11(7)	C26	C27	C28	C29	-176.24(7)
C3	N2	C1	N1	-6.51(10)	C27	C28	C29	N3	-179.64(8)
C3	N2	C13	C14	97.24(9)	C28	C23	C24	C25	0.49(11)
C3	N2	C13	C18	-82.18(10)	C29	N3	C30	C31	52.90(11)
C4	N1	C1	Ru1	11.64(12)	C29	N3	C30	C35	-128.42(9)

**Table 3.6.12 Torsion Angles for cs2913 [Ru] 3.**

A	B	C	D	Angle/°	A	B	C	D	Angle/°
C4	N1	C1	N2	-172.88(8)	C30	N3	C29	C28	-177.26(7)
C4	N1	C2	C3	-177.32(8)	C30	C31	C32	C33	0.09(14)
C4	C5	C6	C7	-2.48(14)	C31	C30	C35	C34	-2.91(13)
C5	C4	C9	C8	-4.59(13)	C31	C32	C33	C34	-1.46(14)
C5	C4	C9	C12	172.55(9)	C31	C32	C33	C36	178.92(9)
C5	C6	C7	C8	0.30(15)	C32	C33	C34	C35	0.65(14)
C5	C6	C7	C11	-177.57(10)	C33	C34	C35	C30	1.52(14)
C6	C7	C8	C9	-0.22(16)	C35	C30	C31	C32	2.12(13)
C7	C8	C9	C4	2.32(15)	C36	C33	C34	C35	-179.72(9)

This report has been created with Olex2, compiled on 2022.04.07 svn.rca3783a0 for OlexSys. Please [let us know](#) if there are any errors or if you would like to have additional features.

**[Ru] 4**

## Experimental

A yellow-brown crystal ( $0.03 \times 0.10 \times 0.12 \text{ mm}^3$ ) was cut from a cluster of intergrown crystals and centered on the goniometer of a Rigaku Oxford Diffraction Synergy-S diffractometer equipped with a HyPix6000HE detector and operating with  $\text{CuK}\alpha$  radiation. The data collection routine, unit cell refinement, and data processing were

carried out with the program CrysAlisPro.<sup>31</sup> The Laue symmetry and systematic absences were consistent with the monoclinic space group  $P2_1/c$ . The structure was solved using SHELXT<sup>32</sup> and refined using SHELXL<sup>33</sup> via Olex2.<sup>34</sup> The final refinement model involved anisotropic displacement parameters for non-hydrogen atoms and a riding model for all hydrogen atoms. Olex2<sup>35</sup> was used for molecular graphics generation.

**Table 3.6.13. Crystal data and structure refinement for cs2849 [Ru] 4.**

Identification code	cs2849
Empirical formula	C <sub>36</sub> H <sub>39</sub> Cl <sub>4</sub> N <sub>3</sub> Ru
Formula weight	756.57
Temperature/K	100.00(10)
Crystal system	monoclinic
Space group	$P2_1/c$
a/Å	18.8082(2)
b/Å	10.19550(10)
c/Å	19.3233(2)
$\alpha/^\circ$	90
$\beta/^\circ$	112.8670(10)
$\gamma/^\circ$	90
Volume/Å <sup>3</sup>	3414.20(6)
Z	4
$\rho_{\text{calc}}/\text{cm}^3$	1.472
$\mu/\text{mm}^{-1}$	6.823
F(000)	1552.0
Crystal size/mm <sup>3</sup>	0.12 × 0.096 × 0.03
Radiation	Cu K $\alpha$ ( $\lambda = 1.54184$ )
2 $\Theta$ range for data collection/ $^\circ$	5.1 to 154.662
Index ranges	-23 ≤ h ≤ 23, -12 ≤ k ≤ 12, -24 ≤ l ≤ 24

(31) CrysAlisPro Software System, v1.171.41.105a, Rigaku Oxford Diffraction, **2021**, Rigaku Corporation, Oxford, UK.

(32) Sheldrick, G. M. "SHELXT – Integrated space-group and crystal structure determination." *Acta Cryst.* **2015**, *A71*, 3–8.

(33) Sheldrick, G. M. "Crystal structure refinement with SHELXL." *Acta Cryst.* **2015**, *C71*, 3–8.

(34) Dolomanov, O.V.; Bourhis, L. J.; Gildea, R. J.; Howard, J. A. K.; Puschmann, H. *J. Appl. Cryst.* **2009**, *42*, 339–341.

(35) Dolomanov, O.V.; Bourhis, L. J.; Gildea, R. J.; Howard, J. A. K.; Puschmann, H. *J. Appl. Cryst.* **2009**, *42*, 339–341.

Reflections collected	79800
Independent reflections	7233 [ $R_{\text{int}} = 0.0562$ , $R_{\text{sigma}} = 0.0231$ ]
Data/restraints/parameters	7233/0/403
Goodness-of-fit on $F^2$	1.066
Final R indexes [ $I \geq 2\sigma(I)$ ]	$R_1 = 0.0411$ , $wR_2 = 0.1137$
Final R indexes [all data]	$R_1 = 0.0424$ , $wR_2 = 0.1150$
Largest diff. peak/hole / $e \text{ \AA}^{-3}$	0.87/-1.65

**Table 3.6.14. Bond Lengths for cs2849 [Ru] 4.**

Atom	Atom	Length/ $\text{\AA}$	Atom	Atom	Length/ $\text{\AA}$
Ru1	C11	2.3437(6)	C13	C18	1.394(3)
Ru1	C12	2.3707(6)	C14	C15	1.399(4)
Ru1	N3	2.0968(19)	C14	C19	1.503(4)
Ru1	C1	2.078(2)	C15	C16	1.392(4)
Ru1	C22	1.839(2)	C16	C17	1.391(4)
N1	C1	1.341(3)	C16	C20	1.506(4)
N1	C2	1.477(3)	C17	C18	1.394(3)
N1	C4	1.434(3)	C18	C21	1.507(3)
N2	C1	1.342(3)	C22	C23	1.449(3)
N2	C3	1.481(3)	C23	C24	1.408(3)
N2	C13	1.431(3)	C23	C28	1.416(3)
N3	C29	1.283(3)	C24	C25	1.385(3)
N3	C30	1.431(3)	C25	C26	1.400(4)
C2	C3	1.528(4)	C26	C27	1.380(4)
C4	C5	1.399(4)	C27	C28	1.399(3)
C4	C9	1.399(4)	C28	C29	1.453(3)
C5	C6	1.397(4)	C30	C31	1.391(4)
C5	C10	1.511(4)	C30	C35	1.392(4)
C6	C7	1.389(5)	C31	C32	1.391(4)
C7	C8	1.386(5)	C32	C33	1.388(4)
C7	C11	1.508(4)	C33	C34	1.386(4)
C8	C9	1.391(4)	C34	C35	1.396(4)
C9	C12	1.512(4)	C13	C36	1.757(4)
C13	C14	1.401(3)	C14	C36	1.770(4)

**Table 3.6.15. Bond Angles for cs2849 [Ru] 4.**

Atom	Atom	Atom	Angle/°	Atom	Atom	Atom	Angle/°
C11	Ru1	C12	162.36(2)	C8	C9	C12	120.0(3)
N3	Ru1	C11	84.94(6)	C14	C13	N2	118.5(2)
N3	Ru1	C12	87.68(6)	C18	C13	N2	119.5(2)
C1	Ru1	C11	89.37(7)	C18	C13	C14	122.0(2)
C1	Ru1	C12	95.35(6)	C13	C14	C19	121.1(2)
C1	Ru1	N3	169.78(9)	C15	C14	C13	118.2(2)
C22	Ru1	C11	98.25(8)	C15	C14	C19	120.6(2)
C22	Ru1	C12	97.70(8)	C16	C15	C14	120.8(2)
C22	Ru1	N3	89.62(9)	C15	C16	C20	120.5(2)
C22	Ru1	C1	99.61(10)	C17	C16	C15	119.4(2)
C1	N1	C2	113.8(2)	C17	C16	C20	120.1(2)
C1	N1	C4	126.4(2)	C16	C17	C18	121.5(2)
C4	N1	C2	118.2(2)	C13	C18	C21	121.4(2)
C1	N2	C3	113.4(2)	C17	C18	C13	118.0(2)
C1	N2	C13	127.7(2)	C17	C18	C21	120.6(2)
C13	N2	C3	118.40(19)	C23	C22	Ru1	127.44(17)
C29	N3	Ru1	125.94(17)	C24	C23	C22	117.9(2)
C29	N3	C30	118.2(2)	C24	C23	C28	118.0(2)
C30	N3	Ru1	115.41(15)	C28	C23	C22	124.1(2)
N1	C1	Ru1	120.19(17)	C25	C24	C23	121.6(2)
N1	C1	N2	106.9(2)	C24	C25	C26	119.9(2)
N2	C1	Ru1	132.75(18)	C27	C26	C25	119.4(2)
N1	C2	C3	101.5(2)	C26	C27	C28	121.5(2)
N2	C3	C2	101.6(2)	C23	C28	C29	122.2(2)
C5	C4	N1	119.2(2)	C27	C28	C23	119.5(2)
C5	C4	C9	121.3(2)	C27	C28	C29	117.9(2)
C9	C4	N1	119.3(2)	N3	C29	C28	124.6(2)
C4	C5	C10	122.4(2)	C31	C30	N3	120.6(2)
C6	C5	C4	118.1(3)	C31	C30	C35	120.3(2)
C6	C5	C10	119.4(3)	C35	C30	N3	119.1(2)
C7	C6	C5	121.9(3)	C30	C31	C32	119.8(3)
C6	C7	C11	121.2(3)	C33	C32	C31	120.3(3)
C8	C7	C6	118.2(3)	C34	C33	C32	119.7(2)
C8	C7	C11	120.6(3)	C33	C34	C35	120.6(3)
C7	C8	C9	122.2(3)	C30	C35	C34	119.2(3)

**Table 3.6.15. Bond Angles for cs2849 [Ru] 4.**

<b>Atom</b>	<b>Atom</b>	<b>Atom</b>	<b>Angle/°</b>	<b>Atom</b>	<b>Atom</b>	<b>Atom</b>	<b>Angle/°</b>
C4	C9	C12	121.7(2)	C13	C36	C14	110.77(19)
C8	C9	C4	118.1(3)				

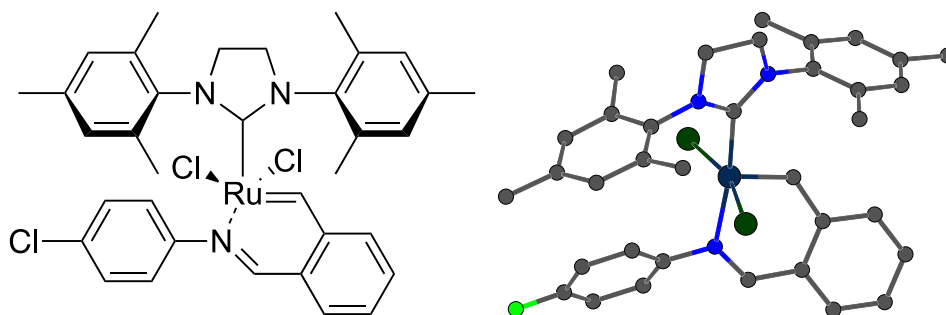
**Table 3.6.16. Torsion Angles for cs2849 [Ru] 4.**

A	B	C	D	Angle/°	A	B	C	D	Angle/°
Ru1	N3	C29	C28	13.3(3)	C7	C8	C9	C4	-2.4(4)
Ru1	N3	C30	C31	-139.88(19)	C7	C8	C9	C12	172.8(3)
Ru1	N3	C30	C35	39.7(3)	C9	C4	C5	C6	-4.6(4)
Ru1	C22	C23	C24	164.97(19)	C9	C4	C5	C10	171.8(2)
Ru1	C22	C23	C28	-16.1(4)	C10	C5	C6	C7	-174.5(3)
C11	Ru1	C22	C23	-60.2(2)	C11	C7	C8	C9	-177.2(3)
C12	Ru1	C22	C23	112.3(2)	C13	N2	C1	Ru1	-2.5(4)
N1	C2	C3	N2	-15.6(3)	C13	N2	C1	N1	-178.1(2)
N1	C4	C5	C6	-179.3(2)	C13	N2	C3	C2	-172.9(2)
N1	C4	C5	C10	-3.0(4)	C13	C14	C15	C16	0.4(4)
N1	C4	C9	C8	179.5(2)	C14	C13	C18	C17	1.3(3)
N1	C4	C9	C12	4.5(4)	C14	C13	C18	C21	179.5(2)
N2	C13	C14	C15	178.3(2)	C14	C15	C16	C17	1.3(4)
N2	C13	C14	C19	1.0(3)	C14	C15	C16	C20	-179.7(2)
N2	C13	C18	C17	-178.8(2)	C15	C16	C17	C18	-1.8(4)
N2	C13	C18	C21	-0.5(3)	C16	C17	C18	C13	0.6(4)
N3	Ru1	C22	C23	24.6(2)	C16	C17	C18	C21	-177.7(2)
N3	C30	C31	C32	-178.9(2)	C18	C13	C14	C15	-1.8(4)
N3	C30	C35	C34	178.3(2)	C18	C13	C14	C19	-179.1(2)
C1	Ru1	C22	C23	-150.9(2)	C19	C14	C15	C16	177.8(2)
C1	N1	C2	C3	14.0(3)	C20	C16	C17	C18	179.1(2)
C1	N1	C4	C5	-107.8(3)	C22	C23	C24	C25	179.5(2)
C1	N1	C4	C9	77.3(3)	C22	C23	C28	C27	-178.6(2)
C1	N2	C3	C2	14.6(3)	C22	C23	C28	C29	-5.0(4)
C1	N2	C13	C14	-89.9(3)	C23	C24	C25	C26	-1.0(4)
C1	N2	C13	C18	90.2(3)	C23	C28	C29	N3	5.1(4)
C2	N1	C1	Ru1	178.31(17)	C24	C23	C28	C27	0.3(3)
C2	N1	C1	N2	-5.5(3)	C24	C23	C28	C29	173.9(2)
C2	N1	C4	C5	87.6(3)	C24	C25	C26	C27	0.6(4)
C2	N1	C4	C9	-87.2(3)	C25	C26	C27	C28	0.2(4)
C3	N2	C1	Ru1	169.19(19)	C26	C27	C28	C23	-0.7(4)
C3	N2	C1	N1	-6.4(3)	C26	C27	C28	C29	-174.6(2)
C3	N2	C13	C14	98.8(3)	C27	C28	C29	N3	178.8(2)
C3	N2	C13	C18	-81.2(3)	C28	C23	C24	C25	0.5(4)
C4	N1	C1	Ru1	13.2(3)	C29	N3	C30	C31	47.4(3)

**Table 3.6.16. Torsion Angles for cs2849 [Ru] 4.**

A	B	C	D	Angle/°	A	B	C	D	Angle/°
C4	N1	C1	N2	-170.6(2)	C29	N3	C30	C35	-133.1(2)
C4	N1	C2	C3	-179.5(2)	C30	N3	C29	C28	-174.7(2)
C4	C5	C6	C7	1.9(4)	C30	C31	C32	C33	0.2(4)
C5	C4	C9	C8	4.8(4)	C31	C30	C35	C34	-2.1(4)
C5	C4	C9	C12	-170.3(2)	C31	C32	C33	C34	-1.3(4)
C5	C6	C7	C8	0.4(4)	C32	C33	C34	C35	0.7(4)
C5	C6	C7	C11	177.4(3)	C33	C34	C35	C30	1.0(4)
C6	C7	C8	C9	-0.2(4)	C35	C30	C31	C32	1.5(4)

This report has been created with Olex2, compiled on 2022.04.07 svn.rca3783a0 for OlexSys. Please [let us know](#) if there are any errors or if you would like to have additional features.



**[Ru] 5**

## Experimental

A blue plate (0.02 x 0.14 x 0.32 mm<sup>3</sup>) was centered on the goniometer of a Rigaku Oxford Diffraction Synergy-S diffractometer equipped with a HyPix6000HE detector and operating with MoK $\alpha$  radiation. The data collection routine, unit cell refinement, and data processing were carried out with the program CrysAlisPro.<sup>36</sup> The Laue symmetry and

---

(36) CrysAlisPro Software System, v1.171.41.105a, Rigaku Oxford Diffraction, 2021, Rigaku Corporation, Oxford, UK.

systematic absences were consistent with the monoclinic space group  $P2_1/c$ . The structure was solved using SHELXT<sup>37</sup> and refined using SHELXL<sup>38</sup> via Olex2.<sup>39</sup> A 2-position disorder model was used for the SIMes ligand, with relative occupancies refining to 0.828(4) and 0.172(4). The atom positions in the disordered region were restrained with the SAME command and the related displacement parameters constrained with EADP. The final refinement model involved anisotropic displacement parameters for all non-hydrogen atoms and a riding model for all hydrogen atoms. Olex2<sup>40</sup> was used for molecular graphics generation.

**Table 3.6.17. Crystal data and structure refinement for cs2907 [Ru] 5.**

Identification code	HA-2-77
Empirical formula	C <sub>35</sub> H <sub>36</sub> Cl <sub>3</sub> N <sub>3</sub> Ru • CHCl <sub>3</sub>
Formula weight	825.45
Temperature/K	99.99(13)
Crystal system	monoclinic
Space group	P2 <sub>1</sub> /c
a/Å	19.1899(3)
b/Å	10.21291(12)
c/Å	19.6967(3)
α/°	90
β/°	112.3088(19)
γ/°	90
Volume/Å <sup>3</sup>	3571.33(10)
Z	4
ρ <sub>calc</sub> /cm <sup>3</sup>	1.535
μ/mm <sup>-1</sup>	0.919
F(000)	1680.0

(37) Sheldrick, G. M. "SHELXT – Integrated space-group and crystal structure determination." *Acta Cryst.* **2015**, *A71*, 3–8.

(38) Sheldrick, G. M. "Crystal structure refinement with SHELXL." *Acta Cryst.* **2015**, *C71*, 3–8.

(39) Dolomanov, O.V.; Bourhis, L. J.; Gildea, R. J.; Howard, J. A. K.; Puschmann, H. *J. Appl. Cryst.* **2009**, *42*, 339–341.

(40) Dolomanov, O.V.; Bourhis, L. J.; Gildea, R. J.; Howard, J. A. K.; Puschmann, H. *J. Appl. Cryst.* **2009**, *42*, 339–341.

Crystal size/mm <sup>3</sup>	0.324 × 0.136 × 0.024
Radiation	Mo K $\alpha$ ( $\lambda$ = 0.71073)
2 $\Theta$ range for data collection/ $^{\circ}$	5.046 to 76.408
Index ranges	-33 $\leq$ h $\leq$ 32, -17 $\leq$ k $\leq$ 17, -33 $\leq$ l $\leq$ 32
Reflections collected	110181
Independent reflections	18792 [ $R_{\text{int}}$ = 0.0509, $R_{\text{sigma}}$ = 0.0402]
Data/restraints/parameters	18792/10/437
Goodness-of-fit on F <sup>2</sup>	1.030
Final R indexes [ $I \geq 2\sigma(I)$ ]	$R_1$ = 0.0415, $wR_2$ = 0.0857
Final R indexes [all data]	$R_1$ = 0.0651, $wR_2$ = 0.0925
Largest diff. peak/hole / e $\text{\AA}^{-3}$	1.33/-1.19

**Table 3.6.18. Bond Lengths for cs2907 [Ru] 5.**

Atom	Atom	Length/ $\text{\AA}$	Atom	Atom	Length/ $\text{\AA}$
Ru1	C11	2.3465(4)	C7	C11	1.511(3)
Ru1	C12	2.3721(4)	C8	C9	1.391(3)
Ru1	C1A	2.065(2)	C9	C12	1.506(3)
Ru1	C1B	2.007(13)	C13	C14	1.391(2)
Ru1	N3	2.0866(12)	C13	C18	1.396(2)
Ru1	C22	1.8291(15)	C14	C15	1.390(3)
C13	C33	1.7325(16)	C14	C19	1.507(3)
C1A	N1A	1.353(3)	C15	C16	1.393(3)
C1A	N2A	1.345(3)	C16	C17	1.388(2)
N1A	C2A	1.470(3)	C16	C20	1.505(2)
N1A	C4	1.434(3)	C17	C18	1.391(2)
C2A	C3A	1.519(3)	C18	C21	1.504(2)
C3A	N2A	1.473(3)	C22	C23	1.451(2)
N2A	C13	1.441(2)	C23	C24	1.403(2)
C1B	N1B	1.352(13)	C23	C28	1.417(2)
C1B	N2B	1.344(13)	C24	C25	1.389(2)
N1B	C2B	1.472(12)	C25	C26	1.393(2)
N1B	C4	1.496(11)	C26	C27	1.382(2)
C2B	C3B	1.536(12)	C27	C28	1.403(2)
C3B	N2B	1.489(11)	C28	C29	1.446(2)
N2B	C13	1.431(9)	C30	C31	1.388(2)
N3	C29	1.2867(19)	C30	C35	1.392(2)
N3	C30	1.4284(19)	C31	C32	1.391(2)

**Table 3.6.18. Bond Lengths for cs2907 [Ru] 5.**

Atom	Atom	Length/Å	Atom	Atom	Length/Å
C4	C5	1.395(3)	C32	C33	1.383(3)
C4	C9	1.398(3)	C33	C34	1.384(2)
C5	C6	1.398(3)	C34	C35	1.383(2)
C5	C10	1.504(3)	C14	C36	1.756(2)
C6	C7	1.387(3)	C15	C36	1.759(2)
C7	C8	1.377(3)	C16	C36	1.755(2)

**Table 3.6.19. Bond Angles for cs2907 [Ru] 5.**

Atom	Atom	Atom	Angle/°	Atom	Atom	Atom	Angle/°
C11	Ru1	C12	162.568(15)	C6	C7	C11	120.3(2)
C1A	Ru1	C11	88.55(6)	C8	C7	C6	118.27(17)
C1A	Ru1	C12	96.18(6)	C8	C7	C11	121.4(2)
C1A	Ru1	N3	169.77(7)	C7	C8	C9	122.48(19)
C1B	Ru1	C11	97.8(4)	C4	C9	C12	123.36(19)
C1B	Ru1	C12	87.1(4)	C8	C9	C4	117.71(18)
C1B	Ru1	N3	170.1(4)	C8	C9	C12	118.9(2)
N3	Ru1	C11	85.58(3)	C14	C13	N2A	121.23(16)
N3	Ru1	C12	87.09(4)	C14	C13	N2B	101.2(5)
C22	Ru1	C11	97.34(5)	C14	C13	C18	122.06(15)
C22	Ru1	C12	98.43(5)	C18	C13	N2A	116.67(17)
C22	Ru1	C1A	99.28(8)	C18	C13	N2B	136.7(5)
C22	Ru1	C1B	98.9(4)	C13	C14	C19	119.90(18)
C22	Ru1	N3	89.79(6)	C15	C14	C13	118.20(15)
N1A	C1A	Ru1	119.73(16)	C15	C14	C19	121.87(18)
N2A	C1A	Ru1	133.59(17)	C14	C15	C16	121.34(16)
N2A	C1A	N1A	106.56(19)	C15	C16	C20	119.41(17)
C1A	N1A	C2A	113.58(19)	C17	C16	C15	118.89(15)
C1A	N1A	C4	126.21(18)	C17	C16	C20	121.69(17)
C4	N1A	C2A	118.60(17)	C16	C17	C18	121.56(15)
N1A	C2A	C3A	101.64(16)	C13	C18	C21	122.42(16)
N2A	C3A	C2A	102.20(16)	C17	C18	C13	117.91(15)
C1A	N2A	C3A	113.23(17)	C17	C18	C21	119.60(16)
C1A	N2A	C13	127.36(17)	C23	C22	Ru1	127.28(11)
C13	N2A	C3A	119.20(16)	C24	C23	C22	117.87(13)
N1B	C1B	Ru1	119.6(9)	C24	C23	C28	118.27(13)

**Table 3.6.19. Bond Angles for cs2907 [Ru] 5.**

Atom	Atom	Atom	Angle/°	Atom	Atom	Atom	Angle/°
N2B	C1B	Ru1	135.0(9)	C28	C23	C22	123.85(13)
N2B	C1B	N1B	105.4(10)	C25	C24	C23	121.56(15)
C1B	N1B	C2B	115.1(10)	C24	C25	C26	119.70(15)
C1B	N1B	C4	127.3(9)	C27	C26	C25	119.93(14)
C2B	N1B	C4	117.6(8)	C26	C27	C28	121.12(15)
N1B	C2B	C3B	102.1(8)	C23	C28	C29	122.80(13)
N2B	C3B	C2B	101.2(7)	C27	C28	C23	119.41(14)
C1B	N2B	C3B	115.2(9)	C27	C28	C29	117.64(13)
C1B	N2B	C13	126.9(9)	N3	C29	C28	123.79(13)
C13	N2B	C3B	113.9(7)	C31	C30	N3	121.66(14)
C29	N3	Ru1	126.70(10)	C31	C30	C35	119.80(14)
C29	N3	C30	118.55(12)	C35	C30	N3	118.52(13)
C30	N3	Ru1	114.24(9)	C30	C31	C32	120.28(16)
C5	C4	N1A	121.86(18)	C33	C32	C31	119.02(15)
C5	C4	N1B	103.4(5)	C32	C33	C13	120.27(13)
C5	C4	C9	121.70(16)	C32	C33	C34	121.20(15)
C9	C4	N1A	115.96(18)	C34	C33	C13	118.51(13)
C9	C4	N1B	134.5(5)	C35	C34	C33	119.51(16)
C4	C5	C6	117.63(17)	C34	C35	C30	120.04(15)
C4	C5	C10	121.54(18)	C14	C36	C15	110.46(10)
C6	C5	C10	120.48(19)	C16	C36	C14	111.48(10)
C7	C6	C5	122.00(18)	C16	C36	C15	110.05(12)

**Table 3.6.20. Torsion Angles for cs2907 [Ru] 5.**

A	B	C	D	Angle/°	A	B	C	D	Angle/°
Ru1	C1A	N1A	C2A	-178.15(17)	C3B	N2B	C13	C18	93.2(10)
Ru1	C1A	N1A	C4	-12.9(3)	N2B	C1B	N1B	C2B	5.0(15)
Ru1	C1A	N2A	C3A	-169.43(18)	N2B	C1B	N1B	C4	-171.5(9)
Ru1	C1A	N2A	C13	5.3(3)	N2B	C13	C14	C15	-175.8(4)
Ru1	C1B	N1B	C2B	-175.7(9)	N2B	C13	C14	C19	2.3(4)
Ru1	C1B	N1B	C4	7.8(16)	N2B	C13	C18	C17	174.6(5)
Ru1	C1B	N2B	C3B	-177.3(11)	N2B	C13	C18	C21	-2.4(6)
Ru1	C1B	N2B	C13	-21.2(19)	N3	Ru1	C22	C23	-24.77(13)

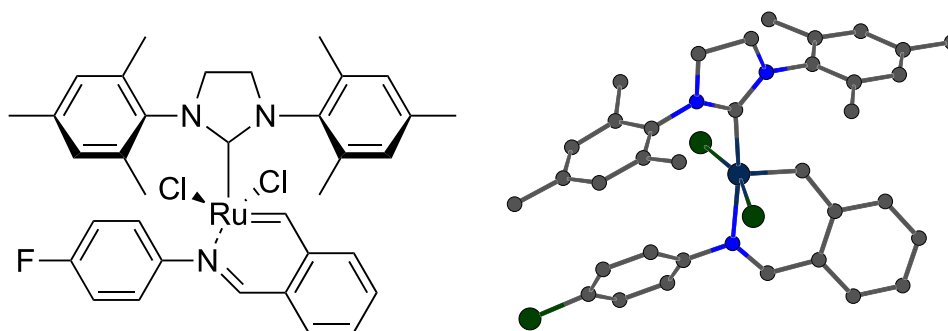
**Table 3.6.20. Torsion Angles for cs2907 [Ru] 5.**

A	B	C	D	Angle/°	A	B	C	D	Angle/°
Ru1	N3	C29	C28	-12.2(2)	N3	C30	C31	C32	178.14(15)
Ru1	N3	C30	C31	136.57(13)	N3	C30	C35	C34	-178.05(14)
Ru1	N3	C30	C35	-41.79(16)	C4	N1A	C2A	C3A	179.7(2)
Ru1	C22	C23	C24	-163.33(12)	C4	N1B	C2B	C3B	167.6(10)
Ru1	C22	C23	C28	17.8(2)	C4	C5	C6	C7	3.0(3)
C11	Ru1	C22	C23	60.74(13)	C5	C4	C9	C8	5.0(3)
C12	Ru1	C22	C23	-111.81(13)	C5	C4	C9	C12	-172.30(19)
C13	C33	C34	C35	175.52(13)	C5	C6	C7	C8	-0.3(3)
C1A	Ru1	C22	C23	150.47(14)	C5	C6	C7	C11	177.25(19)
C1A	N1A	C2A	C3A	-13.9(3)	C6	C7	C8	C9	-0.1(3)
C1A	N1A	C4	C5	-77.7(3)	C7	C8	C9	C4	-2.2(3)
C1A	N1A	C4	C9	110.1(2)	C7	C8	C9	C12	175.2(2)
C1A	N2A	C13	C14	90.2(2)	C9	C4	C5	C6	-5.4(2)
C1A	N2A	C13	C18	-92.3(2)	C9	C4	C5	C10	167.90(17)
N1A	C1A	N2A	C3A	6.4(3)	C10	C5	C6	C7	-170.34(18)
N1A	C1A	N2A	C13	-178.9(2)	C11	C7	C8	C9	-177.6(2)
N1A	C2A	C3A	N2A	15.7(3)	C13	C14	C15	C16	0.1(2)
N1A	C4	C5	C6	-177.16(16)	C14	C13	C18	C17	-2.0(2)
N1A	C4	C5	C10	-3.9(3)	C14	C13	C18	C21	-178.93(16)
N1A	C4	C9	C8	177.22(17)	C14	C15	C16	C17	-1.6(2)
N1A	C4	C9	C12	0.0(3)	C14	C15	C16	C20	179.04(16)
C2A	N1A	C4	C5	86.9(3)	C15	C16	C17	C18	1.4(2)
C2A	N1A	C4	C9	-85.3(3)	C16	C17	C18	C13	0.3(2)
C2A	C3A	N2A	C1A	-14.6(3)	C16	C17	C18	C21	177.38(15)
C2A	C3A	N2A	C13	170.2(2)	C18	C13	C14	C15	1.8(2)
C3A	N2A	C13	C14	-95.4(2)	C18	C13	C14	C19	179.90(16)
C3A	N2A	C13	C18	82.1(2)	C19	C14	C15	C16	-178.02(16)
N2A	C1A	N1A	C2A	5.3(3)	C20	C16	C17	C18	-179.27(15)
N2A	C1A	N1A	C4	170.5(2)	C22	C23	C24	C25	-179.26(14)
N2A	C13	C14	C15	179.18(15)	C22	C23	C28	C27	178.32(14)
N2A	C13	C14	C19	-2.7(2)	C22	C23	C28	C29	3.0(2)
N2A	C13	C18	C17	-179.49(14)	C23	C24	C25	C26	1.1(2)
N2A	C13	C18	C21	3.5(2)	C23	C28	C29	N3	-4.6(2)
C1B	Ru1	C22	C23	159.9(4)	C24	C23	C28	C27	-0.6(2)
C1B	N1B	C2B	C3B	-9.2(16)	C24	C23	C28	C29	-175.88(14)

**Table 3.6.20. Torsion Angles for cs2907 [Ru] 5.**

A	B	C	D	Angle/°	A	B	C	D	Angle/°
C1B	N1B	C4	C5	-98.6(12)	C24	C25	C26	C27	-1.1(2)
C1B	N1B	C4	C9	88.7(12)	C25	C26	C27	C28	0.2(2)
C1B	N2B	C13	C14	113.9(11)	C26	C27	C28	C23	0.6(2)
C1B	N2B	C13	C18	-63.1(13)	C26	C27	C28	C29	176.18(14)
N1B	C1B	N2B	C3B	1.9(15)	C27	C28	C29	N3	179.96(14)
N1B	C1B	N2B	C13	157.9(9)	C28	C23	C24	C25	-0.3(2)
N1B	C2B	C3B	N2B	8.9(14)	C29	N3	C30	C31	-51.0(2)
N1B	C4	C5	C6	-179.3(4)	C29	N3	C30	C35	130.60(15)
N1B	C4	C5	C10	-6.1(4)	C30	N3	C29	C28	176.48(13)
N1B	C4	C9	C8	176.7(6)	C30	C31	C32	C33	0.3(3)
N1B	C4	C9	C12	-0.5(6)	C31	C30	C35	C34	3.6(2)
C2B	N1B	C4	C5	85.0(10)	C31	C32	C33	C13	-175.46(14)
C2B	N1B	C4	C9	-87.8(11)	C31	C32	C33	C34	3.0(3)
C2B	C3B	N2B	C1B	-7.2(15)	C32	C33	C34	C35	-3.0(3)
C2B	C3B	N2B	C13	-166.4(10)	C33	C34	C35	C30	-0.3(2)
C3B	N2B	C13	C14	-89.7(9)	C35	C30	C31	C32	-3.5(2)

This report has been created with Olex2, compiled on 2022.04.07 svn.rca3783a0 for OlexSys. Please [let us know](#) if there are any errors or if you would like to have additional features.

**[Ru] 6**

## Experimental

A blue prism (0.13 x 0.17 x 0.21 mm<sup>3</sup>) was centered on the goniometer of a Rigaku Oxford Diffraction Synergy-S diffractometer equipped with a HyPix6000HE detector and

operating with MoK $\alpha$  radiation. The data collection routine, unit cell refinement, and data processing were carried out with the program CrysAlisPro.<sup>41</sup> The Laue symmetry and systematic absences were consistent with the monoclinic space group  $P2_1/c$ . The structure was solved using SHELXT<sup>42</sup> and refined using SHELXL<sup>43</sup> via Olex2.<sup>44</sup> The final refinement model involved anisotropic displacement parameters for non-hydrogen atoms and a riding model for all hydrogen atoms. Olex2<sup>45</sup> was used for molecular graphics generation.

**Table 3.6.21. Crystal data and structure refinement for cs2931 [Ru] 6.**

Identification code	cs2931
Empirical formula	C <sub>35</sub> H <sub>36</sub> Cl <sub>2</sub> FN <sub>3</sub> Ru • CH <sub>2</sub> Cl <sub>2</sub>
Formula weight	774.56
Temperature/K	100.01(11)
Crystal system	monoclinic
Space group	$P2_1/c$
a/Å	18.8331(2)
b/Å	10.15690(10)
c/Å	19.3756(2)
$\alpha$ /°	90
$\beta$ /°	113.2190(10)
$\gamma$ /°	90
Volume/Å <sup>3</sup>	3406.09(6)
Z	4
$\rho_{\text{calc}}/\text{cm}^3$	1.510
$\mu/\text{mm}^{-1}$	0.810
F(000)	1584.0

(41) CrysAlisPro Software System, v1.171.42.xx, Rigaku Oxford Diffraction, 2022, Rigaku Corporation, Oxford, UK.

(42) Sheldrick, G. M. "SHELXT – Integrated space-group and crystal structure determination." *Acta Cryst.* **2015**, *A71*, 3–8.

(43) Sheldrick, G. M. "Crystal structure refinement with SHELXL." *Acta Cryst.* **2015**, *C71*, 3–8.

(44) Dolomanov, O.V.; Bourhis, L. J.; Gildea, R. J.; Howard, J. A. K.; Puschmann, H. *J. Appl. Cryst.* **2009**, *42*, 339–341.

(45) Dolomanov, O.V.; Bourhis, L. J.; Gildea, R. J.; Howard, J. A. K.; Puschmann, H. *J. Appl. Cryst.* **2009**, *42*, 339–341.

Crystal size/mm <sup>3</sup>	0.21 × 0.17 × 0.13
Radiation	Mo K $\alpha$ ( $\lambda$ = 0.71073)
2 $\theta$ range for data collection/°	5.578 to 76.578
Index ranges	-32 ≤ h ≤ 31, -17 ≤ k ≤ 17, -32 ≤ l ≤ 33
Reflections collected	169607
Independent reflections	17992 [R <sub>int</sub> = 0.0298, R <sub>sigma</sub> = 0.0150]
Data/restraints/parameters	17992/0/412
Goodness-of-fit on F <sup>2</sup>	1.033
Final R indexes [I ≥ 2 $\sigma$ (I)]	R <sub>1</sub> = 0.0214, wR <sub>2</sub> = 0.0550
Final R indexes [all data]	R <sub>1</sub> = 0.0247, wR <sub>2</sub> = 0.0562
Largest diff. peak/hole / e Å <sup>-3</sup>	0.87/-0.75

**Table 3.6.22. Bond Lengths for cs2931 [Ru] 6.**

Atom	Atom	Length/Å	Atom	Atom	Length/Å
Ru1	C11	2.37291(18)	C13	C18	1.4010(10)
Ru1	C12	2.34528(18)	C14	C15	1.3970(11)
Ru1	N3	2.0899(6)	C14	C19	1.5049(11)
Ru1	C1	2.0683(7)	C15	C16	1.3936(11)
Ru1	C22	1.8337(7)	C16	C17	1.3942(11)
F1	C33	1.3526(10)	C16	C20	1.5046(11)
N1	C1	1.3541(9)	C17	C18	1.3959(10)
N1	C2	1.4706(10)	C18	C21	1.5005(10)
N1	C4	1.4292(9)	C22	C23	1.4513(10)
N2	C1	1.3456(9)	C23	C24	1.4064(10)
N2	C3	1.4748(10)	C23	C28	1.4162(10)
N2	C13	1.4274(9)	C24	C25	1.3909(11)
N3	C29	1.2910(9)	C25	C26	1.3934(12)
N3	C30	1.4289(9)	C26	C27	1.3894(11)
C2	C3	1.5207(11)	C27	C28	1.4012(10)
C4	C5	1.4039(11)	C28	C29	1.4492(10)
C4	C9	1.4023(11)	C30	C31	1.3943(11)
C5	C6	1.3943(12)	C30	C35	1.3960(11)
C5	C10	1.5038(12)	C31	C32	1.3932(12)
C6	C7	1.3882(15)	C32	C33	1.3788(14)
C7	C8	1.3908(15)	C33	C34	1.3798(13)
C7	C11	1.5084(13)	C34	C35	1.3917(11)
C8	C9	1.3979(12)	C13	C36	1.7599(12)

**Table 3.6.22. Bond Lengths for cs2931 [Ru] 6.**

Atom	Atom	Length/Å	Atom	Atom	Length/Å
C9	C12	1.5029(13)	C14	C36	1.7685(13)
C13	C14	1.3979(10)			

**Table 3.6.23. Bond Angles for cs2931 [Ru] 6.**

Atom	Atom	Atom	Angle/°	Atom	Atom	Atom	Angle/°
C12	Ru1	C11	162.689(7)	C14	C13	N2	118.65(6)
N3	Ru1	C11	87.534(18)	C14	C13	C18	122.05(6)
N3	Ru1	C12	84.876(18)	C18	C13	N2	119.30(6)
C1	Ru1	C11	95.749(19)	C13	C14	C19	121.07(7)
C1	Ru1	C12	89.21(2)	C15	C14	C13	118.21(7)
C1	Ru1	N3	169.54(3)	C15	C14	C19	120.68(7)
C22	Ru1	C11	97.47(2)	C16	C15	C14	121.17(7)
C22	Ru1	C12	98.04(2)	C15	C16	C17	119.19(7)
C22	Ru1	N3	89.83(3)	C15	C16	C20	120.91(7)
C22	Ru1	C1	99.55(3)	C17	C16	C20	119.89(7)
C1	N1	C2	113.57(6)	C16	C17	C18	121.44(7)
C1	N1	C4	125.75(6)	C13	C18	C21	121.36(6)
C4	N1	C2	118.69(6)	C17	C18	C13	117.91(6)
C1	N2	C3	113.22(6)	C17	C18	C21	120.68(7)
C1	N2	C13	127.11(6)	C23	C22	Ru1	127.48(5)
C13	N2	C3	119.13(6)	C24	C23	C22	117.82(6)
C29	N3	Ru1	126.10(5)	C24	C23	C28	118.22(6)
C29	N3	C30	117.68(6)	C28	C23	C22	123.94(6)
C30	N3	Ru1	115.59(5)	C25	C24	C23	121.42(7)
N1	C1	Ru1	120.08(5)	C24	C25	C26	119.97(7)
N2	C1	Ru1	133.29(5)	C27	C26	C25	119.61(7)
N2	C1	N1	106.48(6)	C26	C27	C28	121.11(7)
N1	C2	C3	101.51(6)	C23	C28	C29	122.59(6)
N2	C3	C2	102.03(6)	C27	C28	C23	119.66(7)
C5	C4	N1	118.97(7)	C27	C28	C29	117.54(6)
C9	C4	N1	119.14(7)	N3	C29	C28	124.21(6)
C9	C4	C5	121.58(7)	C31	C30	N3	121.09(7)

**Table 3.6.23. Bond Angles for cs2931 [Ru] 6.**

<b>Atom</b>	<b>Atom</b>	<b>Atom</b>	<b>Angle/°</b>	<b>Atom</b>	<b>Atom</b>	<b>Atom</b>	<b>Angle/°</b>
C4	C5	C10	122.04(7)	C31	C30	C35	120.01(7)
C6	C5	C4	117.95(8)	C35	C30	N3	118.90(7)
C6	C5	C10	119.83(8)	C32	C31	C30	120.27(8)
C7	C6	C5	122.02(8)	C33	C32	C31	118.29(8)
C6	C7	C8	118.49(8)	F1	C33	C32	118.91(8)
C6	C7	C11	120.45(10)	F1	C33	C34	118.33(9)
C8	C7	C11	121.01(10)	C32	C33	C34	122.77(8)
C7	C8	C9	121.99(8)	C33	C34	C35	118.70(8)
C4	C9	C12	122.49(7)	C34	C35	C30	119.85(8)
C8	C9	C4	117.77(8)	Cl3	C36	Cl4	110.67(6)
C8	C9	C12	119.67(8)				

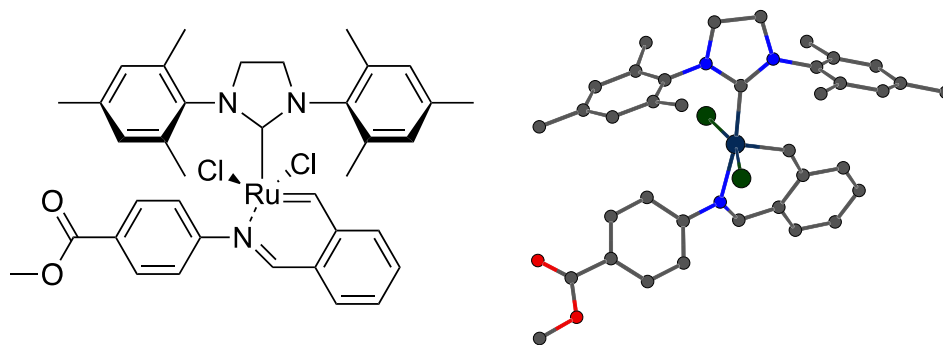
**Table 3.6.24. Torsion Angles for cs2931 [Ru] 6.**

A	B	C	D	Angle/°	A	B	C	D	Angle/°
Ru1	N3	C29	C28	-13.65(10)	C7	C8	C9	C4	-2.66(13)
Ru1	N3	C30	C31	140.58(6)	C7	C8	C9	C12	174.20(8)
Ru1	N3	C30	C35	-39.16(8)	C9	C4	C5	C6	-5.03(12)
Ru1	C22	C23	C24	-165.10(6)	C9	C4	C5	C10	170.07(8)
Ru1	C22	C23	C28	16.22(10)	C10	C5	C6	C7	-173.13(8)
C11	Ru1	C22	C23	-111.76(6)	C11	C7	C8	C9	-177.67(9)
C12	Ru1	C22	C23	60.54(6)	C13	N2	C1	Ru1	2.45(12)
F1	C33	C34	C35	178.11(8)	C13	N2	C1	N1	177.89(7)
N1	C2	C3	N2	16.78(8)	C13	N2	C3	C2	172.45(7)
N1	C4	C5	C6	-178.51(7)	C13	C14	C15	C16	-0.24(11)
N1	C4	C5	C10	-3.40(11)	C14	C13	C18	C17	-1.58(10)
N1	C4	C9	C8	178.77(7)	C14	C13	C18	C21	-179.22(7)
N1	C4	C9	C12	2.00(11)	C14	C15	C16	C17	-1.29(11)
N2	C13	C14	C15	-178.91(6)	C14	C15	C16	C20	179.45(7)
N2	C13	C14	C19	-1.23(10)	C15	C16	C17	C18	1.42(11)
N2	C13	C18	C17	179.04(6)	C16	C17	C18	C13	-0.02(11)
N2	C13	C18	C21	1.39(10)	C16	C17	C18	C21	177.64(7)
N3	Ru1	C22	C23	-24.26(6)	C18	C13	C14	C15	1.71(10)
N3	C30	C31	C32	177.30(7)	C18	C13	C14	C19	179.38(7)
N3	C30	C35	C34	-176.73(7)	C19	C14	C15	C16	-177.92(7)
C1	Ru1	C22	C23	151.09(6)	C20	C16	C17	C18	-179.30(7)
C1	N1	C2	C3	-15.07(9)	C22	C23	C24	C25	-179.52(7)
C1	N1	C4	C5	-77.06(10)	C22	C23	C28	C27	178.78(7)
C1	N1	C4	C9	109.30(9)	C22	C23	C28	C29	4.11(11)
C1	N2	C3	C2	-15.43(9)	C23	C24	C25	C26	0.92(11)
C1	N2	C13	C14	90.16(9)	C23	C28	C29	N3	-4.12(11)
C1	N2	C13	C18	-90.44(9)	C24	C23	C28	C27	0.10(10)
C2	N1	C1	Ru1	-177.80(6)	C24	C23	C28	C29	-174.57(7)
C2	N1	C1	N2	6.03(9)	C24	C25	C26	C27	-0.40(12)
C2	N1	C4	C5	85.78(9)	C25	C26	C27	C28	-0.26(12)
C2	N1	C4	C9	-87.86(9)	C26	C27	C28	C23	0.40(11)
C3	N2	C1	Ru1	-168.92(6)	C26	C27	C28	C29	175.34(7)
C3	N2	C1	N1	6.53(9)	C27	C28	C29	N3	-178.90(7)
C3	N2	C13	C14	-98.93(8)	C28	C23	C24	C25	-0.76(11)
C3	N2	C13	C18	80.47(9)	C29	N3	C30	C31	-47.97(10)

**Table 3.6.24. Torsion Angles for cs2931 [Ru] 6.**

A	B	C	D	Angle/°	A	B	C	D	Angle/°
C4	N1	C1	Ru1	-14.20(10)	C29	N3	C30	C35	132.29(8)
C4	N1	C1	N2	169.63(7)	C30	N3	C29	C28	175.90(7)
C4	N1	C2	C3	-179.93(7)	C30	C31	C32	C33	0.01(13)
C4	C5	C6	C7	2.08(13)	C31	C30	C35	C34	3.52(12)
C5	C4	C9	C8	5.30(12)	C31	C32	C33	F1	-177.55(8)
C5	C4	C9	C12	-171.47(8)	C31	C32	C33	C34	2.48(14)
C5	C6	C7	C8	0.43(14)	C32	C33	C34	C35	-1.92(14)
C5	C6	C7	C11	177.98(9)	C33	C34	C35	C30	-1.13(13)
C6	C7	C8	C9	-0.13(14)	C35	C30	C31	C32	-2.96(12)

This report has been created with Olex2, compiled on 2022.04.07 svn.rca3783a0 for OlexSys. Please [let us know](#) if there are any errors or if you would like to have additional features.

**[Ru] 7**

## Experimental

A brown prism (0.17 x 0.22 x 0.35 mm<sup>3</sup>) was centered on the goniometer of a Rigaku Oxford Diffraction Synergy-S diffractometer equipped with a HyPix6000HE detector and operating with MoK $\alpha$  radiation. The data collection routine, unit cell refinement, and data

processing were carried out with the program CrysAlisPro.<sup>46</sup> The Laue symmetry and systematic absences were consistent with the monoclinic space group  $P2_1/c$ . The structure was solved using SHELXT<sup>47</sup> and refined using SHELXL<sup>48</sup> via Olex2.<sup>49</sup> A 2-position disorder model was used for the 1,3-bis(2,4,6-trimethylphenyl)imidazolidin-2-ylidene ligand, with relative occupancies that refined to 0.737(2) and 0.263(2). The SAME and RIGU commands were used to restrain the metric parameters and anisotropic displacement parameters of the disordered region to be more chemically reasonable. Two disordered/partially evaporated CH<sub>2</sub>Cl<sub>2</sub> molecules were also identified in the asymmetric unit, but attempts to model the disorder were unsuccessful. Therefore, the solvent mask feature of OLEX2 was used. A total of 274 electrons was subtracted from 682 Å<sup>3</sup> total void space in the unit cell (equivalent to ~6 CH<sub>2</sub>Cl<sub>2</sub> 252 electrons) / unit cell). The final refinement model involved anisotropic displacement parameters for non-hydrogen atoms and a riding model for all hydrogen atoms. Olex2<sup>50</sup> was used for molecular graphics generation.

**Table 3.6.25. Crystal data and structure refinement for cs2851 [Ru] 7.**

Identification code	HA-2-31
Empirical formula	C <sub>38.5</sub> Cl <sub>5</sub> H <sub>42</sub> N <sub>3</sub> O <sub>2</sub> Ru
Formula weight	857.07
Temperature/K	100.00(10)
Crystal system	monoclinic
Space group	$P2_1/c$
a/Å	19.7339(3)

(46) CrysAlisPro Software System, v1.171.41.105a, Rigaku Oxford Diffraction, **2021**, Rigaku Corporation, Oxford, UK.

(47) Sheldrick, G. M. "SHELXT – Integrated space-group and crystal structure determination." *Acta Cryst.* **2015**, *A71*, 3–8.

(48) Sheldrick, G. M. "Crystal structure refinement with SHELXL." *Acta Cryst.* **2015**, *C71*, 3–8.

(49) Dolomanov, O.V.; Bourhis, L. J.; Gildea, R. J.; Howard, J. A. K.; Puschmann, H. *J. Appl. Cryst.* **2009**, *42*, 339–341.

(50) Dolomanov, O.V.; Bourhis, L. J.; Gildea, R. J.; Howard, J. A. K.; Puschmann, H. *J. Appl. Cryst.* **2009**, *42*, 339–341.

b/Å	10.11650(10)
c/Å	19.7665(2)
$\alpha$ /°	90
$\beta$ /°	94.5340(10)
$\gamma$ /°	90
Volume/Å <sup>3</sup>	3933.80(8)
Z	4
$\rho_{\text{calc}}$ /cm <sup>3</sup>	1.447
$\mu$ /mm <sup>-1</sup>	0.775
F(000)	1756.0
Crystal size/mm <sup>3</sup>	0.35 × 0.22 × 0.17
Radiation	Mo K $\alpha$ ( $\lambda$ = 0.71073)
2 $\Theta$ range for data collection/°	4.908 to 72.77
Index ranges	-32 ≤ h ≤ 32, -16 ≤ k ≤ 16, -32 ≤ l ≤ 32
Reflections collected	97703
Independent reflections	19037 [R <sub>int</sub> = 0.0359, R <sub>sigma</sub> = 0.0289]
Data/restraints/parameters	19037/417/609
Goodness-of-fit on F <sup>2</sup>	1.093
Final R indexes [I ≥ 2 $\sigma$ (I)]	R <sub>1</sub> = 0.0309, wR <sub>2</sub> = 0.0755
Final R indexes [all data]	R <sub>1</sub> = 0.0431, wR <sub>2</sub> = 0.0788
Largest diff. peak/hole / e Å <sup>-3</sup>	0.76/-0.38

**Table 3.6.26. Bond Lengths for cs2851 [Ru] 7.**

Atom	Atom	Length/Å	Atom	Atom	Length/Å
Ru1	C11	2.3618(3)	N1B	C2B	1.463(6)
Ru1	C12	2.3384(3)	N1B	C4B	1.456(10)
Ru1	C1	2.0601(11)	N2B	C3B	1.475(7)
Ru1	N3	2.0912(8)	C2B	C3B	1.541(7)
Ru1	C22	1.8315(11)	C4B	C5B	1.381(10)
O1	C36	1.2051(18)	C4B	C9B	1.372(9)
O2	C36	1.3365(19)	C5B	C6B	1.397(11)
O2	C37	1.4479(17)	C5B	C10B	1.509(11)
C1	N1A	1.3506(19)	C6B	C7B	1.360(11)
C1	N2A	1.356(3)	C7B	C8B	1.373(11)
C1	N1B	1.409(5)	C7B	C11B	1.528(12)
C1	N2B	1.371(7)	C8B	C9B	1.409(11)
C13	N2A	1.424(3)	C9B	C12B	1.513(10)

**Table 3.6.26. Bond Lengths for cs2851 [Ru] 7.**

Atom	Atom	Length/Å	Atom	Atom	Length/Å
C13	C14A	1.395(3)	C14B	C15B	1.413(9)
C13	C18A	1.410(3)	C14B	C19B	1.463(9)
C13	N2B	1.473(6)	C15B	C16B	1.365(10)
C13	C14B	1.394(9)	C16B	C17B	1.412(10)
C13	C18B	1.393(7)	C16B	C20B	1.539(9)
N1A	C2A	1.472(2)	C17B	C18B	1.359(9)
N1A	C4A	1.431(4)	C18B	C21B	1.522(9)
N2A	C3A	1.471(3)	N3	C29	1.2883(13)
C2A	C3A	1.524(3)	N3	C30	1.4280(13)
C4A	C5A	1.394(4)	C22	C23	1.4498(14)
C4A	C9A	1.392(4)	C23	C24	1.4057(15)
C5A	C6A	1.397(4)	C23	C28	1.4192(13)
C5A	C10A	1.506(4)	C24	C25	1.3864(15)
C6A	C7A	1.395(4)	C25	C26	1.3939(16)
C7A	C8A	1.385(4)	C26	C27	1.3855(16)
C7A	C11A	1.510(4)	C27	C28	1.3979(14)
C8A	C9A	1.405(4)	C28	C29	1.4456(15)
C9A	C12A	1.500(4)	C30	C31	1.3930(15)
C14A	C15A	1.396(3)	C30	C35	1.3923(15)
C14A	C19A	1.506(3)	C31	C32	1.3875(16)
C15A	C16A	1.396(4)	C32	C33	1.3864(17)
C16A	C17A	1.381(4)	C33	C34	1.3927(18)
C16A	C20A	1.512(3)	C33	C36	1.4898(17)
C17A	C18A	1.397(3)	C34	C35	1.3852(17)
C18A	C21A	1.508(3)			

**Table 3.6.27. Bond Angles for cs2851 [Ru] 7.**

Atom	Atom	Atom	Angle/°	Atom	Atom	Atom	Angle/°
C12	Ru1	C11	160.857(11)	C1	N2B	C13	121.3(4)
C1	Ru1	C11	93.01(4)	C1	N2B	C3B	116.6(5)
C1	Ru1	C12	91.30(4)	C13	N2B	C3B	121.3(5)
C1	Ru1	N3	171.23(4)	N1B	C2B	C3B	102.1(4)
N3	Ru1	C11	87.92(2)	N2B	C3B	C2B	101.3(4)
N3	Ru1	C12	85.08(2)	C5B	C4B	N1B	117.3(7)
C22	Ru1	C11	99.81(3)	C9B	C4B	N1B	120.8(7)
C22	Ru1	C12	97.89(3)	C9B	C4B	C5B	121.9(9)
C22	Ru1	C1	99.20(4)	C4B	C5B	C6B	118.0(10)
C22	Ru1	N3	89.22(4)	C4B	C5B	C10B	124.2(8)
C36	O2	C37	115.86(14)	C6B	C5B	C10B	117.5(8)
N1A	C1	Ru1	133.17(10)	C7B	C6B	C5B	123.0(12)
N1A	C1	N2A	105.96(14)	C6B	C7B	C8B	116.3(11)
N2A	C1	Ru1	119.83(11)	C6B	C7B	C11B	124.5(10)
N1B	C1	Ru1	127.7(2)	C8B	C7B	C11B	119.1(9)
N2B	C1	Ru1	119.8(3)	C7B	C8B	C9B	124.1(11)
N2B	C1	N1B	101.9(3)	C4B	C9B	C8B	116.4(9)
C14A	C13	N2A	119.60(15)	C4B	C9B	C12B	119.6(8)
C14A	C13	C18A	121.57(16)	C8B	C9B	C12B	123.9(7)
C18A	C13	N2A	118.67(15)	C13	C14B	C15B	116.4(6)
C14B	C13	N2B	119.2(3)	C13	C14B	C19B	122.9(6)
C18B	C13	N2B	116.4(4)	C15B	C14B	C19B	120.6(8)
C18B	C13	C14B	122.4(4)	C16B	C15B	C14B	121.8(7)
C1	N1A	C2A	113.99(14)	C15B	C16B	C17B	118.4(6)
C1	N1A	C4A	127.5(2)	C15B	C16B	C20B	121.6(9)
C4A	N1A	C2A	118.5(2)	C17B	C16B	C20B	119.9(8)
C1	N2A	C13	126.16(18)	C18B	C17B	C16B	122.0(7)
C1	N2A	C3A	114.10(17)	C13	C18B	C21B	122.0(5)
C13	N2A	C3A	117.97(18)	C17B	C18B	C13	117.8(6)
N1A	C2A	C3A	102.54(14)	C17B	C18B	C21B	120.2(7)
N2A	C3A	C2A	101.64(15)	C29	N3	Ru1	126.67(7)
C5A	C4A	N1A	119.2(2)	C29	N3	C30	117.63(8)
C9A	C4A	N1A	118.1(3)	C30	N3	Ru1	115.47(6)
C9A	C4A	C5A	122.6(3)	C23	C22	Ru1	127.66(7)
C4A	C5A	C6A	117.7(4)	C24	C23	C22	118.19(9)

**Table 3.6.27. Bond Angles for cs2851 [Ru] 7.**

Atom Atom Atom	Angle/°	Atom Atom Atom	Angle/°
C4A C5A C10A	121.3(3)	C24 C23 C28	117.81(9)
C6A C5A C10A	120.9(3)	C28 C23 C22	124.00(9)
C7A C6A C5A	121.1(4)	C25 C24 C23	121.66(10)
C6A C7A C11A	119.3(3)	C24 C25 C26	119.94(10)
C8A C7A C6A	119.8(3)	C27 C26 C25	119.66(10)
C8A C7A C11A	120.9(3)	C26 C27 C28	121.05(10)
C7A C8A C9A	120.6(4)	C23 C28 C29	122.18(9)
C4A C9A C8A	118.1(3)	C27 C28 C23	119.88(9)
C4A C9A C12A	121.4(3)	C27 C28 C29	117.64(9)
C8A C9A C12A	120.5(3)	N3 C29 C28	124.06(9)
C13 C14A C15A	117.8(2)	C31 C30 N3	119.82(9)
C13 C14A C19A	122.3(2)	C35 C30 N3	119.68(9)
C15A C14A C19A	119.6(3)	C35 C30 C31	120.48(10)
C16A C15A C14A	122.1(2)	C32 C31 C30	119.76(10)
C15A C16A C20A	119.9(3)	C33 C32 C31	120.06(11)
C17A C16A C15A	118.5(2)	C32 C33 C34	119.83(11)
C17A C16A C20A	121.5(3)	C32 C33 C36	121.50(12)
C16A C17A C18A	122.0(2)	C34 C33 C36	118.67(12)
C13 C18A C21A	122.16(18)	C35 C34 C33	120.63(11)
C17A C18A C13	117.9(2)	C34 C35 C30	119.15(10)
C17A C18A C21A	119.7(2)	O1 C36 O2	123.92(13)
C1 N1B C2B	113.8(4)	O1 C36 C33	123.92(14)
C1 N1B C4B	125.3(6)	O2 C36 C33	112.15(12)
C4B N1B C2B	115.9(7)		

**Table 3.6.28. Torsion Angles for cs2851 [Ru] 7.**

A	B	C	D	Angle/°	A	B	C	D	Angle/°
Ru1	C1	N1A	C2A	167.74(15)	N1B	C4B	C5B	C6B	-177.6(15)
Ru1	C1	N1A	C4A	-10.4(3)	N1B	C4B	C5B	C10B	-3(2)
Ru1	C1	N2A	C13	16.9(3)	N1B	C4B	C9B	C8B	179.5(12)
Ru1	C1	N2A	C3A	-178.64(15)	N1B	C4B	C9B	C12B	1.0(18)
Ru1	C1	N1B	C2B	-163.9(4)	N2B	C1	N1B	C2B	-20.3(6)
Ru1	C1	N1B	C4B	42.2(7)	N2B	C1	N1B	C4B	-174.2(6)

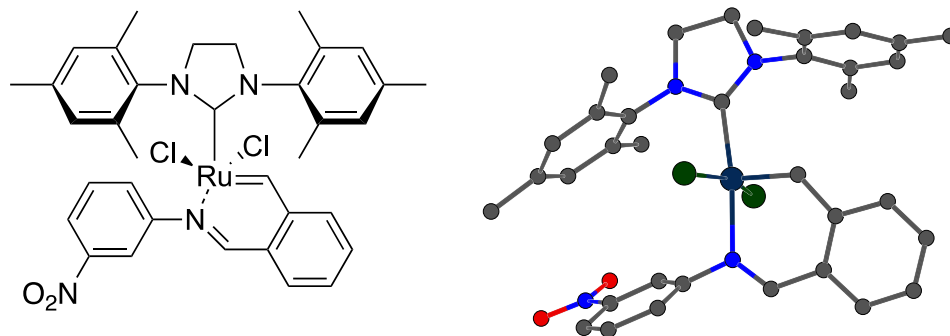
**Table 3.6.28. Torsion Angles for cs2851 [Ru] 7.**

A	B	C	D	Angle/°	A	B	C	D	Angle/°
Ru1	C1	N2B	C13	-32.3(5)	N2B	C13	C14B	C15B	176.2(6)
Ru1	C1	N2B	C3B	157.8(4)	N2B	C13	C14B	C19B	-7.4(11)
Ru1	N3	C29	C28	12.58(14)	N2B	C13	C18B	C17B	-174.5(6)
Ru1	N3	C30	C31	-132.32(9)	N2B	C13	C18B	C21B	5.6(8)
Ru1	N3	C30	C35	45.99(12)	C2B	N1B	C4B	C5B	-93.1(13)
Ru1	C22	C23	C24	164.30(8)	C2B	N1B	C4B	C9B	85.7(14)
Ru1	C22	C23	C28	-16.93(14)	C4B	N1B	C2B	C3B	178.1(6)
Cl1	Ru1	C22	C23	112.94(9)	C4B	C5B	C6B	C7B	-5(3)
Cl2	Ru1	C22	C23	-59.74(9)	C5B	C4B	C9B	C8B	-2(2)
C1	Ru1	C22	C23	-152.36(9)	C5B	C4B	C9B	C12B	179.7(12)
C1	N1A	C2A	C3A	8.1(3)	C5B	C6B	C7B	C8B	4(3)
C1	N1A	C4A	C5A	93.0(4)	C5B	C6B	C7B	C11B	180.0(18)
C1	N1A	C4A	C9A	-88.2(5)	C6B	C7B	C8B	C9B	-2(3)
C1	N2A	C3A	C2A	13.4(3)	C7B	C8B	C9B	C4B	1(2)
C1	N1B	C2B	C3B	21.6(7)	C7B	C8B	C9B	C12B	179.1(14)
C1	N1B	C4B	C5B	60.3(15)	C9B	C4B	C5B	C6B	4(2)
C1	N1B	C4B	C9B	-120.9(11)	C9B	C4B	C5B	C10B	177.9(13)
C1	N2B	C3B	C2B	1.9(7)	C10B	C5B	C6B	C7B	-179.3(18)
C13	N2A	C3A	C2A	179.22(18)	C11B	C7B	C8B	C9B	-178.1(14)
C13	C14A	C15A	C16A	-2.0(4)	C14B	C13	N2B	C1	112.3(6)
C13	N2B	C3B	C2B	-168.0(5)	C14B	C13	N2B	C3B	-78.3(7)
C13	C14B	C15B	C16B	-7.6(12)	C14B	C13	C18B	C17B	-10.9(9)
N1A	C1	N2A	C13	-173.24(17)	C14B	C13	C18B	C21B	169.1(7)
N1A	C1	N2A	C3A	-8.8(2)	C14B	C15B	C16B	C17B	0.3(12)
N1A	C2A	C3A	N2A	-11.8(2)	C14B	C15B	C16B	C20B	-179.8(8)
N1A	C4A	C5A	C6A	179.5(5)	C15B	C16B	C17B	C18B	2.2(12)
N1A	C4A	C5A	C10A	-2.8(7)	C16B	C17B	C18B	C13	2.9(11)
N1A	C4A	C9A	C8A	-179.7(4)	C16B	C17B	C18B	C21B	-177.2(7)
N1A	C4A	C9A	C12A	2.8(6)	C18B	C13	N2B	C1	-83.6(6)
N2A	C1	N1A	C2A	-0.1(2)	C18B	C13	N2B	C3B	85.8(6)
N2A	C1	N1A	C4A	-178.3(2)	C18B	C13	C14B	C15B	13.1(10)
N2A	C13	C14A	C15A	179.8(2)	C18B	C13	C14B	C19B	-170.5(7)
N2A	C13	C14A	C19A	5.6(4)	C19B	C14B	C15B	C16B	176.0(8)
N2A	C13	C18A	C17A	-179.21(18)	C20B	C16B	C17B	C18B	-177.7(8)
N2A	C13	C18A	C21A	-4.2(3)	N3	Ru1	C22	C23	25.18(9)

**Table 3.6.28. Torsion Angles for cs2851 [Ru] 7.**

A	B	C	D	Angle/°	A	B	C	D	Angle/°
C2A	N1A	C4A	C5A	-85.1(5)	N3	C30	C31	C32	-179.65(10)
C2A	N1A	C4A	C9A	93.7(4)	N3	C30	C35	C34	178.42(10)
C4A	N1A	C2A	C3A	-173.5(2)	C22	C23	C24	C25	179.36(9)
C4A	C5A	C6A	C7A	1.0(9)	C22	C23	C28	C27	-178.49(9)
C5A	C4A	C9A	C8A	-1.0(7)	C22	C23	C28	C29	-4.95(15)
C5A	C4A	C9A	C12A	-178.5(4)	C23	C24	C25	C26	-0.92(15)
C5A	C6A	C7A	C8A	-2.6(10)	C23	C28	C29	N3	5.86(15)
C5A	C6A	C7A	C11A	178.6(6)	C24	C23	C28	C27	0.28(14)
C6A	C7A	C8A	C9A	2.4(8)	C24	C23	C28	C29	173.81(9)
C7A	C8A	C9A	C4A	-0.7(7)	C24	C25	C26	C27	0.52(16)
C7A	C8A	C9A	C12A	176.8(5)	C25	C26	C27	C28	0.27(15)
C9A	C4A	C5A	C6A	0.8(8)	C26	C27	C28	C23	-0.67(15)
C9A	C4A	C5A	C10A	178.5(4)	C26	C27	C28	C29	-174.50(9)
C10A	C5A	C6A	C7A	-176.7(6)	C27	C28	C29	N3	179.53(9)
C11A	C7A	C8A	C9A	-178.8(5)	C28	C23	C24	C25	0.52(14)
C14A	C13	N2A	C1	77.8(3)	C29	N3	C30	C31	52.77(13)
C14A	C13	N2A	C3A	-86.1(3)	C29	N3	C30	C35	-128.91(11)
C14A	C13	C18A	C17A	-3.7(3)	C30	N3	C29	C28	-173.15(9)
C14A	C13	C18A	C21A	171.3(2)	C30	C31	C32	C33	0.71(18)
C14A	C15A	C16A	C17A	-1.1(4)	C31	C30	C35	C34	-3.28(17)
C14A	C15A	C16A	C20A	-179.0(2)	C31	C32	C33	C34	-2.20(19)
C15A	C16A	C17A	C18A	1.8(3)	C31	C32	C33	C36	177.39(12)
C16A	C17A	C18A	C13	0.6(3)	C32	C33	C34	C35	0.95(19)
C16A	C17A	C18A	C21A	-174.6(2)	C32	C33	C36	O1	-172.38(15)
C18A	C13	N2A	C1	-106.7(2)	C32	C33	C36	O2	6.42(19)
C18A	C13	N2A	C3A	89.4(2)	C33	C34	C35	C30	1.78(18)
C18A	C13	C14A	C15A	4.4(4)	C34	C33	C36	O1	7.2(2)
C18A	C13	C14A	C19A	-169.8(2)	C34	C33	C36	O2	-173.99(12)
C19A	C14A	C15A	C16A	172.4(2)	C35	C30	C31	C32	2.05(17)
C20A	C16A	C17A	C18A	179.7(2)	C36	C33	C34	C35	-178.66(12)
N1B	C1	N2B	C13	-179.6(4)	C37	O2	C36	O1	-1.6(2)
N1B	C1	N2B	C3B	10.5(6)	C37	O2	C36	C33	179.65(14)
N1B	C2B	C3B	N2B	-13.0(7)					

This report has been created with Olex2, compiled on 2022.04.07 svn.rca3783a0 for OlexSys. Please [let us know](#) if there are any errors or if you would like to have additional features.



[Ru] 8

## Experimental

A yellow-brown plate (0.02 x 0.18 x 0.43 mm<sup>3</sup>) was centered on the goniometer of a Rigaku Oxford Diffraction Synergy-S diffractometer equipped with a HyPix6000HE detector and operating with MoK $\alpha$  radiation. The data collection routine, unit cell refinement, and data processing were carried out with the program CrysAlisPro.<sup>51</sup> The Laue symmetry and systematic absences were consistent with the orthorhombic space group *Pbca*. The structure was solved using SHELXT<sup>52</sup> and refined using SHELXL<sup>53</sup> via Olex2.<sup>54</sup> The final refinement model involved anisotropic displacement parameters for non-hydrogen atoms and a riding model for all hydrogen atoms. Olex2<sup>55</sup> was used for molecular graphics generation.

---

(51) CrysAlisPro Software System, v1.171.41.105a, Rigaku Oxford Diffraction, **2021**, Rigaku Corporation, Oxford, UK.

(52) Sheldrick, G. M. "SHELXT – Integrated space-group and crystal structure determination." *Acta Cryst.* **2015**, *A71*, 3–8.

(53) Sheldrick, G. M. "Crystal structure refinement with SHELXL." *Acta Cryst.* **2015**, *C71*, 3–8.

(54) Dolomanov, O.V.; Bourhis, L. J.; Gildea, R. J.; Howard, J. A. K.; Puschmann, H. *J. Appl. Cryst.* **2009**, *42*, 339–341.

(55) Dolomanov, O.V.; Bourhis, L. J.; Gildea, R. J.; Howard, J. A. K.; Puschmann, H. *J. Appl. Cryst.* **2009**, *42*, 339–341.

**Table 3.6.29. Crystal data and structure refinement for cs2911 [Ru] 8.**

Identification code	HA-2-83
Empirical formula	C <sub>35</sub> H <sub>36</sub> Cl <sub>2</sub> N <sub>4</sub> O <sub>2</sub> Ru
Formula weight	716.65
Temperature/K	99.98(13)
Crystal system	orthorhombic
Space group	Pbca
a/Å	16.4116(2)
b/Å	14.4097(2)
c/Å	27.1079(4)
α/°	90
β/°	90
γ/°	90
Volume/Å <sup>3</sup>	6410.63(16)
Z	8
ρ <sub>calc</sub> /cm <sup>3</sup>	1.485
μ/mm <sup>-1</sup>	0.694
F(000)	2944.0
Crystal size/mm <sup>3</sup>	0.43 × 0.18 × 0.02
Radiation	Mo Kα (λ = 0.71073)
2θ range for data collection/°	5.714 to 61.014
Index ranges	-23 ≤ h ≤ 23, -20 ≤ k ≤ 20, -38 ≤ l ≤ 38
Reflections collected	96404
Independent reflections	9789 [R <sub>int</sub> = 0.0691, R <sub>sigma</sub> = 0.0293]
Data/restraints/parameters	9789/0/403
Goodness-of-fit on F <sup>2</sup>	1.147
Final R indexes [I ≥ 2σ (I)]	R <sub>1</sub> = 0.0401, wR <sub>2</sub> = 0.0877
Final R indexes [all data]	R <sub>1</sub> = 0.0458, wR <sub>2</sub> = 0.0905
Largest diff. peak/hole / e Å <sup>-3</sup>	0.73/-0.59

**Table 3.6.30. Bond Lengths for cs2911 [Ru] 8.**

Atom	Atom	Length/Å	Atom	Atom	Length/Å
Ru1	Cl1	2.3536(5)	C13	C14	1.401(3)
Ru1	Cl2	2.3346(5)	C13	C18	1.398(3)
Ru1	N3	2.1004(16)	C14	C15	1.392(3)
Ru1	C1	2.0581(19)	C14	C19	1.505(3)

**Table 3.6.30. Bond Lengths for cs2911 [Ru] 8.**

Atom	Atom	Length/Å	Atom	Atom	Length/Å
Ru1	C22	1.832(2)	C15	C16	1.389(3)
O2	N4	1.229(3)	C16	C17	1.389(4)
N1	C1	1.352(3)	C16	C20	1.506(3)
N1	C2	1.471(3)	C17	C18	1.397(3)
N1	C4	1.431(2)	C18	C21	1.503(3)
N2	C1	1.345(2)	C22	C23	1.451(3)
N2	C3	1.477(3)	C23	C24	1.406(3)
N2	C13	1.430(3)	C23	C28	1.416(3)
N3	C29	1.283(3)	C24	C25	1.385(3)
N3	C30	1.429(3)	C25	C26	1.383(3)
O1	N4	1.230(2)	C26	C27	1.387(3)
C2	C3	1.529(3)	C27	C28	1.400(3)
C4	C5	1.412(3)	C28	C29	1.447(3)
C4	C9	1.396(3)	C30	C31	1.388(3)
C5	C6	1.391(3)	C30	C35	1.395(3)
C5	C10	1.501(3)	C31	C32	1.384(3)
C6	C7	1.387(3)	C32	C33	1.386(3)
C7	C8	1.390(3)	C32	N4	1.466(3)
C7	C11	1.508(3)	C33	C34	1.385(4)
C8	C9	1.398(3)	C34	C35	1.390(3)
C9	C12	1.503(3)			

**Table 3.6.31. Bond Angles for cs2911 [Ru] 8.**

Atom	Atom	Atom	Angle/°	Atom	Atom	Atom	Angle/°
Cl2	Ru1	Cl1	160.963(18)	C18	C13	N2	118.57(19)
N3	Ru1	Cl1	88.43(4)	C18	C13	C14	121.50(19)
N3	Ru1	Cl2	85.49(4)	C13	C14	C19	120.65(18)
C1	Ru1	Cl1	88.25(5)	C15	C14	C13	118.0(2)
C1	Ru1	Cl2	95.18(5)	C15	C14	C19	121.22(19)
C1	Ru1	N3	171.49(7)	C16	C15	C14	122.1(2)
C22	Ru1	Cl1	98.83(6)	C15	C16	C17	118.4(2)
C22	Ru1	Cl2	99.13(6)	C15	C16	C20	121.1(2)
C22	Ru1	N3	89.48(8)	C17	C16	C20	120.5(2)

**Table 3.6.31. Bond Angles for cs2911 [Ru] 8.**

Atom	Atom	Atom	Angle/°	Atom	Atom	Atom	Angle/°
C22	Ru1	C1	98.77(8)	C16	C17	C18	121.8(2)
C1	N1	C2	114.05(16)	C13	C18	C21	121.0(2)
C1	N1	C4	124.93(16)	C17	C18	C13	118.2(2)
C4	N1	C2	120.73(16)	C17	C18	C21	120.7(2)
C1	N2	C3	113.59(17)	C23	C22	Ru1	128.38(15)
C1	N2	C13	126.45(17)	C24	C23	C22	117.34(18)
C13	N2	C3	118.56(16)	C24	C23	C28	117.92(19)
C29	N3	Ru1	128.54(14)	C28	C23	C22	124.73(18)
C29	N3	C30	117.87(17)	C25	C24	C23	121.5(2)
C30	N3	Ru1	113.59(12)	C26	C25	C24	119.8(2)
N1	C1	Ru1	119.14(14)	C25	C26	C27	120.5(2)
N2	C1	Ru1	132.82(15)	C26	C27	C28	120.2(2)
N2	C1	N1	107.19(16)	C23	C28	C29	122.03(18)
N1	C2	C3	102.35(16)	C27	C28	C23	120.04(19)
N2	C3	C2	102.77(16)	C27	C28	C29	117.86(19)
C5	C4	N1	118.62(18)	N3	C29	C28	123.85(18)
C9	C4	N1	120.08(17)	C31	C30	N3	117.89(16)
C9	C4	C5	121.19(18)	C31	C30	C35	120.55(19)
C4	C5	C10	121.64(19)	C35	C30	N3	121.53(19)
C6	C5	C4	117.76(19)	C32	C31	C30	117.87(18)
C6	C5	C10	120.57(19)	C31	C32	C33	123.2(2)
C7	C6	C5	122.34(19)	C31	C32	N4	117.63(18)
C6	C7	C8	118.18(19)	C33	C32	N4	119.1(2)
C6	C7	C11	121.25(19)	C34	C33	C32	117.6(2)
C8	C7	C11	120.6(2)	C33	C34	C35	121.1(2)
C7	C8	C9	122.0(2)	C34	C35	C30	119.6(2)
C4	C9	C8	118.09(18)	O2	N4	O1	123.3(2)
C4	C9	C12	122.71(18)	O2	N4	C32	118.64(18)
C8	C9	C12	119.13(19)	O1	N4	C32	118.10(19)
C14	C13	N2	119.93(18)				

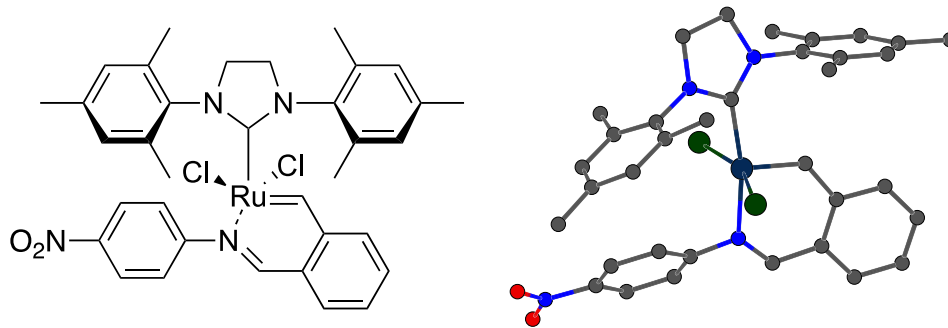
**Table 3.6.32. Torsion Angles for cs2911 [Ru] 8.**

A	B	C	D	Angle/°	A	B	C	D	Angle/°
Ru1	N3	C29	C28	-1.3(3)	C9	C4	C5	C10	-171.42(19)
Ru1	N3	C30	C31	61.0(2)	C10	C5	C6	C7	176.5(2)
Ru1	N3	C30	C35	-117.00(19)	C11	C7	C8	C9	-177.09(19)
Ru1	C22	C23	C24	164.08(14)	C13	N2	C1	Ru1	-25.8(3)
Ru1	C22	C23	C28	-17.1(3)	C13	N2	C1	N1	165.17(18)
C11	Ru1	C22	C23	-69.79(16)	C13	N2	C3	C2	-165.56(18)
C12	Ru1	C22	C23	103.89(16)	C13	C14	C15	C16	0.1(3)
N1	C2	C3	N2	-1.8(2)	C14	C13	C18	C17	0.3(3)
N1	C4	C5	C6	-177.00(18)	C14	C13	C18	C21	-175.8(2)
N1	C4	C5	C10	4.8(3)	C14	C15	C16	C17	0.1(3)
N1	C4	C9	C8	177.16(18)	C14	C15	C16	C20	179.6(2)
N1	C4	C9	C12	-6.0(3)	C15	C16	C17	C18	0.0(3)
N2	C13	C14	C15	179.19(18)	C16	C17	C18	C13	-0.2(3)
N2	C13	C14	C19	-4.7(3)	C16	C17	C18	C21	176.0(2)
N2	C13	C18	C17	-179.13(19)	C18	C13	C14	C15	-0.3(3)
N2	C13	C18	C21	4.7(3)	C18	C13	C14	C19	175.89(19)
N3	Ru1	C22	C23	18.54(17)	C19	C14	C15	C16	-176.06(19)
N3	C30	C31	C32	-178.68(18)	C20	C16	C17	C18	-179.5(2)
N3	C30	C35	C34	178.0(2)	C22	C23	C24	C25	179.06(17)
C1	Ru1	C22	C23	-159.37(16)	C22	C23	C28	C27	-177.60(18)
C1	N1	C2	C3	1.4(2)	C22	C23	C28	C29	-0.7(3)
C1	N1	C4	C5	85.0(2)	C23	C24	C25	C26	-1.7(3)
C1	N1	C4	C9	-98.7(2)	C23	C28	C29	N3	9.3(3)
C1	N2	C3	C2	1.9(2)	C24	C23	C28	C27	1.3(3)
C1	N2	C13	C14	99.7(2)	C24	C23	C28	C29	178.12(17)
C1	N2	C13	C18	-80.8(3)	C24	C25	C26	C27	2.0(3)
C2	N1	C1	Ru1	-171.07(14)	C25	C26	C27	C28	-0.6(3)
C2	N1	C1	N2	-0.3(2)	C26	C27	C28	C23	-1.0(3)
C2	N1	C4	C5	-88.5(2)	C26	C27	C28	C29	-178.03(18)
C2	N1	C4	C9	87.8(2)	C27	C28	C29	N3	-173.80(18)
C3	N2	C1	Ru1	167.96(16)	C28	C23	C24	C25	0.1(3)
C3	N2	C1	N1	-1.1(2)	C29	N3	C30	C31	-119.8(2)
C3	N2	C13	C14	-94.6(2)	C29	N3	C30	C35	62.3(3)
C3	N2	C13	C18	84.8(2)	C30	N3	C29	C28	179.61(18)
C4	N1	C1	Ru1	15.1(3)	C30	C31	C32	C33	0.9(3)

**Table 3.6.32. Torsion Angles for cs2911 [Ru] 8.**

A	B	C	D	Angle/°	A	B	C	D	Angle/°
C4	N1	C1	N2	-174.14(18)	C30	C31	C32	N4	-179.42(18)
C4	N1	C2	C3	175.52(18)	C31	C30	C35	C34	0.1(3)
C4	C5	C6	C7	-1.7(3)	C31	C32	C33	C34	-0.4(3)
C5	C4	C9	C8	-6.7(3)	C31	C32	N4	O2	2.8(3)
C5	C4	C9	C12	170.23(19)	C31	C32	N4	O1	-176.9(2)
C5	C6	C7	C8	-3.1(3)	C32	C33	C34	C35	-0.2(4)
C5	C6	C7	C11	177.2(2)	C33	C32	N4	O2	-177.5(2)
C6	C7	C8	C9	3.3(3)	C33	C32	N4	O1	2.8(3)
C7	C8	C9	C4	1.5(3)	C33	C34	C35	C30	0.4(4)
C7	C8	C9	C12	-175.46(19)	C35	C30	C31	C32	-0.7(3)
C9	C4	C5	C6	6.8(3)	N4	C32	C33	C34	179.9(2)

This report has been created with Olex2, compiled on 2022.04.07 svn.rca3783a0 for OlexSys. Please [let us know](#) if there are any errors or if you would like to have additional features.

**[Ru] 9**

## Experimental

An irregular shaped yellow-brown crystal (0.09 x 0.15 x 0.24 mm<sup>3</sup>) was centered on the goniometer of a Rigaku Oxford Diffraction Synergy-S diffractometer equipped with a HyPix6000HE detector and operating with MoK $\alpha$  radiation. The data collection routine, unit cell refinement, and data processing were carried out with the program CrysAlisPro.<sup>56</sup>

(56) CrysAlisPro Software System, v1.171.42.xx, Rigaku Oxford Diffraction, 2022, Rigaku Corporation, Oxford, UK.

The Laue symmetry was consistent with the triclinic space groups *P*1 and *P*-1. The centrosymmetric space group *P*-1 was chosen. The structure was solved using SHELXT<sup>57</sup> and refined using SHELXL<sup>58</sup> via Olex2.<sup>59</sup> The final refinement model involved anisotropic displacement parameters for non-hydrogen atoms and a riding model for all hydrogen atoms. Olex2<sup>60</sup> was used for molecular graphics generation.

**Table 3.6.33. Crystal data and structure refinement for cs2927 [Ru] 9.**

Identification code	HA-2-54
Empirical formula	C <sub>36</sub> H <sub>38</sub> Cl <sub>4</sub> N <sub>4</sub> O <sub>2</sub> Ru
Formula weight	801.57
Temperature/K	99.97(14)
Crystal system	triclinic
Space group	P-1
<i>a</i> /Å	14.77360(10)
<i>b</i> /Å	15.30140(10)
<i>c</i> /Å	17.1170(2)
$\alpha$ /°	86.9810(10)
$\beta$ /°	86.4960(10)
$\gamma$ /°	68.0610(10)
Volume/Å <sup>3</sup>	3580.63(6)
<i>Z</i>	4
$\rho_{\text{calc}}$ g/cm <sup>3</sup>	1.487
$\mu$ /mm <sup>-1</sup>	0.775
F(000)	1640.0
Crystal size/mm <sup>3</sup>	0.24 × 0.15 × 0.09
Radiation	Mo K $\alpha$ ( $\lambda$ = 0.71073)
2 $\theta$ range for data collection/°	5.416 to 76.46
Index ranges	-24 ≤ <i>h</i> ≤ 24, -26 ≤ <i>k</i> ≤ 25, -29 ≤ <i>l</i> ≤ 29
Reflections collected	253518

(57) Sheldrick, G. M. "SHELXT – Integrated space-group and crystal structure determination." *Acta Cryst.* **2015**, *A71*, 3–8.

(58) Sheldrick, G. M. "Crystal structure refinement with SHELXL." *Acta Cryst.* **2015**, *C71*, 3–8.

(59) Dolomanov, O.V.; Bourhis, L. J.; Gildea, R. J.; Howard, J. A. K.; Puschmann, H. *J. Appl. Cryst.* **2009**, *42*, 339–341.

(60) Dolomanov, O.V.; Bourhis, L. J.; Gildea, R. J.; Howard, J. A. K.; Puschmann, H. *J. Appl. Cryst.* **2009**, *42*, 339–341.

Independent reflections	37825 [ $R_{\text{int}} = 0.0384$ , $R_{\text{sigma}} = 0.0260$ ]
Data/restraints/parameters	37825/0/859
Goodness-of-fit on $F^2$	1.035
Final R indexes [ $I \geq 2\sigma(I)$ ]	$R_1 = 0.0276$ , $wR_2 = 0.0675$
Final R indexes [all data]	$R_1 = 0.0367$ , $wR_2 = 0.0700$
Largest diff. peak/hole / $e \text{ \AA}^{-3}$	0.72/-0.79

**Table 3.6.34. Bond Lengths for cs2927 [Ru] 9.**

Atom	Atom	Length/Å	Atom	Atom	Length/Å
Ru1	Cl1	2.3318(2)	Ru2	N7	2.1117(8)
Ru1	Cl2	2.3487(2)	Ru2	C36	2.0492(9)
Ru1	N3	2.1160(8)	Ru2	C57	1.8323(9)
Ru1	C1	2.0576(9)	O3	N8	1.2247(17)
Ru1	C22	1.8353(10)	O4	N8	1.2253(17)
O1	N4	1.2201(14)	N5	C36	1.3484(12)
O2	N4	1.2245(13)	N5	C37	1.4717(14)
N1	C1	1.3467(12)	N5	C39	1.4300(13)
N1	C2	1.4760(12)	N6	C36	1.3513(12)
N1	C4	1.4347(12)	N6	C38	1.4699(15)
N2	C1	1.3492(12)	N6	C48	1.4350(13)
N2	C3	1.4735(13)	N7	C64	1.2901(12)
N2	C13	1.4292(13)	N7	C65	1.4287(12)
N3	C29	1.2898(12)	N8	C68	1.4665(14)
N3	C30	1.4272(12)	C37	C38	1.5166(17)
N4	C33	1.4656(13)	C39	C40	1.3946(16)
C2	C3	1.5248(15)	C39	C44	1.4000(16)
C4	C5	1.4009(14)	C40	C41	1.3969(16)
C4	C9	1.4038(14)	C40	C45	1.5013(17)
C5	C6	1.4001(14)	C41	C42	1.3916(18)
C5	C10	1.5025(15)	C42	C43	1.3897(19)
C6	C7	1.3851(17)	C42	C46	1.5108(17)
C7	C8	1.3958(17)	C43	C44	1.3955(15)
C7	C11	1.5073(16)	C44	C47	1.5039(18)
C8	C9	1.3931(15)	C48	C49	1.4033(16)
C9	C12	1.5081(15)	C48	C53	1.4003(16)
C13	C14	1.3986(13)	C49	C50	1.3972(15)
C13	C18	1.4050(13)	C49	C54	1.5028(17)
C14	C15	1.3952(14)	C50	C51	1.3857(17)
C14	C19	1.5029(14)	C51	C52	1.3887(17)
C15	C16	1.3937(15)	C51	C55	1.5093(16)
C16	C17	1.3929(15)	C52	C53	1.3978(15)
C16	C20	1.5076(16)	C53	C56	1.5036(17)
C17	C18	1.3895(15)	C57	C58	1.4484(13)
C18	C21	1.5060(15)	C58	C59	1.4080(13)

**Table 3.6.34. Bond Lengths for cs2927 [Ru] 9.**

Atom	Atom	Length/Å	Atom	Atom	Length/Å
C22	C23	1.4520(13)	C58	C63	1.4096(13)
C23	C24	1.4062(13)	C59	C60	1.3842(14)
C23	C28	1.4134(13)	C60	C61	1.3953(16)
C24	C25	1.3856(15)	C61	C62	1.3868(14)
C25	C26	1.3913(17)	C62	C63	1.3989(13)
C26	C27	1.3875(15)	C63	C64	1.4476(13)
C27	C28	1.3995(13)	C65	C66	1.3951(14)
C28	C29	1.4456(13)	C65	C70	1.3969(14)
C30	C31	1.3978(13)	C66	C67	1.3882(15)
C30	C35	1.3969(13)	C67	C68	1.3875(17)
C31	C32	1.3849(13)	C68	C69	1.3826(17)
C32	C33	1.3836(14)	C69	C70	1.3853(14)
C33	C34	1.3848(15)	C15	C71	1.7599(14)
C34	C35	1.3890(15)	C16	C71	1.7607(14)
Ru2	Cl3	2.3382(3)	C17	C72	1.7500(13)
Ru2	Cl4	2.3489(2)	C18	C72	1.7687(15)

**Table 3.6.35. Bond Angles for cs2927 [Ru] 9.**

Atom	Atom	Atom	Angle/°	Atom	Atom	Atom	Angle/°
Cl1	Ru1	Cl2	158.471(9)	N7	Ru2	Cl3	87.58(2)
N3	Ru1	Cl1	85.98(2)	N7	Ru2	Cl4	86.58(2)
N3	Ru1	Cl2	89.10(2)	C36	Ru2	Cl3	86.24(3)
C1	Ru1	Cl1	85.19(3)	C36	Ru2	Cl4	96.80(3)
C1	Ru1	Cl2	96.39(3)	C36	Ru2	N7	170.59(3)
C1	Ru1	N3	168.38(3)	C57	Ru2	Cl3	101.50(3)
C22	Ru1	Cl1	103.17(3)	C57	Ru2	Cl4	98.07(3)
C22	Ru1	Cl2	97.75(3)	C57	Ru2	N7	89.78(4)
C22	Ru1	N3	89.74(4)	C57	Ru2	C36	98.40(4)
C22	Ru1	C1	99.61(4)	C36	N5	C37	113.67(8)
C1	N1	C2	114.08(8)	C36	N5	C39	128.03(8)
C1	N1	C4	126.28(8)	C39	N5	C37	117.45(8)
C4	N1	C2	119.06(8)	C36	N6	C38	114.01(8)
C1	N2	C3	113.47(8)	C36	N6	C48	127.09(8)

**Table 3.6.35. Bond Angles for cs2927 [Ru] 9.**

Atom	Atom	Atom	Angle/°	Atom	Atom	Atom	Angle/°
C1	N2	C13	126.60(8)	C48	N6	C38	118.41(8)
C13	N2	C3	118.93(8)	C64	N7	Ru2	127.62(6)
C29	N3	Ru1	128.62(6)	C64	N7	C65	117.11(8)
C29	N3	C30	117.52(8)	C65	N7	Ru2	115.27(6)
C30	N3	Ru1	113.42(6)	O3	N8	O4	123.66(11)
O1	N4	O2	123.14(10)	O3	N8	C68	117.96(12)
O1	N4	C33	118.42(10)	O4	N8	C68	118.37(12)
O2	N4	C33	118.43(10)	N5	C36	Ru2	132.35(7)
N1	C1	Ru1	119.61(6)	N5	C36	N6	106.70(8)
N1	C1	N2	107.15(8)	N6	C36	Ru2	120.14(7)
N2	C1	Ru1	131.72(7)	N5	C37	C38	102.97(9)
N1	C2	C3	102.10(8)	N6	C38	C37	102.44(9)
N2	C3	C2	103.08(8)	C40	C39	N5	118.61(10)
C5	C4	N1	120.05(9)	C40	C39	C44	121.94(9)
C5	C4	C9	121.21(9)	C44	C39	N5	119.42(10)
C9	C4	N1	118.49(9)	C39	C40	C41	118.01(10)
C4	C5	C10	123.21(9)	C39	C40	C45	120.66(10)
C6	C5	C4	117.76(10)	C41	C40	C45	121.30(11)
C6	C5	C10	119.01(10)	C42	C41	C40	121.74(11)
C7	C6	C5	122.37(10)	C41	C42	C46	121.05(13)
C6	C7	C8	118.21(10)	C43	C42	C41	118.54(10)
C6	C7	C11	120.99(12)	C43	C42	C46	120.41(12)
C8	C7	C11	120.79(12)	C42	C43	C44	121.89(11)
C9	C8	C7	121.68(10)	C39	C44	C47	121.10(10)
C4	C9	C12	121.71(9)	C43	C44	C39	117.85(11)
C8	C9	C4	118.41(10)	C43	C44	C47	120.95(11)
C8	C9	C12	119.84(10)	C49	C48	N6	119.89(10)
C14	C13	N2	120.20(9)	C53	C48	N6	118.59(10)
C14	C13	C18	121.23(9)	C53	C48	C49	121.04(9)
C18	C13	N2	118.57(9)	C48	C49	C54	123.09(10)
C13	C14	C19	121.75(9)	C50	C49	C48	118.06(10)
C15	C14	C13	118.11(9)	C50	C49	C54	118.76(11)
C15	C14	C19	120.14(9)	C51	C50	C49	122.19(11)
C16	C15	C14	122.03(9)	C50	C51	C52	118.25(10)
C15	C16	C20	121.24(10)	C50	C51	C55	121.00(12)

**Table 3.6.35. Bond Angles for cs2927 [Ru] 9.**

Atom	Atom	Atom	Angle/°	Atom	Atom	Atom	Angle/°
C17	C16	C15	118.31(9)	C52	C51	C55	120.70(11)
C17	C16	C20	120.45(10)	C51	C52	C53	121.99(11)
C18	C17	C16	121.73(9)	C48	C53	C56	122.03(10)
C13	C18	C21	120.84(9)	C52	C53	C48	118.22(10)
C17	C18	C13	118.54(9)	C52	C53	C56	119.61(11)
C17	C18	C21	120.60(9)	C58	C57	Ru2	128.91(7)
C23	C22	Ru1	129.60(7)	C59	C58	C57	117.23(8)
C24	C23	C22	117.09(9)	C59	C58	C63	118.15(8)
C24	C23	C28	117.87(9)	C63	C58	C57	124.63(8)
C28	C23	C22	125.02(8)	C60	C59	C58	121.51(9)
C25	C24	C23	121.55(10)	C59	C60	C61	119.75(9)
C24	C25	C26	119.97(10)	C62	C61	C60	119.82(9)
C27	C26	C25	119.84(10)	C61	C62	C63	120.81(9)
C26	C27	C28	120.63(10)	C58	C63	C64	122.93(8)
C23	C28	C29	122.79(8)	C62	C63	C58	119.92(8)
C27	C28	C23	120.14(9)	C62	C63	C64	117.10(8)
C27	C28	C29	117.03(9)	N7	C64	C63	123.92(8)
N3	C29	C28	123.85(8)	C66	C65	N7	118.65(9)
C31	C30	N3	120.23(8)	C66	C65	C70	120.56(9)
C35	C30	N3	119.09(8)	C70	C65	N7	120.75(9)
C35	C30	C31	120.55(9)	C67	C66	C65	119.76(10)
C32	C31	C30	119.93(9)	C68	C67	C66	118.59(10)
C33	C32	C31	118.58(9)	C67	C68	N8	118.32(11)
C32	C33	N4	118.32(9)	C69	C68	N8	119.16(11)
C32	C33	C34	122.61(9)	C69	C68	C67	122.51(9)
C34	C33	N4	119.06(9)	C68	C69	C70	118.72(10)
C33	C34	C35	118.73(9)	C69	C70	C65	119.83(10)
C34	C35	C30	119.59(9)	Cl5	C71	Cl6	111.67(7)
Cl3	Ru2	Cl4	159.539(9)	Cl7	C72	Cl8	112.44(7)

**Table 3.6.36. Torsion Angles for cs2927 [Ru] 9.**

A	B	C	D	Angle/°	A	B	C	D	Angle/°
Ru1	N3	C29	C28	-0.51(13)	Ru2	N7	C64	C63	5.36(14)
Ru1	N3	C30	C31	131.87(8)	Ru2	N7	C65	C66	38.63(12)
Ru1	N3	C30	C35	-44.01(10)	Ru2	N7	C65	C70	-139.29(8)
Ru1	C22	C23	C24	-175.18(8)	Ru2	C57	C58	C59	167.98(8)
Ru1	C22	C23	C28	6.60(15)	Ru2	C57	C58	C63	-12.39(15)
Cl1	Ru1	C22	C23	-92.71(9)	Cl3	Ru2	C57	C58	103.38(9)
Cl2	Ru1	C22	C23	82.16(9)	Cl4	Ru2	C57	C58	-70.62(9)
O1	N4	C33	C32	-175.76(12)	O3	N8	C68	C67	3.03(18)
O1	N4	C33	C34	3.36(17)	O3	N8	C68	C69	-178.10(13)
O2	N4	C33	C32	4.56(15)	O4	N8	C68	C67	-176.22(13)
O2	N4	C33	C34	-176.32(11)	O4	N8	C68	C69	2.65(19)
N1	C2	C3	N2	-3.08(11)	N5	C37	C38	N6	4.10(18)
N1	C4	C5	C6	-179.33(9)	N5	C39	C40	C41	-179.84(9)
N1	C4	C5	C10	-0.59(14)	N5	C39	C40	C45	-1.51(14)
N1	C4	C9	C8	-179.14(9)	N5	C39	C44	C43	179.79(9)
N1	C4	C9	C12	3.23(14)	N5	C39	C44	C47	3.40(15)
N2	C13	C14	C15	-178.33(9)	N6	C48	C49	C50	177.53(10)
N2	C13	C14	C19	1.18(14)	N6	C48	C49	C54	1.13(17)
N2	C13	C18	C17	177.85(8)	N6	C48	C53	C52	-177.73(9)
N2	C13	C18	C21	-0.53(14)	N6	C48	C53	C56	-2.15(15)
N3	Ru1	C22	C23	-6.89(9)	N7	Ru2	C57	C58	15.90(9)
N3	C30	C31	C32	-175.91(9)	N7	C65	C66	C67	-179.53(10)
N3	C30	C35	C34	175.50(9)	N7	C65	C70	C69	179.71(10)
N4	C33	C34	C35	-178.06(10)	N8	C68	C69	C70	-179.71(11)
C1	Ru1	C22	C23	-179.97(9)	C36	Ru2	C57	C58	-168.77(9)
C1	N1	C2	C3	3.56(12)	C36	N5	C37	C38	-2.99(18)
C1	N1	C4	C5	-101.46(12)	C36	N5	C39	C40	77.71(15)
C1	N1	C4	C9	84.26(12)	C36	N5	C39	C44	-103.96(13)
C1	N2	C3	C2	2.04(12)	C36	N6	C38	C37	-4.45(19)
C1	N2	C13	C14	104.98(11)	C36	N6	C48	C49	104.81(13)
C1	N2	C13	C18	-75.62(13)	C36	N6	C48	C53	-83.03(14)
C2	N1	C1	Ru1	-169.95(7)	C37	N5	C36	Ru2	-169.06(11)
C2	N1	C1	N2	-2.42(11)	C37	N5	C36	N6	0.34(15)
C2	N1	C4	C5	87.85(12)	C37	N5	C39	C40	-91.01(14)
C2	N1	C4	C9	-86.43(12)	C37	N5	C39	C44	87.33(14)

**Table 3.6.36. Torsion Angles for cs2927 [Ru] 9.**

A	B	C	D	Angle/°	A	B	C	D	Angle/°
C3	N2	C1	Ru1	165.54(7)	C38	N6	C36	Ru2	173.68(11)
C3	N2	C1	N1	0.10(11)	C38	N6	C36	N5	2.73(16)
C3	N2	C13	C14	-87.26(12)	C38	N6	C48	C49	-83.71(16)
C3	N2	C13	C18	92.15(11)	C38	N6	C48	C53	88.44(15)
C4	N1	C1	Ru1	18.96(13)	C39	N5	C36	Ru2	21.87(18)
C4	N1	C1	N2	-173.51(9)	C39	N5	C36	N6	-168.74(11)
C4	N1	C2	C3	175.34(9)	C39	N5	C37	C38	167.32(13)
C4	C5	C6	C7	-0.11(15)	C39	C40	C41	C42	-0.78(16)
C5	C4	C9	C8	6.64(14)	C40	C39	C44	C43	-1.93(15)
C5	C4	C9	C12	-170.99(9)	C40	C39	C44	C47	-178.32(10)
C5	C6	C7	C8	3.76(16)	C40	C41	C42	C43	-0.18(17)
C5	C6	C7	C11	-176.75(10)	C40	C41	C42	C46	178.79(11)
C6	C7	C8	C9	-2.24(16)	C41	C42	C43	C44	0.11(17)
C7	C8	C9	C4	-2.83(15)	C42	C43	C44	C39	0.91(17)
C7	C8	C9	C12	174.84(10)	C42	C43	C44	C47	177.30(11)
C9	C4	C5	C6	-5.20(14)	C44	C39	C40	C41	1.87(15)
C9	C4	C5	C10	173.53(9)	C44	C39	C40	C45	-179.80(10)
C10	C5	C6	C7	-178.89(10)	C45	C40	C41	C42	-179.10(10)
C11	C7	C8	C9	178.27(10)	C46	C42	C43	C44	-178.87(12)
C13	N2	C1	Ru1	-26.12(14)	C48	N6	C36	Ru2	-14.52(16)
C13	N2	C1	N1	168.44(9)	C48	N6	C36	N5	174.53(11)
C13	N2	C3	C2	-167.27(9)	C48	N6	C38	C37	-177.01(13)
C13	C14	C15	C16	-0.22(15)	C48	C49	C50	C51	-2.23(18)
C14	C13	C18	C17	-2.75(14)	C49	C48	C53	C52	-5.67(15)
C14	C13	C18	C21	178.87(9)	C49	C48	C53	C56	169.91(10)
C14	C15	C16	C17	-1.30(15)	C49	C50	C51	C52	-0.91(19)
C14	C15	C16	C20	178.71(10)	C49	C50	C51	C55	-178.42(13)
C15	C16	C17	C18	0.81(15)	C50	C51	C52	C53	0.81(18)
C16	C17	C18	C13	1.17(14)	C51	C52	C53	C48	2.42(17)
C16	C17	C18	C21	179.55(10)	C51	C52	C53	C56	-173.27(11)
C18	C13	C14	C15	2.28(14)	C53	C48	C49	C50	5.57(16)
C18	C13	C14	C19	-178.21(9)	C53	C48	C49	C54	-170.83(11)
C19	C14	C15	C16	-179.74(10)	C54	C49	C50	C51	174.34(12)
C20	C16	C17	C18	-179.20(10)	C55	C51	C52	C53	178.33(12)
C22	C23	C24	C25	-177.65(10)	C57	C58	C59	C60	-178.94(10)

**Table 3.6.36. Torsion Angles for cs2927 [Ru] 9.**

A	B	C	D	Angle/°	A	B	C	D	Angle/°
C22	C23	C28	C27	177.03(9)	C57	C58	C63	C62	-179.07(9)
C22	C23	C28	C29	-0.50(14)	C57	C58	C63	C64	-1.62(15)
C23	C24	C25	C26	0.13(16)	C58	C59	C60	C61	-2.04(17)
C23	C28	C29	N3	-2.27(14)	C58	C63	C64	N7	4.35(15)
C24	C23	C28	C27	-1.17(13)	C59	C58	C63	C62	0.55(14)
C24	C23	C28	C29	-178.70(9)	C59	C58	C63	C64	178.00(9)
C24	C25	C26	C27	-0.49(17)	C59	C60	C61	C62	0.68(17)
C25	C26	C27	C28	0.00(16)	C60	C61	C62	C63	1.28(17)
C26	C27	C28	C23	0.85(15)	C61	C62	C63	C58	-1.89(15)
C26	C27	C28	C29	178.52(9)	C61	C62	C63	C64	-179.49(10)
C27	C28	C29	N3	-179.87(9)	C62	C63	C64	N7	-178.14(9)
C28	C23	C24	C25	0.70(15)	C63	C58	C59	C60	1.41(15)
C29	N3	C30	C31	-41.13(12)	C64	N7	C65	C66	-140.85(10)
C29	N3	C30	C35	142.99(9)	C64	N7	C65	C70	41.23(13)
C30	N3	C29	C28	171.26(8)	C65	N7	C64	C63	-175.23(9)
C30	C31	C32	C33	0.98(14)	C65	C66	C67	C68	0.15(18)
C31	C30	C35	C34	-0.37(15)	C66	C65	C70	C69	1.83(16)
C31	C32	C33	N4	177.62(9)	C66	C67	C68	N8	179.94(11)
C31	C32	C33	C34	-1.46(16)	C66	C67	C68	C69	1.11(19)
C32	C33	C34	C35	1.01(17)	C67	C68	C69	C70	-0.89(18)
C33	C34	C35	C30	-0.07(16)	C68	C69	C70	C65	-0.59(17)
C35	C30	C31	C32	-0.09(14)	C70	C65	C66	C67	-1.60(17)

This report has been created with Olex2, compiled on 2022.04.07 svn.rca3783a0 for OlexSys. Please [let us know](#) if there are any errors or if you would like to have additional features.

## Experimental Section References

- (1) Niwayama, S.; Cho, H.; Zabet-Moghaddam, M.; Whittlesey, B. R. Remote Exo/Endo Selectivity in Selective Monohydrolysis of Dialkyl Bicyclo[2.2.1]heptane-2,3-dicarboxylate Derivatives. *J. Org. Chem.* **2010**, *75* (11), 3775-3780. DOI: 10.1021/jo100564e.
- (2) Chang, A. B.; Lin, T.-P.; Thompson, N. B.; Luo, S.-X.; Liberman-Martin, A. L.; Chen, H.-Y.; Lee, B.; Grubbs, R. H. Design, Synthesis, and Self-Assembly of Polymers with Tailored Graft Distributions. *J. Am. Chem. Soc.* **2017**, *139* (48), 17683-17693. DOI: 10.1021/jacs.7b10525.

## Chapter 4. Imine-Chelated Ruthenium Olefin Metathesis Inimer

Hanan N. Almuzaini,<sup>a,b</sup> Carla Slebodnick,<sup>a</sup> Michael D. Schulz<sup>a,b</sup>

<sup>a</sup> Department of Chemistry, Virginia Polytechnic Institute and State University,  
Blacksburg, VA 24061

<sup>b</sup> Macromolecules Innovation Institute, Virginia Polytechnic Institute and State  
University, Blacksburg, VA 24061

### 4.1. Abstract

Hyperbranched polymers (HPs) exhibit different material properties compared to their less branched counterparts, but their synthesis is often challenging. Synthesizing HPs via ring-opening metathesis polymerization (ROMP) currently requires multiple reactions or specialized monomers. To enable a more general approach, we synthesized a ROMP inimer (initiator + monomer)—a molecule containing both the initiator and polymerizable group—to enable HP synthesis via self-condensing ROMP in a single step. To test the capabilities of this approach, we monitored the polymerization kinetics of the ROMP inimer with the addition of a ROMP monomer through <sup>1</sup>H NMR experiments. The rate of initiation and propagation affects the branching structure of the polymer. Polymerization with a higher propagation rate produced a polymer with fewer branching units, while increasing the initiation rate increased branching density. This approach enables the synthesis of HPs in a single step while controlling branching density.

### 4.2. Introduction

Hyperbranched polymers (HPs) have distinct chemical and physical properties from their linear counterparts due to their high branching density and abundant end groups, with lower solution viscosity and higher solubility.<sup>1</sup> This polymer topology has attracted

considerable attention for both elucidating structure–property relationships and developing specific applications. Fréchet and coworkers developed self-condensing vinyl polymerization (SCVP) to synthesize HPs in a single step.<sup>2</sup> In this approach, the initiator is combined with a monomer into one chemical entity called an *inimer* (initiator + monomer) (**Figure 4.1.a**). SCVP enables HP synthesis in a controlled manner by altering the monomer-to-inimer ratio, which controls the degree of branching.

Later, this self-condensing polymerization concept was applied to ring-opening polymerization. For instance, hyperbranched polyesters were synthesized by self-condensing ring-opening polymerization (SCROP) using inimers such as 4-(2-hydroxyethyl)- $\epsilon$ -caprolactone (**Figure 4.1.b**).<sup>3</sup> Despite the considerable utility of these self-condensing approaches, this concept has not been applied to olefin metathesis polymerization.

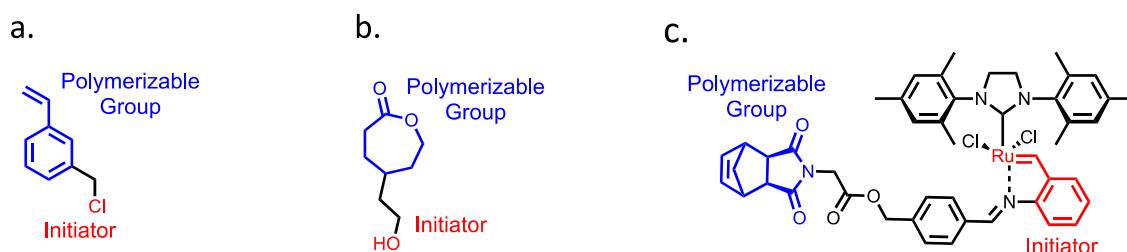


**Figure 4.1. Representative inimers for a. SCVP, b. SCROP, and c. current approach (self-condensing ROMP).**

Ring-opening metathesis polymerization (ROMP) has enabled the controlled synthesis of polyolefins with controlled topologies. Thanks to the development of effective olefin metathesis catalysts, it is now possible to produce precision polyolefins,<sup>4-7</sup> advanced polymer architectures,<sup>8</sup> and functional materials.<sup>9</sup> While some examples of HPs synthesized by ROMP exist,<sup>13,14</sup> the synthesis of a “ROMP-inimer”—a molecule

containing both a ROMP initiator and monomer—has not been reported. Therefore, the synthesis of a ROMP inimer could provide a new approach to preparing HPs by incorporating the concept of self-condensing polymerization into ROMP, thereby enabling the direct synthesis of HPs from any ROMP-active monomers. In this report, we describe the successful synthesis of a ROMP inimer that contains both initiating and propagating sites. The key to this approach is the synthesis of a *latent* olefin metathesis catalyst with a ROMP-polymerizable group appended to the benzylidene ligand (**Figure 4.1.c**).

Latent olefin metathesis catalysts are initially inactive at room temperature, but they can be activated by elevated temperature, changes in pH, mechanical force, or light.<sup>10-12</sup> This characteristic makes them ideal for preparing and handling monomer–catalyst mixtures without unwanted polymerization. In this study, a ROMP monomer was attached to a latent olefin metathesis catalyst via esterification to prevent unwanted polymerization (as shown in **Figure 4.2**). HPs were synthesized by using the ROMP inimer. An additional ROMP monomer was added to form the linear segment of the HPs.

### 4.3. Results and Discussion

The benzylidene ligand (**4**) was synthesized following the synthetic pathway presented in **Figure 4.2.a**. Grubbs second-generation catalyst (**G2**) was reacted with (**4**) to produce a latent olefin metathesis catalyst (**5**). Coupling an acid chloride-functionalized norbornene (**6**) to (**5**) resulted in the ROMP inimer (**7**), which contained both the initiating and propagating site (as shown in **Figure 4.2.a**). The structure of the ROMP inimer was confirmed using proton nuclear magnetic resonance (<sup>1</sup>H NMR) spectroscopy and single-crystal X-ray crystallography as shown in **Figure 4.2**. The presence of carbene (H<sub>a</sub>), imine (H<sub>b</sub>), and olefin (H<sub>c</sub>) peaks in the <sup>1</sup>H NMR spectrum confirmed the synthesis of a ROMP

inimer.  $^1\text{H}$  NMR spectroscopy results showed only the norbornene peaks ( $\text{H}_c$ ) in the alkene region, confirming that the catalysts did not initiate during the coupling step (as shown in **Figure 4.2.b**). The ester linkage was confirmed by the  $\text{H}_d$  and  $\text{H}_e$  peaks.

The synthesis of the trans-chloride isomer ROMP inimer with trigonal bipyramidal geometry was confirmed by single-crystal X-ray crystallography (as depicted in **Figure 4.2.c**). The bond lengths and angles around the ruthenium center were in the same range as other known catalysts containing a chelating imine.<sup>13</sup>

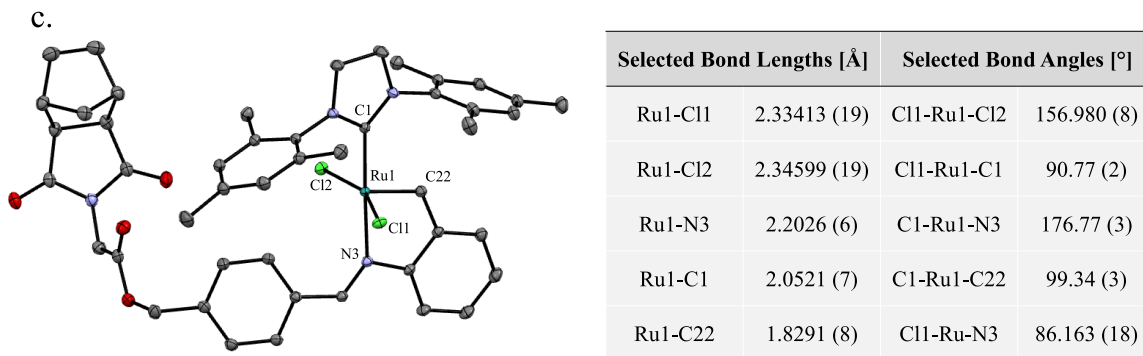
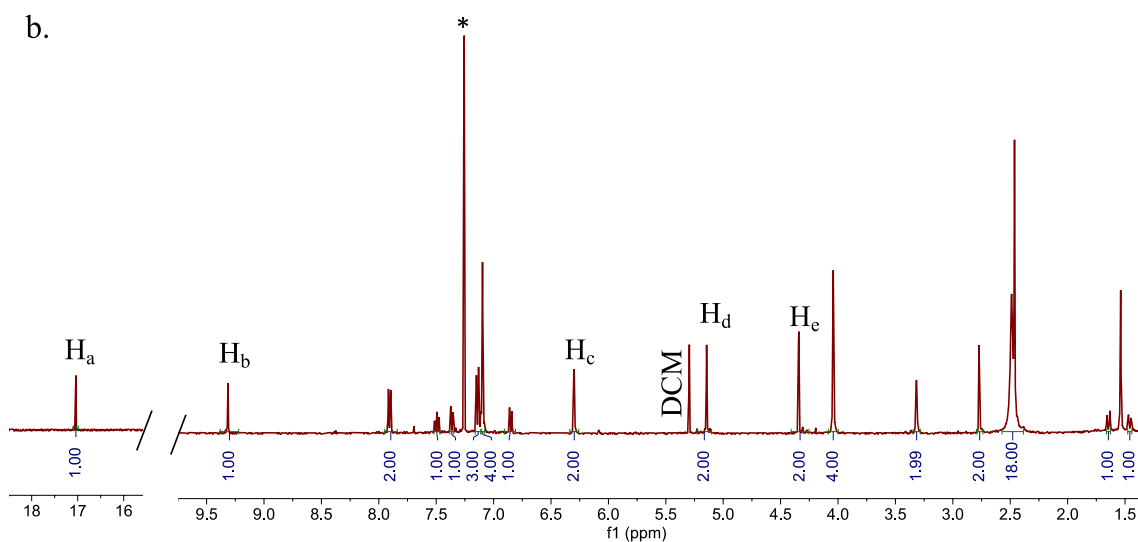
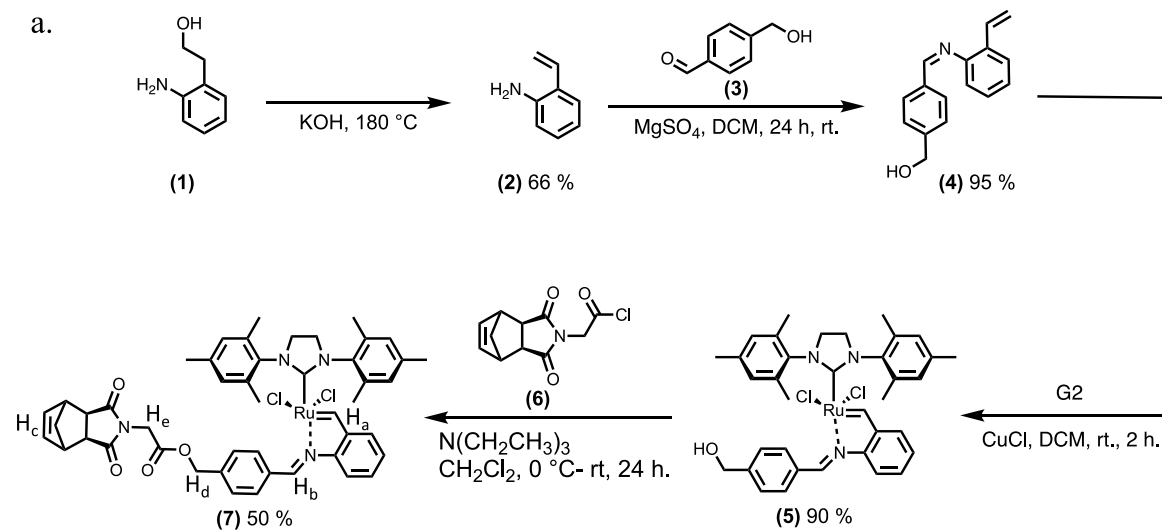


**Figure 4.2.a. Synthesis of ROMP inimer (7), b.  $^1\text{H}$  NMR of (7), and c. crystal structure with selected bond lengths and angles for the synthesis of (7).**

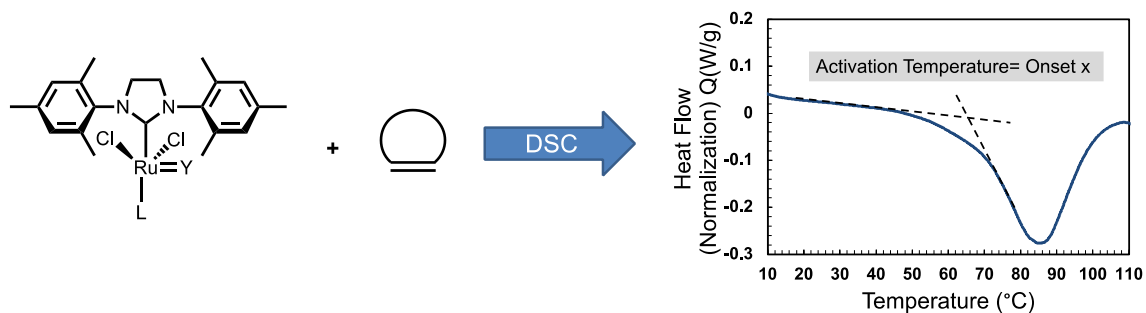
To investigate the inimer activation temperature, we determined the onset of polymerization for several different ROMP monomers. The polymerization was monitored by DSC with a heating ramp of 3 °C/min, and the activation temperature was determined by measuring the onset point of the large exothermic peak associated with polymerization (**Figure 4.3**). The DSC measurement revealed that the inimer exhibited varying activation temperatures when polymerizing the different ROMP monomers. The dependence of the inimer activation temperature on the monomer identity ranged between 48 and 100 °C, with the lowest activation temperature associated with the polymerization of highly reactive norbornene (**M1**). As the reactivity of the ROMP monomer decreased (**M4** and **5**), the activation temperature increased. The presence of a diester functionality on the norbornene increased the inimer activation temperature. Although having two *exo* ester functionalities in monomer (**M2**) increased the activation temperature by only 2 °C, the two *endo* ester groups (**M6**) increased the inimer activation temperature by 52 °C compared to (**M1**) due to steric hindrance.

To investigate the effect of the polymerizable group on the inimer activation temperature, we synthesized the latent olefin metathesis catalyst (**8**). Similar to the ROMP inimer, this olefin metathesis catalyst (**8**) exhibited varied activation temperatures in polymerizing the ROMP monomers. However, (**8**) showed mainly lower activation temperatures, ranging between 48 and 88 °C, compared to the ROMP inimer. The increase in the ROMP inimer activation temperature may be due to the steric hindrance of the polymerizable group.

The DSC measurements suggested that the inimer is inactive below 48 °C. However, polymerization of the ROMP inimer with **M1** in a solution occurred at 25 °C at

a low rate. The polymerization of **M1** (80 equiv.) with the ROMP inimer (1 equiv.) in CDCl<sub>3</sub> was carried out in an NMR tube, and the reaction progress was monitored by <sup>1</sup>H NMR spectroscopy. The conversion was measured by olefin peak integration with 1,2,4,5-tetramethyl benzene as an internal standard. The <sup>1</sup>H NMR spectra showed that 20% of the **M1** was polymerized after 24 h and increased to 66% after 4 days at room temperature.

We also tested the activation of the inimer by UV light by mixing the ROMP inimer (1 equiv.) and **M1** (160 equiv.) in CDCl<sub>3</sub> at room temperature. Similar to room temperature activation, <sup>1</sup>H NMR showed a 15% conversion indicating that the activation was not affected by the UV light.



Initiator	Monomer	M1	M2	M3	M4	M5	M6
<p>ROMP inimer (7)</p> <p>(8)</p>	Activation Temperature (°C)	48	50	60	63	73	100
		48	54	67	58	66	88

**Figure 4.3. ROMP inimer (7) and latent olefin metathesis catalyst (8) activation temperatures were determined by DSC.**

We used self-condensing ROMP to prepare a HP using the ROMP inimer and **M1**. The polymerization process involves an initiation step with the ROMP inimer to form the non-chelated metathesis-active inimer (**Figure 4.4**). The active inimer then proceeds to polymerize both the ROMP inimer polymerizable group and the ROMP monomer, ultimately resulting in the formation of a hyperbranched structure, where the inimer produces branching units and the monomer forms the linear segments (**Figure 4.4**). To

study the polymerization and determine the initiation and propagating rates, we carried out the polymerization of **M1** with the ROMP inimer in toluene- $d_8$  in an NMR tube and monitored the reaction progress using  $^1\text{H}$  NMR spectroscopy.

We conducted two NMR kinetic studies using **M1** as a monomer: at 60 and 80 °C. The two samples were prepared by mixing the inimer (1 equiv.), **M1** (40 equiv.), and triphenylphosphine ( $\text{PPh}_3$ ) (1 equiv.) in toluene- $d_8$ .  $\text{PPh}_3$  was added to enhance the initiation rate, as was reported previously.<sup>14</sup> The first kinetic experiment was carried out by an NMR tube injection in a 600 MHz NMR instrument, and the polymerization progress was monitored at 60 °C.  $^1\text{H}$  NMR spectra were recorded every 4 min. Plotting the polymer olefin peaks (%) versus time (min) showed the low propagation rate of the polymerizable group in the inimer (**a**) compared to **M1** due to the difference in the monomer reactivity. Only 16% of the inimer polymerized after 5 min and slowly polymerized to 67% after 138 min. However, 55% of **M1** was polymerized in the first 5 min and 97% within 86 min. NMR data showed that the carbene inimer peak was still present in significant quantities during the polymerization, indicating that the complex did not decompose but is rather slow to initiate.

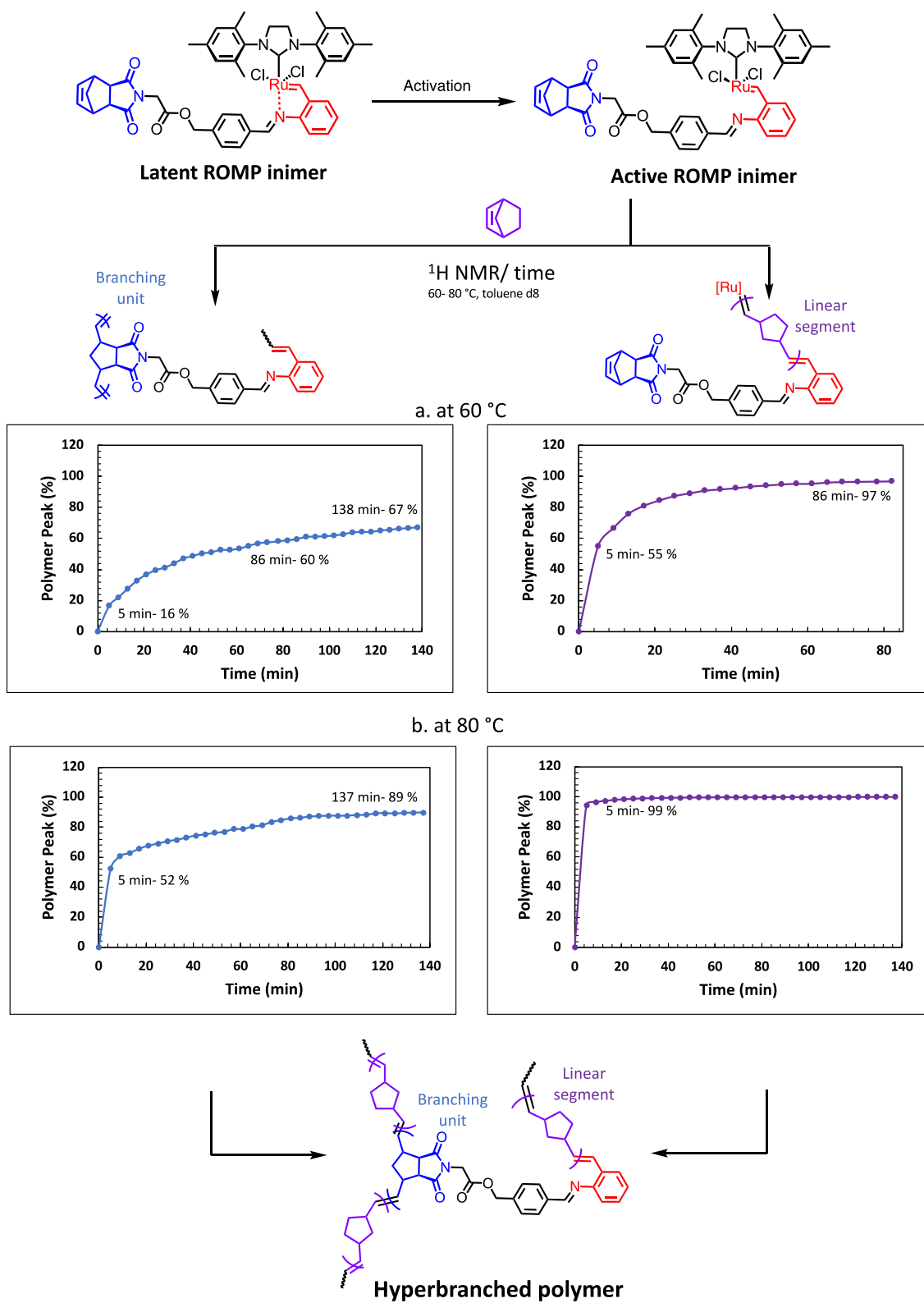
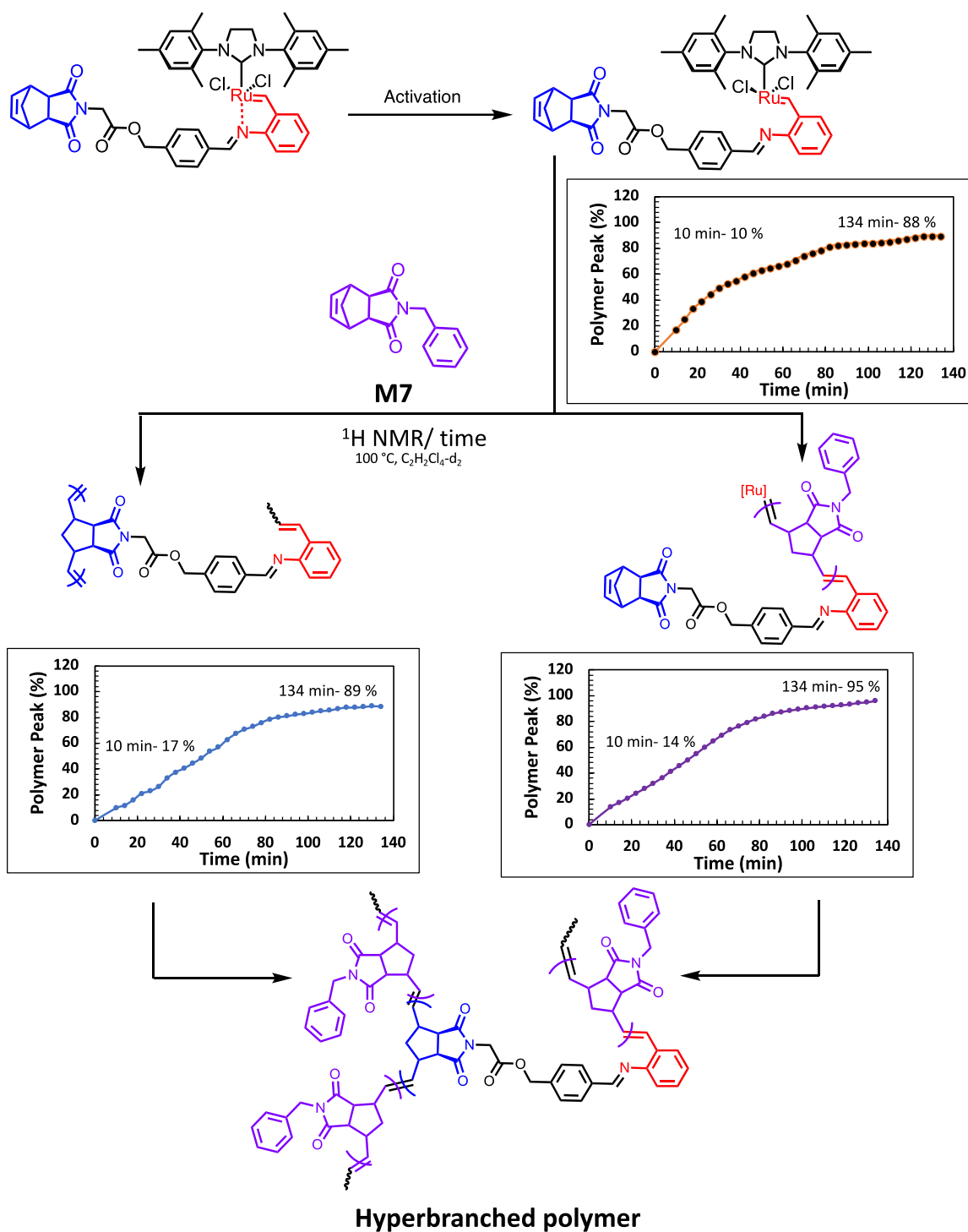


Figure 4.4. Polymerization of M1 and 7 at 60 and 80 °C.

To increase the rate of initiation, we repeated the kinetic experiment at 80 °C. The NMR data revealed an increase in the inimer propagating rate, from 52 % conversion in the first 5 min increasing to 89 % after 137 min. However, **M1** achieved almost full conversion in the first 5 min of the polymerization. The carbene peak remained relatively stable during the polymerization, indicating inimer stability at 80 °C and a low initiation rate. The high rate of monomer propagation and low rate of inimer initiation suggested the formation of a polymer with long linear segments and low branching density.

The initiation rate needs to be enhanced to incorporate a more branching structure in the final HP. Using a monomer with lower reactivity will slow the propagation rate, giving the inimer enough time to initiate. To test this hypothesis, we conducted another kinetic experiment using **M7 (Figure 4.5)**. The activation temperature of the inimer in the polymerization of **M7** is 107 °C, as measured by DSC. This high activation temperature can be explained by the high monomer melting temperature, which is indicated by DSC measurement as an endothermic peak at 105 °C. Lower activation temperatures are possible in solution. To find an accurate inimer activation temperature in polymerizing **M7**, we carried out a <sup>1</sup>H NMR kinetic experiment by mixing the inimer (1 equiv.), **M7**, (20 equiv.), and PPh<sub>3</sub> (1 equiv.) in C<sub>2</sub>D<sub>2</sub>Cl<sub>4</sub> at 80 °C for 1 hour. The <sup>1</sup>H NMR indicates that less than 5% of **M7** polymerized, and no change in the carbene peak was observed, indicating a lower initiation and propagation rate at this temperature. Then, the temperature was increased to 100 °C, and the progress was followed by recording <sup>1</sup>H NMR every 4 min. At 100 °C, both the ROMP inimer polymerizable group and **M7** polymerized at similar rates, starting with 17 and 14%, respectively, after 10 min and increasing to 89 and 95%, after 134 min, respectively.



**Figure 4.5. Polymerization of M7 and ROMP inimer at  $100^\circ\text{C}$ .**

During the polymerization, the carbene peak was shifted, indicating that inimer initiation occurred at a rate similar to the propagation rate.  $^1\text{H}$  NMR analysis revealed that

88% of the inimer was initiated over the course of the polymerization without any sign of inimer degradation. The HP synthesis of M7 exhibited similar initiation and propagation rates, indicating the incorporation of more branching units into the polymer structure. The higher initiation rate in this polymerization suggested polymerization of both the inimer polymerizable group and monomer, with formation of a branching unit at the active site.

Based on  $^1\text{H}$  NMR kinetic studies, we will synthesize a series of HPs having different number-average molecular weight ( $M_n$ ), and polymer degree branching by changing the inimer-to-monomer ratio. Theoretically, increasing the inimer molar ratio will increase the branching units in the final polymer structure, and increasing the monomer molar ratio will lengthen the linear segments, resulting in polymers with lower branching density.

#### **4.4. Conclusion**

Self-condensing ROMP enabled HP synthesis in a single step. The initiation and propagation rates affected the polymer branching density. By enhancing the inimer initiation rate, the branching units increased and the ROMP inimer and monomer polymerized in a controlled manner. This approach introduces a new class of olefin metathesis catalysts, inimers, by the addition of ROMP monomer moieties. The successful ROMP inimer synthesis will enable the synthesis of hyperbranched polymers using any ROMP monomer.

#### 4.5. References

- (1) Zheng, Y.; Li, S.; Weng, Z.; Gao, C. Hyperbranched polymers: advances from synthesis to applications. *Chem. Soc. Rev.* **2015**, *44* (12), 4091-4130. DOI: 10.1039/C4CS00528G.
- (2) Fréchet, J. M. J.; Henmi, M.; Gitsov, I.; Aoshima, S.; Leduc, M. R.; Grubbs, R. B. Self-Condensing Vinyl Polymerization: An Approach to Dendritic Materials. *Science* **1995**, *269* (5227) 1080-1083. doi: 10.1126/science.269.5227.1080.
- (3) Liu, M.; Vladimirov, N.; Fréchet, J. M. A new approach to hyperbranched polymers by ring-opening polymerization of an AB monomer: 4-(2-hydroxyethyl)- $\epsilon$ -caprolactone. *Macromolecules* **1999**, *32* (20), 6881-6884. [doi.org/10.1016/S0032-3861\(01\)00129-X](https://doi.org/10.1016/S0032-3861(01)00129-X)
- (4) Schulz, M. D.; Wagener, K. B. Precision Polymers through ADMET Polymerization. *Macromol. Chem. and Phys* **2014**, *215* (20), 1936-1945. DOI: 10.1002/macp.201400268.  
Schulz, M. D.; Wagener, K. B. ADMET Polymerization. In *Handbook of Metathesis*, Wiley-VCH Verlag GmbH & Co. KGaA, 2015; pp 313-355. Caire da Silva, L.; Rojas, G.; Schulz, M. D.; Wagener, K. B. Acyclic diene metathesis polymerization: History, methods and applications. *Prog. in Polym. Sci.* **2017**, *69*, 79-107. DOI: <https://doi.org/10.1016/j.progpolymsci.2016.12.001>. Atallah, P.; Wagener, K. B.; Schulz, M. D. ADMET: The Future Revealed. *Macromolecules* **2013**, *46* (12), 4735-4741. DOI: 10.1021/ma400067b (accessed 2014/05/09).
- (5) Sheiko, S. S.; Sumerlin, B. S.; Matyjaszewski, K. Cylindrical molecular brushes: Synthesis, characterization, and properties. *Prog. in Polym. Sci.* **2008**, *33* (7), 759-785. DOI: <https://doi.org/10.1016/j.progpolymsci.2008.05.001>.
- (6) Sutthasupa, S.; Shiotsuki, M.; Sanda, F. Recent advances in ring-opening metathesis polymerization, and application to synthesis of functional materials. *Polym J* **2010**, *42* (12), 905-915.
- (7) Teator, A. J.; Bielawski, C. W. Remote control grubbs catalysts that modulate ring-opening metathesis polymerizations. *J. Polym. Sci. Part A: Polym. Chem.* **2017**, *55* (18), 2949-2960. DOI: 10.1002/pola.28665 (accessed 2019/03/15). Monsaert, S.; Lozano Vila, A.; Drozdak, R.; Van Der Voort, P.; Verpoort, F. Latent olefin metathesis catalysts. *Chem. Soc. Rev.* **2009**, *38* (12), 3360-3372, 10.1039/B902345N. DOI: 10.1039/B902345N. Diesendruck, C. E.; Iliashevsky, O.; Ben-Asuly, A.; Goldberg, I.; Lemcoff, N. G. Latent

and Switchable Olefin Metathesis Catalysts. *Macromolecular Symposia* **2010**, 293 (1), 33-38. DOI: 10.1002/masy.200900036.

(8) Slugovc, C.; Burtscher, D.; Stelzer, F.; Mereiter, K. Thermally Switchable Olefin Metathesis Initiators Bearing Chelating Carbenes: Influence of the Chelate's Ring Size. *Organometallics* **2005**, 24 (10), 2255-2258. DOI: 10.1021/om050141f.

(9) Bielawski, C. W.; Grubbs, R. H. Increasing the Initiation Efficiency of Ruthenium-Based Ring-Opening Metathesis Initiators: Effect of Excess Phosphine. *Macromolecules* **2001**, 34 (26), 8838-8840. DOI: 10.1021/ma011214j.

## 4.6. Experimental Section

### Materials

All reactions were performed using oven-dried glassware equipped with a magnetic stir bar under an air atmosphere unless otherwise noted. 2-Aminophenethyl and 4-(hydroxymethyl) benzaldehyde were purchased from Ambeed. Benzaldehyde, cyclooctene, dicyclooctene, and norbornene were purchased from Sigma Aldrich. The Grubbs second-generation catalyst (G2) was donated from Materia and purchased from Ambeed. Deuterated solvents were obtained from Cambridge Isotope Laboratories. Unless otherwise stated, all other reagents were purchased at the highest commercial quality and used without further purification.

### Measurements

$^1\text{H}$  NMR and  $^{13}\text{C}$  NMR data were collected in  $\text{CDCl}_3$ ,  $\text{CD}_2\text{Cl}_2$ , toluene- $d_8$ , and  $\text{C}_2\text{D}_2\text{Cl}_4$  at 25 °C unless otherwise noted using an Agilent U4-DD2 400 MHz, or a Bruker Advance II 500 and 600 MHz NMR instrument. Chemical shifts were reported in ppm and referenced to the  $\text{CHCl}_3$  singlet at 7.26 ppm, TMS singlet at 0 ppm,  $\text{CD}_2\text{Cl}_2$  triplet at 5.32 ppm, toluene singlet at 2.08 ppm, and  $\text{C}_2\text{D}_2\text{Cl}_4$  singlet at 6 ppm for  $^1\text{H}$  NMR.  $^{13}\text{C}$  NMR spectra were referenced to the center peak of the  $\text{CDCl}_3$  triplet at 77.00 ppm, or  $\text{CD}_2\text{Cl}_2$  at 54.00 ppm. The following abbreviations (or combinations thereof) were used to explain the multiplicities: s = singlet, d = doublet, t = triplet, q = quartet, m = multiplet, br = broad, and \* for the deuterated solvent peak.

Catalyst activation temperature was measured by differential scanning calorimetry (DSC) with a DSC Q2500 from TA instruments equipped with an autosampler. Sample

masses ranging from 6–10 mg were crimped in a high-volume pan and lid and then loaded into the cell alongside a reference pan. The method incorporated equilibration at 25 °C and the samples were heated from 25 °C to 150 °C at a rate of 3 °C/ min. The activation temperature was determined as the onset point of the slope from the baseline of an exothermic transition.

**2-Vinylniline (2):** To a 100 mL round-bottom flask equipped with a stir bar, short path distillation head, and tared receiving flask was added 2-aminophenethyl alcohol (1 equiv., 5.0 g) and potassium hydroxide (1 equiv., 2.04 g). The mixture was heated to 180 °C. With continued heating and applied vacuum for 4 h, the clear product distilled over (83–90 °C) to the tared receiving flask (Yield 2.60 g, 66 %).

<sup>1</sup>H NMR (400 MHz, CDCl<sub>3</sub>): δ 7.30 (d, *J* = 7.6 Hz, 1H), 7.10 (t, *J* = 6.8 Hz, 1H), 6.85 – 6.73 (m, 2H), 6.69 (d, *J* = 7.7 Hz, 1H), 5.64 (d, *J* = 17.2 Hz, 1H), 5.33 (d, *J* = 11.0 Hz, 1H), 3.76 (s, 2H). <sup>13</sup>C NMR (101 MHz, CDCl<sub>3</sub>): δ 143.80, 132.89, 128.88, 127.48, 124.24, 119.08, 116.23, 115.84.

**Benzylidene ligand (4):** A round bottom flask was charged with **2** (1 equiv., 0.30 g), 4-(hydroxymethyl)benzaldehyde (1 equiv., 0.33 g), MgSO<sub>4</sub> (1g/1.0 mmol aldehyde, 2.80 g), and DCM (30 mL). The reaction mixture was stirred at room temperature under N<sub>2</sub> for 24 h after which the mixture was filtered and concentrated under reduced pressure. The crude product was used as is (Yield 0.40 g, 95 %).

<sup>1</sup>H NMR (500 MHz, CDCl<sub>3</sub>) δ 8.38 (s, 1H), 7.93 (d, *J* = 8.2 Hz, 2H), 7.59 (dd, *J* = 7.7, 1.5 Hz, 1H), 7.49 (d, *J* = 8.0 Hz, 2H), 7.31 – 7.27 (m, 1H), 7.23 – 7.17 (m, 2H), 6.96 (dd, *J* =

7.8, 1.3 Hz, 1H), 5.75 (dd,  $J = 17.7, 1.4$  Hz, 1H), 5.30 – 5.27 (m, 1H), 4.79 (d,  $J = 5.8$  Hz, 2H).

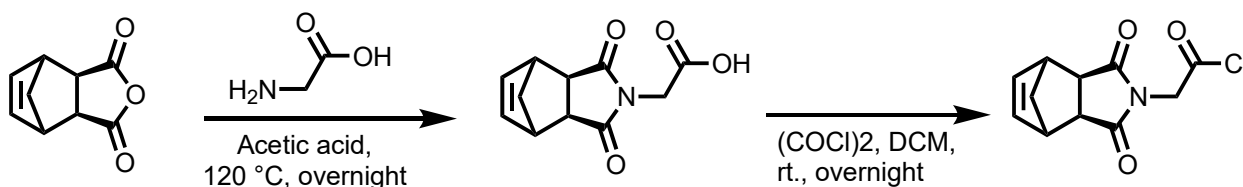
$^{13}\text{C}$  NMR (126 MHz,  $\text{CDCl}_3$ )  $\delta$  159.7, 149.8, 144.3, 135.7, 133.3, 131.3, 129.1, 128.7, 127.1, 125.9, 125.7, 118.4, 114.8, 64.9.

### Latent olefin metathesis catalyst (5)

A round bottom flask was charged with G2 (1 equiv.), and 4 (1 equiv.). DCM was added to the reaction flask under  $\text{N}_2$ . The reaction mixture was stirred at room temperature for 2 h. The solvent was evaporated, and the crude product was precipitated from pentane (Yield 90 %).

$^1\text{H}$  NMR (400 MHz,  $\text{CDCl}_3$ )  $\delta$  17.06 (d,  $J = 0.9$  Hz, 1H), 9.29 (s, 1H), 7.87 (d,  $J = 8.3$  Hz, 2H), 7.50 – 7.45 (m, 1H), 7.36 (d,  $J = 8.1$  Hz, 1H), 7.13 (d,  $J = 22.7$  Hz, 7H), 6.85 (dd,  $J = 7.6, 1.4$  Hz, 1H), 4.67 (s, 2H), 4.04 (s, 4H), 2.49 (d,  $J = 8.2$  Hz, 18H).

### Acid chloride (6)



Norbornene anhydride (1 equiv.), an amino acid (1 equiv.), and acetic acid (15 mL) were placed in a round-bottomed flask equipped with a reflux condenser and refluxed overnight. Then, the reaction mixture was poured into water (100 mL), extracted with DCM, dried with  $\text{MgSO}_4$ , and filtered.

Carboxylic acid functionalized norbornene, 200 mg, was dispersed in 10 mL of dry DCM, 5 equiv. of oxalyl chloride was added, and the mixture was left overnight. The solvent and

excess oxalyl chloride were evaporated on a rotary evaporator, and the residue (acid chloride) was used without further purification or characterization.

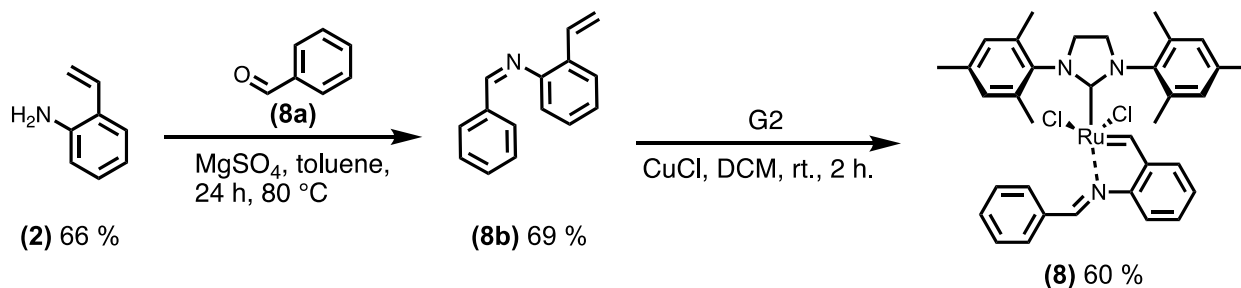
### ROMP inimer (7)

A mixture of catalyst **5** (1 equiv., 300 mg) and triethylamine (1.5 equiv., 65 mg) in DCM was cooled down to 0 °C. Acid chloride **6** (1 equiv., 100 mg) was dissolved in DCM and added dropwise to the catalyst mixture. The reaction mixture was stirred for 2 h under N<sub>2</sub>. Then, the product was isolated by column chromatography (9: 1 hexane: ethyl acetate). (Yield 50 %)

<sup>1</sup>H NMR (500 MHz, CD<sub>2</sub>Cl<sub>2</sub>) δ 17.04 (d, *J* = 0.9 Hz, 1H), 9.38 (s, 1H), 7.96 (d, *J* = 8.2 Hz, 2H), 7.64 – 7.57 (m, 1H), 7.47 (d, *J* = 8.2 Hz, 1H), 7.25 – 7.19 (m, 3H), 7.18 – 7.14 (m, 4H), 6.95 (dd, *J* = 7.6, 1.4 Hz, 1H), 6.35 (t, *J* = 1.9 Hz, 2H), 5.21 (s, 2H), 4.38 (s, 2H), 4.07 (s, 4H), 3.31 (s, 2H), 2.81 (d, *J* = 1.4 Hz, 2H), 2.52 (s, 18H), 1.71 – 1.65 (m, 1H), 1.51 – 1.45 (m, 1H).

<sup>13</sup>C NMR (126 MHz, CD<sub>2</sub>Cl<sub>2</sub>) δ 296.77, 211.41, 177.38, 167.30, 164.16, 143.94, 139.02, 138.82, 138.80, 138.30, 134.97, 130.82, 130.42, 130.11, 129.44, 128.43, 120.44, 117.13, 67.41, 48.41, 45.86, 43.11, 39.83, 21.38.

### Latent olefin metathesis catalyst (8)



**(E)-1-phenyl-N-(2-vinylphenyl)methanimine (8b):** A round bottom flask was charged with **2** (1 equiv., 0.30 g), benzaldehyde (1 equiv., 0.33 g), MgSO<sub>4</sub> (1g/1.0 mmol aldehyde, 2.80 g) and toluene (30 mL). The reaction mixture was stirred at 80 °C under N<sub>2</sub> for 24 h after which the mixture was filtered and concentrated under reduced pressure. The crude product was used (as it is) (Yield 0.40 g, 69 %).

<sup>1</sup>H NMR (400 MHz, cdcl<sub>3</sub>) δ 8.81 (s, 1H), 8.11 (dd, *J* = 7.4, 1.0 Hz, 1H), 7.48 – 7.38 (m, 4H), 7.37 – 7.29 (m, 1H), 7.24 – 7.15 (m, 3H), 6.76 – 6.62 (m, 1H), 5.68 (d, *J* = 17.3 Hz, 1H), 5.47 (dd, *J* = 11.0, 0.7 Hz, 1H).

<sup>13</sup>C NMR (101 MHz, cdcl<sub>3</sub>) δ 192.42, 158.87, 152.44, 139.21, 133.83, 133.06, 131.08, 129.28, 129.15, 127.98, 127.96, 127.07, 125.94, 120.94, 118.55, 118.52, 115.09.

#### **Latent olefin metathesis catalyst (8)**

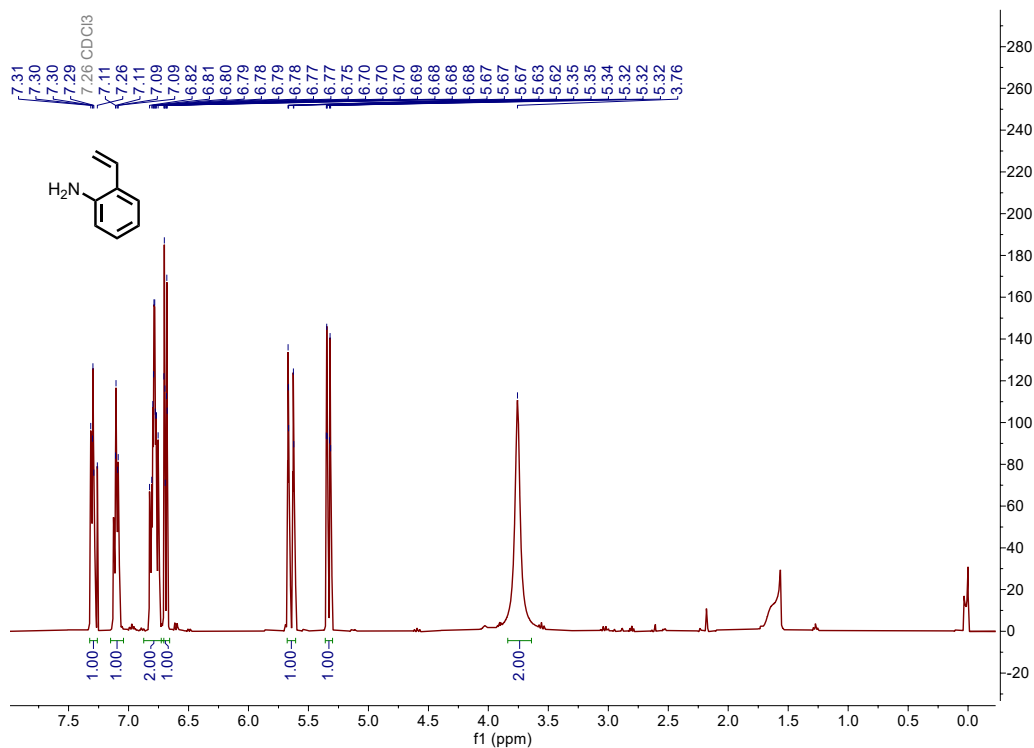
A round bottom flask was charged with G2 (1 equiv.), and **8b** (1 equiv.). DCM was added to the reaction flask under N<sub>2</sub>. The reaction mixture was stirred at room temperature for 2 h. The solvent was evaporated, and the crude product was precipitated from pentane (Yield 90 %).

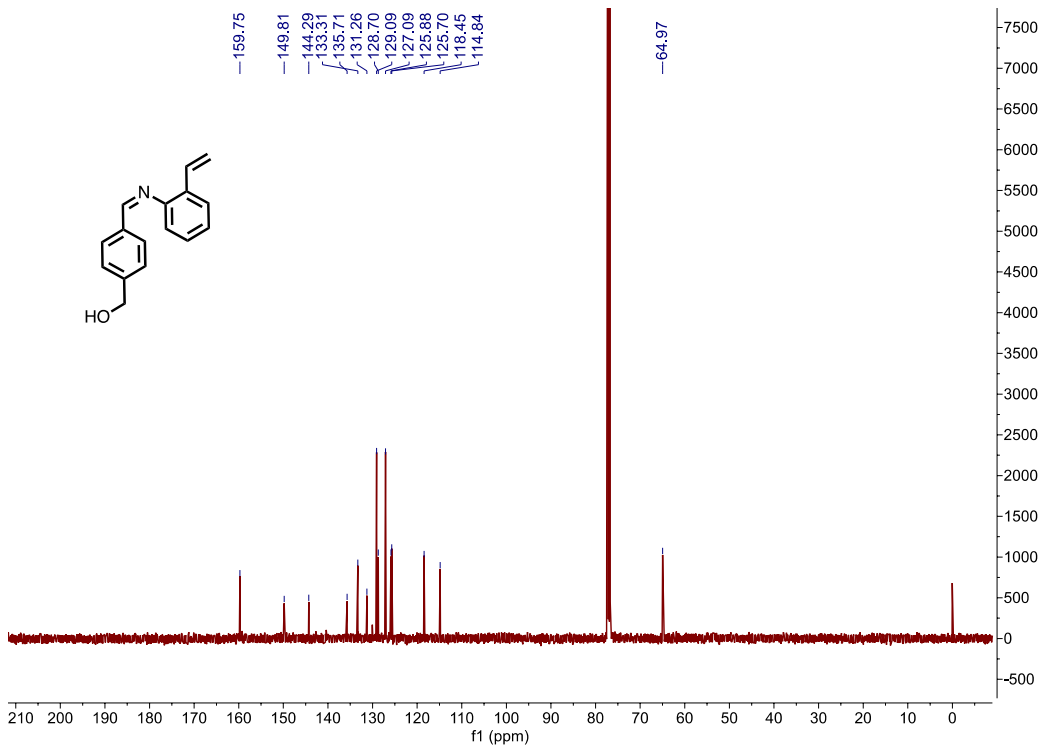
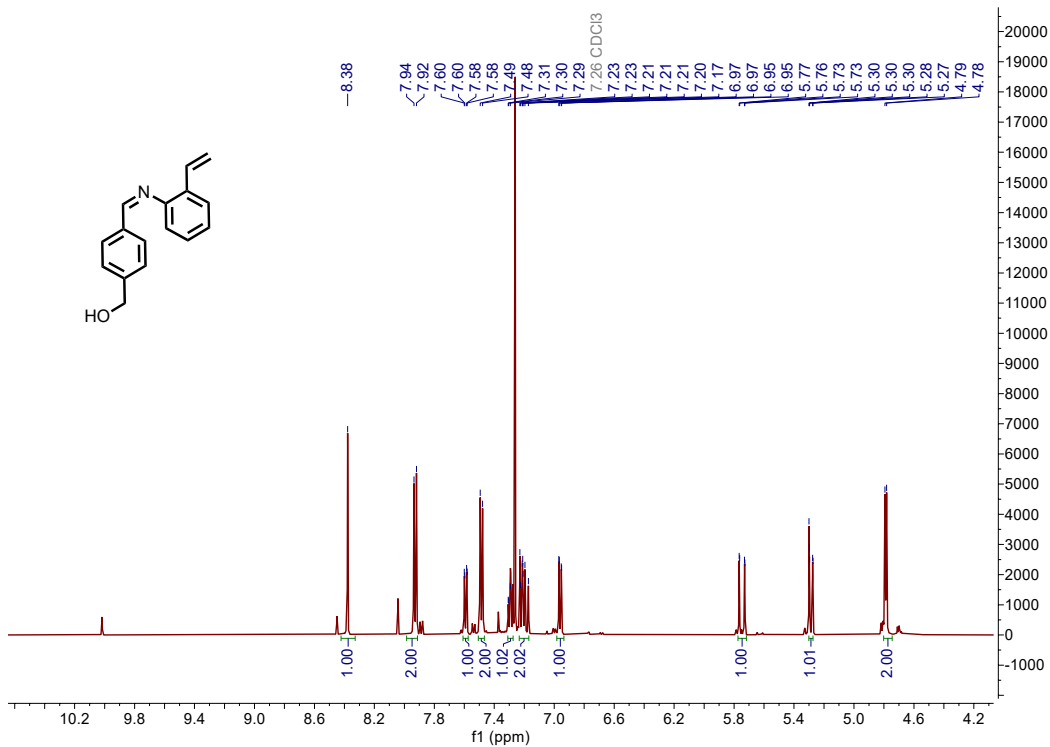
<sup>1</sup>H NMR (500 MHz, CD<sub>2</sub>Cl<sub>2</sub>) δ 18.72 (s, 1H), 8.67 (s, 1H), 7.86 – 6.98 (m, 10H), 6.83 (d, *J* = 7.8 Hz, 1H), 4.10 (s, 4H), 2.49 (d, *J* = 18.9 Hz, 18H).

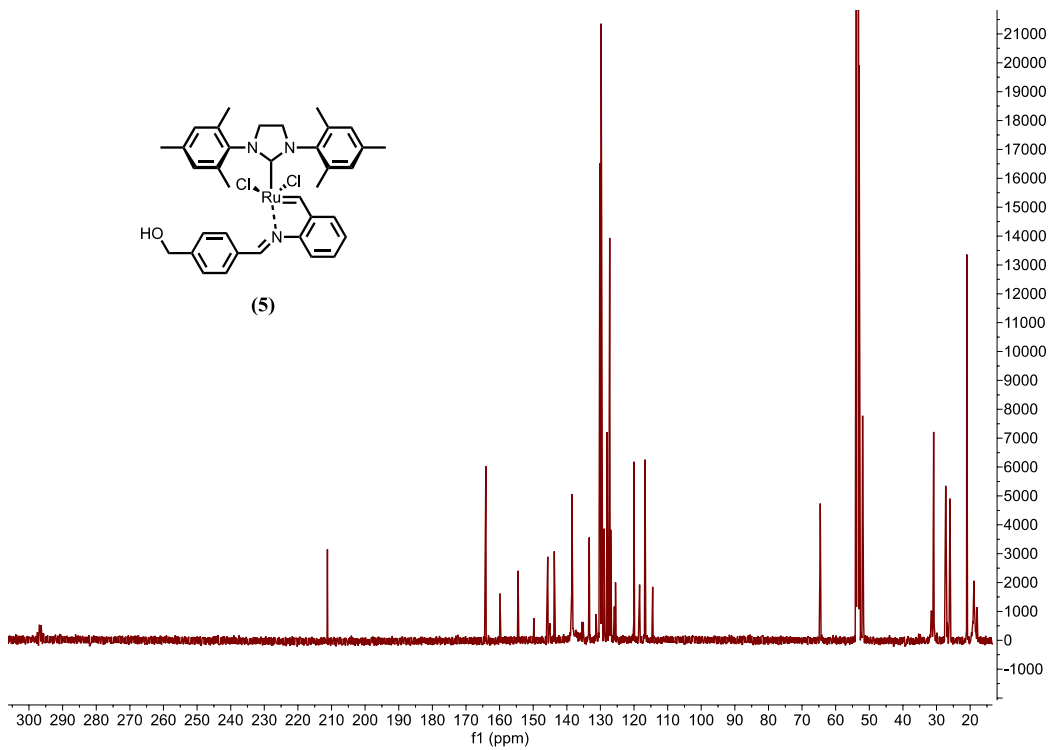
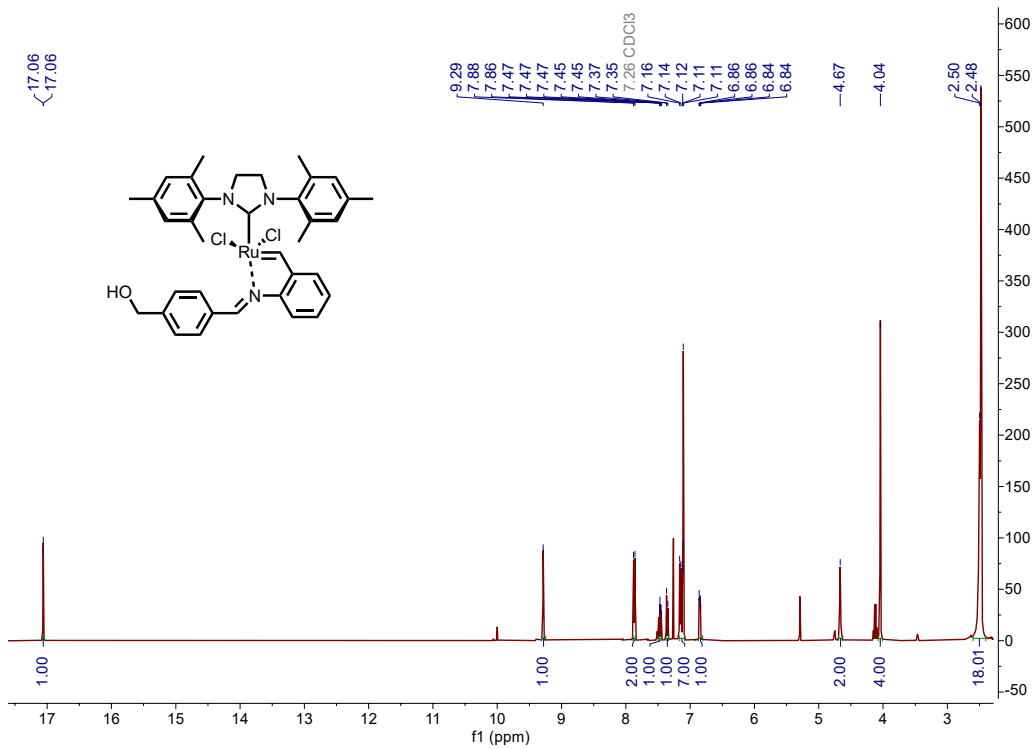
#### **Synthesis of ROMP monomer M2, 3, and 6**

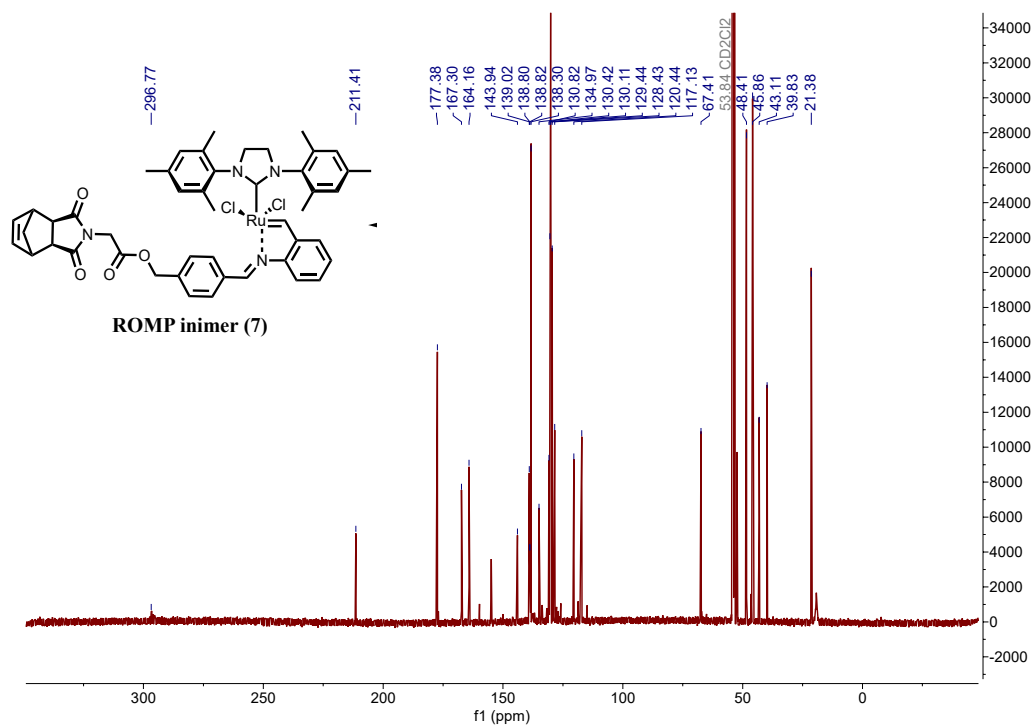
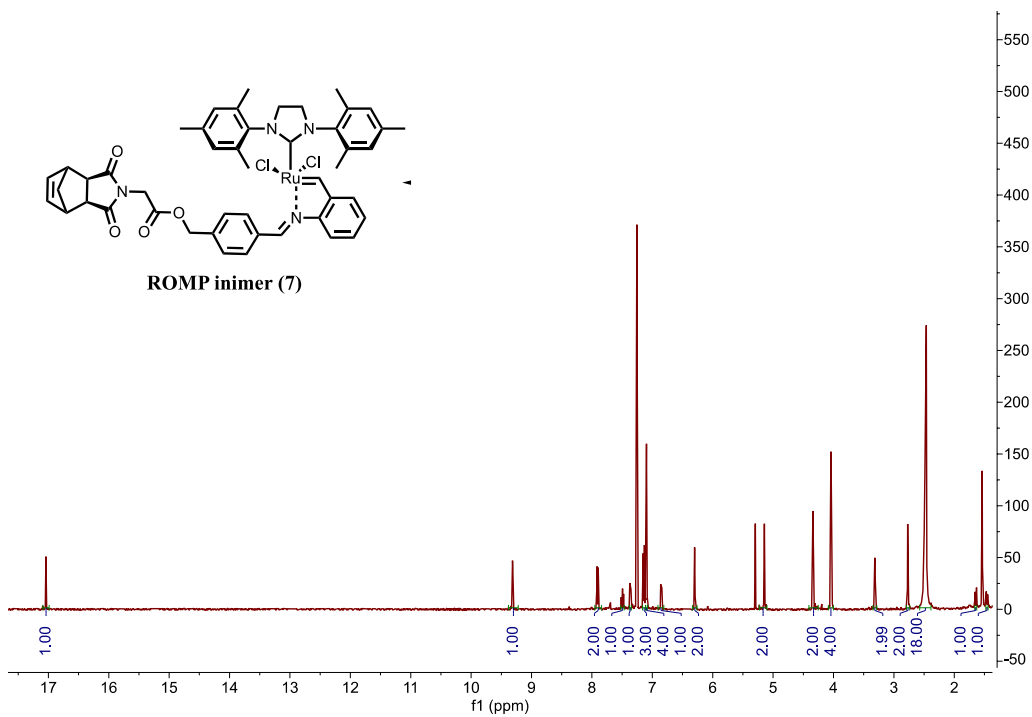
Monomers were synthesized following a literature procedure and characterized by <sup>1</sup>H NMR.<sup>1,2</sup> **M2** <sup>1</sup>H NMR (400 MHz, CDCl<sub>3</sub>): δ 6.19 (s, 2H), 4.08 (dd, *J* = 11.0, 7.2 Hz, 4H), 3.09 – 3.03 (m, 2H), 2.58 (d, *J* = 1.9 Hz, 2H), 2.14 – 2.10 (m, 1H), 1.47 (dt, *J* = 9.0, 1.8 Hz, 1H), 1.23 (t, *J* = 7.1 Hz, 6H). **M3** <sup>1</sup>H NMR (400 MHz, CDCl<sub>3</sub>): δ 6.33 – 6.24 (m, 1H), 6.17

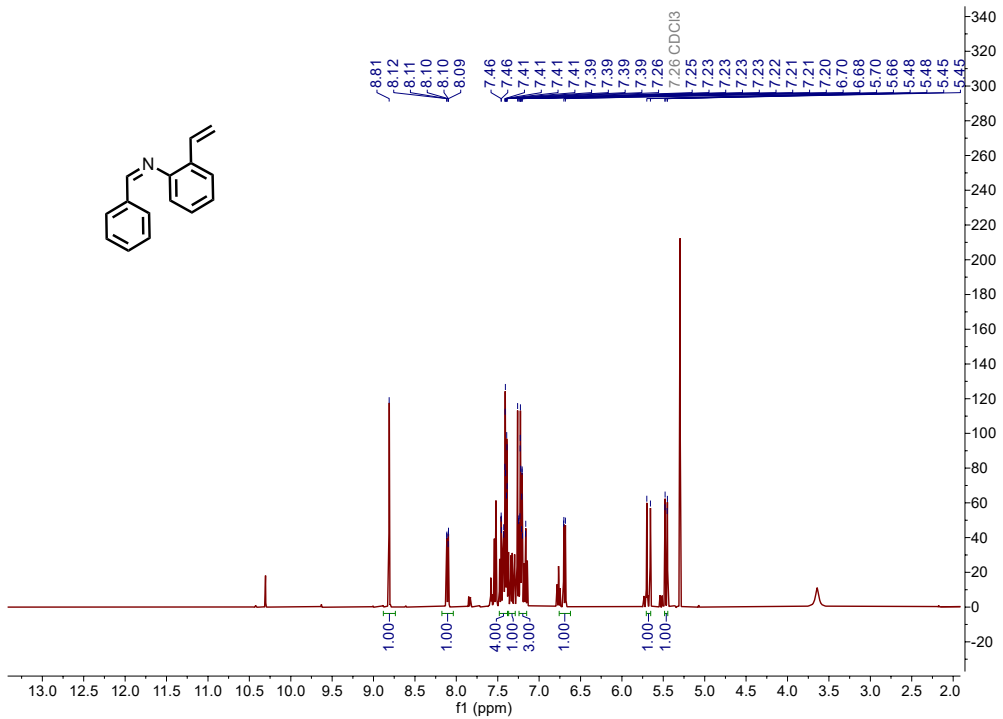
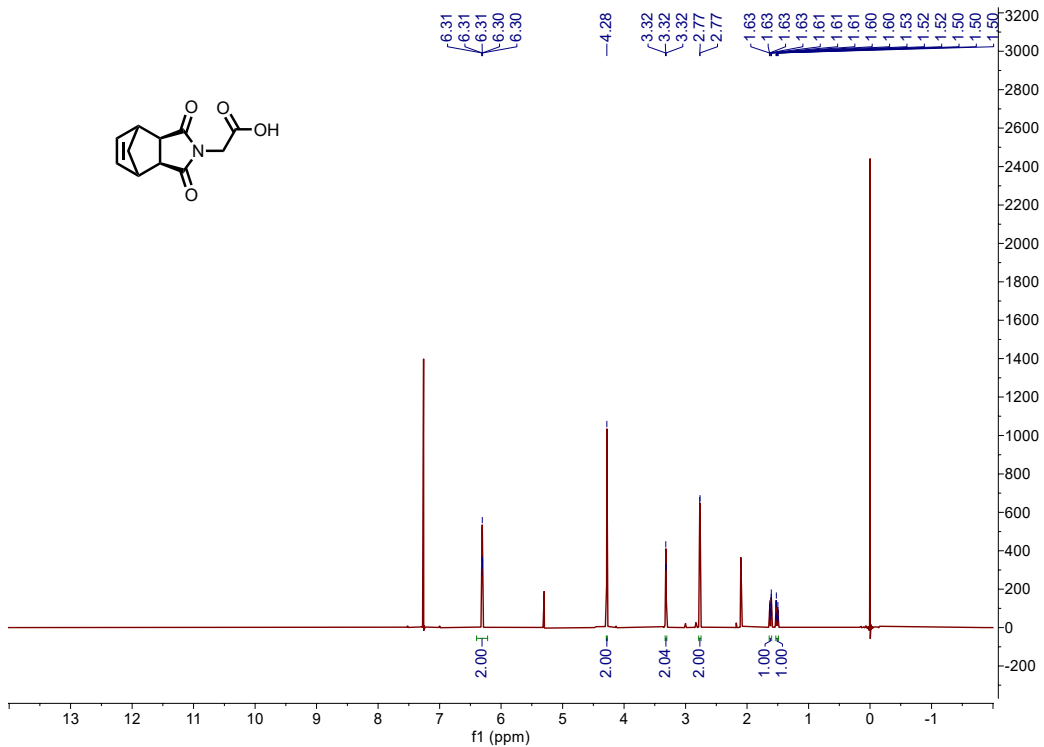
– 5.99 (m, 1H), 3.71 (d,  $J = 3.1$  Hz, 3H), 3.64 (d,  $J = 3.1$  Hz, 3H), 3.43 – 3.33 (m, 1H), 3.28 – 3.24 (m, 1H), 3.12 (dtd,  $J = 3.2, 1.6, 0.8$  Hz, 1H), 2.68 (ddd,  $J = 2.9, 1.6, 0.9$  Hz, 1H), 1.63 – 1.60 (m, 1H), 1.48 – 1.44 (m, 1H). **M6**  $^1\text{H}$  NMR (400 MHz,  $\text{CDCl}_3$ ):  $\delta$  6.23 (s, 2H), 4.04 (dddd,  $J = 11.0, 5.4, 2.5, 1.6$  Hz, 4H), 3.29 – 3.20 (m, 2H), 3.16 – 3.11 (m, 2H), 1.46 – 1.42 (m, 1H), 1.30 (dt,  $J = 8.5, 1.6$  Hz, 1H), 1.22 – 1.17 (m, 6H).

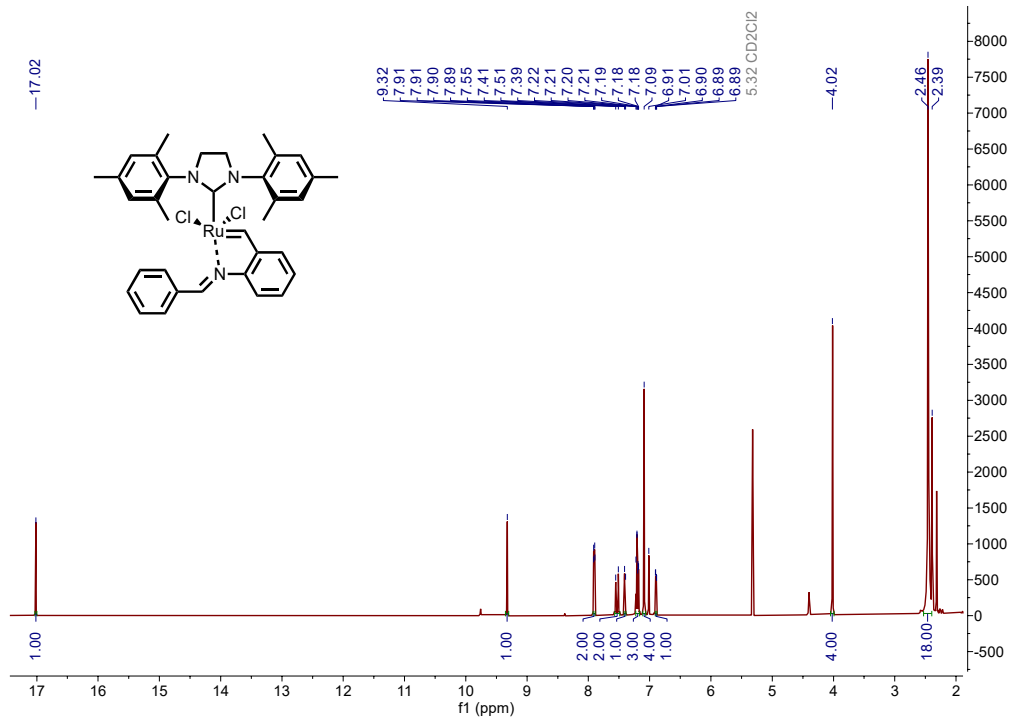
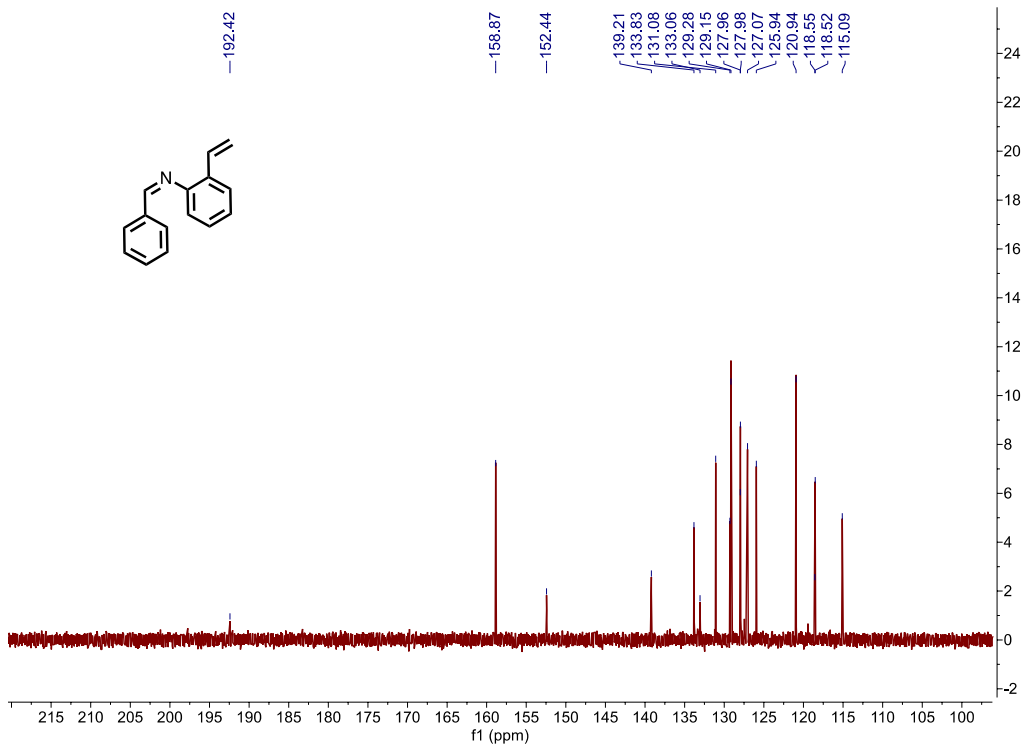


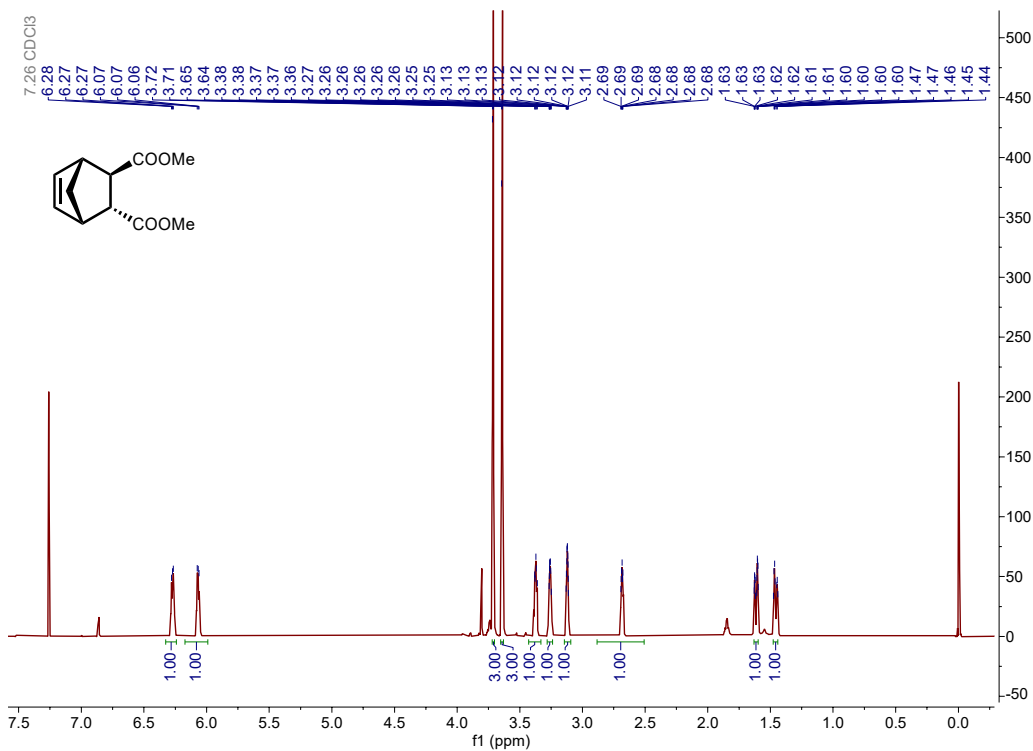
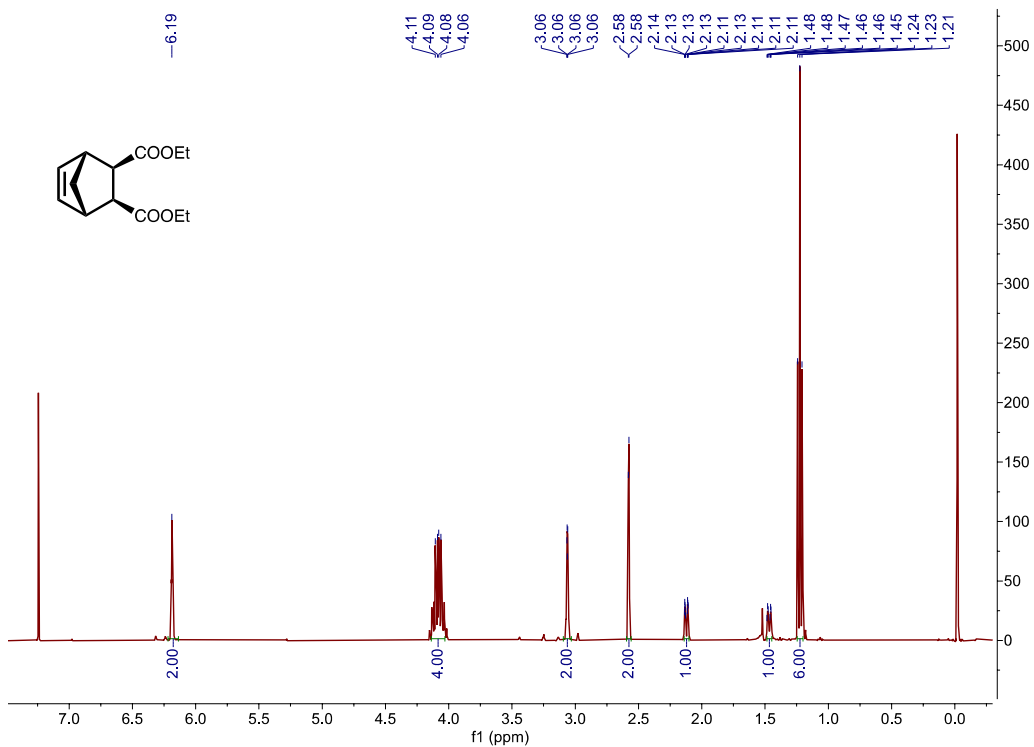


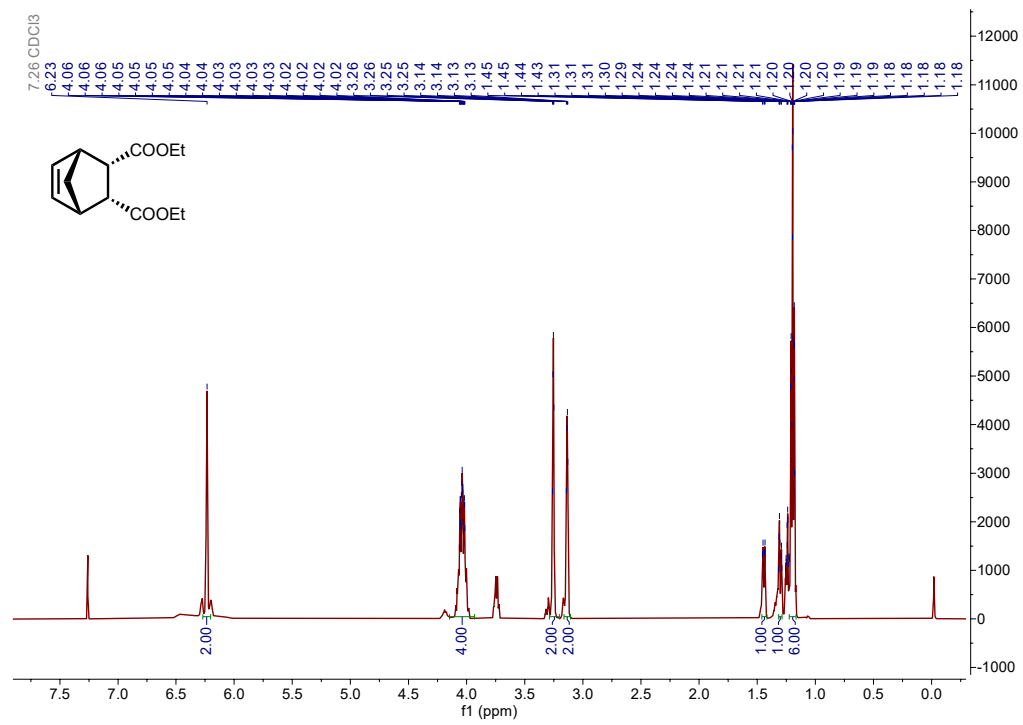








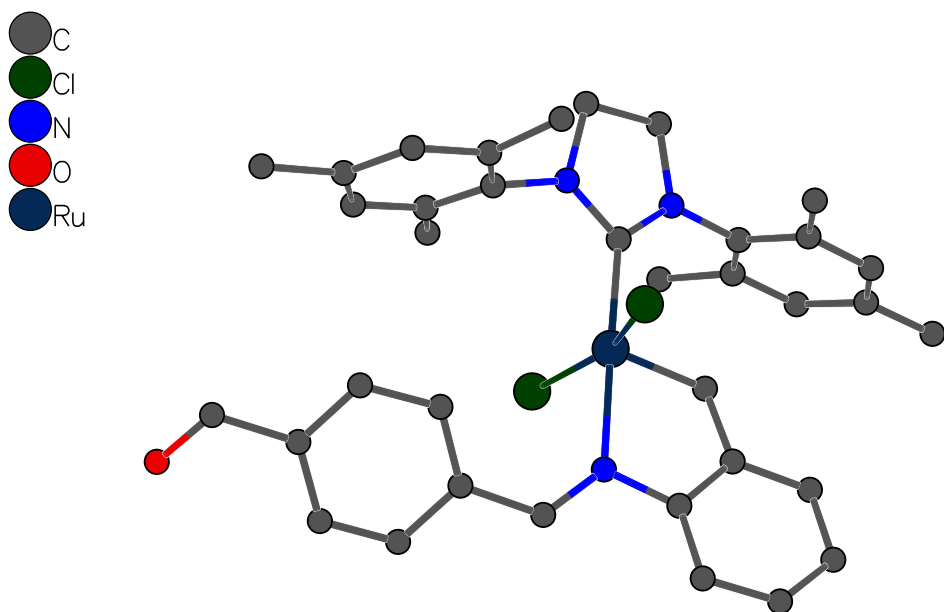




## Crystal Structure

**Acknowledgements:** We thank the support of the National Science Foundation under CHE-1726077 for crystallography experiments.

Crystal structure of (5)



(5)

## Experimental

A small yellow plate (0.01 x 0.05 x 0.06 mm<sup>3</sup>) was centered on the goniometer of a Rigaku Oxford Diffraction Synergy-S diffractometer equipped with a HyPix6000HE detector and operating with CuK $\alpha$  radiation. The data collection routine, unit cell refinement, and data processing were carried out with the program CrysAlisPro.<sup>61</sup> The Laue symmetry was consistent with the triclinic space groups P1 and P-1. The

---

(61) CrysAlisPro Software System, v1.171.42.xx, Rigaku Oxford Diffraction, 2022, Rigaku Corporation, Oxford, UK.

centrosymmetric space group P-1 was chosen. The structure was solved using SHELXT<sup>62</sup> and refined using SHELXL<sup>63</sup> via Olex2.<sup>64</sup> After modeling the metal complex, the largest difference peaks were appearing in a small void and were presumably disordered/mostly evaporated CH<sub>2</sub>Cl<sub>2</sub>. A total of 8 e<sup>-</sup> was subtracted from a void space of 43 Å<sup>3</sup>/asymmetric unit, equivalent to ~0.4CH<sub>2</sub>Cl<sub>2</sub>/unit cell. The final refinement model involved anisotropic displacement parameters for all non-hydrogen atoms with a universal RIGU restraint. A riding model was used for all hydrogen atoms. Olex2<sup>65</sup> was used for molecular graphics generation.

**Table 4.6.1. Crystal data and structure refinement for cs3029-catalyst (5).**

Identification code	HA-2-66
Empirical formula	C <sub>36</sub> H <sub>39</sub> Cl <sub>2</sub> N <sub>3</sub> ORu • 0.1(CH <sub>2</sub> Cl <sub>2</sub> )
Formula weight	710.16
Temperature/K	100.0(2)
Crystal system	triclinic
Space group	P-1
a/Å	14.3662(7)
b/Å	14.5676(10)
c/Å	16.0240(18)
α/°	80.507(8)
β/°	87.035(6)

---

(62) Sheldrick, G. M. "SHELXT – Integrated space-group and crystal structure determination." *Acta Cryst.* **2015**, *A71*, 3–8.

(63) Sheldrick, G. M. "Crystal structure refinement with SHELXL." *Acta Cryst.* **2015**, *C71*, 3–8.

(64) Dolomanov, O.V.; Bourhis, L. J.; Gildea, R. J.; Howard, J. A. K.; Puschmann, H. *J. Appl. Cryst.* **2009**, *42*, 339–341.

(65) Dolomanov, O.V.; Bourhis, L. J.; Gildea, R. J.; Howard, J. A. K.; Puschmann, H. *J. Appl. Cryst.* **2009**, *42*, 339–341.

$\gamma/^\circ$	84.684(5)
Volume/ $\text{\AA}^3$	3291.1(5)
Z	4
$\rho_{\text{calc}}/\text{cm}^3$	1.433
$\mu/\text{mm}^{-1}$	5.751
F(000)	1465.0
Crystal size/ $\text{mm}^3$	$0.062 \times 0.048 \times 0.01$
Radiation	Cu K $\alpha$ ( $\lambda = 1.54184$ )
2 $\Theta$ range for data collection/ $^\circ$	6.174 to 136.664
Index ranges	$-17 \leq h \leq 13, -17 \leq k \leq 17, -19 \leq l \leq 19$
Reflections collected	35853
Independent reflections	11550 [ $R_{\text{int}} = 0.1923, R_{\text{sigma}} = 0.1915$ ]
Data/restraints/parameters	11550/706/789
Goodness-of-fit on $F^2$	1.048
Final R indexes [ $I \geq 2\sigma(I)$ ]	$R_1 = 0.0978, wR_2 = 0.2418$
Final R indexes [all data]	$R_1 = 0.1720, wR_2 = 0.2891$
Largest diff. peak/hole / $e \text{\AA}^{-3}$	2.94/-2.16

#### Crystal Data as a Footnote

**Crystal Data for cs3029.**  $\text{C}_{36.1}\text{H}_{39.2}\text{Cl}_{2.2}\text{N}_3\text{ORu}$  ( $M = 710.16 \text{ g/mol}$ ): triclinic, space group P-1 (no. 2),  $a = 14.3662(7) \text{ \AA}$ ,  $b = 14.5676(10) \text{ \AA}$ ,  $c = 16.0240(18) \text{ \AA}$ ,  $\alpha = 80.507(8)^\circ$ ,  $\beta = 87.035(6)^\circ$ ,  $\gamma = 84.684(5)^\circ$ ,  $V = 3291.1(5) \text{ \AA}^3$ ,  $Z = 4$ ,  $T = 100.0(2) \text{ K}$ ,  $\mu(\text{Cu K}\alpha) = 5.751 \text{ mm}^{-1}$ ,  $D_{\text{calc}} = 1.433 \text{ g/cm}^3$ , 35853 reflections measured ( $6.174^\circ \leq 2\Theta \leq 136.664^\circ$ ), 11550 unique ( $R_{\text{int}} = 0.1923, R_{\text{sigma}} = 0.1915$ ) which were used in all calculations. The final  $R_1$  was 0.0978 ( $I > 2\sigma(I)$ ) and  $wR_2$  was 0.2891 (all data).

**Table 4.6.2. Bond Lengths for cs3029-catalyst (5).**

<b>Atom</b>	<b>Atom</b>	<b>Length/Å</b>	<b>Atom</b>	<b>Atom</b>	<b>Length/Å</b>
Ru1	Cl4	2.352 (3)	C24	C59	1.40 (2)
Ru1	Cl3	2.345 (3)	N5	C48	1.355 (16)
Ru1	N6	2.187 (9)	C26	C53	1.399 (18)
Ru1	C50	2.045 (11)	C28	C15	1.51 (2)
Ru1	C35	1.810 (12)	C30	C70	1.388 (17)
Ru2	Cl1	2.338 (3)	C30	C5	1.371 (17)
Ru2	Cl2	2.355 (3)	C32	C34	1.37 (2)
Ru2	N4	2.167 (13)	C32	C57	1.38 (2)
Ru2	C48	2.038 (14)	C34	C56	1.417 (17)
Ru2	C66	1.838 (13)	C36	C68	1.37 (2)
N4	C8	1.404 (17)	C38	C44	1.508 (18)
N4	C39	1.305 (18)	C44	N3	1.474 (15)
O1	C51	1.413 (17)	C46	C15	1.41 (2)
N6	C10	1.315 (15)	C50	N3	1.371 (15)
N6	C22	1.435 (14)	C52	C11	1.403 (18)
N7	C16	1.444 (15)	C52	C27	1.382 (19)
N7	C38	1.464 (16)	C54	C57	1.37 (2)
N7	C50	1.357 (15)	C56	C66	1.43 (2)
C37	C16	1.38 (2)	C60	C68	1.39 (3)
C37	C36	1.439 (18)	C60	C41	1.40 (2)
C37	C2	1.50 (2)	C62	C11	1.389 (18)
O3	C9	1.401 (16)	C62	C67	1.395 (18)

**Table 4.6.2. Bond Lengths for cs3029-catalyst (5).**

Atom	Atom	Length/Å	Atom	Atom	Length/Å
N2	C48	1.374 (15)	C64	C27	1.406 (18)
N2	C64	1.441 (16)	C64	C67	1.372 (17)
N2	C65	1.46 (2)	C68	C1	1.52 (2)
C4	N5	1.497 (19)	C70	C35	1.466 (16)
C4	C65	1.529 (18)	C72	C49	1.387 (19)
C6	C26	1.355 (17)	C19	C29	1.499 (19)
C6	C13	1.400 (19)	C39	C23	1.476 (18)
C8	C54	1.39 (2)	C5	C45	1.409 (17)
C8	C56	1.408 (19)	C41	C31	1.50 (3)
C10	C53	1.428 (16)	C21	C47	1.383 (17)
C12	C14	1.45 (2)	C21	C69	1.539 (16)
C12	C40	1.49 (2)	C43	C11	1.488 (17)
C12	C42	1.420 (19)	C45	C63	1.369 (17)
C14	N3	1.429 (16)	C23	C49	1.40 (2)
C14	C15	1.37 (2)	C23	C71	1.408 (19)
C16	C41	1.38 (2)	C47	C7	1.375 (18)
C18	C42	1.37 (2)	C3	C7	1.381 (18)
C18	C46	1.41 (2)	C3	C29	1.390 (18)
C18	C58	1.526 (19)	C25	C53	1.415 (18)
C20	N5	1.444 (14)	C25	C33	1.403 (17)
C20	C21	1.385 (17)	C51	C13	1.516 (17)
C20	C29	1.409 (17)	C13	C33	1.39 (2)

**Table 4.6.2. Bond Lengths for cs3029-catalyst (5).**

<b>Atom</b>	<b>Atom</b>	<b>Length/Å</b>	<b>Atom</b>	<b>Atom</b>	<b>Length/Å</b>
C22	C70	1.392 (16)	C27	C17	1.496 (17)
C22	C63	1.399 (16)	C55	C67	1.518 (17)
C24	C72	1.399 (19)	C7	C61	1.488 (17)
C24	C9	1.511 (18)	C59	C71	1.361 (19)

**Table 4.6.3. Bond Angles for cs3029-catalyst (5).**

Atom Atom Atom	Angle/°	Atom Atom Atom	Angle/°
Cl3 Ru1 Cl4	156.58 (11)	N5 C48 Ru2	123.1 (8)
N6 Ru1 Cl4	89.8 (3)	N5 C48 N2	105.6 (11)
N6 Ru1 Cl3	86.3 (3)	N7 C50 Ru1	130.9 (8)
C50 Ru1 Cl4	88.1 (4)	N7 C50 N3	106.1 (9)
C50 Ru1 Cl3	96.3 (4)	N3 C50 Ru1	122.2 (7)
C50 Ru1 N6	177.2 (5)	C27 C52 C11	123.2 (11)
C35 Ru1 Cl4	102.7 (5)	C57 C54 C8	117.1 (16)
C35 Ru1 Cl3	99.4 (5)	C8 C56 C34	119.5 (13)
C35 Ru1 N6	80.4 (4)	C8 C56 C66	116.4 (11)
C35 Ru1 C50	98.3 (5)	C34 C56 C66	124.0 (12)
Cl1 Ru2 Cl2	158.16 (11)	C68 C60 C41	120.4 (14)
N4 Ru2 Cl1	88.4 (3)	C11 C62 C67	122.2 (11)
N4 Ru2 Cl2	87.0 (3)	C27 C64 N2	117.9 (10)
C48 Ru2 Cl1	91.1 (3)	C67 C64 N2	119.1 (10)
C48 Ru2 Cl2	93.7 (3)	C67 C64 C27	123.0 (11)
C48 Ru2 N4	179.0 (4)	C56 C66 Ru2	118.6 (9)
C66 Ru2 Cl1	101.0 (3)	C36 C68 C60	120.4 (13)
C66 Ru2 Cl2	99.1 (4)	C36 C68 C1	119.6 (18)
C66 Ru2 N4	79.4 (5)	C60 C68 C1	120.0 (17)
C66 Ru2 C48	99.9 (5)	C22 C70 C35	115.3 (10)
C8 N4 Ru2	110.8 (9)	C30 C70 C22	120.0 (10)
C39 N4 Ru2	131.7 (9)	C30 C70 C35	124.7 (10)

**Table 4.6.3. Bond Angles for cs3029-catalyst (5).**

<b>Atom Atom Atom</b>	<b>Angle/°</b>	<b>Atom Atom Atom</b>	<b>Angle/°</b>
C39 N4 C8	116.9 (13)	C49 C72 C24	121.2 (14)
C10 N6 Ru1	132.6 (7)	O3 C9 C24	114.0 (11)
C10 N6 C22	116.8 (9)	N4 C39 C23	124.7 (15)
C22 N6 Ru1	109.2 (7)	C30 C5 C45	118.9 (11)
C16 N7 C38	116.8 (9)	C14 N3 C44	119.2 (9)
C50 N7 C16	128.2 (9)	C50 N3 C14	126.6 (9)
C50 N7 C38	114.0 (10)	C50 N3 C44	112.9 (9)
C16 C37 C36	117.3 (13)	C16 C41 C60	118.7 (15)
C16 C37 C2	123.6 (12)	C16 C41 C31	121.0 (14)
C36 C37 C2	119.1 (13)	C60 C41 C31	120.2 (14)
C48 N2 C64	128.4 (12)	C20 C21 C69	122.0 (10)
C48 N2 C65	114.4 (10)	C47 C21 C20	119.4 (10)
C64 N2 C65	116.9 (10)	C47 C21 C69	118.5 (10)
N5 C4 C65	101.6 (11)	C52 C11 C43	121.1 (11)
C26 C6 C13	121.9 (12)	C62 C11 C52	117.1 (11)
N4 C8 C56	111.9 (12)	C62 C11 C43	121.8 (11)
C54 C8 N4	127.5 (13)	C63 C45 C5	121.3 (11)
C54 C8 C56	120.6 (12)	C49 C23 C39	124.7 (12)
N6 C10 C53	127.3 (10)	C49 C23 C71	118.3 (12)
C14 C12 C40	123.3 (12)	C71 C23 C39	117.0 (14)
C42 C12 C14	115.8 (15)	C7 C47 C21	122.0 (11)
C42 C12 C40	120.7 (14)	C7 C3 C29	123.0 (11)

**Table 4.6.3. Bond Angles for cs3029-catalyst (5).**

Atom Atom Atom	Angle/°	Atom Atom Atom	Angle/°
N3 C14 C12	116.4 (13)	C72 C49 C23	120.1 (13)
C15 C14 C12	121.4 (12)	C33 C25 C53	119.8 (12)
C15 C14 N3	121.8 (14)	O1 C51 C13	113.2 (11)
C37 C16 N7	116.2 (12)	C6 C13 C51	119.4 (12)
C41 C16 N7	120.9 (13)	C33 C13 C6	118.3 (11)
C41 C16 C37	122.9 (12)	C33 C13 C51	122.3 (11)
C42 C18 C46	121.4 (13)	C26 C53 C10	116.8 (11)
C42 C18 C58	120.2 (16)	C26 C53 C25	118.4 (10)
C46 C18 C58	118.3 (16)	C25 C53 C10	124.7 (12)
C21 C20 N5	120.8 (10)	C52 C27 C64	116.5 (11)
C21 C20 C29	120.3 (11)	C52 C27 C17	121.4 (11)
C29 C20 N5	117.9 (10)	C64 C27 C17	122.1 (11)
C70 C22 N6	113.7 (9)	C47 C7 C3	117.6 (11)
C70 C22 C63	119.8 (10)	C47 C7 C61	120.3 (11)
C63 C22 N6	126.4 (10)	C3 C7 C61	122.0 (11)
C72 C24 C9	118.5 (13)	C54 C57 C32	124.5 (16)
C72 C24 C59	118.2 (12)	C20 C29 C19	123.3 (11)
C59 C24 C9	123.3 (12)	C3 C29 C20	117.5 (11)
C20 N5 C4	117.1 (10)	C3 C29 C19	119.1 (11)
C48 N5 C4	114.7 (9)	C71 C59 C24	120.9 (12)
C48 N5 C20	128.1 (12)	C14 C15 C28	120.2 (13)
C6 C26 C53	121.0 (12)	C14 C15 C46	121.0 (16)

**Table 4.6.3. Bond Angles for cs3029-catalyst (5).**

<b>Atom Atom Atom</b>	<b>Angle/°</b>	<b>Atom Atom Atom</b>	<b>Angle/°</b>
C5 C30 C70	120.6 (11)	C46 C15 C28	118.6 (16)
C34 C32 C57	118.7 (13)	C45 C63 C22	119.2 (11)
C32 C34 C56	119.7 (13)	N2 C65 C4	103.6 (11)
C68 C36 C37	120.2 (14)	C13 C33 C25	120.6 (12)
N7 C38 C44	102.6 (10)	C62 C67 C55	119.5 (10)
C18 C42 C12	121.9 (15)	C64 C67 C62	118.0 (11)
N3 C44 C38	103.3 (9)	C64 C67 C55	122.4 (11)
C18 C46 C15	118.1 (16)	C70 C35 Ru1	119.9 (8)
N2 C48 Ru2	131.3 (8)	C59 C71 C23	121.3 (14)

**Table 4.6.4. Torsion Angles for cs3029-catalyst (5).**

A	B	C	D	Angle/°	A	B	C	D	Angle/°
Ru1	N6	C10	C53	18 (2)	C40	C12	C42	C18	175.7 (12)
Ru1	N6	C22	C70	9.7 (14)	C42	C12	C14	N3	176.9 (10)
Ru1	N6	C22	C63	-171.4 (12)	C42	C12	C14	C15	4.0 (17)
Ru1	C50	N3	C14	-23 (2)	C42	C18	C46	C15	-0.2 (19)
Ru1	C50	N3	C44	170.7 (11)	C46	C18	C42	C12	-2.4 (19)
Ru2	N4	C8	C54	167.1 (13)	C48	Ru2	C66	C56	165.6 (9)
Ru2	N4	C8	C56	-13.4 (13)	C48	N2	C64	C27	-86.8 (16)
Ru2	N4	C39	C23	-18.0 (19)	C48	N2	C64	C67	93.7 (15)
Cl1	Ru2	C66	C56	72.5 (9)	C48	N2	C65	C4	-1.4 (12)
Cl4	Ru1	C35	C70	97.6 (11)	C50	Ru1	C35	C70	-172.4 (12)
Cl2	Ru2	C66	C56	-99.0 (9)	C50	N7	C16	C37	-103.3 (15)
Cl3	Ru1	C35	C70	-74.5 (12)	C50	N7	C16	C41	75.3 (18)
N4	Ru2	C66	C56	-13.7 (9)	C50	N7	C38	C44	10.9 (19)
N4	C8	C54	C57	-179.9 (14)	C54	C8	C56	C34	0.5 (19)
N4	C8	C56	C34	-179.0 (10)	C54	C8	C56	C66	-176.9 (13)
N4	C8	C56	C66	3.6 (16)	C56	C8	C54	C57	1 (2)
N4	C39	C23	C49	-21 (2)	C58	C18	C42	C12	178.7 (12)
N4	C39	C23	C71	161.8 (13)	C58	C18	C46	C15	178.8 (12)
O1	C51	C13	C6	173.5 (12)	C64	N2	C48	Ru2	-2.5 (15)
O1	C51	C13	C33	-5.7 (18)	C64	N2	C48	N5	177.2 (10)
N6	Ru1	C35	C70	10.0 (11)	C64	N2	C65	C4	-176.3 (9)
N6	C10	C53	C26	-161.4 (12)	C68	C60	C41	C16	-0.1 (18)

**Table 4.6.4. Torsion Angles for cs3029-catalyst (5).**

A	B	C	D	Angle/°	A	B	C	D	Angle/°
N6	C10	C53	C25	21 (2)	C68	C60	C41	C31	-176.5 (13)
N6	C22	C70	C30	177.3 (13)	C70	C22	C63	C45	-1 (2)
N6	C22	C70	C35	-2.8 (18)	C70	C30	C5	C45	-2 (2)
N6	C22	C63	C45	-179.6 (14)	C72	C24	C9	O3	157.2 (11)
N7	C16	C41	C60	-178.2 (11)	C72	C24	C59	C71	-1.7 (18)
N7	C16	C41	C31	-1.8 (18)	C9	C24	C72	C49	179.6 (12)
N7	C38	C44	N3	-9.5 (18)	C9	C24	C59	C71	-178.3 (12)
N7	C50	N3	C14	166.7 (14)	C39	N4	C8	C54	-20 (2)
N7	C50	N3	C44	0.2 (17)	C39	N4	C8	C56	159.2 (11)
C37	C16	C41	C60	0.3 (17)	C39	C23	C49	C72	-178.1 (12)
C37	C16	C41	C31	176.7 (12)	C39	C23	C71	C59	179.4 (12)
C37	C36	C68	C60	1.4 (18)	C5	C30	C70	C22	3 (2)
C37	C36	C68	C1	-177.8 (12)	C5	C30	C70	C35	-176.6 (14)
N2	C64	C27	C52	-178.6 (13)	C5	C45	C63	C22	2 (2)
N2	C64	C27	C17	3 (2)	N3	C14	C15	C28	-3.3 (18)
N2	C64	C67	C62	179.3 (13)	N3	C14	C15	C46	-179.2 (11)
N2	C64	C67	C55	-3 (2)	C41	C60	C68	C36	-0.8 (19)
C4	N5	C48	Ru2	176.3 (7)	C41	C60	C68	C1	178.4 (13)
C4	N5	C48	N2	-3.4 (11)	C21	C20	N5	C4	90.6 (15)
C6	C26	C53	C10	-178.2 (12)	C21	C20	N5	C48	-85.8 (17)
C6	C26	C53	C25	-0.1 (19)	C21	C20	C29	C19	-173.9 (14)
C6	C13	C33	C25	-0.4 (19)	C21	C20	C29	C3	3 (2)

**Table 4.6.4. Torsion Angles for cs3029-catalyst (5).**

A	B	C	D	Angle/°	A	B	C	D	Angle/°
C8	N4	C39	C23	171.2 (12)	C21	C47	C7	C3	-3 (2)
C8	C54	C57	C32	-2 (3)	C21	C47	C7	C61	177.0 (15)
C8	C56	C66	Ru2	10.6 (14)	C11	C52	C27	C64	-1 (2)
C10	N6	C22	C70	-158.5 (12)	C11	C52	C27	C17	177.8 (14)
C10	N6	C22	C63	20 (2)	C11	C62	C67	C64	-1 (2)
C12	C14	N3	C44	-83.7 (17)	C11	C62	C67	C55	-178.3 (14)
C12	C14	N3	C50	110.5 (15)	C49	C23	C71	C59	2.1 (19)
C12	C14	C15	C28	169.2 (12)	C51	C13	C33	C25	178.8 (12)
C12	C14	C15	C46	-6.7 (19)	C13	C6	C26	C53	0 (2)
C14	C12	C42	C18	0.5 (18)	C53	C25	C33	C13	0.1 (19)
C16	N7	C38	C44	-179.9 (13)	C27	C52	C11	C62	0 (2)
C16	N7	C50	Ru1	16 (2)	C27	C52	C11	C43	179.3 (15)
C16	N7	C50	N3	-174.9 (13)	C27	C64	C67	C62	0 (2)
C16	C37	C36	C68	-1.2 (16)	C27	C64	C67	C55	177.4 (14)
C18	C46	C15	C14	4.7 (19)	C7	C3	C29	C20	-2 (2)
C18	C46	C15	C28	-171.3 (12)	C7	C3	C29	C19	175.7 (15)
C20	N5	C48	Ru2	-7.2 (15)	C57	C32	C34	C56	-0.5 (19)
C20	N5	C48	N2	173.2 (10)	C29	C20	N5	C4	-77.8 (15)
C20	C21	C47	C7	5 (2)	C29	C20	N5	C48	105.8 (15)
C22	N6	C10	C53	-176.9 (13)	C29	C20	C21	C47	-5 (2)
C22	C70	C35	Ru1	-7.6 (18)	C29	C20	C21	C69	172.5 (14)
C24	C72	C49	C23	-1.4 (19)	C29	C3	C7	C47	2 (2)

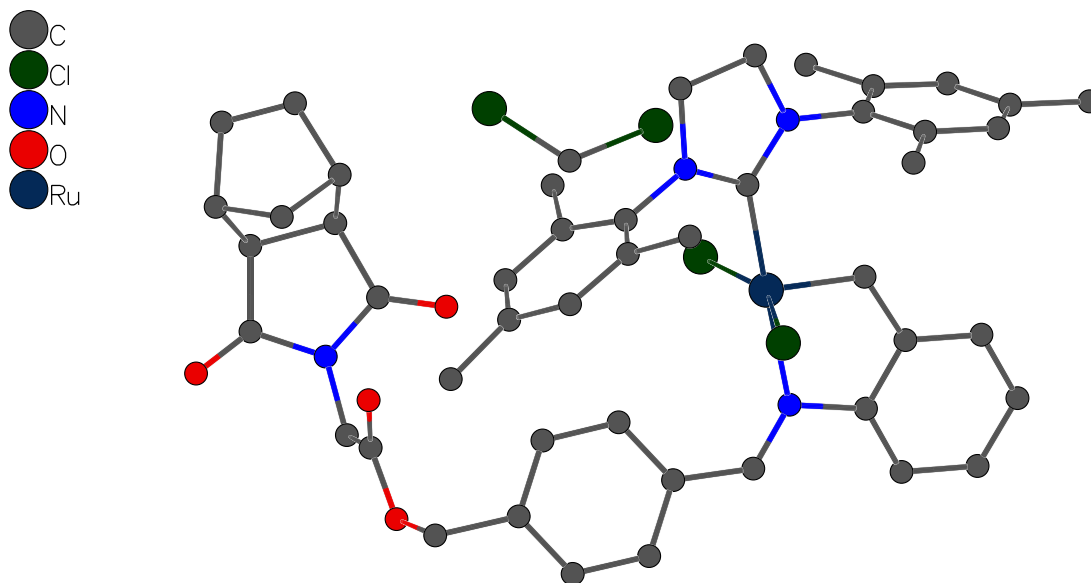
**Table 4.6.4. Torsion Angles for cs3029-catalyst (5).**

A	B	C	D	Angle/°	A	B	C	D	Angle/°
C24	C59	C71	C23	-1 (2)	C29	C3	C7	C61	-178.8 (15)
N5	C4	C65	N2	-0.6 (11)	C59	C24	C72	C49	2.7 (18)
N5	C20	C21	C47	-173.0 (13)	C59	C24	C9	O3	-26.2 (18)
N5	C20	C21	C69	4 (2)	C15	C14	N3	C44	89.1 (16)
N5	C20	C29	C19	-5 (2)	C15	C14	N3	C50	-76.7 (19)
N5	C20	C29	C3	171.6 (13)	C63	C22	C70	C30	-2 (2)
C26	C6	C13	C51	-178.7 (13)	C63	C22	C70	C35	178.2 (13)
C26	C6	C13	C33	1 (2)	C2	C37	C16	N7	2.0 (16)
C30	C70	C35	Ru1	172.2 (12)	C2	C37	C16	C41	-176.6 (11)
C30	C5	C45	C63	0 (2)	C2	C37	C36	C68	175.9 (11)
C32	C34	C56	C8	-0.6 (17)	C65	N2	C48	Ru2	-176.7 (8)
C32	C34	C56	C66	176.6 (11)	C65	N2	C48	N5	2.9 (12)
C34	C32	C57	C54	2 (2)	C65	N2	C64	C27	87.3 (15)
C34	C56	C66	Ru2	-166.6 (9)	C65	N2	C64	C67	-92.2 (15)
C36	C37	C16	N7	178.9 (9)	C65	C4	N5	C20	-174.4 (9)
C36	C37	C16	C41	0.3 (16)	C65	C4	N5	C48	2.5 (12)
C38	N7	C16	C37	89.2 (16)	C33	C25	C53	C10	178.1 (12)
C38	N7	C16	C41	-92.1 (15)	C33	C25	C53	C26	0.2 (18)
C38	N7	C50	Ru1	-176.6 (12)	C67	C62	C11	C52	1 (2)
C38	N7	C50	N3	-7.2 (18)	C67	C62	C11	C43	-178.5 (15)
C38	C44	N3	C14	-161.3 (15)	C67	C64	C27	C52	1 (2)
C38	C44	N3	C50	6.3 (19)	C67	C64	C27	C17	-177.8 (14)

**Table 4.6.4. Torsion Angles for cs3029-catalyst (5).**

<b>A</b>	<b>B</b>	<b>C</b>	<b>D</b>	<b>Angle/°</b>	<b>A</b>	<b>B</b>	<b>C</b>	<b>D</b>	<b>Angle/°</b>
C40	C12	C14	N3	1.8 (18)	C69	C21	C47	C7	-172.4 (14)
C40	C12	C14	C15	-171.1 (12)	C71	C23	C49	C72	-1.0 (19)

This report has been created with Olex2, compiled on 2023.03.06 svn.rbb2c1857 for OlexSys. Please [let us know](#) if there are any errors or if you would like to have additional features.



(7)

## Experimental

A yellow-brown plate (0.08 x 0.21 x 0.31 mm<sup>3</sup>) was centered on the goniometer of a Rigaku Oxford Diffraction Synergy-S diffractometer equipped with a HyPix6000HE detector and operating with MoK $\alpha$  radiation. The data collection routine, unit cell refinement, and data processing were carried out with the program CrysAlisPro.<sup>66</sup> The Laue symmetry and systematic absences were consistent with the monoclinic space group  $P2_1/n$ . The structure was solved using SHELXT<sup>67</sup> and refined using SHELXL<sup>68</sup> via Olex2.<sup>69</sup> A 2-position disorder model was used for the CH<sub>2</sub>Cl<sub>2</sub> molecule with relative

(66) CrysAlisPro Software System, v1.171.41.105a, Rigaku Oxford Diffraction, 2021, Rigaku Corporation, Oxford, UK.

(67) Sheldrick, G. M. "SHELXT – Integrated space-group and crystal structure determination." *Acta Cryst.* **2015**, *A71*, 3–8.

(68) Sheldrick, G. M. "Crystal structure refinement with SHELXL." *Acta Cryst.* **2015**, *C71*, 3–8.

(69) Dolomanov, O.V.; Bourhis, L. J.; Gildea, R. J.; Howard, J. A. K.; Puschmann, H. *J. Appl. Cryst.* **2009**, *42*, 339–341.

occupancies that refined to 0.529(17) and 0.471(17); the SADI restraint was used to maintain chemically reasonable bond lengths and angles. The final refinement model involved anisotropic displacement parameters for non-hydrogen atoms and a riding model for all hydrogen atoms. Olex2<sup>70</sup> was used for molecular graphics generation.

**Table 4.6.5. Crystal data and structure refinement for cs2915-inimer (7).**

Identification code	cs2915
Empirical formula	C <sub>47</sub> H <sub>48</sub> Cl <sub>2</sub> N <sub>4</sub> O <sub>4</sub> Ru • CH <sub>2</sub> Cl <sub>2</sub>
Formula weight	989.79
Temperature/K	99.99(10)
Crystal system	monoclinic
Space group	P2 <sub>1</sub> /n
a/Å	14.32290(10)
b/Å	14.54890(10)
c/Å	21.7287(2)
α/°	90
β/°	100.7450(10)
γ/°	90
Volume/Å <sup>3</sup>	4448.49(6)
Z	4
ρ <sub>calc</sub> /cm <sup>3</sup>	1.478
μ/mm <sup>-1</sup>	0.642
F(000)	2040.0
Crystal size/mm <sup>3</sup>	0.31 × 0.21 × 0.08
Radiation	Mo Kα (λ = 0.71073)

---

(70) Dolomanov, O.V.; Bourhis, L. J.; Gildea, R. J.; Howard, J. A. K.; Puschmann, H. *J. Appl. Cryst.* **2009**, *42*, 339–341.

2 $\Theta$ range for data collection/ $^{\circ}$	5.164 to 76.61
Index ranges	$-24 \leq h \leq 24$ , $-25 \leq k \leq 24$ , $-37 \leq l \leq 37$
Reflections collected	267023
Independent reflections	23715 [ $R_{\text{int}} = 0.0433$ , $R_{\text{sigma}} = 0.0210$ ]
Data/restraints/parameters	23715/3/575
Goodness-of-fit on $F^2$	1.051
Final R indexes [ $I \geq 2\sigma(I)$ ]	$R_1 = 0.0250$ , $wR_2 = 0.0635$
Final R indexes [all data]	$R_1 = 0.0311$ , $wR_2 = 0.0654$
Largest diff. peak/hole / $e \text{ \AA}^{-3}$	0.66/-0.45

**Table 4.6.6. Bond Lengths for cs2915-inimer (7).**

Atom	Atom	Length/ $\text{\AA}$	Atom	Atom	Length/ $\text{\AA}$
Ru1	C11	2.33413(19)	C15	C16	1.3874(13)
Ru1	C12	2.34599(19)	C16	C17	1.3976(13)
Ru1	N3	2.2026(6)	C16	C20	1.5061(13)
Ru1	C1	2.0521(7)	C17	C18	1.3937(12)
Ru1	C22	1.8291(8)	C18	C21	1.5048(12)
O1	C36	1.4573(11)	C22	C23	1.4459(11)
O1	C37	1.3439(11)	C23	C24	1.4007(11)
O2	C37	1.2043(11)	C23	C28	1.3965(11)
O3	C39	1.2140(11)	C24	C25	1.3892(12)
O4	C46	1.2096(10)	C25	C26	1.3929(14)
N1	C1	1.3483(10)	C26	C27	1.3941(12)
N1	C2	1.4759(11)	C27	C28	1.3976(11)
N1	C4	1.4277(10)	C29	C30	1.4550(11)
N2	C1	1.3549(9)	C30	C31	1.4030(11)
N2	C3	1.4733(10)	C30	C35	1.3990(11)
N2	C13	1.4312(10)	C31	C32	1.3880(12)

**Table 4.6.6. Bond Lengths for cs2915-inimer (7).**

Atom	Atom	Length/Å	Atom	Atom	Length/Å
N3	C28	1.4291(10)	C32	C33	1.3883(12)
N3	C29	1.2935(10)	C33	C34	1.3998(12)
N4	C38	1.4438(12)	C33	C36	1.5054(12)
N4	C39	1.3879(11)	C34	C35	1.3841(12)
N4	C46	1.3904(11)	C37	C38	1.5139(12)
C2	C3	1.5199(12)	C39	C40	1.5110(13)
C4	C5	1.3944(11)	C40	C41	1.5672(12)
C4	C9	1.4019(12)	C40	C45	1.5434(12)
C5	C6	1.4005(11)	C41	C42	1.5173(14)
C5	C10	1.5061(12)	C41	C47	1.5450(13)
C6	C7	1.3914(12)	C42	C43	1.3327(16)
C7	C8	1.3959(12)	C43	C44	1.5141(14)
C7	C11	1.5035(12)	C44	C45	1.5660(12)
C8	C9	1.3920(12)	C44	C47	1.5387(12)
C9	C12	1.5068(12)	C45	C46	1.5102(12)
C13	C14	1.4005(11)	C48	Cl3A	1.742(3)
C13	C18	1.4056(11)	C48	Cl4A	1.824(2)
C14	C15	1.3985(11)	C48	Cl3B	1.811(4)
C14	C19	1.5047(12)	C48	Cl4B	1.683(4)

**Table 4.6.7. Bond Angles for cs2915-inimer (7).**

Atom	Atom	Atom	Angle/°	Atom	Atom	Atom	Angle/°
Cl1	Ru1	Cl2	156.980(8)	C13	C18	C21	122.20(7)
N3	Ru1	Cl1	86.163(18)	C17	C18	C13	118.35(8)

**Table 4.6.7. Bond Angles for cs2915-inimer (7).**

Atom	Atom	Atom	Angle/°	Atom	Atom	Atom	Angle/°
N3	Ru1	Cl2	91.236(18)	C17	C18	C21	119.44(8)
C1	Ru1	Cl1	90.77(2)	C23	C22	Ru1	119.60(6)
C1	Ru1	Cl2	91.98(2)	C24	C23	C22	122.59(7)
C1	Ru1	N3	176.77(3)	C28	C23	C22	117.04(7)
C22	Ru1	Cl1	102.22(3)	C28	C23	C24	120.36(7)
C22	Ru1	Cl2	99.87(3)	C25	C24	C23	119.61(8)
C22	Ru1	N3	80.34(3)	C24	C25	C26	119.75(8)
C22	Ru1	C1	99.34(3)	C25	C26	C27	121.23(8)
C37	O1	C36	116.14(7)	C26	C27	C28	118.94(8)
C1	N1	C2	114.22(6)	C23	C28	N3	113.16(6)
C1	N1	C4	126.65(6)	C23	C28	C27	120.08(7)
C4	N1	C2	118.02(6)	C27	C28	N3	126.76(7)
C1	N2	C3	113.92(6)	N3	C29	C30	127.91(7)
C1	N2	C13	127.34(6)	C31	C30	C29	115.96(7)
C13	N2	C3	118.72(6)	C35	C30	C29	125.10(7)
C28	N3	Ru1	109.82(5)	C35	C30	C31	118.73(7)
C29	N3	Ru1	132.35(5)	C32	C31	C30	120.86(7)
C29	N3	C28	116.67(6)	C31	C32	C33	120.31(7)
C39	N4	C38	122.87(7)	C32	C33	C34	118.90(8)
C39	N4	C46	113.29(7)	C32	C33	C36	120.54(7)
C46	N4	C38	123.24(7)	C34	C33	C36	120.53(8)
N1	C1	Ru1	130.73(5)	C35	C34	C33	121.18(8)
N1	C1	N2	106.43(6)	C34	C35	C30	120.00(8)
N2	C1	Ru1	122.81(5)	O1	C36	C33	109.82(7)
N1	C2	C3	102.40(6)	O1	C37	C38	109.87(7)

**Table 4.6.7. Bond Angles for cs2915-inimer (7).**

Atom Atom Atom	Angle/°	Atom Atom Atom	Angle/°
N2 C3 C2	102.70(6)	O2 C37 O1	125.05(8)
C5 C4 N1	119.23(7)	O2 C37 C38	125.05(8)
C5 C4 C9	121.91(7)	N4 C38 C37	109.96(7)
C9 C4 N1	118.83(7)	O3 C39 N4	123.87(9)
C4 C5 C6	118.07(7)	O3 C39 C40	127.80(8)
C4 C5 C10	120.93(7)	N4 C39 C40	108.32(7)
C6 C5 C10	120.96(8)	C39 C40 C41	112.99(7)
C7 C6 C5	121.49(8)	C39 C40 C45	105.04(7)
C6 C7 C8	118.81(7)	C45 C40 C41	102.76(7)
C6 C7 C11	121.15(8)	C42 C41 C40	104.49(7)
C8 C7 C11	120.04(8)	C42 C41 C47	100.22(8)
C9 C8 C7	121.56(8)	C47 C41 C40	101.07(7)
C4 C9 C12	121.52(7)	C43 C42 C41	107.42(9)
C8 C9 C4	118.12(8)	C42 C43 C44	107.81(9)
C8 C9 C12	120.18(8)	C43 C44 C45	104.74(8)
C14 C13 N2	119.80(7)	C43 C44 C47	100.43(7)
C14 C13 C18	120.89(7)	C47 C44 C45	100.54(7)
C18 C13 N2	119.04(7)	C40 C45 C44	103.31(7)
C13 C14 C19	122.55(7)	C46 C45 C40	104.77(7)
C15 C14 C13	118.31(7)	C46 C45 C44	112.19(7)
C15 C14 C19	119.08(7)	O4 C46 N4	123.89(8)
C16 C15 C14	122.01(8)	O4 C46 C45	127.67(8)
C15 C16 C17	118.17(8)	N4 C46 C45	108.43(7)
C15 C16 C20	121.10(9)	C44 C47 C41	93.73(7)
C17 C16 C20	120.72(9)	Cl3A C48 Cl4A	111.93(13)

**Table 4.6.7. Bond Angles for cs2915-inimer (7).**

<b>Atom Atom Atom</b>	<b>Angle/°</b>	<b>Atom Atom Atom</b>	<b>Angle/°</b>
C18 C17 C16	121.82(8)	C14B C48 C13B	107.3(3)

**Table 4.6.8. Torsion Angles for cs2915-inimer (7).**

A	B	C	D	Angle/°	A	B	C	D	Angle/°
Ru1	N3	C28	C23	-0.53(8)	C18	C13	C14	C19	171.05(7)
Ru1	N3	C28	C27	179.92(7)	C19	C14	C15	C16	-176.77(8)
Ru1	N3	C29	C30	21.66(12)	C20	C16	C17	C18	174.76(8)
Ru1	C22	C23	C24	-177.53(6)	C22	C23	C24	C25	179.45(8)
Ru1	C22	C23	C28	1.82(10)	C22	C23	C28	N3	-0.64(10)
Cl1	Ru1	C22	C23	82.32(6)	C22	C23	C28	C27	178.95(7)
Cl2	Ru1	C22	C23	-91.15(6)	C23	C24	C25	C26	0.95(13)
O1	C37	C38	N4	-174.76(7)	C24	C23	C28	N3	178.73(7)
O2	C37	C38	N4	3.47(12)	C24	C23	C28	C27	-1.68(12)
O3	C39	C40	C41	-67.04(12)	C24	C25	C26	C27	-0.48(14)
O3	C39	C40	C45	-178.29(9)	C25	C26	C27	C28	-1.07(14)
N1	C2	C3	N2	5.48(9)	C26	C27	C28	N3	-178.34(8)
N1	C4	C5	C6	-175.58(7)	C26	C27	C28	C23	2.13(12)
N1	C4	C5	C10	2.01(11)	C28	N3	C29	C30	-172.07(7)
N1	C4	C9	C8	175.91(7)	C28	C23	C24	C25	0.12(12)
N1	C4	C9	C12	0.83(12)	C29	N3	C28	C23	-169.79(7)
N2	C13	C14	C15	179.77(7)	C29	N3	C28	C27	10.66(11)
N2	C13	C14	C19	-2.93(11)	C29	C30	C31	C32	-173.92(7)
N2	C13	C18	C17	-179.20(7)	C29	C30	C35	C34	173.28(8)
N2	C13	C18	C21	2.19(11)	C30	C31	C32	C33	0.05(12)
N3	Ru1	C22	C23	-1.58(6)	C31	C30	C35	C34	-1.18(13)
N3	C29	C30	C31	-177.81(8)	C31	C32	C33	C34	-0.98(13)
N3	C29	C30	C35	7.59(13)	C31	C32	C33	C36	177.22(8)
N4	C39	C40	C41	111.76(8)	C32	C33	C34	C35	0.84(14)
N4	C39	C40	C45	0.51(9)	C32	C33	C36	O1	-107.42(9)

**Table 4.6.8. Torsion Angles for cs2915-inimer (7).**

A	B	C	D	Angle/°	A	B	C	D	Angle/°
C1	Ru1	C22	C23	175.16(6)	C33	C34	C35	C30	0.25(15)
C1	N1	C2	C3	-4.87(10)	C34	C33	C36	O1	70.75(11)
C1	N1	C4	C5	99.01(10)	C35	C30	C31	C32	1.04(12)
C1	N1	C4	C9	-79.05(10)	C36	O1	C37	O2	-9.82(12)
C1	N2	C3	C2	-5.11(10)	C36	O1	C37	C38	168.41(7)
C1	N2	C13	C14	-87.99(10)	C36	C33	C34	C35	-177.36(9)
C1	N2	C13	C18	97.92(9)	C37	O1	C36	C33	-87.42(9)
C2	N1	C1	Ru1	179.91(6)	C38	N4	C39	O3	4.55(14)
C2	N1	C1	N2	1.86(10)	C38	N4	C39	C40	-174.30(7)
C2	N1	C4	C5	-93.79(9)	C38	N4	C46	O4	-4.57(13)
C2	N1	C4	C9	88.15(10)	C38	N4	C46	C45	175.45(7)
C3	N2	C1	Ru1	-175.99(6)	C39	N4	C38	C37	70.20(10)
C3	N2	C1	N1	2.25(9)	C39	N4	C46	O4	-175.95(8)
C3	N2	C13	C14	90.04(9)	C39	N4	C46	C45	4.07(9)
C3	N2	C13	C18	-84.05(9)	C39	C40	C41	C42	178.95(8)
C4	N1	C1	Ru1	-12.47(12)	C39	C40	C41	C47	-77.32(8)
C4	N1	C1	N2	169.48(8)	C39	C40	C45	C44	119.38(7)
C4	N1	C2	C3	-173.64(8)	C39	C40	C45	C46	1.74(8)
C4	C5	C6	C7	-1.11(12)	C40	C41	C42	C43	70.85(10)
C5	C4	C9	C8	-2.10(12)	C40	C41	C47	C44	-57.14(8)
C5	C4	C9	C12	-177.18(8)	C40	C45	C46	O4	176.58(8)
C5	C6	C7	C8	-0.45(12)	C40	C45	C46	N4	-3.44(9)
C5	C6	C7	C11	-179.50(8)	C41	C40	C45	C44	0.98(8)
C6	C7	C8	C9	0.79(13)	C41	C40	C45	C46	-116.65(7)
C7	C8	C9	C4	0.45(12)	C41	C42	C43	C44	0.41(11)

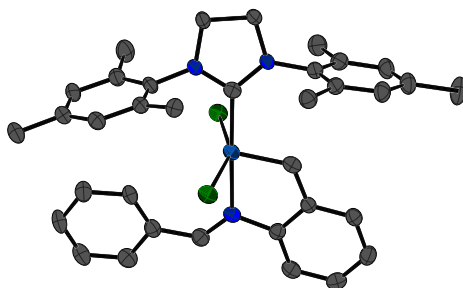
**Table 4.6.8. Torsion Angles for cs2915-inimer (7).**

A	B	C	D	Angle/°	A	B	C	D	Angle/°
C7	C8	C9	C12	175.60(8)	C42	C41	C47	C44	49.98(8)
C9	C4	C5	C6	2.42(12)	C42	C43	C44	C45	-70.91(10)
C9	C4	C5	C10	-179.99(8)	C42	C43	C44	C47	33.02(10)
C10	C5	C6	C7	-178.70(8)	C43	C44	C45	C40	66.74(8)
C11	C7	C8	C9	179.85(8)	C43	C44	C45	C46	179.04(7)
C13	N2	C1	Ru1	2.12(11)	C43	C44	C47	C41	-49.77(8)
C13	N2	C1	N1	-179.64(7)	C44	C45	C46	O4	65.19(11)
C13	N2	C3	C2	176.60(7)	C44	C45	C46	N4	-114.83(8)
C13	C14	C15	C16	0.63(12)	C45	C40	C41	C42	-68.40(9)
C14	C13	C18	C17	6.78(11)	C45	C40	C41	C47	35.33(8)
C14	C13	C18	C21	-171.83(7)	C45	C44	C47	C41	57.53(8)
C14	C15	C16	C17	4.25(13)	C46	N4	C38	C37	-100.37(9)
C14	C15	C16	C20	-174.19(8)	C46	N4	C39	O3	175.98(8)
C15	C16	C17	C18	-3.69(13)	C46	N4	C39	C40	-2.88(10)
C16	C17	C18	C13	-1.71(12)	C47	C41	C42	C43	-33.51(10)
C16	C17	C18	C21	176.94(8)	C47	C44	C45	C40	-37.11(8)
C18	C13	C14	C15	-6.25(11)	C47	C44	C45	C46	75.19(8)

**Chapter 4.**

This report has been created with Olex2, compiled on 2022.04.07 svn.rca3783a0 for OlexSys.

Please [let us know](#) if there are any errors or if you would like to have additional features.



(8)

## Experimental

A brownish-yellow plate (0.03 x 0.09 x 0.12 mm<sup>3</sup>) was centered on the goniometer of a Rigaku Oxford Diffraction Synergy-S diffractometer equipped with a HyPix6000HE detector and operating with CuK $\alpha$  radiation. The data collection routine, unit cell refinement, and data processing were carried out with the program CrysAlisPro.<sup>71</sup> The Laue symmetry and systematic absences were consistent with the monoclinic space group *I2/a*. The structure was solved using SHELXT<sup>72</sup> and refined using SHELXL<sup>73</sup> via Olex2.<sup>74</sup> The final refinement model involved anisotropic displacement parameters for non-hydrogen atoms and a riding model for all hydrogen atoms. The difference electron density map from the final structure model suggested there is a small amount of whole molecule disorder and showed a relatively large difference peak of 3.3 e-/Å<sup>3</sup> where Ru would reside. Refinement of the Ru as disordered suggest the minor conformation of the molecule

---

(71) CrysAlisPro Software System, v1.171.42.xx, Rigaku Oxford Diffraction, **2022**, Rigaku Corporation, Oxford, UK.

(72) Sheldrick, G. M. "SHELXT – Integrated space-group and crystal structure determination." *Acta Cryst.* **2015**, *A71*, 3–8.

(73) Sheldrick, G. M. "Crystal structure refinement with SHELXL." *Acta Cryst.* **2015**, *C71*, 3–8.

(74) Dolomanov, O.V.; Bourhis, L. J.; Gildea, R. J.; Howard, J. A. K.; Puschmann, H. *J. Appl. Cryst.* **2009**, *42*, 339–341.

amounts to ~5% occupancy. With such a low occupancy, only the major conformation was used the structure model. Olex2<sup>75</sup> was used for molecular graphics generation.

**Table 4.6.9. Crystal data and structure refinement for cs2925-catalyst (8).**

Identification code	cs2925
Empirical formula	C <sub>35</sub> H <sub>37</sub> Cl <sub>2</sub> N <sub>3</sub> Ru
Formula weight	671.64
Temperature/K	99.98(10)
Crystal system	monoclinic
Space group	<i>I</i> 2/a
<i>a</i> /Å	23.2621(3)
<i>b</i> /Å	10.15680(10)
<i>c</i> /Å	27.3417(4)
$\alpha$ /°	90
$\beta$ /°	100.7970(10)
$\gamma$ /°	90
Volume/Å <sup>3</sup>	6345.62(14)
<i>Z</i>	8
$\rho_{\text{calc}}/\text{cm}^3$	1.406
$\mu/\text{mm}^{-1}$	5.758
F(000)	2768.0
Crystal size/mm <sup>3</sup>	0.12 × 0.09 × 0.03
Radiation	Cu K $\alpha$ ( $\lambda$ = 1.54184)
2 $\Theta$ range for data collection/°	7.738 to 154.558
Index ranges	-29 ≤ <i>h</i> ≤ 29, -12 ≤ <i>k</i> ≤ 12, -34 ≤ <i>l</i> ≤ 34
Reflections collected	54791
Independent reflections	6639 [ <i>R</i> <sub>int</sub> = 0.0609, <i>R</i> <sub>sigma</sub> = 0.0326]
Data/restraints/parameters	6639/0/376
Goodness-of-fit on F <sup>2</sup>	1.033
Final <i>R</i> indexes [ <i>I</i> ≥ 2 $\sigma$ ( <i>I</i> )]	<i>R</i> <sub>1</sub> = 0.0581, <i>wR</i> <sub>2</sub> = 0.1374
Final <i>R</i> indexes [all data]	<i>R</i> <sub>1</sub> = 0.0620, <i>wR</i> <sub>2</sub> = 0.1400
Largest diff. peak/hole / e Å <sup>-3</sup>	3.31/-1.74

**Table 4.6.10. Bond Lengths for cs2925-catalyst (8).**

Atom	Atom	Length/Å	Atom	Atom	Length/Å
Ru1	Cl1	2.3307 (11)	C13	C14	1.402 (6)

(75) Dolomanov, O. V.; Bourhis, L. J.; Gildea, R. J.; Howard, J. A. K.; Puschmann, H. *J. Appl. Cryst.* **2009**, *42*, 339–341.

**Table 4.6.10. Bond Lengths for cs2925-catalyst (8).**

Atom	Atom	Length/Å	Atom	Atom	Length/Å
Ru1	C12	2.3511 (10)	C13	C18	1.396 (6)
Ru1	N3	2.174 (4)	C14	C15	1.399 (6)
Ru1	C1	2.051 (4)	C14	C19	1.498 (6)
Ru1	C22	1.846 (5)	C15	C16	1.385 (7)
N1	C1	1.345 (5)	C16	C17	1.386 (7)
N1	C2	1.476 (5)	C16	C20	1.518 (6)
N1	C4	1.447 (5)	C17	C18	1.408 (6)
N2	C1	1.349 (6)	C18	C21	1.507 (7)
N2	C3	1.473 (5)	C22	C23	1.450 (6)
N2	C13	1.441 (5)	C23	C24	1.401 (6)
N3	C28	1.442 (5)	C23	C28	1.396 (6)
N3	C29	1.286 (6)	C24	C25	1.390 (7)
C2	C3	1.526 (5)	C25	C26	1.398 (7)
C4	C5	1.398 (7)	C26	C27	1.387 (7)
C4	C9	1.398 (6)	C27	C28	1.387 (6)
C5	C6	1.400 (6)	C29	C30	1.450 (6)
C5	C10	1.504 (6)	C30	C31	1.398 (7)
C6	C7	1.382 (7)	C30	C35	1.397 (6)
C7	C8	1.391 (8)	C31	C32	1.392 (6)
C7	C11	1.514 (7)	C32	C33	1.391 (7)
C8	C9	1.408 (6)	C33	C34	1.377 (8)
C9	C12	1.502 (7)	C34	C35	1.377 (7)

**Table 4.6.11. Bond Angles for cs2925-catalyst (8).**

Atom	Atom	Atom	Angle/°	Atom	Atom	Atom	Angle/°
C11	Ru1	C12	152.53 (4)	C4	C9	C12	122.5 (4)
N3	Ru1	C11	86.80 (10)	C8	C9	C12	120.1 (4)
N3	Ru1	C12	89.16 (10)	C14	C13	N2	118.0 (4)
C1	Ru1	C11	98.35 (12)	C18	C13	N2	119.6 (4)
C1	Ru1	C12	86.13 (12)	C18	C13	C14	121.8 (4)
C1	Ru1	N3	174.84 (15)	C13	C14	C19	122.2 (4)
C22	Ru1	C11	98.12 (14)	C15	C14	C13	117.8 (4)
C22	Ru1	C12	108.06 (14)	C15	C14	C19	119.9 (4)
C22	Ru1	N3	80.99 (17)	C16	C15	C14	121.9 (4)
C22	Ru1	C1	98.48 (19)	C15	C16	C17	118.7 (4)
C1	N1	C2	113.5 (3)	C15	C16	C20	120.8 (5)
C1	N1	C4	129.9 (4)	C17	C16	C20	120.5 (4)
C4	N1	C2	115.3 (3)	C16	C17	C18	121.8 (4)
C1	N2	C3	114.1 (3)	C13	C18	C17	117.7 (4)
C1	N2	C13	127.6 (4)	C13	C18	C21	123.1 (4)
C13	N2	C3	117.7 (3)	C17	C18	C21	119.2 (4)
C28	N3	Ru1	110.5 (3)	C23	C22	Ru1	118.2 (3)
C29	N3	Ru1	132.1 (3)	C24	C23	C22	121.9 (4)
C29	N3	C28	117.4 (4)	C28	C23	C22	117.8 (4)
N1	C1	Ru1	128.3 (3)	C28	C23	C24	120.3 (4)
N1	C1	N2	107.1 (4)	C25	C24	C23	119.5 (4)
N2	C1	Ru1	123.4 (3)	C24	C25	C26	119.4 (4)
N1	C2	C3	102.9 (3)	C27	C26	C25	121.3 (4)
N2	C3	C2	102.2 (3)	C26	C27	C28	119.1 (4)
C5	C4	N1	118.1 (4)	C23	C28	N3	112.4 (4)
C9	C4	N1	119.7 (4)	C27	C28	N3	127.3 (4)
C9	C4	C5	122.2 (4)	C27	C28	C23	120.3 (4)
C4	C5	C6	117.8 (4)	N3	C29	C30	128.2 (4)
C4	C5	C10	121.0 (4)	C31	C30	C29	127.3 (4)
C6	C5	C10	121.1 (4)	C35	C30	C29	113.9 (4)
C7	C6	C5	122.3 (5)	C35	C30	C31	118.8 (4)
C6	C7	C8	118.3 (4)	C32	C31	C30	119.7 (4)
C6	C7	C11	121.4 (5)	C33	C32	C31	120.2 (5)
C8	C7	C11	120.4 (5)	C34	C33	C32	120.2 (4)
C7	C8	C9	122.1 (4)	C35	C34	C33	119.8 (4)
C4	C9	C8	117.4 (4)	C34	C35	C30	121.3 (5)

**Table 4.6.12. Torsion Angles for cs2925-catalyst (8).**

A	B	C	D	Angle/°	A	B	C	D	Angle/°
Ru1	N3	C28	C23	2.8 (4)	C7	C8	C9	C4	-0.4 (7)
Ru1	N3	C28	C27	-177.2 (4)	C7	C8	C9	C12	-179.8 (5)
Ru1	N3	C29	C30	-2.9 (7)	C9	C4	C5	C6	1.3 (7)
Ru1	C22	C23	C24	179.9 (3)	C9	C4	C5	C10	-174.9 (4)
Ru1	C22	C23	C28	1.0 (5)	C10	C5	C6	C7	175.1 (5)
C11	Ru1	C22	C23	86.0 (3)	C11	C7	C8	C9	179.8 (5)
C12	Ru1	C22	C23	-85.6 (3)	C13	N2	C1	Ru1	21.2 (6)
N1	C2	C3	N2	4.4 (4)	C13	N2	C1	N1	-170.3 (4)
N1	C4	C5	C6	-176.5 (4)	C13	N2	C3	C2	168.4 (4)
N1	C4	C5	C10	7.3 (6)	C13	C14	C15	C16	-2.7 (7)
N1	C4	C9	C8	177.1 (4)	C14	C13	C18	C17	-3.8 (7)
N1	C4	C9	C12	-3.4 (7)	C14	C13	C18	C21	173.0 (5)
N2	C13	C14	C15	177.3 (4)	C14	C15	C16	C17	-1.6 (7)
N2	C13	C14	C19	1.1 (7)	C14	C15	C16	C20	179.2 (5)
N2	C13	C18	C17	-175.6 (4)	C15	C16	C17	C18	3.3 (7)
N2	C13	C18	C21	1.3 (7)	C16	C17	C18	C13	-0.7 (7)
N3	Ru1	C22	C23	0.6 (3)	C16	C17	C18	C21	-177.7 (5)
N3	C29	C30	C31	-5.6 (8)	C18	C13	C14	C15	5.5 (7)
N3	C29	C30	C35	175.5 (5)	C18	C13	C14	C19	-170.8 (4)
C1	Ru1	C22	C23	-174.2 (3)	C19	C14	C15	C16	173.6 (4)
C1	N1	C2	C3	-4.9 (5)	C20	C16	C17	C18	-177.4 (5)
C1	N1	C4	C5	-81.8 (6)	C22	C23	C24	C25	-178.4 (4)
C1	N1	C4	C9	100.4 (6)	C22	C23	C28	N3	-2.6 (6)
C1	N2	C3	C2	-3.0 (5)	C22	C23	C28	C27	177.4 (4)
C1	N2	C13	C14	80.8 (6)	C23	C24	C25	C26	0.7 (7)
C1	N2	C13	C18	-107.2 (5)	C24	C23	C28	N3	178.5 (4)
C2	N1	C1	Ru1	171.0 (3)	C24	C23	C28	C27	-1.5 (6)
C2	N1	C1	N2	3.2 (5)	C24	C25	C26	C27	-0.9 (7)
C2	N1	C4	C5	84.3 (5)	C25	C26	C27	C28	-0.1 (7)
C2	N1	C4	C9	-93.5 (5)	C26	C27	C28	N3	-178.7 (4)
C3	N2	C1	Ru1	-168.4 (3)	C26	C27	C28	C23	1.3 (7)
C3	N2	C1	N1	0.1 (5)	C28	N3	C29	C30	177.9 (4)
C3	N2	C13	C14	-89.2 (5)	C28	C23	C24	C25	0.5 (6)
C3	N2	C13	C18	82.8 (5)	C29	N3	C28	C23	-177.8 (4)
C4	N1	C1	Ru1	-22.8 (7)	C29	N3	C28	C27	2.2 (6)
C4	N1	C1	N2	169.5 (4)	C29	C30	C31	C32	-178.6 (5)
C4	N1	C2	C3	-173.3 (4)	C29	C30	C35	C34	179.4 (4)
C4	C5	C6	C7	-1.1 (7)	C30	C31	C32	C33	-0.6 (7)
C5	C4	C9	C8	-0.6 (7)	C31	C30	C35	C34	0.4 (7)
C5	C4	C9	C12	178.8 (4)	C31	C32	C33	C34	0.1 (8)

**Table 4.6.12. Torsion Angles for cs2925-catalyst (8).**

A	B	C	D	Angle/°	A	B	C	D	Angle/°
C5	C6	C7	C8	0.2 (8)	C32	C33	C34	C35	0.6 (8)
C5	C6	C7	C11	-179.1 (5)	C33	C34	C35	C30	-0.9 (8)
C6	C7	C8	C9	0.6 (8)	C35	C30	C31	C32	0.3 (7)

This report has been created with Olex2, compiled on 2022.04.07 svn.rca3783a0 for OlexSys. Please [let us know](#) if there are any errors or if you would like to have additional features.

## Chapter 5. Synthesis of Azo and Imine Ring-Opening Metathesis Polymerization

### Inimers

Hanan N. Almuzaini,<sup>a,b</sup> Grace Dinges,<sup>a,b</sup> Carla Slebodnick,<sup>a</sup> Michael D. Schulz<sup>a,b</sup>

<sup>a</sup> Department of Chemistry, Virginia Polytechnic Institute and State University,  
Blacksburg, VA 24061

<sup>b</sup> Macromolecules Innovation Institute, Virginia Polytechnic Institute and State  
University, Blacksburg, VA 24061

#### 5.1. Abstract

Ring-opening metathesis polymerization (ROMP) is a great tool for synthesizing polyolefin materials with different topologies, including hyperbranched polymers (HPs) — polymers with irregular branching and many end groups. However, current methods for synthesizing HPs via ROMP require multiple reactions or specialized monomers. To provide a more general approach, we synthesized a series of ROMP inimers (initiator + monomer), which contain both the initiator and a polymerizable group, enabling HP synthesis via self-condensing ROMP in a single step. To test the capabilities of this approach, we synthesized hyperbranched polyoctenamer. Using Differential Scanning Calorimetry (DSC), we demonstrated that the physical properties of HPs could be modulated by varying the degree of branching (DB). For example, the melting temperature ( $T_m$ ), which ranged between 30 and 44°C, decreased as the DB increased. The identity and activity of the inimer controlled the HP stereochemistry, and inimers that activated at high temperatures produced polymers with higher cis content. This approach enables the direct synthesis of HPs from any ROMP active monomers, allowing the design of unique materials.

## 5.2. Introduction

Ring-opening metathesis polymerization (ROMP) is a type of olefin metathesis reaction that involves ring-opening of an unsaturated cyclic monomer to synthesize polyolefins. The development of effective ruthenium-based olefin metathesis catalysts has enabled the synthesis of advanced polymers and functional materials due to their relative stability, ease of use, and tolerance for most organic functional groups.<sup>1-6</sup> However, synthesizing hyperbranched polymers (HPs)—polymers with irregular branching structures and a high number of end groups—via ROMP is challenging. For example, HPs have been synthesized using a multifunctional ROMP monomer, such as dicyclopentadiene;<sup>7</sup> however, this polymerization required the addition of monoterpenes, d-limonene, limonene oxide, or  $\beta$ -pinene to prevent cross-linking.<sup>7</sup> HPs have also been synthesized by combining two polymerization approaches (ring-opening metathesis and cross-metathesis) using a single monomer containing a cyclic olefin for ring-opening metathesis and a terminal olefin for cross-metathesis.<sup>8</sup> Although examples of hyperbranched ROMP polymers were synthesized, there are some disadvantages, such as requiring multiple reactions or specialized monomers. To enable a more general hyperbranched ROMP polymer synthesis, we aimed to combine the ROMP initiator (an olefin metathesis catalyst) and polymerizable group (an unsaturated cyclic monomer) in a single molecular “*inimer*” (**Figure 5.1.c**). This inimer will enable self-condensing polymerization to produce HP in a single step.<sup>9</sup>

Self-condensing polymerization as a concept was first applied to vinyl polymerization and called self-condensing vinyl polymerization (SCVP) (**Figure 5.1.a**). SCVP inimer (**a**) undergoes an activation step to initiate radical polymerization of the

monomer and inimer. The self-condensation concept was then applied to ring-opening polymerization (ROP) to synthesize HPs using a self-condensing ring-opening polymerization (SCROP) inimer. For example, hyperbranched polyesters were synthesized by SCROP using an inimer such as 4-(2-hydroxyethyl)- $\epsilon$ -caprolactone (**Figure 5.1.b**).<sup>10</sup> This self-condensing approach enables HP synthesis in a one-step reaction with the polymer branching structure controlled by adjusting the inimer-to-monomer ratio. Although self-condensing polymerization simplifies hyperbranched polymer synthesis, self-condensing ROMP has not yet been developed.

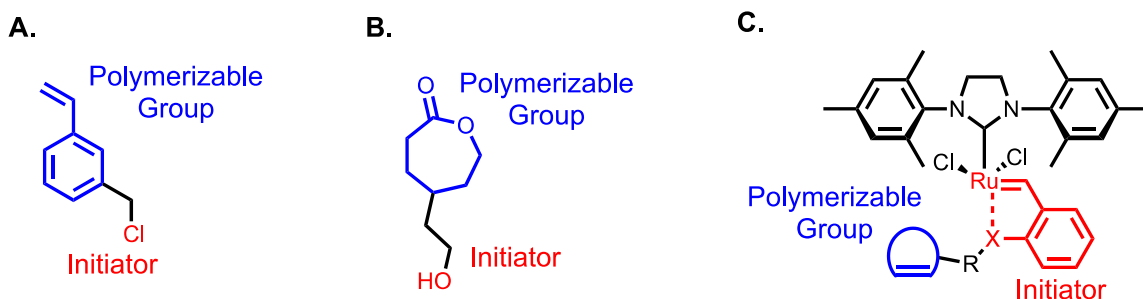


**Figure 5.1. Examples of inimers for A. SCVP, B. SCROP, and C. Current approach: self-condensing ROMP.**

Applying self-condensing polymerization to ROMP requires a coupling reaction between the initiator (olefin metathesis catalyst) and ROMP monomer (cyclic olefin) without prematurely initiating polymerization. A modified latent olefin metathesis catalyst, which is a precatalyst showing no reactivity at room temperature, can be used to avoid initiating polymerization (**Figure 5.2**). The latent olefin metathesis catalyst can be modified to have a functional group on the benzylidene ligand that enables the ROMP monomer coupling reaction. After the coupling reaction, the ROMP inimer can initiate self-condensing polymerization (**Figure 5.2**). The ROMP inimer polymerization forms the

branching units, while the monomer polymerization forms the linear segments. Branching density can be controlled by adjusting the inimer-to-monomer ratio. Increasing the monomer molar ratio will increase the linear segment, while increasing the inimer molar ratio will increase branching. Different HPs can also be synthesized by varying the ROMP inimer and monomer structures. Additionally, the inimer-monomer linkage enables the synthesis of degradable HPs.

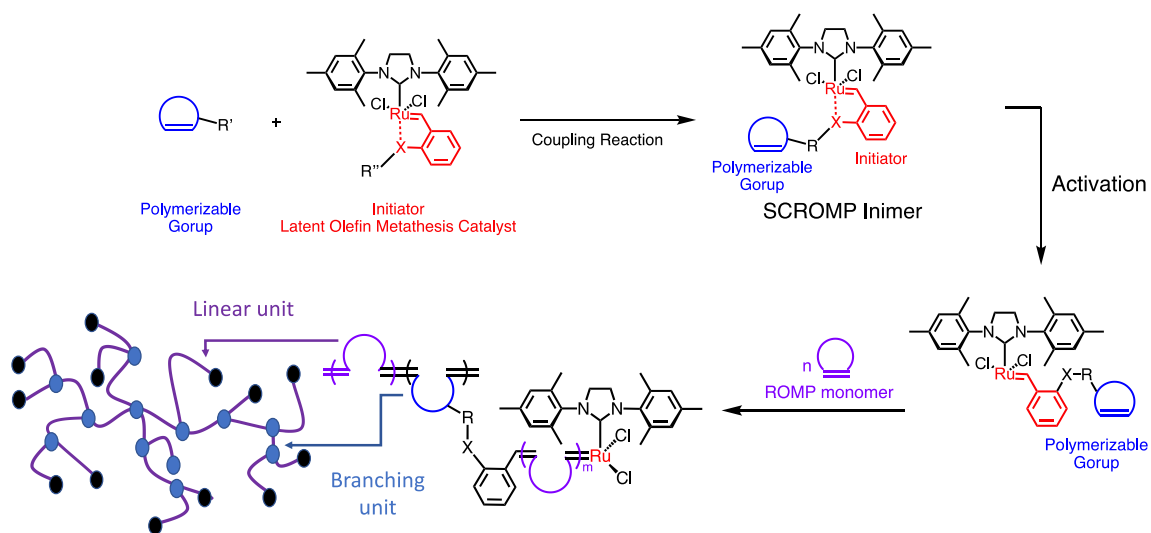


**Figure 5.2. Synthesis of ROMP inimer to synthesize HPs.**

Here, our aim was to synthesize a series of ROMP inimers with different chelating and polymerizable groups to study their activity and the properties of the resulting HPs. We synthesized inimers with a six-member chelating ring containing an imine (**Inimer 1** and **2** in **Figure 5.3**) and azo (**inimer 3, 4, 5** in **Figure 5.3**) chelating group. These inimers have a different chelation atom, polymerizable group, and chain length.

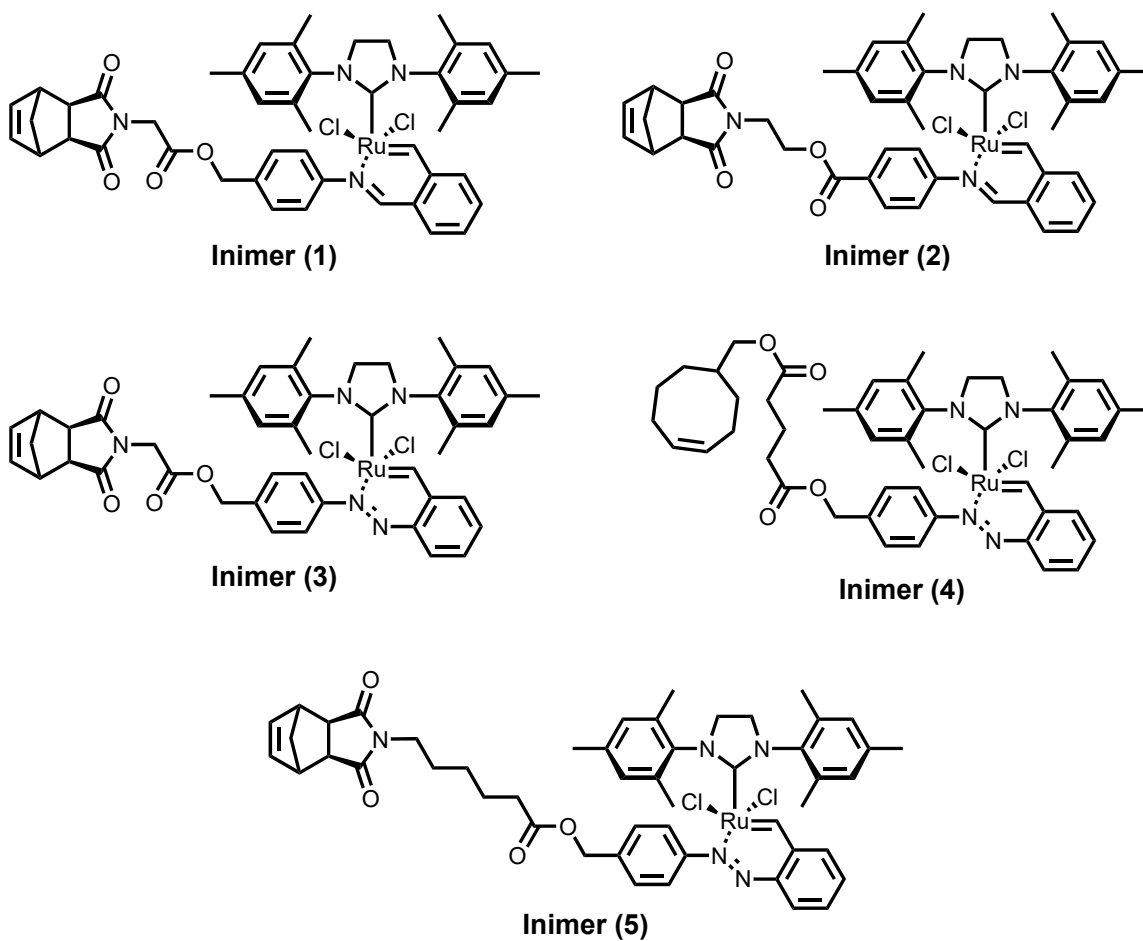


**Figure 5.3. ROMP inimer structures.**

### 5.3. Results and Discussions

#### **Inimer (1): Synthesis and characterization**

The benzylidene ligand (**4**) was synthesized as illustrated in **Figure 5.4**. Grubbs second-generation catalyst (**G2**) was reacted with (**4**) to produce a latent olefin metathesis catalyst (**5**). Catalyst (**5**) is unstable and easily undergoes an oxidation reaction, forming an aldehyde-functionalized catalyst (**7**) due to the presence of Cu(I)Cl as an oxidizing agent.<sup>11</sup> The two catalysts were isolated by column chromatography, and <sup>1</sup>H NMR spectroscopy confirmed the catalyst oxidation with a 1:1 ratio of alcohol to aldehyde products. The

alcohol-functionalized catalyst can further oxidize over time in a solution. Single-crystal X-ray diffraction confirmed the oxidation of the catalyst and only showed catalyst (7) (Figure 5.5). An attempt was made to synthesize catalyst (5) without Cu(I)Cl, but the catalyst was slower to form, though with less aldehyde-catalyst byproduct formation. Even though the oxidation was much slower in the absence of Cu(I)Cl, this result suggests that G2 may also oxidize this complex. To test this hypothesis, G2 (0.5 equiv.) was added to benzyl alcohol in CD<sub>2</sub>Cl<sub>2</sub>. The <sup>1</sup>H NMR spectroscopy showed an aldehyde peak (4 %) after keeping the solution overnight at room temperature. This result suggests the ability of the olefin metathesis catalysts to oxidize alcohol-functionalized products.

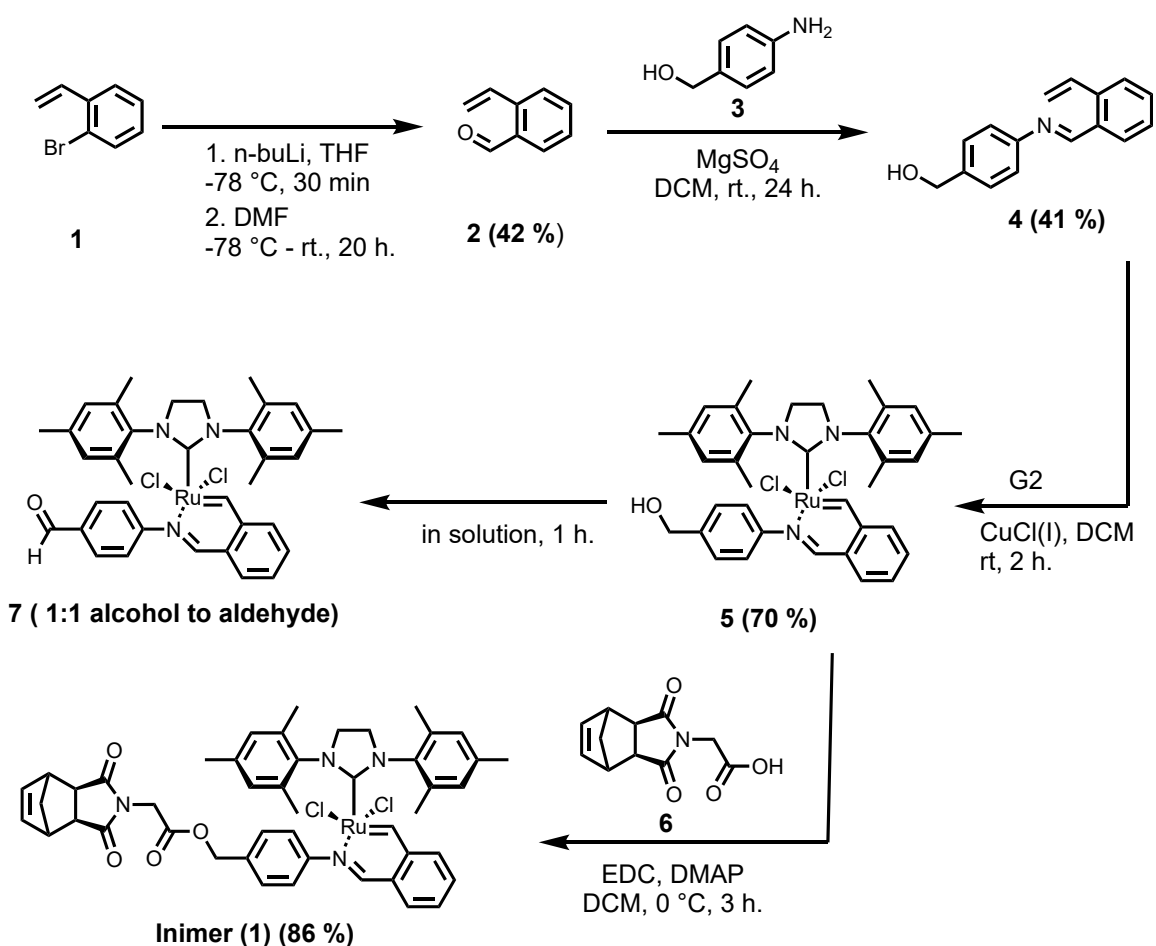
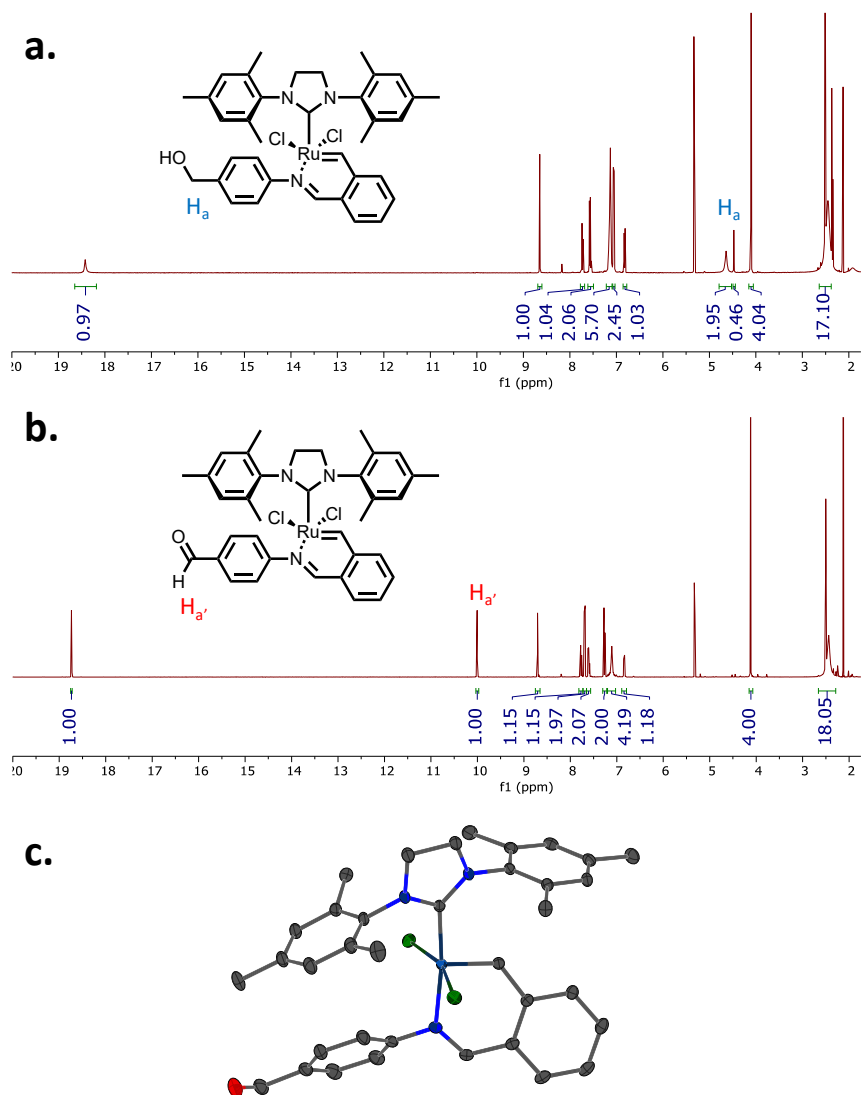


Figure 5.4. Synthesis of inimer (1).



**Figure 5.5.  $^1\text{H}$  NMR spectroscopy and crystal structure confirmed catalyst (5) oxidation.**

The coupling of carboxylic acid-functionalized norbornene (**6**) to the latent catalyst (**5**) resulted in the formation of the ROMP **inimer** (**1**), which contains both the initiating and propagating site. The structure of the ROMP inimer was confirmed by  $^1\text{H}$  NMR spectroscopy and single-crystal X-ray diffraction, as shown in **Figure 5.6**. The imine-chelated ruthenium olefin metathesis ROMP inimer was found to have an imine linkage

(H<sub>b</sub>), a carbene benzylidene ligand (H<sub>a</sub>), an NHC ligand (H<sub>e</sub>), and an ester linkage (H<sub>d</sub>), which were confirmed by <sup>1</sup>H NMR spectroscopy. The inimer only exhibited norbornene peaks (H<sub>c</sub>) in the alkene region of the NMR spectrum, indicating that the catalyst did not initiate during the coupling step.

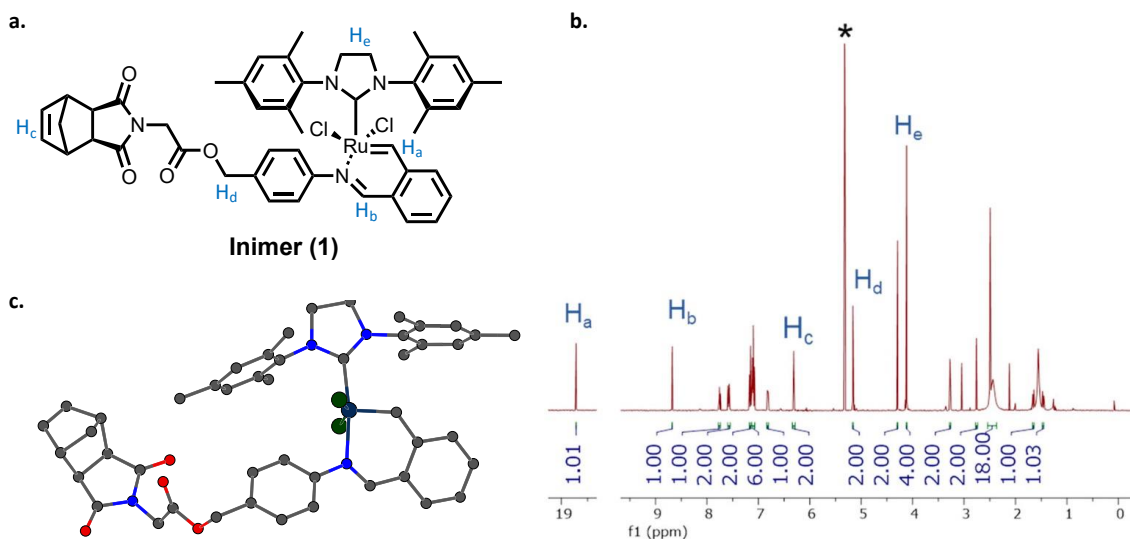


**Figure 5.6. a. inimer (1) structure, b. <sup>1</sup>H NMR spectroscopy, and c. crystal structure confirmed inimer (1) synthesis.**

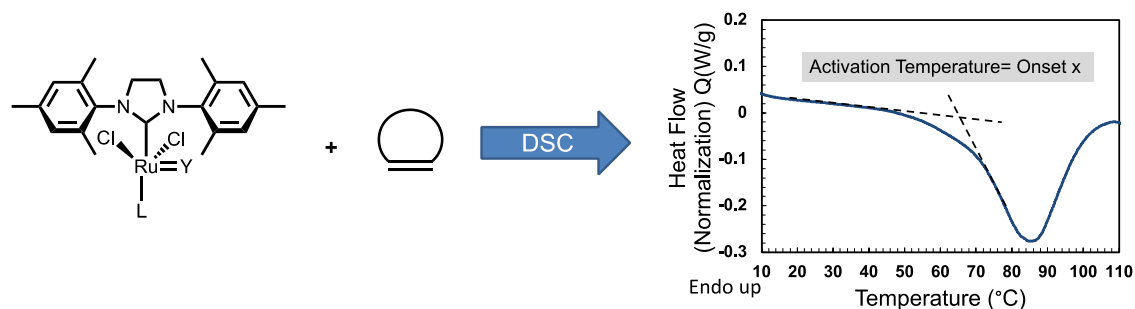
The activity and stability of the ROMP inimer were probed by polymerizing cyclooctene. The first attempt involved the polymerization of cyclooctene (80 equiv.) with the ROMP inimer (1 equiv.) in toluene-d<sub>8</sub>, in the presence of triphenylphosphine (PPh<sub>3</sub>) (1 equiv.). PPh<sub>3</sub> was added to improve catalyst stability and reactivity, and to slow down the propagating step, as reported in previous studies.<sup>12, 13</sup> The ROMP inimer was completely inactive at room temperature.

Remarkably, solutions of ROMP inimer in the presence of cyclooctene could be stored for more than 10 days without any sign of polymerization or decomposition of the

complex, demonstrating the high latency as well as the exceptional stability of this ROMP inimer. Furthermore, this inimer can be stored in CD<sub>2</sub>Cl<sub>2</sub> for at least 90 days without any sign of decomposition detected by <sup>1</sup>H NMR spectroscopy.

Differential scanning calorimetry (DSC) was used to measure the activation temperature of the ROMP inimer, which is the temperature at which the polymerization is initiated under specific conditions. A mixture of a ROMP monomer in the presence of the ROMP inimer was combined in a DSC pan and heated (3 °C/ min). The exotherm of the reaction was measured as a function of temperature. The activation temperature for the inimer was determined as the temperature at which exothermic heat flow was observed (refer to **Figure 5.7**). The activation temperature of the inimer varied depending on the identity of the monomer and ranged between 64–92 °C. The lowest activation temperature was associated with norbornene polymerization, and the highest activation temperature was associated with cyclooctene polymerization.

To study the effect of the polymerizable group on the inimer reactivity, **[Ru] 1** was synthesized. Similar to **inimer (1)**, the activation temperature of **[Ru] 1** varied and ranged between 50–90 °C, showing mainly lower activation temperatures compared to the inimer, potentially due to the absence of the bulky polymerizable group (refer to **Figure 5.7**). Although **inimer (1)** was activated at higher temperatures, it was activated at a lower temperature in polymerizing **M3** compared to **[Ru] 1**.



Initiator	Monomer	M1	M2	M3	M4	M5	M6
 Inimer (1)	 [Ru] 1	64	65	69	90	92	90
		50	70	93	51	75	90

**Figure 5.7. ROMP inimer and [Ru] 1 activation temperature.**

To investigate the ability of self-condensing ROMP to control the degree of branching (DB) of polymers, a series of HPs were synthesized using different inimer-to-monomer molar ratios (**Table 5.1**). As each inimer becomes a branch point in the final polymer, **HP (1)**, prepared with 20 equiv. cyclooctene, was expected to have the highest DB. Increasing the monomer molar ratio resulted in HPs with longer linear segments and fewer dendritic units, leading to a decrease in DB. DSC was used to illustrate the differences in properties based on DB. Self-condensing ROMP of the inimer with cyclooctene produced semi-crystalline HPs with  $T_m$  ranging between 30 and 45°C (refer to

**Table 1).** As the monomer molar ratio increased, the crystallization and  $T_m$  of the HPs increased, indicating that the DB was decreasing.

**Table 5.1. Hyperbranched polymers were synthesized via self-condensing ROMP.**

Sample	COE equiv.	target segment $M_n$	conv. <sup>a</sup> (%)	$M_n$ <sup>b</sup> (KDa)	$M_w$ <sup>b</sup> (KDa)	$\bar{D}$ <sup>b</sup>	$T_c$ <sup>c</sup> (°C)	$T_m$ <sup>c</sup> (°C)	Trans/cis
HP 1	20	2640	99	37.0	49.6	1.34	8.0	30	60/40
HP 2	40	4840	99	25.7	36.4	1.42	8.4	32	60/40
HP 3	60	7040	99	50.2	72.2	1.44	13	37	61/39
HP 4	80	9240	99	60.2	80.8	1.34	16	39	60/40
HP 5	160	18040	99	103	139	1.35	23	43	60/40
HP 6	200	22440	96	73.6	103	1.40	24	44	60/40
LP <sup>c</sup>	680	75000	98	25.5	39.5	1.56	43	60	80/20
Crosslinked	50	5850	100	-	-	-	-	-	-
Crosslinked	500	58500	100	-	-	-	-	-	-

<sup>a</sup> Determined by <sup>1</sup>H NMR spectroscopy, <sup>b</sup> determined by SEC, and <sup>c</sup> determined by DSC. <sup>e</sup> Grubbs third-generation catalyst was used to prepare the linear polymer.

The self-condensing ROMP approach produced polymers that are completely soluble in organic solvents like toluene, DCM, THF, and chloroform, which suggests that this approach can prevent the formation of insoluble crosslinked materials. To explore an alternative method for synthesizing hyperbranched ROMP polymers, an A<sub>2</sub> ROMP monomer was synthesized (**Table 5.1**). However, when the A<sub>2</sub> monomer was added (1 equiv.) to cyclooctene (50 equiv.) and Grubbs II catalyst, immediate gelation occurred, which could not be avoided even with a cyclooctene-to-A<sub>2</sub> monomer loading of 500:1. In contrast, gelation was not observed when using the self-condensing ROMP approach, even at equivalent DB.

To further illustrate the effect of branching units on the properties of the polymer, a linear polyoctenamer with  $M_n = 25.5$  KDa (**Table 5.1. LP**) was synthesized. The materials prepared via self-condensing ROMP exhibited lower melting and crystallization temperatures than the linear polymer (**Table 5.1**). However, the trans/cis ratio in the HPs (60/40) differed from the linear polymer (80/20). As previously reported, the identity of the olefin metathesis catalyst can affect the polymer stereochemistry,<sup>14</sup> so a latent olefin metathesis catalyst **[Ru] 2** (**Figure 5.8**) was synthesized. **[Ru] 2** has a structure similar to ROMP **inimer (1)** but with a phthalimide group instead of the polymerizable norbornene group. Single-crystal x-ray crystallography confirmed the synthesis of the catalyst. However, the activation temperature of **[Ru] 2** to polymerize cyclooctene was higher than the inimer by 28 °C (**Table 5.2**). This result can be explained by the absence of the norbornene polymerizable group, which may lower the activation temperature of the inimer.

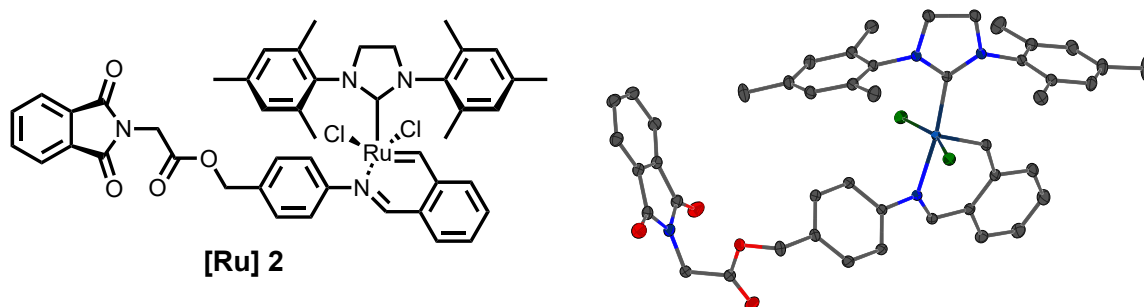
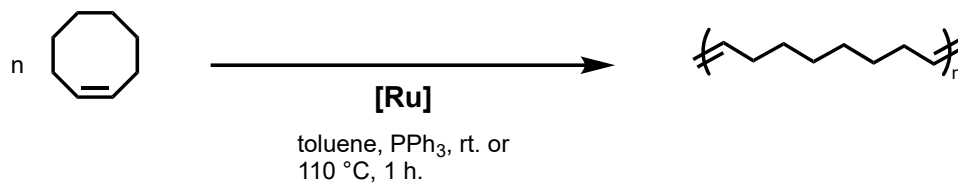


**Figure 5.8.** Crystal structure of **[Ru] 2**.

**Table 5.2. Activation temperature of the catalysts and polymer stereochemistry in percentage (%).**



Initiator	Activation Temperature (°C)	Trans/ cis
G2	rt.	80/20
[Ru] 1	75	50/50
Inimer (1)	92	60/40
[Ru] 2	120	40/60

Then linear polyoctenamer was synthesized using catalysts **[Ru] 1** and **2** (**Table 5.2**). The trans-to-cis ratio of the synthesized polymers was measured by using the olefin peaks in the  $^1\text{H}$  NMR spectrum. The polymerization results clearly demonstrated that the stereochemistry of the polymer was influenced by the catalyst identity. Higher cis content was observed in the polymer synthesized with **[Ru] 2**.

## Inimer (2): Synthesis and characterization

We attempted to decrease the activation temperature of the inimer to test the possibility of controlling HP stereochemistry. For this purpose, we synthesized latent olefin metathesis catalysts functionalized with carboxylic acid (**10**) (**Figure 5.9**). Then, we esterified the latent catalyst with the polymerizable group (**11**) to produce **inimer (2)**. We hypothesized that the carbonyl carbon attached to the chelating phenyl would withdraw the electron density away from the imine, weakening the Ru-N chelation and increasing the catalyst activity.

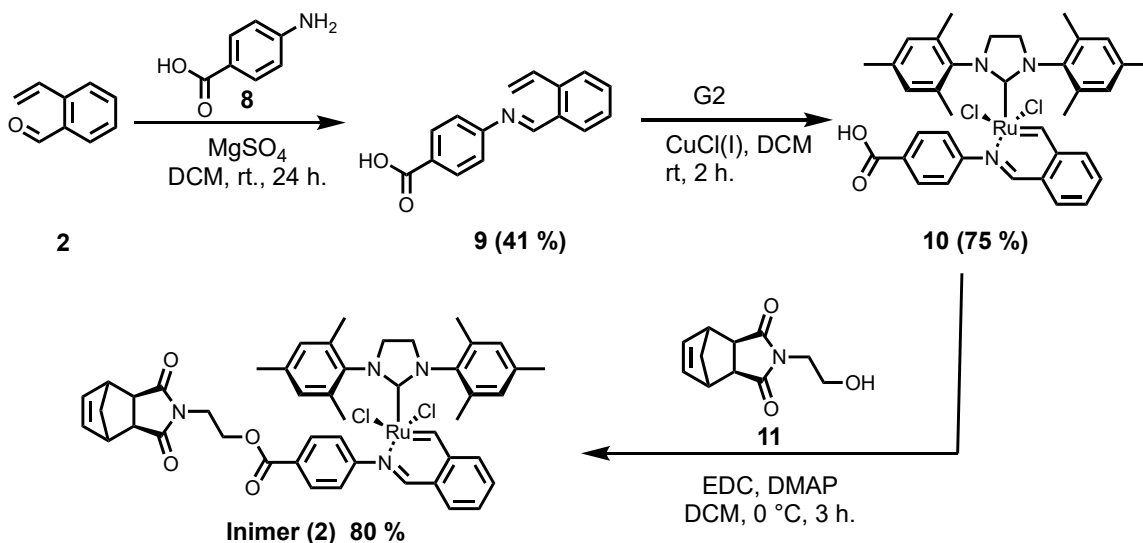


**Figure 5.9. ROMP inimer (2) synthesis.**

We conducted a  $^1\text{H}$  NMR kinetic study to measure the activation temperature of **Inimer (2)** in polymerizing cyclooctene. The study involved varying temperatures from room temperature to  $100\text{ }^\circ\text{C}$  with increasing the temperature  $10\text{ }^\circ\text{C}$  every 20 min. To prepare a polymerization sample, we mixed **inimer (2)** (1 equiv.), cyclooctene (80 equiv.), and

PPh<sub>3</sub> (1 equiv.) in toluene-d<sub>8</sub>. The <sup>1</sup>H NMR spectra showed no polymerization at or below 80 °C. However, we observed cyclooctene polymerization at 100 °C, with 40% conversion in 20 min (**Figure 5.10**). The <sup>1</sup>H NMR results confirmed the high stability of the inimer in the presence of cyclooctene even at 80 °C. The NMR kinetic study results showed a higher activation temperature, despite the presence of the carbonyl group attached to phenyl group. However, **Inimer (2)** produced a polymer with higher cis isomer content (43/ 65 trans/ cis) compared to **inimer (1)** (60/ 40 trans/ cis).

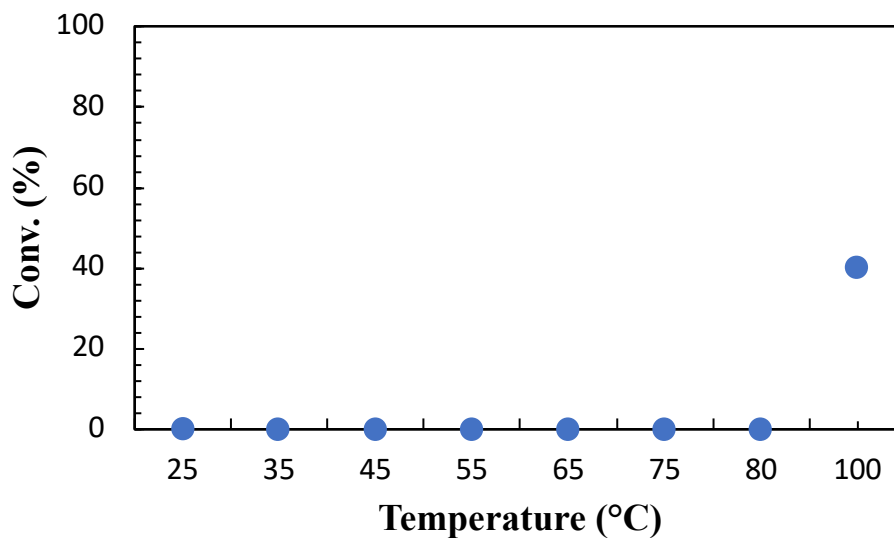
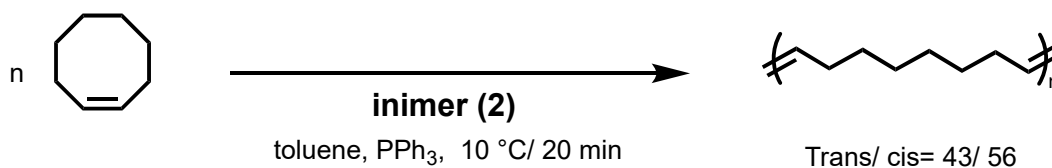


**Figure 5.10.** <sup>1</sup>H NMR kinetic experiment determined inimer (2) activation temperature.

### **Inimer (3-5): Synthesis and characterization**

The azo benzylidene ligand (**16**) was synthesized following the synthetic procedure shown in **Figure 5.11**. We then synthesized an azo-chelated ruthenium olefin metathesis catalyst (**17**) with two isomers: a major isomer that has a six-member chelating ring and a minor isomer that has a five-member chelating ring (**Figure 5.11**).

The minor isomer underwent isomerization in solution to the major thermodynamic isomer, which was detected by  $^1\text{H}$  NMR spectroscopy. After 24 h in  $\text{CD}_2\text{Cl}_2$ , the minor isomer peaks disappeared, and only the major isomer peaks were observed in the  $^1\text{H}$  NMR spectra (**Figure 5.12**). The six-membered-ring chelated olefin metathesis catalyst structure was confirmed by single-crystal X-ray crystallography (**Figure 5.12**). The isomers and isomerization result are consistent with previous work on preparing azo-chelated latent olefin metathesis catalysts.<sup>15</sup>

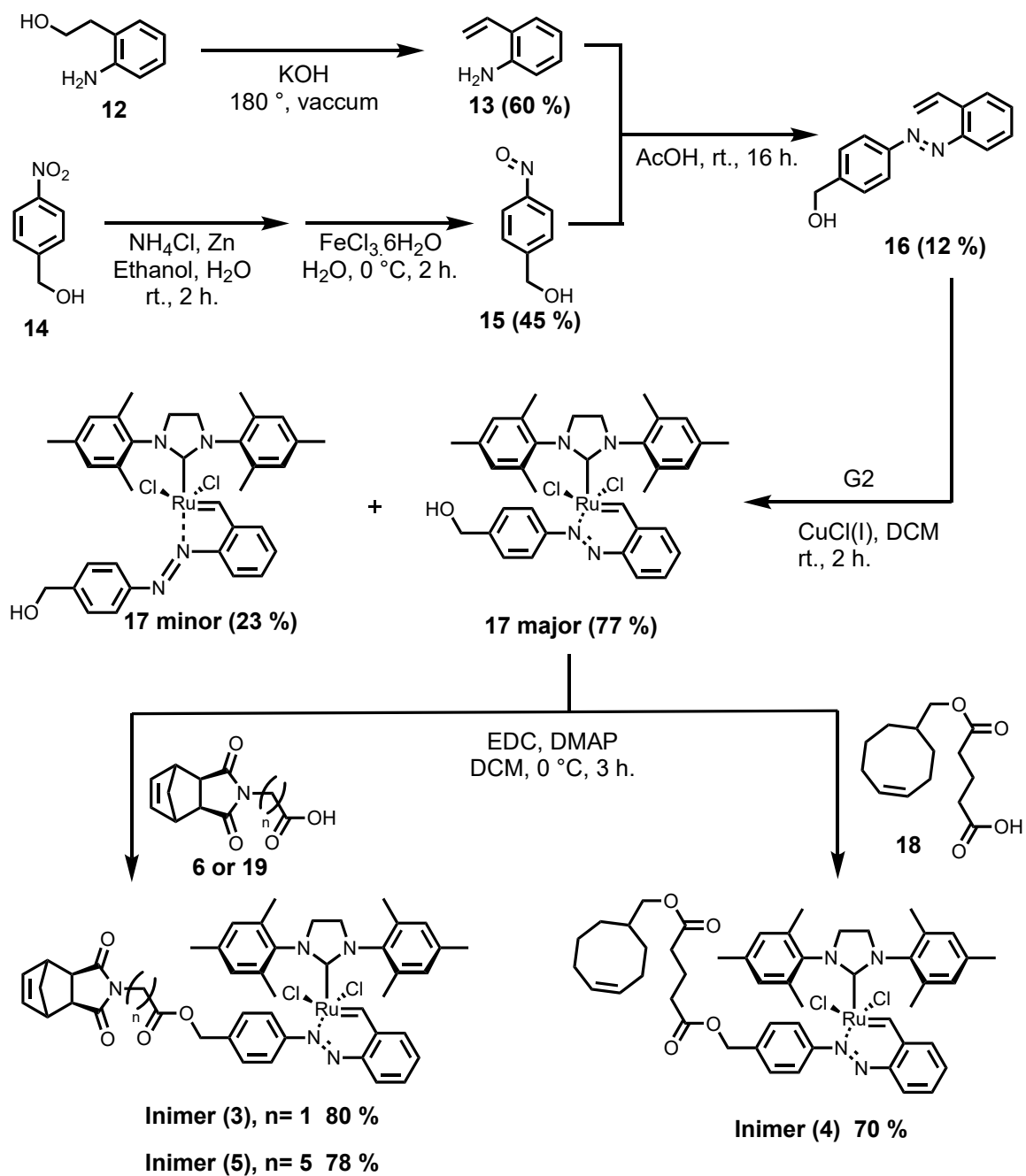
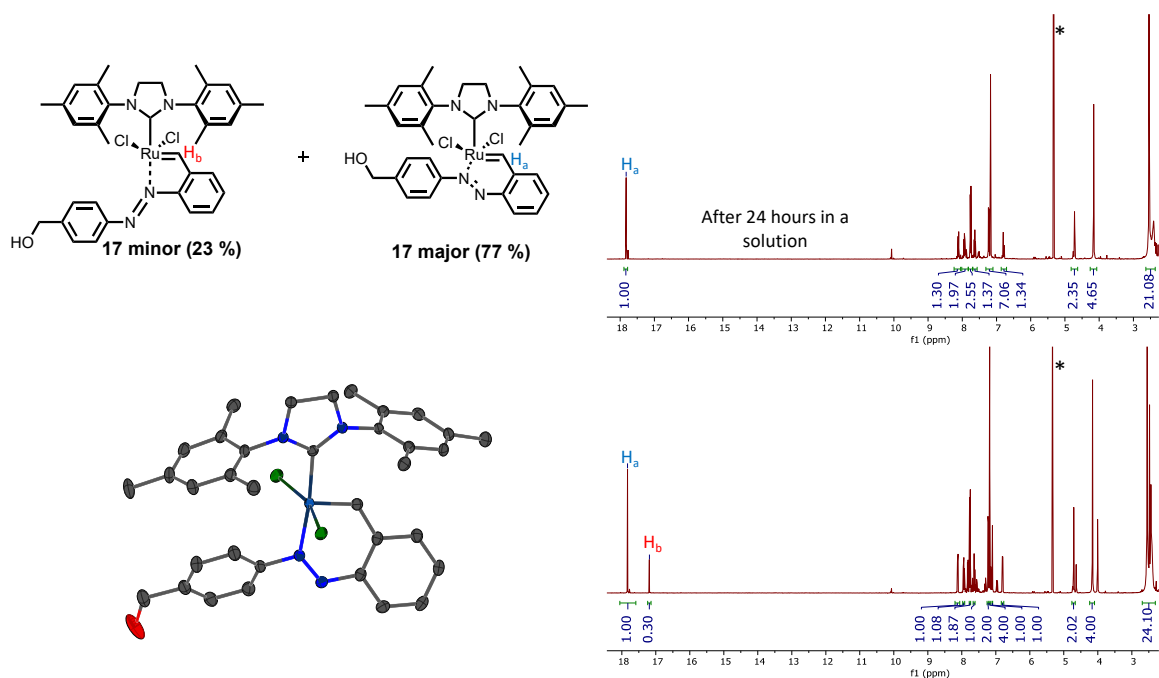


Figure 5.11. Inimer (3), (4), and (5) synthesis.



**Figure 5.12. Isomerization of (17).**

Catalyst (**17**) reacted with (**6**), (**18**), and (**19**) to prepare ROMP **inimers** (**3**), (**4**), and (**5**), respectively (**Figure 5.11**). These **inimers** have an azo-chelated ruthenium initiator with a different polymerizable group. The synthesis of **inimers** (**3**) and (**4**) was confirmed by both  $^1\text{H}$  NMR spectroscopy and single-crystal X-ray crystallography (**Figure 5.13**). The synthesis of **Inimer** (**5**) was confirmed by  $^1\text{H}$  NMR spectroscopy, but this compound did not crystallize, presumably due to the presence of a long aliphatic ester linkage chain.

The  $^1\text{H}$  NMR spectroscopy analysis of the three **inimers** confirmed the synthesis of a single molecule containing a ruthenium initiator with a polymerizable group. No initiation or polymerization was observed during the coupling reaction, and the ester linkage was also confirmed by  $^1\text{H}$  NMR analysis.

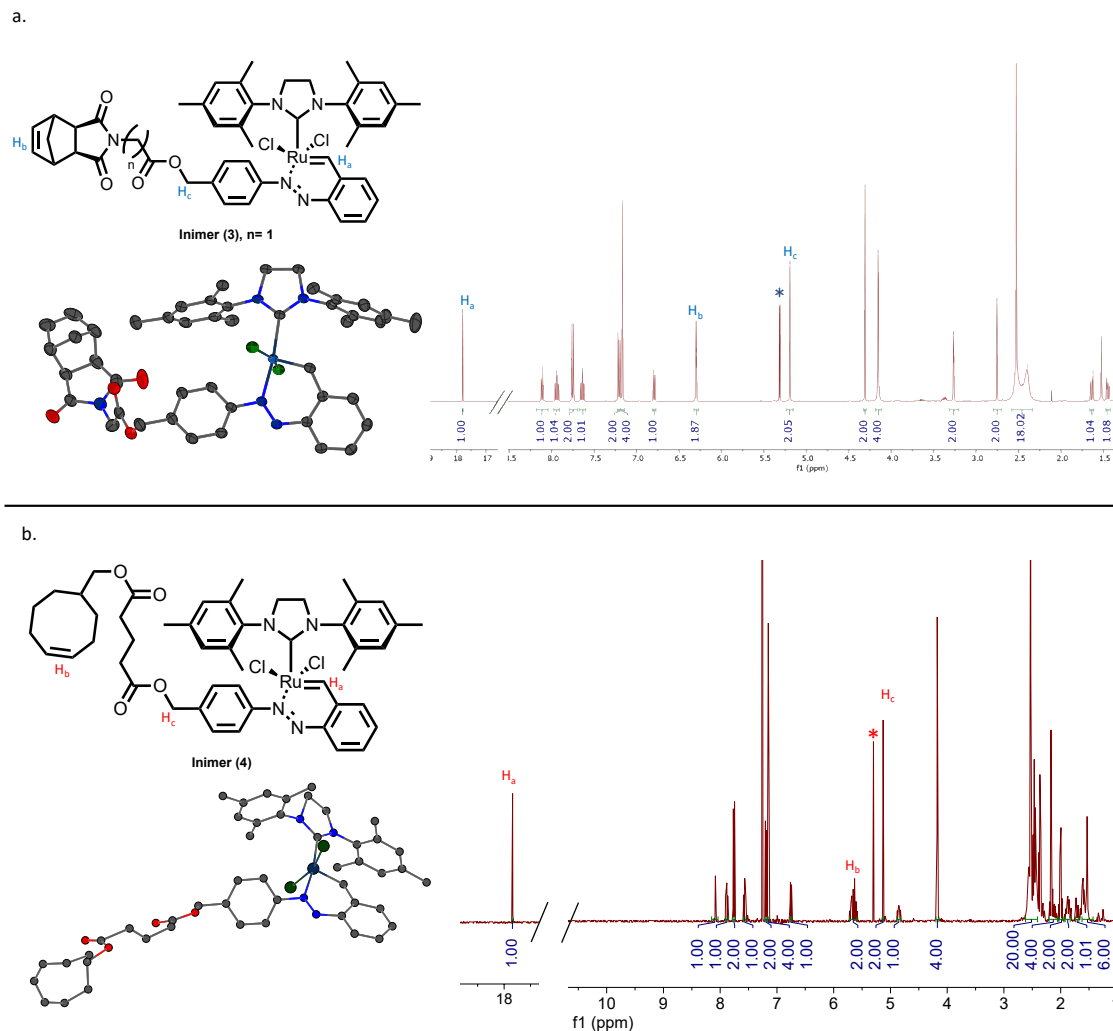


**Figure 5.13.  $^1\text{H}$  NMR and crystal structure confirm the inimer (3) and (4) synthesis.**

**Inimer (3)** was highly stable in DCM at room temperature for at least four months without any signs of decomposition detected by  $^1\text{H}$  NMR spectroscopy. It also showed no reactivity at room temperature in the presence of cyclooctene in  $\text{CDCl}_3$  for over three months. However, this ROMP inimer initiates when heated.

To determine the inimer activation temperature, we performed DSC analysis. We mixed the ROMP inimer (1 equiv.) with norbornene (100 equiv.) in a DSC pan and applied

a heating ramp of 10 °C/ min. The inimer activation temperature was 81 °C, which was the temperature at which the exothermic heat flow was observed (**Figure 5.14**).

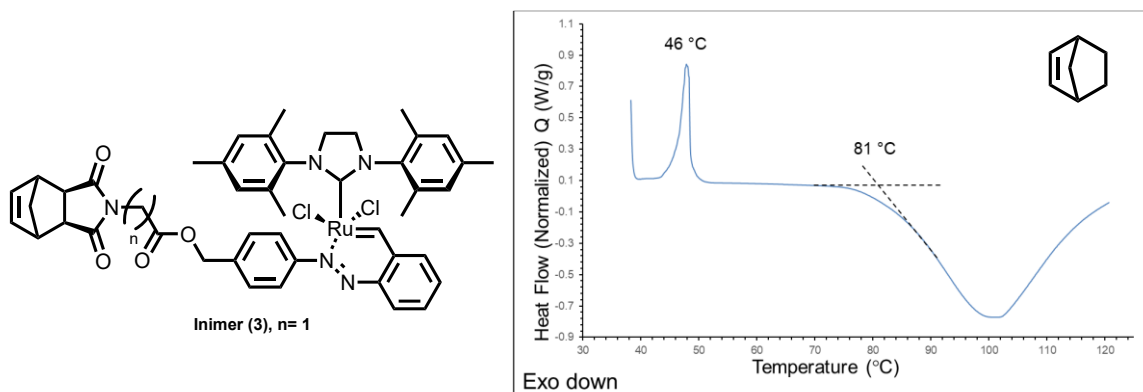


**Figure 5.14. Inimer (3) activation temperature**

We also determined the activation temperature of **inimer (3)** using  $^1\text{H}$  NMR spectroscopy. We mixed **inimer (3)** (1 equiv.) with cyclooctene (120 equiv.) and  $\text{PPh}_3$  (1 equiv.) in toluene- $d_8$  in an NMR tube. The temperature was increased by 10 °C every 10 min from room temperature to 100 °C. We observed monomer conversion at 80 °C, but the polymerization rate increased with increasing the reaction temperature. At 80 °C, 50% conversion of cyclooctene was achieved after 70 min, while 99% conversion of cyclooctene was achieved in 70 min at 100 °C. The resulting hyperbranched polyoctenamer had a 75:25 trans-to-cis ratio.

We synthesized HPs by combining **inimer (3)** with cyclooctene (1:120), and  $^1\text{H}$  NMR spectroscopy confirmed polymerization via self-condensing ROMP. The number-average molecular weight ( $M_n$ ) was determined using gel permeation chromatography (GPC) in THF, and it was found to be  $M_n = 78,300 \text{ g mol}^{-1}$  with a  $\mathcal{D}$  of 1.67. DSC analysis revealed that the resulting HP was semi-crystalline, with  $T_m = 48 \text{ °C}$ . Furthermore, thermogravimetric analysis (TGA) showed that the HP had high thermal stability, as only

5% of its mass was lost when the temperature increased to 160 °C. It is important to note that the ROMP **inimer (3)** used in this process resulted in HPs without the formation of insoluble crosslinks.

**Inimer (4)** activity was studied in the polymerization of cyclooctene. After 4 h at 100 °C, <sup>1</sup>H NMR spectroscopy showed 98% conversion. The resulting HP had a stereochemistry of 75% trans and 25% cis, which was similar to the HP synthesized by **inimer (3)**. We also attempted to test the activation of **inimer (4)** using UV-Vis spectroscopy in the polymerization of cyclooctene at room temperature. However, the inimer did not activate, and no polymer was observed even after 24 h.

The activation of **inimer (5)** was studied in the polymerization of norbornene. When a mixture of **inimer (5)** (1 equiv.) and norbornene (50 equiv.) in toluene was analyzed using <sup>1</sup>H NMR spectroscopy, no polymerization was observed after 1 h at room temperature. However, after 24 h at room temperature, 28% of the norbornene was polymerized. The conversion increased to 99% in a polymerization carried out at 80 °C in 2 h. <sup>1</sup>H NMR suggested that **inimer (5)** had activity at room temperature but at a lower rate.

#### 5.4. Conclusion

Examples of ROMP inimers were synthesized with azo and imine-chelated ruthenium complexes to prepare HPs via self-condensing ROMP. These inimers were characterized by using <sup>1</sup>H NMR spectroscopy and single-crystal X-ray crystallography, which confirmed the synthesis of each inimer without prematurely initiating polymerization. The inimers showed variable activation temperature based on their chelation group. We were able to synthesize a series of HPs with controlled the polymer

branching density and stereochemistry. While the self-condensing ROMP approach allows the synthesis of the HP in a single step, further inimer structure modifications are in development to prepare a variety of HPs with different properties.

## 5.5. References

- (1) Schulz, M. D.; Wagener, K. B. Precision Polymers through ADMET Polymerization. *Macromol. Chem. and Phys.* **2014**, *215* (20), 1936-1945. DOI: 10.1002/macp.201400268.
- (2) Schulz, M. D.; Wagener, K. B. ADMET Polymerization. In *Handbook of Metathesis*, Wiley-VCH Verlag GmbH & Co. KGaA, 2015; pp 313-355.
- (3) Caire da Silva, L.; Rojas, G.; Schulz, M. D.; Wagener, K. B. Acyclic diene metathesis polymerization: History, methods and applications. *Prog. Polym. Sci.* **2017**, *69*, 79-107. DOI: <https://doi.org/10.1016/j.progpolymsci.2016.12.001>.
- (4) Atallah, P.; Wagener, K. B.; Schulz, M. D. ADMET: The Future Revealed. *Macromolecules* **2013**, *46* (12), 4735-4741. DOI: 10.1021/ma400067b (accessed 2014/05/09).
- (5) Sheiko, S. S.; Sumerlin, B. S.; Matyjaszewski, K. Cylindrical molecular brushes: Synthesis, characterization, and properties. *Prog. Polym. Sci.* **2008**, *33* (7), 759-785. DOI: <https://doi.org/10.1016/j.progpolymsci.2008.05.001>.
- (6) Sutthasupa, S.; Shiotsuki, M.; Sanda, F. Recent advances in ring-opening metathesis polymerization, and application to synthesis of functional materials. *Polym J* **2010**, *42* (12), 905-915.
- (7) Mathers, R. T.; Damodaran, K.; Rendos, M. G.; Lavrich, M. S. Functional Hyperbranched Polymers Using Ring-Opening Metathesis Polymerization of Dicyclopentadiene with Monoterpenes. *Macromolecules* **2009**, *42* (5), 1512-1518. DOI: 10.1021/ma802441t.
- (8) Ren, N.; Zhu, X. Hybrid Polymerization of Ring-Opening Metathesis and Cross-Metathesis for Polyolefins with Tunable Architectures. *Macromolecules* **2018**, *51* (23), 9555-9561. DOI: 10.1021/acs.macromol.8b02135.
- (9) Fréchet, J. M. J.; Henmi, M.; Gitsov, I.; Aoshima, S.; Leduc, M. R.; Grubbs, R. B. Self-Condensing Vinyl Polymerization: An Approach to Dendritic Materials. *Science* **1995**, *269* (5227), 1080, 10.1126/science.269.5227.1080.
- (10) Liu, M.; Vladimirov, N.; Fréchet, J. M. A new approach to hyperbranched polymers by ring-opening polymerization of an AB monomer: 4-(2-hydroxyethyl)- $\epsilon$ -caprolactone. *Macromolecules* **1999**, *32* (20), 6881-6884.
- (11) Mannam, S.; Sekar, G. CuCl catalyzed selective oxidation of primary alcohols to carboxylic acids with tert-butyl hydroperoxide at room temperature. *Tetrahedron Lett.* **2008**, *49* (15), 2457-2460. DOI: <https://doi.org/10.1016/j.tetlet.2008.02.031>.
- (12) Schmid, T. E.; Bantreil, X.; Citadelle, C. A.; Slawin, A. M. Z.; Cazin, C. S. J. Phosphites as ligands in ruthenium-benzylidene catalysts for olefin metathesis. *Chem. Commun.* **2011**, *47* (25), 7060-7062, 10.1039/C1CC10825E. DOI: 10.1039/C1CC10825E.
- (13) Robertson, I. D.; Dean, L. M.; Rudebusch, G. E.; Sottos, N. R.; White, S. R.; Moore, J. S. Alkyl Phosphite Inhibitors for Frontal Ring-Opening Metathesis Polymerization Greatly Increase Pot Life. *ACS Macro Lett.* **2017**, *6* (6), 609-612. DOI: 10.1021/acsmacrolett.7b00270.
- (14) Spring, A. M.; Yu, F.; Qiu, F.; Yamamoto, K.; Yokoyama, S. The preparation of well-controlled poly(N-cyclohexyl-exo-norbornene-5,6-dicarboximide) polymers. *Polym. J.* **2014**, *46* (9), 576-583. DOI: 10.1038/pj.2014.26.

(15) Sashuk, V.; Danylyuk, O. A Thermo- and Photo-Switchable Ruthenium Initiator For Olefin Metathesis. *Chem. Eur. J.* **2016**, *22* (19), 6528-6531. DOI: <https://doi.org/10.1002/chem.201600776>.

## 5.6. Experimental Section

### Materials

All reactions were performed using oven-dried glassware equipped with a magnetic stir bar under air atmosphere unless otherwise noted. 2-Aminophenethyl alcohol was purchased from Ambeed, while 4-nitrobenzyl alcohol, ammonium chloride, iron chloride hexahydrate, and copper (I) chloride were obtained from Oakwood. *cis*-5-Norbornene-*endo*-2,3-dicarboxylic anhydride was purchased from Sigma Aldrich. G2 was donated by Materia and purchased from Sigma-Aldrich and Ambeed. CDCl<sub>3</sub>, CD<sub>2</sub>Cl<sub>2</sub>, and toluene-d<sub>8</sub> were obtained from Cambridge Isotope Laboratories. All other reagents were purchased from commercial suppliers and used without further purification.

### Measurements

<sup>1</sup>H NMR and <sup>13</sup>C NMR data were collected at 25 °C in CDCl<sub>3</sub>, CD<sub>2</sub>Cl<sub>2</sub>, or toluene-d<sub>8</sub> unless otherwise noted using an Agilent U4-DD2 400 MHz or a Bruker Avance II 500 MHz NMR instrument. Chemical shifts were reported in parts per million (ppm) and referenced to the CHCl<sub>3</sub> singlet at 7.26 ppm, CD<sub>2</sub>Cl<sub>2</sub> triplet at 5.32 ppm, or toluene-d<sub>8</sub> singlet at 7.00 ppm for <sup>1</sup>H NMR. <sup>13</sup>C NMR spectra referenced to the center peak of the CDCl<sub>3</sub> triplet at 77.00 ppm, or CD<sub>2</sub>Cl<sub>2</sub> at 54.00 ppm.

### Experimental Procedures

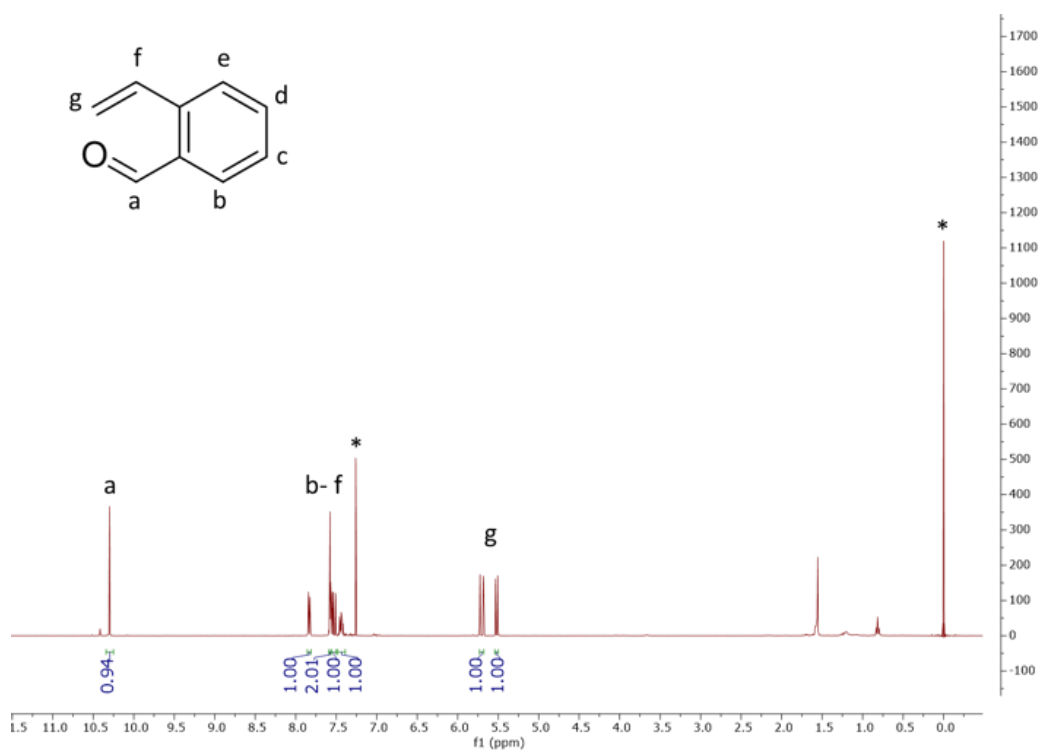
#### 2-vinylbenzaldehyde (2)

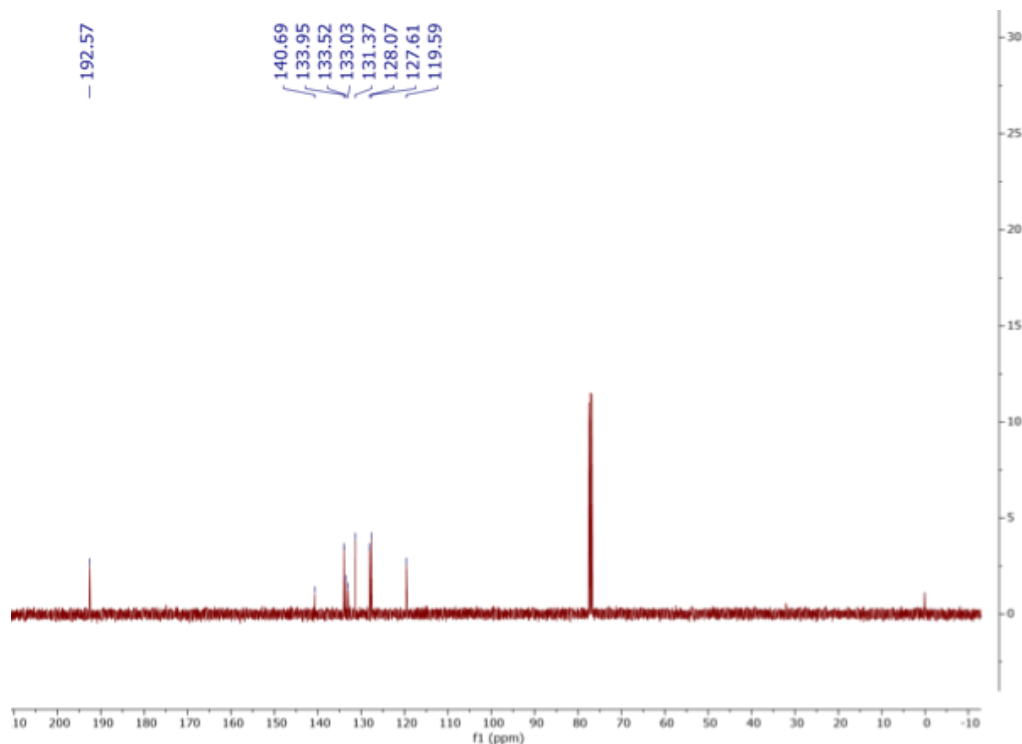
*n*-BuLi (1.1 equiv., 770 mg) in 1 M hexane was added to a solution of 2-Bromostyrene (1 equiv., 2 g) in 50 mL of THF at -78 °C and stirred for 30 min. Then, DMF (15 equiv., 1 mL) was added dropwise. The reaction mixture was stirred for 20 h while the temperature was increased to room temperature (rt). The organic layer was washed with brine, dried over MgSO<sub>4</sub>, and filtered. The

crude product was purified by column chromatography (1:9 acetone: hexane) to produce the product as a clear liquid (600 mg, 41 %).  $^1\text{H}$  NMR and  $^{13}\text{C}$  NMR data matched that from literature report.<sup>1</sup>

$^1\text{H}$  NMR (400 MHz,  $\text{CDCl}_3\text{-d}$ )  $\delta$  10.30 (s, 1H), 7.86 – 7.81 (m, 1H), 7.58 (t,  $J = 1.7$  Hz, 2H), 7.57 – 7.49 (m, 1H), 7.48 – 7.40 (m, 1H), 5.70 (dd,  $J = 17.4, 1.2$  Hz, 1H), 5.52 (dd,  $J = 11.0, 1.2$  Hz, 1H).

$^{13}\text{C}$  NMR (101 MHz,  $\text{CDCl}_3$ )  $\delta$  192.5, 140.7, 133.9, 133.5, 133.0, 131.4, 128.1, 127.6, 119.6.



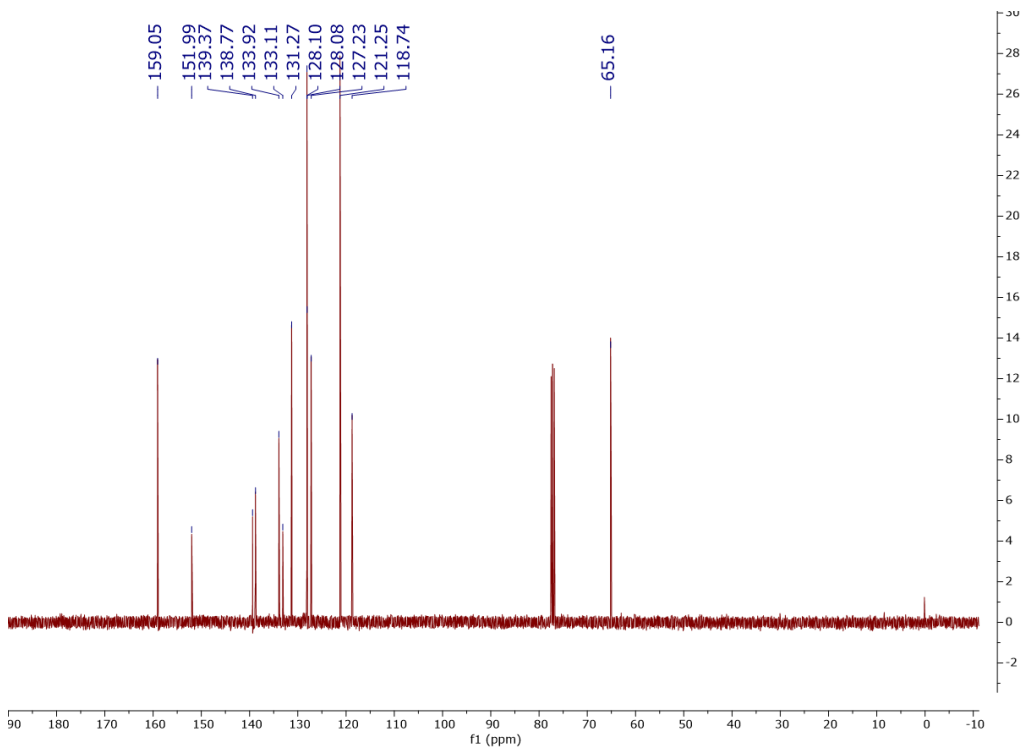
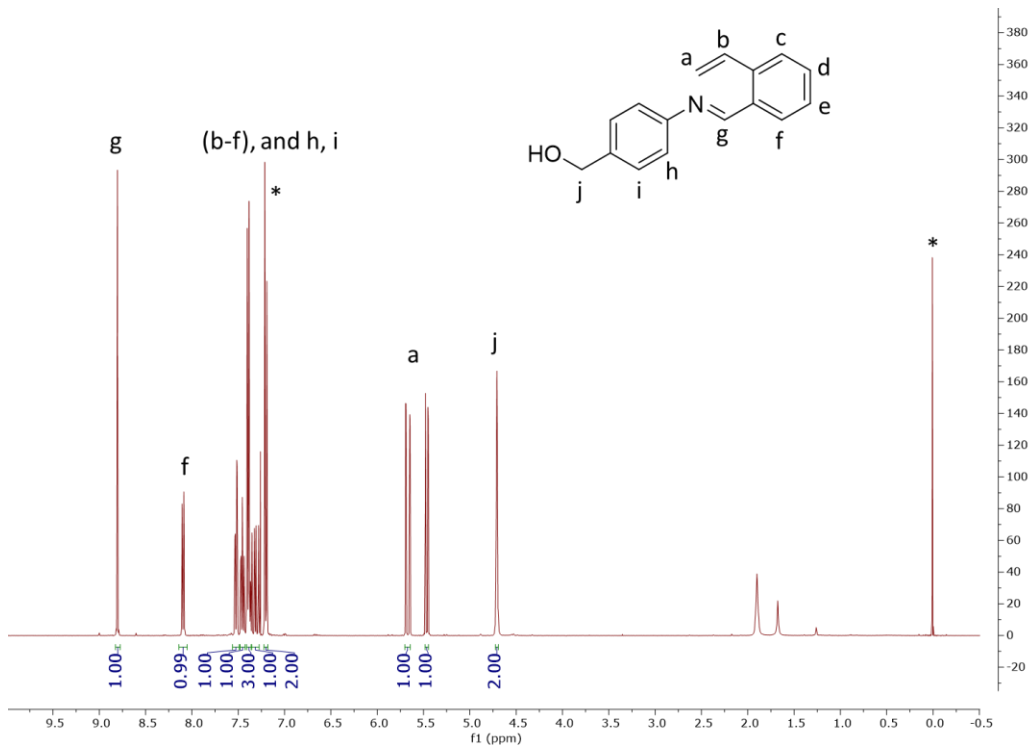


#### Benzylidene ligand (4)

A round bottom flask was charged with **2** (1 equiv., 300 mg), (4-aminophenyl) methanol (1.1 equiv., 307.50 mg), MgSO<sub>4</sub> (1g/1.0 mmol aldehyde, 2.20 g) and CH<sub>2</sub>Cl<sub>2</sub> (10 mL). The reaction mixture was stirred at rt under N<sub>2</sub> for 24 h after which the mixture was filtered and concentrated under reduced pressure. The crude product was purified by chromatography (2:8 acetone: hexane) to provide the imines as a pale oil (225 mg, 42%).

**<sup>1</sup>H NMR** (400 MHz, CDCl<sub>3</sub>) δ 8.80 (s, 1H), 8.09 (dd, J = 7.7, 1.4 Hz, 1H), 7.52 (ddt, J = 7.8, 1.3, 0.6 Hz, 1H), 7.45 (ddd, J = 7.8, 1.5, 0.6 Hz, 1H), 7.43 – 7.36 (m, 3H), 7.32 (dd, J = 17.3, 11.0 Hz, 1H), 7.24 – 7.16 (m, 2H), 5.67 (dd, J = 17.4, 1.2 Hz, 1H), 5.46 (dd, J = 11.0, 1.3 Hz, 1H), 4.71 (s, 2H).

**<sup>13</sup>C NMR** (101 MHz, CDCl<sub>3</sub>) δ 159.1, 151.9, 139.4, 138.8, 133.9, 133.1, 131.3, 128.10, 128.08, 127.2, 121.2, 118.7, 65.2.

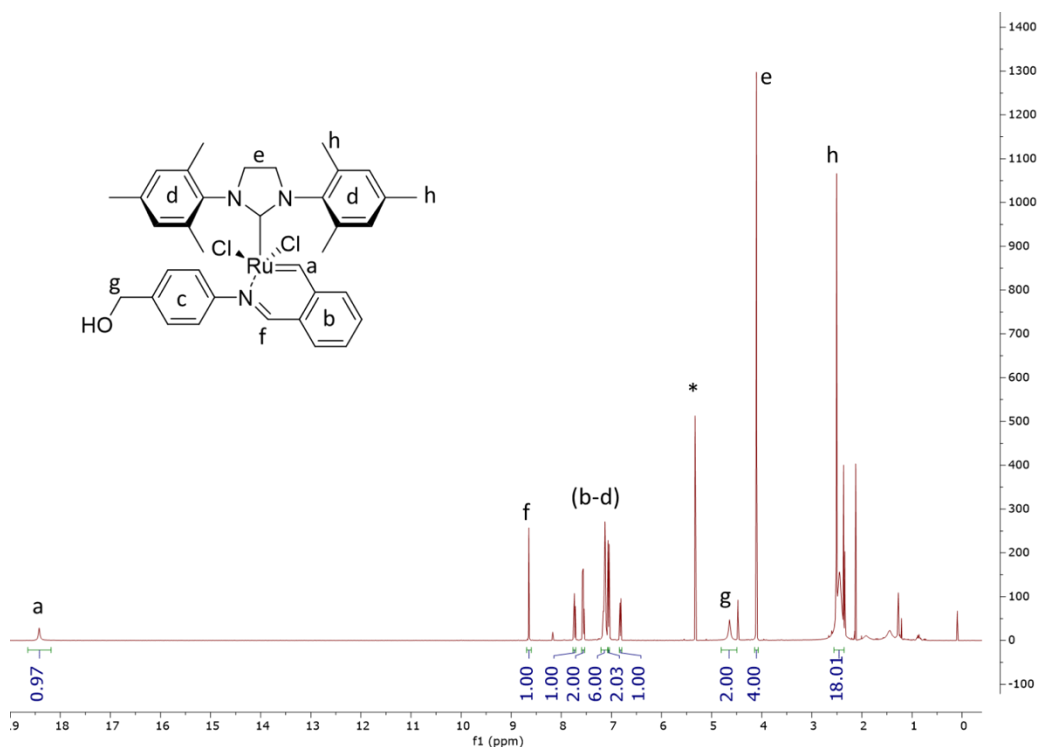


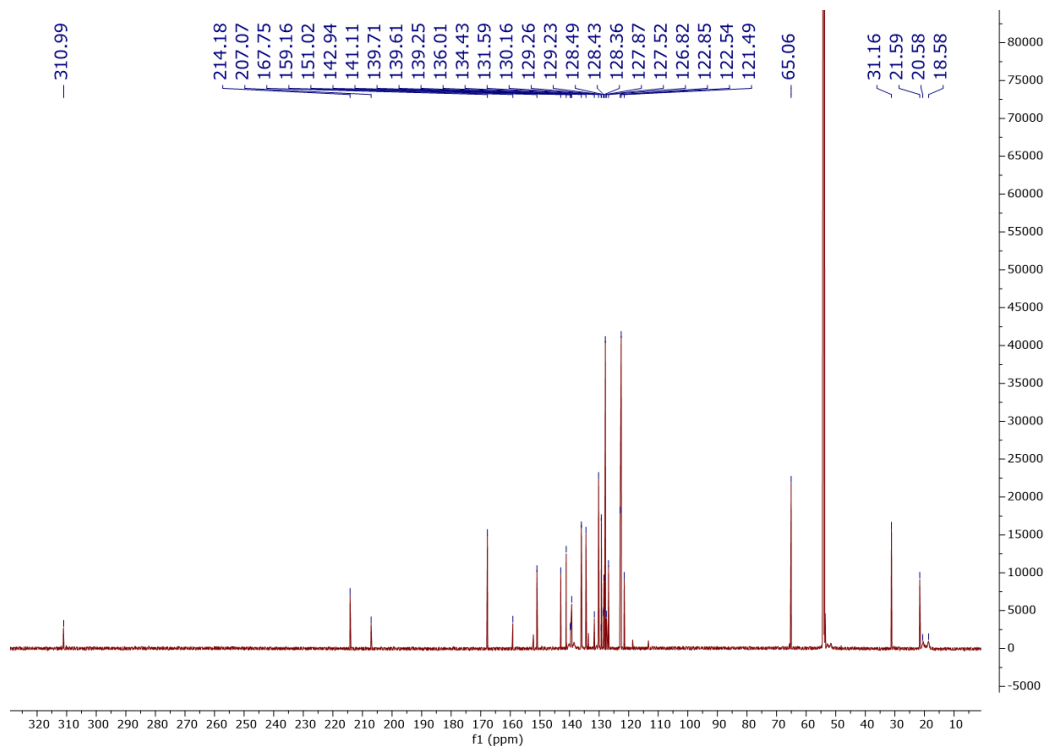
## Latent olefin metathesis catalyst (5)

A Schlenk flask was charged with **4** (1.2 equiv., 100 mg), G2 (1 equiv., 310 mg), and Cu(I)Cl (1 equiv., 35 mg) in a 15 mL of CH<sub>2</sub>Cl<sub>2</sub> under N<sub>2</sub> atmosphere. The reaction mixture was stirred at rt for 2 h. Removal of the solvent in a vacuum and purifying the product by flash chromatography (1:9 DCM: acetone) yielded the catalyst as a green solid (70 %).

<sup>1</sup>H NMR (400 MHz, CD<sub>2</sub>Cl<sub>2</sub>) δ 18.42 (s, 1H), 8.65 (s, 1H), 7.74 (td, J = 7.5, 1.2 Hz, 1H), 7.61 – 7.53 (m, 2H), 7.13 (d, J = 5.1 Hz, 6H), 7.06 (d, J = 8.4 Hz, 2H), 6.88 – 6.75 (m, 1H), 4.64 (s, 2H), 4.10 (s, 4H), 2.51 (s, 6H), 2.49 – 2.39 (m, 14H).

<sup>13</sup>C NMR (126 MHz, CD<sub>2</sub>Cl<sub>2</sub>) δ 213.2, 206.7, 170.9, 167.3, 150.3, 142.6, 140.7, 138.7, 135.56, 135.00, 133.9, 130.1, 129.84, 129.67, 128.7, 127.3, 126.3, 122.3, 121.9, 64.35, 60.3, 30.6, 21.1, 20.8, 14.1.





## Monomer 6

### Isomerization of *cis*-5-norbornene-*endo*-2,3-dicarboxylic anhydride

The *exo* adduct was prepared by heating the *endo* adduct at 180 °C under a condenser for 24 h. The reaction mixture was cooled to 120 °C, toluene was added, the reaction was cooled to rt, and the precipitated pale-yellow crystals were collected and dried. Then, toluene was added to the collected crystals and the mixture was heated to reflux until all crystals were dissolved. After cooling to rt, the precipitated crystals were collected. The procedure was repeated until the purity of *exo*-5-norbornene-2,3-dicarboxylic anhydride was more than 98% as evaluated by <sup>1</sup>H NMR (white solid, yield 70%).

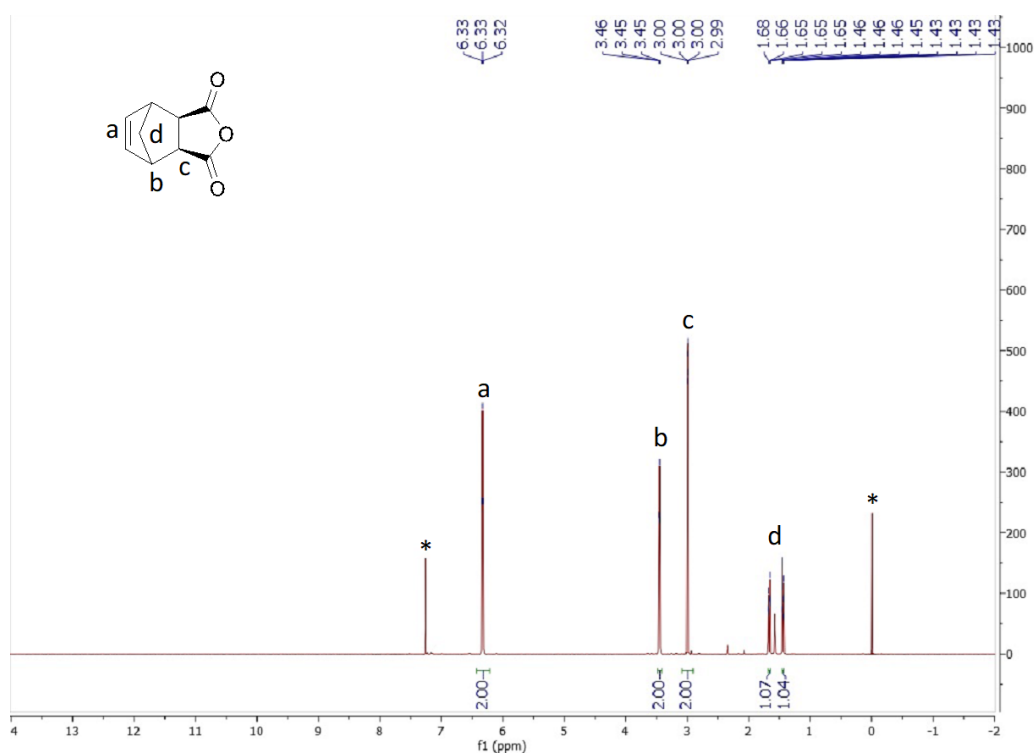
**<sup>1</sup>H NMR** (400 MHz, CDCl<sub>3</sub>): δ 6.33 (t, J = 1.9 Hz, 2H), 3.48 – 3.43 (m, 2H), 3.00 (dd, J = 1.7, 0.4 Hz, 2H), 1.67 (ddd, J = 10.3, 2.4, 1.0 Hz, 1H), 1.44 (dtd, J = 10.2, 1.5, 0.7 Hz, 1H).

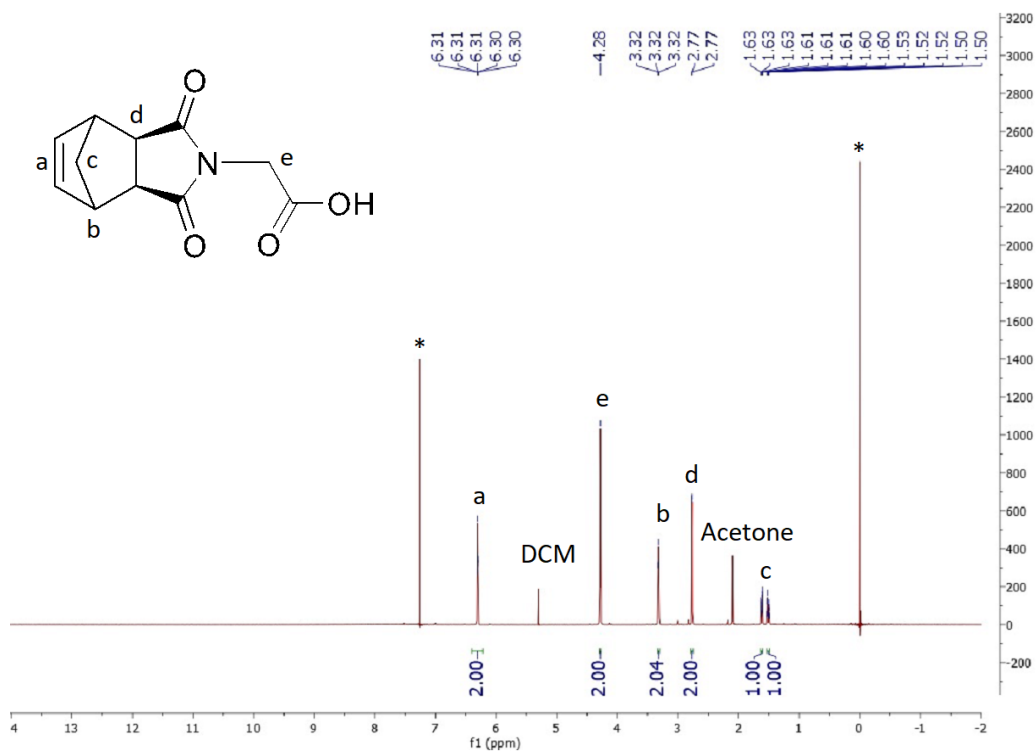
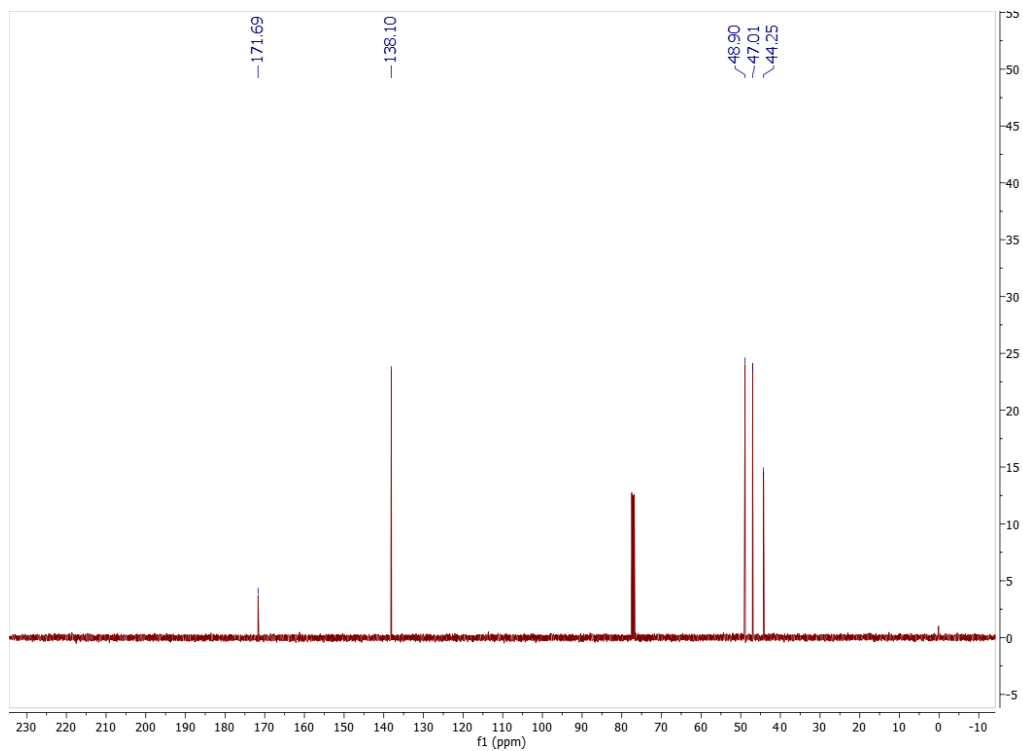
**<sup>13</sup>C NMR** (101 MHz, CDCl<sub>3</sub>): δ 171.7, 138.1, 48.9, 47.0, 44.25.

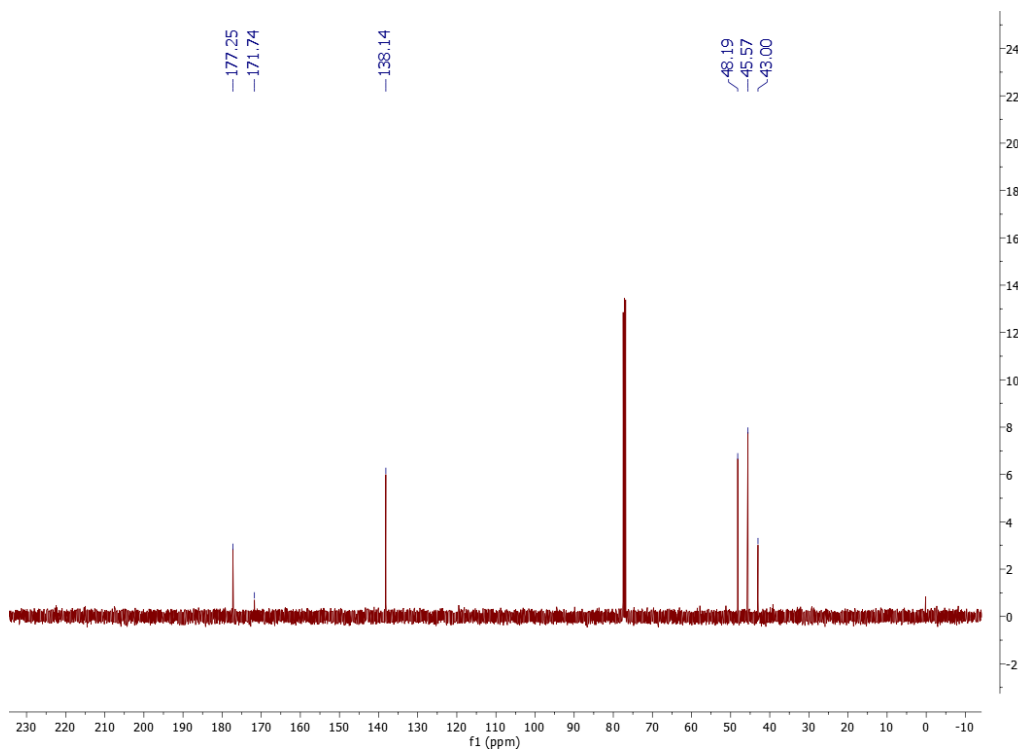
Then, a mixture of (1 equiv., 2 g, 12.18 mmol) of *exo* anhydride and glycine (1 equiv., 914 mg, 12.18 mmol) was boiled under a condenser in 20 mL of glacial acetic acid for 24 h. The reaction mixture was cooled to rt and the solvent was removed in a vacuum. DI water (20 mL) was added to the residue and extracted with DCM. The organic layer was dried, the solvent was evaporated, and the white solid product was recrystallized from ethyl acetate: hexane (3:7) (yield 2.16 g, 80%, white crystal).

**<sup>1</sup>H NMR** (400 MHz, CDCl<sub>3</sub>): 6.33 – 6.28 (m, 2H), 4.28 (s, 2H), 3.35 – 3.29 (m, 2H), 2.77 (d, J = 1.4 Hz, 2H), 1.64 – 1.60 (m, 1H), 1.51 (dt, J = 10.0, 1.6 Hz, 1H).

**<sup>13</sup>C NMR** (101 MHz, CDCl<sub>3</sub>): δ 177.25, 171.74, 138.14, 48.19, 45.57, 43.00.





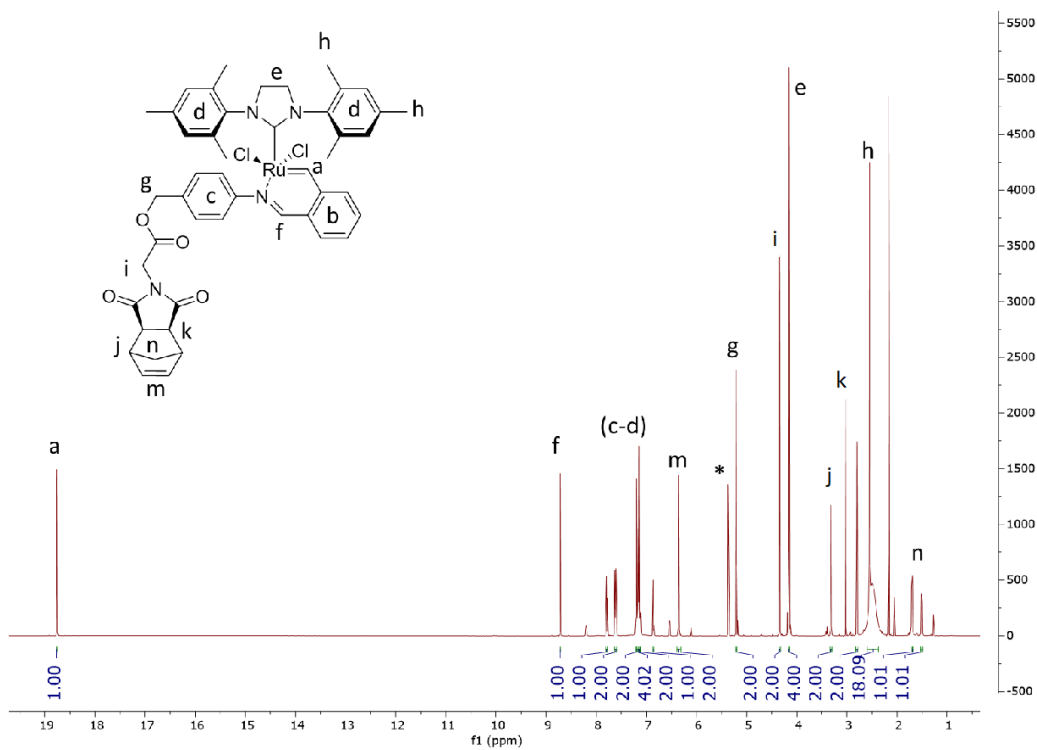


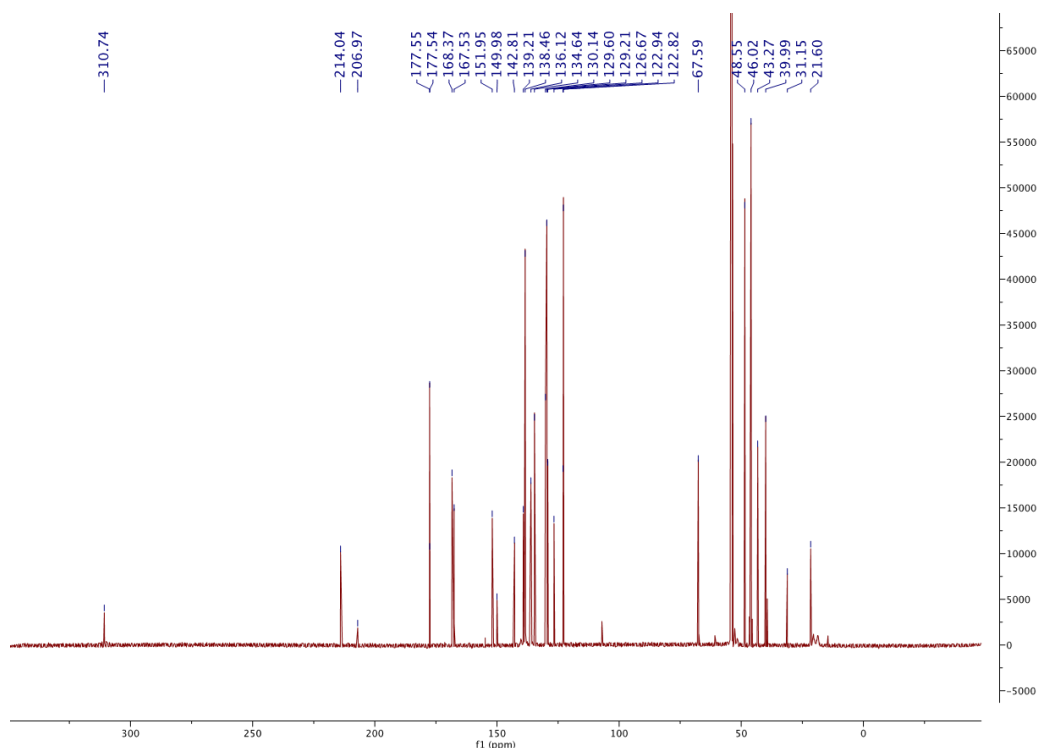
### ROMP inimer (1)

A mixture of the latent olefin metathesis catalyst **5** (1 equiv.) and DMAP (10 equiv.) in DCM was stirred under N<sub>2</sub> atmosphere for 20 min at 0 °C. Then, a mixture of the ROMP monomer **6** (2 equiv.) with EDC (1.5 equiv.) in DCM was added dropwise. The reaction mixture was stirred for 2 h with holding the temperature below 5 °C. The mixture was filtered through silica plug and the crude product was purified by column chromatography (DCM: acetone 2:8) (yield g, 86 %).

**<sup>1</sup>H NMR** (500 MHz, CD<sub>2</sub>Cl<sub>2</sub>) δ 18.76 (s, 1H), 8.72 (s, 1H), 7.79 (td, J = 7.5, 1.2 Hz, 1H), 7.65 – 7.57 (m, 2H), 7.21 (d, J = 8.4 Hz, 2H), 7.16 (s, 4H), 7.13 (d, J = 8.3 Hz, 2H), 6.86 (d, J = 7.6 Hz, 1H), 6.36 (t, J = 1.9 Hz, 2H), 5.21 (s, 2H), 4.34 (s, 2H), 4.16 (s, 4H), 3.32 (t, J = 1.8 Hz, 2H), 2.80 (d, J = 1.4 Hz, 2H), 2.54 (s, 18H), 1.70 (d, J = 9.9 Hz, 1H), 1.51 (d, J = 13.0 Hz, 1H).

$^{13}\text{C}$  NMR (126 MHz,  $\text{CD}_2\text{Cl}_2$ )  $\delta$  310.82, 310.74, 214.04, 206.97, 177.55, 177.54, 168.37, 167.53, 151.95, 149.98, 142.81, 139.21, 138.46, 136.12, 134.64, 130.14, 129.60, 129.21, 126.67, 122.94, 122.82, 67.59, 48.55, 46.02, 43.27, 39.99, 31.15, 21.60.



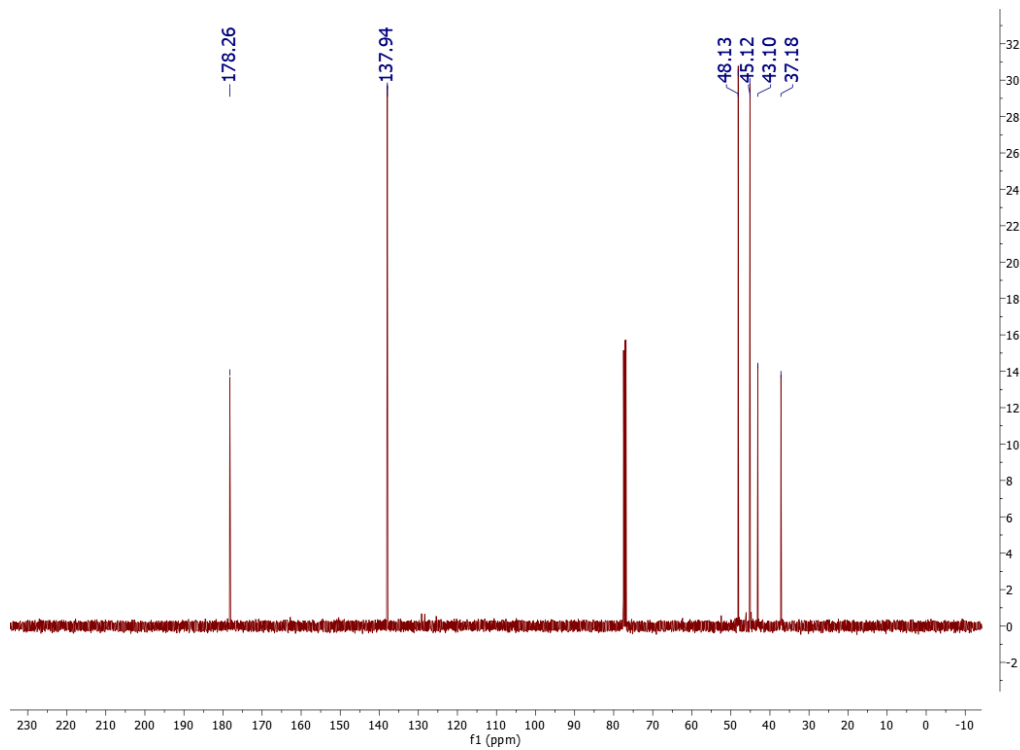
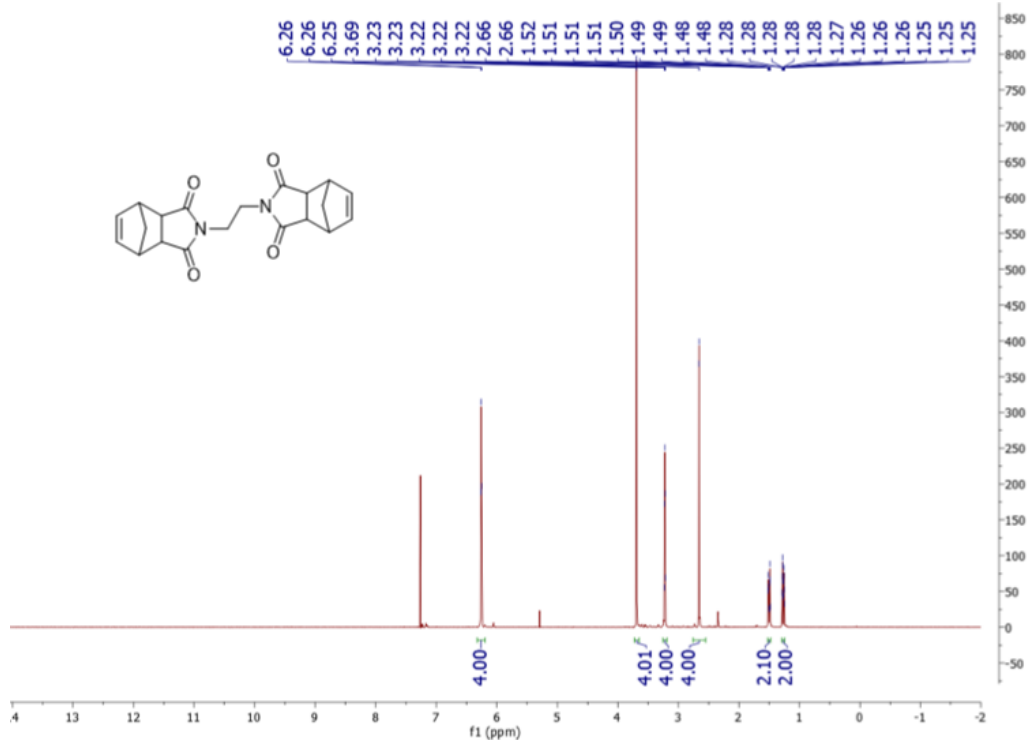


## A2 ROMP monomer

*Exo* norbornene (2 equiv., 1 g) was dissolved in toluene. Ethyldiamine (1 equiv., 183 mg) was added slowly. The reaction mixture was heated to 120 °C and stirred overnight under a condenser. Then, the reaction mixture was cooled to rt. The solvent was evaporated. The crude product was redissolved in DCM and washed with H<sub>2</sub>SO<sub>4</sub> and DI water. The organic layers were collected, dried over MgSO<sub>4</sub>, filtered, and the solvent was evaporated to give a white crystalline solid as the final product (970 mg, 90%)

<sup>1</sup>H NMR (400 MHz, CDCl<sub>3</sub>) δ 6.26 (t, J = 1.9 Hz, 1H), 3.69 (s, 1H), 3.22 (p, J = 1.7 Hz, 1H), 2.66 (d, J = 1.4 Hz, 1H), 1.54 – 1.47 (m, 1H), 1.27 (ddq, J = 10.0, 1.6, 0.8 Hz, 1H).

<sup>13</sup>C NMR (101 MHz, CDCl<sub>3</sub>) δ 178.3, 137.9, 48.1, 45.1, 43.1, 37.2.

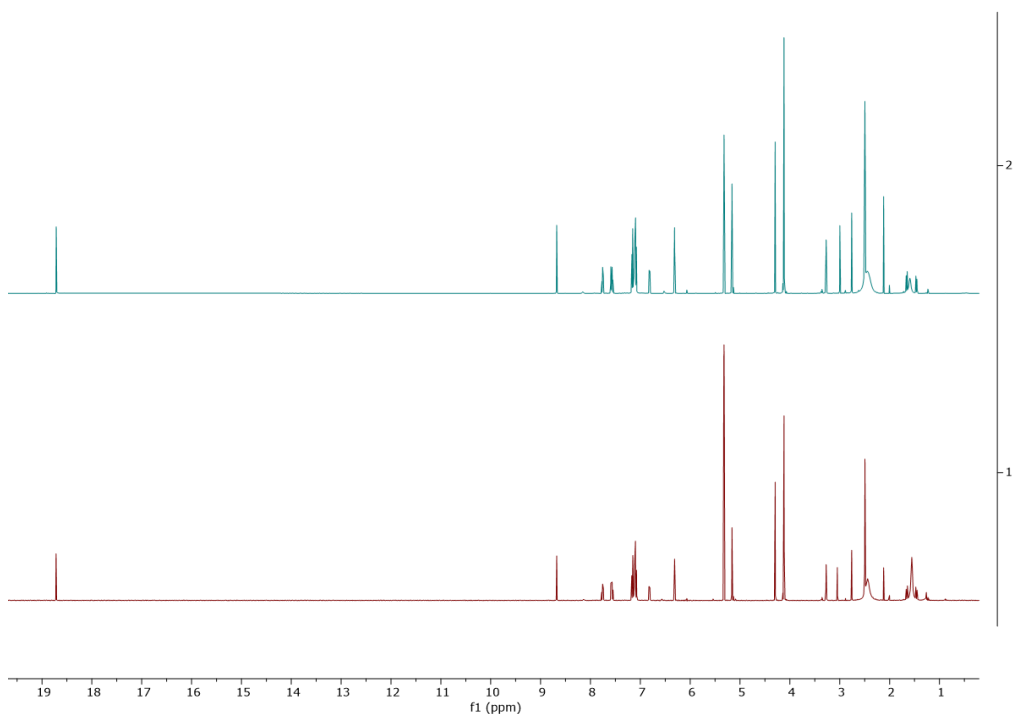


### Demonstration of ROMP inimer (1) latency

Cyclooctene was added to a solution of ROMP inimer in toluene-d8 in a screw cap NMR tube under N<sub>2</sub>. The sample was set at rt for 10 days. Data was recorded using 32 scans with a D1 delay time. Progress of the reaction was monitored through the appearance of the alkene signals of polycyclooctene (5.38 and 5.34 ppm).

### Demonstration of ROMP inimer (1) stability

An NMR tube was charged with 10 mg of ROMP inimer in CD<sub>2</sub>Cl<sub>2</sub>. The sample was kept at rt under air. After 90 days, <sup>1</sup>H NMR for the sample did not show any sign of decomposition.



<sup>1</sup>H NMR spectra of (a) before and (b) after standing ROMP inimer at rt for 90 days in CD<sub>2</sub>Cl<sub>2</sub> (open to air).

## Synthesis of the HPs

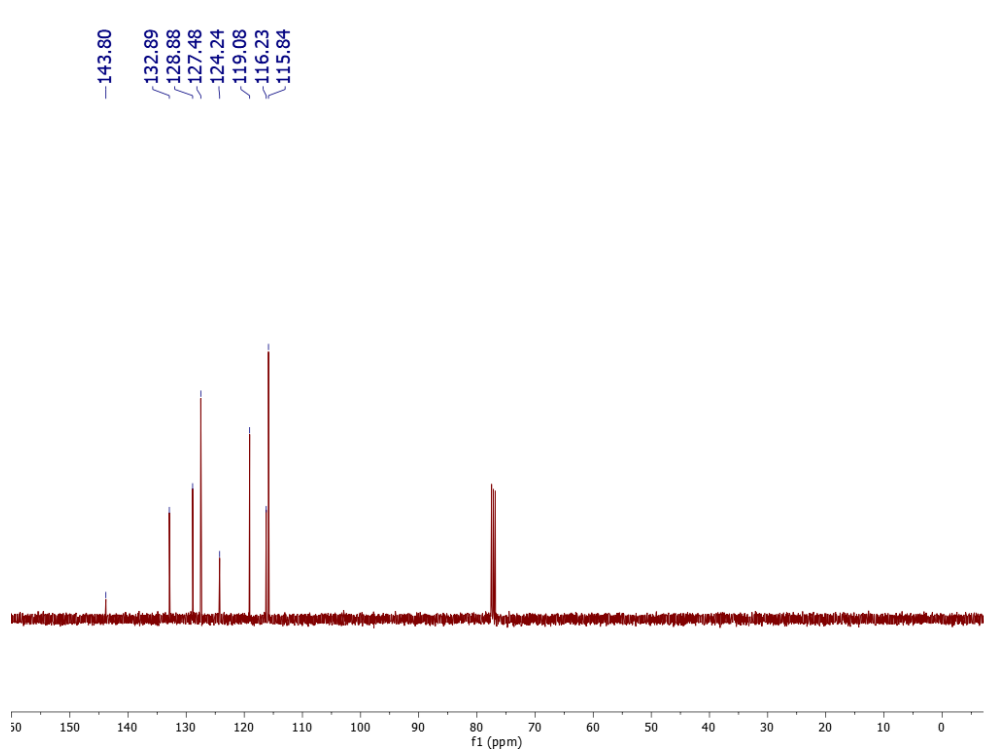
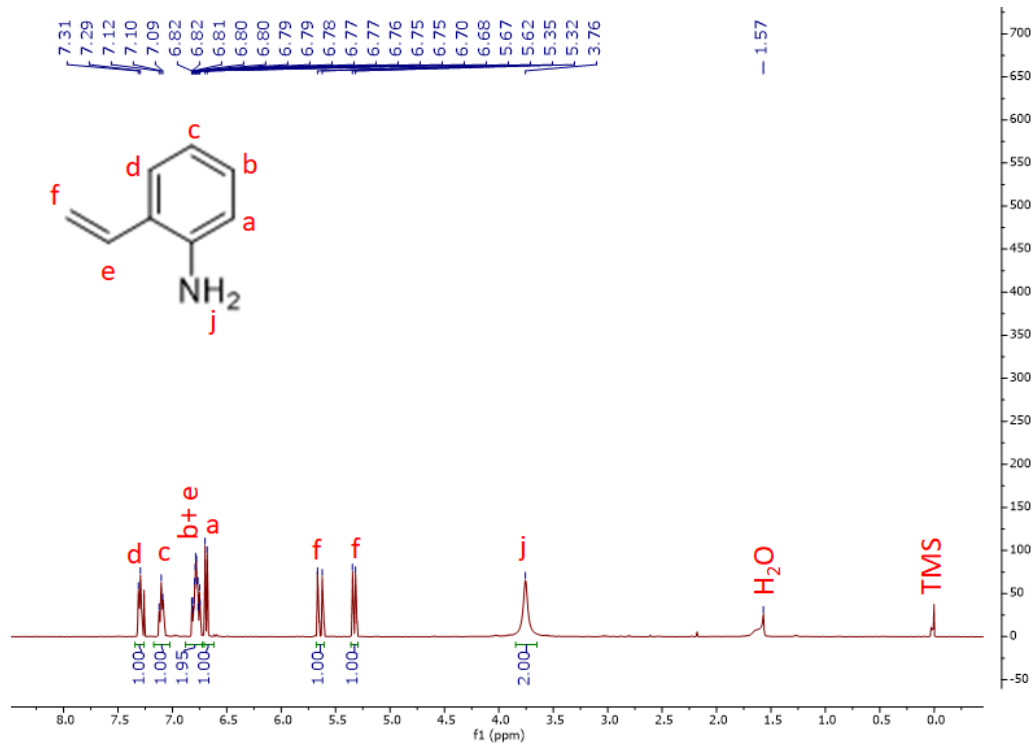
All HPs were prepared by adding a mixture of (1 equiv.) ROMP inimer and (1 equiv.) PPh<sub>3</sub> in toluene to cyclooctene. The reaction mixture was heated to 110 °C for 1 h. The monomer conversion was followed by <sup>1</sup>H NMR spectroscopy. The HPs were terminated by addition of ethyl vinyl ether. The polymers were passed through a silica plug and precipitated in methanol.

### 2-vinylniline (13)

In a 100 mL round-bottom flask equipped with a stir bar, short path distillation head, and tared receiving flask was added 2-aminophenethyl alcohol (1 equiv., 5.0 g, 36.5 mmol) and potassium hydroxide (1 equiv., 2.04 g, 36.5 mmol). The mixture was heated to 180 °C. With continued heating and applied vacuum for 4 h, the clear product distilled over (83–90 °C) to the tared receiving flask (yield 2.60 g, 60 %). <sup>1</sup>H NMR data matched that from a literature report.<sup>1</sup>

**<sup>1</sup>H NMR** (400 MHz, CDCl<sub>3</sub>): δ 7.30 (d, J = 7.6 Hz, 1H), 7.10 (t, J = 6.8 Hz, 1H), 6.85 – 6.73 (m, 2H), 6.69 (d, J = 7.7 Hz, 1H), 5.64 (d, J = 17.2 Hz, 1H), 5.33 (d, J = 11.0 Hz, 1H), 3.76 (s, 2H).

**<sup>13</sup>C NMR** (101 MHz, CDCl<sub>3</sub>): δ 143.8, 132.9, 128.9, 127.5, 124.2, 119.1, 116.2, 115.8.

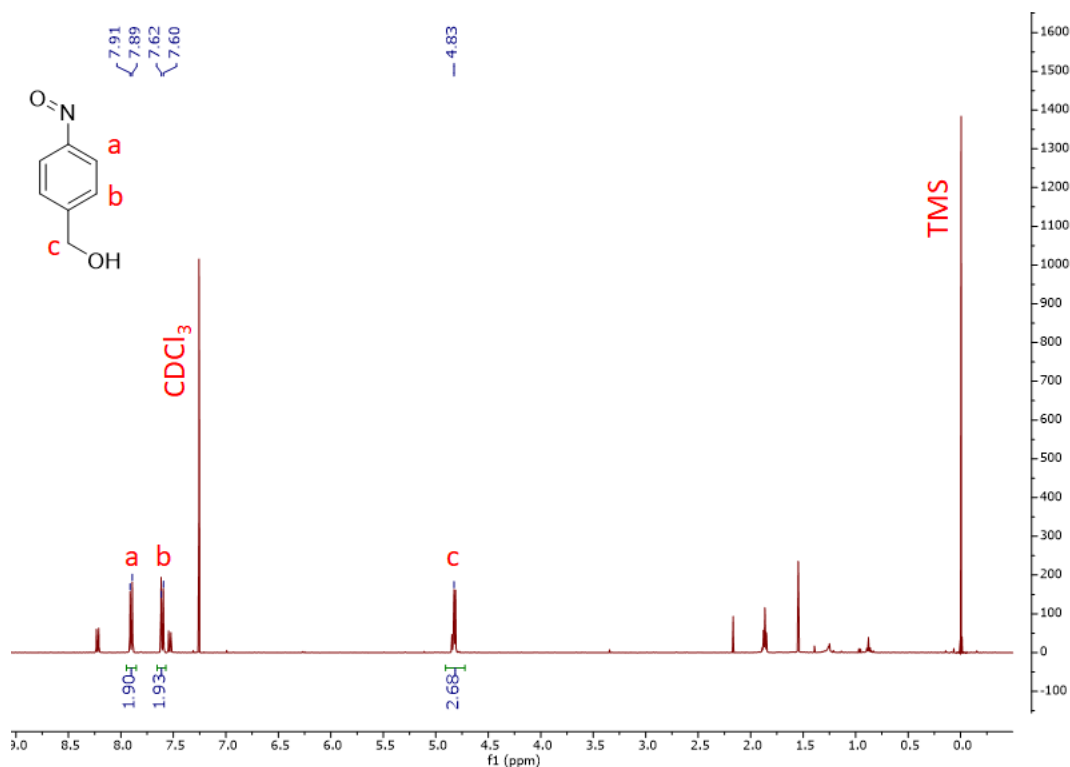


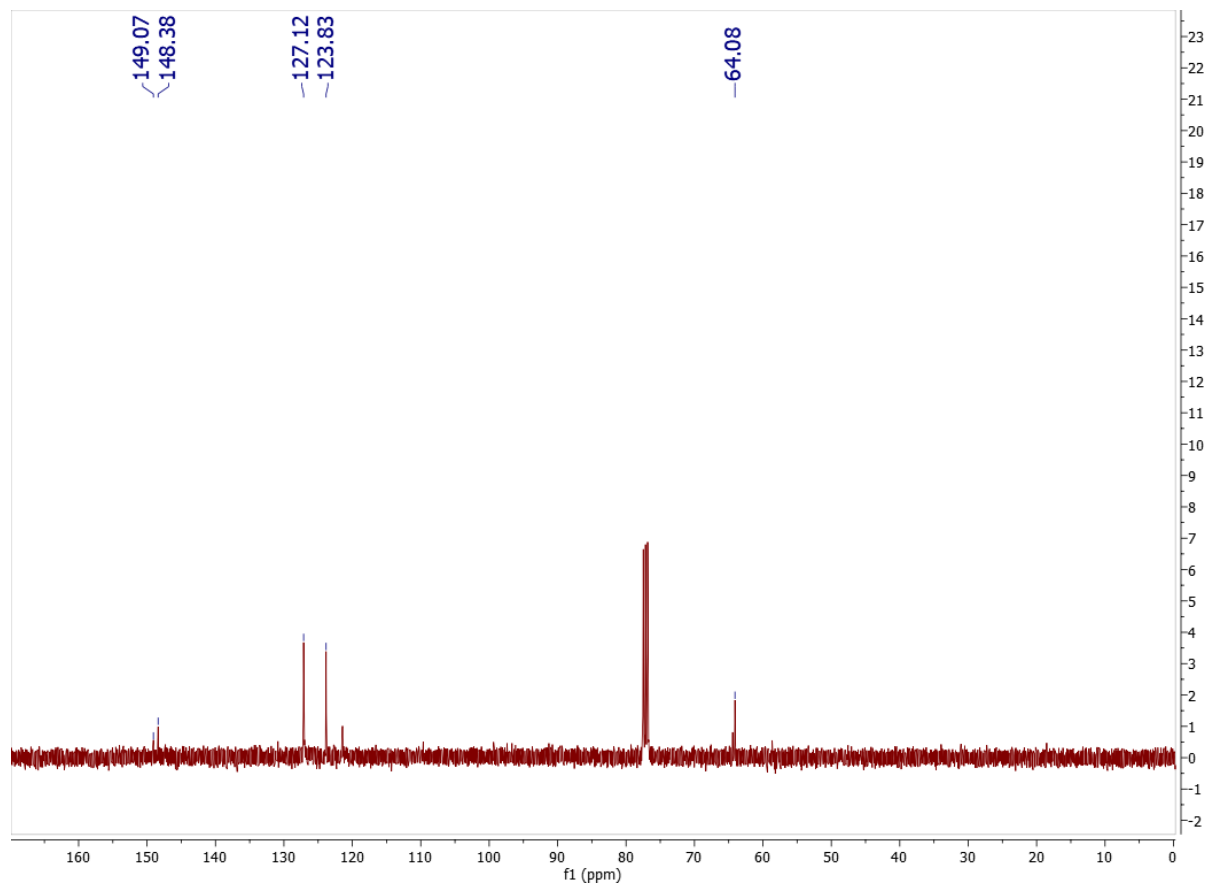
(4-nitrosophenyl)methanol (15)

4-Nitrobenzyl alcohol (1 equiv., 3.50 g, 22.86 mmol) was dissolved in ethanol and ammonium chloride (1.4 equiv., 1.60 g, 29.90 mmol) in water and zinc powder (3 equiv., 4.10 g, 62.71 mmol) were added. After 2 h the reaction mixture was filtered. The solution was added dropwise to another solution of iron chloride hexahydrate (1.2 equiv., 6.80 g, 25.15 mmol) in water and ethanol at  $-5\text{ }^{\circ}\text{C}$  and it was stirred for another 1 h with keeping the temperature below  $0\text{ }^{\circ}\text{C}$ . The solution was diluted with brine and extracted with dichloromethane. The organic layer was washed with water, dried over  $\text{NaSO}_4$  and filtered. After removing the solvent under reduced pressure, the crude product was obtained, which was used without further purification (yield 1.42 g, 45%).

$^1\text{H}$  NMR (400 MHz,  $\text{CDCl}_3$ ):  $\delta$  7.90 (d,  $J = 8.4$  Hz, 3H), 7.61 (d,  $J = 7.9$  Hz, 2H), 4.83 (s, 2H).

$^{13}\text{C}$  NMR (101 MHz,  $\text{CDCl}_3$ ):  $\delta$  149.1, 148.4, 127.1, 123.8, 64.1.





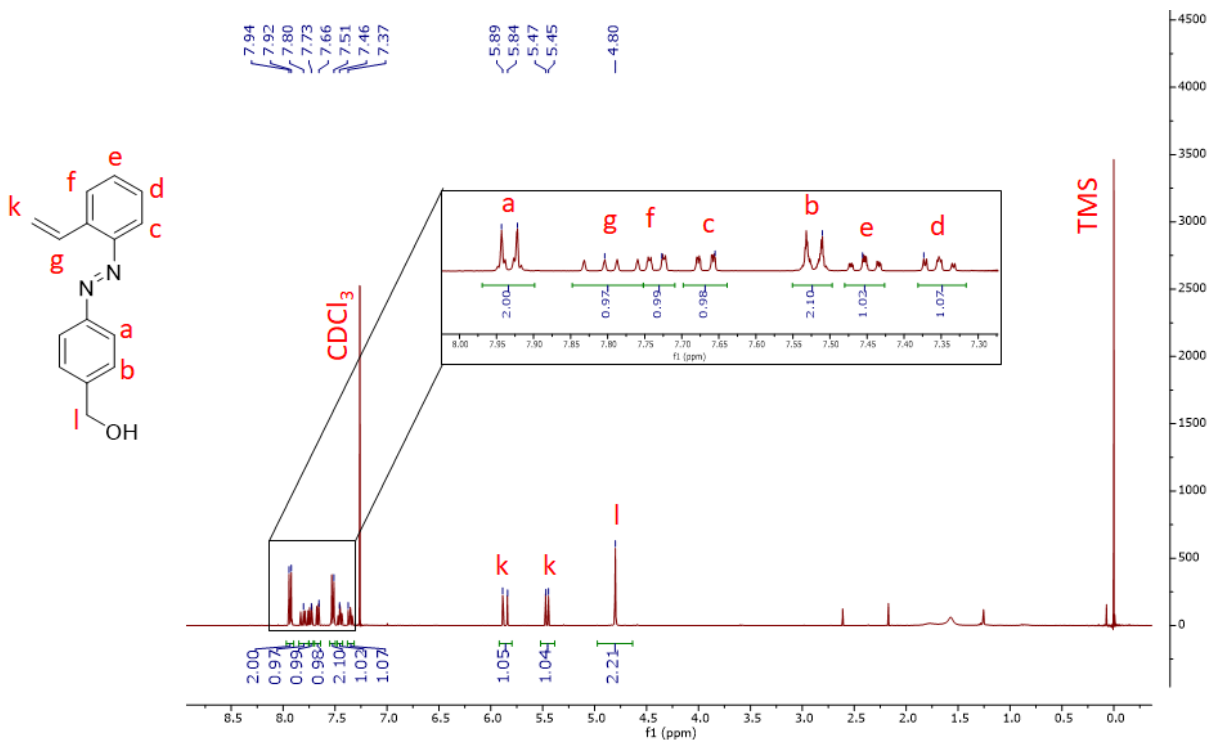
### Benzylidene ligand (16)

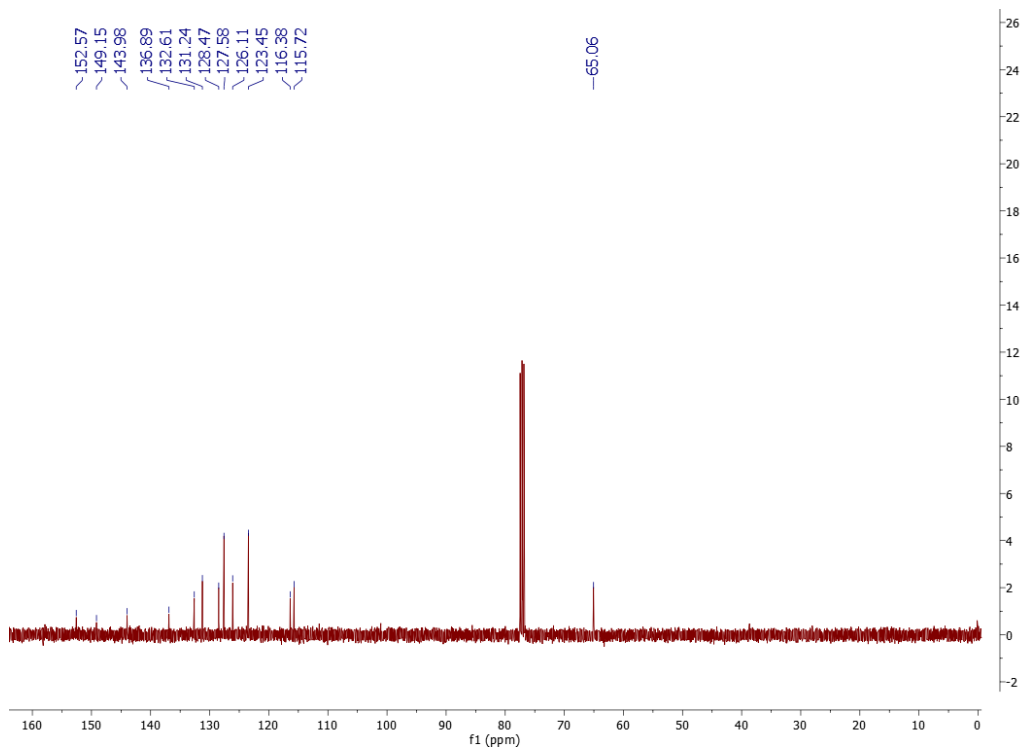
(4-Nitrosophenyl) methanol (2 equiv., 1.40 g, 10.20 mmol) and 2-vinylaniline (1 equiv., 610 mg, 5.12 mmol) were mixed in acetic acid and stirred overnight under nitrogen atmosphere at room temperature. The acetic acid was evaporated, and the crude product was redissolved in DCM and extracted with water. The organic layer was dried over  $\text{Na}_2\text{SO}_4$ . Then the solvent was evaporated, and the remaining residue was purified by flash chromatography (cyclohexane/ acetone 8:2) to afford the product (yield 150 mg, 12 %).

$^1\text{H}$  NMR (400 MHz,  $\text{CDCl}_3$ ):  $\delta$  7.93 (d,  $J = 8.6$  Hz, 2H), 7.80 (dd,  $J = 17.8, 11.2$  Hz, 1H), 7.75 – 7.71 (m, 1H), 7.67 (ddd,  $J = 8.1, 1.4, 0.5$  Hz, 1H), 7.56 – 7.49 (m, 2H), 7.45 (dddd,  $J = 8.5, 7.2,$

1.4, 0.6 Hz, 1H), 7.35 (ddd, J = 8.5, 7.2, 1.4 Hz, 1H), 5.86 (dd, J = 17.8, 1.2 Hz, 1H), 5.46 (dd, J = 11.1, 1.2 Hz, 1H).

$^{13}\text{C}$  NMR (101 MHz,  $\text{CDCl}_3$ ):  $\delta$  152.3, 148.8, 143.7, 136.6, 132.3, 130.9, 128.2, 127.3, 125.8, 123.1, 116.1, 115.4, 64.7.



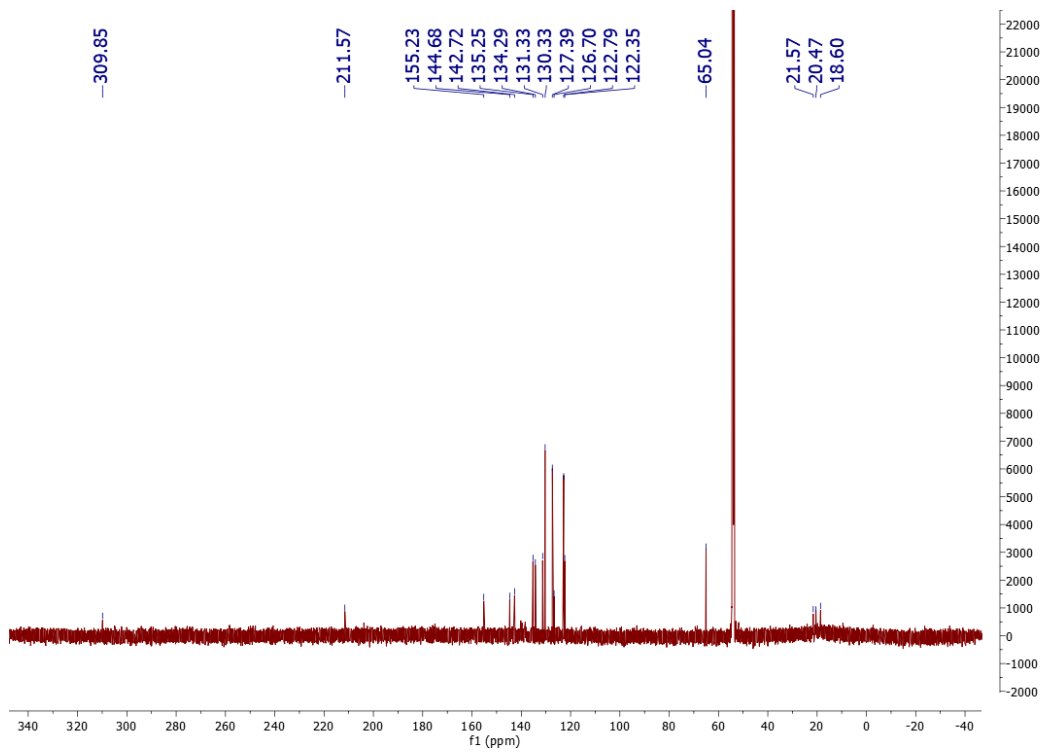
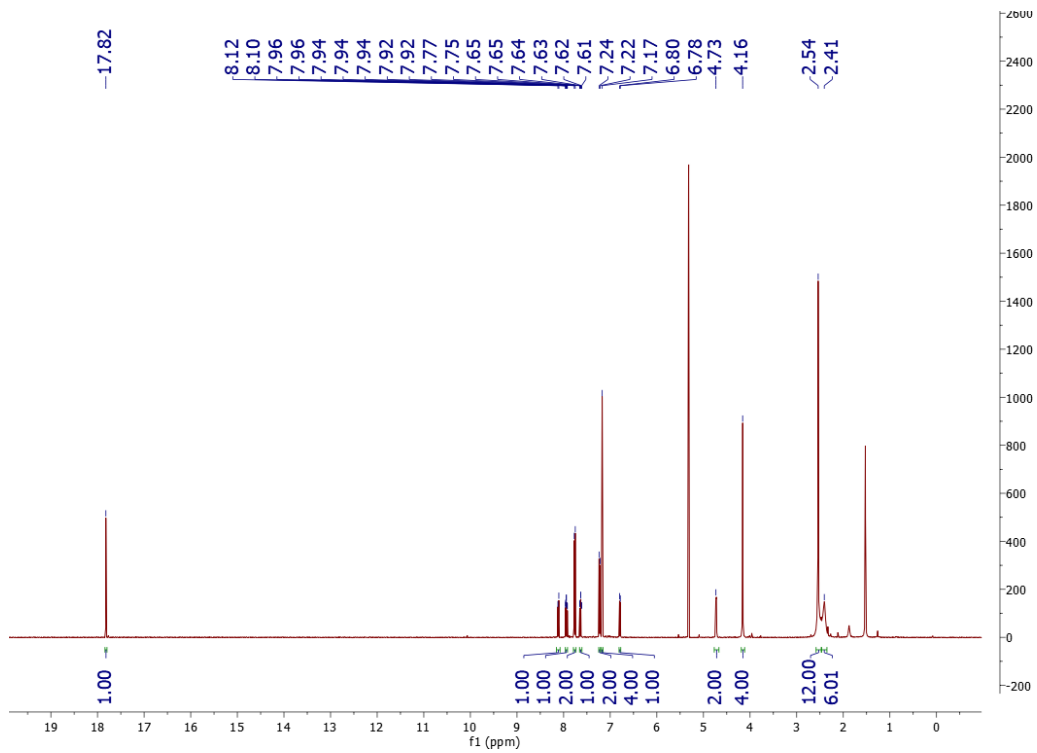


### Latent olefin metathesis catalyst (17)

A dry Schlenk flask charged with Grubbs II (1 equiv., 356 mg, 0.42 mmol), and copper(I) chloride (1 equiv., 42 mg, 0.42 mmol) was filled with N<sub>2</sub>. Benzylidene ligand (3a) (1.5 equiv., 150 mg, 0.63 mmol) was dissolved in dichloromethane (5 mL) and added through a syringe to the flask. The mixture was stirred at room temperature for 4 h. Next the reaction mixture was concentrated in vacuo and the residue was chromatographed (DCM: acetone =8:2) to afford (4a) as a brown microcrystalline solid (yield 207 mg, 70 %).

<sup>1</sup>H NMR (400 MHz, CD<sub>2</sub>Cl<sub>2</sub>) δ 17.82 (s, 1H), 8.11 (d, J = 7.8 Hz, 1H), 7.98 – 7.90 (m, 1H), 7.76 (d, J = 8.5 Hz, 2H), 7.68 – 7.59 (m, 1H), 7.23 (d, J = 8.7 Hz, 2H), 7.17 (s, 4H), 6.79 (d, J = 6.4 Hz, 1H), 4.73 (s, 2H), 4.16 (s, 4H), 2.54 (s, 12H), 2.41 (s, 6H).

<sup>13</sup>C NMR (151 MHz, CD<sub>2</sub>Cl<sub>2</sub>) δ 309.8, 211.6, 155.2, 144.7, 142.7, 135.2, 134.3, 131.3, 130.3, 127.4, 126.7, 122.8, 122.3, 65.0, 21.6, 20.5, 18.6.

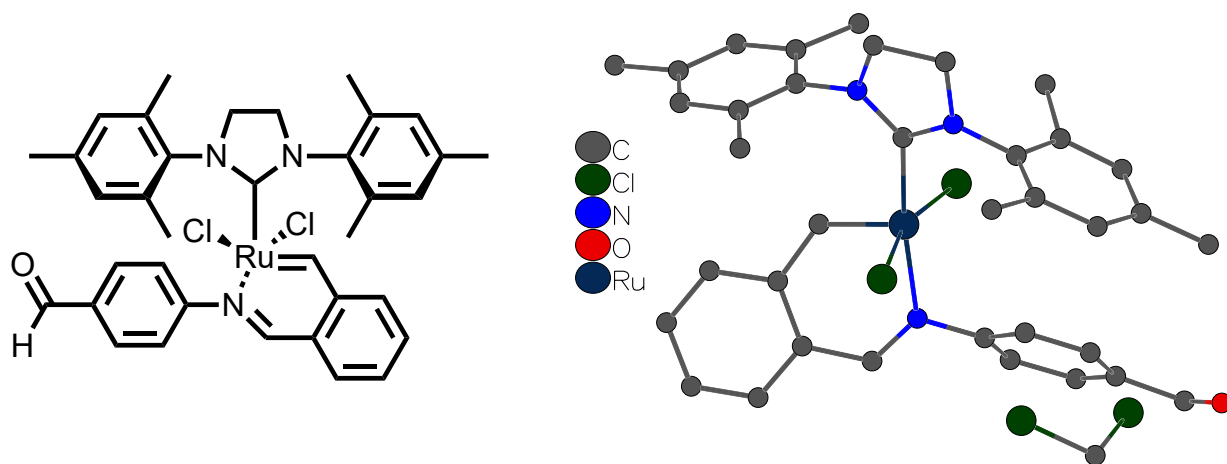


### **ROMP inimer (3)**

The ROMP monomer (5a) was esterified (using EDC and DMAP) with the latent olefin metathesis catalyst (4a) to give the ROMP inimer (6a). A mixture of the latent olefin metathesis catalyst (4a) (1 equiv., g, mmol) and DMAP (1 equiv., g, mmol) in DCM was stirred under N<sub>2</sub> atmosphere for 20 min at 0 °C. Then, a mixture of the ROMP monomer (5a) (2 equiv., g, mmol) with EDC (1.5 equiv., g, mmol) in DCM was added dropwise. The reaction mixture was stirred for 2 h with holding the temperature below 5 °C. The mixture was filtered through silica plug and the crude product was purified by column chromatography (DCM/ acetone 2:8) (yield g, 80 %).

## Crystal Structure Determination

**Acknowledgements:** We thank the support of the National Science Foundation under CHE-1726077 for crystallography experiments.



(7)

## Experimental

A brown plate (0.04 x 0.15 x 0.21 mm<sup>3</sup>) was centered on the goniometer of a Rigaku Oxford Diffraction Synergy-S diffractometer equipped with a HyPix6000HE detector and operating with MoK $\alpha$  radiation. The data collection routine, unit cell refinement, and data processing were carried out with the program CrysAlisPro.<sup>76</sup> The Laue symmetry and systematic absences were consistent with the monoclinic space group  $P2_1/c$ . The structure was solved using SHELXT<sup>77</sup> and refined using SHELXL<sup>78</sup> via Olex2.<sup>79</sup> Two-position disorder models were used for the ethylene backbone of the imidazolidine as well as both

(76) CrysAlisPro Software System, v1.171.41.105a, Rigaku Oxford Diffraction, **2021**, Rigaku Corporation, Oxford, UK.

(77) Sheldrick, G. M. "SHELXT – Integrated space-group and crystal structure determination." *Acta Cryst.* **2015**, *A71*, 3–8.

(78) Sheldrick, G. M. "Crystal structure refinement with SHELXL." *Acta Cryst.* **2015**, *C71*, 3–8.

(79) Dolomanov, O. V.; Bourhis, L. J.; Gildea, R. J.; Howard, J. A. K.; Puschmann, H. *J. Appl. Cryst.* **2009**, *42*, 339–341.

CH<sub>2</sub>Cl<sub>2</sub> groups. Relative occupancies refined to 0.693(7) and 0.307(7) for the ethylene backbone. The CH<sub>2</sub>Cl<sub>2</sub> occupancies refined to 0.789(3) and 0.211(3), and 0.602(8) and 0.398(8). The final refinement model involved anisotropic displacement parameters for non-hydrogen atoms and a riding model for all hydrogen atoms. Olex2<sup>80</sup> was used for molecular graphics generation.

**Table 5.6.1. Crystal data and structure refinement for cs2745-catalyst 7.**

Identification code	cs2745
Empirical formula	C <sub>37</sub> H <sub>39</sub> Cl <sub>4</sub> N <sub>3</sub> ORu
Formula weight	784.58
Temperature/K	100.00(13)
Crystal system	monoclinic
Space group	P2 <sub>1</sub> /c
a/Å	19.4909(2)
b/Å	10.17350(10)
c/Å	35.4085(4)
α/°	90
β/°	97.9620(10)
γ/°	90
Volume/Å <sup>3</sup>	6953.49(13)
Z	8
ρ <sub>calc</sub> /cm <sup>3</sup>	1.499
μ/mm <sup>-1</sup>	0.793
F(000)	3216.0
Crystal size/mm <sup>3</sup>	0.21 × 0.15 × 0.04
Radiation	Mo Kα (λ = 0.71073)
2θ range for data collection/°	5.22 to 76.628
Index ranges	-33 ≤ h ≤ 32, -17 ≤ k ≤ 17, -61 ≤ l ≤ 59

---

(80) Dolomanov, O.V.; Bourhis, L. J.; Gildea, R. J.; Howard, J. A. K.; Puschmann, H. *J. Appl. Cryst.* **2009**, *42*, 339–341.

Reflections collected	214279
Independent reflections	36805 [ $R_{\text{int}} = 0.0452$ , $R_{\text{sigma}} = 0.0334$ ]
Data/restraints/parameters	36805/58/874
Goodness-of-fit on $F^2$	1.034
Final R indexes [ $I \geq 2\sigma(I)$ ]	$R_1 = 0.0361$ , $wR_2 = 0.0892$
Final R indexes [all data]	$R_1 = 0.0553$ , $wR_2 = 0.0960$
Largest diff. peak/hole / $e \text{ \AA}^{-3}$	1.47/-0.78

**Table 5.6.2. Bond Lengths for cs2745-catalyst 7.**

Atom	Atom	Length/Å	Atom	Atom	Length/Å
Ru1	Cl1	2.3772(3)	N4	C37	1.3510(16)
Ru1	Cl2	2.3487(3)	N4	C38A	1.471(7)
Ru1	N3	2.0866(10)	N4	C38B	1.493(3)
Ru1	C1	2.0596(11)	N4	C40	1.4298(17)
Ru1	C22	1.8333(12)	N5	C37	1.3438(17)
O1	C36	1.209(2)	N5	C39A	1.480(10)
N1	C1	1.3509(15)	N5	C39B	1.481(4)
N1	C3	1.4700(17)	N5	C49	1.4254(16)
N1	C13	1.4312(16)	N6	C65	1.2915(15)
N2	C1	1.3459(15)	N6	C66	1.4243(16)
N2	C2	1.4734(16)	C38A	C39A	1.507(12)
N2	C4	1.4279(15)	C38B	C39B	1.523(5)
N3	C29	1.2871(16)	C40	C41	1.398(2)
N3	C30	1.4269(16)	C40	C45	1.401(2)
C2	C3	1.5210(18)	C41	C42	1.401(2)
C4	C5	1.3989(17)	C41	C46	1.504(2)

**Table 5.6.2. Bond Lengths for cs2745-catalyst 7.**

<b>Atom</b>	<b>Atom</b>	<b>Length/Å</b>	<b>Atom</b>	<b>Atom</b>	<b>Length/Å</b>
C4	C9	1.3984(16)	C42	C43	1.388(2)
C5	C6	1.3942(18)	C43	C44	1.386(2)
C5	C10	1.5033(18)	C43	C47	1.511(2)
C6	C7	1.3937(19)	C44	C45	1.396(2)
C7	C8	1.3929(18)	C45	C48	1.506(2)
C7	C11	1.5047(18)	C49	C50	1.3992(18)
C8	C9	1.3959(17)	C49	C54	1.3973(19)
C9	C12	1.5029(18)	C50	C51	1.3950(19)
C13	C14	1.4054(19)	C50	C55	1.5024(19)
C13	C18	1.3980(19)	C51	C52	1.392(2)
C14	C15	1.3945(18)	C52	C53	1.388(2)
C14	C19	1.504(2)	C52	C56	1.507(2)
C15	C16	1.393(2)	C53	C54	1.391(2)
C16	C17	1.391(2)	C54	C57	1.506(2)
C16	C20	1.505(2)	C58	C59	1.4529(16)
C17	C18	1.3970(19)	C59	C60	1.4049(16)
C18	C21	1.505(2)	C59	C64	1.4164(17)
C22	C23	1.4490(16)	C60	C61	1.3898(17)
C23	C24	1.4066(17)	C61	C62	1.393(2)
C23	C28	1.4173(17)	C62	C63	1.3856(18)
C24	C25	1.3902(17)	C63	C64	1.4013(16)
C25	C26	1.394(2)	C64	C65	1.4445(17)
C26	C27	1.381(2)	C66	C67	1.3939(18)
C27	C28	1.4016(17)	C66	C71	1.3989(18)
C28	C29	1.4491(18)	C67	C68	1.3896(18)
C30	C31	1.3949(19)	C68	C69	1.3860(19)

**Table 5.6.2. Bond Lengths for cs2745-catalyst 7.**

Atom	Atom	Length/Å	Atom	Atom	Length/Å
C30	C35	1.3922(18)	C69	C70	1.3995(19)
C31	C32	1.3861(19)	C69	C72	1.4754(18)
C32	C33	1.397(2)	C70	C71	1.3793(18)
C33	C34	1.388(2)	Cl5	C73A	1.774(5)
C33	C36	1.481(2)	Cl5	C73B	1.73(2)
C34	C35	1.392(2)	C73A	Cl6A	1.768(4)
Ru2	Cl3	2.3612(3)	C73B	Cl6B	1.723(19)
Ru2	Cl4	2.3463(3)	C74	Cl7A	1.748(3)
Ru2	N6	2.0848(10)	C74	Cl8A	1.720(3)
Ru2	C37	2.0578(12)	C74	Cl7B	1.719(4)
Ru2	C58	1.8316(12)	C74	Cl8B	1.807(4)
O2	C72	1.2137(19)			

**Table 5.6.3. Bond Angles for cs2745-catalyst 7.**

Atom	Atom	Atom	Angle/°	Atom	Atom	Atom	Angle/°
Cl2	Ru1	Cl1	163.388(12)	C37	Ru2	N6	170.52(4)
N3	Ru1	Cl1	86.56(3)	C58	Ru2	Cl3	98.91(4)
N3	Ru1	Cl2	85.90(3)	C58	Ru2	Cl4	98.24(4)
C1	Ru1	Cl1	97.65(3)	C58	Ru2	N6	89.58(5)
C1	Ru1	Cl2	87.49(3)	C58	Ru2	C37	99.90(5)
C1	Ru1	N3	169.45(5)	C37	N4	C38A	113.6(3)
C22	Ru1	Cl1	98.14(4)	C37	N4	C38B	112.99(14)
C22	Ru1	Cl2	96.58(4)	C37	N4	C40	127.44(11)
C22	Ru1	N3	89.55(5)	C40	N4	C38A	116.5(3)

**Table 5.6.3. Bond Angles for cs2745-catalyst 7.**

Atom	Atom	Atom	Angle/°	Atom	Atom	Atom	Angle/°
C22	Ru1	C1	99.37(5)	C40	N4	C38B	118.94(14)
C1	N1	C3	113.78(10)	C37	N5	C39A	111.1(4)
C1	N1	C13	124.60(10)	C37	N5	C39B	114.27(17)
C13	N1	C3	119.79(10)	C37	N5	C49	127.86(11)
C1	N2	C2	113.16(10)	C49	N5	C39A	117.5(4)
C1	N2	C4	126.85(10)	C49	N5	C39B	117.76(17)
C4	N2	C2	119.91(10)	C65	N6	Ru2	127.48(9)
C29	N3	Ru1	126.65(9)	C65	N6	C66	118.36(10)
C29	N3	C30	118.76(11)	C66	N6	Ru2	113.87(7)
C30	N3	Ru1	114.07(8)	N4	C37	Ru2	120.09(9)
N1	C1	Ru1	119.14(8)	N5	C37	Ru2	132.80(9)
N2	C1	Ru1	133.54(9)	N5	C37	N4	106.88(11)
N2	C1	N1	106.79(10)	N4	C38A	C39A	100.9(6)
N2	C2	C3	102.51(10)	N5	C39A	C38A	104.8(7)
N1	C3	C2	101.70(10)	N4	C38B	C39B	102.2(2)
C5	C4	N2	118.41(11)	N5	C39B	C38B	102.2(2)
C9	C4	N2	119.67(11)	C41	C40	N4	119.07(13)
C9	C4	C5	121.92(11)	C41	C40	C45	121.14(12)
C4	C5	C10	121.02(12)	C45	C40	N4	119.37(14)
C6	C5	C4	118.24(11)	C40	C41	C42	118.13(13)
C6	C5	C10	120.66(12)	C40	C41	C46	121.86(15)
C7	C6	C5	121.31(12)	C42	C41	C46	119.91(15)
C6	C7	C11	120.65(12)	C43	C42	C41	121.89(14)
C8	C7	C6	119.02(11)	C42	C43	C47	121.26(15)
C8	C7	C11	120.33(12)	C44	C43	C42	118.28(13)
C7	C8	C9	121.49(11)	C44	C43	C47	120.43(14)

**Table 5.6.3. Bond Angles for cs2745-catalyst 7.**

Atom	Atom	Atom	Angle/°	Atom	Atom	Atom	Angle/°
C4	C9	C12	121.23(11)	C43	C44	C45	122.16(13)
C8	C9	C4	118.02(11)	C40	C45	C48	122.40(14)
C8	C9	C12	120.68(11)	C44	C45	C40	118.15(13)
C14	C13	N1	118.82(12)	C44	C45	C48	119.36(14)
C18	C13	N1	119.42(12)	C50	C49	N5	119.38(12)
C18	C13	C14	121.47(11)	C54	C49	N5	118.91(12)
C13	C14	C19	121.56(12)	C54	C49	C50	121.70(12)
C15	C14	C13	118.17(13)	C49	C50	C55	121.12(13)
C15	C14	C19	120.00(13)	C51	C50	C49	118.23(12)
C16	C15	C14	121.73(13)	C51	C50	C55	120.58(13)
C15	C16	C20	120.64(14)	C52	C51	C50	121.20(13)
C17	C16	C15	118.40(13)	C51	C52	C56	120.14(15)
C17	C16	C20	120.94(14)	C53	C52	C51	119.03(12)
C16	C17	C18	122.12(14)	C53	C52	C56	120.83(15)
C13	C18	C21	122.45(12)	C52	C53	C54	121.68(13)
C17	C18	C13	117.89(13)	C49	C54	C57	121.45(13)
C17	C18	C21	119.60(13)	C53	C54	C49	118.11(12)
C23	C22	Ru1	127.01(9)	C53	C54	C57	120.38(14)
C24	C23	C22	117.77(11)	C59	C58	Ru2	127.76(9)
C24	C23	C28	118.26(11)	C60	C59	C58	117.82(11)
C28	C23	C22	123.97(11)	C60	C59	C64	117.97(10)
C25	C24	C23	121.37(12)	C64	C59	C58	124.20(10)
C24	C25	C26	119.77(12)	C61	C60	C59	121.60(12)
C27	C26	C25	119.93(12)	C60	C61	C62	119.94(12)
C26	C27	C28	121.17(13)	C63	C62	C61	119.58(11)
C23	C28	C29	122.57(11)	C62	C63	C64	121.15(12)

**Table 5.6.3. Bond Angles for cs2745-catalyst 7.**

Atom	Atom	Atom	Angle/°	Atom	Atom	Atom	Angle/°
C27	C28	C23	119.49(12)	C59	C64	C65	122.49(10)
C27	C28	C29	117.72(11)	C63	C64	C59	119.74(11)
N3	C29	C28	123.71(11)	C63	C64	C65	117.62(11)
C31	C30	N3	118.49(11)	N6	C65	C64	123.73(11)
C35	C30	N3	120.97(12)	C67	C66	N6	121.05(11)
C35	C30	C31	120.51(12)	C67	C66	C71	120.31(11)
C32	C31	C30	119.72(13)	C71	C66	N6	118.62(11)
C31	C32	C33	120.07(14)	C68	C67	C66	119.40(12)
C32	C33	C36	119.99(15)	C69	C68	C67	120.31(12)
C34	C33	C32	119.81(13)	C68	C69	C70	120.12(12)
C34	C33	C36	120.17(14)	C68	C69	C72	119.54(13)
C33	C34	C35	120.50(13)	C70	C69	C72	120.33(13)
C34	C35	C30	119.31(14)	C71	C70	C69	119.90(12)
O1	C36	C33	124.73(17)	C70	C71	C66	119.86(12)
Cl4	Ru2	Cl3	161.404(12)	O2	C72	C69	124.41(14)
N6	Ru2	Cl3	87.56(3)	Cl6A	C73A	Cl5	111.4(2)
N6	Ru2	Cl4	85.42(3)	Cl6B	C73B	Cl5	109.5(11)
C37	Ru2	Cl3	90.60(4)	Cl8A	C74	Cl7A	110.23(15)
C37	Ru2	Cl4	93.49(4)	Cl7B	C74	Cl8B	108.9(2)

**Table 5.6.4. Torsion Angles for cs2745-catalyst 7.**

A	B	C	D	Angle/°	A	B	C	D	Angle/°
Ru1	N3	C29	C28	12.28(18)	N4	C38A	C39A	N5	2.8(6)
Ru1	N3	C30	C31	51.49(14)	N4	C38B	C39B	N5	-9.6(3)

**Table 5.6.4. Torsion Angles for cs2745-catalyst 7.**

<b>A</b>	<b>B</b>	<b>C</b>	<b>D</b>	<b>Angle/°</b>	<b>A</b>	<b>B</b>	<b>C</b>	<b>D</b>	<b>Angle/°</b>
Ru1	N3	C30	C35	-126.59(11)	N4	C40	C41	C42	-178.69(13)
Ru1	C22	C23	C24	162.70(9)	N4	C40	C41	C46	-2.4(2)
Ru1	C22	C23	C28	-18.49(17)	N4	C40	C45	C44	177.44(12)
Cl1	Ru1	C22	C23	112.68(10)	N4	C40	C45	C48	1.0(2)
Cl2	Ru1	C22	C23	-59.60(11)	N5	C49	C50	C51	-178.92(11)
N1	C13	C14	C15	179.22(11)	N5	C49	C50	C55	-1.92(19)
N1	C13	C14	C19	5.22(18)	N5	C49	C54	C53	179.85(12)
N1	C13	C18	C17	-178.89(12)	N5	C49	C54	C57	2.63(19)
N1	C13	C18	C21	-1.57(19)	N6	Ru2	C58	C59	22.59(11)
N2	C2	C3	N1	-13.51(15)	N6	C66	C67	C68	-178.88(11)
N2	C4	C5	C6	178.81(11)	N6	C66	C71	C70	178.45(12)
N2	C4	C5	C10	2.15(17)	C37	Ru2	C58	C59	-157.76(11)
N2	C4	C9	C8	-179.20(11)	C37	N4	C38A	C39A	-12.5(7)
N2	C4	C9	C12	-2.29(17)	C37	N4	C38B	C39B	12.8(3)
N3	Ru1	C22	C23	26.22(11)	C37	N4	C40	C41	-93.11(19)
N3	C30	C31	C32	178.83(12)	C37	N4	C40	C45	94.29(19)
N3	C30	C35	C34	-179.55(12)	C37	N5	C39A	C38A	7.3(6)
C1	Ru1	C22	C23	-148.12(10)	C37	N5	C39B	C38B	4.8(3)
C1	N1	C3	C2	12.10(16)	C37	N5	C49	C50	77.83(19)
C1	N1	C13	C14	74.20(16)	C37	N5	C49	C54	-103.08(17)
C1	N1	C13	C18	-111.82(15)	C38A	N4	C37	Ru2	-167.1(5)
C1	N2	C2	C3	12.42(15)	C38A	N4	C37	N5	17.7(5)
C1	N2	C4	C5	-84.75(16)	C38A	N4	C40	C41	67.9(5)
C1	N2	C4	C9	95.19(15)	C38A	N4	C40	C45	-104.7(5)
C2	N2	C1	Ru1	165.98(10)	C39A	N5	C37	Ru2	170.5(4)
C2	N2	C1	N1	-5.27(15)	C39A	N5	C37	N4	-15.0(4)

**Table 5.6.4. Torsion Angles for cs2745-catalyst 7.**

<b>A</b>	<b>B</b>	<b>C</b>	<b>D</b>	<b>Angle/°</b>	<b>A</b>	<b>B</b>	<b>C</b>	<b>D</b>	<b>Angle/°</b>
C2	N2	C4	C5	98.63(14)	C39A	N5	C49	C50	-79.0(4)
C2	N2	C4	C9	-81.44(15)	C39A	N5	C49	C54	100.1(4)
C3	N1	C1	Ru1	-177.59(10)	C38B	N4	C37	Ru2	165.1(2)
C3	N1	C1	N2	-4.84(15)	C38B	N4	C37	N5	-10.2(3)
C3	N1	C13	C14	-89.40(16)	C38B	N4	C40	C41	96.7(3)
C3	N1	C13	C18	84.57(16)	C38B	N4	C40	C45	-75.9(3)
C4	N2	C1	Ru1	-10.8(2)	C39B	N5	C37	Ru2	-171.4(2)
C4	N2	C1	N1	177.91(11)	C39B	N5	C37	N4	3.0(2)
C4	N2	C2	C3	-170.51(12)	C39B	N5	C49	C50	-98.2(2)
C4	C5	C6	C7	0.25(19)	C39B	N5	C49	C54	80.9(2)
C5	C4	C9	C8	0.73(18)	C40	N4	C37	Ru2	-5.6(2)
C5	C4	C9	C12	177.65(12)	C40	N4	C37	N5	179.13(15)
C5	C6	C7	C8	0.98(19)	C40	N4	C38A	C39A	-176.1(4)
C5	C6	C7	C11	-178.77(12)	C40	N4	C38B	C39B	-175.68(19)
C6	C7	C8	C9	-1.39(19)	C40	C41	C42	C43	3.7(2)
C7	C8	C9	C4	0.55(18)	C41	C40	C45	C44	5.0(2)
C7	C8	C9	C12	-176.38(12)	C41	C40	C45	C48	-171.48(14)
C9	C4	C5	C6	-1.12(18)	C41	C42	C43	C44	0.0(2)
C9	C4	C5	C10	-177.78(12)	C41	C42	C43	C47	177.86(15)
C10	C5	C6	C7	176.92(12)	C42	C43	C44	C45	-1.3(2)
C11	C7	C8	C9	178.36(12)	C43	C44	C45	C40	-1.1(2)
C13	N1	C1	Ru1	17.94(17)	C43	C44	C45	C48	175.47(14)
C13	N1	C1	N2	-169.31(12)	C45	C40	C41	C42	-6.2(2)
C13	N1	C3	C2	177.40(12)	C45	C40	C41	C46	170.09(15)
C13	C14	C15	C16	-2.6(2)	C46	C41	C42	C43	-172.72(16)
C14	C13	C18	C17	-5.08(19)	C47	C43	C44	C45	-179.19(14)

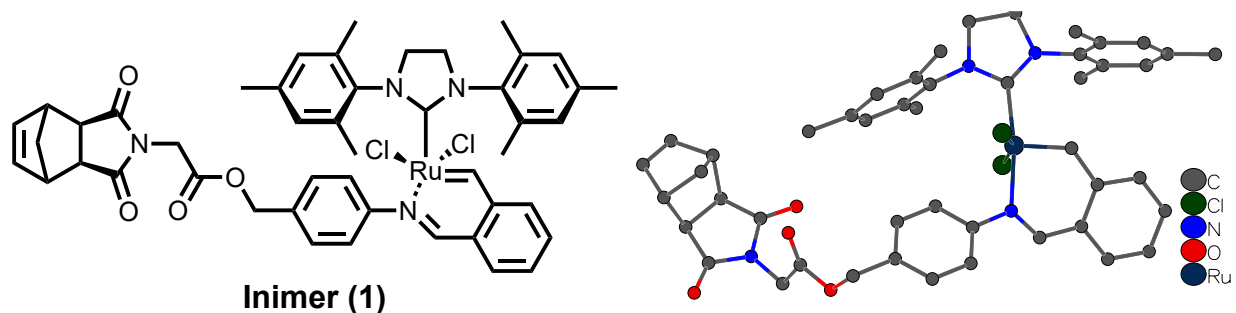
**Table 5.6.4. Torsion Angles for cs2745-catalyst 7.**

<b>A</b>	<b>B</b>	<b>C</b>	<b>D</b>	<b>Angle/°</b>	<b>A</b>	<b>B</b>	<b>C</b>	<b>D</b>	<b>Angle/°</b>
C14	C13	C18	C21	172.24(13)	C49	N5	C37	Ru2	12.5(2)
C14	C15	C16	C17	-0.4(2)	C49	N5	C37	N4	-173.07(14)
C14	C15	C16	C20	-178.62(14)	C49	N5	C39A	C38A	167.8(4)
C15	C16	C17	C18	0.7(2)	C49	N5	C39B	C38B	-178.7(2)
C16	C17	C18	C13	2.0(2)	C49	C50	C51	C52	-1.07(19)
C16	C17	C18	C21	-175.41(14)	C50	C49	C54	C53	-1.08(19)
C18	C13	C14	C15	5.38(19)	C50	C49	C54	C57	-178.30(12)
C18	C13	C14	C19	-168.63(12)	C50	C51	C52	C53	-0.8(2)
C19	C14	C15	C16	171.52(13)	C50	C51	C52	C56	179.00(13)
C20	C16	C17	C18	178.92(14)	C51	C52	C53	C54	1.8(2)
C22	C23	C24	C25	179.47(12)	C52	C53	C54	C49	-0.8(2)
C22	C23	C28	C27	-178.53(12)	C52	C53	C54	C57	176.41(13)
C22	C23	C28	C29	-4.00(19)	C54	C49	C50	C51	2.02(19)
C23	C24	C25	C26	-1.1(2)	C54	C49	C50	C55	179.02(12)
C23	C28	C29	N3	5.9(2)	C55	C50	C51	C52	-178.08(13)
C24	C23	C28	C27	0.27(17)	C56	C52	C53	C54	-178.01(13)
C24	C23	C28	C29	174.81(11)	C58	C59	C60	C61	179.50(11)
C24	C25	C26	C27	0.7(2)	C58	C59	C64	C63	-178.57(11)
C25	C26	C27	C28	0.2(2)	C58	C59	C64	C65	-3.04(18)
C26	C27	C28	C23	-0.67(19)	C59	C60	C61	C62	-0.82(19)
C26	C27	C28	C29	-175.47(12)	C59	C64	C65	N6	4.99(19)
C27	C28	C29	N3	-179.46(12)	C60	C59	C64	C63	0.47(17)
C28	C23	C24	C25	0.59(18)	C60	C59	C64	C65	176.01(11)
C29	N3	C30	C31	-120.84(14)	C60	C61	C62	C63	0.37(19)
C29	N3	C30	C35	61.09(17)	C61	C62	C63	C64	0.50(19)
C30	N3	C29	C28	-176.47(11)	C62	C63	C64	C59	-0.93(18)

**Table 5.6.4. Torsion Angles for cs2745-catalyst 7.**

<b>A</b>	<b>B</b>	<b>C</b>	<b>D</b>	<b>Angle/°</b>	<b>A</b>	<b>B</b>	<b>C</b>	<b>D</b>	<b>Angle/°</b>
C30	C31	C32	C33	1.3(2)	C62	C63	C64	C65	-176.67(12)
C31	C30	C35	C34	2.4(2)	C63	C64	C65	N6	-179.39(12)
C31	C32	C33	C34	1.2(2)	C64	C59	C60	C61	0.39(18)
C31	C32	C33	C36	-176.49(14)	C65	N6	C66	C67	50.42(17)
C32	C33	C34	C35	-1.9(2)	C65	N6	C66	C71	-131.35(13)
C32	C33	C36	O1	0.6(2)	C66	N6	C65	C64	-176.16(11)
C33	C34	C35	C30	0.1(2)	C66	C67	C68	C69	-0.4(2)
C34	C33	C36	O1	-177.07(16)	C67	C66	C71	C70	-3.30(19)
C35	C30	C31	C32	-3.1(2)	C67	C68	C69	C70	-1.8(2)
C36	C33	C34	C35	175.81(13)	C67	C68	C69	C72	177.43(12)
Ru2	N6	C65	C64	10.38(18)	C68	C69	C70	C71	1.4(2)
Ru2	N6	C66	C67	-135.25(10)	C68	C69	C72	O2	-179.55(14)
Ru2	N6	C66	C71	42.98(14)	C69	C70	C71	C66	1.1(2)
Ru2	C58	C59	C60	164.64(9)	C70	C69	C72	O2	-0.3(2)
Ru2	C58	C59	C64	-16.32(18)	C71	C66	C67	C68	2.92(19)
Cl3	Ru2	C58	C59	110.06(10)	C72	C69	C70	C71	-177.80(12)
Cl4	Ru2	C58	C59	-62.72(11)					

This report has been created with Olex2, compiled on 2021.08.20 svn.r13c46975 for OlexSys. Please [let us know](#) if there are any errors or if you would like to have additional features.



## Experimental

A yellow-brown plate (0.03 x 0.16 x 0.39 mm<sup>3</sup>) was centered on the goniometer of a Rigaku Oxford Diffraction Synergy-S diffractometer equipped with a HyPix6000HE detector and operating with MoK $\alpha$  radiation. The data collection routine, unit cell refinement, and data processing were carried out with the program CrysAlisPro.<sup>81</sup> The Laue symmetry and systematic absences were consistent with the monoclinic space group  $P2_1/n$ . The structure was solved using SHELXT<sup>82</sup> and refined using SHELXL<sup>83</sup> via Olex2.<sup>84</sup> After modeling the main molecule, residual electron density suggested the presence of disordered CH<sub>2</sub>Cl<sub>2</sub> and hexanes. A satisfactory model for the solvent could not be obtained. The solvent mask feature of Olex2 was used and calculated 55.5 e<sup>-</sup> and 216 Å<sup>3</sup> void space per asymmetric unit (222 e<sup>-</sup> in 864 Å<sup>3</sup> per unit cell), approximated as 1CH<sub>2</sub>Cl<sub>2</sub> and ½C<sub>6</sub>H<sub>14</sub>, corresponding to 67 e<sup>-</sup>/asymmetric unit. The final refinement model involved anisotropic displacement parameters for non-hydrogen atoms and a riding model for all hydrogen atoms. *Add/update when preparing publication:* Olex2<sup>85</sup> AND/OR Mercury<sup>86</sup> was used for molecular graphics generation.

(81) CrysAlisPro Software System, v1.171.41.105a, Rigaku Oxford Diffraction, **2021**, Rigaku Corporation, Oxford, UK.

(82) Sheldrick, G. M. "SHELXT – Integrated space-group and crystal structure determination." *Acta Cryst.* **2015**, *A71*, 3–8.

(83) Sheldrick, G. M. "Crystal structure refinement with SHELXL." *Acta Cryst.* **2015**, *C71*, 3–8.

(84) Dolomanov, O.V.; Bourhis, L. J.; Gildea, R. J.; Howard, J. A. K.; Puschmann, H. *J. Appl. Cryst.* **2009**, *42*, 339–341.

(85) Dolomanov, O.V.; Bourhis, L. J.; Gildea, R. J.; Howard, J. A. K.; Puschmann, H. *J. Appl. Cryst.* **2009**, *42*, 339–341.

(86) Macrae, C. F.; Sovago, I.; Cottrell, S. J.; Galek, P. T. A.; McCabe, P.; Pidcock, E.; Platings, M.; Shields, G. P.; Stevens, J. S.; Towler M.; Wood, P. A. *J. Appl. Cryst.* **2020**, *53*, 226–235. [DOI: 10.1107/S1600576719014092].

**Table 5.6.5. Crystal data and structure refinement for cs2743-inimer (1).**

Identification code	HA-61
Empirical formula	C <sub>47</sub> H <sub>48</sub> Cl <sub>2</sub> N <sub>4</sub> O <sub>4</sub> Ru•CH <sub>2</sub> Cl <sub>2</sub> •0.5(C <sub>6</sub> H <sub>14</sub> )
Formula weight	1032.87
Temperature/K	99.99(13)
Crystal system	monoclinic
Space group	P2 <sub>1</sub> /n
a/Å	19.1975(3)
b/Å	10.02560(10)
c/Å	25.2080(5)
α/°	90
β/°	105.677(2)
γ/°	90
Volume/Å <sup>3</sup>	4671.21(13)
Z	4
ρ <sub>calc</sub> /cm <sup>3</sup>	1.409
μ/mm <sup>-1</sup>	0.615
F(000)	1872.0
Crystal size/mm <sup>3</sup>	0.39 × 0.16 × 0.03
Radiation	Mo Kα (λ = 0.71073)
2θ range for data collection/°	5.116 to 67.444
Index ranges	-24 ≤ h ≤ 29, -15 ≤ k ≤ 14, -38 ≤ l ≤ 37
Reflections collected	100321
Independent reflections	16658 [R <sub>int</sub> = 0.0363, R <sub>sigma</sub> = 0.0280]
Data/restraints/parameters	16658/0/529
Goodness-of-fit on F <sup>2</sup>	1.037
Final R indexes [I ≥ 2σ (I)]	R <sub>1</sub> = 0.0358, wR <sub>2</sub> = 0.0877

Final R indexes [all data]

$R_1 = 0.0463$ ,  $wR_2 = 0.0913$

Largest diff. peak/hole /  $e \text{ \AA}^{-3}$

1.40/-0.66

**Table 5.6.6. Bond Lengths for cs2743-inimer (1).**

Atom	Atom	Length/Å	Atom	Atom	Length/Å
Ru1	C11	2.3444(3)	C14	C15	1.387(3)
Ru1	C12	2.3461(4)	C14	C19	1.505(2)
Ru1	N3	2.1057(12)	C15	C16	1.390(3)
Ru1	C1	2.0582(14)	C16	C17	1.388(3)
Ru1	C22	1.8264(15)	C16	C20	1.520(3)
O1	C36	1.454(3)	C17	C18	1.390(2)
O1	C37	1.337(3)	C18	C21	1.499(2)
O2	C37	1.193(3)	C22	C23	1.451(2)
O3	C39	1.203(3)	C23	C24	1.400(2)
O4	C46	1.220(3)	C23	C28	1.417(2)
N1	C1	1.3440(19)	C24	C25	1.392(2)
N1	C3	1.4811(19)	C25	C26	1.386(3)
N1	C13	1.430(2)	C26	C27	1.382(2)
N2	C1	1.3491(19)	C27	C28	1.398(2)
N2	C2	1.4729(19)	C28	C29	1.440(2)
N2	C4	1.425(2)	C30	C31	1.397(2)
N3	C29	1.2914(19)	C30	C35	1.393(2)
N3	C30	1.424(2)	C31	C32	1.382(2)
N4	C38	1.444(4)	C32	C33	1.394(3)
N4	C39	1.386(2)	C33	C34	1.388(3)
N4	C46	1.391(4)	C33	C36	1.507(3)
C2	C3	1.519(2)	C34	C35	1.386(3)
C4	C5	1.412(2)	C37	C38	1.513(3)
C4	C9	1.397(3)	C39	C40	1.491(3)
C5	C6	1.388(3)	C40	C41	1.543(3)
C5	C10	1.507(3)	C40	C45	1.551(3)

**Table 5.6.6. Bond Lengths for cs2743-inimer (1).**

<b>Atom</b>	<b>Atom</b>	<b>Length/Å</b>	<b>Atom</b>	<b>Atom</b>	<b>Length/Å</b>
C6	C7	1.378(4)	C41	C42	1.506(4)
C7	C8	1.398(3)	C41	C47	1.543(3)
C7	C11	1.513(3)	C42	C43	1.268(5)
C8	C9	1.392(3)	C43	C44	1.488(5)
C9	C12	1.507(2)	C44	C45	1.561(4)
C13	C14	1.398(2)	C44	C47	1.574(4)
C13	C18	1.401(2)	C45	C46	1.462(5)

**Table 5.6.7. Bond Angles for cs2743-inimer (1).**

Atom	Atom	Atom	Angle/°	Atom	Atom	Atom	Angle/°
C11	Ru1	C12	160.783(15)	C16	C17	C18	121.92(18)
N3	Ru1	C11	85.08(3)	C13	C18	C21	121.20(15)
N3	Ru1	C12	88.59(4)	C17	C18	C13	117.86(15)
C1	Ru1	C11	89.69(4)	C17	C18	C21	120.92(15)
C1	Ru1	C12	93.91(4)	C23	C22	Ru1	126.73(11)
C1	Ru1	N3	170.66(5)	C24	C23	C22	118.20(14)
C22	Ru1	C11	98.82(5)	C24	C23	C28	118.26(14)
C22	Ru1	C12	99.30(5)	C28	C23	C22	123.50(14)
C22	Ru1	N3	89.92(6)	C25	C24	C23	120.89(16)
C22	Ru1	C1	98.54(6)	C26	C25	C24	120.42(16)
C37	O1	C36	117.30(18)	C27	C26	C25	119.60(15)
C1	N1	C3	113.85(13)	C26	C27	C28	121.01(16)
C1	N1	C13	128.64(12)	C23	C28	C29	122.75(14)
C13	N1	C3	117.41(12)	C27	C28	C23	119.74(15)
C1	N2	C2	113.88(13)	C27	C28	C29	117.37(14)
C1	N2	C4	126.89(13)	N3	C29	C28	124.80(13)
C4	N2	C2	118.47(13)	C31	C30	N3	118.51(14)
C29	N3	Ru1	123.73(11)	C35	C30	N3	122.45(14)
C29	N3	C30	117.80(13)	C35	C30	C31	119.04(15)
C30	N3	Ru1	117.59(9)	C32	C31	C30	120.27(16)
C39	N4	C38	122.4(2)	C31	C32	C33	120.83(18)
C39	N4	C46	113.2(2)	C32	C33	C36	119.66(19)
C46	N4	C38	123.9(2)	C34	C33	C32	118.63(17)
N1	C1	Ru1	132.69(11)	C34	C33	C36	121.70(18)
N1	C1	N2	106.93(12)	C35	C34	C33	120.99(17)
N2	C1	Ru1	120.06(11)	C34	C35	C30	120.16(16)

**Table 5.6.7. Bond Angles for cs2743-inimer (1).**

Atom	Atom	Atom	Angle/°	Atom	Atom	Atom	Angle/°
N2	C2	C3	102.71(12)	O1	C36	C33	108.4(2)
N1	C3	C2	102.42(12)	O1	C37	C38	109.4(2)
C5	C4	N2	119.47(17)	O2	C37	O1	126.0(2)
C9	C4	N2	118.88(14)	O2	C37	C38	124.6(2)
C9	C4	C5	121.28(17)	N4	C38	C37	111.3(2)
C4	C5	C10	122.44(18)	O3	C39	N4	123.6(2)
C6	C5	C4	118.0(2)	O3	C39	C40	128.52(19)
C6	C5	C10	119.57(17)	N4	C39	C40	107.90(19)
C7	C6	C5	122.18(19)	C39	C40	C41	113.22(19)
C6	C7	C8	118.7(2)	C39	C40	C45	104.6(2)
C6	C7	C11	121.0(2)	C41	C40	C45	102.91(18)
C8	C7	C11	120.3(3)	C42	C41	C40	103.7(2)
C9	C8	C7	121.7(2)	C42	C41	C47	100.4(2)
C4	C9	C12	122.34(16)	C47	C41	C40	102.09(19)
C8	C9	C4	118.11(18)	C43	C42	C41	109.0(3)
C8	C9	C12	119.43(19)	C42	C43	C44	108.7(3)
C14	C13	N1	119.57(14)	C43	C44	C45	105.6(2)
C14	C13	C18	121.77(15)	C43	C44	C47	100.5(3)
C18	C13	N1	118.62(14)	C45	C44	C47	99.9(2)
C13	C14	C19	120.90(16)	C40	C45	C44	102.5(2)
C15	C14	C13	118.04(16)	C46	C45	C40	105.4(2)
C15	C14	C19	121.05(16)	C46	C45	C44	113.1(2)
C14	C15	C16	121.85(18)	O4	C46	N4	121.6(3)
C15	C16	C20	120.6(2)	O4	C46	C45	129.9(3)
C17	C16	C15	118.56(19)	N4	C46	C45	108.54(19)
C17	C16	C20	120.8(2)	C41	C47	C44	91.6(2)

**Table 5.6.8. Torsion Angles for cs2743-Inimer (1).**

A	B	C	D	Angle/°	A	B	C	D	Angle/°
Ru1	N3	C29	C28	16.3(2)	C18	C13	C14	C19	179.84(15)
Ru1	N3	C30	C31	26.81(18)	C19	C14	C15	C16	-179.8(2)
Ru1	N3	C30	C35	-152.63(12)	C20	C16	C17	C18	-179.4(3)
Ru1	C22	C23	C24	161.91(12)	C22	C23	C24	C25	-174.26(14)
Ru1	C22	C23	C28	-15.5(2)	C22	C23	C28	C27	175.24(13)
Cl1	Ru1	C22	C23	-57.14(13)	C22	C23	C28	C29	-9.3(2)
Cl2	Ru1	C22	C23	116.42(12)	C23	C24	C25	C26	-1.9(2)
O1	C37	C38	N4	-176.8(2)	C23	C28	C29	N3	7.1(2)
O2	C37	C38	N4	3.8(4)	C24	C23	C28	C27	-2.2(2)
O3	C39	C40	C41	68.9(3)	C24	C23	C28	C29	173.28(13)
O3	C39	C40	C45	-179.8(2)	C24	C25	C26	C27	-0.7(2)
N1	C13	C14	C15	178.33(15)	C25	C26	C27	C28	1.8(2)
N1	C13	C14	C19	-2.7(2)	C26	C27	C28	C23	-0.3(2)
N1	C13	C18	C17	-177.99(15)	C26	C27	C28	C29	-176.06(14)
N1	C13	C18	C21	3.9(2)	C27	C28	C29	N3	-177.36(14)
N2	C2	C3	N1	-4.16(15)	C28	C23	C24	C25	3.3(2)
N2	C4	C5	C6	-177.12(15)	C29	N3	C30	C31	-142.82(15)
N2	C4	C5	C10	0.7(2)	C29	N3	C30	C35	37.7(2)
N2	C4	C9	C8	177.15(16)	C30	N3	C29	C28	-174.74(13)
N2	C4	C9	C12	1.1(2)	C30	C31	C32	C33	-0.5(3)
N3	Ru1	C22	C23	27.87(13)	C31	C30	C35	C34	2.9(2)
N3	C30	C31	C32	178.51(16)	C31	C32	C33	C34	2.1(3)
N3	C30	C35	C34	-177.64(15)	C31	C32	C33	C36	-177.3(2)
N4	C39	C40	C41	-111.31(18)	C32	C33	C34	C35	-1.2(3)
N4	C39	C40	C45	0.0(2)	C32	C33	C36	O1	67.1(3)

**Table 5.6.8. Torsion Angles for cs2743-Inimer (1).**

A	B	C	D	Angle/°	A	B	C	D	Angle/°
C1	Ru1	C22	C23	-148.16(13)	C33	C34	C35	C30	-1.3(3)
C1	N1	C3	C2	3.14(16)	C34	C33	C36	O1	-112.3(2)
C1	N1	C13	C14	96.92(18)	C35	C30	C31	C32	-2.0(3)
C1	N1	C13	C18	-85.55(19)	C36	O1	C37	O2	-3.6(3)
C1	N2	C2	C3	4.44(17)	C36	O1	C37	C38	177.1(2)
C1	N2	C4	C5	-101.02(18)	C36	C33	C34	C35	178.17(19)
C1	N2	C4	C9	85.92(19)	C37	O1	C36	C33	-102.9(2)
C2	N2	C1	Ru1	-176.96(10)	C38	N4	C39	O3	-4.9(3)
C2	N2	C1	N1	-2.62(17)	C38	N4	C39	C40	175.27(18)
C2	N2	C4	C5	89.63(18)	C38	N4	C46	O4	2.5(3)
C2	N2	C4	C9	-83.42(19)	C38	N4	C46	C45	-177.1(2)
C3	N1	C1	Ru1	172.83(10)	C39	N4	C38	C37	-98.3(2)
C3	N1	C1	N2	-0.50(16)	C39	N4	C46	O4	174.5(2)
C3	N1	C13	C14	-86.94(17)	C39	N4	C46	C45	-5.1(2)
C3	N1	C13	C18	90.59(17)	C39	C40	C41	C42	-179.40(19)
C4	N2	C1	Ru1	13.3(2)	C39	C40	C41	C47	76.6(2)
C4	N2	C1	N1	-172.38(14)	C39	C40	C45	C44	-121.4(2)
C4	N2	C2	C3	175.13(13)	C39	C40	C45	C46	-2.8(2)
C4	C5	C6	C7	2.4(3)	C40	C41	C42	C43	-71.4(3)
C5	C4	C9	C8	4.2(3)	C40	C41	C47	C44	58.1(2)
C5	C4	C9	C12	-171.77(16)	C40	C45	C46	O4	-174.8(2)
C5	C6	C7	C8	-0.5(3)	C40	C45	C46	N4	4.7(2)
C5	C6	C7	C11	177.7(2)	C41	C40	C45	C44	-2.8(3)
C6	C7	C8	C9	0.5(3)	C41	C40	C45	C46	115.7(2)
C7	C8	C9	C4	-2.3(3)	C41	C42	C43	C44	0.2(4)
C7	C8	C9	C12	173.79(19)	C42	C41	C47	C44	-48.5(3)

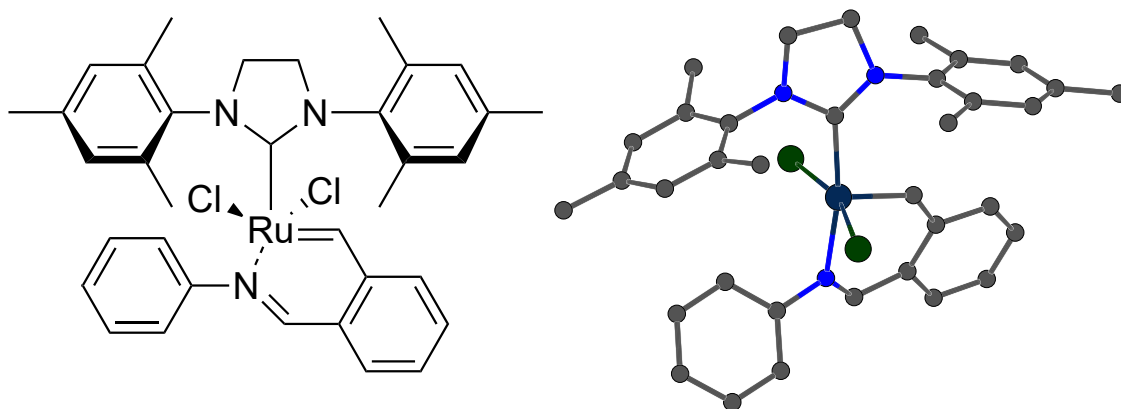
**Table 5.6.8. Torsion Angles for cs2743-Inimer (1).**

A	B	C	D	Angle/°	A	B	C	D	Angle/°
C9	C4	C5	C6	-4.2(2)	C42	C43	C44	C45	70.1(4)
C9	C4	C5	C10	173.56(16)	C42	C43	C44	C47	-33.4(3)
C10	C5	C6	C7	-175.51(19)	C43	C44	C45	C40	-64.5(3)
C11	C7	C8	C9	-177.7(2)	C43	C44	C45	C46	-177.5(3)
C13	N1	C1	Ru1	-10.9(2)	C43	C44	C47	C41	49.0(2)
C13	N1	C1	N2	175.76(13)	C44	C45	C46	O4	-63.6(4)
C13	N1	C3	C2	-173.57(12)	C44	C45	C46	N4	115.9(2)
C13	C14	C15	C16	-0.9(3)	C45	C40	C41	C42	68.2(2)
C14	C13	C18	C17	-0.5(2)	C45	C40	C41	C47	-35.8(3)
C14	C13	C18	C21	-178.60(15)	C45	C44	C47	C41	-59.1(2)
C14	C15	C16	C17	0.5(3)	C46	N4	C38	C37	73.0(3)
C14	C15	C16	C20	179.8(3)	C46	N4	C39	O3	-177.11(19)
C15	C16	C17	C18	-0.1(3)	C46	N4	C39	C40	3.1(2)
C16	C17	C18	C13	0.1(3)	C47	C41	C42	C43	33.9(3)
C16	C17	C18	C21	178.20(19)	C47	C44	C45	C40	39.4(3)
C18	C13	C14	C15	0.9(2)	C47	C44	C45	C46	-73.6(3)

**Table 5.6.9. Solvent masks information for cs2743-inimer (1).**

Number	X	Y	Z	Volume	Electron count	Content
1	0.000	-0.871	0.500	432.5	111.3	2CH <sub>2</sub> Cl <sub>2</sub> ,1C <sub>6</sub> H <sub>14</sub>
2	0.500	-0.019	0.000	432.5	111.3	2CH <sub>2</sub> Cl <sub>2</sub> ,1C <sub>6</sub> H <sub>14</sub>

This report has been created with Olex2, compiled on 2021.08.20 svn.r13c46975 for OlexSys. Please [let us know](#) if there are any errors or if you would like to have additional features.



[Ru] 1

## Experimental

A yellow-brown crystal ( $0.03 \times 0.10 \times 0.12 \text{ mm}^3$ ) was cut from a cluster of intergrown crystals and centered on the goniometer of a Rigaku Oxford Diffraction Synergy-S diffractometer equipped with a HyPix6000HE detector and operating with  $\text{CuK}\alpha$  radiation. The data collection routine, unit cell refinement, and data processing were carried out with the program CrysAlisPro.<sup>87</sup> The Laue symmetry and systematic absences were consistent with the monoclinic space group  $P2_1/c$ . The structure was solved using SHELXT<sup>88</sup> and refined using SHELXL<sup>89</sup> via Olex2.<sup>90</sup> The final refinement model involved anisotropic displacement parameters for non-hydrogen atoms and a riding model for all hydrogen atoms. Olex2<sup>91</sup> was used for molecular graphics generation.

**Table 5.6.10. Crystal data and structure refinement for cs2849-[Ru] 1.**

Identification code	cs2849
Empirical formula	$\text{C}_{36}\text{H}_{39}\text{Cl}_4\text{N}_3\text{Ru}$
Formula weight	756.57

- 
- (87) CrysAlisPro Software System, v1.171.41.105a, Rigaku Oxford Diffraction, **2021**, Rigaku Corporation, Oxford, UK.  
 (88) Sheldrick, G. M. "SHELXT – Integrated space-group and crystal structure determination." *Acta Cryst.* **2015**, *A71*, 3–8.  
 (89) Sheldrick, G. M. "Crystal structure refinement with SHELXL." *Acta Cryst.* **2015**, *C71*, 3–8.  
 (90) Dolomanov, O.V.; Bourhis, L. J.; Gildea, R. J.; Howard, J. A. K.; Puschmann, H. *J. Appl. Cryst.* **2009**, *42*, 339–341.  
 (91) Dolomanov, O.V.; Bourhis, L. J.; Gildea, R. J.; Howard, J. A. K.; Puschmann, H. *J. Appl. Cryst.* **2009**, *42*, 339–341.

Temperature/K	100.00(10)
Crystal system	monoclinic
Space group	<i>P2<sub>1</sub>/c</i>
<i>a</i> /Å	18.8082(2)
<i>b</i> /Å	10.19550(10)
<i>c</i> /Å	19.3233(2)
$\alpha$ /°	90
$\beta$ /°	112.8670(10)
$\gamma$ /°	90
Volume/Å <sup>3</sup>	3414.20(6)
<i>Z</i>	4
$\rho_{\text{calc}}/\text{cm}^3$	1.472
$\mu/\text{mm}^{-1}$	6.823
<i>F</i> (000)	1552.0
Crystal size/mm <sup>3</sup>	0.12 × 0.096 × 0.03
Radiation	Cu K $\alpha$ ( $\lambda$ = 1.54184)
2 $\Theta$ range for data collection/°	5.1 to 154.662
Index ranges	-23 ≤ <i>h</i> ≤ 23, -12 ≤ <i>k</i> ≤ 12, -24 ≤ <i>l</i> ≤ 24
Reflections collected	79800
Independent reflections	7233 [ <i>R</i> <sub>int</sub> = 0.0562, <i>R</i> <sub>sigma</sub> = 0.0231]
Data/restraints/parameters	7233/0/403
Goodness-of-fit on <i>F</i> <sup>2</sup>	1.066
Final <i>R</i> indexes [ <i>I</i> ≥ 2 $\sigma$ ( <i>I</i> )]	<i>R</i> <sub>1</sub> = 0.0411, <i>wR</i> <sub>2</sub> = 0.1137
Final <i>R</i> indexes [all data]	<i>R</i> <sub>1</sub> = 0.0424, <i>wR</i> <sub>2</sub> = 0.1150
Largest diff. peak/hole / e Å <sup>-3</sup>	0.87/-1.65

**Table 5.6.11. Bond Lengths for cs2849-[Ru] 1.**

Atom	Atom	Length/Å	Atom	Atom	Length/Å
Ru1	C11	2.3437(6)	C13	C18	1.394(3)
Ru1	C12	2.3707(6)	C14	C15	1.399(4)
Ru1	N3	2.0968(19)	C14	C19	1.503(4)
Ru1	C1	2.078(2)	C15	C16	1.392(4)
Ru1	C22	1.839(2)	C16	C17	1.391(4)
N1	C1	1.341(3)	C16	C20	1.506(4)
N1	C2	1.477(3)	C17	C18	1.394(3)
N1	C4	1.434(3)	C18	C21	1.507(3)
N2	C1	1.342(3)	C22	C23	1.449(3)
N2	C3	1.481(3)	C23	C24	1.408(3)
N2	C13	1.431(3)	C23	C28	1.416(3)
N3	C29	1.283(3)	C24	C25	1.385(3)
N3	C30	1.431(3)	C25	C26	1.400(4)
C2	C3	1.528(4)	C26	C27	1.380(4)
C4	C5	1.399(4)	C27	C28	1.399(3)
C4	C9	1.399(4)	C28	C29	1.453(3)
C5	C6	1.397(4)	C30	C31	1.391(4)
C5	C10	1.511(4)	C30	C35	1.392(4)
C6	C7	1.389(5)	C31	C32	1.391(4)
C7	C8	1.386(5)	C32	C33	1.388(4)
C7	C11	1.508(4)	C33	C34	1.386(4)
C8	C9	1.391(4)	C34	C35	1.396(4)
C9	C12	1.512(4)	C13	C36	1.757(4)
C13	C14	1.401(3)	C14	C36	1.770(4)

**Table 5.6.12. Bond Angles for cs2849-[Ru] 1.**

Atom	Atom	Atom	Angle/°	Atom	Atom	Atom	Angle/°
C11	Ru1	C12	162.36(2)	C8	C9	C12	120.0(3)
N3	Ru1	C11	84.94(6)	C14	C13	N2	118.5(2)
N3	Ru1	C12	87.68(6)	C18	C13	N2	119.5(2)
C1	Ru1	C11	89.37(7)	C18	C13	C14	122.0(2)
C1	Ru1	C12	95.35(6)	C13	C14	C19	121.1(2)
C1	Ru1	N3	169.78(9)	C15	C14	C13	118.2(2)
C22	Ru1	C11	98.25(8)	C15	C14	C19	120.6(2)
C22	Ru1	C12	97.70(8)	C16	C15	C14	120.8(2)
C22	Ru1	N3	89.62(9)	C15	C16	C20	120.5(2)
C22	Ru1	C1	99.61(10)	C17	C16	C15	119.4(2)
C1	N1	C2	113.8(2)	C17	C16	C20	120.1(2)
C1	N1	C4	126.4(2)	C16	C17	C18	121.5(2)
C4	N1	C2	118.2(2)	C13	C18	C21	121.4(2)
C1	N2	C3	113.4(2)	C17	C18	C13	118.0(2)
C1	N2	C13	127.7(2)	C17	C18	C21	120.6(2)
C13	N2	C3	118.40(19)	C23	C22	Ru1	127.44(17)
C29	N3	Ru1	125.94(17)	C24	C23	C22	117.9(2)
C29	N3	C30	118.2(2)	C24	C23	C28	118.0(2)
C30	N3	Ru1	115.41(15)	C28	C23	C22	124.1(2)
N1	C1	Ru1	120.19(17)	C25	C24	C23	121.6(2)
N1	C1	N2	106.9(2)	C24	C25	C26	119.9(2)
N2	C1	Ru1	132.75(18)	C27	C26	C25	119.4(2)
N1	C2	C3	101.5(2)	C26	C27	C28	121.5(2)
N2	C3	C2	101.6(2)	C23	C28	C29	122.2(2)
C5	C4	N1	119.2(2)	C27	C28	C23	119.5(2)
C5	C4	C9	121.3(2)	C27	C28	C29	117.9(2)

**Table 5.6.12. Bond Angles for cs2849-[Ru] 1.**

<b>Atom Atom Atom</b>	<b>Angle/°</b>	<b>Atom Atom Atom</b>	<b>Angle/°</b>
C9 C4 N1	119.3(2)	N3 C29 C28	124.6(2)
C4 C5 C10	122.4(2)	C31 C30 N3	120.6(2)
C6 C5 C4	118.1(3)	C31 C30 C35	120.3(2)
C6 C5 C10	119.4(3)	C35 C30 N3	119.1(2)
C7 C6 C5	121.9(3)	C30 C31 C32	119.8(3)
C6 C7 C11	121.2(3)	C33 C32 C31	120.3(3)
C8 C7 C6	118.2(3)	C34 C33 C32	119.7(2)
C8 C7 C11	120.6(3)	C33 C34 C35	120.6(3)
C7 C8 C9	122.2(3)	C30 C35 C34	119.2(3)
C4 C9 C12	121.7(2)	Cl3 C36 Cl4	110.77(19)
C8 C9 C4	118.1(3)		

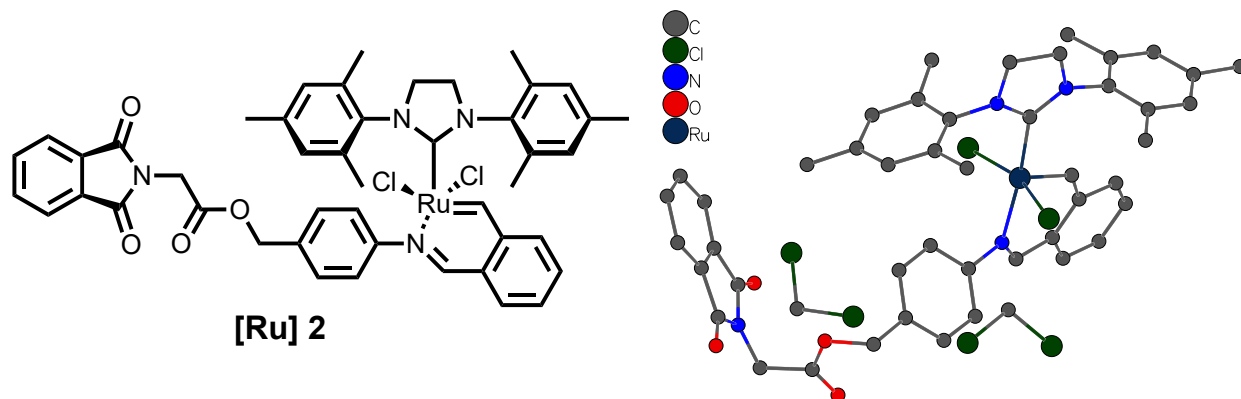
**Table 5.6.13. Torsion Angles for cs2849-[Ru] 1.**

A	B	C	D	Angle/°	A	B	C	D	Angle/°
Ru1	N3	C29	C28	13.3(3)	C7	C8	C9	C4	-2.4(4)
Ru1	N3	C30	C31	-139.88(19)	C7	C8	C9	C12	172.8(3)
Ru1	N3	C30	C35	39.7(3)	C9	C4	C5	C6	-4.6(4)
Ru1	C22	C23	C24	164.97(19)	C9	C4	C5	C10	171.8(2)
Ru1	C22	C23	C28	-16.1(4)	C10	C5	C6	C7	-174.5(3)
C11	Ru1	C22	C23	-60.2(2)	C11	C7	C8	C9	-177.2(3)
C12	Ru1	C22	C23	112.3(2)	C13	N2	C1	Ru1	-2.5(4)
N1	C2	C3	N2	-15.6(3)	C13	N2	C1	N1	-178.1(2)
N1	C4	C5	C6	-179.3(2)	C13	N2	C3	C2	-172.9(2)
N1	C4	C5	C10	-3.0(4)	C13	C14	C15	C16	0.4(4)
N1	C4	C9	C8	179.5(2)	C14	C13	C18	C17	1.3(3)
N1	C4	C9	C12	4.5(4)	C14	C13	C18	C21	179.5(2)
N2	C13	C14	C15	178.3(2)	C14	C15	C16	C17	1.3(4)
N2	C13	C14	C19	1.0(3)	C14	C15	C16	C20	-179.7(2)
N2	C13	C18	C17	-178.8(2)	C15	C16	C17	C18	-1.8(4)
N2	C13	C18	C21	-0.5(3)	C16	C17	C18	C13	0.6(4)
N3	Ru1	C22	C23	24.6(2)	C16	C17	C18	C21	-177.7(2)
N3	C30	C31	C32	-178.9(2)	C18	C13	C14	C15	-1.8(4)
N3	C30	C35	C34	178.3(2)	C18	C13	C14	C19	-179.1(2)
C1	Ru1	C22	C23	-150.9(2)	C19	C14	C15	C16	177.8(2)
C1	N1	C2	C3	14.0(3)	C20	C16	C17	C18	179.1(2)
C1	N1	C4	C5	-107.8(3)	C22	C23	C24	C25	179.5(2)
C1	N1	C4	C9	77.3(3)	C22	C23	C28	C27	-178.6(2)
C1	N2	C3	C2	14.6(3)	C22	C23	C28	C29	-5.0(4)
C1	N2	C13	C14	-89.9(3)	C23	C24	C25	C26	-1.0(4)
C1	N2	C13	C18	90.2(3)	C23	C28	C29	N3	5.1(4)

**Table 5.6.13. Torsion Angles for cs2849-[Ru] 1.**

A	B	C	D	Angle/°	A	B	C	D	Angle/°
C2	N1	C1	Ru1	178.31(17)	C24	C23	C28	C27	0.3(3)
C2	N1	C1	N2	-5.5(3)	C24	C23	C28	C29	173.9(2)
C2	N1	C4	C5	87.6(3)	C24	C25	C26	C27	0.6(4)
C2	N1	C4	C9	-87.2(3)	C25	C26	C27	C28	0.2(4)
C3	N2	C1	Ru1	169.19(19)	C26	C27	C28	C23	-0.7(4)
C3	N2	C1	N1	-6.4(3)	C26	C27	C28	C29	-174.6(2)
C3	N2	C13	C14	98.8(3)	C27	C28	C29	N3	178.8(2)
C3	N2	C13	C18	-81.2(3)	C28	C23	C24	C25	0.5(4)
C4	N1	C1	Ru1	13.2(3)	C29	N3	C30	C31	47.4(3)
C4	N1	C1	N2	-170.6(2)	C29	N3	C30	C35	-133.1(2)
C4	N1	C2	C3	-179.5(2)	C30	N3	C29	C28	-174.7(2)
C4	C5	C6	C7	1.9(4)	C30	C31	C32	C33	0.2(4)
C5	C4	C9	C8	4.8(4)	C31	C30	C35	C34	-2.1(4)
C5	C4	C9	C12	-170.3(2)	C31	C32	C33	C34	-1.3(4)
C5	C6	C7	C8	0.4(4)	C32	C33	C34	C35	0.7(4)
C5	C6	C7	C11	177.4(3)	C33	C34	C35	C30	1.0(4)
C6	C7	C8	C9	-0.2(4)	C35	C30	C31	C32	1.5(4)

This report has been created with Olex2, compiled on 2022.04.07 svn.rca3783a0 for OlexSys. Please [let us know](#) if there are any errors or if you would like to have additional features.



## Experimental

A green prism (0.17 x 0.30 x 0.39 mm<sup>3</sup>) was centered on the goniometer of a Rigaku Oxford Diffraction Synergy-S diffractometer equipped with a HyPix6000HE detector and operating with MoK $\alpha$  radiation. The data collection routine, unit cell refinement, and data processing were carried out with the program CrysAlisPro.<sup>92</sup> The Laue symmetry and systematic absences were consistent with the monoclinic space group  $P2_1/n$ . The structure was solved using SHELXT<sup>93</sup> and refined using SHELXL<sup>94</sup> via Olex2.<sup>95</sup> The asymmetric unit comprised the ruthenium complex two CH<sub>2</sub>Cl<sub>2</sub> molecule. A 2-position disorder model was used on one CH<sub>2</sub>Cl<sub>2</sub> molecule with relative occupancies that refined to 0.920(4) and 0.080(4). The final refinement model involved anisotropic displacement parameters for non-hydrogen atoms and a riding model for all hydrogen atoms. Olex2<sup>96</sup> was used for molecular graphics generation.

**Table 5.6.14. Crystal data and structure refinement for cs2809-[Ru] 2.**

Identification code	HA-2-12-1
Empirical formula	C <sub>48</sub> H <sub>48</sub> Cl <sub>6</sub> N <sub>4</sub> O <sub>4</sub> Ru

- (92) CrysAlisPro Software System, v1.171.41.105a, Rigaku Oxford Diffraction, **2021**, Rigaku Corporation, Oxford, UK.  
 (93) Sheldrick, G. M. "SHELXT – Integrated space-group and crystal structure determination." *Acta Cryst.* **2015**, *A71*, 3–8.  
 (94) Sheldrick, G. M. "Crystal structure refinement with SHELXL." *Acta Cryst.* **2015**, *C71*, 3–8.  
 (95) Dolomanov, O.V.; Bourhis, L. J.; Gildea, R. J.; Howard, J. A. K.; Puschmann, H. *J. Appl. Cryst.* **2009**, *42*, 339–341.  
 (96) Dolomanov, O.V.; Bourhis, L. J.; Gildea, R. J.; Howard, J. A. K.; Puschmann, H. *J. Appl. Cryst.* **2009**, *42*, 339–341.

Formula weight	1058.67
Temperature/K	100.00(10)
Crystal system	monoclinic
Space group	P2 <sub>1</sub> /n
a/Å	19.63423(17)
b/Å	13.07725(10)
c/Å	19.76928(18)
α/°	90
β/°	110.5333(10)
γ/°	90
Volume/Å <sup>3</sup>	4753.51(8)
Z	4
ρ <sub>calc</sub> /cm <sup>3</sup>	1.479
μ/mm <sup>-1</sup>	0.715
F(000)	2168.0
Crystal size/mm <sup>3</sup>	0.39 × 0.3 × 0.17
Radiation	Mo Kα (λ = 0.71073)
2θ range for data collection/°	4.782 to 76.624
Index ranges	-34 ≤ h ≤ 33, -22 ≤ k ≤ 22, -34 ≤ l ≤ 34
Reflections collected	235821
Independent reflections	25572 [R <sub>int</sub> = 0.0418, R <sub>sigma</sub> = 0.0230]
Data/restraints/parameters	25572/0/581
Goodness-of-fit on F <sup>2</sup>	1.026
Final R indexes [I ≥ 2σ (I)]	R <sub>1</sub> = 0.0272, wR <sub>2</sub> = 0.0669
Final R indexes [all data]	R <sub>1</sub> = 0.0341, wR <sub>2</sub> = 0.0690
Largest diff. peak/hole / e Å <sup>-3</sup>	0.73/-0.56

**Table 5.6.15. Bond Lengths for cs2809-[Ru] 2.**

Atom	Atom	Length/Å	Atom	Atom	Length/Å
Ru1	C11	2.3601(2)	C15	C16	1.3943(13)
Ru1	C12	2.3451(2)	C16	C17	1.3901(14)
Ru1	N3	2.0934(7)	C16	C20	1.5025(13)
Ru1	C1	2.0636(8)	C17	C18	1.3970(12)
Ru1	C22	1.8293(8)	C18	C21	1.5040(14)
O1	C36	1.4586(11)	C22	C23	1.4520(12)
O1	C37	1.3363(11)	C23	C24	1.4066(12)
O2	C37	1.2010(11)	C23	C28	1.4165(12)
O3	C39	1.2106(11)	C24	C25	1.3884(13)
O4	C46	1.2084(11)	C25	C26	1.3937(15)
N1	C1	1.3423(10)	C26	C27	1.3873(13)
N1	C2	1.4800(11)	C27	C28	1.4046(12)
N1	C4	1.4281(11)	C28	C29	1.4499(11)
N2	C1	1.3545(10)	C30	C31	1.3900(12)
N2	C3	1.4690(11)	C30	C35	1.3981(12)
N2	C13	1.4315(11)	C31	C32	1.3907(12)
N3	C29	1.2896(10)	C32	C33	1.3923(12)
N3	C30	1.4297(10)	C33	C34	1.3956(12)
N4	C38	1.4391(11)	C33	C36	1.5033(12)
N4	C39	1.3956(11)	C34	C35	1.3906(12)
N4	C46	1.3953(11)	C37	C38	1.5163(12)
C2	C3	1.5200(13)	C39	C40	1.4860(12)
C4	C5	1.3984(12)	C40	C41	1.3853(13)
C4	C9	1.3979(12)	C40	C45	1.3906(12)
C5	C6	1.3932(12)	C41	C42	1.3968(14)
C5	C10	1.5005(13)	C42	C43	1.3921(15)

**Table 5.6.15. Bond Lengths for cs2809-[Ru] 2.**

Atom	Atom	Length/Å	Atom	Atom	Length/Å
C6	C7	1.3893(15)	C43	C44	1.3970(15)
C7	C8	1.3906(15)	C44	C45	1.3828(13)
C7	C11	1.5061(14)	C45	C46	1.4851(13)
C8	C9	1.3964(13)	Cl3A	C47	1.7633(12)
C9	C12	1.5047(14)	Cl3B	C47	1.779(7)
C13	C14	1.4050(12)	Cl4A	C47	1.7708(12)
C13	C18	1.4033(12)	Cl4B	C47	1.738(6)
C14	C15	1.3944(12)	Cl5	C48	1.7630(12)
C14	C19	1.5054(13)	Cl6	C48	1.7657(13)

**Table 5.6.16. Bond Angles for cs2809-[Ru] 2.**

Atom	Atom	Atom	Angle/°	Atom	Atom	Atom	Angle/°
Cl2	Ru1	Cl1	161.224(8)	C17	C16	C20	121.81(9)
N3	Ru1	Cl1	88.40(2)	C16	C17	C18	121.97(8)
N3	Ru1	Cl2	83.75(2)	C13	C18	C21	122.19(8)
C1	Ru1	Cl1	87.48(2)	C17	C18	C13	117.88(8)
C1	Ru1	Cl2	97.72(2)	C17	C18	C21	119.89(8)
C1	Ru1	N3	170.89(3)	C23	C22	Ru1	127.02(6)
C22	Ru1	Cl1	101.03(3)	C24	C23	C22	117.27(8)
C22	Ru1	Cl2	96.04(3)	C24	C23	C28	118.30(8)
C22	Ru1	N3	90.20(3)	C28	C23	C22	124.42(7)
C22	Ru1	C1	98.56(3)	C25	C24	C23	121.42(9)
C37	O1	C36	115.53(7)	C24	C25	C26	119.97(9)
C1	N1	C2	113.69(7)	C27	C26	C25	119.75(8)
C1	N1	C4	129.17(7)	C26	C27	C28	121.02(8)

**Table 5.6.16. Bond Angles for cs2809-[Ru] 2.**

Atom	Atom	Atom	Angle/°	Atom	Atom	Atom	Angle/°
C4	N1	C2	117.13(7)	C23	C28	C29	122.78(7)
C1	N2	C3	114.07(7)	C27	C28	C23	119.52(8)
C1	N2	C13	125.00(7)	C27	C28	C29	117.57(7)
C13	N2	C3	119.36(7)	N3	C29	C28	123.62(7)
C29	N3	Ru1	126.87(6)	C31	C30	N3	120.60(7)
C29	N3	C30	118.47(7)	C31	C30	C35	120.13(7)
C30	N3	Ru1	114.55(5)	C35	C30	N3	119.13(7)
C39	N4	C38	122.64(7)	C30	C31	C32	119.64(8)
C46	N4	C38	125.04(7)	C31	C32	C33	120.94(8)
C46	N4	C39	112.15(7)	C32	C33	C34	118.94(8)
N1	C1	Ru1	133.67(6)	C32	C33	C36	119.76(8)
N1	C1	N2	106.76(7)	C34	C33	C36	121.22(8)
N2	C1	Ru1	118.89(6)	C35	C34	C33	120.72(8)
N1	C2	C3	102.64(7)	C34	C35	C30	119.61(8)
N2	C3	C2	102.35(7)	O1	C36	C33	112.36(7)
C5	C4	N1	119.40(8)	O1	C37	C38	111.78(7)
C9	C4	N1	118.78(8)	O2	C37	O1	125.26(8)
C9	C4	C5	121.69(8)	O2	C37	C38	122.91(8)
C4	C5	C10	121.40(8)	N4	C38	C37	114.43(7)
C6	C5	C4	118.12(8)	O3	C39	N4	123.70(8)
C6	C5	C10	120.48(8)	O3	C39	C40	130.35(9)
C7	C6	C5	121.73(9)	N4	C39	C40	105.94(7)
C6	C7	C8	118.72(8)	C41	C40	C39	130.68(8)
C6	C7	C11	120.17(10)	C41	C40	C45	121.54(8)
C8	C7	C11	121.09(10)	C45	C40	C39	107.78(7)
C7	C8	C9	121.58(9)	C40	C41	C42	117.14(9)

**Table 5.6.16. Bond Angles for cs2809-[Ru] 2.**

Atom	Atom	Atom	Angle/°	Atom	Atom	Atom	Angle/°
C4	C9	C12	121.01(8)	C43	C42	C41	121.17(9)
C8	C9	C4	118.10(8)	C42	C43	C44	121.36(9)
C8	C9	C12	120.87(9)	C45	C44	C43	117.06(9)
C14	C13	N2	118.74(8)	C40	C45	C46	108.49(7)
C18	C13	N2	119.41(8)	C44	C45	C40	121.71(8)
C18	C13	C14	121.56(8)	C44	C45	C46	129.79(8)
C13	C14	C19	122.15(8)	O4	C46	N4	124.91(9)
C15	C14	C13	117.93(8)	O4	C46	C45	129.54(8)
C15	C14	C19	119.79(8)	N4	C46	C45	105.54(7)
C16	C15	C14	121.89(9)	Cl3A	C47	Cl4A	111.12(7)
C15	C16	C20	119.70(9)	Cl4B	C47	Cl3B	114.5(3)
C17	C16	C15	118.49(8)	Cl5	C48	Cl6	111.05(6)

**Table 5.6.17. Torsion Angles for cs2809-[Ru] 2.**

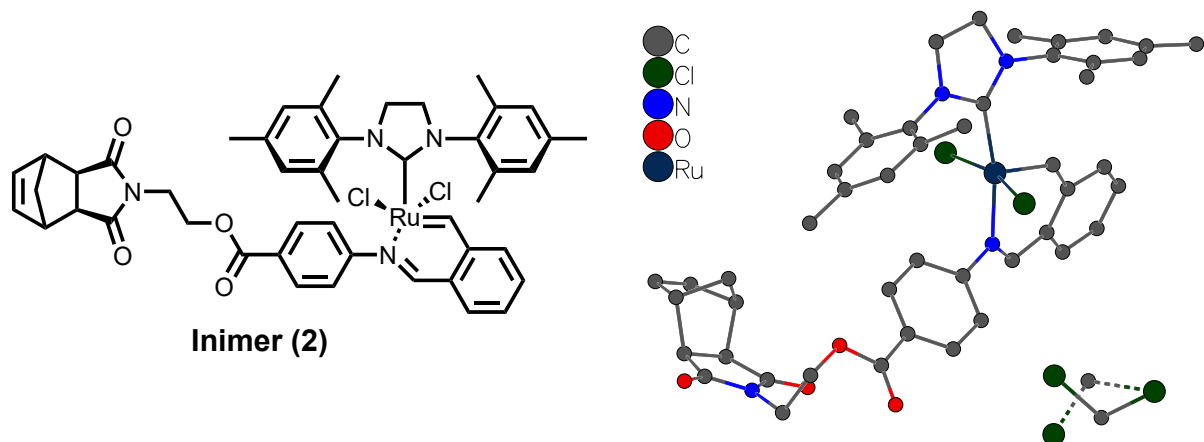
A	B	C	D	Angle/°	A	B	C	D	Angle/°
Ru1	N3	C29	C28	-9.34(12)	C14	C15	C16	C20	178.56(9)
Ru1	N3	C30	C31	134.16(7)	C15	C16	C17	C18	2.88(14)
Ru1	N3	C30	C35	-41.67(9)	C16	C17	C18	C13	0.51(13)
Ru1	C22	C23	C24	-163.87(7)	C16	C17	C18	C21	-177.43(9)
Ru1	C22	C23	C28	16.87(13)	C18	C13	C14	C15	5.96(12)
Cl1	Ru1	C22	C23	-111.80(8)	C18	C13	C14	C19	-170.00(8)
Cl2	Ru1	C22	C23	60.35(8)	C19	C14	C15	C16	173.65(8)
O1	C37	C38	N4	-24.92(11)	C20	C16	C17	C18	-177.59(9)
O2	C37	C38	N4	157.65(9)	C22	C23	C24	C25	179.63(9)
O3	C39	C40	C41	1.21(17)	C22	C23	C28	C27	179.53(8)

**Table 5.6.17. Torsion Angles for cs2809-[Ru] 2.**

A	B	C	D	Angle/°	A	B	C	D	Angle/°
O3	C39	C40	C45	-179.19(10)	C22	C23	C28	C29	3.67(13)
N1	C2	C3	N2	-6.53(10)	C23	C24	C25	C26	0.94(16)
N1	C4	C5	C6	175.27(8)	C23	C28	C29	N3	-6.40(13)
N1	C4	C5	C10	-5.38(12)	C24	C23	C28	C27	0.27(12)
N1	C4	C9	C8	-173.83(8)	C24	C23	C28	C29	-175.59(8)
N1	C4	C9	C12	7.64(13)	C24	C25	C26	C27	-0.03(16)
N2	C13	C14	C15	179.72(7)	C25	C26	C27	C28	-0.76(15)
N2	C13	C14	C19	3.77(12)	C26	C27	C28	C23	0.63(13)
N2	C13	C18	C17	-178.76(8)	C26	C27	C28	C29	176.70(9)
N2	C13	C18	C21	-0.87(12)	C27	C28	C29	N3	177.67(8)
N3	Ru1	C22	C23	-23.38(8)	C28	C23	C24	C25	-1.05(14)
N3	C30	C31	C32	-175.64(8)	C29	N3	C30	C31	-49.53(11)
N3	C30	C35	C34	176.59(8)	C29	N3	C30	C35	134.63(8)
N4	C39	C40	C41	-179.56(9)	C30	N3	C29	C28	174.87(7)
N4	C39	C40	C45	0.04(10)	C30	C31	C32	C33	-0.72(13)
C1	Ru1	C22	C23	159.12(8)	C31	C30	C35	C34	0.74(13)
C1	N1	C2	C3	5.84(11)	C31	C32	C33	C34	0.38(13)
C1	N1	C4	C5	95.60(11)	C31	C32	C33	C36	177.17(8)
C1	N1	C4	C9	-88.53(11)	C32	C33	C34	C35	0.53(13)
C1	N2	C3	C2	6.05(11)	C32	C33	C36	O1	127.08(9)
C1	N2	C13	C14	78.62(11)	C33	C34	C35	C30	-1.08(13)
C1	N2	C13	C18	-107.48(10)	C34	C33	C36	O1	-56.21(11)
C2	N1	C1	Ru1	167.79(7)	C35	C30	C31	C32	0.16(13)
C2	N1	C1	N2	-2.28(10)	C36	O1	C37	O2	4.05(13)
C2	N1	C4	C5	-85.55(10)	C36	O1	C37	C38	-173.31(7)
C2	N1	C4	C9	90.32(10)	C36	C33	C34	C35	-176.21(8)

**Table 5.6.17. Torsion Angles for cs2809-[Ru] 2.**

A	B	C	D	Angle/°	A	B	C	D	Angle/°
C3	N2	C1	Ru1	-174.43(6)	C37	O1	C36	C33	-80.05(10)
C3	N2	C1	N1	-2.62(10)	C38	N4	C39	O3	-3.34(14)
C3	N2	C13	C14	-86.22(10)	C38	N4	C39	C40	177.37(7)
C3	N2	C13	C18	87.68(11)	C38	N4	C46	O4	0.91(14)
C4	N1	C1	Ru1	-13.33(14)	C38	N4	C46	C45	-178.30(8)
C4	N1	C1	N2	176.61(8)	C39	N4	C38	C37	-82.63(10)
C4	N1	C2	C3	-173.19(8)	C39	N4	C46	O4	176.25(9)
C4	C5	C6	C7	-1.93(13)	C39	N4	C46	C45	-2.96(10)
C5	C4	C9	C8	1.94(13)	C39	C40	C41	C42	-178.74(9)
C5	C4	C9	C12	-176.59(9)	C39	C40	C45	C44	179.03(8)
C5	C6	C7	C8	2.75(14)	C39	C40	C45	C46	-1.80(10)
C5	C6	C7	C11	-175.60(10)	C40	C41	C42	C43	-1.01(14)
C6	C7	C8	C9	-1.20(15)	C40	C45	C46	O4	-176.26(9)
C7	C8	C9	C4	-1.09(14)	C40	C45	C46	N4	2.90(9)
C7	C8	C9	C12	177.44(10)	C41	C40	C45	C44	-1.32(14)
C9	C4	C5	C6	-0.48(12)	C41	C40	C45	C46	177.84(8)
C9	C4	C5	C10	178.88(8)	C41	C42	C43	C44	-0.11(15)
C10	C5	C6	C7	178.71(9)	C42	C43	C44	C45	0.55(14)
C11	C7	C8	C9	177.14(10)	C43	C44	C45	C40	0.15(14)
C13	N2	C1	Ru1	20.03(11)	C43	C44	C45	C46	-178.82(9)
C13	N2	C1	N1	-168.16(8)	C44	C45	C46	O4	2.82(16)
C13	N2	C3	C2	172.48(8)	C44	C45	C46	N4	-178.03(9)
C13	C14	C15	C16	-2.40(13)	C45	C40	C41	C42	1.71(13)
C14	C13	C18	C17	-5.04(12)	C46	N4	C38	C37	92.25(10)
C14	C13	C18	C21	172.86(8)	C46	N4	C39	O3	-178.81(9)
C14	C15	C16	C17	-1.90(14)	C46	N4	C39	C40	1.90(10)



## Experimental

A brown prism (0.04 x 0.14 x 0.22 mm<sup>3</sup>) was centered on the goniometer of a Rigaku Oxford Diffraction Synergy-S diffractometer equipped with a HyPix6000HE detector and operating with MoK $\alpha$  radiation. The data collection routine, unit cell refinement, and data processing were carried out with the program CrysAlisPro.<sup>97</sup> The Laue symmetry was consistent with the triclinic space groups P1 and P-1. The centrosymmetric space group P-1 was chosen. The structure was solved using SHELXT<sup>98</sup> and refined using SHELXL<sup>99</sup> via Olex2.<sup>100</sup> A 2-position model was used for a disordered CH<sub>2</sub>Cl<sub>2</sub> molecule with relative occupancies that refined to 0.6303(19) and 0.3697(19). The final refinement model involved anisotropic displacement

(97) CrysAlisPro Software System, v1.171.42.xx, Rigaku Oxford Diffraction, **2022**, Rigaku Corporation, Oxford, UK.

(98) Sheldrick, G. M. "SHELXT – Integrated space-group and crystal structure determination." *Acta Cryst.* **2015**, *A71*, 3–8.

(99) Sheldrick, G. M. "Crystal structure refinement with SHELXL." *Acta Cryst.* **2015**, *C71*, 3–8.

(100) Dolomanov, O.V.; Bourhis, L. J.; Gildea, R. J.; Howard, J. A. K.; Puschmann, H. *J. Appl. Cryst.* **2009**, *42*, 339–341.

parameters for non-hydrogen atoms and a riding model for all hydrogen atoms. Olex2<sup>101</sup> was used for molecular graphics generation.

**Table 5.6.18. Crystal data and structure refinement for cs3021-inimer (2).**

Identification code	HA-2-61
Empirical formula	C <sub>48</sub> H <sub>50</sub> Cl <sub>4</sub> N <sub>4</sub> O <sub>4</sub> Ru
Formula weight	989.79
Temperature/K	99.97(13)
Crystal system	triclinic
Space group	P-1
a/Å	10.41900(10)
b/Å	14.4166(2)
c/Å	15.3529(2)
α/°	96.6040(10)
β/°	103.0170(10)
γ/°	91.3660(10)
Volume/Å <sup>3</sup>	2228.99(5)
Z	2
ρ <sub>calc</sub> /cm <sup>3</sup>	1.475
μ/mm <sup>1</sup>	0.641
F(000)	1020.0
Crystal size/mm <sup>3</sup>	0.22 × 0.14 × 0.043
Radiation	Mo Kα (λ = 0.71073)
2θ range for data collection/°	6.322 to 76.408
Index ranges	-17 ≤ h ≤ 17, -24 ≤ k ≤ 24, -25 ≤ l ≤ 26
Reflections collected	136110
Independent reflections	23450 [R <sub>int</sub> = 0.0453, R <sub>sigma</sub> = 0.0339]
Data/restraints/parameters	23450/0/575

---

(101) Dolomanov, O.V.; Bourhis, L. J.; Gildea, R. J.; Howard, J. A. K.; Puschmann, H. *J. Appl. Cryst.* **2009**, *42*, 339–341.

Goodness-of-fit on F2            1.044  
 Final R indexes [ $I \geq 2\sigma(I)$ ]    R1 = 0.0389, wR2 = 0.0978  
 Final R indexes [all data]        R1 = 0.0500, wR2 = 0.1021  
 Largest diff. peak/hole / e Å<sup>-3</sup>        1.72/-1.62

Crystal data as a footnote:

Crystal Data for cs3021. C<sub>48</sub>H<sub>50</sub>Cl<sub>4</sub>N<sub>4</sub>O<sub>4</sub>Ru (M = 989.79 g/mol): triclinic, space group P-1 (no. 2), a = 10.41900(10) Å, b = 14.4166(2) Å, c = 15.3529(2) Å, α = 96.6040(10)°, β = 103.0170(10)°, γ = 91.3660(10)°, V = 2228.99(5) Å<sup>3</sup>, Z = 2, T = 99.97(13) K, μ(Mo Kα) = 0.641 mm<sup>-1</sup>, D<sub>calc</sub> = 1.475 g/cm<sup>3</sup>, 136110 reflections measured (6.322° ≤ 2θ ≤ 76.408°), 23450 unique (R<sub>int</sub> = 0.0453, R<sub>sigma</sub> = 0.0339) which were used in all calculations. The final R1 was 0.0389 (I > 2σ(I)) and wR2 was 0.1021 (all data).

**Table 5.6.19. Bond Lengths for cs3021-inimer (2).**

Atom	Atom	Length/Å	Atom	Atom	Length/Å
Ru1	Cl1	2.3579(3)	C15	C16	1.395(2)
Ru1	Cl2	2.3522(3)	C16	C17	1.391(2)
Ru1	N3	2.0862(10)	C16	C20	1.5059(19)
Ru1	C1	2.0613(11)	C17	C18	1.3967(17)
Ru1	C22	1.8308(12)	C18	C21	1.5068(19)
O1	C36	1.2091(18)	C22	C23	1.4535(16)
O2	C36	1.3506(17)	C23	C24	1.4077(17)
O2	C37	1.4441(16)	C23	C28	1.4148(17)
O3	C39	1.2104(19)	C24	C25	1.3911(18)

O4	C46	1.205(2)	C25	C26	1.392(2)
N1	C1	1.3511(14)	C26	C27	1.386(2)
N1	C2	1.4715(15)	C27	C28	1.4036(17)
N1	C4	1.4348(15)	C28	C29	1.4515(18)
N2	C1	1.3428(14)	C30	C31	1.3978(18)
N2	C3	1.4758(15)	C30	C35	1.3930(18)
N2	C13	1.4273(15)	C31	C32	1.3878(18)
N3	C29	1.2880(16)	C32	C33	1.3963(19)
N3	C30	1.4246(16)	C33	C34	1.3891(18)
N4	C38	1.446(2)	C33	C36	1.4830(18)
N4	C39	1.385(2)	C34	C35	1.3855(18)
N4	C46	1.393(2)	C37	C38	1.523(2)
C2	C3	1.5238(17)	C39	C40	1.515(3)
C4	C5	1.4035(17)	C40	C41	1.572(3)
C4	C9	1.3990(17)	C40	C45	1.539(2)
C5	C6	1.3952(17)	C41	C42	1.516(3)
C5	C10	1.5017(18)	C41	C47	1.545(2)
C6	C7	1.3940(18)	C42	C43	1.317(4)
C7	C8	1.3876(18)	C43	C44	1.522(4)
C7	C11	1.5097(17)	C44	C45	1.571(2)
C8	C9	1.3991(16)	C44	C47	1.542(3)
C9	C12	1.5003(18)	C45	C46	1.504(3)
C13	C14	1.3970(17)	C13	C48A	1.699(3)
C13	C18	1.3969(18)	C13	C48B	1.987(6)
C14	C15	1.3983(18)	C14A	C48A	1.756(3)
C14	C19	1.500(2)	C14B	C48B	1.759(8)

**Table 5.6.20. Bond Angles for cs3021-inimer (2).**

Atom	Atom	Atom	Angle/°	Atom	Atom	Atom	Angle/°
Cl2	Ru1	Cl1	163.730(13)	C13	C18	C21	120.81(11)

N3	Ru1	Cl1	88.41(3)	C17	C18	C13	118.01(12)
N3	Ru1	Cl2	86.20(3)	C17	C18	C21	121.11(12)
C1	Ru1	Cl1	94.78(3)	C23	C22	Ru1	125.72(9)
C1	Ru1	Cl2	87.90(3)	C24	C23	C22	117.87(11)
C1	Ru1	N3	169.13(4)	C24	C23	C28	118.07(11)
C22	Ru1	Cl1	98.80(4)	C28	C23	C22	124.06(11)
C22	Ru1	Cl2	96.45(4)	C25	C24	C23	121.32(12)
C22	Ru1	N3	89.10(5)	C24	C25	C26	119.97(12)
C22	Ru1	C1	100.64(5)	C27	C26	C25	119.81(12)
C36	O2	C37	115.74(11)	C26	C27	C28	120.84(13)
C1	N1	C2	113.62(9)	C23	C28	C29	122.34(11)
C1	N1	C4	126.54(10)	C27	C28	C23	119.84(12)
C4	N1	C2	118.85(9)	C27	C28	C29	117.62(11)
C1	N2	C3	114.16(9)	N3	C29	C28	122.90(11)
C1	N2	C13	126.19(10)	C31	C30	N3	118.94(11)
C13	N2	C3	119.41(9)	C35	C30	N3	120.50(11)
C29	N3	Ru1	126.76(9)	C35	C30	C31	120.38(12)
C29	N3	C30	118.58(11)	C32	C31	C30	119.84(12)
C30	N3	Ru1	114.56(8)	C31	C32	C33	119.87(12)
C39	N4	C38	123.44(13)	C32	C33	C36	122.81(12)
C39	N4	C46	112.76(15)	C34	C33	C32	119.76(12)
C46	N4	C38	123.79(14)	C34	C33	C36	117.41(12)
N1	C1	Ru1	119.50(8)	C35	C34	C33	120.85(12)
N2	C1	Ru1	132.75(8)	C34	C35	C30	119.27(12)
N2	C1	N1	106.99(9)	O1	C36	O2	123.03(12)
N1	C2	C3	102.87(9)	O1	C36	C33	124.26(13)
N2	C3	C2	102.18(9)	O2	C36	C33	112.68(12)
C5	C4	N1	118.49(11)	O2	C37	C38	110.34(12)
C9	C4	N1	119.78(11)	N4	C38	C37	112.21(13)
C9	C4	C5	121.21(10)	O3	C39	N4	123.80(17)

C4	C5	C10	121.15(11)	O3	C39	C40	127.25(16)
C6	C5	C4	118.35(11)	N4	C39	C40	108.93(13)
C6	C5	C10	120.41(11)	C39	C40	C41	112.66(14)
C7	C6	C5	121.73(11)	C39	C40	C45	104.38(15)
C6	C7	C11	120.71(12)	C45	C40	C41	103.17(13)
C8	C7	C6	118.42(11)	C42	C41	C40	104.76(15)
C8	C7	C11	120.85(12)	C42	C41	C47	100.52(16)
C7	C8	C9	121.99(12)	C47	C41	C40	100.65(15)
C4	C9	C8	118.16(11)	C43	C42	C41	107.3(2)
C4	C9	C12	121.79(11)	C42	C43	C44	108.42(19)
C8	C9	C12	119.83(11)	C43	C44	C45	105.35(15)
C14	C13	N2	119.38(11)	C43	C44	C47	99.82(19)
C18	C13	N2	118.42(11)	C47	C44	C45	100.30(13)
C18	C13	C14	122.19(11)	C40	C45	C44	102.98(15)
C13	C14	C15	117.55(12)	C46	C45	C40	105.34(14)
C13	C14	C19	120.88(11)	C46	C45	C44	112.30(14)
C15	C14	C19	121.49(12)	O4	C46	N4	123.78(19)
C16	C15	C14	122.03(13)	O4	C46	C45	127.62(16)
C15	C16	C20	120.91(14)	N4	C46	C45	108.58(14)
C17	C16	C15	118.36(12)	C44	C47	C41	93.55(14)
C17	C16	C20	120.71(14)	Cl3	C48A	Cl4A	108.72(17)
C16	C17	C18	121.74(13)	Cl4B	C48B	Cl3	111.1(3)

**Table 5.6.21. Torsion Angles for cs3021-inimer (2).**

A	B	C	D	Angle/°	A	B	C	D	Angle/°
Ru1	N3	C29	C28	-10.46(19)	C20	C16	C17	C18	177.22(14)
Ru1	N3	C30	C31	-45.92(15)	C22	C23	C24	C25	176.00(12)
Ru1	N3	C30	C35	129.30(11)	C22	C23	C28	C27	-178.36(12)
Ru1	C22	C23	C24	-158.31(10)	C22	C23	C28	C29	6.8(2)
Ru1	C22	C23	C28	21.44(18)	C23	C24	C25	C26	2.6(2)

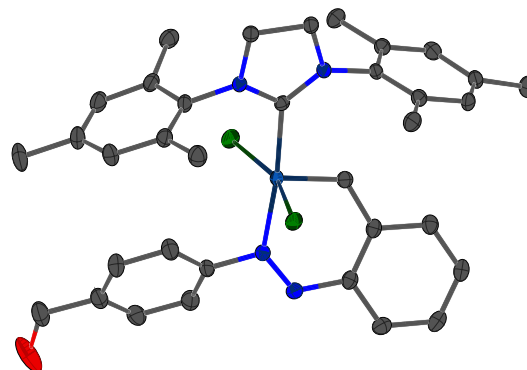
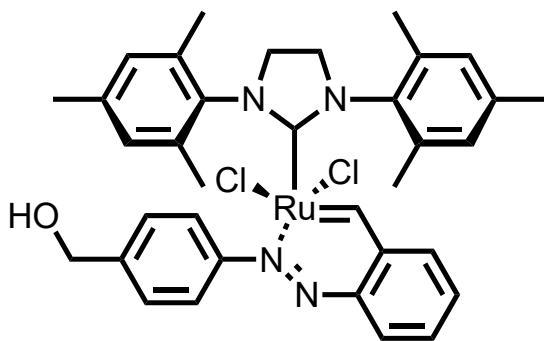
Cl1	Ru1	C22	C23	-118.98(10)	C23	C28	C29	N3	-11.1(2)
Cl2	Ru1	C22	C23	55.35(11)	C24	C23	C28	C27	1.39(19)
O2	C37	C38	N4	57.61(17)	C24	C23	C28	C29	-173.47(12)
O3	C39	C40	C41	-68.0(2)	C24	C25	C26	C27	1.1(2)
O3	C39	C40	C45	-179.20(16)	C25	C26	C27	C28	-3.5(2)
N1	C2	C3	N2	4.01(13)	C26	C27	C28	C23	2.2(2)
N1	C4	C5	C6	-176.02(10)	C26	C27	C28	C29	177.28(13)
N1	C4	C5	C10	0.35(16)	C27	C28	C29	N3	173.97(13)
N1	C4	C9	C8	176.11(10)	C28	C23	C24	C25	-3.76(19)
N1	C4	C9	C12	1.48(17)	C29	N3	C30	C31	130.77(14)
N2	C13	C14	C15	179.38(11)	C29	N3	C30	C35	-54.00(18)
N2	C13	C14	C19	2.50(18)	C30	N3	C29	C28	173.29(12)
N2	C13	C18	C17	-177.24(11)	C30	C31	C32	C33	-0.5(2)
N2	C13	C18	C21	-0.30(17)	C31	C30	C35	C34	0.6(2)
N3	Ru1	C22	C23	-30.73(11)	C31	C32	C33	C34	1.3(2)
N3	C30	C31	C32	174.72(13)	C31	C32	C33	C36	-177.14(13)
N3	C30	C35	C34	-174.52(12)	C32	C33	C34	C35	-1.2(2)
N4	C39	C40	C41	110.38(15)	C32	C33	C36	O1	-177.36(14)
N4	C39	C40	C45	-0.84(16)	C32	C33	C36	O2	4.34(19)
C1	Ru1	C22	C23	144.42(10)	C33	C34	C35	C30	0.2(2)
C1	N1	C2	C3	-3.84(15)	C34	C33	C36	O1	4.1(2)
C1	N1	C4	C5	-85.01(15)	C34	C33	C36	O2	-174.18(12)
C1	N1	C4	C9	103.12(15)	C35	C30	C31	C32	-0.5(2)
C1	N2	C3	C2	-3.46(15)	C36	O2	C37	C38	77.99(16)
C1	N2	C13	C14	-101.19(14)	C36	C33	C34	C35	177.34(13)
C1	N2	C13	C18	79.01(16)	C37	O2	C36	O1	5.3(2)
C2	N1	C1	Ru1	173.05(9)	C37	O2	C36	C33	-176.38(11)
C2	N1	C1	N2	1.81(15)	C38	N4	C39	O3	-0.4(2)
C2	N1	C4	C5	82.87(14)	C38	N4	C39	C40	-178.88(13)
C2	N1	C4	C9	-89.00(14)	C38	N4	C46	O4	1.4(2)

C3	N2	C1	Ru1	-168.40(10)		C38	N4	C46	C45	179.85(13)
C3	N2	C1	N1	1.21(14)		C39	N4	C38	C37	88.95(17)
C3	N2	C13	C14	84.88(15)		C39	N4	C46	O4	-177.32(15)
C3	N2	C13	C18	-94.91(14)		C39	N4	C46	C45	1.13(17)
C4	N1	C1	Ru1	-18.53(17)		C39	C40	C41	C42	179.39(15)
C4	N1	C1	N2	170.22(11)		C39	C40	C41	C47	-76.62(17)
C4	N1	C2	C3	-173.23(11)		C39	C40	C45	C44	119.27(15)
C4	C5	C6	C7	1.34(17)		C39	C40	C45	C46	1.43(15)
C5	C4	C9	C8	4.47(17)		C40	C41	C42	C43	70.79(18)
C5	C4	C9	C12	-170.17(11)		C40	C41	C47	C44	-57.38(17)
C5	C6	C7	C8	1.25(18)		C40	C45	C46	O4	176.79(16)
C5	C6	C7	C11	179.54(11)		C40	C45	C46	N4	-1.58(16)
C6	C7	C8	C9	-1.03(18)		C41	C40	C45	C44	1.34(18)
C7	C8	C9	C4	-1.77(17)		C41	C40	C45	C46	-116.50(14)
C7	C8	C9	C12	172.97(11)		C41	C42	C43	C44	0.0(2)
C9	C4	C5	C6	-4.26(17)		C42	C41	C47	C44	50.00(18)
C9	C4	C5	C10	172.10(11)		C42	C43	C44	C45	-70.3(2)
C10	C5	C6	C7	-175.05(11)		C42	C43	C44	C47	33.34(18)
C11	C7	C8	C9	-179.32(11)		C43	C44	C45	C40	65.60(18)
C13	N2	C1	Ru1	17.40(19)		C43	C44	C45	C46	178.43(16)
C13	N2	C1	N1	-172.99(11)		C43	C44	C47	C41	-49.51(16)
C13	N2	C3	C2	171.17(11)		C44	C45	C46	O4	65.4(2)
C13	C14	C15	C16	-2.39(19)		C44	C45	C46	N4	-112.94(15)
C14	C13	C18	C17	2.97(18)		C45	C40	C41	C42	-68.64(18)
C14	C13	C18	C21	179.91(12)		C45	C40	C41	C47	35.34(17)
C14	C15	C16	C17	3.3(2)	C45	C44	C47	C41		58.22(18)
C14	C15	C16	C20	-174.94(14)		C46	N4	C38	C37	-89.64(17)
C15	C16	C17	C18	-1.0(2)	C46	N4	C39	O3		178.28(15)
C16	C17	C18	C13	-2.00(19)		C46	N4	C39	C40	-0.16(17)
C16	C17	C18	C21	-178.93(13)		C47	C41	C42	C43	-33.29(19)

C18	C13	C14	C15	-0.83(18)	C47	C44	C45	C40	-37.67(19)
C18	C13	C14	C19	-177.71(12)	C47	C44	C45	C46	75.15(19)
C19	C14	C15	C16	174.46(13)					

This report has been created with Olex2, compiled on 2023.03.06 svn.rbb2c1857 for OlexSys.

Please let us know if there are any errors or if you would like to have additional features.



(17)

## Experimental

A brown plate (0.04 x 0.17 x 0.22 mm<sup>3</sup>) was centered on a Rigaku Oxford Diffraction Synergy-S diffractometer equipped with a HyPix6000HE detector and operating with CuK $\alpha$  radiation. The crystal screening, data collection, unit cell refinement, and data processing were carried out with the program CrysAlisPro.<sup>102</sup> The Laue symmetry and systematic absences were consistent with the monoclinic space groups *I2/a* and *Ia*. The centrosymmetric space group *I2/a*

---

(102) CrysAlisPro Software System, v1.171.40.68a, Rigaku Oxford Diffraction, 2020, Rigaku Corporation, Oxford, UK.

was chosen. The structure was solved using SHELXT<sup>103</sup> and refined using SHELXL<sup>104</sup> via Olex2.<sup>105</sup> The final refinement model involved anisotropic displacement parameters for non-hydrogen atoms and a riding model for all hydrogen atoms. Olex2<sup>106</sup> was used for molecular graphics generation.

**Table 5.6.22.** Crystal data and structure refinement for cs2583-catalyst 17.

Identification code	HA-52	
Empirical formula	C <sub>35</sub> H <sub>38</sub> Cl <sub>2</sub> N <sub>4</sub> ORu •CH <sub>2</sub> Cl <sub>2</sub>	
Formula weight	787.59	
Temperature	100.00(12) K	
Wavelength	1.54184 Å	
Crystal system	Monoclinic	
Space group	C 1 2/c 1	
Unit cell dimensions	$a = 28.8949(7) \text{ \AA}$	$\alpha = 90^\circ$ .
	$b = 9.8707(2) \text{ \AA}$	$\beta = 119.907(3)^\circ$ .
	$c = 27.8656(6) \text{ \AA}$	$\gamma = 90^\circ$ .
Volume	6889.3(3) Å <sup>3</sup>	
Z	8	
Density (calculated)	1.519 g/cm <sup>3</sup>	
Absorption coefficient	6.819 mm <sup>-1</sup>	
F(000)	3232	
Crystal size	0.224 x 0.174 x 0.038 mm <sup>3</sup>	
Theta range for data collection	3.529 to 76.934°	
Index ranges	$-36 \leq h \leq 36, -11 \leq k \leq 12, -35 \leq l \leq 35$	

(103) Sheldrick, G. M. "SHELXT – Integrated space-group and crystal structure determination." *Acta Cryst.* **2015**, *A71*, 3–8.

(104) Sheldrick, G. M. "Crystal structure refinement with SHELXL." *Acta Cryst.* **2015**, *C71*, 3–8.

(105) Dolomanov, O.V.; Bourhis, L. J.; Gildea, R. J.; Howard, J. A. K.; Puschmann, H. *J. Appl. Cryst.* **2009**, *42*, 339–341.

(106) Dolomanov, O.V.; Bourhis, L. J.; Gildea, R. J.; Howard, J. A. K.; Puschmann, H. *J. Appl. Cryst.* **2009**, *42*, 339–341.

Reflections collected	54759
Independent reflections	7186 [R(int) = 0.0486]
Completeness to theta = 67.684°	99.5 %
Absorption correction	Gaussian
Max. and min. transmission	1.000 and 0.342
Refinement method	Full-matrix least-squares on F <sup>2</sup>
Data / restraints / parameters	7186 / 0 / 422
Goodness-of-fit on F <sup>2</sup>	1.041
Final R indices [I > 2σ (I)]	R1 = 0.0358, wR2 = 0.0974
R indices (all data)	R1 = 0.0382, wR2 = 0.0993
Extinction coefficient	n/a
Largest diff. peak and hole	0.906 and -1.154 e•Å <sup>-3</sup>

---

**Table 5.6.23.** Bond lengths [Å] and angles [°] for cs2583-catalyst 17.

Ru(1)-Cl(1)	2.3485(5)	C(2)-C(3)	1.390(3)	C(20)-C(21)	1.396(4)
Ru(1)-Cl(2)	2.3340(5)	C(3)-C(4)	1.390(4)	C(21)-C(22)	1.377(4)
Ru(1)-N(1)	2.0402(19)	C(4)-C(5)	1.392(4)	C(21)-C(25)	1.513(3)
Ru(1)-C(14)	1.838(2)	C(4)-C(7)	1.504(3)	C(22)-C(23)	1.393(3)
Ru(1)-C(15)	2.112(2)	C(5)-C(6)	1.386(4)	C(23)-C(26)	1.497(3)
O(1)-C(7)	1.341(4)	C(8)-C(9)	1.404(3)	C(27)-C(28)	1.398(3)
N(1)-N(2)	1.275(3)	C(8)-C(13)	1.407(3)	C(27)-C(32)	1.404(3)
N(1)-C(1)	1.439(3)	C(9)-C(10)	1.383(3)	C(28)-C(29)	1.392(3)
N(2)-C(8)	1.398(3)	C(10)-C(11)	1.391(4)	C(28)-C(33)	1.511(3)
N(3)-C(15)	1.343(3)	C(11)-C(12)	1.384(3)	C(29)-C(30)	1.403(4)
N(3)-C(16)	1.477(3)	C(12)-C(13)	1.407(3)	C(30)-C(31)	1.393(4)
N(3)-C(18)	1.440(3)	C(13)-C(14)	1.447(3)	C(30)-C(34)	1.508(3)
N(4)-C(15)	1.339(3)	C(16)-C(17)	1.528(3)	C(31)-C(32)	1.394(3)
N(4)-C(17)	1.481(3)	C(18)-C(19)	1.394(3)	C(32)-C(35)	1.508(3)
N(4)-C(27)	1.435(3)	C(18)-C(23)	1.417(3)	Cl(3)-C(36)	1.754(3)
C(1)-C(2)	1.389(3)	C(19)-C(20)	1.401(3)	Cl(4)-C(36)	1.763(3)
C(1)-C(6)	1.387(3)	C(19)-C(24)	1.509(3)		
Cl(2)-Ru(1)-Cl(1)	161.00(2)	C(15)-N(3)-C(16)	113.89(18)		
N(1)-Ru(1)-Cl(1)	87.66(5)	C(15)-N(3)-C(18)	126.22(19)		
N(1)-Ru(1)-Cl(2)	89.37(5)	C(18)-N(3)-C(16)	119.27(18)		
N(1)-Ru(1)-C(15)	171.66(8)	C(15)-N(4)-C(17)	113.89(18)		
C(14)-Ru(1)-Cl(1)	99.73(7)	C(15)-N(4)-C(27)	126.62(18)		
C(14)-Ru(1)-Cl(2)	98.96(7)	C(27)-N(4)-C(17)	119.19(17)		
C(14)-Ru(1)-N(1)	88.84(9)	C(2)-C(1)-N(1)	118.8(2)		
C(14)-Ru(1)-C(15)	98.90(9)	C(6)-C(1)-N(1)	120.5(2)		
C(15)-Ru(1)-Cl(1)	87.95(6)	C(6)-C(1)-C(2)	120.6(2)		
C(15)-Ru(1)-Cl(2)	92.48(6)	C(1)-C(2)-C(3)	119.2(2)		
N(2)-N(1)-Ru(1)	132.04(15)	C(2)-C(3)-C(4)	120.6(2)		
N(2)-N(1)-C(1)	111.72(19)	C(3)-C(4)-C(5)	119.5(2)		
C(1)-N(1)-Ru(1)	116.12(15)	C(3)-C(4)-C(7)	119.4(2)		
N(1)-N(2)-C(8)	118.20(19)	C(5)-C(4)-C(7)	121.1(2)		

C(6)-C(5)-C(4)	120.2(2)	C(20)-C(19)-C(24)	119.2(2)
C(5)-C(6)-C(1)	119.8(2)	C(21)-C(20)-C(19)	121.6(3)
O(1)-C(7)-C(4)	116.4(3)	C(20)-C(21)-C(25)	121.1(3)
N(2)-C(8)-C(9)	113.8(2)	C(22)-C(21)-C(20)	118.6(2)
N(2)-C(8)-C(13)	125.9(2)	C(22)-C(21)-C(25)	120.3(3)
C(9)-C(8)-C(13)	120.3(2)	C(21)-C(22)-C(23)	122.6(2)
C(10)-C(9)-C(8)	120.4(2)	C(18)-C(23)-C(26)	122.9(2)
C(9)-C(10)-C(11)	120.0(2)	C(22)-C(23)-C(18)	117.4(2)
C(12)-C(11)-C(10)	120.1(2)	C(22)-C(23)-C(26)	119.6(2)
C(11)-C(12)-C(13)	121.3(2)	C(28)-C(27)-N(4)	118.82(19)
C(8)-C(13)-C(12)	117.9(2)	C(28)-C(27)-C(32)	121.6(2)
C(8)-C(13)-C(14)	124.0(2)	C(32)-C(27)-N(4)	119.6(2)
C(12)-C(13)-C(14)	118.0(2)	C(27)-C(28)-C(33)	121.4(2)
C(13)-C(14)-Ru(1)	125.03(17)	C(29)-C(28)-C(27)	118.2(2)
N(3)-C(15)-Ru(1)	120.12(15)	C(29)-C(28)-C(33)	120.4(2)
N(4)-C(15)-Ru(1)	132.05(16)	C(28)-C(29)-C(30)	121.9(2)
N(4)-C(15)-N(3)	107.40(19)	C(29)-C(30)-C(34)	120.4(2)
N(3)-C(16)-C(17)	102.41(17)	C(31)-C(30)-C(29)	118.2(2)
N(4)-C(17)-C(16)	102.29(17)	C(31)-C(30)-C(34)	121.4(2)
C(19)-C(18)-N(3)	119.6(2)	C(30)-C(31)-C(32)	121.9(2)
C(19)-C(18)-C(23)	121.5(2)	C(27)-C(32)-C(35)	120.9(2)
C(23)-C(18)-N(3)	118.6(2)	C(31)-C(32)-C(27)	118.2(2)
C(18)-C(19)-C(20)	118.1(2)	C(31)-C(32)-C(35)	120.9(2)
C(18)-C(19)-C(24)	122.7(2)	Cl(3)-C(36)-Cl(4)	111.83(16)

---

**Table 5.6.24.** Torsion angles [°] for cs2583-catalyst 17.

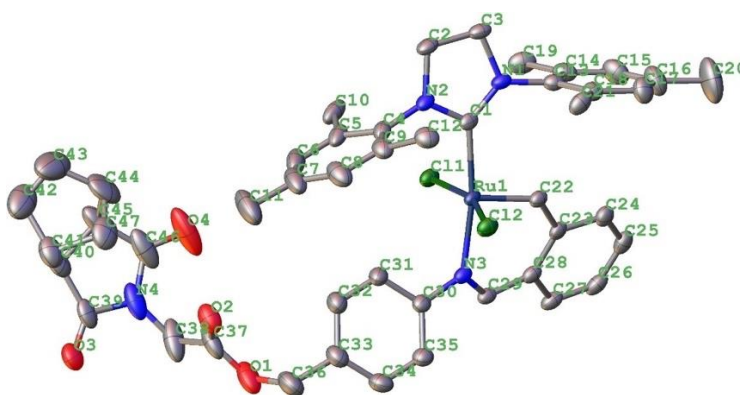
Ru(1)-N(1)-N(2)-C(8)	-10.3(3)	C(5)-C(4)-C(7)-O(1)	15.9(4)
Ru(1)-N(1)-C(1)-C(2)	-32.3(3)	C(6)-C(1)-C(2)-C(3)	3.1(4)
Ru(1)-N(1)-C(1)-C(6)	146.19(19)	C(7)-C(4)-C(5)-C(6)	179.9(2)
Cl(1)-Ru(1)-C(14)-C(13)	64.20(19)	C(8)-C(9)-C(10)-C(11)	-2.7(4)
Cl(2)-Ru(1)-C(14)-C(13)	-112.41(18)	C(8)-C(13)-C(14)-Ru(1)	14.5(3)
N(1)-Ru(1)-C(14)-C(13)	-23.23(19)	C(9)-C(8)-C(13)-C(12)	1.9(3)
N(1)-N(2)-C(8)-C(9)	173.4(2)	C(9)-C(8)-C(13)-C(14)	-175.2(2)
N(1)-N(2)-C(8)-C(13)	-10.2(3)	C(9)-C(10)-C(11)-C(12)	1.1(4)
N(1)-C(1)-C(2)-C(3)	-178.5(2)	C(10)-C(11)-C(12)-C(13)	2.2(4)
N(1)-C(1)-C(6)-C(5)	179.6(2)	C(11)-C(12)-C(13)-C(8)	-3.6(3)
N(2)-N(1)-C(1)-C(2)	144.1(2)	C(11)-C(12)-C(13)-C(14)	173.7(2)
N(2)-N(1)-C(1)-C(6)	-37.4(3)	C(12)-C(13)-C(14)-Ru(1)	-162.68(17)
N(2)-C(8)-C(9)-C(10)	177.8(2)	C(13)-C(8)-C(9)-C(10)	1.2(3)
N(2)-C(8)-C(13)-C(12)	-174.3(2)	C(15)-Ru(1)-C(14)-C(13)	153.63(18)
N(2)-C(8)-C(13)-C(14)	8.6(4)	C(15)-N(3)-C(16)-C(17)	-3.1(2)
N(3)-C(16)-C(17)-N(4)	3.1(2)	C(15)-N(3)-C(18)-C(19)	101.4(3)
N(3)-C(18)-C(19)-C(20)	178.5(2)	C(15)-N(3)-C(18)-C(23)	-84.7(3)
N(3)-C(18)-C(19)-C(24)	0.4(4)	C(15)-N(4)-C(17)-C(16)	-2.6(2)
N(3)-C(18)-C(23)-C(22)	180.0(2)	C(15)-N(4)-C(27)-C(28)	81.5(3)
N(3)-C(18)-C(23)-C(26)	-3.8(3)	C(15)-N(4)-C(27)-C(32)	-97.9(3)
N(4)-C(27)-C(28)-C(29)	-176.8(2)	C(16)-N(3)-C(15)-Ru(1)	175.00(14)
N(4)-C(27)-C(28)-C(33)	0.8(3)	C(16)-N(3)-C(15)-N(4)	1.7(2)
N(4)-C(27)-C(32)-C(31)	175.8(2)	C(16)-N(3)-C(18)-C(19)	-88.1(3)
N(4)-C(27)-C(32)-C(35)	-3.7(3)	C(16)-N(3)-C(18)-C(23)	85.8(3)
C(1)-N(1)-N(2)-C(8)	174.03(19)	C(17)-N(4)-C(15)-Ru(1)	-171.54(16)
C(1)-C(2)-C(3)-C(4)	-2.0(4)	C(17)-N(4)-C(15)-N(3)	0.7(2)
C(2)-C(1)-C(6)-C(5)	-1.9(4)	C(17)-N(4)-C(27)-C(28)	-91.9(2)
C(2)-C(3)-C(4)-C(5)	-0.2(4)	C(17)-N(4)-C(27)-C(32)	88.7(3)
C(2)-C(3)-C(4)-C(7)	-178.8(2)	C(18)-N(3)-C(15)-Ru(1)	-14.1(3)
C(3)-C(4)-C(5)-C(6)	1.4(4)	C(18)-N(3)-C(15)-N(4)	172.5(2)
C(3)-C(4)-C(7)-O(1)	-165.7(3)	C(18)-N(3)-C(16)-C(17)	-174.71(19)
C(4)-C(5)-C(6)-C(1)	-0.3(4)	C(18)-C(19)-C(20)-C(21)	-0.3(4)

C(19)-C(18)-C(23)-C(22)	-6.2(4)
C(19)-C(18)-C(23)-C(26)	169.9(2)
C(19)-C(20)-C(21)-C(22)	-2.3(4)
C(19)-C(20)-C(21)-C(25)	178.9(3)
C(20)-C(21)-C(22)-C(23)	0.7(4)
C(21)-C(22)-C(23)-C(18)	3.5(4)
C(21)-C(22)-C(23)-C(26)	-172.9(2)
C(23)-C(18)-C(19)-C(20)	4.7(4)
C(23)-C(18)-C(19)-C(24)	-173.3(2)
C(24)-C(19)-C(20)-C(21)	177.7(3)
C(25)-C(21)-C(22)-C(23)	179.5(3)
C(27)-N(4)-C(15)-Ru(1)	14.8(3)
C(27)-N(4)-C(15)-N(3)	-173.01(19)
C(27)-N(4)-C(17)-C(16)	171.66(18)
C(27)-C(28)-C(29)-C(30)	1.0(4)
C(28)-C(27)-C(32)-C(31)	-3.6(3)
C(28)-C(27)-C(32)-C(35)	176.9(2)
C(28)-C(29)-C(30)-C(31)	-3.3(4)
C(28)-C(29)-C(30)-C(34)	175.0(2)
C(29)-C(30)-C(31)-C(32)	2.3(4)
C(30)-C(31)-C(32)-C(27)	1.1(3)
C(30)-C(31)-C(32)-C(35)	-179.4(2)
C(32)-C(27)-C(28)-C(29)	2.6(3)
C(32)-C(27)-C(28)-C(33)	-179.8(2)
C(33)-C(28)-C(29)-C(30)	-176.7(2)
C(34)-C(30)-C(31)-C(32)	-176.0(2)

**Table 5.6.25.** Hydrogen bonds for cs2583-catalyst 17 [ $\text{\AA}$  and  $^\circ$ ].

D-H...A	d(D-H)	d(H...A)	d(D...A)	$\angle(\text{DHA})$
O(1)-H(1)...N(2)#1	0.84	2.20	3.008(3)	162.0

Symmetry transformations used to generate equivalent atoms: #1  $-x+1, y, -z+1/2$



inimer (**3**)

Crystals of the ROMP inimer (**3**) were obtained by layering saturated solutions in  $\text{CH}_2\text{Cl}_2$  with hexane and subsequent diffusion at  $-18^\circ\text{C}$ . The inimer crystallized as an unsolvated yellow-brown plate. A yellow-brown plate ( $0.03 \times 0.16 \times 0.39 \text{ mm}^3$ ) was centered on the goniometer of a Rigaku Oxford Diffraction Synergy-S diffractometer equipped with a HyPix6000HE detector and operating with MoK $\alpha$  radiation. The data collection routine, unit cell refinement, and data processing were carried out with the program CrysAlisPro.<sup>1</sup> The Laue symmetry and systematic absences were consistent with the monoclinic space group  $P2_1/n$ . The structure was solved using SHELXT2 and refined

using SHELXL3 via Olex2.<sup>4</sup> After modeling the main molecule, residual electron density suggested the presence of disordered CH<sub>2</sub>Cl<sub>2</sub> and hexanes. A satisfactory model for the solvent could not be obtained. The solvent mask feature of Olex2 was used and calculated 55.5 e<sup>-</sup> and 216 Å<sup>3</sup> void space per asymmetric unit (222 e<sup>-</sup> in 864 Å<sup>3</sup> per unit cell), approximated as 1CH<sub>2</sub>Cl<sub>2</sub> and ½C<sub>6</sub>H<sub>14</sub>, corresponding to 67 e<sup>-</sup>/asymmetric unit. The final refinement model involved anisotropic displacement parameters for non-hydrogen atoms and a riding model for all hydrogen atoms. Olex2<sup>5</sup> was used for molecular graphics generation.

**Table 5.6.26. Crystal data and structure refinement for cs2743-inimer (3).**

Identification code	HA-61
Empirical formula	C <sub>47</sub> H <sub>48</sub> Cl <sub>2</sub> N <sub>4</sub> O <sub>4</sub> Ru•CH <sub>2</sub> Cl <sub>2</sub> •0.5(C <sub>6</sub> H <sub>14</sub> )
Formula weight	1032.87
Temperature/K	99.99(13)
Crystal system	monoclinic
Space group	P2 <sub>1</sub> /n
a/Å	19.1975(3)
b/Å	10.02560(10)
c/Å	25.2080(5)
α/°	90
β/°	105.677(2)
γ/°	90

Volume/Å <sup>3</sup>	4671.21(13)
Z	4
ρ <sub>calc</sub> /cm <sup>3</sup>	1.409
μ/mm <sup>1</sup>	0.615
F(000)	1872.0
Crystal size/mm <sup>3</sup>	0.39 × 0.16 × 0.03
Radiation	Mo Kα (λ = 0.71073)
2θ range for data collection/°	5.116 to 67.444
Index ranges	-24 ≤ h ≤ 29, -15 ≤ k ≤ 14, -38 ≤ l ≤ 37
Reflections collected	100321
Independent reflections	16658 [R <sub>int</sub> = 0.0363, R <sub>sigma</sub> = 0.0280]
Data/restraints/parameters	16658/0/529
Goodness-of-fit on F <sup>2</sup>	1.037
Final R indexes [I ≥ 2σ (I)]	R <sub>1</sub> = 0.0358, wR <sub>2</sub> = 0.0877
Final R indexes [all data]	R <sub>1</sub> = 0.0463, wR <sub>2</sub> = 0.0913
Largest diff. peak/hole / e Å <sup>-3</sup>	1.40/-0.66

**Table 5.6.27. Bond Lengths for cs2743-inimer (3).**

Atom	Atom	Length/Å	Atom	Atom	Length/Å
Ru1	C11	2.3444(3)	C14	C15	1.387(3)
Ru1	C12	2.3461(4)	C14	C19	1.505(2)
Ru1	N3	2.1057(12)	C15	C16	1.390(3)

Ru1	C1	2.0582(14)	C16	C17	1.388(3)
Ru1	C22	1.8264(15)	C16	C20	1.520(3)
O1	C36	1.454(3)	C17	C18	1.390(2)
O1	C37	1.337(3)	C18	C21	1.499(2)
O2	C37	1.193(3)	C22	C23	1.451(2)
O3	C39	1.203(3)	C23	C24	1.400(2)
O4	C46	1.220(3)	C23	C28	1.417(2)
N1	C1	1.3440(19)	C24	C25	1.392(2)
N1	C3	1.4811(19)	C25	C26	1.386(3)
N1	C13	1.430(2)	C26	C27	1.382(2)
N2	C1	1.3491(19)	C27	C28	1.398(2)
N2	C2	1.4729(19)	C28	C29	1.440(2)
N2	C4	1.425(2)	C30	C31	1.397(2)
N3	C29	1.2914(19)	C30	C35	1.393(2)
N3	C30	1.424(2)	C31	C32	1.382(2)
N4	C38	1.444(4)	C32	C33	1.394(3)
N4	C39	1.386(2)	C33	C34	1.388(3)
N4	C46	1.391(4)	C33	C36	1.507(3)
C2	C3	1.519(2)	C34	C35	1.386(3)
C4	C5	1.412(2)	C37	C38	1.513(3)
C4	C9	1.397(3)	C39	C40	1.491(3)
C5	C6	1.388(3)	C40	C41	1.543(3)

C5	C10	1.507(3)	C40	C45	1.551(3)
C6	C7	1.378(4)	C41	C42	1.506(4)
C7	C8	1.398(3)	C41	C47	1.543(3)
C7	C11	1.513(3)	C42	C43	1.268(5)
C8	C9	1.392(3)	C43	C44	1.488(5)
C9	C12	1.507(2)	C44	C45	1.561(4)
C13	C14	1.398(2)	C44	C47	1.574(4)
C13	C18	1.401(2)	C45	C46	1.462(5)

**Table 5.6.28. Bond Angles for cs2743-inimer (3).**

Atom	Atom	Atom	Angle/°	Atom	Atom	Atom	Angle/°
C11	Ru1	C12	160.783(15)	C16	C17	C18	121.92(18)
N3	Ru1	C11	85.08(3)	C13	C18	C21	121.20(15)
N3	Ru1	C12	88.59(4)	C17	C18	C13	117.86(15)
C1	Ru1	C11	89.69(4)	C17	C18	C21	120.92(15)
C1	Ru1	C12	93.91(4)	C23	C22	Ru1	126.73(11)
C1	Ru1	N3	170.66(5)	C24	C23	C22	118.20(14)
C22	Ru1	C11	98.82(5)	C24	C23	C28	118.26(14)
C22	Ru1	C12	99.30(5)	C28	C23	C22	123.50(14)
C22	Ru1	N3	89.92(6)	C25	C24	C23	120.89(16)
C22	Ru1	C1	98.54(6)	C26	C25	C24	120.42(16)
C37	O1	C36	117.30(18)	C27	C26	C25	119.60(15)
C1	N1	C3	113.85(13)	C26	C27	C28	121.01(16)
C1	N1	C13	128.64(12)	C23	C28	C29	122.75(14)
C13	N1	C3	117.41(12)	C27	C28	C23	119.74(15)
C1	N2	C2	113.88(13)	C27	C28	C29	117.37(14)

C1	N2	C4	126.89(13)	N3	C29	C28	124.80(13)
C4	N2	C2	118.47(13)	C31	C30	N3	118.51(14)
C29	N3	Ru1	123.73(11)	C35	C30	N3	122.45(14)
C29	N3	C30	117.80(13)	C35	C30	C31	119.04(15)
C30	N3	Ru1	117.59(9)	C32	C31	C30	120.27(16)
C39	N4	C38	122.4(2)	C31	C32	C33	120.83(18)
C39	N4	C46	113.2(2)	C32	C33	C36	119.66(19)
C46	N4	C38	123.9(2)	C34	C33	C32	118.63(17)
N1	C1	Ru1	132.69(11)	C34	C33	C36	121.70(18)
N1	C1	N2	106.93(12)	C35	C34	C33	120.99(17)
N2	C1	Ru1	120.06(11)	C34	C35	C30	120.16(16)
N2	C2	C3	102.71(12)	O1	C36	C33	108.4(2)
N1	C3	C2	102.42(12)	O1	C37	C38	109.4(2)
C5	C4	N2	119.47(17)	O2	C37	O1	126.0(2)
C9	C4	N2	118.88(14)	O2	C37	C38	124.6(2)
C9	C4	C5	121.28(17)	N4	C38	C37	111.3(2)
C4	C5	C10	122.44(18)	O3	C39	N4	123.6(2)
C6	C5	C4	118.0(2)	O3	C39	C40	128.52(19)
C6	C5	C10	119.57(17)	N4	C39	C40	107.90(19)
C7	C6	C5	122.18(19)	C39	C40	C41	113.22(19)
C6	C7	C8	118.7(2)	C39	C40	C45	104.6(2)
C6	C7	C11	121.0(2)	C41	C40	C45	102.91(18)
C8	C7	C11	120.3(3)	C42	C41	C40	103.7(2)
C9	C8	C7	121.7(2)	C42	C41	C47	100.4(2)
C4	C9	C12	122.34(16)	C47	C41	C40	102.09(19)
C8	C9	C4	118.11(18)	C43	C42	C41	109.0(3)
C8	C9	C12	119.43(19)	C42	C43	C44	108.7(3)
C14	C13	N1	119.57(14)	C43	C44	C45	105.6(2)
C14	C13	C18	121.77(15)	C43	C44	C47	100.5(3)
C18	C13	N1	118.62(14)	C45	C44	C47	99.9(2)

C13	C14	C19	120.90(16)	C40	C45	C44	102.5(2)
C15	C14	C13	118.04(16)	C46	C45	C40	105.4(2)
C15	C14	C19	121.05(16)	C46	C45	C44	113.1(2)
C14	C15	C16	121.85(18)	O4	C46	N4	121.6(3)
C15	C16	C20	120.6(2)	O4	C46	C45	129.9(3)
C17	C16	C15	118.56(19)	N4	C46	C45	108.54(19)
C17	C16	C20	120.8(2)	C41	C47	C44	91.6(2)

**Table 5.6.29. Torsion Angles for cs2743-inimer (17).**

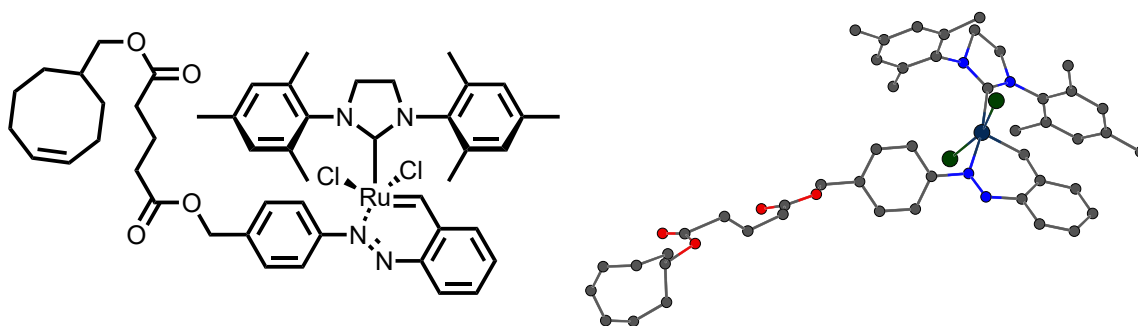
A	B	C	D	Angle/°	A	B	C	D	Angle/°
Ru1	N3	C29	C28	16.3(2)	C18	C13	C14	C19	179.84(15)
Ru1	N3	C30	C31	26.81(18)	C19	C14	C15	C16	-179.8(2)
Ru1	N3	C30	C35	-152.63(12)	C20	C16	C17	C18	-179.4(3)
Ru1	C22	C23	C24	161.91(12)	C22	C23	C24	C25	-174.26(14)
Ru1	C22	C23	C28	-15.5(2)	C22	C23	C28	C27	175.24(13)
Cl1	Ru1	C22	C23	-57.14(13)	C22	C23	C28	C29	-9.3(2)
Cl2	Ru1	C22	C23	116.42(12)	C23	C24	C25	C26	-1.9(2)
O1	C37	C38	N4	-176.8(2)	C23	C28	C29	N3	7.1(2)
O2	C37	C38	N4	3.8(4)	C24	C23	C28	C27	-2.2(2)
O3	C39	C40	C41	68.9(3)	C24	C23	C28	C29	173.28(13)
O3	C39	C40	C45	-179.8(2)	C24	C25	C26	C27	-0.7(2)
N1	C13	C14	C15	178.33(15)	C25	C26	C27	C28	1.8(2)
N1	C13	C14	C19	-2.7(2)	C26	C27	C28	C23	-0.3(2)
N1	C13	C18	C17	-177.99(15)	C26	C27	C28	C29	-176.06(14)
N1	C13	C18	C21	3.9(2)	C27	C28	C29	N3	-177.36(14)
N2	C2	C3	N1	-4.16(15)	C28	C23	C24	C25	3.3(2)
N2	C4	C5	C6	-177.12(15)	C29	N3	C30	C31	-142.82(15)
N2	C4	C5	C10	0.7(2)	C29	N3	C30	C35	37.7(2)
N2	C4	C9	C8	177.15(16)	C30	N3	C29	C28	-174.74(13)
N2	C4	C9	C12	1.1(2)	C30	C31	C32	C33	-0.5(3)

N3 Ru1 C22 C23 27.87(13)	C31 C30 C35 C34 2.9(2)
N3 C30 C31 C32 178.51(16)	C31 C32 C33 C34 2.1(3)
N3 C30 C35 C34 -177.64(15)	C31 C32 C33 C36 -177.3(2)
N4 C39 C40 C41 -111.31(18)	C32 C33 C34 C35 -1.2(3)
N4 C39 C40 C45 0.0(2)	C32 C33 C36 O1 67.1(3)
C1 Ru1 C22 C23 -148.16(13)	C33 C34 C35 C30 -1.3(3)
C1 N1 C3 C2 3.14(16)	C34 C33 C36 O1 -112.3(2)
C1 N1 C13 C14 96.92(18)	C35 C30 C31 C32 -2.0(3)
C1 N1 C13 C18 -85.55(19)	C36 O1 C37 O2 -3.6(3)
C1 N2 C2 C3 4.44(17)	C36 O1 C37 C38 177.1(2)
C1 N2 C4 C5 -101.02(18)	C36 C33 C34 C35 178.17(19)
C1 N2 C4 C9 85.92(19)	C37 O1 C36 C33 -102.9(2)
C2 N2 C1 Ru1 -176.96(10)	C38 N4 C39 O3 -4.9(3)
C2 N2 C1 N1 -2.62(17)	C38 N4 C39 C40 175.27(18)
C2 N2 C4 C5 89.63(18)	C38 N4 C46 O4 2.5(3)
C2 N2 C4 C9 -83.42(19)	C38 N4 C46 C45 -177.1(2)
C3 N1 C1 Ru1 172.83(10)	C39 N4 C38 C37 -98.3(2)
C3 N1 C1 N2 -0.50(16)	C39 N4 C46 O4 174.5(2)
C3 N1 C13 C14 -86.94(17)	C39 N4 C46 C45 -5.1(2)
C3 N1 C13 C18 90.59(17)	C39 C40 C41 C42 -179.40(19)
C4 N2 C1 Ru1 13.3(2)	C39 C40 C41 C47 76.6(2)
C4 N2 C1 N1 -172.38(14)	C39 C40 C45 C44 -121.4(2)
C4 N2 C2 C3 175.13(13)	C39 C40 C45 C46 -2.8(2)
C4 C5 C6 C7 2.4(3)	C40 C41 C42 C43 -71.4(3)
C5 C4 C9 C8 4.2(3)	C40 C41 C47 C44 58.1(2)
C5 C4 C9 C12 -171.77(16)	C40 C45 C46 O4 -174.8(2)
C5 C6 C7 C8 -0.5(3)	C40 C45 C46 N4 4.7(2)
C5 C6 C7 C11 177.7(2)	C41 C40 C45 C44 -2.8(3)
C6 C7 C8 C9 0.5(3)	C41 C40 C45 C46 115.7(2)
C7 C8 C9 C4 -2.3(3)	C41 C42 C43 C44 0.2(4)

C7 C8 C9 C12	173.79(19)	C42 C41 C47 C44	-48.5(3)
C9 C4 C5 C6	-4.2(2)	C42 C43 C44 C45	70.1(4)
C9 C4 C5 C10	173.56(16)	C42 C43 C44 C47	-33.4(3)
C10 C5 C6 C7	-175.51(19)	C43 C44 C45 C40	-64.5(3)
C11 C7 C8 C9	-177.7(2)	C43 C44 C45 C46	-177.5(3)
C13 N1 C1 Ru1	-10.9(2)	C43 C44 C47 C41	49.0(2)
C13 N1 C1 N2	175.76(13)	C44 C45 C46 O4	-63.6(4)
C13 N1 C3 C2	-173.57(12)	C44 C45 C46 N4	115.9(2)
C13 C14 C15 C16	-0.9(3)	C45 C40 C41 C42	68.2(2)
C14 C13 C18 C17	-0.5(2)	C45 C40 C41 C47	-35.8(3)
C14 C13 C18 C21	-178.60(15)	C45 C44 C47 C41	-59.1(2)
C14 C15 C16 C17	0.5(3)	C46 N4 C38 C37	73.0(3)
C14 C15 C16 C20	179.8(3)	C46 N4 C39 O3	-177.11(19)
C15 C16 C17 C18	-0.1(3)	C46 N4 C39 C40	3.1(2)
C16 C17 C18 C13	0.1(3)	C47 C41 C42 C43	33.9(3)
C16 C17 C18 C21	178.20(19)	C47 C44 C45 C40	39.4(3)
C18 C13 C14 C15	0.9(2)	C47 C44 C45 C46	-73.6(3)

**Table 5.6.30. Solvent masks information for cs2743-inimer (3).**

Number	X	Y	Z	Volume	Electron count	Content
1	0.000	-0.871	0.500	432.5	111.3	2CH <sub>2</sub> Cl <sub>2</sub> ,1C <sub>6</sub> H <sub>14</sub>
2	0.500	-0.019	0.000	432.5	111.3	2CH <sub>2</sub> Cl <sub>2</sub> ,1C <sub>6</sub> H <sub>14</sub>



**Inimer (4)**

## Experimental

Orange-brown plates were grown from  $\text{CH}_2\text{Cl}_2$ /hexanes. The chosen crystal ( $0.03 \times 0.17 \times 0.21 \text{ mm}^3$ ) was centered on the goniometer of a Rigaku Oxford Diffraction Synergy-S diffractometer equipped with a HyPix6000HE detector and operating with  $\text{CuK}\alpha$  radiation. The data collection routine, unit cell refinement, and data processing were carried out with the program CrysAlisPro.<sup>107</sup> The Laue symmetry and systematic absences were consistent with the monoclinic space group  $P2_1/c$ . The structure was solved using SHELXT<sup>108</sup> and refined using SHELXL<sup>109</sup> via Olex2.<sup>110</sup>

The structure solution revealed the ruthenium coordination environment, but not the ligand sidechain with the esters and the cyclohexene. The difference electron density

---

CrysAlisPro Software System, v1.171.41.105a, Rigaku Oxford Diffraction, **2021**, Rigaku Corporation, Oxford, UK.

Sheldrick, G. M. "SHELXT – Integrated space-group and crystal structure determination." *Acta Cryst.* **2015**, *A71*, 3–8.

Sheldrick, G. M. "Crystal structure refinement with SHELXL." *Acta Cryst.* **2015**, *C71*, 3–8.

Dolomanov, O. V.; Bourhis, L. J.; Gildea, R. J.; Howard, J. A. K.; Puschmann, H. *J. Appl. Cryst.* **2009**, *42*, 339–341.

map from the preliminary refinement cycles revealed a highly disordered sidechain and additional electron density suggesting the presence of disordered CH<sub>2</sub>Cl<sub>2</sub> and hexanes. A reasonable disorder model was not obtained for the sidechain or the solvent. The proximity of the sidechain to the solvate region likely allowed for many orientations of this fragment and/or substantial motion. No disorder model was used for the sidechain resulting in very large anisotropic displacement ellipsoids and unreliable/unreasonable metric parameters. For the disordered solvent, the solvent mask feature of OLEX2 was used (Figure 1). A total of 72 e<sup>-</sup> was subtracted from 238 Å<sup>3</sup> masked space per asymmetric unit (estimated as one CH<sub>2</sub>Cl<sub>2</sub> and one C<sub>6</sub>H<sub>14</sub> corresponding to 92 e<sup>-</sup>/asymmetric unit). The final refinement model involved anisotropic displacement parameters for non-hydrogen atoms and a riding model for all hydrogen atoms. Olex2<sup>111</sup> was used for molecular graphics generation.

---

Dolomanov, O.V.; Bourhis, L. J.; Gildea, R. J.; Howard, J. A. K.; Puschmann, H. *J. Appl. Cryst.* **2009**, *42*, 339–341.

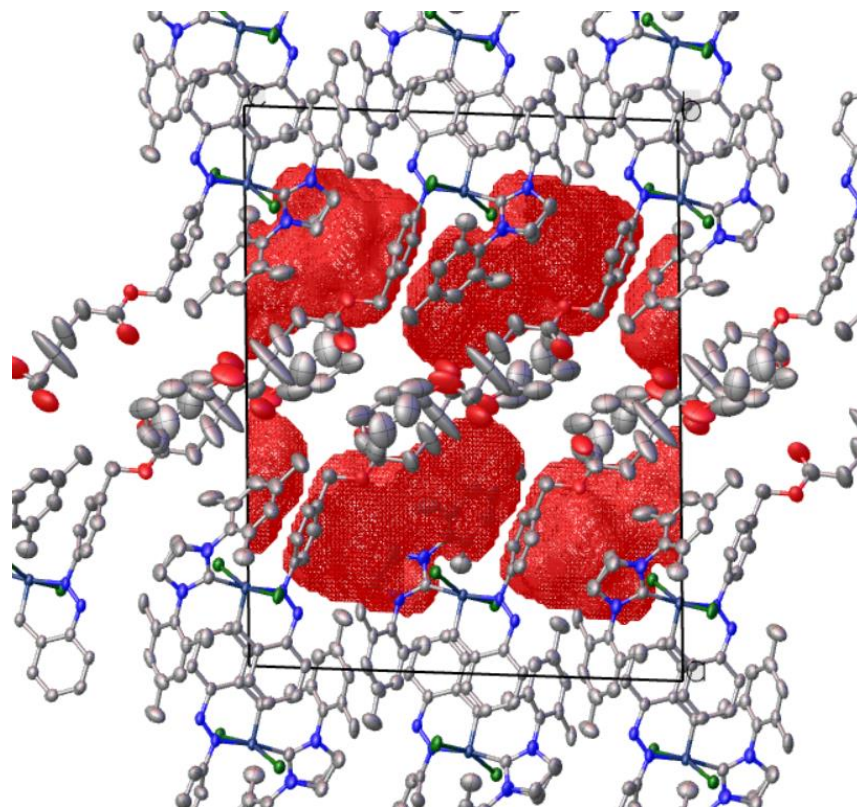


**Figure 5.6.1.** cs2681-inimer (4) unit cell viewed down the *b*-axis. The red surfaces represent the solvent mas region. The sidechain containing the esters and the cyclohexene extends into this solvent region and the resultant disorder could not be modeled effectively.

**Table 5.6.31. Crystal data and structure refinement for cs2681-inimer (4).**

Identification code	HA-99
Empirical formula	C <sub>48</sub> H <sub>56</sub> Cl <sub>2</sub> N <sub>4</sub> O <sub>4</sub> Ru
Formula weight	924.93
Temperature/K	100.00(13)
Crystal system	monoclinic
Space group	<i>P</i> 2 <sub>1</sub> / <i>c</i>
<i>a</i> /Å	24.7428(2)
<i>b</i> /Å	10.54000(10)
<i>c</i> /Å	19.13780(10)

$\alpha/^\circ$	90
$\beta/^\circ$	92.5130(10)
$\gamma/^\circ$	90
Volume/ $\text{\AA}^3$	4986.13(7)
Z	4
$\rho_{\text{calc}}/\text{cm}^3$	1.232
$\mu/\text{mm}^{-1}$	3.870
F(000)	1928.0
Crystal size/ $\text{mm}^3$	$0.21 \times 0.17 \times 0.03$
Radiation	Cu K $\alpha$ ( $\lambda = 1.54184$ )
$2\Theta$ range for data collection/ $^\circ$	7.152 to 155.222
Index ranges	$-31 \leq h \leq 31, -13 \leq k \leq 13, -19 \leq l \leq 24$
Reflections collected	97367
Independent reflections	10517 [ $R_{\text{int}} = 0.0725, R_{\text{sigma}} = 0.0358$ ]
Data/restraints/parameters	10517/0/542
Goodness-of-fit on $F^2$	1.084
Final R indexes [ $I \geq 2\sigma(I)$ ]	$R_1 = 0.0534, wR_2 = 0.1532$
Final R indexes [all data]	$R_1 = 0.0597, wR_2 = 0.1600$
Largest diff. peak/hole / $e \text{\AA}^{-3}$	0.98/-1.36

**Table 5.6.32. Bond Lengths for cs2681-inimer (4).**

Atom	Atom	Length/Å	Atom	Atom	Length/Å
Ru1	C11	2.3608(8)	C14	C15	1.386(5)
Ru1	C12	2.3381(8)	C14	C19	1.509(5)
Ru1	N4	2.038(2)	C15	C16	1.392(5)
Ru1	C1	2.103(3)	C16	C17	1.380(6)
Ru1	C22	1.840(3)	C16	C20	1.512(6)
O1	C35	1.445(5)	C17	C18	1.381(6)
O1	C36	1.327(5)	C18	C21	1.498(5)
O2	C36	1.188(6)	C22	C23	1.441(4)
O3	C40	0.971(11)	C23	C24	1.405(4)
O4	C40	1.354(11)	C23	C28	1.420(4)
O4	C41	1.613(11)	C24	C25	1.380(4)
N1	C1	1.342(4)	C25	C26	1.401(5)
N1	C3	1.477(5)	C26	C27	1.369(5)
N1	C13	1.426(4)	C27	C28	1.401(4)
N2	C1	1.340(4)	C29	C30	1.381(5)
N2	C2A	1.59(3)	C29	C34	1.386(5)
N2	C2B	1.462(12)	C30	C31	1.394(6)
N2	C4	1.438(5)	C31	C32	1.385(7)
N3	N4	1.268(3)	C32	C33	1.383(7)
N3	C28	1.392(4)	C32	C35	1.499(6)
N4	C29	1.444(4)	C33	C34	1.389(6)
C2A	C3	1.56(3)	C36	C37	1.487(7)
C2B	C3	1.498(14)	C37	C38	1.538(8)
C4	C5	1.369(7)	C40	C39	1.678(15)
C4	C9	1.408(7)	C41	C42	1.497(13)
C5	C6	1.407(7)	C41	C48	1.485(13)

**Table 5.6.32. Bond Lengths for cs2681-inimer (4).**

<b>Atom</b>	<b>Atom</b>	<b>Length/Å</b>	<b>Atom</b>	<b>Atom</b>	<b>Length/Å</b>
C5	C10	1.511(9)	C42	C43	1.587(15)
C6	C7	1.383(9)	C43	C44	1.360(12)
C7	C8	1.371(9)	C44	C45	1.294(11)
C7	C11	1.531(7)	C45	C46	1.345(14)
C8	C9	1.387(6)	C46	C47	1.418(15)
C9	C12	1.515(7)	C47	C48	1.461(15)
C13	C14	1.393(5)	C38	C39	1.116(17)
C13	C18	1.403(4)			

**Table 5.6.33. Bond Angles for cs2681-inimer (4).**

<b>Atom Atom Atom</b>	<b>Angle/°</b>	<b>Atom Atom Atom</b>	<b>Angle/°</b>
C12 Ru1 C11	162.35(3)	C15 C14 C19	120.7(3)
N4 Ru1 C11	89.67(7)	C14 C15 C16	121.6(3)
N4 Ru1 C12	87.64(7)	C15 C16 C20	120.3(4)
N4 Ru1 C1	171.43(11)	C17 C16 C15	118.8(3)
C1 Ru1 C11	87.13(9)	C17 C16 C20	120.9(4)
C1 Ru1 C12	93.01(9)	C16 C17 C18	121.8(3)
C22 Ru1 C11	98.23(10)	C13 C18 C21	121.5(4)
C22 Ru1 C12	99.12(10)	C17 C18 C13	118.2(3)
C22 Ru1 N4	88.21(12)	C17 C18 C21	120.3(3)
C22 Ru1 C1	100.12(13)	C23 C22 Ru1	125.8(2)
C36 O1 C35	116.4(3)	C24 C23 C22	118.1(3)
C40 O4 C41	113.6(7)	C24 C23 C28	118.0(3)
C1 N1 C3	113.1(3)	C28 C23 C22	123.9(3)
C1 N1 C13	127.5(3)	C25 C24 C23	121.6(3)
C13 N1 C3	119.0(3)	C24 C25 C26	119.6(3)
C1 N2 C2A	113.0(11)	C27 C26 C25	120.0(3)
C1 N2 C2B	113.2(6)	C26 C27 C28	121.3(3)
C1 N2 C4	127.6(3)	N3 C28 C23	125.7(3)
C4 N2 C2A	115.7(10)	N3 C28 C27	114.6(3)
C4 N2 C2B	119.3(6)	C27 C28 C23	119.4(3)
N4 N3 C28	117.9(2)	C30 C29 N4	119.3(3)
N3 N4 Ru1	133.8(2)	C30 C29 C34	120.8(3)
N3 N4 C29	112.3(2)	C34 C29 N4	119.8(3)
C29 N4 Ru1	113.90(19)	C29 C30 C31	119.1(4)
N1 C1 Ru1	130.8(2)	C32 C31 C30	121.3(4)
N2 C1 Ru1	121.0(2)	C31 C32 C35	121.2(5)

**Table 5.6.33. Bond Angles for cs2681-inimer (4).**

<b>Atom Atom Atom</b>	<b>Angle/°</b>	<b>Atom Atom Atom</b>	<b>Angle/°</b>
N2 C1 N1	107.2(3)	C33 C32 C31	118.3(4)
C3 C2A N2	95.1(13)	C33 C32 C35	120.5(5)
N2 C2B C3	103.4(8)	C32 C33 C34	121.7(5)
N1 C3 C2A	104.0(9)	C29 C34 C33	118.8(4)
N1 C3 C2B	102.5(5)	O1 C35 C32	106.9(3)
C5 C4 N2	119.7(4)	O1 C36 C37	111.9(4)
C5 C4 C9	122.2(4)	O2 C36 O1	123.1(5)
C9 C4 N2	117.7(4)	O2 C36 C37	125.0(5)
C4 C5 C6	117.7(5)	C36 C37 C38	113.1(6)
C4 C5 C10	122.0(5)	O3 C40 O4	135.7(13)
C6 C5 C10	120.2(5)	O3 C40 C39	133.8(14)
C7 C6 C5	121.5(5)	O4 C40 C39	90.0(10)
C6 C7 C11	121.1(6)	C42 C41 O4	110.0(6)
C8 C7 C6	119.0(5)	C48 C41 O4	110.4(8)
C8 C7 C11	119.9(7)	C48 C41 C42	113.7(10)
C7 C8 C9	121.8(5)	C41 C42 C43	117.0(6)
C4 C9 C12	122.7(4)	C44 C43 C42	120.0(9)
C8 C9 C4	117.6(5)	C45 C44 C43	125.5(10)
C8 C9 C12	119.6(5)	C44 C45 C46	130.2(10)
C14 C13 N1	119.6(3)	C45 C46 C47	123.6(11)
C14 C13 C18	121.5(3)	C46 C47 C48	128.1(10)
C18 C13 N1	118.9(3)	C47 C48 C41	117.5(8)
C13 C14 C19	121.2(3)	C39 C38 C37	125.8(12)
C15 C14 C13	118.1(3)	C38 C39 C40	126.4(12)

**Table 5.6.34. Torsion Angles for cs2681-inimer (4).**

A	B	C	D	Angle/°	A	B	C	D	Angle/°
Ru1	N4	C29	C30	42.2(3)	C7	C8	C9	C12	-176.3(4)
Ru1	N4	C29	C34	-135.8(2)	C9	C4	C5	C6	4.9(6)
Ru1	C22	C23	C24	166.0(2)	C9	C4	C5	C10	-169.9(5)
Ru1	C22	C23	C28	-15.4(4)	C10	C5	C6	C7	173.6(5)
Cl1	Ru1	C22	C23	110.9(3)	C11	C7	C8	C9	179.2(5)
Cl2	Ru1	C22	C23	-65.8(3)	C13	N1	C1	Ru1	21.5(5)
O1	C36	C37	C38	173.9(7)	C13	N1	C1	N2	-169.6(3)
O2	C36	C37	C38	-3.3(12)	C13	N1	C3	C2A	153.3(13)
O3	C40	C39	C38	101(3)	C13	N1	C3	C2B	175.3(9)
O4	C40	C39	C38	-86(2)	C13	C14	C15	C16	-1.0(5)
O4	C41	C42	C43	-169.0(8)	C14	C13	C18	C17	-1.7(4)
O4	C41	C48	C47	144.4(11)	C14	C13	C18	C21	-179.5(3)
N1	C13	C14	C15	-178.0(3)	C14	C15	C16	C17	-0.8(5)
N1	C13	C14	C19	-0.2(4)	C14	C15	C16	C20	178.9(3)
N1	C13	C18	C17	178.6(3)	C15	C16	C17	C18	1.5(5)
N1	C13	C18	C21	0.9(4)	C16	C17	C18	C13	-0.2(5)
N2	C2A	C3	N1	24.4(16)	C16	C17	C18	C21	177.6(3)
N2	C2B	C3	N1	-5.8(13)	C18	C13	C14	C15	2.3(4)
N2	C4	C5	C6	177.3(3)	C18	C13	C14	C19	-179.9(3)
N2	C4	C5	C10	2.5(6)	C19	C14	C15	C16	-178.8(3)
N2	C4	C9	C8	-177.2(3)	C20	C16	C17	C18	-178.3(3)
N2	C4	C9	C12	-0.2(6)	C22	C23	C24	C25	180.0(3)
N3	N4	C29	C30	-136.8(3)	C22	C23	C28	N3	-5.7(4)
N3	N4	C29	C34	45.2(4)	C22	C23	C28	C27	-179.6(3)
N4	Ru1	C22	C23	21.5(3)	C23	C24	C25	C26	-0.9(4)
N4	N3	C28	C23	9.5(4)	C24	C23	C28	N3	172.9(3)

**Table 5.6.34. Torsion Angles for cs2681-inimer (4).**

A	B	C	D	Angle/°	A	B	C	D	Angle/°
N4	N3	C28	C27	-176.4(2)	C24	C23	C28	C27	-1.0(4)
N4	C29	C30	C31	180.0(3)	C24	C25	C26	C27	0.1(4)
N4	C29	C34	C33	179.9(3)	C25	C26	C27	C28	0.2(4)
C1	Ru1	C22	C23	-160.6(3)	C26	C27	C28	N3	-174.2(3)
C1	N1	C3	C2A	-19.8(13)	C26	C27	C28	C23	0.3(4)
C1	N1	C3	C2B	2.2(10)	C28	N3	N4	Ru1	7.1(4)
C1	N1	C13	C14	71.9(4)	C28	N3	N4	C29	-174.2(2)
C1	N1	C13	C18	-108.4(4)	C28	C23	C24	C25	1.3(4)
C1	N2	C2A	C3	-25.8(18)	C29	C30	C31	C32	1.1(6)
C1	N2	C2B	C3	8.3(14)	C30	C29	C34	C33	1.9(5)
C1	N2	C4	C5	99.5(5)	C30	C31	C32	C33	-0.1(6)
C1	N2	C4	C9	-87.8(5)	C30	C31	C32	C35	179.3(4)
C2AN2	C1	Ru1		-173.9(12)	C31	C32	C33	C34	0.0(6)
C2AN2	C1	N1		15.9(12)	C31	C32	C35	O1	97.5(5)
C2AN2	C4	C5		-104.0(13)	C32	C33	C34	C29	-0.9(6)
C2AN2	C4	C9		68.7(13)	C33	C32	C35	O1	-83.2(5)
C2BN2	C1	Ru1		163.1(9)	C34	C29	C30	C31	-2.0(5)
C2BN2	C1	N1		-7.1(10)	C35	O1	C36	O2	-2.9(9)
C2BN2	C4	C5		-80.4(11)	C35	O1	C36	C37	179.8(6)
C2BN2	C4	C9		92.3(10)	C35	C32	C33	C34	-179.4(4)
C3	N1	C1	Ru1	-166.1(3)	C36	O1	C35	C32	166.5(5)
C3	N1	C1	N2	2.9(5)	C36	C37	C38	C39	93.0(19)
C3	N1	C13	C14	-100.1(4)	C37	C38	C39	C40	-173.0(12)
C3	N1	C13	C18	79.6(4)	C40	O4	C41	C42	144.2(9)
C4	N2	C1	Ru1	-16.8(6)	C40	O4	C41	C48	-89.5(11)
C4	N2	C1	N1	172.9(4)	C41	O4	C40	O3	-8(3)

**Table 5.6.34. Torsion Angles for cs2681-inimer (4).**

A	B	C	D	Angle/°	A	B	C	D	Angle/°
C4	N2	C2A	C3	174.2(8)	C41	O4	C40	C39	179.6(8)
C4	N2	C2B	C3	-171.7(7)	C41	C42	C43	C44	32.8(14)
C4	C5	C6	C7	-1.3(7)	C42	C41	C48	C47	-91.4(12)
C5	C4	C9	C8	-4.7(6)	C42	C43	C44	C45	-74.3(15)
C5	C4	C9	C12	172.3(4)	C43	C44	C45	C46	-5.8(17)
C5	C6	C7	C8	-2.4(7)	C44	C45	C46	C47	71.6(17)
C5	C6	C7	C11	-179.0(5)	C45	C46	C47	C48	-52(2)
C6	C7	C8	C9	2.6(7)	C46	C47	C48	C41	50(2)
C7	C8	C9	C4	0.8(7)	C48	C41	C42	C43	66.5(11)

**Table 5.6.35. Solvent masks information for cs2681-inimer (4).**

Number	X	Y	Z	Volume	Electron count	Content
1	0.279	0.564	0.856	237.6	71.8	1 dichloromethane,1 hexane
2	0.279	0.936	0.356	237.6	71.7	1 dichloromethane,1 hexane
3	0.721	0.436	0.144	237.6	74.4	1 dichloromethane,1 hexane
4	0.721	0.064	0.644	237.6	74.5	1 dichloromethane,1 hexane

This report has been created with Olex2, compiled on 2020.11.12 svn.r5f609507 for OlexSys. Please [let us know](#) if there are any errors or if you would like to have additional features.

## Experimental Section References

1. Kleine, T.; Bergander, K.; Fröhlich, R.; Wibbeling, B.; Würthwein, E.-U., Ring-Closure Reactions of 1,2-Diaza-4,5-benzoheptatrienyl Metal Compounds: Experiment and Theory. *J. Org. Chem.* 2011, 76 (7), 1979-1991.

## Chapter 6. Synthesis and Characterization of Bimetallic Olefin Metathesis

### Catalysts

Hanan N. Almuzaini,<sup>a,b</sup> Carla Slebodnick,<sup>a</sup> Michael D. Schulz<sup>a,b</sup>

<sup>a</sup> Department of Chemistry, Virginia Polytechnic Institute and State University,  
Blacksburg, VA 24061

<sup>b</sup> Macromolecules Innovation Institute, Virginia Polytechnic Institute and State  
University, Blacksburg, VA 24061

#### 6.1. Abstract

This section summarizes the main achievements and other attempts to synthesize and characterize bimetallic ruthenium olefin metathesis catalysts. A single-crystal X-ray diffraction measurement confirmed the synthesis of a bimetallic complex containing a chelating sulfur and two chelating oxygens of a carboxylate (per ruthenium atom) forming an octahedral geometry around two ruthenium centers. Other attempts to prepare ether- or imine-chelated bimetallic complexes were unsuccessful due to product degradation or the formation of a monometallic complex. The advantage of synthesizing this class of complexes is the potential ability to prepare a cyclic polymer (a polymer with a cyclic structure and a lack of end and branching groups), which often have higher stability and distinct physical and chemical properties compared to linear and branched polymers. This bimetallic catalyst has a cyclic structure that can insert itself into the ring-opening metathesis polymerization (ROMP) monomer by alkene metathesis to produce a large cycle structure. The successful synthesis of this complex provides a route for a new catalyst class having a functional group capable of chelating the metal center to form a bimetallic complex. Hence, this class of catalysts could enable the synthesis of new materials with

wide applications. Furthermore, studies of the activity and stability of these complexes are needed to investigate the effect of carboxylic acid chelation and the bimetallic structure on the catalyst behavior.

## 6.2. Introduction

Progress in developing novel ruthenium-based olefin metathesis catalysts is ongoing, with a focus on improving catalyst activity, selectivity, and stability.<sup>1-3</sup> Modification of catalyst activity by varying the sterics, electronics, or chelating properties of ligands enabled the synthesis of varying materials with different topologies having distinct physical and chemical properties.<sup>4-7</sup> Bimetallic metathesis catalysts have also been developed to enhance selectivity and reactivity. For example, Lemcoff and co-workers reported the synthesis of a homo-di-nuclear ruthenium complex **[Ru] 1** with a dimeric N-heterocyclic carbene (NHC) ligand (**Figure 6.1**).<sup>8</sup> This complex showed high selectivity in dimer ring-closing metathesis of 1,12-tridecadiene to form a 22-membered-ring product following the suggested mechanism in **Figure 6.1**. This bimetallic complex prevented the formation of acyclic diene metathesis (ADMET) products and mono ring-closing metathesis. The high selectivity toward the metathesis product was attributed to the cooperation of the two ruthenium centers.<sup>8</sup> Each ruthenium center binds one of the olefinic end groups of the diene substrate, which is then combined with end groups of the second diene molecule to form the final product with a 22-membered-ring (**Figure 6.1**).<sup>8</sup> In comparison, using monometallic catalysts in this metathesis reaction produced a high ADMET product with a low dimer product.<sup>8</sup>



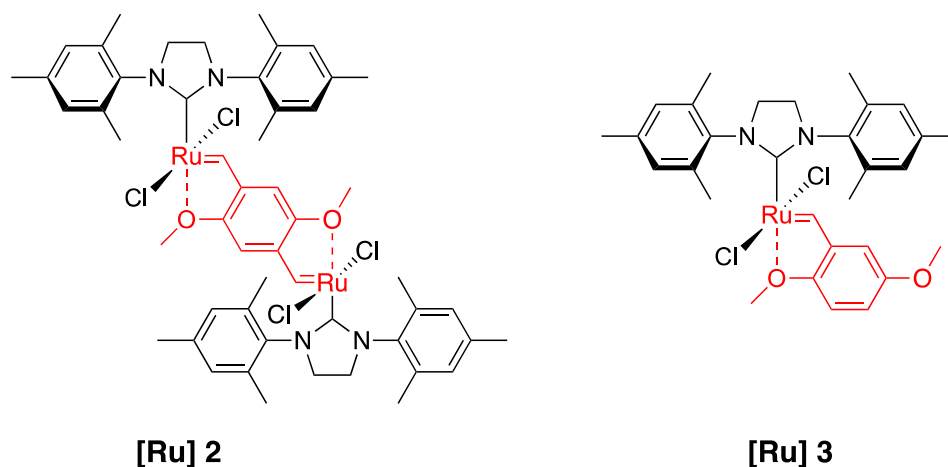


**Figure 6. A bimetallic catalyst [Ru]2 was synthesized to increase catalyst activity of the corresponding monometallic catalyst [Ru]3.<sup>9</sup>**

Here, we developed a novel approach to synthesize bimetallic ruthenium olefin metathesis catalysts by introducing a carboxylic acid functionality to the catalyst benzylidene ligand. First, we designed a sulfur-benzylidene ligand functionalized with a carboxylic acid. The carbene exchange reaction of this benzylidene ligand with Grubbs second-generation catalyst released 2 equivalents of HCl to produce a dimer complex having two ruthenium centers, each with a chelating sulfur, Cl, NHC, and two oxygens of the carboxylic acid group. The dimerization of this complex resulted in a cyclic structure containing the two Ru initiation centers and two chelating benzylidene ligands. We hypothesized that upon the ROMP monomer addition, this catalyst will insert itself into the ROMP monomer by alkene metathesis to produce a cycle having both the bimetallic ruthenium catalyst and the monomer. Propagation can continue with subsequent monomers further expanding the cycle until an intramolecular backbiting reaction produces a separate cyclic polymer.

Cyclic polymers are a class of polymers having a ring structure with a lack of end and branching groups. Although cyclic polymers showed distinct physical and chemical properties compared with linear and branching polymers, this topology remains uncommon.<sup>13-15</sup> The synthesis of cyclic polyolefins requires specific initiators and conditions, and usually requires a multistep purification. For example, cyclic polyolefins have been achieved based on NHC ligand modification (**Figure 6.3**).<sup>13, 16</sup> The NHC ligand modification allowed the synthesis of a cyclic polymer by attaching the omega chain ends of the growing polymer to the metal complex throughout the entire polymerization process. We hypothesized that the bimetallic complex could follow a similar mechanism of growing a cyclic polymer via ring expansion by attaching the omega chain end to the benzylidene ligand instead of the NHC ligand (**Figure 6.3**).

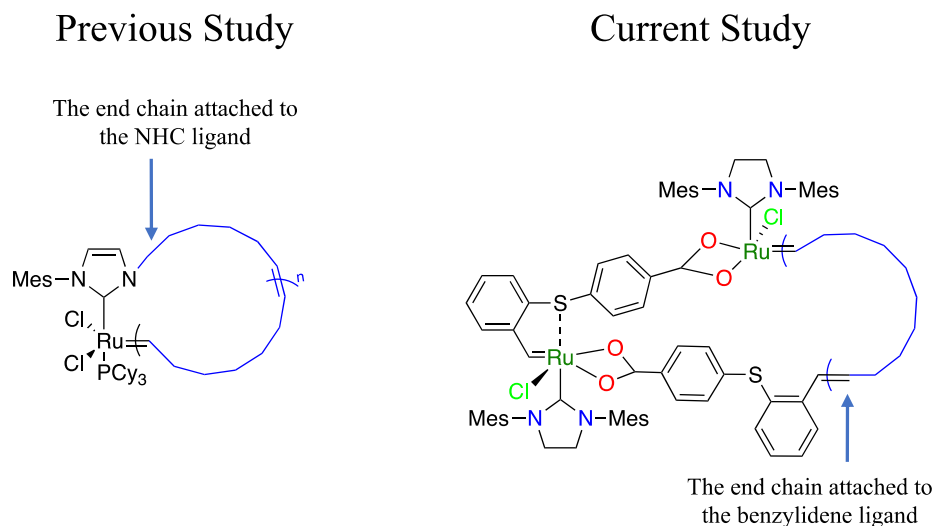


**Figure 6.3. Olefin metathesis catalysts with a cyclic functionality to prepare cyclic polymers via a ring expansion approach.**

### 6.3. Results and Discussion

The synthesis of the bimetallic complex is illustrated in **Figure 6.4**. Commercially available 4-mercaptobenzoic acid reacted with 2-fluorobenzaldehyde under basic conditions to form **3** with an aldehyde, which further underwent a Wittig reaction to form the benzylidene ligand **4**. Reacting the benzylidene ligand with Grubbs second-generation catalyst (**G2**) at 40 °C in dichloromethane (DCM) produced a bimetallic complex **5** instead of a monometallic complex **6** (**Figure 6.4**). The resulting product **5** was isolated and purified by column chromatography. The purified product was characterized by single-crystal X-ray crystallography and <sup>1</sup>H NMR spectroscopy. X-ray crystallography confirmed catalyst dimerization. The catalyst crystal structure showed the chelation of two oxygen atoms with each ruthenium center, forming a cyclic bimetallic catalyst (**Figure 6.5**). The catalyst analysis by <sup>1</sup>H NMR did not show dimerization due to the high symmetry of the catalyst.

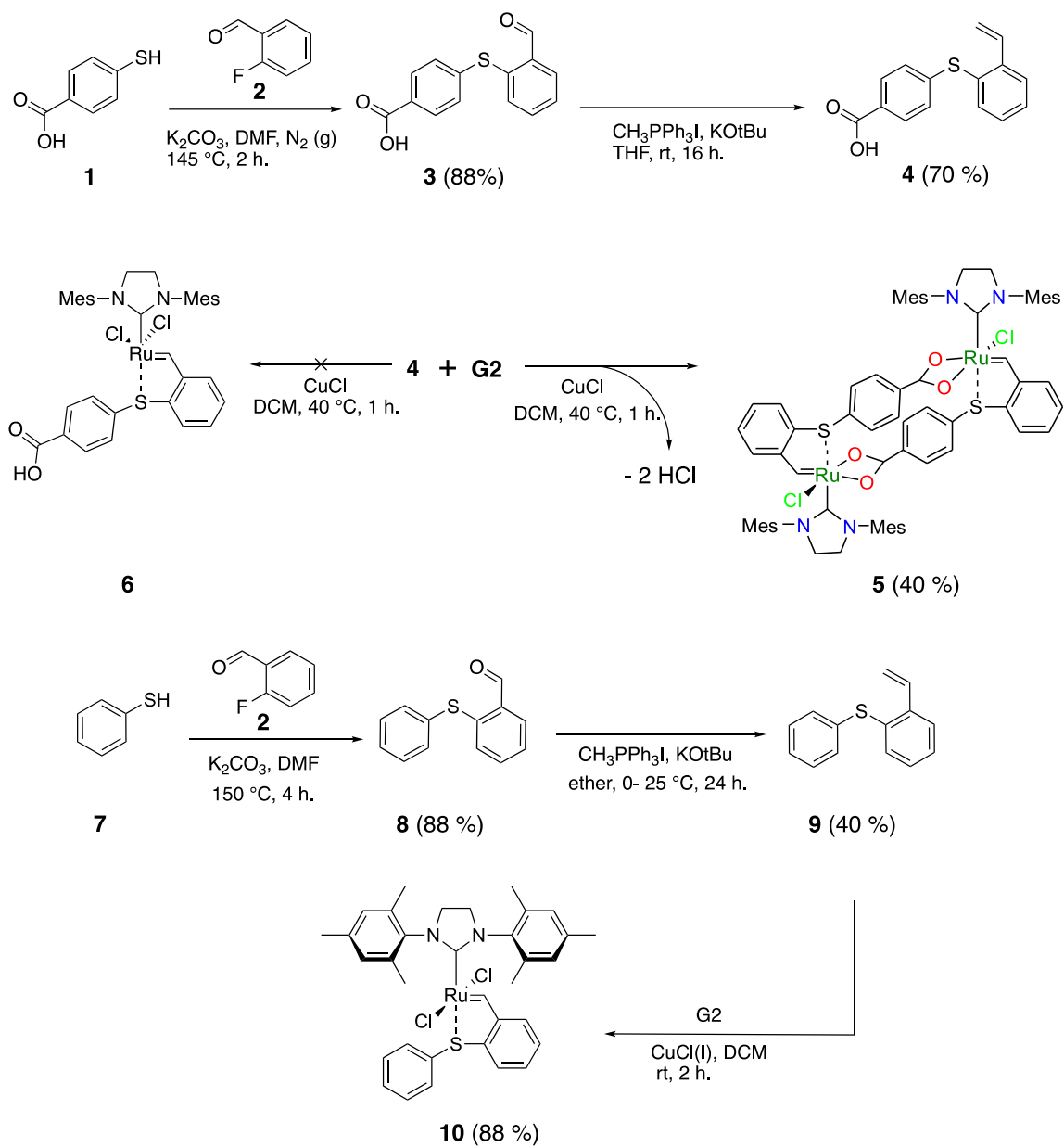
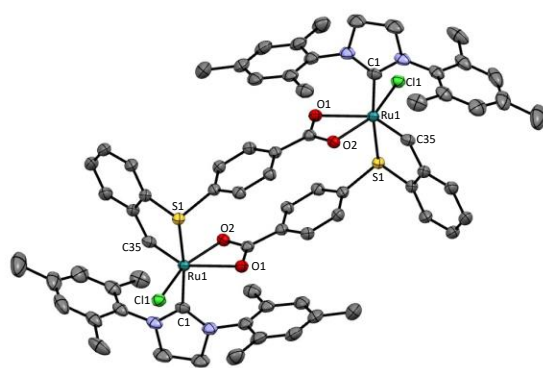
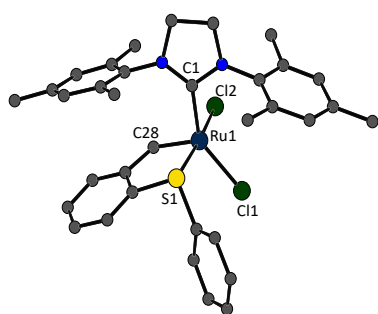


**Figure 6. Synthesis of a bimetallic and monometallic catalyst.**



5

Selected Bond Lengths [Å]		Selected Bond Angles [°]	
Ru1-Cl1	2.3445(4)	Cl1-Ru1-S1	84.847(14)
Ru1-S1	2.4482(4)	Cl1-Ru1-O1	98.60(3)
Ru1-O1	2.3577(13)	O1-Ru1-S1	82.40(3)
Ru1-O2	2.0893(11)	O2-Ru1-S1	92.79(3)
Ru1-C1	2.0647(16)	C35-Ru1-C1	108.47(5)
Ru1-C35	1.8480(18)	C1-Ru1-S1	171.99(5)



10

Selected Bond Lengths [Å]		Selected Bond Angles [°]	
Ru-Cl1	2.3844(3)	Cl1-Ru1-Cl2	89.430(14)
Ru-Cl2	2.3529(4)	S1-Ru1-Cl1	173.230(13)
Ru1-S1	2.3386(3)	C1-Ru1-Cl1	89.37(4)
Ru1-C1	2.0158(12)	C1-Ru1-S1	92.76(4)
Ru1-C28	1.8391(13)	C28-Ru1-C1	98.24(5)

**Figure 6 Crystal structures of the synthesized bimetallic and monometallic complexes.**

After successfully synthesizing the bimetallic complex **5**, we synthesized a monometallic sulfur chelating ruthenium olefin metathesis catalyst (**10**, **Figure 6.4**) to compare the catalyst geometry and predict the catalyst reactivity. To synthesize the monometallic complex, we started with the commercially available thiophenol, which reacted with 2-fluorobenzaldehyde under basic conditions to form the thiol linkage in compound **8**. Using Wittig reagents, we prepared the styrene benzylidene ligand **9** from the aldehyde **8**. The carbene exchange reaction of **9** with **G2** produced the monometallic catalyst **10**. The catalyst structure was confirmed with  $^1\text{H}$  NMR spectroscopy and X-ray crystallography (**Figure 6.5**). Then, we used the crystal structure to compare the geometry

of the monometallic and the bimetallic complexes. The bimetallic catalyst showed an octahedral geometry around the two ruthenium centers. Each ruthenium has a Cl, an NHC ligand, chelating S and the two oxygens of the carboxyl group. The crystal structure of the monometallic catalyst showed the formation of a *cis* isomer chelating two chlorine ligands on the same side in a plane. The crystal analysis confirmed a trigonal bipyramidal geometry around the ruthenium center. The two complexes showed similar bond lengths, but the Ru-S bond length was increased by 0.10 Å with the formation of the bimetallic complex. The presence of different bond angles could be attributed to the differences in catalysts' geometry.

Furthermore, we attempted to synthesize a series of bimetallic catalysts with different chelating heteroatoms. The first attempt was based on the Hoveyda–Grubbs ruthenium olefin metathesis catalyst chelating ether group **14** (Figure 6.6). We synthesized the benzylidene by reacting 2-fluorobenzaldehyde **2** and 4-hydroxybenzoate **11**. Then, we prepared the styrene product **12** by a Wittig reaction of **11**. **G2** reacted with the benzylidene ligand to prepare the bimetallic complex **14**. However, we could not isolate the product after several attempts. The failure to isolate the product was explained by the <sup>1</sup>H NMR results, which showed catalyst decomposition, suggesting that the bimetallic catalyst may not be stable with releasing HCl. Hence, modified reaction conditions may be required to overcome the failure in isolating the product.

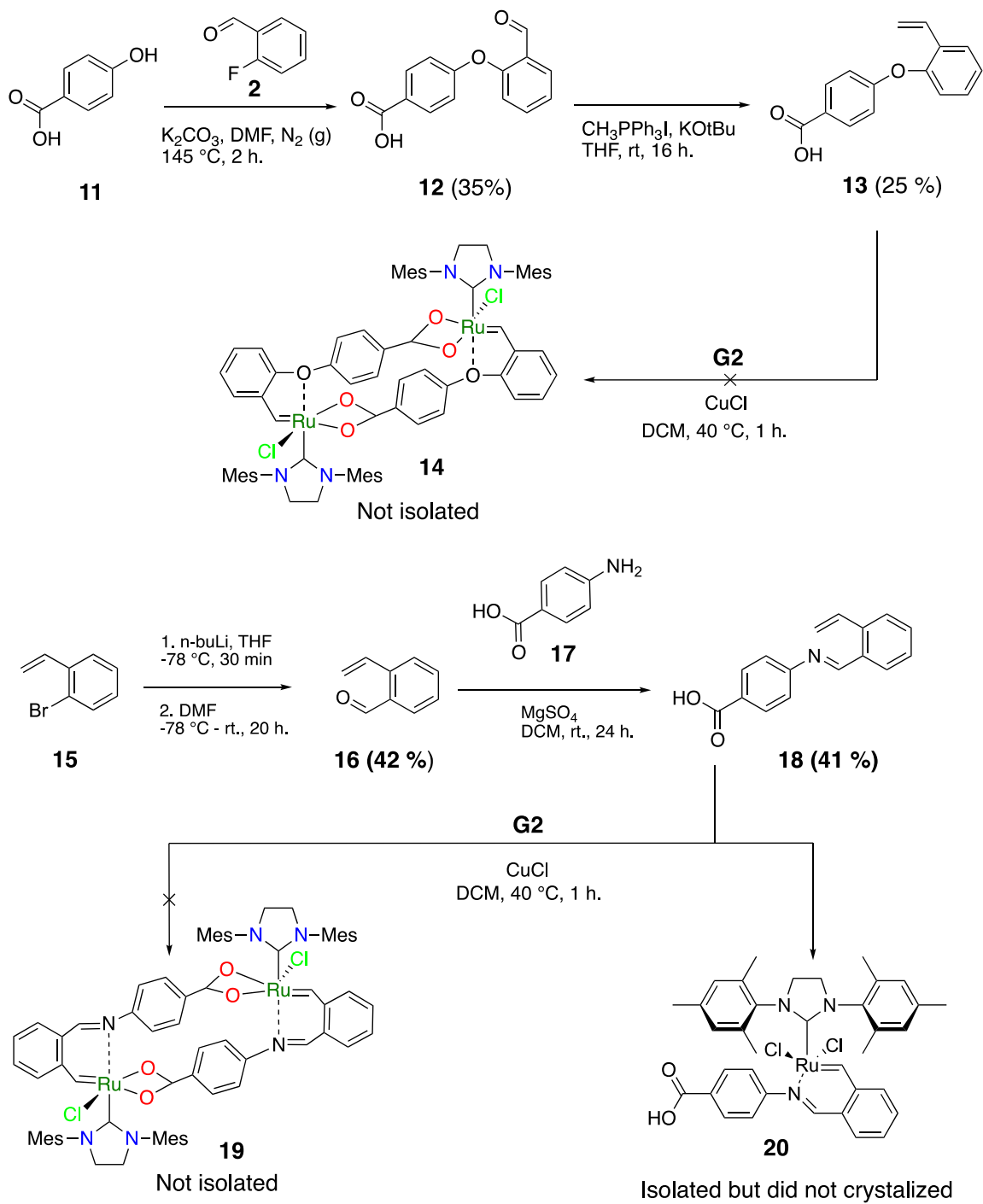


**Figure 6. Attempts to synthesize bimetallic complexes.**

Another attempt was to prepare a bimetallic complex with imine chelation **19** (**Figure 6.6**). We successfully synthesized the benzylidene ligand **18** by mixing 2-vinyl benzaldehyde **16** with 4-amino benzoic acid **17**. Afterward, the benzylidene ligand underwent a carbene exchange reaction with **G2** (**Figure 6.6**). The  $^1\text{H}$  NMR analysis confirmed the isolation of a catalyst with imine chelation. However, we could not confirm the bimetallic synthesis by  $^1\text{H}$  NMR due to the possibility of having symmetrical protons. This complex did not grow a crystal and decomposed during crystallization attempts, suggesting the low stability of this complex. One way to confirm the catalyst structure is by adding an alcohol to test the possibility of ester linkage formation (**Figure 6.7**). We allowed the isolated product to react with **21**. After purification by column chromatography,  $^1\text{H}$  NMR data confirmed the synthesis of a catalyst having an ester linkage due to shifts of methyl proton peaks (**Figure 6.7**). This result confirmed the monometallic catalyst synthesis having a free carboxylic acid group, since the free acid group reacted with an alcohol to form the ester linkage.

A possible explanation of forming a bimetallic sulfur- and monometallic amine-chelated ruthenium complexes is the *cis* and *trans* catalysts isomers. The *cis* sulfur-ruthenium complex has the two chlorine ligands in the same plane, reducing the benzylidene steric effect and allowing the carboxylic acid chelation and releasing the chlorine ligand. The imine-ruthenium complex showed a *trans* chlorine isomer confirmed by the  $^1\text{H}$  NMR. Having the two chlorine ligands in a different plane increases the benzylidene ligand steric hinderance, which could limit the carboxylic acid chelation.

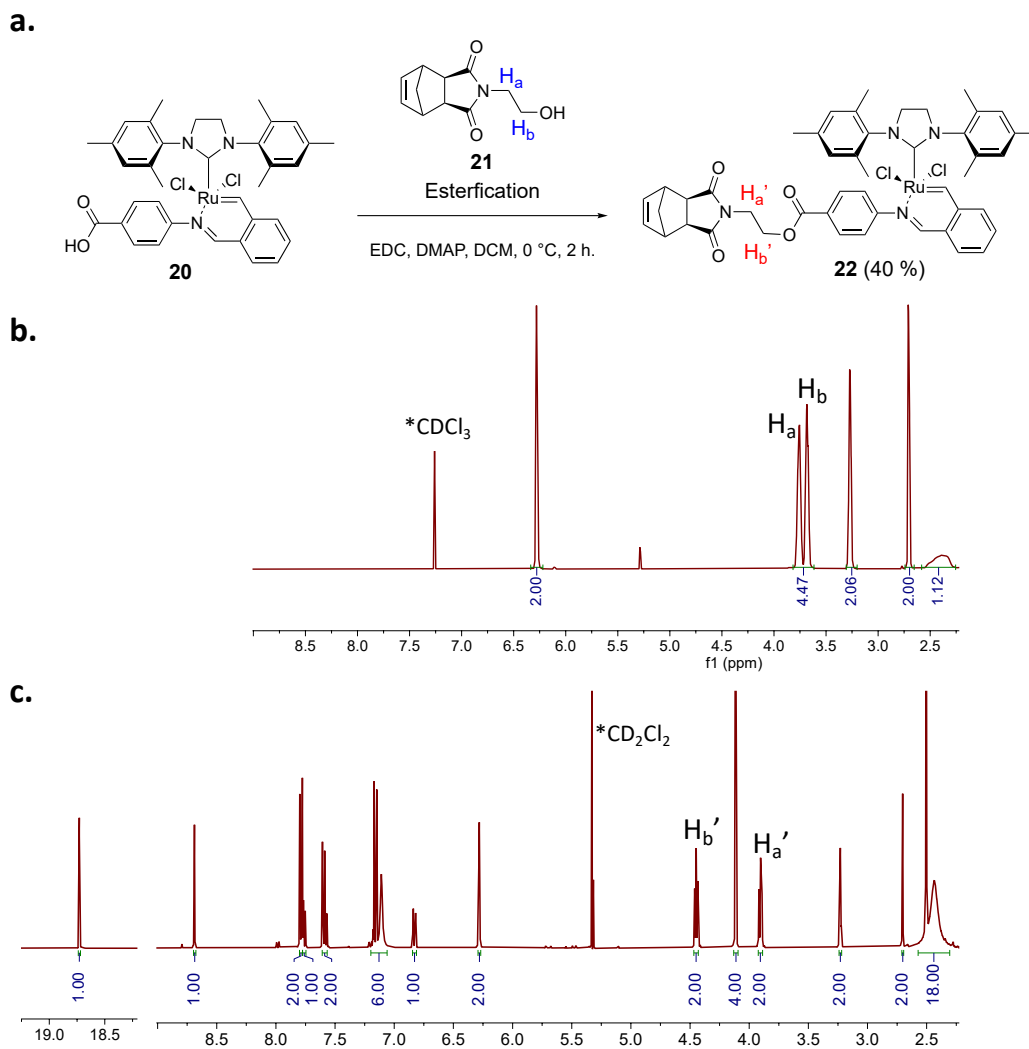


**Figure 6. a. Esterification of the monometallic synthesis, and  $^1\text{H}$  NMR of b. 21, and c. 22 showed the protons shift.**

#### 6.4. Conclusions and Future Work

Here, we introduced a new approach to preparing a bimetallic complex. The formation of this bimetallic catalyst could enable the synthesis of cyclic polymers via a ring expansion mechanism. In the future, we will investigate the ability of the catalyst to form cyclic polymers. We will characterize the polymers by matrix-assisted laser desorption ionization (MALDI) to confirm the absence of the end groups. We will also design and synthesize

other bimetallic complexes with different chelation ligands to expand the class of bimetallic catalysts.

## 6.5. References

- (1) Rogalski, S.; Pietraszuk, C. Application of Olefin Metathesis in the Synthesis of Carbo- and Heteroaromatic Compounds—Recent Advances. *Molecules* **2023**, *28* (4), 1680.
- (2) Bano, T.; Zahoor, A. F.; Rasool, N.; Irfan, M.; Mansha, A. Recent trends in Grubbs catalysis toward the synthesis of natural products: a review. *J. Iran. Chem. Soc.* **2022**, *19* (6), 2131-2170. DOI: 10.1007/s13738-021-02463-x.
- (3) Kajetanowicz, A.; Grela, K. Nitro and Other Electron Withdrawing Group Activated Ruthenium Catalysts for Olefin Metathesis Reactions. *Angew. Chem., Int. Ed. Engl.* **2021**, *60* (25), 13738-13756. DOI: <https://doi.org/10.1002/anie.202008150>.
- (4) Eivgi, O.; Phatake, R. S.; Nechmad, N. B.; Lemcoff, N. G. Light-Activated Olefin Metathesis: Catalyst Development, Synthesis, and Applications. *Acc. Chem. Res.* **2020**, *53* (10), 2456-2471. DOI: 10.1021/acs.accounts.0c00495.
- (5) Duan, Y.; Wang, T.; Xie, Q.; Yu, X.; Guo, W.; Wang, J.; Liu, G. Highly efficient nitrogen chelated ruthenium carbene metathesis catalysts. *Dalton Trans.* **2016**, *45* (48), 19441-19448, 10.1039/C6DT03899A. DOI: 10.1039/C6DT03899A.
- (6) Hejl, A.; Day, M. W.; Grubbs, R. H. Latent Olefin Metathesis Catalysts Featuring Chelating Alkylidenes. *Organometallics* **2006**, *25* (26), 6149-6154. DOI: 10.1021/om060620u.
- (7) Kost, T.; Sigalov, M.; Goldberg, I.; Ben-Asuly, A.; Lemcoff, N. G. Latent sulfur chelated ruthenium catalysts: Steric acceleration effects on olefin metathesis. *J. Organomet. Chem.* **2008**, *693* (12), 2200-2203. DOI: <https://doi.org/10.1016/j.jorganchem.2008.03.028>.
- (8) Tzur, E.; Ben-Asuly, A.; Diesendruck, C. E.; Goldberg, I.; Lemcoff, N. G. Homodinuclear Ruthenium Catalysts for Dimer Ring-Closing Metathesis. *Angew. Chem. Int. Ed.* **2008**, *47* (34), 6422-6425. DOI: <https://doi.org/10.1002/anie.200801626>.
- (9) Grudzień, K.; Malinska, M.; Barbasiewicz, M. Synthesis and Properties of Bimetallic Hoveyda–Grubbs Metathesis Catalysts. *Organometallics* **2012**, *31* (9), 3636-3646. DOI: 10.1021/om3001372.
- (10) Frenzel, U.; Nuyken, O. Ruthenium-based metathesis initiators: Development and use in ring-opening metathesis polymerization. *J. Polym. Sci., Part A-1: Polym. Chem.* **2002**, *40* (17), 2895-2916. DOI: <https://doi.org/10.1002/pola.10324>.
- (11) Dias, E. L.; Grubbs, R. H. Synthesis and Investigation of Homo- and Heterobimetallic Ruthenium Olefin Metathesis Catalysts Exhibiting Increased Activities. *Organometallics* **1998**, *17* (13), 2758-2767. DOI: 10.1021/om9708788.
- (12) Borguet, Y.; Sauvage, X.; Zaragoza, G.; Demonceau, A.; Delaude, L. Synthesis and Catalytic Evaluation in Olefin Metathesis of a Second-Generation Homobimetallic Ruthenium–Arene Complex Bearing a Vinylidene Ligand. *Organometallics* **2011**, *30* (10), 2730-2738. DOI: 10.1021/om2001074.

- (13) Edwards, J. P.; Wolf, W. J.; Grubbs, R. H. The synthesis of cyclic polymers by olefin metathesis: Achievements and challenges. *J. Polym. Sci., Part A: Polym. Chem.* **2019**, *57* (3), 228-242. DOI: <https://doi.org/10.1002/pola.29253>.
- (14) Chen, C.; Weil, T. Cyclic polymers: synthesis, characteristics, and emerging applications. *Mater. Horiz.* **2022**, *7* (10), 1121-1135, 10.1039/D2NH00242F. DOI: 10.1039/D2NH00242F.
- (15) Liénard, R.; De Winter, J.; Coulembier, O. Cyclic polymers: Advances in their synthesis, properties, and biomedical applications. *J. Polym. Sci.* **2020**, *58* (11), 1481-1502. DOI: <https://doi.org/10.1002/pol.20200236>.
- (16) Bielawski, C. W.; Benitez, D.; Grubbs, R. H. An "Endless" Route to Cyclic Polymers. *sci.* **2002**, *297* (5589), 2041-2044. DOI: doi:10.1126/science.1075401.

## 6.6. Experimental Section

### Materials

All reactions were performed using oven-dried glassware equipped with a magnetic stir bar under an air atmosphere unless otherwise noted. 2-fluorobenzaldehyde and 4-hydroxybenzoic acid were obtained from Oakwood. 4-aminobenzoic acid, 4-mercaptobenzoic acid, G2, 2-bromostyrene were purchased from Ambeed. CDCl<sub>3</sub> and CD<sub>2</sub>Cl<sub>2</sub> were obtained from Cambridge Isotope Laboratories. All other reagents were purchased from commercial suppliers and used without further purification.

### Measurements

<sup>1</sup>H NMR and <sup>13</sup>C NMR data were collected at 25 °C in CDCl<sub>3</sub> or CD<sub>2</sub>Cl<sub>2</sub> unless otherwise noted using an Agilent U4-DD2 400 MHz or a Bruker Avance II 500 MHz NMR instrument. Chemical shifts were reported in parts per million (ppm) and referenced to the CHCl<sub>3</sub> singlet at 7.26 ppm and CD<sub>2</sub>Cl<sub>2</sub> triplet at 5.32 ppm for <sup>1</sup>H NMR. <sup>13</sup>C NMR spectra referenced to the center peak of the CDCl<sub>3</sub> triplet at 77.00 ppm, or CD<sub>2</sub>Cl<sub>2</sub> at 54.00 ppm.

### Experimental Procedures

**3:** 2-Fluorobenzaldehyde (**2**) (1 equiv., 3 g) was added to potassium carbonate (2.1 equiv., 7 g), and 4-mercaptobenzoic acid (1 equiv., 3.7 g) in 40 mL DMF. The mixture was stirred at 180 °C for 4 h under an N<sub>2</sub> atmosphere. After cooling, the mixture was poured into 50 mL DI water and extracted with DCM (3×50 mL). The extracts were dried over MgSO<sub>4</sub>, and the solvent was removed under reduced pressure. The crude product was used without any further purification (Yield 88 %). <sup>1</sup>H NMR (400 MHz, CDCl<sub>3</sub>, ppm): δ 10.44 (s, 1H), 8.03 (d, *J* = 8.5 Hz, 2H), 8.01 – 7.96 (m, 1H), 7.56 (td, *J* = 7.5, 1.8 Hz, 1H), 7.54 – 7.47 (m, 1H), 7.41 (dd, *J* = 7.7, 1.3 Hz, 1H), 7.32 (d, *J* = 8.6 Hz, 2H).

$^{13}\text{C}$  NMR (101 MHz,  $\text{cdCl}_3$ )  $\delta$  191.44, 168.69, 163.30, 141.32, 137.95, 135.20, 134.54, 133.15, 131.09, 130.86, 129.96, 129.29, 128.13.

**4:** Methyltriphenylphosphonium iodide (1.4 equiv., 4.3 g) was dissolved in 50 mL of diethyl ether. Potassium *tert*-butoxide (1.5 equiv., 1.3g) was added in one portion at 0 °C. After stirring for 20 min under  $\text{N}_2$  atmosphere, **3** (1 equiv., 2 g) in 15 mL of diethyl ether was added dropwise at 0 °C and the reaction mixture was warmed to room temperature and stirred overnight. The mixture was poured into 50 mL DI water and extracted with ether (3×30 mL). The extract was dried over  $\text{MgSO}_4$ , and the solvent was removed under reduced pressure. The crude product was further purified by chromatography on silica gel (hexane-acetone gradient 9:1 to 7:3) to yield **4** as a colorless oil (Yield 70 %).  $^1\text{H}$  NMR (400 MHz,  $\text{CDCl}_3$ )  $\delta$  7.91 (d,  $J$  = 8.8 Hz, 2H), 7.71 (d,  $J$  = 9.3 Hz, 1H), 7.55 (d,  $J$  = 7.7 Hz, 1H), 7.45 (t,  $J$  = 6.9 Hz, 1H), 7.35 – 7.29 (m, 1H), 7.17 (dd,  $J$  = 17.5, 11.0 Hz, 1H), 7.07 (d,  $J$  = 8.7 Hz, 2H), 5.73 (d,  $J$  = 17.4 Hz, 1H), 5.32 – 5.25 (m, 1H).

$^{13}\text{C}$  NMR (101 MHz,  $\text{CDCl}_3$ )  $\delta$  170.13, 145.05, 141.44, 136.22, 134.42, 133.90, 132.89, 132.61, 132.20, 132.10, 132.05, 132.02, 131.92, 131.89, 131.57, 130.63, 130.52, 129.90, 129.85, 129.57, 128.82, 128.76, 128.64, 128.59, 128.47, 126.87, 126.48, 126.36, 116.76.

**5:** A round bottom flask was charged with G2 (1 equiv., 135 mg) and  $\text{Cu}(\text{I})\text{Cl}$  (1 equiv., 13 mg) benzylidene ligand **4** (1 equiv., 40 mg). DCM (10 ml) was added to the reaction flask under  $\text{N}_2$ . The reaction mixture was stirred at room temperature for 2 h. The solvent was evaporated, and the crude product was purified by column chromatography (Yield 40 %).

**8:** 2-Fluorbenzaldehyde (**2**) (1 equiv., 5.00 g) was added to potassium carbonate (2.1 equiv., 11.70 g), and thiophenol (1 equiv., 4.44 g) in 40 mL DMF. The mixture was stirred at 150 °C for 4 h under an N<sub>2</sub> atmosphere. After cooling, the mixture was poured into 50 mL DI water and extracted with DCM (3×50 mL). The extracts were dried over MgSO<sub>4</sub>, and the solvent was removed under reduced pressure. The crude product was used without any further purification (Yield 7.6 g, 88 %). <sup>1</sup>H NMR (400 MHz, CDCl<sub>3</sub>, ppm): δ 10.37 (s, 1H), 7.89 – 7.82 (m, 1H), 7.43 – 7.30 (m, 7H), 7.08 (dd, J = 7.9, 1.2 Hz, 1H).

**9:** Methyltriphenylphosphonium iodide (1.4 equiv., 20.07 g) was dissolved in 50 mL of diethyl ether. Potassium *tert*-butoxide (1.5 equiv., 6.00 g) was added in one portion at 0 °C. After stirring for 20 min under N<sub>2</sub> atmosphere, **8** (1 equiv., 7.6 g) in 15 mL of diethyl ether was added dropwise at 0 °C and the reaction mixture was warmed to room temperature and stirred overnight. The mixture was poured into 50 mL DI water and extracted with ether (3×30 mL). The extract was dried over MgSO<sub>4</sub>, and the solvent was removed under reduced pressure. The crude product was further purified by chromatography on silica gel (hexane-acetone gradient 9:1 to 7:3) to yield **9** as a colorless oil (Yield 3.05 g, 40 %). <sup>1</sup>H NMR (400 MHz, CDCl<sub>3</sub>) δ 7.65 – 7.57 (m, 1H), 7.42 – 7.08 (m, 9H), 5.70 (dd, J = 17.4, 1.2 Hz, 1H), 5.29 (dd, J = 11.0, 1.3 Hz, 1H). <sup>13</sup>C NMR (101 MHz, CDCl<sub>3</sub>) δ 139.81, 136.55, 134.60, 133.88, 132.77, 129.45, 129.11, 128.51, 128.30, 126.33, 126.18, 116.24.

**10:** A round bottom flask was charged with G2 (1 equiv., 182 mg) and Cu(I)Cl (1 equiv., 21 mg) benzylidene ligand **9** (1 equiv., 50 mg). DCM (10 ml) was added to the reaction flask under N<sub>2</sub>. The reaction mixture was stirred at room temperature for 2 h. The solvent was evaporated, and the crude product was purified by column chromatography (Yield 88 %).

**12:** 2-Fluorbenzaldehyde (**2**) (1 equiv., 3 g) was added to potassium carbonate (2.5 equiv., 8.35 g), and 4-hydroxybenzoic acid (**11**) (1 equiv., 3.9 g) in 40 mL DMF. The mixture was stirred at 180 °C for 4 h under an N<sub>2</sub> atmosphere. After cooling, the mixture was poured into 50 mL DI water and extracted with DCM (3×50 mL). The extracts were dried over MgSO<sub>4</sub>, and the solvent was removed under reduced pressure. The crude product was used without any further purification (Yield 35 %).

<sup>1</sup>H NMR (400 MHz, CDCl<sub>3</sub>) δ 12.02 (s, 1H), 10.24 (s, 1H), 8.05 – 7.91 (m, 3H), 7.84 – 7.69 (m, 1H), 7.43 (d, *J* = 6.8 Hz, 1H), 7.11 (t, *J* = 7.3 Hz, 1H), 6.86 (dd, *J* = 17.4, 8.2 Hz, 4H).

<sup>13</sup>C NMR (101 MHz, CDCl<sub>3</sub>) δ 188.73, 188.71, 163.00, 158.33, 135.92, 132.17, 132.03, 128.60, 127.32, 124.40, 119.79, 117.71, 115.11.

**13:** Methyltriphenylphosphonium iodide (1.2 equiv., 2.6 g) was dissolved in 50 mL of diethyl ether. Potassium *tert*-butoxide (1.5 equiv., 900 mg) was added in one portion at 0 °C. After stirring for 20 min under N<sub>2</sub> atmosphere, **12** (1 equiv., 1.3 g) in 15 mL of diethyl ether was added dropwise at 0 °C and the reaction mixture was warmed to room temperature and stirred overnight. The mixture was poured into 50 mL DI water and extracted with ether (3×30 mL). The extract was dried over MgSO<sub>4</sub>, and the solvent was removed under reduced pressure. The crude product was further purified by chromatography on silica gel (hexane-acetone gradient 9:1 to 7:3) to yield **9** (Yield 25 %).

<sup>1</sup>H NMR (400 MHz, cdcl<sub>3</sub>) δ 11.62 (s, 1H), 8.07 (q, *J* = 4.8 Hz, 2H), 7.65 (dd, *J* = 7.7, 1.6 Hz, 1H), 7.38 – 7.20 (m, 2H), 7.02 (dd, *J* = 8.0, 1.3 Hz, 1H), 6.98 – 6.91 (m, 2H), 6.86 (dd, *J* = 17.7, 11.1 Hz, 1H), 5.79 (dd, *J* = 17.7, 1.1 Hz, 1H), 5.28 (dd, *J* = 11.1, 1.1 Hz, 1H).

$^{13}\text{C}$  NMR (101 MHz,  $\text{CDCl}_3$ )  $\delta$  168.54, 161.94, 132.72, 132.16, 132.08, 132.06, 132.04, 132.01, 131.89, 131.86, 131.69, 130.60, 130.51, 130.50, 130.35, 129.23, 128.75, 128.63, 128.59, 128.47, 128.46, 126.80, 125.13, 124.95, 121.24, 116.27, 115.93.

**16:** *n*-BuLi (1.1 equiv., 770 mg) in 1 M hexane was added to a solution of 2-Bromostyrene **15** (1 equiv., 2 g) in 50 mL of THF at  $-78\text{ }^\circ\text{C}$  and stirred for 30 min. Then, DMF (15 equiv., 1 mL) was added dropwise. The reaction mixture was stirred for 20 h while the temperature was increased to room temperature (rt). The organic layer was washed with brine, dried over  $\text{MgSO}_4$ , and filtered. The crude product was purified by column chromatography (1:9 acetone: hexane) to produce the pure product as a clear liquid (600 mg, 41 %).  $^1\text{H}$  NMR and  $^{13}\text{C}$  NMR data matched that from literature report.<sup>1</sup>

$^1\text{H}$  NMR (400 MHz,  $\text{CDCl}_3$ -d)  $\delta$  10.30 (s, 1H), 7.86 – 7.81 (m, 1H), 7.58 (t,  $J = 1.7$  Hz, 2H), 7.57 – 7.49 (m, 1H), 7.48 – 7.40 (m, 1H), 5.70 (dd,  $J = 17.4, 1.2$  Hz, 1H), 5.52 (dd,  $J = 11.0, 1.2$  Hz, 1H).

$^{13}\text{C}$  NMR (101 MHz,  $\text{CDCl}_3$ )  $\delta$  192.57, 140.69, 133.95, 133.52, 133.03, 131.37, 128.07, 127.61, 119.59.

**18:** A round bottom flask was charged with **17** (1 equiv., 0.20 g), **16** (1 equiv., 0.19 g),  $\text{MgSO}_4$  (1g/1.0 mmol aldehyde, 0.7 g) and DCM (30 mL). The reaction mixture was stirred at room temperature under  $\text{N}_2$  for 24 h after which the mixture was filtered and concentrated under reduced pressure. The crude product was used (as it is) (Yield 41 %).

$^1\text{H}$  NMR (400 MHz, DMSO)  $\delta$  8.90 (s, 1H), 8.06 (dd,  $J = 7.8, 1.5$  Hz, 1H), 8.02 – 7.95 (m, 2H), 7.70 – 7.64 (m, 1H), 7.60 – 7.52 (m, 2H), 7.48 – 7.41 (m, 1H), 7.36 – 7.29 (m, 2H), 5.79 (dd,  $J = 17.3, 1.4$  Hz, 1H), 5.47 (dd,  $J = 11.0, 1.3$  Hz, 1H).

$^{13}\text{C}$  NMR (101 MHz,  $\text{CD}_2\text{Cl}_2$ )  $\delta$  192.73, 171.90, 160.86, 157.88, 140.04, 134.07, 132.99, 132.03, 131.87, 128.69, 128.37, 127.55, 126.75, 121.27, 119.00.

**20:** A round bottom flask was charged with G2 (1 equiv., 168 mg) and  $\text{Cu(I)Cl}$  (1 equiv., 19 mg) benzylidene ligand **18** (1 equiv., 60 mg). DCM (10 mL) was added to the reaction flask under  $\text{N}_2$ . The reaction mixture was stirred at room temperature for 2 h. The solvent was evaporated, and the crude product was purified by column chromatography (Yield 61 %).

$^1\text{H}$  NMR (400 MHz,  $\text{CDCl}_3$ )  $\delta$  18.59 (s, 1H), 8.65 (s, 1H), 7.90 (d,  $J = 8.0$  Hz, 2H), 7.70 (t,  $J = 7.4$  Hz, 1H), 7.55 – 7.49 (m, 2H), 7.19 – 7.07 (m, 6H), 6.81 (d,  $J = 7.8$  Hz, 1H), 4.13 (s, 4H), 2.48 (d,  $J = 17.4$  Hz, 18H).

**21:** *cis*-5-Norbornene-*exo*-2,3-dicarboxylic anhydride (1 equiv., 2 g) was dissolved in 8 mL toluene purged with  $\text{N}_2$  gas. Then, 2-aminoethanol (1 equiv., 1.12 g) and  $\text{Et}_3\text{N}$  (10 equiv., 0.25 g) were added, and the flask was fitted with a Dean-Stark trap and a condenser. The reaction mixture was refluxed in oil bath at 120 °C for 15 h. The solvent was evaporated under reduced pressure. The product was purified by column chromatography to give a white solid (Yield 90 %).

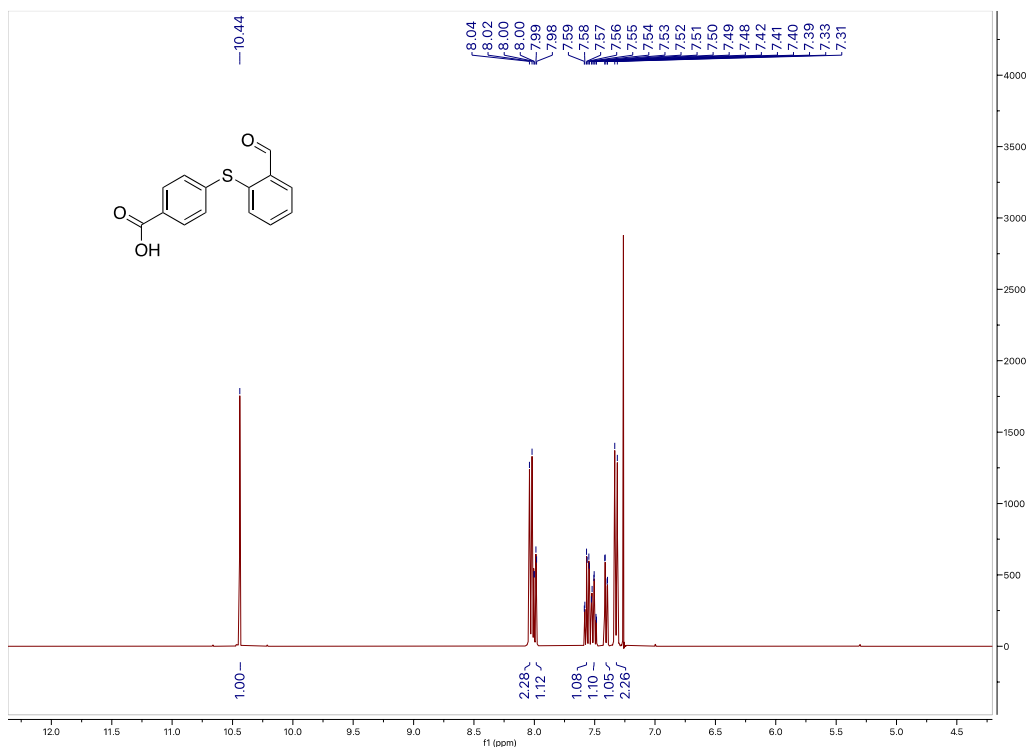
$^1\text{H}$  NMR (400 MHz,  $\text{CDCl}_3$ )  $\delta$  6.28 (d,  $J = 1.8$  Hz, 2H), 3.82 – 3.61 (m, 4H), 3.31 – 3.20 (m, 2H), 2.74 – 2.65 (m, 2H), 1.50 (ddt,  $J = 8.8, 3.3, 1.8$  Hz, 1H), 1.39 – 1.29 (m, 1H).

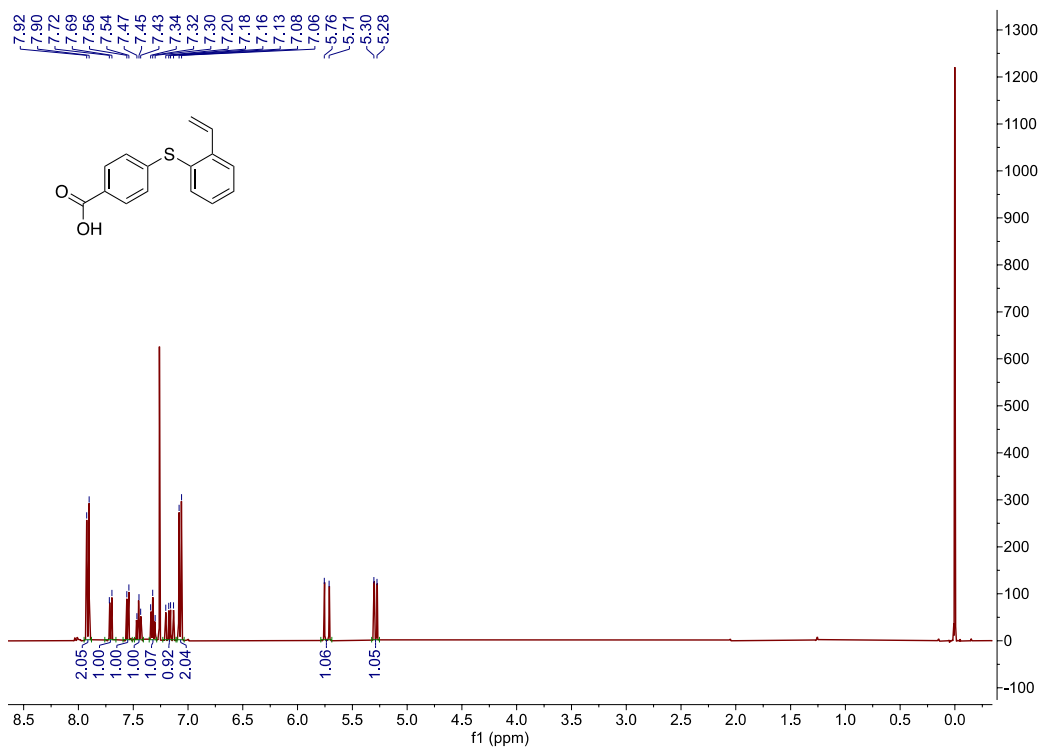
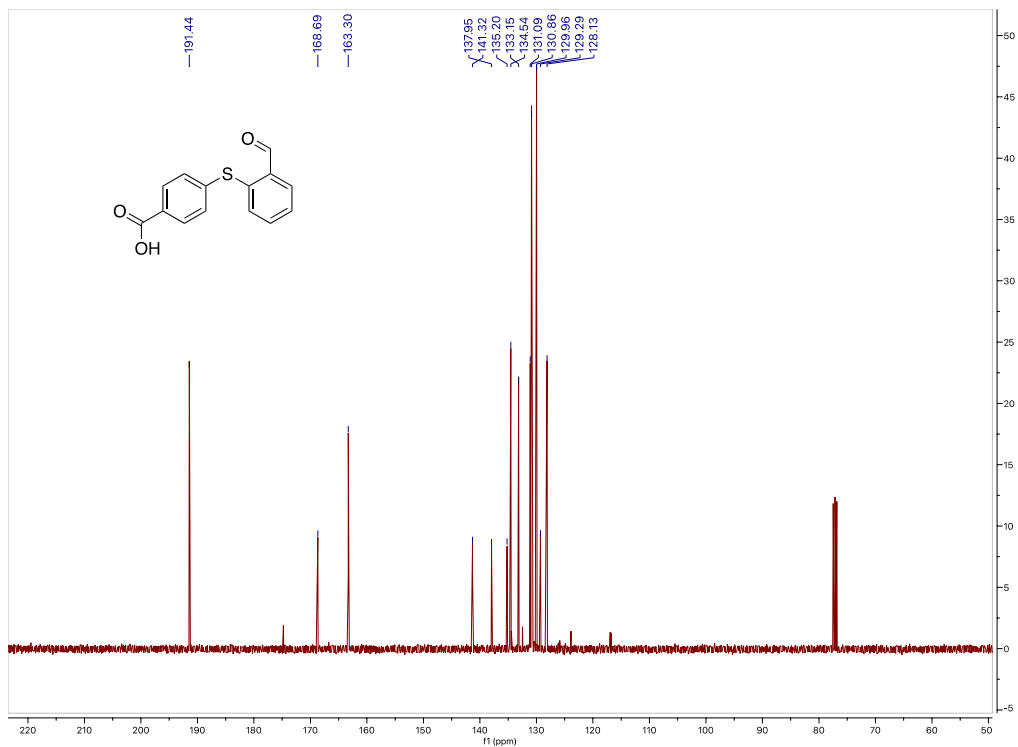
**22:** A mixture of the olefin metathesis catalyst **21** (1 equiv., 100 mg) and DMAP (10 equiv., 170 mg) in DCM was stirred under  $\text{N}_2$  atmosphere for 20 min at 0 °C. Then, a mixture of

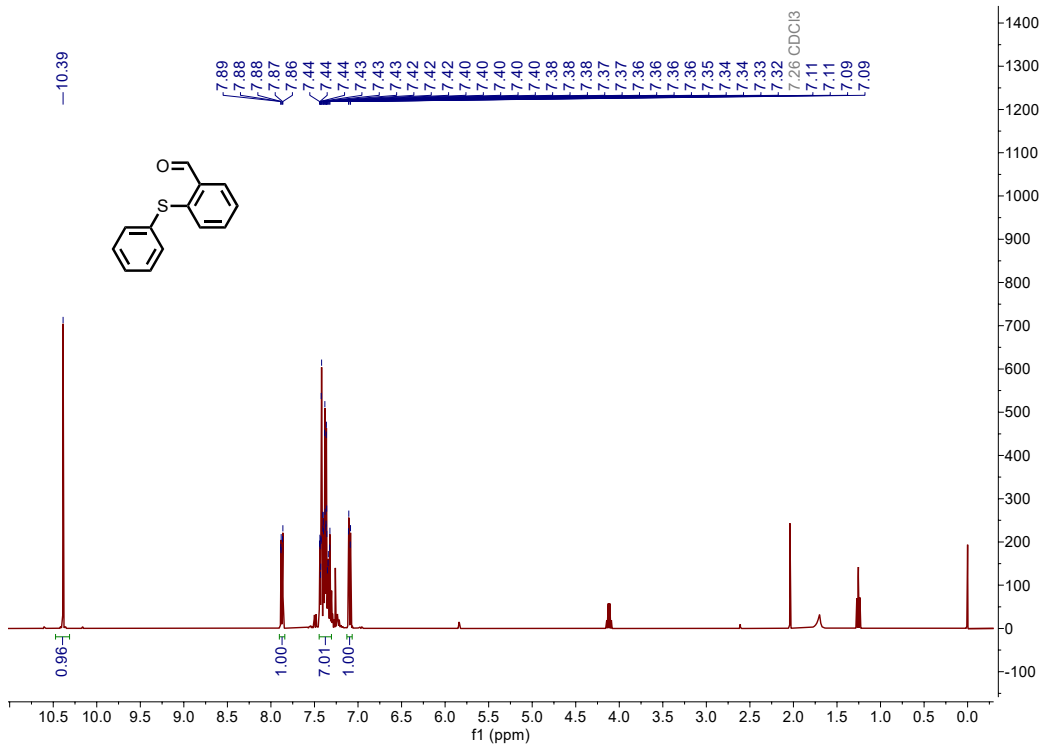
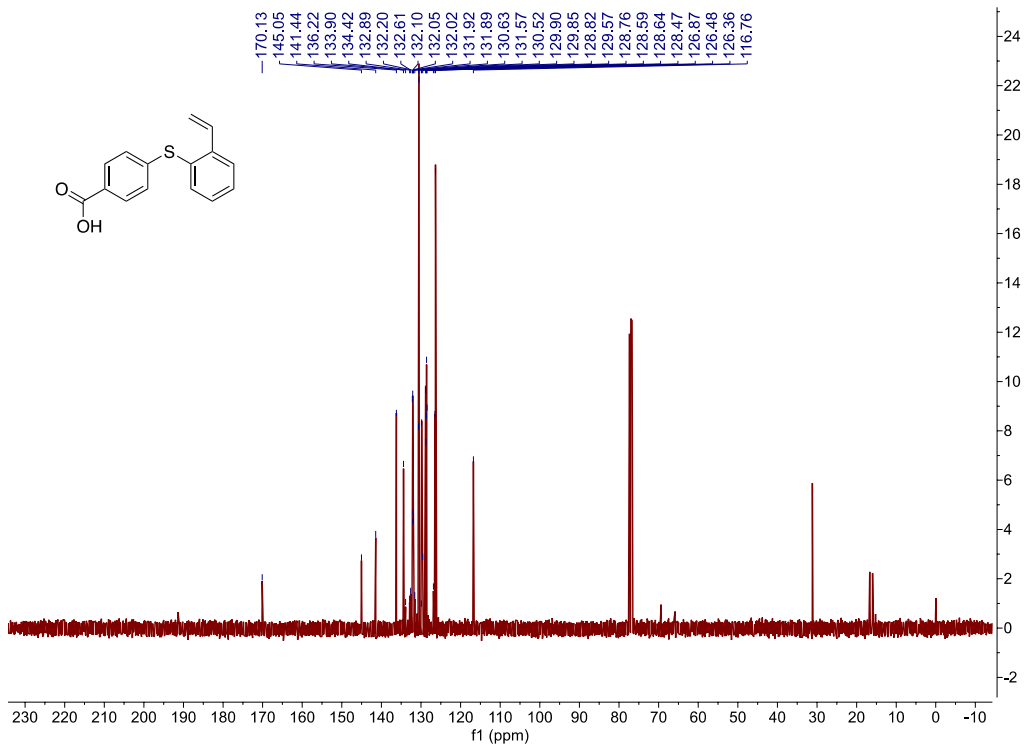
the ROMP monomer **21** (1.2 equiv., 34.70 mg) with EDC (1.5 equiv., 53 mg) in DCM was added dropwise. The reaction mixture was stirred for 2 h with holding the temperature below 5 °C. The mixture was filtered through silica plug and the crude product was purified by column chromatography (DCM: acetone 2:8) (yield 40 %).

<sup>1</sup>H NMR (400 MHz, cd<sub>2</sub>cl<sub>2</sub>) δ 18.73 (s, 1H), 8.69 (t, *J* = 0.5 Hz, 1H), 7.80 – 7.77 (m, 2H), 7.78 – 7.75 (m, 1H), 7.61 – 7.57 (m, 2H), 7.20 – 7.06 (m, 6H), 6.84 – 6.81 (m, 1H), 6.29 – 6.27 (m, 2H), 4.45 (dd, *J* = 6.0, 5.0 Hz, 2H), 4.11 (s, 4H), 3.91 (d, *J* = 0.8 Hz, 2H), 3.24 – 3.22 (m, 2H), 2.70 (d, *J* = 1.4 Hz, 2H), 2.50 (s, 18H), 1.45 (dt, *J* = 9.8, 1.6 Hz, 1H), 1.29 – 1.26 (m, 1H).

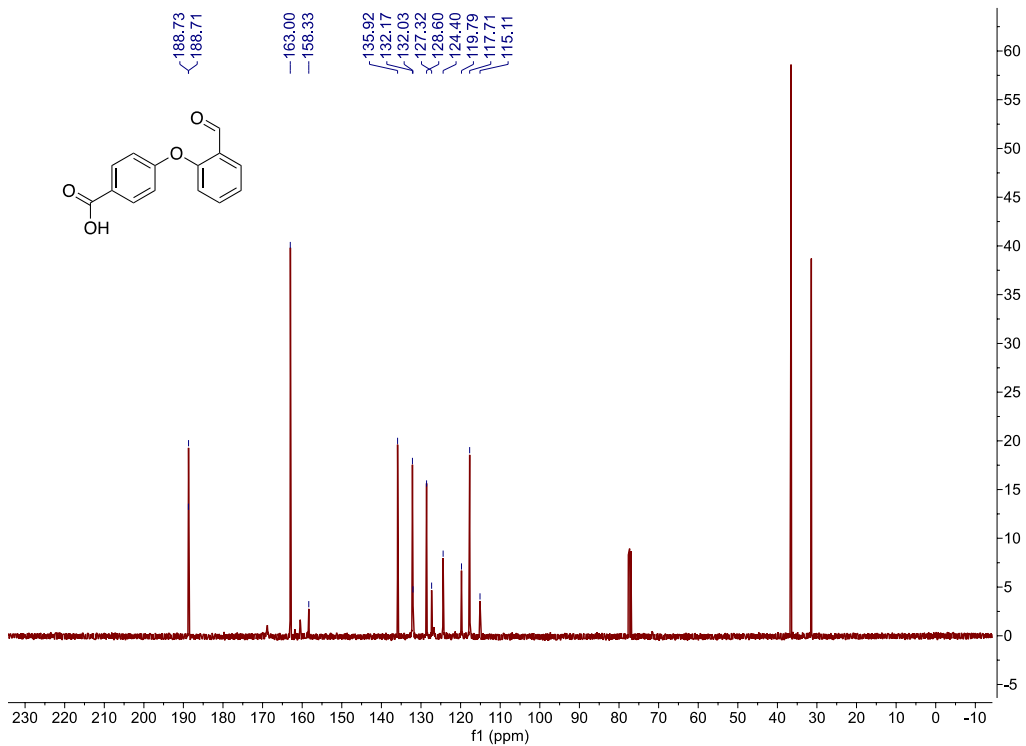
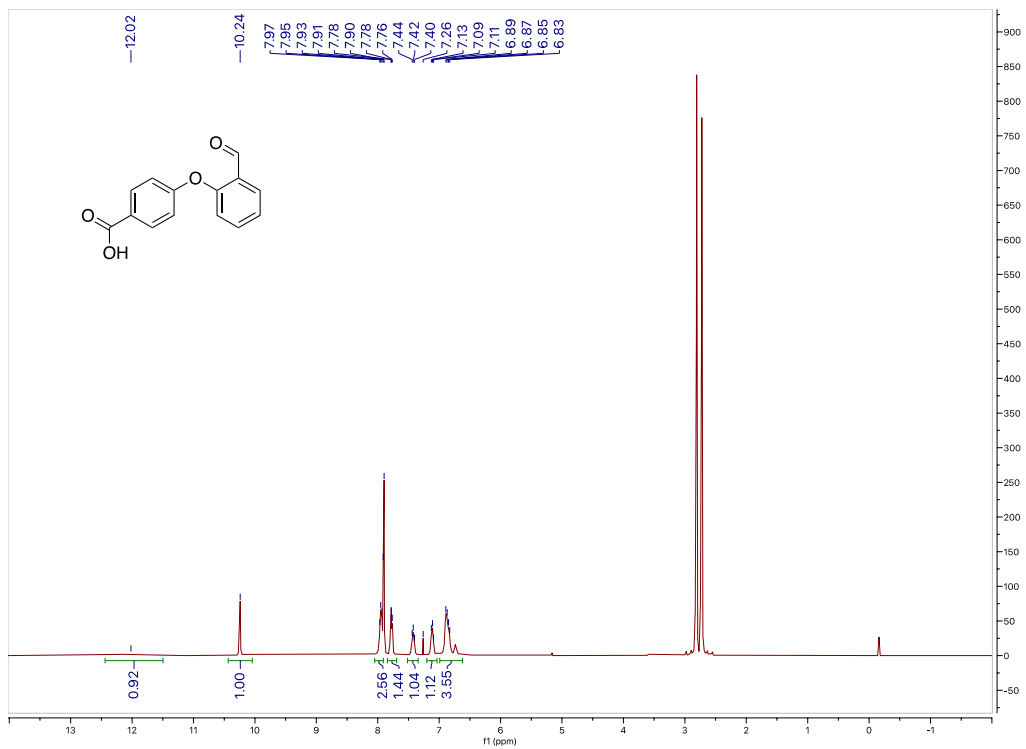
### NMR characterization

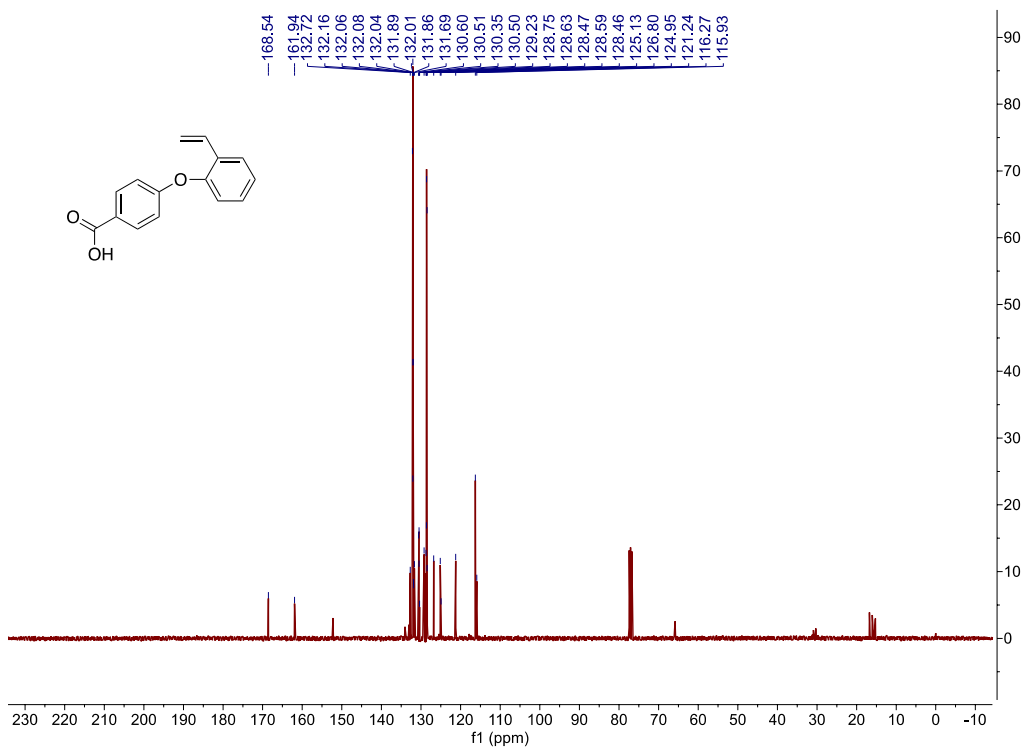
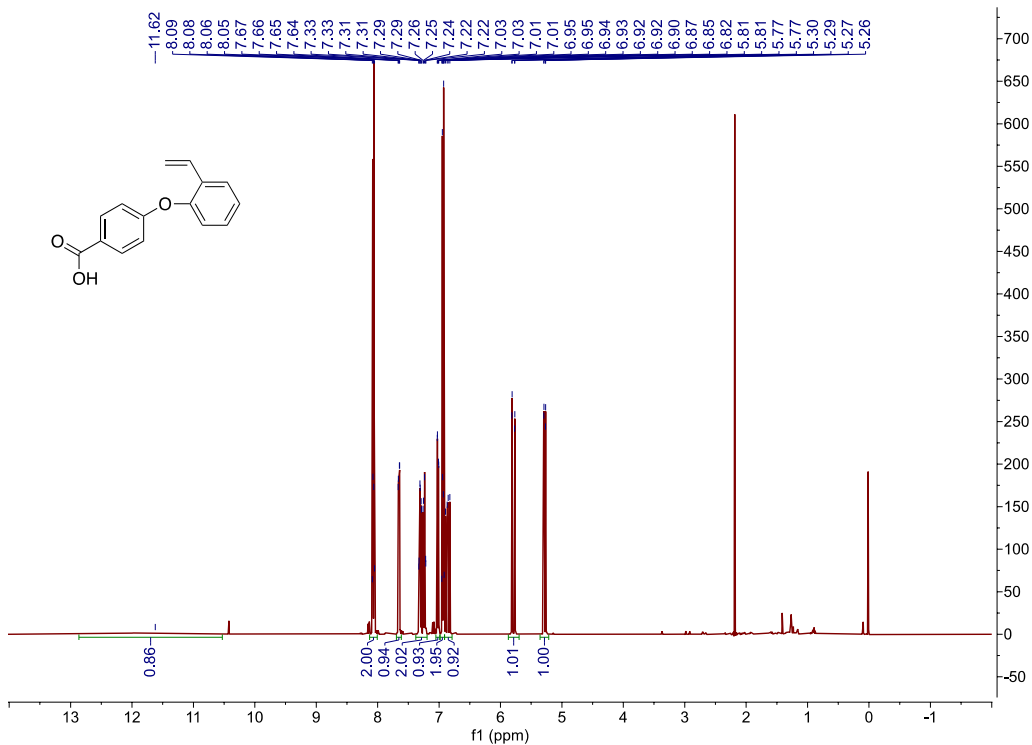


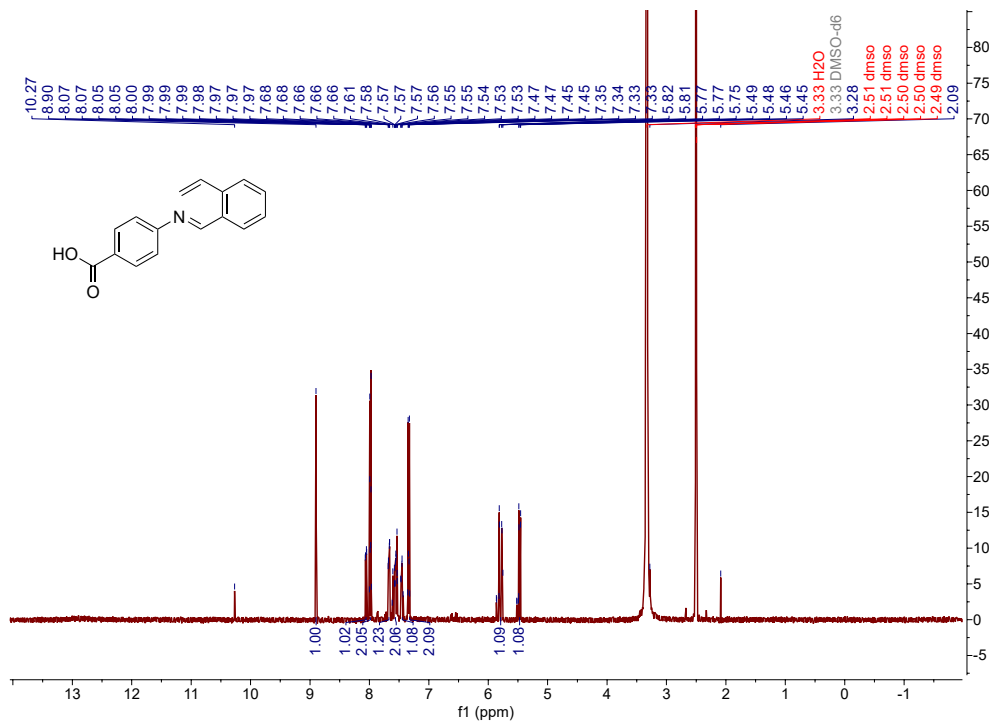
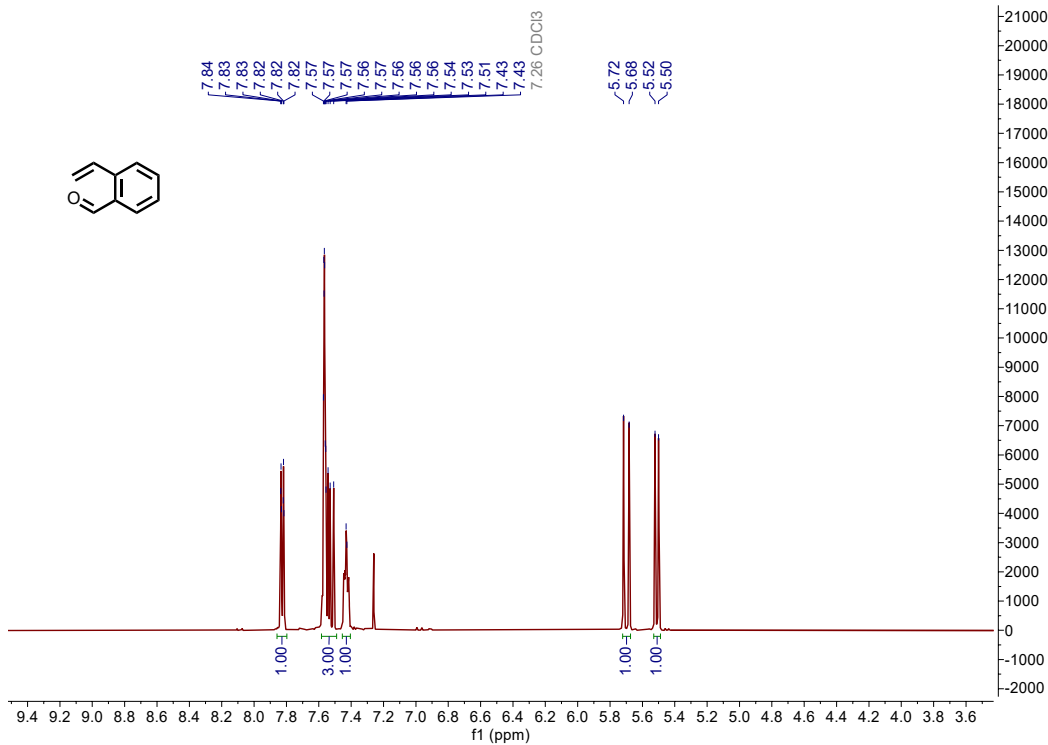


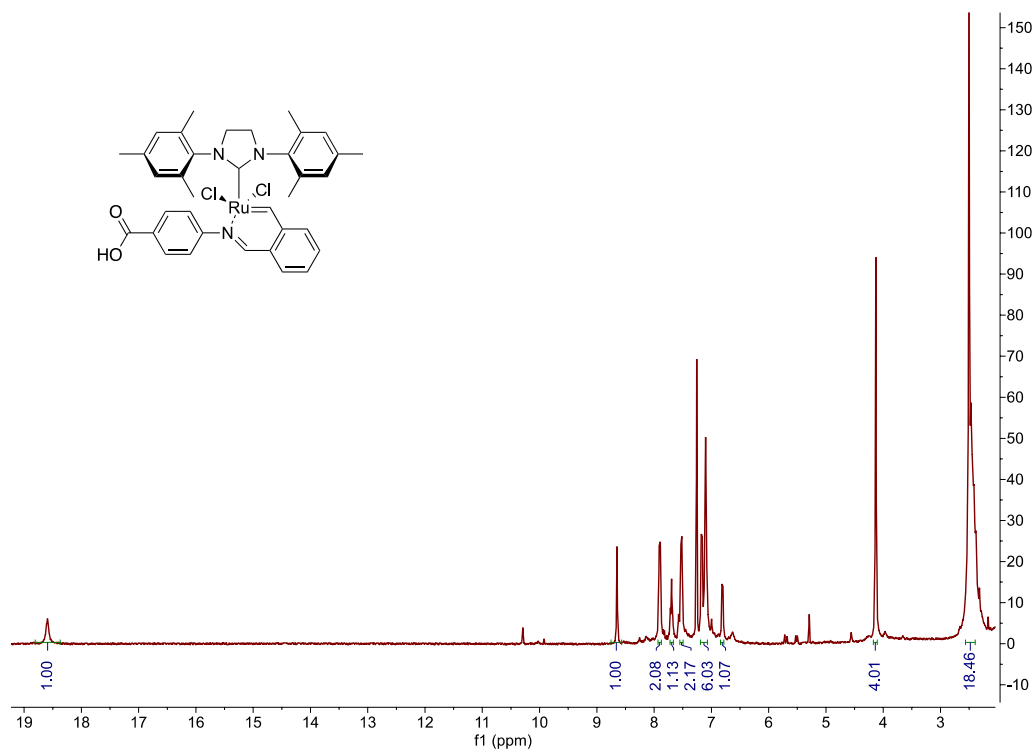
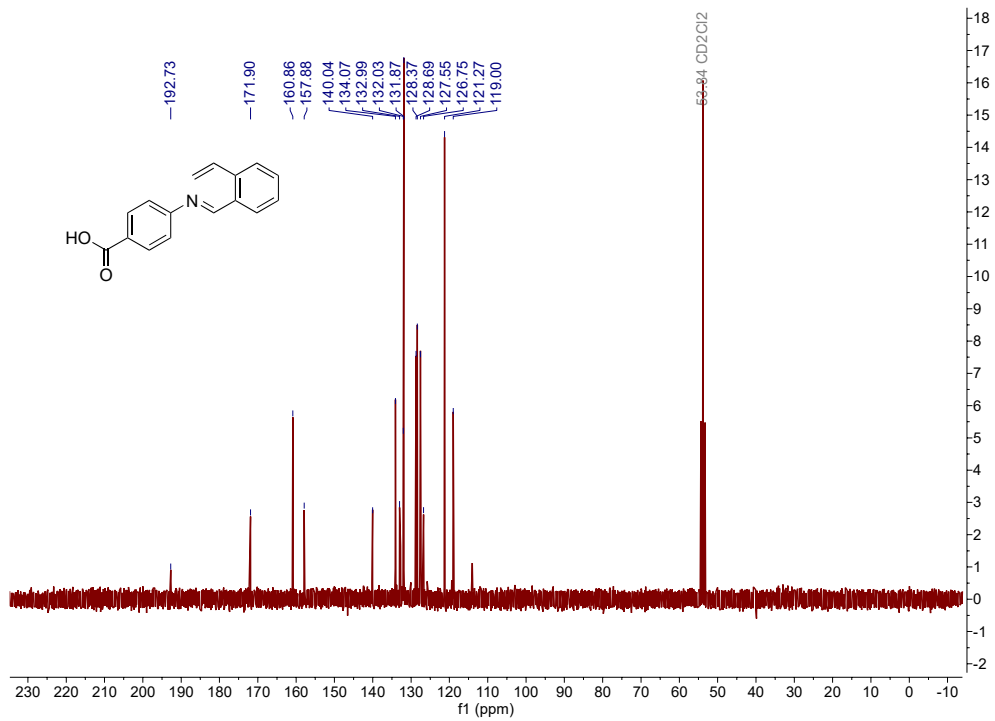


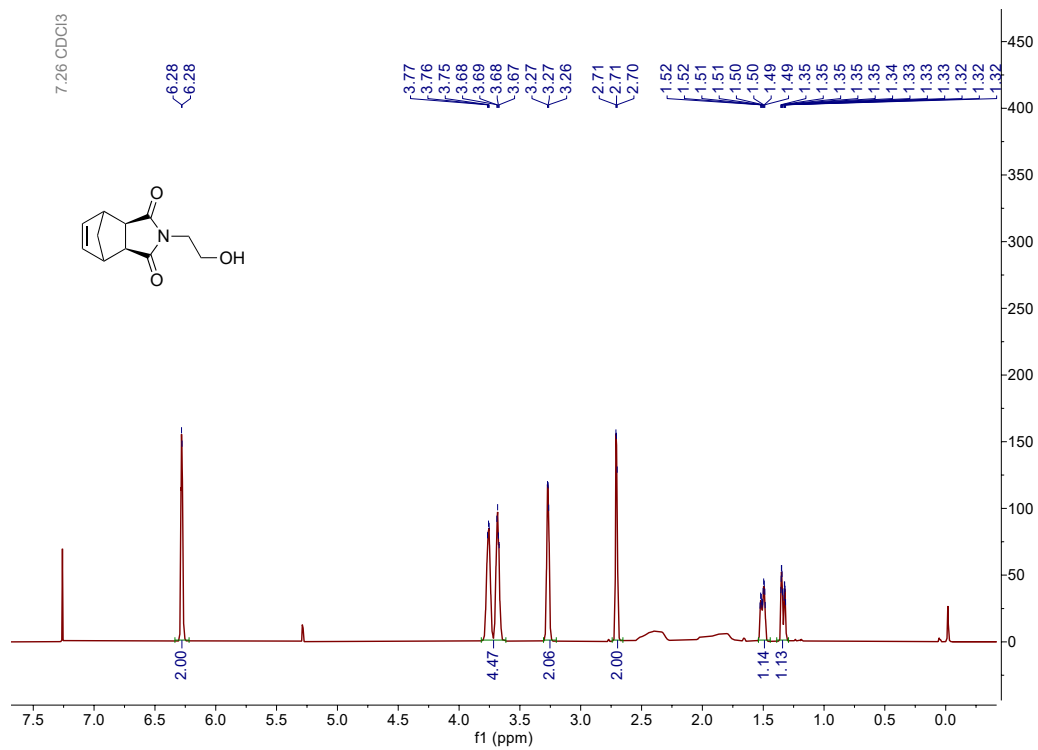
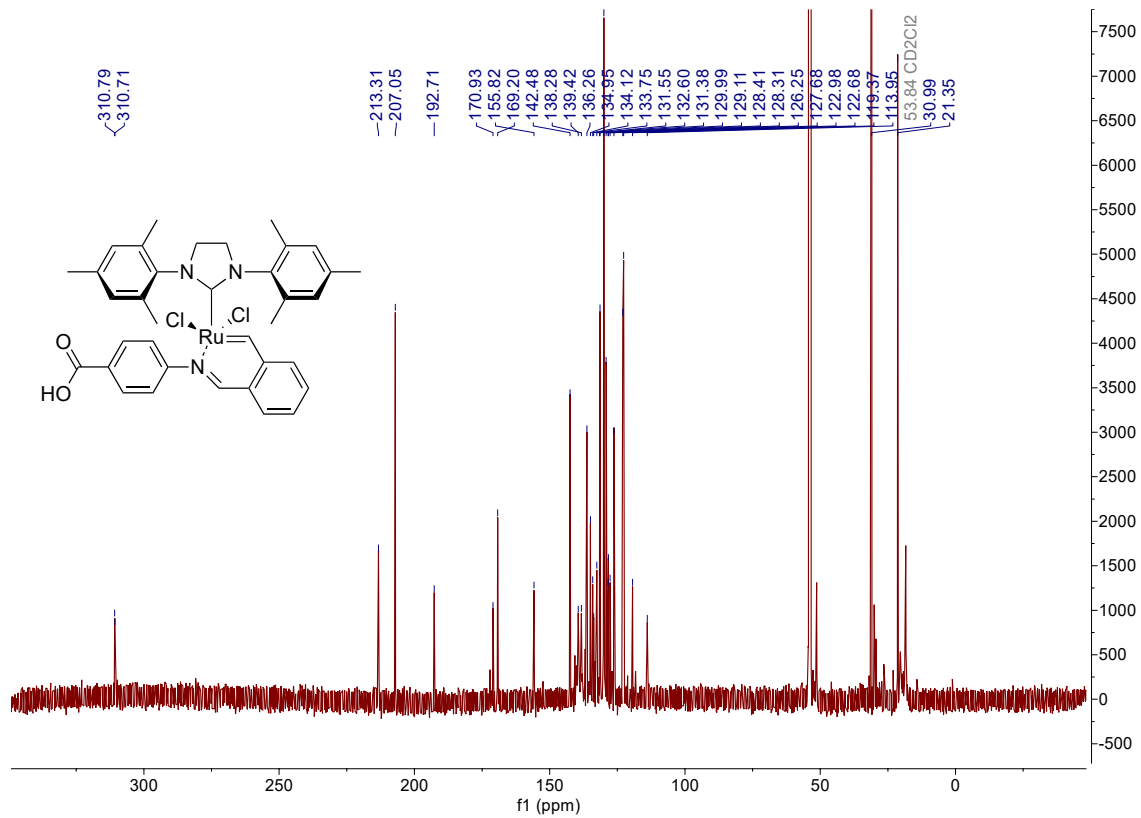


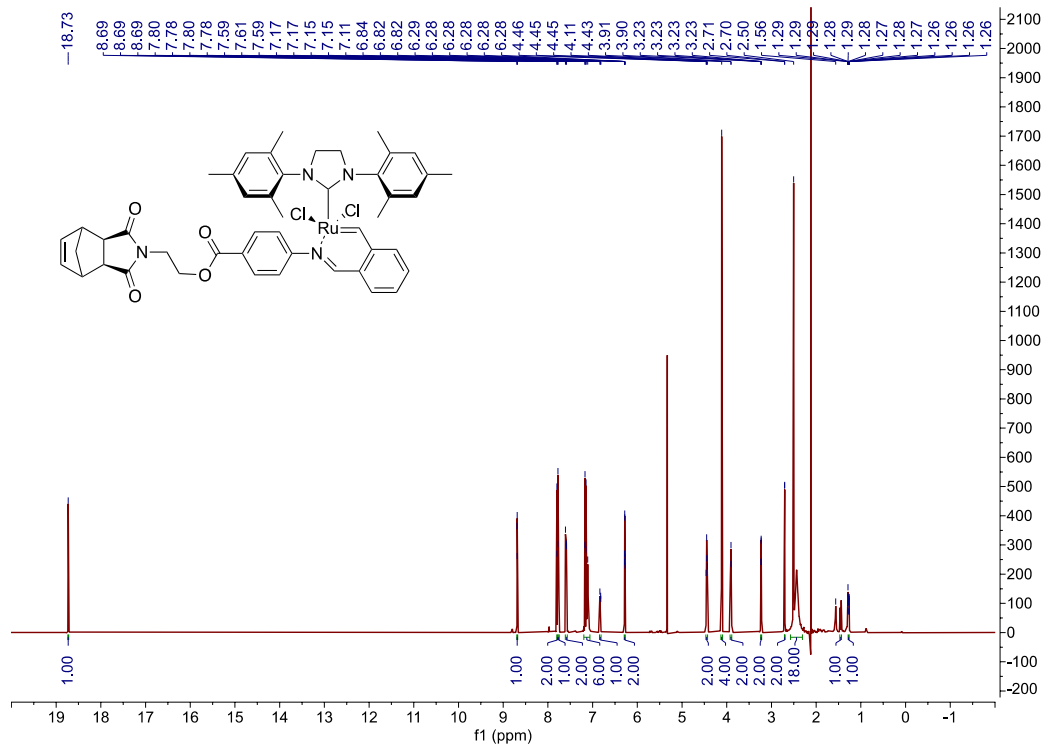






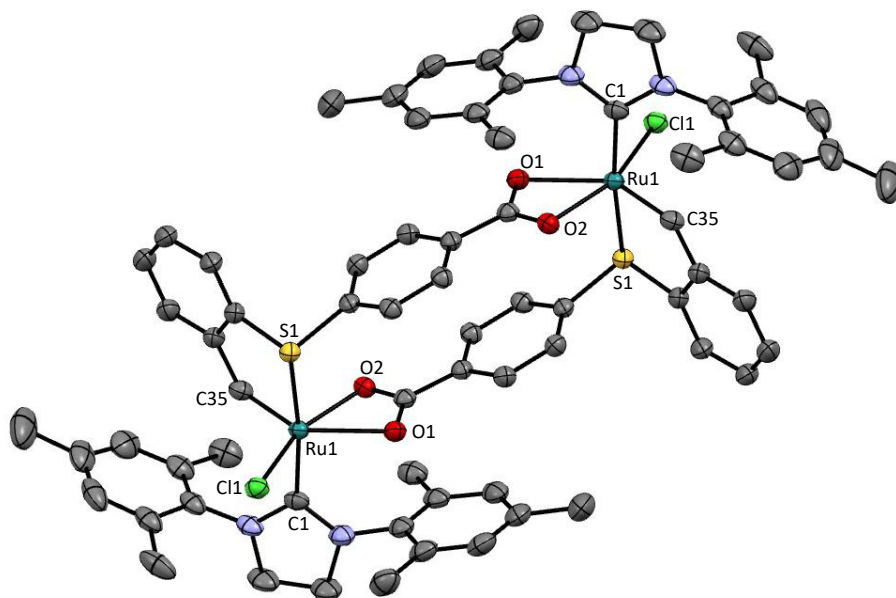






## Crystal Structure Determination

**Acknowledgements:** We thank the support of the National Science Foundation under CHE-1726077 for crystallography experiments.



(5)

## Experimental

A brown prism ( $0.138 \times 0.372 \times 0.453 \text{ mm}^3$ ) was centered on the goniometer of a Rigaku Oxford Diffraction Synergy-S diffractometer equipped with a HyPix6000HE detector and operating with  $\text{MoK}\alpha$  radiation. The data collection routine, unit cell refinement, and data processing were carried out with the program CrysAlisPro.<sup>112</sup> The

---

(107) CrysAlisPro Software System, v1.171.40.53, Rigaku Oxford Diffraction, 2019, Rigaku Corporation, Oxford, UK.

Laue symmetry and systematic absences were consistent with the monoclinic space group  $P2_1/n$ . The structure was solved using SHELXT<sup>113</sup> and refined using SHELXL<sup>114</sup> via Olex2.<sup>115</sup> After identifying the main entity, the difference electron density map suggested the presence of one CH<sub>2</sub>Cl<sub>2</sub> and at least one hexane in the asymmetric unit. Attempts to model the disordered solvent were unsuccessful, so the solvent mask feature of OLEX2 was used. Two symmetry equivalent solvent regions of volume 687.4 Å<sup>3</sup> were identified; 258.7 electrons was subtracted from each solvent region, roughly corresponding to two CH<sub>2</sub>Cl<sub>2</sub> (42 e-/molecule) and 3-4 C<sub>6</sub>H<sub>14</sub> (50 e-/molecule) per void. The final refinement model involved anisotropic displacement parameters for non-hydrogen atoms and a riding model for all hydrogen atoms. Olex2<sup>116</sup> was used for molecular graphics generation.

**Table 6.6.1.** Crystal data and structure refinement for cs2577-catalyst 5.

Identification code	HA-1-40-P1	
Empirical formula	C <sub>70</sub> H <sub>70</sub> Cl <sub>2</sub> N <sub>4</sub> O <sub>4</sub> Ru <sub>2</sub> S <sub>2</sub>	
Formula weight	1368.46	
Temperature	100.00(11) K	
Wavelength	0.71073 Å	
Crystal system	Monoclinic	
Space group	$P 1 2_1/n 1$	
Unit cell dimensions	$a = 13.6427(3)$ Å	$\alpha = 90^\circ$
	$b = 22.6856(3)$ Å	$\beta = 114.873(3)^\circ$
	$c = 14.4186(3)$ Å	$\gamma = 90^\circ$

(108) Sheldrick, G. M. "SHELXT – Integrated space-group and crystal structure determination." *Acta Cryst.* **2015**, *A71*, 3–8.

(109) Sheldrick, G. M. "Crystal structure refinement with SHELXL." *Acta Cryst.* **2015**, *C71*, 3-8.

(110) Dolomanov, O.V.; Bourhis, L. J.; Gildea, R. J.; Howard, J. A. K.; Puschmann, H. *J. Appl. Cryst.* **2009**, *42*, 339–341.

(111) Dolomanov, O.V.; Bourhis, L. J.; Gildea, R. J.; Howard, J. A. K.; Puschmann, H. *J. Appl. Cryst.* **2009**, *42*, 339–341.

Volume	4048.53(16) Å <sup>3</sup>
Z	2
Density (calculated)	1.123 Mg/m <sup>3</sup>
Absorption coefficient	0.531 mm <sup>-1</sup>
F(000)	1408
Crystal size	0.453 x 0.372 x 0.138 mm <sup>3</sup>
Theta range for data collection	2.700 to 35.705°.
Index ranges	-21 ≤ h ≤ 21, -35 ≤ k ≤ 37, -21 ≤ l ≤ 23
Reflections collected	90613
Independent reflections	17221 [R(int) = 0.0465]
Completeness to theta = 25.242°	99.7 %
Absorption correction	Gaussian
Max. and min. transmission	1.000 and 0.206
Refinement method	Full-matrix least-squares on F <sup>2</sup>
Data / restraints / parameters	17221 / 0 / 385
Goodness-of-fit on F <sup>2</sup>	1.059
Final R indices [I>2σ(I)]	R1 = 0.0427, wR2 = 0.1211
R indices (all data)	R1 = 0.0578, wR2 = 0.1269
Extinction coefficient	n/a
Largest diff. peak and hole	1.545 and -0.449 e.Å <sup>-3</sup>

**Table 6.6.2.** Bond lengths [Å] and angles [°] for cs2577-catalyst 5.

Ru(1)-Cl(1)	2.3445(4)
Ru(1)-S(1)	2.4482(4)
Ru(1)-O(1)#1	2.3577(13)
Ru(1)-O(2)#1	2.0893(11)
Ru(1)-C(1)	2.0647(16)
Ru(1)-C(35)	1.8480(18)
S(1)-C(22)	1.7860(17)
S(1)-C(29)	1.7766(17)
O(1)-C(28)	1.2571(19)

O(2)-C(28)	1.280(2)
N(1)-C(1)	1.355(2)
N(1)-C(2)	1.474(2)
N(1)-C(4)	1.427(3)
N(2)-C(1)	1.344(2)
N(2)-C(3)	1.481(2)
N(2)-C(13)	1.434(3)
C(2)-C(3)	1.502(3)
C(4)-C(5)	1.408(3)
C(4)-C(9)	1.407(3)
C(5)-C(6)	1.389(3)
C(5)-C(10)	1.502(3)
C(6)-C(7)	1.394(4)
C(7)-C(8)	1.375(4)
C(7)-C(11)	1.505(4)
C(8)-C(9)	1.390(3)
C(9)-C(12)	1.499(3)
C(13)-C(14)	1.402(3)
C(13)-C(18)	1.390(3)
C(14)-C(15)	1.406(3)
C(14)-C(19)	1.495(3)
C(15)-C(16)	1.369(3)
C(16)-C(17)	1.392(3)
C(16)-C(20)	1.519(3)
C(17)-C(18)	1.388(3)
C(18)-C(21)	1.510(3)
C(22)-C(23)	1.393(2)
C(22)-C(27)	1.390(2)
C(23)-C(24)	1.382(2)
C(24)-C(25)	1.401(2)
C(25)-C(26)	1.381(2)

C(25)-C(28) 1.493(2)  
C(26)-C(27) 1.387(2)  
C(29)-C(30) 1.397(2)  
C(29)-C(34) 1.391(2)  
C(30)-C(31) 1.390(3)  
C(31)-C(32) 1.364(3)  
C(32)-C(33) 1.391(3)  
C(33)-C(34) 1.394(2)  
C(34)-C(35) 1.465(2)  
Cl(1)-Ru(1)-S(1) 84.847(14)  
Cl(1)-Ru(1)-O(1)#1 98.60(3)  
O(1)#1-Ru(1)-S(1) 82.40(3)  
O(2)#1-Ru(1)-Cl(1) 157.35(3)  
O(2)#1-Ru(1)-S(1) 92.79(3)  
O(2)#1-Ru(1)-O(1)#1 58.79(4)  
C(1)-Ru(1)-Cl(1) 88.15(4)  
C(1)-Ru(1)-S(1) 171.99(5)  
C(1)-Ru(1)-O(1)#1 102.52(6)  
C(1)-Ru(1)-O(2)#1 95.17(5)  
C(35)-Ru(1)-Cl(1) 108.47(5)  
C(35)-Ru(1)-S(1) 83.78(5)  
C(35)-Ru(1)-O(1)#1 148.24(6)  
C(35)-Ru(1)-O(2)#1 93.60(6)  
C(35)-Ru(1)-C(1) 94.79(7)  
C(22)-S(1)-Ru(1) 111.79(5)  
C(29)-S(1)-Ru(1) 97.11(6)  
C(29)-S(1)-C(22) 102.39(8)  
C(28)-O(1)-Ru(1)#1 84.72(10)  
C(28)-O(2)-Ru(1)#1 96.34(9)  
C(1)-N(1)-C(2) 113.27(16)  
C(1)-N(1)-C(4) 128.97(14)

C(4)-N(1)-C(2)	117.20(16)
C(1)-N(2)-C(3)	113.72(16)
C(1)-N(2)-C(13)	129.15(15)
C(13)-N(2)-C(3)	117.13(15)
N(1)-C(1)-Ru(1)	128.18(13)
N(2)-C(1)-Ru(1)	124.42(13)
N(2)-C(1)-N(1)	106.80(14)
N(1)-C(2)-C(3)	103.24(16)
N(2)-C(3)-C(2)	102.54(16)
C(5)-C(4)-N(1)	119.23(17)
C(9)-C(4)-N(1)	120.56(18)
C(9)-C(4)-C(5)	120.0(2)
C(4)-C(5)-C(10)	121.3(2)
C(6)-C(5)-C(4)	119.0(2)
C(6)-C(5)-C(10)	119.7(2)
C(5)-C(6)-C(7)	121.7(2)
C(6)-C(7)-C(11)	121.7(3)
C(8)-C(7)-C(6)	117.7(2)
C(8)-C(7)-C(11)	120.7(3)
C(7)-C(8)-C(9)	123.4(2)
C(4)-C(9)-C(12)	122.1(2)
C(8)-C(9)-C(4)	117.8(2)
C(8)-C(9)-C(12)	120.1(2)
C(14)-C(13)-N(2)	118.48(17)
C(18)-C(13)-N(2)	119.45(17)
C(18)-C(13)-C(14)	121.96(19)
C(13)-C(14)-C(15)	116.91(18)
C(13)-C(14)-C(19)	121.43(18)
C(15)-C(14)-C(19)	121.64(18)
C(16)-C(15)-C(14)	122.43(19)
C(15)-C(16)-C(17)	118.8(2)

C(15)-C(16)-C(20) 120.8(2)  
C(17)-C(16)-C(20) 120.4(2)  
C(18)-C(17)-C(16) 121.4(2)  
C(13)-C(18)-C(21) 121.6(2)  
C(17)-C(18)-C(13) 118.48(19)  
C(17)-C(18)-C(21) 119.9(2)  
C(23)-C(22)-S(1) 122.41(13)  
C(27)-C(22)-S(1) 116.48(12)  
C(27)-C(22)-C(23) 120.84(15)  
C(24)-C(23)-C(22) 119.44(16)  
C(23)-C(24)-C(25) 119.92(15)  
C(24)-C(25)-C(28) 119.25(14)  
C(26)-C(25)-C(24) 120.04(15)  
C(26)-C(25)-C(28) 120.58(15)  
C(25)-C(26)-C(27) 120.44(15)  
C(26)-C(27)-C(22) 119.23(15)  
O(1)-C(28)-Ru(1)#1 66.10(9)  
O(1)-C(28)-O(2) 119.86(15)  
O(1)-C(28)-C(25) 121.96(15)  
O(2)-C(28)-Ru(1)#1 53.97(8)  
O(2)-C(28)-C(25) 118.11(14)  
C(25)-C(28)-Ru(1)#1 1169.34(11)  
C(30)-C(29)-S(1) 121.86(14)  
C(34)-C(29)-S(1) 115.61(12)  
C(34)-C(29)-C(30) 122.46(16)  
C(31)-C(30)-C(29) 117.59(18)  
C(32)-C(31)-C(30) 121.28(17)  
C(31)-C(32)-C(33) 120.49(18)  
C(32)-C(33)-C(34) 120.36(18)  
C(29)-C(34)-C(33) 117.82(16)  
C(29)-C(34)-C(35) 119.64(15)

C(33)-C(34)-C(35) 122.54(16)

C(34)-C(35)-Ru(1) 123.76(12)

Symmetry transformations used to generate equivalent atoms: #1 -x+1,-y+1,-z

**Table 6.6.3.** Torsion angles [°] for cs2577-catalyst 5

---

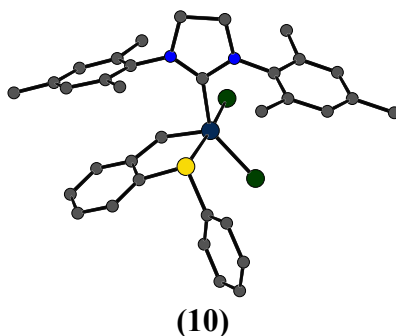
Ru(1)-S(1)-C(22)-C(23)	70.37(14)
Ru(1)-S(1)-C(22)-C(27)	-103.68(12)
Ru(1)-S(1)-C(29)-C(30)	179.25(14)
Ru(1)-S(1)-C(29)-C(34)	2.23(13)
Ru(1)#1-O(1)-C(28)-O(2)	4.96(13)
Ru(1)#1-O(1)-C(28)-C(25)	-172.10(14)
Ru(1)#1-O(2)-C(28)-O(1)	-5.61(15)
Ru(1)#1-O(2)-C(28)-C(25)	171.57(12)
Cl(1)-Ru(1)-C(35)-C(34)	81.03(14)
S(1)-Ru(1)-C(35)-C(34)	-1.40(13)
S(1)-C(22)-C(23)-C(24)	-171.27(13)
S(1)-C(22)-C(27)-C(26)	170.91(12)
S(1)-C(29)-C(30)-C(31)	-176.76(13)
S(1)-C(29)-C(34)-C(33)	176.54(13)
S(1)-C(29)-C(34)-C(35)	-3.7(2)
O(1)#1-Ru(1)-C(35)-C(34)	-66.0(2)
O(2)#1-Ru(1)-C(35)-C(34)	-93.82(14)
N(1)-C(2)-C(3)-N(2)	-6.2(2)
N(1)-C(4)-C(5)-C(6)	-178.33(17)
N(1)-C(4)-C(5)-C(10)	0.3(3)
N(1)-C(4)-C(9)-C(8)	177.45(16)
N(1)-C(4)-C(9)-C(12)	-4.7(3)
N(2)-C(13)-C(14)-C(15)	-178.11(15)
N(2)-C(13)-C(14)-C(19)	3.7(2)
N(2)-C(13)-C(18)-C(17)	177.63(16)
N(2)-C(13)-C(18)-C(21)	-3.7(3)
C(1)-Ru(1)-C(35)-C(34)	170.68(14)

C(1)-N(1)-C(2)-C(3)	5.1(2)
C(1)-N(1)-C(4)-C(5)	85.2(2)
C(1)-N(1)-C(4)-C(9)	-99.7(2)
C(1)-N(2)-C(3)-C(2)	6.1(2)
C(1)-N(2)-C(13)-C(14)	-88.9(2)
C(1)-N(2)-C(13)-C(18)	94.9(2)
C(2)-N(1)-C(1)-Ru(1)	-172.81(14)
C(2)-N(1)-C(1)-N(2)	-1.4(2)
C(2)-N(1)-C(4)-C(5)	-85.6(2)
C(2)-N(1)-C(4)-C(9)	89.5(2)
C(3)-N(2)-C(1)-Ru(1)	168.68(13)
C(3)-N(2)-C(1)-N(1)	-3.1(2)
C(3)-N(2)-C(13)-C(14)	90.4(2)
C(3)-N(2)-C(13)-C(18)	-85.8(2)
C(4)-N(1)-C(1)-Ru(1)	16.1(3)
C(4)-N(1)-C(1)-N(2)	-172.52(17)
C(4)-N(1)-C(2)-C(3)	177.31(16)
C(4)-C(5)-C(6)-C(7)	-0.5(3)
C(5)-C(4)-C(9)-C(8)	-7.5(3)
C(5)-C(4)-C(9)-C(12)	170.31(17)
C(5)-C(6)-C(7)-C(8)	-4.4(3)
C(5)-C(6)-C(7)-C(11)	176.1(2)
C(6)-C(7)-C(8)-C(9)	3.4(3)
C(7)-C(8)-C(9)-C(4)	2.5(3)
C(7)-C(8)-C(9)-C(12)	-175.4(2)
C(9)-C(4)-C(5)-C(6)	6.6(3)
C(9)-C(4)-C(5)-C(10)	-174.77(17)
C(10)-C(5)-C(6)-C(7)	-179.16(19)
C(11)-C(7)-C(8)-C(9)	-177.1(2)
C(13)-N(2)-C(1)-Ru(1)	-12.0(3)
C(13)-N(2)-C(1)-N(1)	176.25(17)

C(13)-N(2)-C(3)-C(2)	-173.34(17)
C(13)-C(14)-C(15)-C(16)	1.4(3)
C(14)-C(13)-C(18)-C(17)	1.5(3)
C(14)-C(13)-C(18)-C(21)	-179.82(18)
C(14)-C(15)-C(16)-C(17)	-0.3(3)
C(14)-C(15)-C(16)-C(20)	-179.02(18)
C(15)-C(16)-C(17)-C(18)	-0.2(3)
C(16)-C(17)-C(18)-C(13)	-0.4(3)
C(16)-C(17)-C(18)-C(21)	-179.06(19)
C(18)-C(13)-C(14)-C(15)	-2.0(3)
C(18)-C(13)-C(14)-C(19)	179.84(17)
C(19)-C(14)-C(15)-C(16)	179.53(17)
C(20)-C(16)-C(17)-C(18)	178.52(19)
C(22)-S(1)-C(29)-C(30)	-66.51(16)
C(22)-S(1)-C(29)-C(34)	116.46(13)
C(22)-C(23)-C(24)-C(25)	0.4(2)
C(23)-C(22)-C(27)-C(26)	-3.2(2)
C(23)-C(24)-C(25)-C(26)	-2.5(2)
C(23)-C(24)-C(25)-C(28)	173.36(15)
C(24)-C(25)-C(26)-C(27)	1.8(2)
C(24)-C(25)-C(28)-Ru(1)#1	-133.8(6)
C(24)-C(25)-C(28)-O(1)	3.4(2)
C(24)-C(25)-C(28)-O(2)	-173.70(14)
C(25)-C(26)-C(27)-C(22)	1.1(2)
C(26)-C(25)-C(28)-Ru(1)#1	42.0(7)
C(26)-C(25)-C(28)-O(1)	179.26(14)
C(26)-C(25)-C(28)-O(2)	2.1(2)
C(27)-C(22)-C(23)-C(24)	2.5(2)
C(28)-C(25)-C(26)-C(27)	-174.02(15)
C(29)-S(1)-C(22)-C(23)	-32.58(15)
C(29)-S(1)-C(22)-C(27)	153.36(13)

C(29)-C(30)-C(31)-C(32)	0.5(3)
C(29)-C(34)-C(35)-Ru(1)	3.5(2)
C(30)-C(29)-C(34)-C(33)	-0.5(3)
C(30)-C(29)-C(34)-C(35)	179.31(15)
C(30)-C(31)-C(32)-C(33)	-0.6(3)
C(31)-C(32)-C(33)-C(34)	0.2(3)
C(32)-C(33)-C(34)-C(29)	0.3(3)
C(32)-C(33)-C(34)-C(35)	-179.42(17)
C(33)-C(34)-C(35)-Ru(1)	-176.75(13)
C(34)-C(29)-C(30)-C(31)	0.1(3)

Symmetry transformations used to generate equivalent atoms: #1 -x+1,-y+1,-z



## Experimental

A brown prism (0.11 x 0.23 x 0.26 mm<sup>3</sup>) was centered on the goniometer of a Rigaku Oxford Diffraction Synergy-S diffractometer equipped with a HyPix6000HE detector and operating with MoK $\alpha$  radiation. The data collection routine, unit cell refinement, and data processing were carried out with the program CrysAlisPro.<sup>117</sup> The Laue symmetry and systematic absences were consistent with the monoclinic space group

---

(112) CrysAlisPro Software System, v1.171.41.105a, Rigaku Oxford Diffraction, **2021**, Rigaku Corporation, Oxford, UK.

*P2<sub>1</sub>/c*. The structure was solved using SHELXT<sup>118</sup> and refined using SHELXL<sup>119</sup> via Olex2.<sup>120</sup> The final refinement model involved anisotropic displacement parameters for non-hydrogen atoms and a riding model for all hydrogen atoms. A CH<sub>2</sub>Cl<sub>2</sub> solvate was modeled with 2-position disorder with relative occupancies that refined to 0.708(3) and 0.292(3); the bond lengths and ellipsoids were restrained DFIX and SIMU, respectively. In addition, anisotropic displacement parameters on a phenyl ring and a mesityl ring were elongated and somewhat irregular in shape; these are attributed to dynamic disorder at the data collection temperature of 200 K. Just below 200 K, the crystals undergo a phase transition and crack into many pieces. The phase transition likely results from the dynamic groups freezing into position. Olex2<sup>121</sup> was used for molecular graphics generation.

---

(113) Sheldrick, G. M. "SHELXT – Integrated space-group and crystal structure determination." *Acta Cryst.* **2015**, *A71*, 3–8.

(114) Sheldrick, G. M. "Crystal structure refinement with SHELXL." *Acta Cryst.* **2015**, *C71*, 3–8.

(115) Dolomanov, O.V.; Bourhis, L. J.; Gildea, R. J.; Howard, J. A. K.; Puschmann, H. *J. Appl. Cryst.* **2009**, **42**, 339–341.

(116) Dolomanov, O.V.; Bourhis, L. J.; Gildea, R. J.; Howard, J. A. K.; Puschmann, H. *J. Appl. Cryst.* **2009**, **42**, 339–341.

**Table 6.6.4. Crystal data and structure refinement for cs2903- catalyst 10.**

Identification code	HA-2-75
Empirical formula	C <sub>34</sub> H <sub>36</sub> Cl <sub>2</sub> N <sub>2</sub> RuS • CH <sub>2</sub> Cl <sub>2</sub>
Formula weight	761.60
Temperature/K	200.00(15)
Crystal system	monoclinic
Space group	P2 <sub>1</sub> /c
a/Å	8.08610(10)
b/Å	18.3296(3)
c/Å	24.0578(3)
α/°	90
β/°	98.9570(10)
γ/°	90
Volume/Å <sup>3</sup>	3522.24(9)
Z	4
ρ <sub>calc</sub> /cm <sup>3</sup>	1.436
μ/mm <sup>-1</sup>	0.835
F(000)	1560.0
Crystal size/mm <sup>3</sup>	0.26 × 0.23 × 0.11
Radiation	Mo Kα (λ = 0.71073)
2θ range for data collection/°	5.564 to 76.65
Index ranges	-13 ≤ h ≤ 13, -31 ≤ k ≤ 30, -40 ≤ l ≤ 40
Reflections collected	109895
Independent reflections	18426 [R <sub>int</sub> = 0.0314, R <sub>sigma</sub> = 0.0245]
Data/restraints/parameters	18426/52/413
Goodness-of-fit on F <sup>2</sup>	1.054
Final R indexes [I ≥ 2σ (I)]	R <sub>1</sub> = 0.0365, wR <sub>2</sub> = 0.0970
Final R indexes [all data]	R <sub>1</sub> = 0.0522, wR <sub>2</sub> = 0.1029
Largest diff. peak/hole / e Å <sup>-3</sup>	1.13/-0.85

**Table 6.6.5. Bond Lengths for cs2903-catalyst 10.**

Atom	Atom	Length/Å	Atom	Atom	Length/Å
Ru1	C11	2.3844(3)	C14	C15	1.385(3)
Ru1	C12	2.3529(4)	C14	C19	1.505(3)
Ru1	S1	2.3386(3)	C15	C16	1.389(3)
Ru1	C1	2.0158(12)	C16	C17	1.377(3)
Ru1	C28	1.8391(13)	C16	C20	1.513(3)
S1	C22	1.7806(15)	C17	C18	1.385(2)
S1	C29	1.7857(15)	C18	C21	1.503(2)
N1	C1	1.3395(16)	C22	C23	1.388(2)
N1	C2	1.4744(18)	C22	C27	1.390(2)
N1	C4	1.4257(18)	C23	C24	1.386(3)
N2	C1	1.3378(17)	C24	C25	1.379(3)
N2	C3	1.4774(18)	C25	C26	1.389(2)
N2	C13	1.4311(19)	C26	C27	1.403(2)
C2	C3	1.502(3)	C27	C28	1.4570(19)
C4	C5	1.397(2)	C29	C30	1.371(2)
C4	C9	1.398(2)	C29	C34	1.388(2)
C5	C6	1.393(2)	C30	C31	1.393(3)
C5	C10	1.503(2)	C31	C32	1.362(3)
C6	C7	1.380(2)	C32	C33	1.373(3)
C7	C8	1.389(2)	C33	C34	1.386(2)
C7	C11	1.499(2)	C13	C35A	1.775(6)
C8	C9	1.395(2)	C13	C35B	1.673(16)
C9	C12	1.506(2)	C35A	C14A	1.760(7)
C13	C14	1.393(2)	C35B	C14B	1.787(15)
C13	C18	1.398(2)			

**Table 6.6.6. Bond Angles for cs2903-catalyst 10.**

Atom	Atom	Atom	Angle/°	Atom	Atom	Atom	Angle/°
C12	Ru1	Cl1	89.430(14)	C8	C9	C12	120.35(15)
S1	Ru1	Cl1	173.230(13)	C14	C13	N2	118.98(14)
S1	Ru1	Cl2	92.533(14)	C14	C13	C18	121.22(14)
C1	Ru1	Cl1	89.37(4)	C18	C13	N2	119.51(14)
C1	Ru1	Cl2	144.63(4)	C13	C14	C19	122.10(17)
C1	Ru1	S1	92.76(4)	C15	C14	C13	118.12(17)
C28	Ru1	Cl1	89.82(4)	C15	C14	C19	119.73(17)
C28	Ru1	Cl2	117.11(4)	C14	C15	C16	122.10(19)
C28	Ru1	S1	83.52(4)	C15	C16	C20	120.3(2)
C28	Ru1	C1	98.24(5)	C17	C16	C15	118.06(19)
C22	S1	Ru1	99.36(5)	C17	C16	C20	121.6(2)
C22	S1	C29	100.61(7)	C16	C17	C18	122.33(18)
C29	S1	Ru1	117.07(5)	C13	C18	C21	122.51(15)
C1	N1	C2	112.38(12)	C17	C18	C13	118.04(16)
C1	N1	C4	127.90(11)	C17	C18	C21	119.37(15)
C4	N1	C2	119.59(12)	C23	C22	S1	123.76(14)
C1	N2	C3	113.08(12)	C23	C22	C27	122.23(15)
C1	N2	C13	126.01(11)	C27	C22	S1	114.00(10)
C13	N2	C3	120.48(12)	C24	C23	C22	117.97(19)
N1	C1	Ru1	133.67(10)	C25	C24	C23	121.32(17)
N2	C1	Ru1	118.14(9)	C24	C25	C26	120.33(17)
N2	C1	N1	108.16(11)	C25	C26	C27	119.62(17)
N1	C2	C3	103.43(12)	C22	C27	C26	118.50(14)
N2	C3	C2	102.34(11)	C22	C27	C28	117.39(13)
C5	C4	N1	119.73(13)	C26	C27	C28	124.04(15)
C5	C4	C9	121.63(13)	C27	C28	Ru1	124.88(11)

**Table 6.6.6. Bond Angles for cs2903-catalyst 10.**

Atom	Atom	Atom	Angle/°	Atom	Atom	Atom	Angle/°
C9	C4	N1	118.51(13)	C30	C29	S1	117.62(12)
C4	C5	C10	121.77(14)	C30	C29	C34	120.25(15)
C6	C5	C4	117.92(14)	C34	C29	S1	122.11(13)
C6	C5	C10	120.30(14)	C29	C30	C31	119.55(18)
C7	C6	C5	121.95(15)	C32	C31	C30	120.6(2)
C6	C7	C8	118.79(15)	C31	C32	C33	119.68(18)
C6	C7	C11	120.51(17)	C32	C33	C34	120.83(17)
C8	C7	C11	120.70(17)	C33	C34	C29	119.05(17)
C7	C8	C9	121.54(15)	Cl4A	C35A	Cl3	114.4(3)
C4	C9	C12	121.65(15)	Cl3	C35B	Cl4B	94.6(8)
C8	C9	C4	118.00(14)				

**Table 6.6.7. Torsion Angles for cs2903-catalyst 10.**

A	B	C	D	Angle/°	A	B	C	D	Angle/°
Ru1	S1	C22	C23	172.84(13)	C5	C6	C7	C11	-179.92(16)
Ru1	S1	C22	C27	-8.16(10)	C6	C7	C8	C9	-2.3(2)
Ru1	S1	C29	C30	119.35(16)	C7	C8	C9	C4	0.9(2)
Ru1	S1	C29	C34	-62.14(15)	C7	C8	C9	C12	-178.71(14)
Cl1	Ru1	C28	C27	171.56(10)	C9	C4	C5	C6	-4.98(19)
Cl2	Ru1	C28	C27	82.30(11)	C9	C4	C5	C10	173.81(13)
S1	Ru1	C28	C27	-7.23(10)	C10	C5	C6	C7	-175.25(14)
S1	C22	C23	C24	179.79(13)	C11	C7	C8	C9	177.61(16)
S1	C22	C27	C26	-178.31(10)	C13	N2	C1	Ru1	-7.38(19)
S1	C22	C27	C28	4.60(15)	C13	N2	C1	N1	174.39(13)
S1	C29	C30	C31	178.8(2)	C13	N2	C3	C2	-179.03(15)

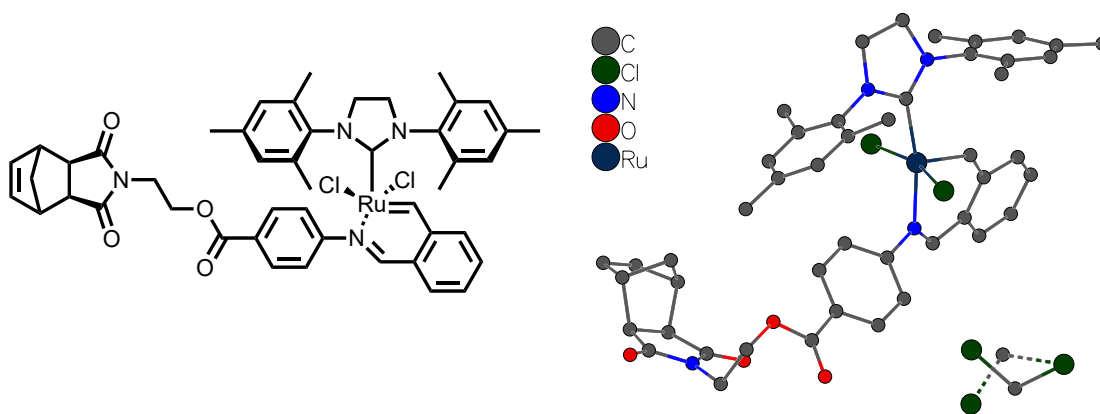
**Table 6.6.7. Torsion Angles for cs2903-catalyst 10.**

A	B	C	D	Angle/°	A	B	C	D	Angle/°
S1	C29	C34	C33	-177.61(14)	C13	C14	C15	C16	-0.7(4)
N1	C2	C3	N2	7.33(18)	C14	C13	C18	C17	-4.2(3)
N1	C4	C5	C6	179.24(12)	C14	C13	C18	C21	172.34(16)
N1	C4	C5	C10	-1.97(19)	C14	C15	C16	C17	-1.6(5)
N1	C4	C9	C8	178.63(12)	C14	C15	C16	C20	179.3(3)
N1	C4	C9	C12	-1.74(19)	C15	C16	C17	C18	1.0(5)
N2	C13	C14	C15	177.41(19)	C16	C17	C18	C13	1.8(3)
N2	C13	C14	C19	0.1(3)	C16	C17	C18	C21	-174.8(2)
N2	C13	C18	C17	-177.92(16)	C18	C13	C14	C15	3.7(3)
N2	C13	C18	C21	-1.4(2)	C18	C13	C14	C19	-173.70(17)
C1	Ru1	C28	C27	-99.10(11)	C19	C14	C15	C16	176.7(3)
C1	N1	C2	C3	-7.1(2)	C20	C16	C17	C18	-179.9(3)
C1	N1	C4	C5	-84.61(18)	C22	S1	C29	C30	-134.29(17)
C1	N1	C4	C9	99.47(17)	C22	S1	C29	C34	44.22(15)
C1	N2	C3	C2	-6.16(18)	C22	C23	C24	C25	-1.7(3)
C1	N2	C13	C14	107.38(18)	C22	C27	C28	Ru1	3.55(16)
C1	N2	C13	C18	-78.8(2)	C23	C22	C27	C26	0.7(2)
C2	N1	C1	Ru1	-174.47(13)	C23	C22	C27	C28	-176.38(13)
C2	N1	C1	N2	3.38(18)	C23	C24	C25	C26	0.9(3)
C2	N1	C4	C5	91.00(17)	C24	C25	C26	C27	0.7(3)
C2	N1	C4	C9	-84.91(18)	C25	C26	C27	C22	-1.5(2)
C3	N2	C1	Ru1	-179.79(10)	C25	C26	C27	C28	175.40(14)
C3	N2	C1	N1	1.98(17)	C26	C27	C28	Ru1	-173.37(11)
C3	N2	C13	C14	-80.7(2)	C27	C22	C23	C24	0.9(2)
C3	N2	C13	C18	93.13(18)	C29	S1	C22	C23	52.83(14)
C4	N1	C1	Ru1	1.4(2)	C29	S1	C22	C27	-128.16(11)
C4	N1	C1	N2	179.26(13)	C29	C30	C31	C32	-0.9(5)

**Table 6.6.7. Torsion Angles for cs2903-catalyst 10.**

A	B	C	D	Angle/°	A	B	C	D	Angle/°
C4	N1	C2	C3	176.69(14)	C30	C29	C34	C33	0.9(3)
C4	C5	C6	C7	3.6(2)	C30	C31	C32	C33	0.4(4)
C5	C4	C9	C8	2.80(19)	C31	C32	C33	C34	0.7(4)
C5	C4	C9	C12	-177.57(13)	C32	C33	C34	C29	-1.4(3)
C5	C6	C7	C8	0.0(2)	C34	C29	C30	C31	0.3(4)

This report has been created with Olex2, compiled on 2022.04.07 svn.rca3783a0 for OlexSys. Please [let us know](#) if there are any errors or if you would like to have additional features.



(22)

## Experimental

A brown prism (0.04 x 0.14 x 0.22 mm<sup>3</sup>) was centered on the goniometer of a Rigaku Oxford Diffraction Synergy-S diffractometer equipped with a HyPix6000HE detector and operating with MoK $\alpha$  radiation. The data collection routine, unit cell

refinement, and data processing were carried out with the program CrysAlisPro.<sup>122</sup> The Laue symmetry was consistent with the triclinic space groups P1 and P-1. The centrosymmetric space group P-1 was chosen. The structure was solved using SHELXT<sup>123</sup> and refined using SHELXL<sup>124</sup> via Olex2.<sup>125</sup> A 2-position model was used for a disordered CH<sub>2</sub>Cl<sub>2</sub> molecule with relative occupancies that refined to 0.6303(19) and 0.3697(19). The final refinement model involved anisotropic displacement parameters for non-hydrogen atoms and a riding model for all hydrogen atoms. Olex2<sup>126</sup> was used for molecular graphics generation.

**Table 6.6.8. Crystal data and structure refinement for cs3021- (22).**

Identification code	HA-2-61
Empirical formula	C <sub>48</sub> H <sub>50</sub> Cl <sub>4</sub> N <sub>4</sub> O <sub>4</sub> Ru
Formula weight	989.79
Temperature/K	99.97(13)
Crystal system	triclinic
Space group	P-1
a/Å	10.41900(10)
b/Å	14.4166(2)
c/Å	15.3529(2)
α/°	96.6040(10)
β/°	103.0170(10)
γ/°	91.3660(10)
Volume/Å <sup>3</sup>	2228.99(5)
Z	2

---

(117) CrysAlisPro Software System, v1.171.42.xx, Rigaku Oxford Diffraction, **2022**, Rigaku Corporation, Oxford, UK.

(118) Sheldrick, G. M. "SHELXT – Integrated space-group and crystal structure determination." *Acta Cryst.* **2015**, *A71*, 3–8.

(119) Sheldrick, G. M. "Crystal structure refinement with SHELXL." *Acta Cryst.* **2015**, *C71*, 3–8.

(120) Dolomanov, O.V.; Bourhis, L. J.; Gildea, R. J.; Howard, J. A. K.; Puschmann, H. *J. Appl. Cryst.* **2009**, *42*, 339–341.

(121) Dolomanov, O.V.; Bourhis, L. J.; Gildea, R. J.; Howard, J. A. K.; Puschmann, H. *J. Appl. Cryst.* **2009**, *42*, 339–341.

$\rho_{\text{calc}}/\text{cm}^3$  1.475  
 $\mu/\text{mm}^{-1}$  0.641  
 $F(000)$  1020.0  
 Crystal size/ $\text{mm}^3$   $0.22 \times 0.14 \times 0.043$   
 Radiation Mo  $K\alpha$  ( $\lambda = 0.71073$ )  
 $2\theta$  range for data collection/ $^\circ$  6.322 to 76.408  
 Index ranges  $-17 \leq h \leq 17$ ,  $-24 \leq k \leq 24$ ,  $-25 \leq l \leq 26$   
 Reflections collected 136110  
 Independent reflections 23450 [Rint = 0.0453, Rsigma = 0.0339]  
 Data/restraints/parameters 23450/0/575  
 Goodness-of-fit on  $F^2$  1.044  
 Final R indexes [ $I \geq 2\sigma(I)$ ] R1 = 0.0389, wR2 = 0.0978  
 Final R indexes [all data] R1 = 0.0500, wR2 = 0.1021  
 Largest diff. peak/hole /  $e \text{ \AA}^{-3}$  1.72/-1.62

Crystal data as a footnote:

Crystal Data for cs3021.  $\text{C}_{48}\text{H}_{50}\text{Cl}_{14}\text{N}_{4}\text{O}_{4}\text{Ru}$  ( $M = 989.79 \text{ g/mol}$ ): triclinic, space group P-1 (no. 2),  $a = 10.41900(10) \text{ \AA}$ ,  $b = 14.4166(2) \text{ \AA}$ ,  $c = 15.3529(2) \text{ \AA}$ ,  $\alpha = 96.6040(10)^\circ$ ,  $\beta = 103.0170(10)^\circ$ ,  $\gamma = 91.3660(10)^\circ$ ,  $V = 2228.99(5) \text{ \AA}^3$ ,  $Z = 2$ ,  $T = 99.97(13) \text{ K}$ ,  $\mu(\text{Mo } K\alpha) = 0.641 \text{ mm}^{-1}$ ,  $D_{\text{calc}} = 1.475 \text{ g/cm}^3$ , 136110 reflections measured ( $6.322^\circ \leq 2\theta \leq 76.408^\circ$ ), 23450 unique (Rint = 0.0453, Rsigma = 0.0339) which were used in all calculations. The final R1 was 0.0389 ( $I > 2\sigma(I)$ ) and wR2 was 0.1021 (all data).

**Table 6.6.9. Bond Lengths for cs3021- (22).**

Atom	Atom	Length/ $\text{\AA}$	Atom	Atom	Length/ $\text{\AA}$
------	------	----------------------	------	------	----------------------

Ru1	C11	2.3579(3)	C15	C16	1.395(2)
Ru1	C12	2.3522(3)	C16	C17	1.391(2)
Ru1	N3	2.0862(10)	C16	C20	1.5059(19)
Ru1	C1	2.0613(11)	C17	C18	1.3967(17)
Ru1	C22	1.8308(12)	C18	C21	1.5068(19)
O1	C36	1.2091(18)	C22	C23	1.4535(16)
O2	C36	1.3506(17)	C23	C24	1.4077(17)
O2	C37	1.4441(16)	C23	C28	1.4148(17)
O3	C39	1.2104(19)	C24	C25	1.3911(18)
O4	C46	1.205(2)	C25	C26	1.392(2)
N1	C1	1.3511(14)	C26	C27	1.386(2)
N1	C2	1.4715(15)	C27	C28	1.4036(17)
N1	C4	1.4348(15)	C28	C29	1.4515(18)
N2	C1	1.3428(14)	C30	C31	1.3978(18)
N2	C3	1.4758(15)	C30	C35	1.3930(18)
N2	C13	1.4273(15)	C31	C32	1.3878(18)
N3	C29	1.2880(16)	C32	C33	1.3963(19)
N3	C30	1.4246(16)	C33	C34	1.3891(18)
N4	C38	1.446(2)	C33	C36	1.4830(18)
N4	C39	1.385(2)	C34	C35	1.3855(18)
N4	C46	1.393(2)	C37	C38	1.523(2)
C2	C3	1.5238(17)	C39	C40	1.515(3)
C4	C5	1.4035(17)	C40	C41	1.572(3)
C4	C9	1.3990(17)	C40	C45	1.539(2)
C5	C6	1.3952(17)	C41	C42	1.516(3)
C5	C10	1.5017(18)	C41	C47	1.545(2)
C6	C7	1.3940(18)	C42	C43	1.317(4)
C7	C8	1.3876(18)	C43	C44	1.522(4)
C7	C11	1.5097(17)	C44	C45	1.571(2)
C8	C9	1.3991(16)	C44	C47	1.542(3)
C9	C12	1.5003(18)	C45	C46	1.504(3)

C13	C14	1.3970(17)	C13	C48A	1.699(3)
C13	C18	1.3969(18)	C13	C48B	1.987(6)
C14	C15	1.3983(18)	C14A	C48A	1.756(3)
C14	C19	1.500(2)	C14B	C48B	1.759(8)

**Table 6.6.10. Bond Angles for cs3021- (22).**

Atom	Atom	Atom	Angle/°	Atom	Atom	Atom	Angle/°
Cl2	Ru1	Cl1	163.730(13)	C13	C18	C21	120.81(11)
N3	Ru1	Cl1	88.41(3)	C17	C18	C13	118.01(12)
N3	Ru1	Cl2	86.20(3)	C17	C18	C21	121.11(12)
C1	Ru1	Cl1	94.78(3)	C23	C22	Ru1	125.72(9)
C1	Ru1	Cl2	87.90(3)	C24	C23	C22	117.87(11)
C1	Ru1	N3	169.13(4)	C24	C23	C28	118.07(11)
C22	Ru1	Cl1	98.80(4)	C28	C23	C22	124.06(11)
C22	Ru1	Cl2	96.45(4)	C25	C24	C23	121.32(12)
C22	Ru1	N3	89.10(5)	C24	C25	C26	119.97(12)
C22	Ru1	C1	100.64(5)	C27	C26	C25	119.81(12)
C36	O2	C37	115.74(11)	C26	C27	C28	120.84(13)
C1	N1	C2	113.62(9)	C23	C28	C29	122.34(11)
C1	N1	C4	126.54(10)	C27	C28	C23	119.84(12)
C4	N1	C2	118.85(9)	C27	C28	C29	117.62(11)
C1	N2	C3	114.16(9)	N3	C29	C28	122.90(11)
C1	N2	C13	126.19(10)	C31	C30	N3	118.94(11)
C13	N2	C3	119.41(9)	C35	C30	N3	120.50(11)
C29	N3	Ru1	126.76(9)	C35	C30	C31	120.38(12)
C29	N3	C30	118.58(11)	C32	C31	C30	119.84(12)
C30	N3	Ru1	114.56(8)	C31	C32	C33	119.87(12)
C39	N4	C38	123.44(13)	C32	C33	C36	122.81(12)
C39	N4	C46	112.76(15)	C34	C33	C32	119.76(12)
C46	N4	C38	123.79(14)	C34	C33	C36	117.41(12)
N1	C1	Ru1	119.50(8)	C35	C34	C33	120.85(12)

N2	C1	Ru1	132.75(8)	C34	C35	C30	119.27(12)
N2	C1	N1	106.99(9)	O1	C36	O2	123.03(12)
N1	C2	C3	102.87(9)	O1	C36	C33	124.26(13)
N2	C3	C2	102.18(9)	O2	C36	C33	112.68(12)
C5	C4	N1	118.49(11)	O2	C37	C38	110.34(12)
C9	C4	N1	119.78(11)	N4	C38	C37	112.21(13)
C9	C4	C5	121.21(10)	O3	C39	N4	123.80(17)
C4	C5	C10	121.15(11)	O3	C39	C40	127.25(16)
C6	C5	C4	118.35(11)	N4	C39	C40	108.93(13)
C6	C5	C10	120.41(11)	C39	C40	C41	112.66(14)
C7	C6	C5	121.73(11)	C39	C40	C45	104.38(15)
C6	C7	C11	120.71(12)	C45	C40	C41	103.17(13)
C8	C7	C6	118.42(11)	C42	C41	C40	104.76(15)
C8	C7	C11	120.85(12)	C42	C41	C47	100.52(16)
C7	C8	C9	121.99(12)	C47	C41	C40	100.65(15)
C4	C9	C8	118.16(11)	C43	C42	C41	107.3(2)
C4	C9	C12	121.79(11)	C42	C43	C44	108.42(19)
C8	C9	C12	119.83(11)	C43	C44	C45	105.35(15)
C14	C13	N2	119.38(11)	C43	C44	C47	99.82(19)
C18	C13	N2	118.42(11)	C47	C44	C45	100.30(13)
C18	C13	C14	122.19(11)	C40	C45	C44	102.98(15)
C13	C14	C15	117.55(12)	C46	C45	C40	105.34(14)
C13	C14	C19	120.88(11)	C46	C45	C44	112.30(14)
C15	C14	C19	121.49(12)	O4	C46	N4	123.78(19)
C16	C15	C14	122.03(13)	O4	C46	C45	127.62(16)
C15	C16	C20	120.91(14)	N4	C46	C45	108.58(14)
C17	C16	C15	118.36(12)	C44	C47	C41	93.55(14)
C17	C16	C20	120.71(14)	Cl3	C48A	Cl4A	108.72(17)
C16	C17	C18	121.74(13)	Cl4B	C48B	Cl3	111.1(3)

**Table 6.6.11. Torsion Angles for cs3021-inimer (22).**

A	B	C	D	Angle/°	A	B	C	D	
				Angle/°					
Ru1	N3	C29	C28	-10.46(19)	C20	C16	C17	C18	
				177.22(14)					
Ru1	N3	C30	C31	-45.92(15)	C22	C23	C24	C25	
				176.00(12)					
Ru1	N3	C30	C35	129.30(11)	C22	C23	C28	C27	-
				178.36(12)					
Ru1	C22	C23	C24	-158.31(10)	C22	C23	C28	C29	6.8(2)
Ru1	C22	C23	C28	21.44(18)	C23	C24	C25	C26	2.6(2)
Cl1	Ru1	C22	C23	-118.98(10)	C23	C28	C29	N3	-
				11.1(2)					
Cl2	Ru1	C22	C23	55.35(11)	C24	C23	C28	C27	
				1.39(19)					
O2	C37	C38	N4	57.61(17)	C24	C23	C28	C29	-
				173.47(12)					
O3	C39	C40	C41	-68.0(2)	C24	C25	C26	C27	1.1(2)
O3	C39	C40	C45	-179.20(16)	C25	C26	C27	C28	-3.5(2)
N1	C2	C3	N2	4.01(13)	C26	C27	C28	C23	2.2(2)
N1	C4	C5	C6	-176.02(10)	C26	C27	C28	C29	
				177.28(13)					
N1	C4	C5	C10	0.35(16)	C27	C28	C29	N3	
				173.97(13)					
N1	C4	C9	C8	176.11(10)	C28	C23	C24	C25	-
				3.76(19)					
N1	C4	C9	C12	1.48(17)	C29	N3	C30	C31	
				130.77(14)					
N2	C13	C14	C15	179.38(11)	C29	N3	C30	C35	-
				54.00(18)					
N2	C13	C14	C19	2.50(18)	C30	N3	C29	C28	
				173.29(12)					

N2	C13	C18	C17	-177.24(11)	C30	C31	C32	C33	-0.5(2)
N2	C13	C18	C21	-0.30(17)	C31	C30	C35	C34	0.6(2)
N3	Ru1	C22	C23	-30.73(11)	C31	C32	C33	C34	1.3(2)
N3	C30	C31	C32	174.72(13)	C31	C32	C33	C36	-
177.14(13)									
N3	C30	C35	C34	-174.52(12)	C32	C33	C34	C35	-1.2(2)
N4	C39	C40	C41	110.38(15)	C32	C33	C36	O1	-
177.36(14)									
N4	C39	C40	C45	-0.84(16)	C32	C33	C36	O2	
4.34(19)									
C1	Ru1	C22	C23	144.42(10)	C33	C34	C35	C30	0.2(2)
C1	N1	C2	C3	-3.84(15)	C34	C33	C36	O1	4.1(2)
C1	N1	C4	C5	-85.01(15)	C34	C33	C36	O2	-
174.18(12)									
C1	N1	C4	C9	103.12(15)	C35	C30	C31	C32	-0.5(2)
C1	N2	C3	C2	-3.46(15)	C36	O2	C37	C38	
77.99(16)									
C1	N2	C13	C14	-101.19(14)	C36	C33	C34	C35	
177.34(13)									
C1	N2	C13	C18	79.01(16)	C37	O2	C36	O1	5.3(2)
C2	N1	C1	Ru1	173.05(9)	C37	O2	C36	C33	-
176.38(11)									
C2	N1	C1	N2	1.81(15)	C38	N4	C39	O3	-0.4(2)
C2	N1	C4	C5	82.87(14)	C38	N4	C39	C40	-
178.88(13)									
C2	N1	C4	C9	-89.00(14)	C38	N4	C46	O4	1.4(2)
C3	N2	C1	Ru1	-168.40(10)	C38	N4	C46	C45	
179.85(13)									
C3	N2	C1	N1	1.21(14)	C39	N4	C38	C37	
88.95(17)									

C3	N2	C13	C14	84.88(15)	C39	N4	C46	O4	-
177.32(15)									
C3	N2	C13	C18	-94.91(14)	C39	N4	C46	C45	
1.13(17)									
C4	N1	C1	Ru1	-18.53(17)	C39	C40	C41	C42	
179.39(15)									
C4	N1	C1	N2	170.22(11)	C39	C40	C41	C47	-
76.62(17)									
C4	N1	C2	C3	-173.23(11)	C39	C40	C45	C44	
119.27(15)									
C4	C5	C6	C7	1.34(17)	C39	C40	C45	C46	
1.43(15)									
C5	C4	C9	C8	4.47(17)	C40	C41	C42	C43	
70.79(18)									
C5	C4	C9	C12	-170.17(11)	C40	C41	C47	C44	-
57.38(17)									
C5	C6	C7	C8	1.25(18)	C40	C45	C46	O4	
176.79(16)									
C5	C6	C7	C11	179.54(11)	C40	C45	C46	N4	-
1.58(16)									
C6	C7	C8	C9	-1.03(18)	C41	C40	C45	C44	
1.34(18)									
C7	C8	C9	C4	-1.77(17)	C41	C40	C45	C46	-
116.50(14)									
C7	C8	C9	C12	172.97(11)	C41	C42	C43	C44	0.0(2)
C9	C4	C5	C6	-4.26(17)	C42	C41	C47	C44	
50.00(18)									
C9	C4	C5	C10	172.10(11)	C42	C43	C44	C45	-
70.3(2)									
C10	C5	C6	C7	-175.05(11)	C42	C43	C44	C47	
33.34(18)									

C11	C7	C8	C9	-179.32(11)		C43	C44	C45	C40	
				65.60(18)						
C13	N2	C1	Ru1	17.40(19)		C43	C44	C45	C46	
				178.43(16)						
C13	N2	C1	N1	-172.99(11)		C43	C44	C47	C41	-
				49.51(16)						
C13	N2	C3	C2	171.17(11)		C44	C45	C46	O4	65.4(2)
C13	C14	C15	C16	-2.39(19)		C44	C45	C46	N4	-
				112.94(15)						
C14	C13	C18	C17	2.97(18)		C45	C40	C41	C42	-
				68.64(18)						
C14	C13	C18	C21	179.91(12)		C45	C40	C41	C47	
				35.34(17)						
C14	C15	C16	C17	3.3(2)	C45	C44	C47	C41	58.22(18)	
C14	C15	C16	C20	-174.94(14)		C46	N4	C38	C37	-
				89.64(17)						
C15	C16	C17	C18	-1.0(2)	C46	N4	C39	O3	178.28(15)	
C16	C17	C18	C13	-2.00(19)		C46	N4	C39	C40	-
				0.16(17)						
C16	C17	C18	C21	-178.93(13)		C47	C41	C42	C43	-
				33.29(19)						
C18	C13	C14	C15	-0.83(18)		C47	C44	C45	C40	-
				37.67(19)						
C18	C13	C14	C19	-177.71(12)		C47	C44	C45	C46	
				75.15(19)						
C19	C14	C15	C16	174.46(13)						

This report has been created with Olex2, compiled on 2023.03.06 svn.rbb2c1857 for OlexSys. Please let us know if there are any errors or if you would like to have additional features.

## Chapter 7. Synthesis and Characterization of Copper-Ruthenium Olefin Metathesis

### Catalysts

Hanan N. Almuzaini,<sup>a,b</sup> Carla Slebodnick,<sup>a</sup> Michael D. Schulz<sup>a,b</sup>

<sup>a</sup> Department of Chemistry, Virginia Polytechnic Institute and State University,  
Blacksburg, VA 24061

<sup>b</sup> Macromolecules Innovation Institute, Virginia Polytechnic Institute and State  
University, Blacksburg, VA 24061

#### 7.1. Abstract

Copper(I) halides are often added to olefin metathesis reactions to inhibit catalyst degradation, control product isomerization, enhance catalyst activation, or facilitate catalyst dimerization. In each of these examples, however, the copper salt is presumed to operate as an independent species, separate from the ruthenium center. We have discovered, however, that certain copper salts can form complexes with the ruthenium catalyst itself, forming hetero-bimetallic copper-ruthenium olefin metathesis catalysts. We confirmed the formation of two complexes through single-crystal X-ray crystallography and <sup>1</sup>H NMR spectroscopy. The crystal structure revealed the presence of a four-member ring containing ruthenium, carbon, copper, and chloride or bromide. To study the activity of these bimetallic complexes, we measured the catalyst activation temperature in ring-opening metathesis polymerization (ROMP) using different ROMP monomers. The catalyst activation was affected by both the catalyst and monomer identity, with the activation temperature for the complex with copper addition differing by up to 12 °C compared to the complex without copper. The formation of these copper-ruthenium

bimetallic complexes suggests the possibility of multi-metallic olefin metathesis catalysts, potentially with different activity and properties than their traditional counterparts.

## 7.2. Introduction

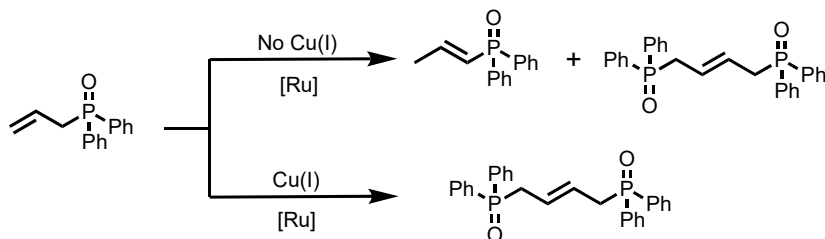
The development of well-defined ruthenium-based olefin metathesis catalysts has opened up synthetic access to a wide range of organic molecules and macromolecular structures.<sup>1, 2</sup> However, ongoing catalyst modification aims to improve catalyst stability, reactivity, and selectivity.<sup>1</sup> The influence of copper halide additives on olefin metathesis reactions has been studied to stabilize and enhance catalyst reactivity.<sup>3, 4</sup> For example, phosphine-chelated ruthenium complexes degrade under thermal activation due to the formation of phosphorus by-products.<sup>5</sup> Therefore, additives such as copper (I) halides are added to stabilize olefin metathesis catalysts. Copper(I) salts act as phosphine sponges, isolating phosphorus by-products and inhibiting catalyst degradation.<sup>6</sup>

Thuo and co-workers reported the effect of copper(I) halide addition to a metathesis reaction occurring in polar protic solvents with phosphine-based Grubbs catalysts.<sup>3</sup> Cross-metathesis with copper halide addition selectively produces cross-metathesis olefin and limits the formation of isomerized by-products (**Figure 7.1. a**).<sup>3</sup>

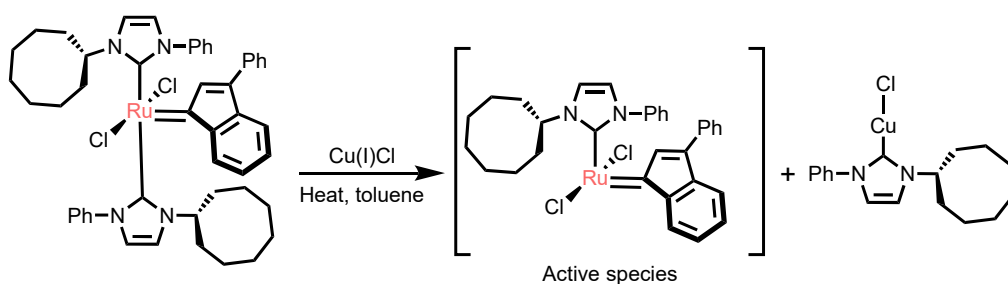
Most recently, Dorcet and co-workers studied the activation conditions of ruthenium-indenylidene catalysts containing two unsymmetrical unsaturated NHC ligands.<sup>4</sup> This catalyst showed high stability and low reactivity in ring-closing metathesis, even at 80 °C, but becomes highly active at 30 °C with the addition of copper salt. Copper(I) chloride traps the NHC ligand to release the active ruthenium species through a trans-metalation process (**Figure 7.1. b**).<sup>4</sup> Furthermore, copper(I) chloride dimerized an indenylidene

complex, forming two bridging chloride donors (**Figure 7.1. c**).<sup>7</sup> The dimerized complex initiates faster, 250 times faster than the single metallic catalyst.<sup>7</sup>

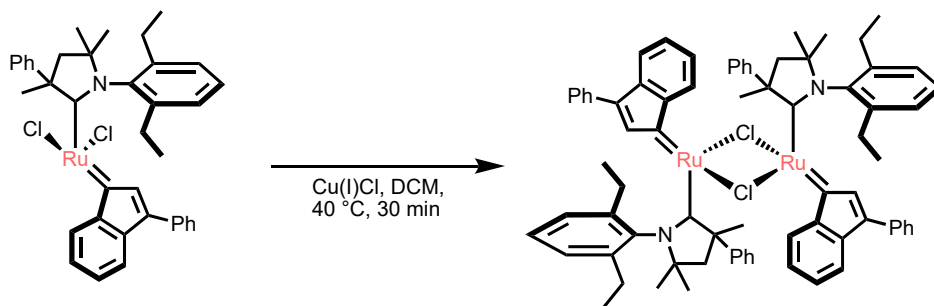
**a.** limit isomerized by-products



**b.** activate olefin metathesis catalysts



**c.** dimerize olefin metathesis catalysts



**This Work:**

**d.** synthesize bimetallic olefin metathesis catalysts

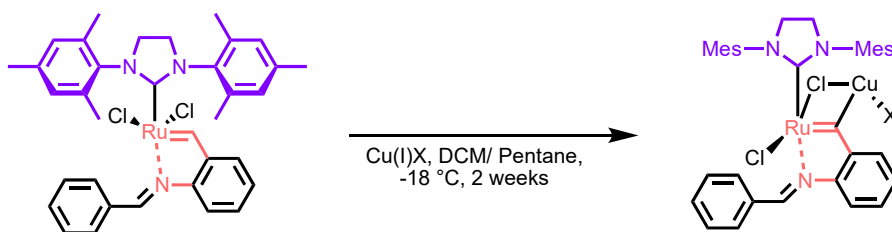


**Figure 7.7.2. Copper halide addition to olefin metathesis and catalysts.**

Due to the interesting chemistry of copper (I) halides with olefin metathesis catalysts, we investigated the effect of treating imine-chelated ruthenium olefin metathesis catalysts with different copper(I) salts (**Figure 7.1. d**). This catalyst has a five-member chelating imine ring and was synthesized without the addition of copper halide.<sup>8</sup> It showed high stability in the presence of olefins at room temperature but was activated upon heating.<sup>8</sup> We synthesized this complex with the addition of copper (I) chloride, bromide, and iodide. We also synthesized the first generation of the imine-chelated catalyst by reacting Grubbs' first-generation catalyst (G1) and imine benzylidene ligand with Cu(I) Cl addition. The result of copper halide addition demonstrated the ability of copper to insert into the catalyst structure to produce a bimetallic complex.

### 7.3. Results and Dissections

The imine benzylidene ligand **3c** was synthesized following a literature procedure (**Figure 7.2**).<sup>8</sup> The benzylidene ligand underwent a carbene exchange reaction with G1 and second-generation Grubbs catalysts (G2) with the addition of copper (I) halide. After the formation of the catalyst, which was indicated by the color change from red to green, the product was precipitated in pentane. Confirmation of the synthesis of the catalysts was done by <sup>1</sup>H NMR spectroscopy, which showed the addition of P(Cy)<sub>3</sub> by-products. Catalyst single crystals were grown from dichloromethane (DCM)/pentane at -18 °C and room temperature.

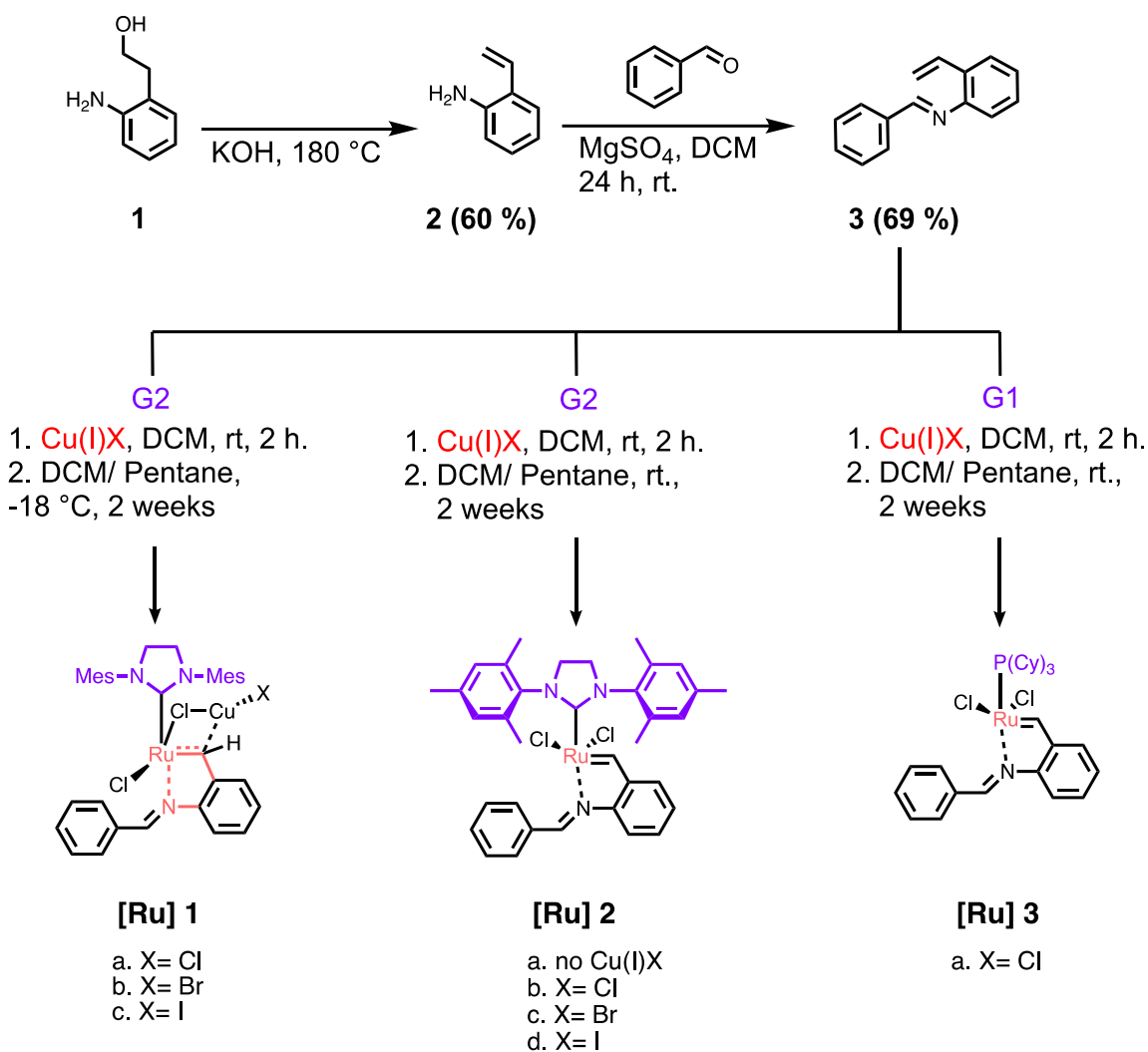


**Figure 7.2. Different conditions to synthesize bimetallic catalysts.**

X-ray crystallography showed different results based on the crystallization conditions and copper halides used. First, catalysts were synthesized by reacting the benzylidene ligand **3c** with G2 and copper chloride or bromide, and they were crystallized at  $-18\text{ }^\circ\text{C}$  to produce hetero-bimetallic copper-ruthenium catalysts: **[Ru] 1a** and **1b** (Figure 7.2). Crystal analysis of **[Ru] 1a** presents copper-ruthenium complex 93.3% of the time, and the other 6.7% was the complex without copper addition. However, **[Ru] 1b**, underwent a halide exchange reaction and copper insertion to form three halogen sites that were modeled with Cl/Br site disorder with relative occupancies refined to

0.717(3)/0.283(3) for the C11/Br1 site, 0.626(3)/0.374(3) for the C12/Br2 site, and 0.420(3)/0.580(3) for the C13/Br3 site.

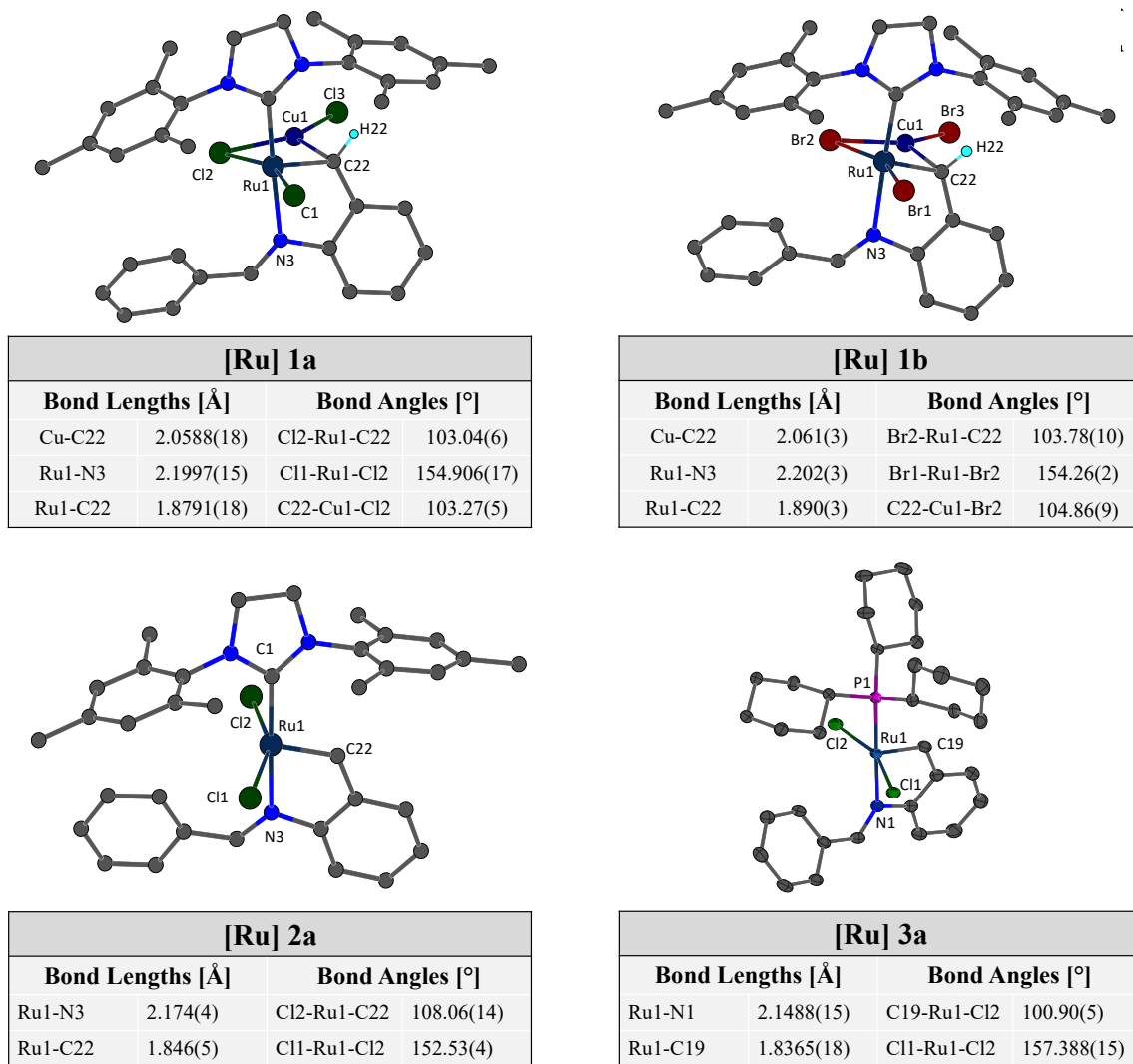


**Figure 7.3.** Catalysts' crystal structures and selected bond lengths and angles.

After X-ray crystal analysis, we collected the crystal to do  $^1\text{H}$  NMR spectroscopy analysis. NMR spectroscopy confirmed both the synthesis of the bimetallic **[Ru] 1a** and **1b** and the halide exchange reaction of **[Ru] 1b**. The carbene and imine peaks became broader after the copper insertion into the two complexes (**Figure 7.4**). Additionally,  $^1\text{H}$

NMR of **[Ru] 1b** showed a multi-imine peak indicating the presence of a mixture of halide-catalysts.

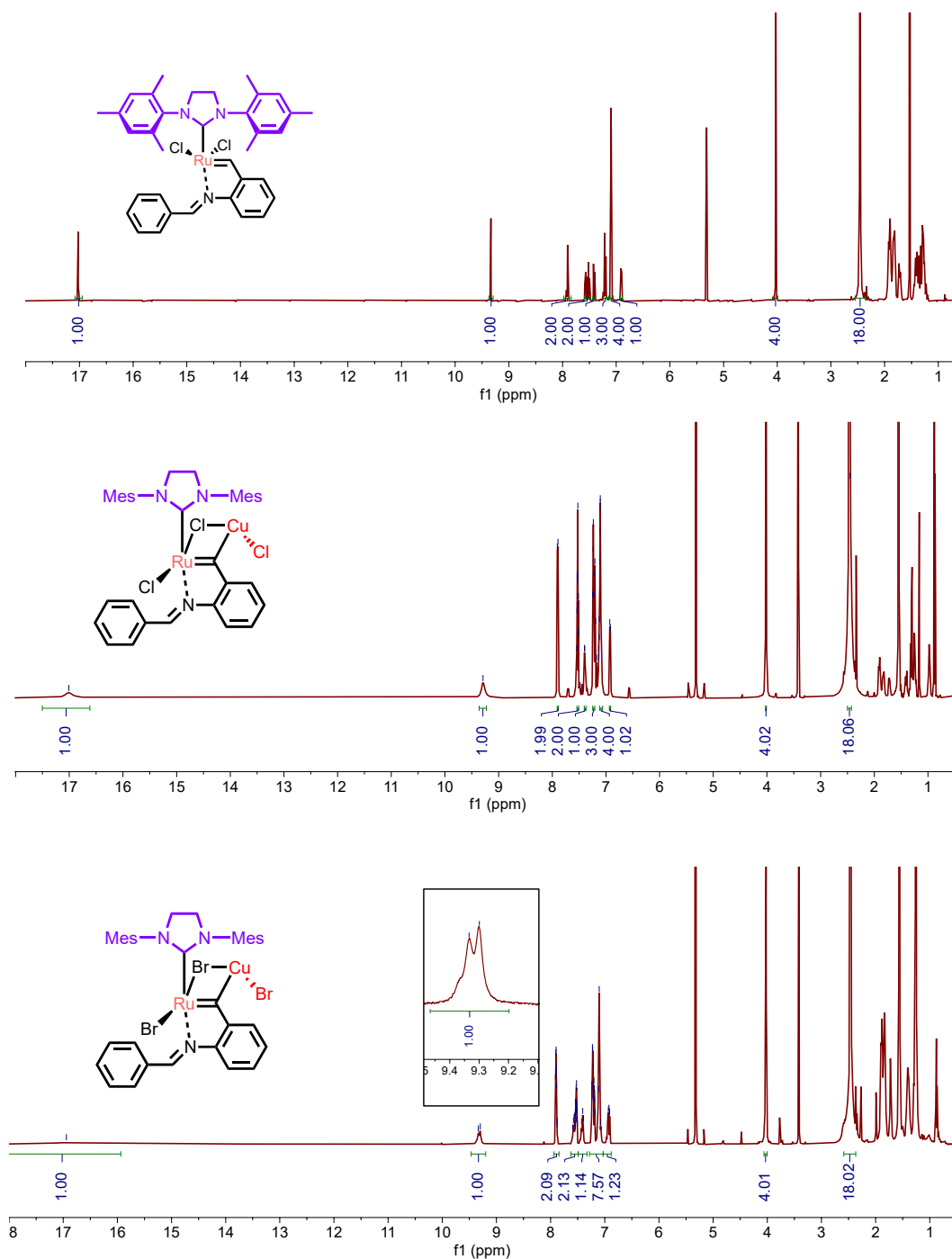


Figure 7.4.  $^1\text{H}$  NMR spectra of **[Ru] 1a**, **[Ru] 1b**, and **[Ru] 2a**.

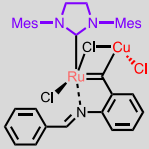
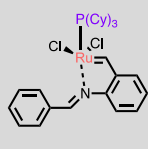
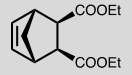
Crystals grown at room temperature (**[Ru] 2b** and **2c**) showed a monometallic catalyst having only ruthenium. The attempt to grow crystals for both **[Ru] 1c** and **2d** was unsuccessful due to the large size of iodine atoms. Additionally, crystals grown at room temperature and at -18 °C (**[Ru] 2a** and **3a**) showed monometallic catalysts without copper halide insertion.

**Figure 7.3** presents the catalyst crystal structures and selected bond lengths and angles for the synthesized complexes. These complexes showed similar bond lengths and angles around the ruthenium center. However, the Cl2-Ru1-C22 angle in **[Ru] 2a** is wider than Cl2-Ru1-C19 in **[Ru] 3a** by 8°. The broader angle can explain the ability of copper to insert in **[Ru] 2a** but not **[Ru] 3a**. After copper insertion, the Cl2-Ru1-C22 and Br1-Ru1-C22 angle decreased to 103.04(6) and 103.78(10) in **[Ru] 1a** and **1b** respectively, but it is still wider than the angle in **[Ru] 3a** (100.90(5) °). This result suggests that **[Ru] 3a** is not able to undergo copper insertion even with crystallization at a lower temperature.

We then investigated the activation temperature of these complexes in ring-opening metathesis polymerization using differential scanning calorimetry (DSC), which indicated an exothermic peak associated with polymerization. The measurements showed that copper insertion affects the catalyst's activity. The differences in activation temperature between **[Ru] 1a** and **[Ru] 2a** can be up to 13 °C and are influenced by both catalyst and monomer identity. Both complexes were activated at 48 °C when polymerizing norbornene (**M1**) due to the monomer's melting temperature, which prevents any activity below that temperature. **[Ru] 3a** exhibited higher catalyst latency and activity due to the phosphorus ligand chelation, which tends to increase catalyst stability. A higher activation temperature was

measured for [Ru] 3a when polymerizing the three monomers, up to 51 °C compared to [Ru] 1a.

**Table 7.1. Catalysts' activation temperature measured by DSC.**

Catalysts				
Monomer		[Ru] 1a	[Ru] 2a	[Ru] 3a
Identity	Melting point (°C)	Activation Temperature (°C)		
M1 	44- 47	48	48	97
M2 	8	67	54	105
M3 	-16	57	66	108

#### 7.4. Conclusions and Future Work

We have successfully synthesized novel olefin metathesis catalysts with a copper-ruthenium bimetallic four-member ring using Cu(I)Cl and Cu(I)Br, but not with Cu(I)I due to the larger atomic size of iodine. X-ray crystallography analysis confirmed the insertion of a copper halide into one of the chlorine ligands, forming the four-member ring. However, the catalyst with a phosphorus ligand did not show any copper insertion. The successful synthesis of these complexes presents an opportunity to explore their reactivity and develop new catalysts with interesting structures.

For future work, we aim to study the activation mechanism to better understand copper's role in the catalyst's activity. Additionally, we plan to investigate the ability of

copper to insert into other catalysts with different chelating ligands and functionality to expand this catalyst family.

## 7.5. References

- (1) Bano, T.; Zahoor, A. F.; Rasool, N.; Irfan, M.; Mansha, A. Recent trends in Grubbs catalysis toward the synthesis of natural products: a review. *J. Iran. Chem. Soc.* **2022**, *19* (6), 2131-2170. DOI: 10.1007/s13738-021-02463-x.
- (2) Eivgi, O.; Phatake, R. S.; Nechmad, N. B.; Lemcoff, N. G. Light-Activated Olefin Metathesis: Catalyst Development, Synthesis, and Applications. *Acc. Chem. Res.* **2020**, *53* (10), 2456-2471. DOI: 10.1021/acs.accounts.0c00495.
- (3) Schulz, M. D.; Atkinson, M. B. J.; Elsey, R. J.; Thuo, M. M. Copper(I) halides inhibit olefin isomerized by-products from phosphine-based Grubbs' metathesis catalysts in polar protic solvents. *Transit. Met. Chem.* **2014**, *39* (7), 763-767. DOI: 10.1007/s11243-014-9858-1.
- (4) Kamal, F.; Colombel-Rouen, S.; Dumas, A.; Guégan, J.-P.; Roisnel, T.; Dorcet, V.; Baslé, O.; Rouen, M.; Mauduit, M. Activation of olefin metathesis complexes containing unsymmetrical unsaturated N-heterocyclic carbenes by copper and gold transmetalation. *Chem. Commun.* **2019**, *55* (77), 11583-11586, 10.1039/C9CC05776E. DOI: 10.1039/C9CC05776E.
- (5) Hong, S. H.; Day, M. W.; Grubbs, R. H. Decomposition of a Key Intermediate in Ruthenium-Catalyzed Olefin Metathesis Reactions. *J. Am. Chem. Soc.* **2004**, *126* (24), 7414-7415. DOI: 10.1021/ja0488380.
- (6) Ulman, M.; Grubbs, R. H. Ruthenium Carbene-Based Olefin Metathesis Initiators: Catalyst Decomposition and Longevity. *J. Org. Chem.* **1999**, *64* (19), 7202-7207. DOI: 10.1021/jo9908703.
- (7) Nascimento, D. L.; Gawin, A.; Gawin, R.; Guńka, P. A.; Zachara, J.; Skowerski, K.; Fogg, D. E. Integrating Activity with Accessibility in Olefin Metathesis: An Unprecedentedly Reactive Ruthenium-Indenylidene Catalyst. *J. Am. Chem. Soc.* **2019**, *141* (27), 10626-10631. DOI: 10.1021/jacs.9b05362.
- (8) Slugovc, C.; Burtscher, D.; Stelzer, F.; Mereiter, K. Thermally Switchable Olefin Metathesis Initiators Bearing Chelating Carbenes: Influence of the Chelate's Ring Size. *Organometallics* **2005**, *24* (10), 2255-2258. DOI: 10.1021/om050141f.

## 7.6. EXPERIMENTAL SECTION

### General methods

All reactions were performed with oven-dried glassware equipped with a magnetic stir bar under an air atmosphere unless otherwise noted. 2-aminophenethyl alcohol was purchased from AmBeed. The Grubbs second-generation catalyst (G2) was donated from Materia and purchased from AmBeed and the Grubbs first-generation catalyst was purchased from Aldrich. Deuterated solvents were obtained from Cambridge Isotope Laboratories. Unless otherwise stated, all other reagents were purchased at the highest commercial quality and used without further purification.

### Measurements

$^1\text{H}$  NMR and  $^{13}\text{C}$  NMR data were collected at 25 °C unless otherwise noted using Agilent U4-DD2 400 MHz, and Bruker Advance II 500 MHz NMR instruments and obtained in  $\text{CDCl}_3$  or  $\text{CD}_2\text{Cl}_2$ . Chemical shifts are reported in ppm and referenced to the  $\text{CHCl}_3$  singlet at 7.26 ppm, TMS singlet at 0 ppm, or  $\text{CD}_2\text{Cl}_2$  triplet at 5.32 ppm for  $^1\text{H}$  NMR.  $^{13}\text{C}$  NMR spectra were referenced to the center peak of the  $\text{CDCl}_3$  triplet at 77.00 ppm, or  $\text{CD}_2\text{Cl}_2$  at 54.00 ppm. The following abbreviations (or combinations thereof) were used to explain the multiplicities: s = singlet, d = doublet, t = triplet, q = quartet, m = multiplet, br = broad, and \* for the deuterated solvent peak.

Catalyst activation temperature was measured with differential scanning calorimetry (DSC) with a DSC Q2500 from TA instruments equipped with an autosampler. Sample masses ranging from 6–10 mg were crimped in a high-volume pan and lid and then loaded into the cell alongside a reference pan. The method incorporated equilibrate at 25 °C and the samples were heated from 25 °C to 150 °C at a rate of 3 °C/ min. The activation

temperature was determined as the onset point of the slope from the baseline of an exothermic transition.

**2-Vinylaniline (2):** To a 100 mL round-bottom flask equipped with a stir bar, short path distillation head, and tared receiving flask was added 2-aminophenethyl alcohol (**1**) (1 equiv., 5.0 g) and potassium hydroxide (1 equiv., 2.04 g). The mixture was heated to 180 °C. With continued heating and applied vacuum for 4 h, the clear product distilled over (83-90 °C) to the tared receiving flask (Yield 2.60 g, 60 %). <sup>1</sup>H NMR (400 MHz, CDCl<sub>3</sub>): δ 7.30 (d, J = 7.6 Hz, 1H), 7.10 (t, J = 6.8 Hz, 1H), 6.85 – 6.73 (m, 2H), 6.69 (d, J = 7.7 Hz, 1H), 5.64 (d, J = 17.2 Hz, 1H), 5.33 (d, J = 11.0 Hz, 1H), 3.76 (s, 2H). <sup>13</sup>C NMR (101 MHz, CDCl<sub>3</sub>): δ 143.80, 132.89, 128.88, 127.48, 124.24, 119.08, 116.23, 115.84.

**(E)-1-phenyl-N-(2-vinylphenyl)methanimine (3):** A round bottom flask was charged with **2** (1 equiv., 0.30 g), benzaldehyde (1 equiv., 0.33 g), MgSO<sub>4</sub> (1g/1.0 mmol aldehyde, 2.80 g) and DCM (30 mL). The reaction mixture was stirred at room temperature under N<sub>2</sub> for 24 h after which the mixture was filtered and concentrated under reduced pressure. The crude product was used (as it is) (Yield 0.40 g, 69 %).

### Synthesis of catalysts [Ru]1-3

A round bottom flask was charged with G1 or G2 (1 equiv.), Cu(I)X (1 equiv.), and benzylidene ligand **3** (1 equiv.). DCM was added to the reaction flask under N<sub>2</sub>. The reaction mixture was stirred at rt for 2 h. The solvent was evaporated, and the crude product was isolated from pentane.

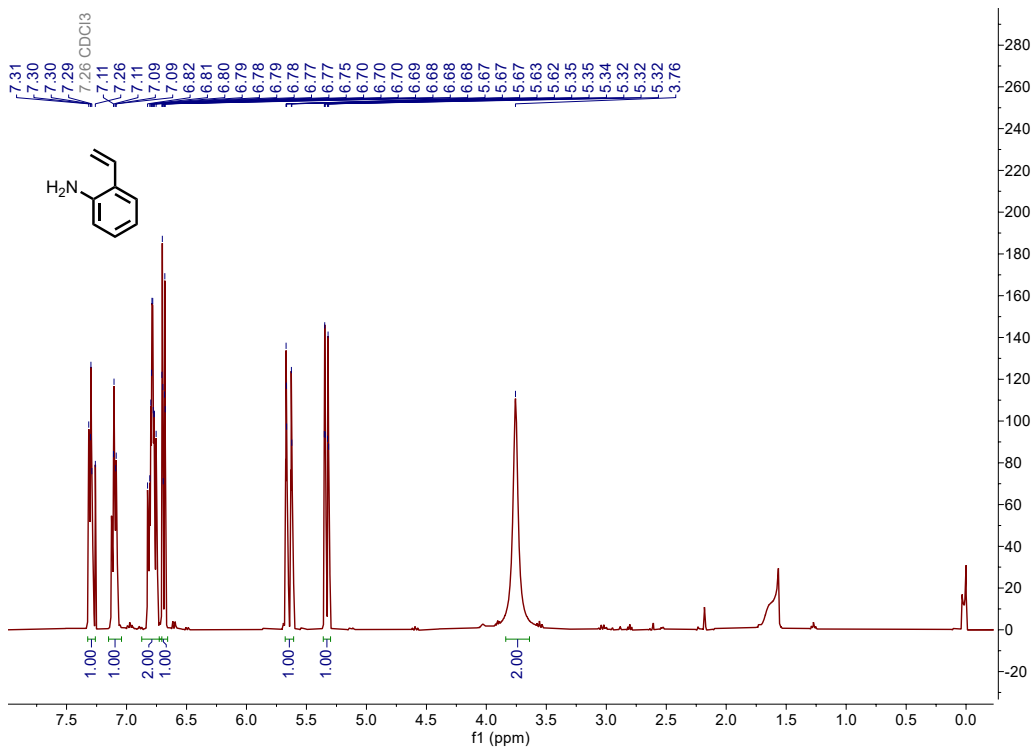
**[Ru] 1a:**  $^1\text{H}$  NMR (600 MHz,  $\text{CD}_2\text{Cl}_2$ )  $\delta$  17.01 (s, 1H), 7.90 (d,  $J = 7.6$  Hz, 2H), 7.56 – 7.50 (m, 2H), 7.39 (s, 1H), 7.25 – 7.22 (m, 2H), 7.21 – 7.17 (m, 1H), 7.15 – 7.06 (m, 4H), 6.92 (d,  $J = 7.6$  Hz, 1H), 4.02 (s, 4H), 2.47 (s, 18H).

**[Ru] 1b:**  $^1\text{H}$  NMR (600 MHz,  $\text{CD}_2\text{Cl}_2$ )  $\delta$  16.94 (s, 1H), 9.32 (d,  $J = 20.9$  Hz, 1H), 7.94 – 7.85 (m, 2H), 7.62 – 7.49 (m, 2H), 7.41 (t,  $J = 10.7$  Hz, 1H), 7.28 – 7.03 (m, 8H), 6.93 (dd,  $J = 14.2, 8.0$  Hz, 1H), 4.02 (s, 4H), 2.47 (s, 18H).

**[Ru] 2:** (Yield 60 %)  $^1\text{H}$  NMR (400 MHz,  $\text{CDCl}_3$ ):  $\delta$  17.02 (s, 1H), 9.32 (s, 1H), 7.92 – 7.89 (m, 2H), 7.53 (d,  $J = 22.2$  Hz, 2H), 7.40 (d,  $J = 8.1$  Hz, 1H), 7.23 – 7.17 (m, 3H), 7.09 (s, 4H), 6.90 (dd,  $J = 7.6, 1.4$  Hz, 1H), 4.02 (s, 4H), 2.46 (s, 18H).

**[Ru] 3:**

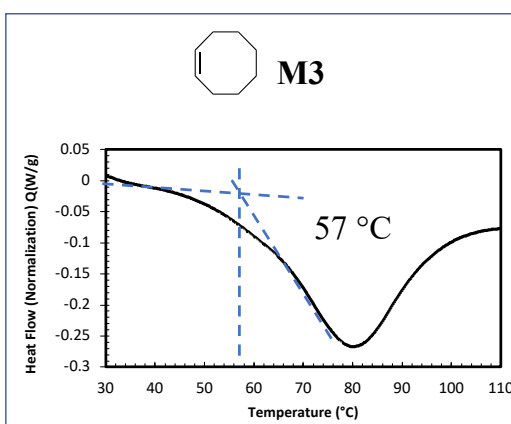
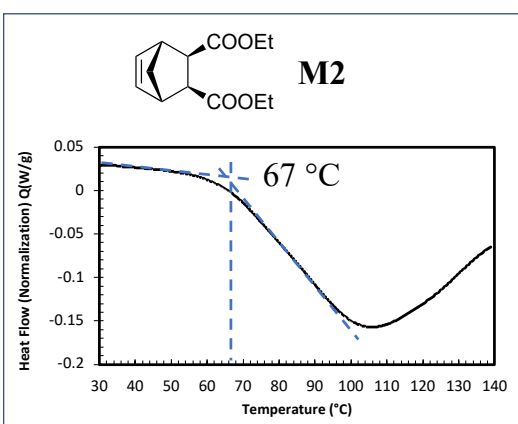
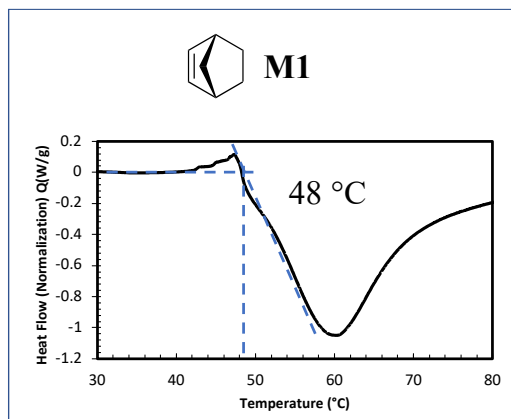
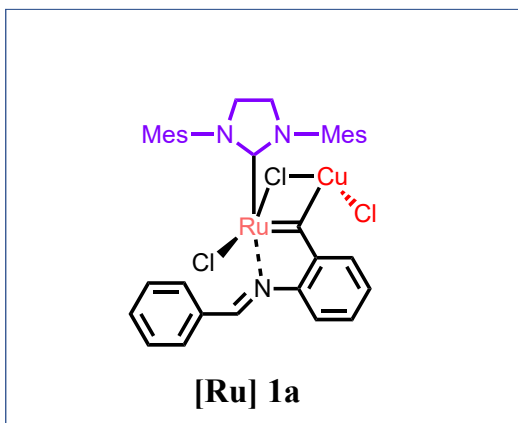
# NMR Characterization

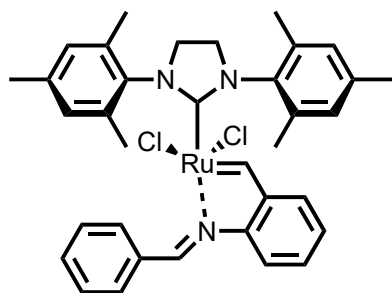






## DSC Traces for the Catalysts' Activation Temperature

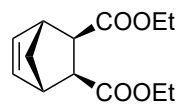
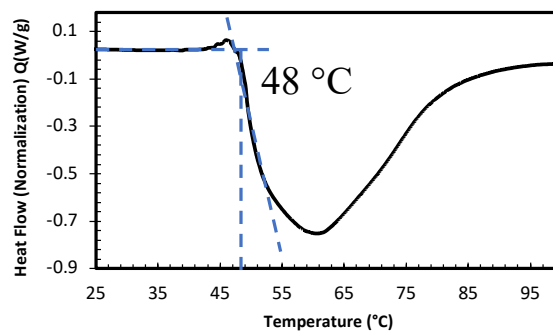




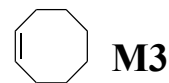
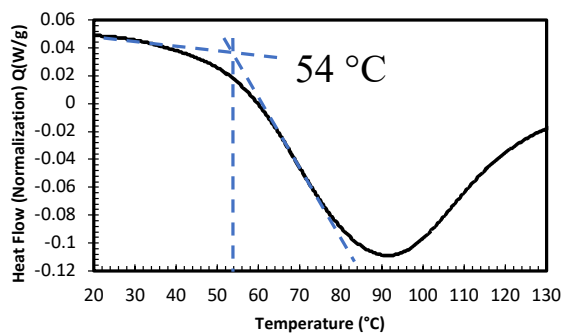
**[Ru] 2a**



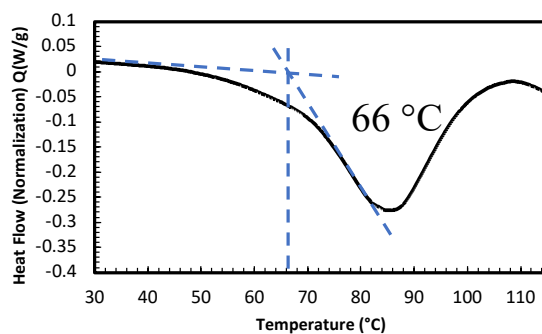
**M1**

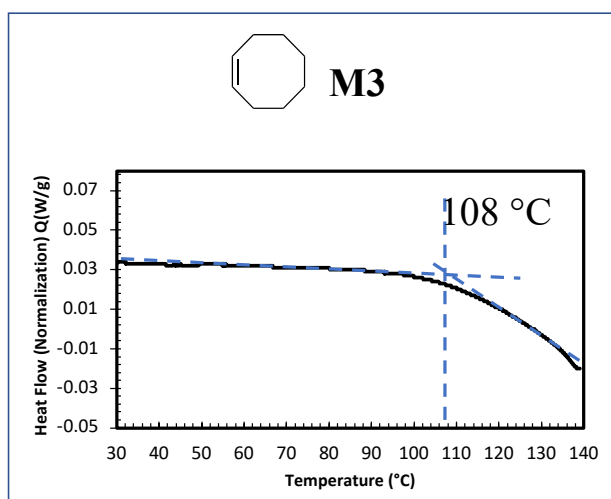
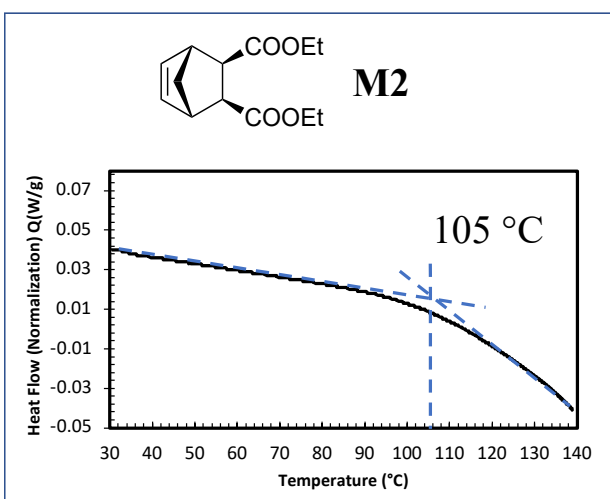
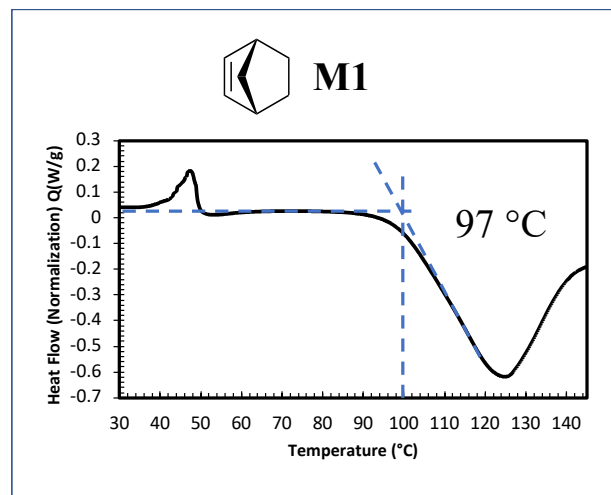
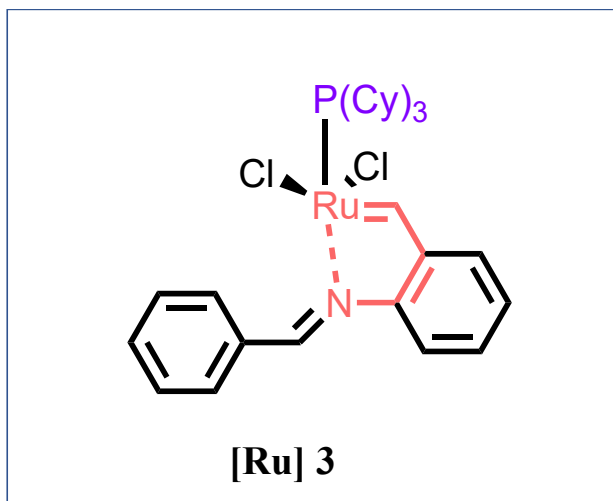


**M2**



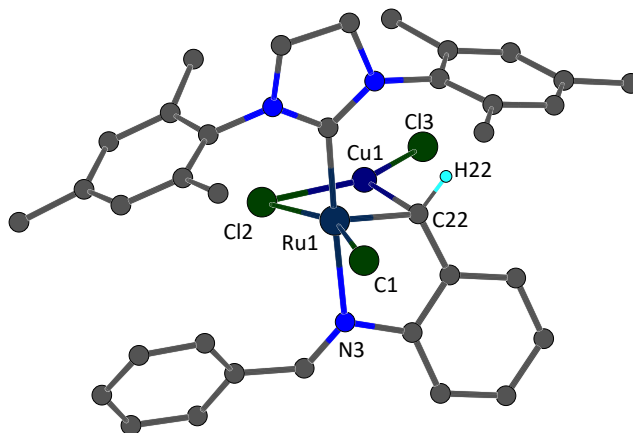
**M3**





## Crystal Structure Determination

**Acknowledgements:** We thank the support of the National Science Foundation under CHE-1726077 for crystallography experiments.



**[Ru] 1a**

## Experimental

A yellow-brown plate (0.01 x 0.16 x 0.22 mm<sup>3</sup>) was centered on the goniometer of a Rigaku Oxford Diffraction Synergy-S diffractometer equipped with a HyPix6000HE detector and operating with MoK $\alpha$  radiation. The data collection routine, unit cell refinement, and data processing were carried out with the program CrysAlisPro.<sup>127</sup> The Laue symmetry and systematic absences were consistent with the orthorhombic space group *Pbca*. The structure was solved using SHELXT<sup>128</sup> and refined using SHELXL<sup>129</sup> via Olex2.<sup>130</sup> When all atoms were refined as fully occupied, the difference electron density map indicated significant negative electron density at Cu1. Therefore, the occupancies of

---

(122) CrysAlisPro Software System, v1.171.41.105a, Rigaku Oxford Diffraction, **2021**, Rigaku Corporation, Oxford, UK.

(123) Sheldrick, G. M. "SHELXT – Integrated space-group and crystal structure determination." *Acta Cryst.* **2015**, *A71*, 3–8.

(124) Sheldrick, G. M. "Crystal structure refinement with SHELXL." *Acta Cryst.* **2015**, *C71*, 3–8.

(125) Dolomanov, O.V.; Bourhis, L. J.; Gildea, R. J.; Howard, J. A. K.; Puschmann, H. *J. Appl. Cryst.* **2009**, *42*, 339–341.

Cu1 and Cl3 were fixed to be equal but allowed to refine; the occupancies refined to 0.9330(12). The final refinement model involved anisotropic displacement parameters for non-hydrogen atoms. A riding model was used for all H-atoms except the hydrogen of the carbene, which was located from the difference electron density map and the position and isotropic displacement parameter were refined independently. Olex2<sup>131</sup> was used for molecular graphics generation.

**Table 7.6.1. Crystal data and structure refinement for cs2905-[Ru] 1a.**

Identification code	HA-2-72
Empirical formula	C <sub>35</sub> H <sub>37</sub> Cl <sub>2.93</sub> Cu <sub>0.93</sub> N <sub>3</sub> Ru
Formula weight	763.95
Temperature/K	100.0(2)
Crystal system	orthorhombic
Space group	<i>Pbca</i>
<i>a</i> /Å	18.9117(2)
<i>b</i> /Å	14.9901(2)
<i>c</i> /Å	23.0481(3)
$\alpha$ /°	90
$\beta$ /°	90
$\gamma$ /°	90
Volume/Å <sup>3</sup>	6533.87(14)
<i>Z</i>	8
$\rho_{\text{calc}}$ /cm <sup>3</sup>	1.553
$\mu$ /mm <sup>-1</sup>	1.340
<i>F</i> (000)	3111.0

---

(126) Dolomanov, O.V.; Bourhis, L. J.; Gildea, R. J.; Howard, J. A. K.; Puschmann, H. *J. Appl. Cryst.* **2009**, *42*, 339–341.

Crystal size/mm <sup>3</sup>	0.22 × 0.16 × 0.01
Radiation	Mo K $\alpha$ ( $\lambda$ = 0.71073)
2 $\Theta$ range for data collection/ $^{\circ}$	4.952 to 61.016
Index ranges	-25 $\leq$ h $\leq$ 27, -21 $\leq$ k $\leq$ 21, -32 $\leq$ l $\leq$ 32
Reflections collected	135069
Independent reflections	9976 [R <sub>int</sub> = 0.0569, R <sub>sigma</sub> = 0.0242]
Data/restraints/parameters	9976/0/399
Goodness-of-fit on F <sup>2</sup>	1.111
Final R indexes [I $\geq$ 2 $\sigma$ (I)]	R <sub>1</sub> = 0.0335, wR <sub>2</sub> = 0.0659
Final R indexes [all data]	R <sub>1</sub> = 0.0423, wR <sub>2</sub> = 0.0683
Largest diff. peak/hole / e $\text{\AA}^{-3}$	0.72/-0.44

**Table 7.6.2. Bond Lengths for cs2905-[Ru] 1a.**

Atom	Atom	Length/ $\text{\AA}$	Atom	Atom	Length/ $\text{\AA}$
Ru1	Cl2	2.3739(5)	C27	C26	1.384(3)
Ru1	Cl1	2.3227(5)	C5	C6	1.396(3)
Ru1	N3	2.1997(15)	C5	C10	1.509(3)
Ru1	C22	1.8791(18)	C18	C13	1.396(3)
Ru1	C1	2.0486(17)	C18	C21	1.504(3)
Cu1	Cl2	2.2039(5)	C18	C17	1.394(3)
Cu1	Cl3	2.1399(5)	C26	C25	1.394(3)
Cu1	C22	2.0588(18)	C13	C14	1.403(3)
N1	C1	1.348(2)	C29	C30	1.456(3)
N1	C13	1.435(2)	C30	C35	1.403(3)
N1	C2	1.473(2)	C30	C31	1.391(3)
N3	C28	1.436(2)	C8	C7	1.395(3)
N3	C29	1.290(2)	C6	C7	1.391(3)

**Table 7.6.2. Bond Lengths for cs2905-[Ru] 1a.**

Atom	Atom	Length/Å	Atom	Atom	Length/Å
N2	C1	1.355(2)	C2	C3	1.523(3)
N2	C4	1.433(2)	C14	C19	1.506(3)
N2	C3	1.479(2)	C14	C15	1.394(3)
C22	C23	1.456(2)	C7	C11	1.509(3)
C23	C28	1.398(2)	C35	C34	1.383(3)
C23	C24	1.399(3)	C33	C32	1.390(3)
C28	C27	1.394(2)	C33	C34	1.380(3)
C4	C9	1.401(3)	C17	C16	1.392(3)
C4	C5	1.402(3)	C16	C15	1.392(3)
C9	C12	1.503(3)	C16	C20	1.508(3)
C9	C8	1.393(3)	C31	C32	1.387(3)
C24	C25	1.389(3)			

**Table 7.6.3. Bond Angles for cs2905-[Ru] 1a.**

Atom	Atom	Atom	Angle/°	Atom	Atom	Atom	Angle/°
C11	Ru1	C12	154.906(17)	C8	C9	C4	118.39(18)
N3	Ru1	C12	87.14(4)	C8	C9	C12	120.42(17)
N3	Ru1	C11	87.00(4)	C25	C24	C23	119.70(17)
C22	Ru1	C12	103.04(6)	C26	C27	C28	119.00(17)
C22	Ru1	C11	100.03(6)	C4	C5	C10	121.50(17)
C22	Ru1	N3	80.64(7)	C6	C5	C4	118.51(17)
C22	Ru1	C1	99.23(7)	C6	C5	C10	119.99(17)
C1	Ru1	C12	96.60(5)	C13	C18	C21	122.32(17)
C1	Ru1	C11	89.27(5)	C17	C18	C13	118.02(18)
C1	Ru1	N3	176.17(6)	C17	C18	C21	119.60(18)
C13	Cu1	C12	142.28(2)	C27	C26	C25	121.39(17)
C22	Cu1	C12	103.27(5)	C18	C13	N1	120.23(17)
C22	Cu1	C13	113.97(5)	C18	C13	C14	121.40(17)
Cu1	C12	Ru1	69.250(14)	C14	C13	N1	118.16(17)
C1	N1	C13	125.48(15)	C24	C25	C26	119.59(17)
C1	N1	C2	113.93(15)	N3	C29	C30	128.76(17)
C13	N1	C2	120.14(15)	C35	C30	C29	115.85(17)
C28	N3	Ru1	108.93(11)	C31	C30	C29	124.54(17)
C29	N3	Ru1	134.29(13)	C31	C30	C35	119.41(18)
C29	N3	C28	116.03(15)	C9	C8	C7	121.90(18)
C1	N2	C4	126.73(15)	C7	C6	C5	121.69(18)
C1	N2	C3	113.32(15)	N1	C2	C3	102.28(15)
C4	N2	C3	119.06(15)	C13	C14	C19	122.21(18)
Ru1	C22	Cu1	82.69(7)	C15	C14	C13	117.98(18)
C23	C22	Ru1	117.22(13)	C15	C14	C19	119.80(18)

**Table 7.6.3. Bond Angles for cs2905-[Ru] 1a.**

Atom	Atom	Atom	Angle/°	Atom	Atom	Atom	Angle/°
C23	C22	Cu1	107.64(12)	N2	C3	C2	102.37(15)
N1	C1	Ru1	121.45(13)	C8	C7	C11	120.32(18)
N1	C1	N2	106.78(15)	C6	C7	C8	118.35(18)
N2	C1	Ru1	131.11(13)	C6	C7	C11	121.33(19)
C28	C23	C22	117.19(16)	C34	C35	C30	120.50(19)
C28	C23	C24	119.97(16)	C34	C33	C32	120.3(2)
C24	C23	C22	122.81(17)	C16	C17	C18	122.01(19)
C23	C28	N3	114.09(15)	C17	C16	C15	118.15(18)
C27	C28	N3	125.59(16)	C17	C16	C20	121.4(2)
C27	C28	C23	120.32(16)	C15	C16	C20	120.5(2)
C9	C4	N2	119.39(16)	C32	C31	C30	119.61(19)
C9	C4	C5	121.02(17)	C31	C32	C33	120.4(2)
C5	C4	N2	119.58(16)	C16	C15	C14	121.89(19)
C4	C9	C12	121.17(17)	C33	C34	C35	119.6(2)

**Table 7.6.4. Torsion Angles for cs2905-[Ru] 1a.**

A	B	C	D	Angle/°	A	B	C	D	Angle/°
Ru1	N3	C28	C23	-11.41(18)	C9	C8	C7	C6	1.7(3)
Ru1	N3	C28	C27	167.89(15)	C9	C8	C7	C11	-178.70(18)
Ru1	N3	C29	C30	-14.5(3)	C24	C23	C28	N3	-178.50(16)
Ru1	C22	C23	C28	8.2(2)	C24	C23	C28	C27	2.2(3)
Ru1	C22	C23	C24	-169.70(14)	C27	C26	C25	C24	-0.3(3)
Cu1	C22	C23	C28	-82.56(17)	C5	C4	C9	C12	177.53(17)
Cu1	C22	C23	C24	99.53(17)	C5	C4	C9	C8	-4.0(3)
Cl2	Ru1	C22	Cu1	10.19(6)	C5	C6	C7	C8	-1.5(3)

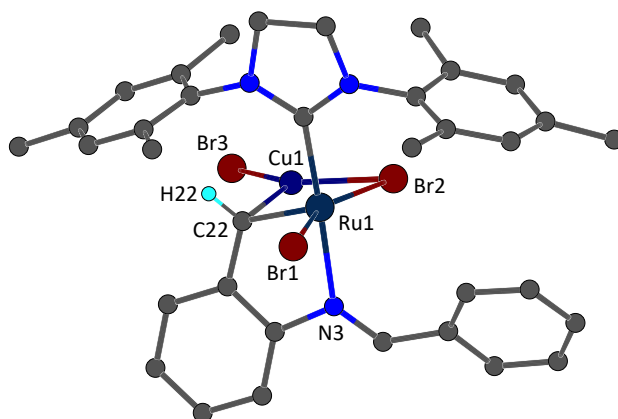
**Table 7.6.4. Torsion Angles for cs2905-[Ru] 1a.**

A	B	C	D	Angle/°	A	B	C	D	Angle/°
C12	Ru1	C22	C23	-95.92(13)	C5	C6	C7	C11	178.95(18)
C11	Ru1	C22	Cu1	-179.74(4)	C18	C13	C14	C19	171.24(18)
C11	Ru1	C22	C23	74.15(13)	C18	C13	C14	C15	-7.7(3)
N1	C13	C14	C19	-3.5(3)	C18	C17	C16	C15	-3.9(3)
N1	C13	C14	C15	177.60(17)	C18	C17	C16	C20	176.24(19)
N1	C2	C3	N2	-10.8(2)	C13	N1	C1	Ru1	-20.4(2)
N3	Ru1	C22	Cu1	95.03(6)	C13	N1	C1	N2	167.91(17)
N3	Ru1	C22	C23	-11.09(13)	C13	N1	C2	C3	-162.65(17)
N3	C28	C27	C26	179.06(17)	C13	C18	C17	C16	-1.5(3)
N3	C29	C30	C35	158.93(19)	C13	C14	C15	C16	2.0(3)
N3	C29	C30	C31	-26.3(3)	C29	N3	C28	C23	160.11(16)
N2	C4	C9	C12	-2.5(3)	C29	N3	C28	C27	-20.6(3)
N2	C4	C9	C8	176.05(16)	C29	C30	C35	C34	178.48(18)
N2	C4	C5	C6	-175.82(16)	C29	C30	C31	C32	-175.20(19)
N2	C4	C5	C10	3.8(3)	C30	C35	C34	C33	-3.2(3)
C22	C23	C28	N3	3.5(2)	C30	C31	C32	C33	-2.4(3)
C22	C23	C28	C27	-175.81(16)	C12	C9	C8	C7	179.48(17)
C22	C23	C24	C25	176.17(17)	C21	C18	C13	N1	4.7(3)
C1	Ru1	C22	Cu1	-88.85(6)	C21	C18	C13	C14	-169.91(18)
C1	Ru1	C22	C23	165.04(13)	C21	C18	C17	C16	175.92(18)
C1	N1	C13	C18	100.7(2)	C2	N1	C1	Ru1	167.35(13)
C1	N1	C13	C14	-84.6(2)	C2	N1	C1	N2	-4.3(2)
C1	N1	C2	C3	10.0(2)	C2	N1	C13	C18	-87.6(2)
C1	N2	C4	C9	-95.6(2)	C2	N1	C13	C14	87.2(2)
C1	N2	C4	C5	84.4(2)	C19	C14	C15	C16	-176.97(19)

**Table 7.6.4. Torsion Angles for cs2905-[Ru] 1a.**

A	B	C	D	Angle/°	A	B	C	D	Angle/°
C1	N2	C3	C2	9.7(2)	C3	N2	C1	Ru1	-174.35(14)
C23	C28	C27	C26	-1.7(3)	C3	N2	C1	N1	-3.8(2)
C23	C24	C25	C26	0.7(3)	C3	N2	C4	C9	95.9(2)
C28	N3	C29	C30	176.75(17)	C3	N2	C4	C5	-84.1(2)
C28	C23	C24	C25	-1.7(3)	C35	C30	C31	C32	-0.6(3)
C28	C27	C26	C25	0.7(3)	C17	C18	C13	N1	-177.95(16)
C4	N2	C1	Ru1	16.6(3)	C17	C18	C13	C14	7.4(3)
C4	N2	C1	N1	-172.87(17)	C17	C16	C15	C14	3.7(3)
C4	N2	C3	C2	179.66(17)	C10	C5	C6	C7	178.93(18)
C4	C9	C8	C7	1.0(3)	C31	C30	C35	C34	3.4(3)
C4	C5	C6	C7	-1.4(3)	C32	C33	C34	C35	0.2(3)
C9	C4	C5	C6	4.2(3)	C34	C33	C32	C31	2.7(3)
C9	C4	C5	C10	-176.17(17)	C20	C16	C15	C14	-176.50(19)

This report has been created with Olex2, compiled on 2022.04.07 svn.rca3783a0 for OlexSys. Please [let us know](#) if there are any errors or if you would like to have additional features.



**[Ru] 1b**

## Experimental

A brown plate (0.01 x 0.10 x 0.16 mm<sup>3</sup>) was centered on the goniometer of a Rigaku Oxford Diffraction Synergy-S diffractometer equipped with a HyPix6000HE detector and operating with CuK $\alpha$  radiation. The data collection routine, unit cell refinement, and data processing were carried out with the program CrysAlisPro.<sup>132</sup> The Laue symmetry and systematic absences were consistent with the orthorhombic space group *Pbca*. The structure was solved using SHELXT<sup>133</sup> and refined using SHELXL<sup>134</sup> via Olex2.<sup>135</sup> The three halogen sites were modeled with Cl/Br site disorder and EXYZ and EADP commands where used to constrain the Cl/Br positions and anisotropic displacement parameters to be equal. The relative occupancies refined to 0.717(3)/0.283(3) for the Cl1/Br1 site, 0.626(3)/0.374(3) for the Cl2/Br2 site, and 0.420(3)/0.580(3) for the Cl3/Br3 site. The final

---

(127) CrysAlisPro Software System, v1.171.42.xx, Rigaku Oxford Diffraction, **2022**, Rigaku Corporation, Oxford, UK.

(128) Sheldrick, G. M. "SHELXT – Integrated space-group and crystal structure determination." *Acta Cryst.* **2015**, *A71*, 3–8.

(129) Sheldrick, G. M. "Crystal structure refinement with SHELXL." *Acta Cryst.* **2015**, *C71*, 3–8.

(130) Dolomanov, O.V.; Bourhis, L. J.; Gildea, R. J.; Howard, J. A. K.; Puschmann, H. *J. Appl. Cryst.* **2009**, *42*, 339–341.

refinement model involved anisotropic displacement parameters for non-hydrogen atoms and a riding model for all hydrogen atoms except H22, which was located and refined independently. Olex2<sup>136</sup> was used for molecular graphics generation.

**Table 7.6.5. Crystal data and structure refinement for cs3007A1-[Ru] 1b.**

Identification code	HA-2-103_plate
Empirical formula	C <sub>35</sub> H <sub>37</sub> Br <sub>1.24</sub> Cl <sub>1.76</sub> CuN <sub>3</sub> Ru
Formula weight	825.65
Temperature/K	99.98(10)
Crystal system	orthorhombic
Space group	Pbca
a/Å	19.0876(2)
b/Å	15.01780(10)
c/Å	23.1814(2)
α/°	90
β/°	90
γ/°	90
Volume/Å <sup>3</sup>	6645.04(10)
Z	8
ρ <sub>calc</sub> /cm <sup>3</sup>	1.651
μ/mm <sup>-1</sup>	7.736
F(000)	3314.0
Crystal size/mm <sup>3</sup>	0.16 × 0.097 × 0.012
Radiation	Cu Kα (λ = 1.54184)
2θ range for data collection/°	7.628 to 154.828

---

(131) Dolomanov, O.V.; Bourhis, L. J.; Gildea, R. J.; Howard, J. A. K.; Puschmann, H. *J. Appl. Cryst.* **2009**, *42*, 339–341.

Index ranges	-24 ≤ h ≤ 23, -18 ≤ k ≤ 18, -28 ≤ l ≤ 29
Reflections collected	44831
Independent reflections	7008 [R <sub>int</sub> = 0.0486, R <sub>sigma</sub> = 0.0334]
Data/restraints/parameters	7008/0/401
Goodness-of-fit on F <sup>2</sup>	1.039
Final R indexes [I ≥ 2σ (I)]	R <sub>1</sub> = 0.0314, wR <sub>2</sub> = 0.0800
Final R indexes [all data]	R <sub>1</sub> = 0.0331, wR <sub>2</sub> = 0.0811
Largest diff. peak/hole / e Å <sup>-3</sup>	0.53/-1.00

**Table 7.6.6. Bond Lengths for cs3007A1-[Ru] 1b.**

Atom	Atom	Length/Å	Atom	Atom	Length/Å
Ru1	Br1	2.3787(4)	C7	C11	1.506(4)
Ru1	Br2	2.4475(4)	C8	C9	1.390(4)
Ru1	Cl1	2.3787(4)	C9	C12	1.503(4)
Ru1	Cl2	2.4475(4)	C13	C14	1.407(4)
Ru1	N3	2.199(2)	C13	C18	1.399(4)
Ru1	C1	2.058(2)	C14	C15	1.397(4)
Ru1	C22	1.889(2)	C14	C19	1.501(4)
Br2	Cu1	2.2648(5)	C15	C16	1.397(4)
Br3	Cu1	2.2321(5)	C16	C17	1.389(4)
Cu1	Cl2	2.2648(5)	C16	C20	1.507(4)
Cu1	Cl3	2.2321(5)	C17	C18	1.396(4)
Cu1	C22	2.062(2)	C18	C21	1.506(4)
N1	C1	1.349(3)	C22	C23	1.457(3)
N1	C2	1.479(3)	C23	C24	1.399(3)
N1	C4	1.430(3)	C23	C28	1.401(3)

**Table 7.6.6. Bond Lengths for cs3007A1-[Ru] 1b.**

Atom	Atom	Length/Å	Atom	Atom	Length/Å
N2	C1	1.350(3)	C24	C25	1.390(4)
N2	C3	1.478(3)	C25	C26	1.395(4)
N2	C13	1.433(3)	C26	C27	1.390(3)
N3	C28	1.438(3)	C27	C28	1.393(3)
N3	C29	1.292(3)	C29	C30	1.458(3)
C2	C3	1.520(4)	C30	C31	1.401(4)
C4	C5	1.408(3)	C30	C35	1.391(4)
C4	C9	1.396(4)	C31	C32	1.385(4)
C5	C6	1.391(4)	C32	C33	1.381(4)
C5	C10	1.511(4)	C33	C34	1.392(5)
C6	C7	1.397(4)	C34	C35	1.387(4)
C7	C8	1.393(4)			

**Table 7.6.7. Bond Angles for cs3007A1-[Ru] 1b.**

Atom	Atom	Atom	Angle/°	Atom	Atom	Atom	Angle/°
Br1	Ru1	Br2	154.204(16)	C5	C6	C7	122.0(2)
Cl1	Ru1	Cl2	154.204(16)	C6	C7	C11	121.3(2)
N3	Ru1	Br1	86.92(5)	C8	C7	C6	118.0(2)
N3	Ru1	Br2	87.05(5)	C8	C7	C11	120.7(3)
N3	Ru1	Cl1	86.92(5)	C9	C8	C7	122.0(2)
N3	Ru1	Cl2	87.05(5)	C4	C9	C12	121.2(2)
C1	Ru1	Br1	89.13(6)	C8	C9	C4	118.7(2)
C1	Ru1	Br2	96.88(7)	C8	C9	C12	120.1(2)
C1	Ru1	Cl1	89.13(6)	C14	C13	N2	118.1(2)

**Table 7.6.7. Bond Angles for cs3007A1-[Ru] 1b.**

Atom	Atom	Atom	Angle/°	Atom	Atom	Atom	Angle/°
C1	Ru1	Cl2	96.88(7)	C18	C13	N2	120.3(2)
C1	Ru1	N3	175.96(8)	C18	C13	C14	121.4(2)
C22	Ru1	Br1	99.93(7)	C13	C14	C19	122.1(3)
C22	Ru1	Br2	103.80(7)	C15	C14	C13	118.1(3)
C22	Ru1	Cl1	99.93(7)	C15	C14	C19	119.8(3)
C22	Ru1	Cl2	103.80(7)	C14	C15	C16	121.7(3)
C22	Ru1	N3	80.72(9)	C15	C16	C20	120.7(3)
C22	Ru1	C1	99.14(10)	C17	C16	C15	118.2(2)
Cu1	Br2	Ru1	67.168(14)	C17	C16	C20	121.2(3)
Br3	Cu1	Br2	141.27(2)	C16	C17	C18	122.3(3)
Cl3	Cu1	Cl2	141.27(2)	C13	C18	C21	122.1(2)
C22	Cu1	Br2	104.79(7)	C17	C18	C13	117.9(2)
C22	Cu1	Br3	113.55(7)	C17	C18	C21	119.9(2)
C22	Cu1	Cl2	104.79(7)	Ru1	C22	Cu1	82.62(9)
C22	Cu1	Cl3	113.55(7)	C23	C22	Ru1	116.93(17)
Cu1	Cl2	Ru1	67.168(14)	C23	C22	Cu1	106.95(15)
C1	N1	C2	113.2(2)	C24	C23	C22	122.5(2)
C1	N1	C4	127.0(2)	C24	C23	C28	120.1(2)
C4	N1	C2	119.0(2)	C28	C23	C22	117.3(2)
C1	N2	C3	113.5(2)	C25	C24	C23	119.7(2)
C1	N2	C13	126.0(2)	C24	C25	C26	119.6(2)
C13	N2	C3	120.0(2)	C27	C26	C25	121.4(2)
C28	N3	Ru1	109.10(14)	C26	C27	C28	118.9(2)
C29	N3	Ru1	134.46(17)	C23	C28	N3	114.1(2)
C29	N3	C28	115.6(2)	C27	C28	N3	125.7(2)

**Table 7.6.7. Bond Angles for cs3007A1-[Ru] 1b.**

Atom	Atom	Atom	Angle/°	Atom	Atom	Atom	Angle/°
N1	C1	Ru1	131.14(17)	C27	C28	C23	120.2(2)
N1	C1	N2	107.2(2)	N3	C29	C30	128.8(2)
N2	C1	Ru1	120.98(16)	C31	C30	C29	115.9(2)
N1	C2	C3	102.7(2)	C35	C30	C29	124.6(2)
N2	C3	C2	102.2(2)	C35	C30	C31	119.4(2)
C5	C4	N1	119.2(2)	C32	C31	C30	120.7(2)
C9	C4	N1	119.9(2)	C33	C32	C31	119.6(3)
C9	C4	C5	121.0(2)	C32	C33	C34	120.1(3)
C4	C5	C10	121.7(2)	C35	C34	C33	120.6(3)
C6	C5	C4	118.2(2)	C34	C35	C30	119.5(3)
C6	C5	C10	120.1(2)				

**Table 7.6.8. Torsion Angles for cs3007A1-[Ru] 1b.**

A	B	C	D	Angle/°	A	B	C	D	Angle/°
Ru1	N3	C28	C23	10.9(2)	C5	C4	C9	C8	4.4(4)
Ru1	N3	C28	C27	-167.68(19)	C5	C4	C9	C12	-176.5(2)
Ru1	N3	C29	C30	15.3(4)	C5	C6	C7	C8	2.0(4)
Ru1	C22	C23	C24	170.11(18)	C5	C6	C7	C11	-178.8(2)
Ru1	C22	C23	C28	-8.1(3)	C6	C7	C8	C9	-2.1(4)
Br1	Ru1	C22	Cu1	-179.72(5)	C7	C8	C9	C4	-1.0(4)
Br1	Ru1	C22	C23	-74.41(17)	C7	C8	C9	C12	179.9(2)
Br2	Ru1	C22	Cu1	-9.91(8)	C9	C4	C5	C6	-4.6(4)
Br2	Ru1	C22	C23	95.39(17)	C9	C4	C5	C10	176.3(2)
Cu1	C22	C23	C24	-99.7(2)	C10	C5	C6	C7	-179.5(2)

**Table 7.6.8. Torsion Angles for cs3007A1-[Ru] 1b.**

A	B	C	D	Angle/°	A	B	C	D	Angle/°
Cu1	C22	C23	C28	82.2(2)	C11	C7	C8	C9	178.6(2)
Cl1	Ru1	C22	Cu1	-179.72(5)	C13	N2	C1	Ru1	20.7(3)
Cl1	Ru1	C22	C23	-74.41(17)	C13	N2	C1	N1	-167.8(2)
Cl2	Ru1	C22	Cu1	-9.91(8)	C13	N2	C3	C2	162.9(2)
Cl2	Ru1	C22	C23	95.39(17)	C13	C14	C15	C16	-1.7(4)
N1	C2	C3	N2	10.5(3)	C14	C13	C18	C17	-6.9(4)
N1	C4	C5	C6	175.3(2)	C14	C13	C18	C21	169.4(2)
N1	C4	C5	C10	-3.8(3)	C14	C15	C16	C17	-4.0(4)
N1	C4	C9	C8	-175.4(2)	C14	C15	C16	C20	175.9(3)
N1	C4	C9	C12	3.6(3)	C15	C16	C17	C18	4.4(4)
N2	C13	C14	C15	-177.7(2)	C16	C17	C18	C13	0.9(4)
N2	C13	C14	C19	3.9(4)	C16	C17	C18	C21	-175.5(3)
N2	C13	C18	C17	178.2(2)	C18	C13	C14	C15	7.3(4)
N2	C13	C18	C21	-5.4(4)	C18	C13	C14	C19	-171.0(3)
N3	Ru1	C22	Cu1	-94.53(8)	C19	C14	C15	C16	176.7(3)
N3	Ru1	C22	C23	10.78(17)	C20	C16	C17	C18	-175.5(3)
N3	C29	C30	C31	-160.4(3)	C22	C23	C24	C25	-176.4(2)
N3	C29	C30	C35	23.8(4)	C22	C23	C28	N3	-3.2(3)
C1	Ru1	C22	Cu1	89.56(9)	C22	C23	C28	C27	175.5(2)
C1	Ru1	C22	C23	-165.14(17)	C23	C24	C25	C26	-0.4(4)
C1	N1	C2	C3	-9.4(3)	C24	C23	C28	N3	178.6(2)
C1	N1	C4	C5	-84.3(3)	C24	C23	C28	C27	-2.7(3)
C1	N1	C4	C9	95.6(3)	C24	C25	C26	C27	0.1(4)
C1	N2	C3	C2	-9.6(3)	C25	C26	C27	C28	-1.1(4)
C1	N2	C13	C14	84.1(3)	C26	C27	C28	N3	-179.1(2)

**Table 7.6.8. Torsion Angles for cs3007A1-[Ru] 1b.**

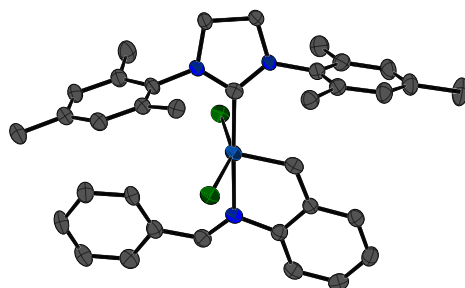
A	B	C	D	Angle/°	A	B	C	D	Angle/°
C1	N2	C13	C18	-100.9(3)	C26	C27	C28	C23	2.4(3)
C2	N1	C1	Ru1	173.91(18)	C28	N3	C29	C30	-176.4(2)
C2	N1	C1	N2	3.7(3)	C28	C23	C24	C25	1.8(3)
C2	N1	C4	C5	84.8(3)	C29	N3	C28	C23	-160.3(2)
C2	N1	C4	C9	-95.4(3)	C29	N3	C28	C27	21.1(3)
C3	N2	C1	Ru1	-167.32(17)	C29	C30	C31	C32	-178.1(2)
C3	N2	C1	N1	4.1(3)	C29	C30	C35	C34	175.6(3)
C3	N2	C13	C14	-87.4(3)	C30	C31	C32	C33	2.0(4)
C3	N2	C13	C18	87.6(3)	C31	C30	C35	C34	-0.1(4)
C4	N1	C1	Ru1	-16.5(4)	C31	C32	C33	C34	0.2(4)
C4	N1	C1	N2	173.2(2)	C32	C33	C34	C35	-2.4(5)
C4	N1	C2	C3	-179.8(2)	C33	C34	C35	C30	2.3(5)
C4	C5	C6	C7	1.3(4)	C35	C30	C31	C32	-2.1(4)

**Table 7.6.9. Atomic Occupancy for cs3007A1-[Ru] 1b.**

Atom	Occupancy	Atom	Occupancy	Atom	Occupancy
Br1	0.283(3)	Br2	0.374(3)	Br3	0.580(3)
Cl1	0.717(3)	Cl2	0.626(3)	Cl3	0.420(3)

This report has been created with Olex2, compiled on 2023.03.06 svn.rbb2c1857 for

OlexSys. Please [let us know](#) if there are any errors or if you would like to have additional features.



[Ru] 2a

## Experimental

A brownish-yellow plate (0.03 x 0.09 x 0.12 mm<sup>3</sup>) was centered on the goniometer of a Rigaku Oxford Diffraction Synergy-S diffractometer equipped with a HyPix6000HE detector and operating with CuK $\alpha$  radiation. The data collection routine, unit cell refinement, and data processing were carried out with the program CrysAlisPro.<sup>137</sup> The Laue symmetry and systematic absences were consistent with the monoclinic space group *I*2/*a*. The structure was solved using SHELXT<sup>138</sup> and refined using SHELXL<sup>139</sup> via Olex2.<sup>140</sup> The final refinement model involved anisotropic displacement parameters for non-hydrogen atoms and a riding model for all hydrogen atoms. The difference electron density map from the final structure model suggested there is a small amount of whole molecule disorder and showed a relatively large difference peak of 3.3 e-/Å<sup>3</sup> where Ru would reside. Refinement of the Ru as disordered suggest the minor conformation of the

---

(132) CrysAlisPro Software System, v1.171.42.xx, Rigaku Oxford Diffraction, **2022**, Rigaku Corporation, Oxford, UK.

(133) Sheldrick, G. M. "SHELXT – Integrated space-group and crystal structure determination." *Acta Cryst.* **2015**, *A71*, 3–8.

(134) Sheldrick, G. M. "Crystal structure refinement with SHELXL." *Acta Cryst.* **2015**, *C71*, 3–8.

(135) Dolomanov, O.V.; Bourhis, L. J.; Gildea, R. J.; Howard, J. A. K.; Puschmann, H. *J. Appl. Cryst.* **2009**, *42*, 339–341.

molecule amounts to ~5% occupancy. With such a low occupancy, only the major conformation was used the structure model. Olex2<sup>141</sup> was used for molecular graphics generation.

**Table 7.6.10. Crystal data and structure refinement for cs2925-[Ru] 2a**

Identification code	cs2925
Empirical formula	C <sub>35</sub> H <sub>37</sub> Cl <sub>2</sub> N <sub>3</sub> Ru
Formula weight	671.64
Temperature/K	99.98(10)
Crystal system	monoclinic
Space group	<i>I</i> 2/ <i>a</i>
<i>a</i> /Å	23.2621(3)
<i>b</i> /Å	10.15680(10)
<i>c</i> /Å	27.3417(4)
$\alpha$ /°	90
$\beta$ /°	100.7970(10)
$\gamma$ /°	90
Volume/Å <sup>3</sup>	6345.62(14)
<i>Z</i>	8
$\rho_{\text{calc}}$ /cm <sup>3</sup>	1.406
$\mu$ /mm <sup>-1</sup>	5.758
F(000)	2768.0
Crystal size/mm <sup>3</sup>	0.12 × 0.09 × 0.03
Radiation	Cu K $\alpha$ ( $\lambda$ = 1.54184)
2 $\theta$ range for data collection/°	7.738 to 154.558
Index ranges	-29 ≤ <i>h</i> ≤ 29, -12 ≤ <i>k</i> ≤ 12, -34 ≤ <i>l</i> ≤ 34
Reflections collected	54791

---

(136) Dolomanov, O.V.; Bourhis, L. J.; Gildea, R. J.; Howard, J. A. K.; Puschmann, H. *J. Appl. Cryst.* **2009**, *42*, 339–341.

Independent reflections	6639 [R <sub>int</sub> = 0.0609, R <sub>sigma</sub> = 0.0326]
Data/restraints/parameters	6639/0/376
Goodness-of-fit on F <sup>2</sup>	1.033
Final R indexes [I >= 2σ (I)]	R <sub>1</sub> = 0.0581, wR <sub>2</sub> = 0.1374
Final R indexes [all data]	R <sub>1</sub> = 0.0620, wR <sub>2</sub> = 0.1400
Largest diff. peak/hole / e Å <sup>-3</sup>	3.31/-1.74

**Table 7.6.11. Bond Lengths for cs2925-[Ru] 2a.**

Atom	Atom	Length/Å	Atom	Atom	Length/Å
Ru1	C11	2.3307(11)	C13	C14	1.402(6)
Ru1	C12	2.3511(10)	C13	C18	1.396(6)
Ru1	N3	2.174(4)	C14	C15	1.399(6)
Ru1	C1	2.051(4)	C14	C19	1.498(6)
Ru1	C22	1.846(5)	C15	C16	1.385(7)
N1	C1	1.345(5)	C16	C17	1.386(7)
N1	C2	1.476(5)	C16	C20	1.518(6)
N1	C4	1.447(5)	C17	C18	1.408(6)
N2	C1	1.349(6)	C18	C21	1.507(7)
N2	C3	1.473(5)	C22	C23	1.450(6)
N2	C13	1.441(5)	C23	C24	1.401(6)
N3	C28	1.442(5)	C23	C28	1.396(6)
N3	C29	1.286(6)	C24	C25	1.390(7)
C2	C3	1.526(5)	C25	C26	1.398(7)
C4	C5	1.398(7)	C26	C27	1.387(7)
C4	C9	1.398(6)	C27	C28	1.387(6)
C5	C6	1.400(6)	C29	C30	1.450(6)
C5	C10	1.504(6)	C30	C31	1.398(7)
C6	C7	1.382(7)	C30	C35	1.397(6)

**Table 7.6.11. Bond Lengths for cs2925-[Ru] 2a.**

<b>Atom</b>	<b>Atom</b>	<b>Length/Å</b>	<b>Atom</b>	<b>Atom</b>	<b>Length/Å</b>
C7	C8	1.391(8)	C31	C32	1.392(6)
C7	C11	1.514(7)	C32	C33	1.391(7)
C8	C9	1.408(6)	C33	C34	1.377(8)
C9	C12	1.502(7)	C34	C35	1.377(7)

**Table 7.6.12. Bond Angles for cs2925-[Ru] 2a.**

Atom	Atom	Atom	Angle/°	Atom	Atom	Atom	Angle/°
C11	Ru1	C12	152.53(4)	C4	C9	C12	122.5(4)
N3	Ru1	C11	86.80(10)	C8	C9	C12	120.1(4)
N3	Ru1	C12	89.16(10)	C14	C13	N2	118.0(4)
C1	Ru1	C11	98.35(12)	C18	C13	N2	119.6(4)
C1	Ru1	C12	86.13(12)	C18	C13	C14	121.8(4)
C1	Ru1	N3	174.84(15)	C13	C14	C19	122.2(4)
C22	Ru1	C11	98.12(14)	C15	C14	C13	117.8(4)
C22	Ru1	C12	108.06(14)	C15	C14	C19	119.9(4)
C22	Ru1	N3	80.99(17)	C16	C15	C14	121.9(4)
C22	Ru1	C1	98.48(19)	C15	C16	C17	118.7(4)
C1	N1	C2	113.5(3)	C15	C16	C20	120.8(5)
C1	N1	C4	129.9(4)	C17	C16	C20	120.5(4)
C4	N1	C2	115.3(3)	C16	C17	C18	121.8(4)
C1	N2	C3	114.1(3)	C13	C18	C17	117.7(4)
C1	N2	C13	127.6(4)	C13	C18	C21	123.1(4)
C13	N2	C3	117.7(3)	C17	C18	C21	119.2(4)
C28	N3	Ru1	110.5(3)	C23	C22	Ru1	118.2(3)
C29	N3	Ru1	132.1(3)	C24	C23	C22	121.9(4)
C29	N3	C28	117.4(4)	C28	C23	C22	117.8(4)
N1	C1	Ru1	128.3(3)	C28	C23	C24	120.3(4)
N1	C1	N2	107.1(4)	C25	C24	C23	119.5(4)
N2	C1	Ru1	123.4(3)	C24	C25	C26	119.4(4)
N1	C2	C3	102.9(3)	C27	C26	C25	121.3(4)
N2	C3	C2	102.2(3)	C26	C27	C28	119.1(4)
C5	C4	N1	118.1(4)	C23	C28	N3	112.4(4)
C9	C4	N1	119.7(4)	C27	C28	N3	127.3(4)
C9	C4	C5	122.2(4)	C27	C28	C23	120.3(4)

**Table 7.6.12. Bond Angles for cs2925-[Ru] 2a.**

<b>Atom</b>	<b>Atom</b>	<b>Atom</b>	<b>Angle/°</b>	<b>Atom</b>	<b>Atom</b>	<b>Atom</b>	<b>Angle/°</b>
C4	C5	C6	117.8(4)	N3	C29	C30	128.2(4)
C4	C5	C10	121.0(4)	C31	C30	C29	127.3(4)
C6	C5	C10	121.1(4)	C35	C30	C29	113.9(4)
C7	C6	C5	122.3(5)	C35	C30	C31	118.8(4)
C6	C7	C8	118.3(4)	C32	C31	C30	119.7(4)
C6	C7	C11	121.4(5)	C33	C32	C31	120.2(5)
C8	C7	C11	120.4(5)	C34	C33	C32	120.2(4)
C7	C8	C9	122.1(4)	C35	C34	C33	119.8(4)
C4	C9	C8	117.4(4)	C34	C35	C30	121.3(5)

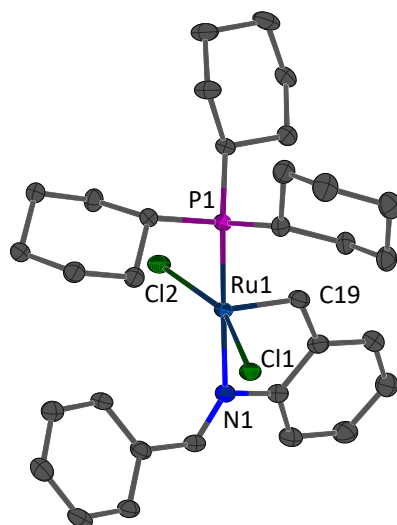
**Table 7.6.13. Torsion Angles for cs2925-[Ru] 2a.**

A	B	C	D	Angle/°	A	B	C	D	Angle/°
Ru1	N3	C28	C23	2.8(4)	C7	C8	C9	C4	-0.4(7)
Ru1	N3	C28	C27	-177.2(4)	C7	C8	C9	C12	-179.8(5)
Ru1	N3	C29	C30	-2.9(7)	C9	C4	C5	C6	1.3(7)
Ru1	C22	C23	C24	179.9(3)	C9	C4	C5	C10	-174.9(4)
Ru1	C22	C23	C28	1.0(5)	C10	C5	C6	C7	175.1(5)
Cl1	Ru1	C22	C23	86.0(3)	C11	C7	C8	C9	179.8(5)
Cl2	Ru1	C22	C23	-85.6(3)	C13	N2	C1	Ru1	21.2(6)
N1	C2	C3	N2	4.4(4)	C13	N2	C1	N1	-170.3(4)
N1	C4	C5	C6	-176.5(4)	C13	N2	C3	C2	168.4(4)
N1	C4	C5	C10	7.3(6)	C13	C14	C15	C16	-2.7(7)
N1	C4	C9	C8	177.1(4)	C14	C13	C18	C17	-3.8(7)
N1	C4	C9	C12	-3.4(7)	C14	C13	C18	C21	173.0(5)
N2	C13	C14	C15	177.3(4)	C14	C15	C16	C17	-1.6(7)
N2	C13	C14	C19	1.1(7)	C14	C15	C16	C20	179.2(5)
N2	C13	C18	C17	-175.6(4)	C15	C16	C17	C18	3.3(7)
N2	C13	C18	C21	1.3(7)	C16	C17	C18	C13	-0.7(7)
N3	Ru1	C22	C23	0.6(3)	C16	C17	C18	C21	-177.7(5)
N3	C29	C30	C31	-5.6(8)	C18	C13	C14	C15	5.5(7)
N3	C29	C30	C35	175.5(5)	C18	C13	C14	C19	-170.8(4)
C1	Ru1	C22	C23	-174.2(3)	C19	C14	C15	C16	173.6(4)
C1	N1	C2	C3	-4.9(5)	C20	C16	C17	C18	-177.4(5)
C1	N1	C4	C5	-81.8(6)	C22	C23	C24	C25	-178.4(4)
C1	N1	C4	C9	100.4(6)	C22	C23	C28	N3	-2.6(6)
C1	N2	C3	C2	-3.0(5)	C22	C23	C28	C27	177.4(4)
C1	N2	C13	C14	80.8(6)	C23	C24	C25	C26	0.7(7)
C1	N2	C13	C18	-107.2(5)	C24	C23	C28	N3	178.5(4)
C2	N1	C1	Ru1	171.0(3)	C24	C23	C28	C27	-1.5(6)

**Table 7.6.13. Torsion Angles for cs2925-[Ru] 2a.**

A	B	C	D	Angle/°	A	B	C	D	Angle/°
C2	N1	C1	N2	3.2(5)	C24	C25	C26	C27	-0.9(7)
C2	N1	C4	C5	84.3(5)	C25	C26	C27	C28	-0.1(7)
C2	N1	C4	C9	-93.5(5)	C26	C27	C28	N3	-178.7(4)
C3	N2	C1	Ru1	-168.4(3)	C26	C27	C28	C23	1.3(7)
C3	N2	C1	N1	0.1(5)	C28	N3	C29	C30	177.9(4)
C3	N2	C13	C14	-89.2(5)	C28	C23	C24	C25	0.5(6)
C3	N2	C13	C18	82.8(5)	C29	N3	C28	C23	-177.8(4)
C4	N1	C1	Ru1	-22.8(7)	C29	N3	C28	C27	2.2(6)
C4	N1	C1	N2	169.5(4)	C29	C30	C31	C32	-178.6(5)
C4	N1	C2	C3	-173.3(4)	C29	C30	C35	C34	179.4(4)
C4	C5	C6	C7	-1.1(7)	C30	C31	C32	C33	-0.6(7)
C5	C4	C9	C8	-0.6(7)	C31	C30	C35	C34	0.4(7)
C5	C4	C9	C12	178.8(4)	C31	C32	C33	C34	0.1(8)
C5	C6	C7	C8	0.2(8)	C32	C33	C34	C35	0.6(8)
C5	C6	C7	C11	-179.1(5)	C33	C34	C35	C30	-0.9(8)
C6	C7	C8	C9	0.6(8)	C35	C30	C31	C32	0.3(7)

This report has been created with Olex2, compiled on 2022.04.07 svn.rca3783a0 for OlexSys. Please [let us know](#) if there are any errors or if you would like to have additional features.



[Ru] 3a

## Experimental

A yellow plank (0.01 x 0.05 x 0.31 mm<sup>3</sup>) was centered on the goniometer of a Rigaku Oxford Diffraction Synergy-S diffractometer equipped with a HyPix6000HE detector and operating with CuK $\alpha$  radiation. The data collection routine, unit cell refinement, and data processing were carried out with the program CrysAlisPro.<sup>142</sup> The Laue symmetry and systematic absences were consistent with the monoclinic space group  $P2_1/c$ . The structure was solved using SHELXT<sup>143</sup> and refined using SHELXL<sup>144</sup> via Olex2.<sup>145</sup> In addition to the main molecule, there was evidence of a severely disordered pentane molecule in the asymmetric unit. The solvent mask feature of Olex2 was used and

---

(137) CrysAlisPro Software System, v1.171.42.xx, Rigaku Oxford Diffraction, **2022**, Rigaku Corporation, Oxford, UK.

(138) Sheldrick, G. M. "SHELXT – Integrated space-group and crystal structure determination." *Acta Cryst.* **2015**, *A71*, 3–8.

(139) Sheldrick, G. M. "Crystal structure refinement with SHELXL." *Acta Cryst.* **2015**, *C71*, 3–8.

(140) Dolomanov, O.V.; Bourhis, L. J.; Gildea, R. J.; Howard, J. A. K.; Puschmann, H. *J. Appl. Cryst.* **2009**, *42*, 339–341.

total of 180 e<sup>-</sup> was subtracted from 802 Å<sup>3</sup> total void space in the unit cell. This was approximated as 4 pentane molecules (168 e<sup>-</sup>) per unit cell and giving one pentane per asymmetric unit. The final refinement model involved anisotropic displacement parameters for non-hydrogen atoms and a riding model for all hydrogen atoms. Olex2<sup>146</sup> was used for molecular graphics generation.

**Table 7.6.14. Crystal data and structure refinement for cs2921-[Ru] 3a.**

Identification code	HA-2-70
Empirical formula	C <sub>37</sub> H <sub>56</sub> NPCl <sub>2</sub> Ru
Formula weight	717.76
Temperature/K	99.99(11)
Crystal system	monoclinic
Space group	P2 <sub>1</sub> /c
a/Å	15.30222(11)
b/Å	26.4763(2)
c/Å	9.07431(7)
α/°	90
β/°	105.2125(8)
γ/°	90
Volume/Å <sup>3</sup>	3547.59(5)
Z	4

---

(141) Dolomanov, O.V.; Bourhis, L. J.; Gildea, R. J.; Howard, J. A. K.; Puschmann, H. *J. Appl. Cryst.* **2009**, *42*, 339–341.

$\rho_{\text{calc}}/\text{cm}^3$	1.344
$\mu/\text{mm}^{-1}$	5.570
F(000)	1512.0
Crystal size/ $\text{mm}^3$	$0.31 \times 0.05 \times 0.01$
Radiation	Cu K $\alpha$ ( $\lambda = 1.54184$ )
$2\Theta$ range for data collection/ $^\circ$	5.986 to 154.464
Index ranges	$-19 \leq h \leq 19, -33 \leq k \leq 32, -11 \leq l \leq 10$
Reflections collected	55473
Independent reflections	7419 [ $R_{\text{int}} = 0.0419, R_{\text{sigma}} = 0.0243$ ]
Data/restraints/parameters	7419/0/334
Goodness-of-fit on $F^2$	1.078
Final R indexes [ $I \geq 2\sigma(I)$ ]	$R_1 = 0.0258, wR_2 = 0.0697$
Final R indexes [all data]	$R_1 = 0.0275, wR_2 = 0.0706$
Largest diff. peak/hole / $e \text{ \AA}^{-3}$	0.63/-0.53

**Table 7.6.15. Bond Lengths for cs2921-[Ru] 3a.**

Atom	Atom	Length/ $\text{\AA}$	Atom	Atom	Length/ $\text{\AA}$
Ru1	C11	2.3459(4)	C25	C20	1.406(3)
Ru1	C12	2.3469(4)	C25	C24	1.394(3)
Ru1	P1	2.3369(4)	C13	C14	1.533(2)
Ru1	N1	2.1488(15)	C20	C21	1.402(3)

**Table 7.6.15. Bond Lengths for cs2921-[Ru] 3a.**

Atom	Atom	Length/Å	Atom	Atom	Length/Å
Ru1	C19	1.8365(18)	C20	C19	1.453(2)
P1	C1	1.8636(17)	C6	C5	1.531(2)
P1	C7	1.8681(17)	C24	C23	1.387(3)
P1	C13	1.8581(17)	C31	C30	1.383(3)
N1	C25	1.426(2)	C31	C32	1.386(3)
N1	C26	1.286(2)	C17	C16	1.524(3)
C1	C6	1.539(2)	C14	C15	1.539(3)
C1	C2	1.541(2)	C30	C29	1.396(3)
C7	C12	1.535(2)	C21	C22	1.379(3)
C7	C8	1.537(2)	C11	C12	1.535(3)
C3	C2	1.529(2)	C11	C10	1.525(3)
C3	C4	1.522(2)	C4	C5	1.526(3)
C27	C32	1.395(3)	C28	C29	1.383(3)
C27	C26	1.462(3)	C23	C22	1.396(3)
C27	C28	1.400(3)	C8	C9	1.536(3)
C18	C13	1.536(2)	C16	C15	1.530(3)
C18	C17	1.530(2)	C10	C9	1.525(3)

**Table 7.6.16. Bond Angles for cs2921-[Ru] 3a.**

Atom	Atom	Atom	Angle/°	Atom	Atom	Atom	Angle/°
C11	Ru1	C12	157.488(15)	C24	C25	C20	120.80(17)
P1	Ru1	C11	90.613(15)	C18	C13	P1	113.93(12)
P1	Ru1	C12	92.759(15)	C14	C13	P1	117.57(12)
N1	Ru1	C11	86.23(4)	C14	C13	C18	109.75(14)
N1	Ru1	C12	90.10(4)	C25	C20	C19	116.77(16)
N1	Ru1	P1	176.84(4)	C21	C20	C25	118.81(17)
C19	Ru1	C11	100.57(5)	C21	C20	C19	124.42(17)
C19	Ru1	C12	100.90(5)	C5	C6	C1	111.71(15)
C19	Ru1	P1	98.75(6)	C23	C24	C25	119.11(17)
C19	Ru1	N1	82.02(7)	C3	C2	C1	110.17(14)
C1	P1	Ru1	110.49(6)	C30	C31	C32	119.92(17)
C1	P1	C7	102.35(8)	C16	C17	C18	111.69(16)
C7	P1	Ru1	116.52(6)	C13	C14	C15	110.77(16)
C13	P1	Ru1	112.69(6)	C31	C30	C29	120.04(18)
C13	P1	C1	102.44(8)	C31	C32	C27	120.36(17)
C13	P1	C7	110.92(8)	C22	C21	C20	120.37(18)
C25	N1	Ru1	109.94(11)	C10	C11	C12	111.82(16)
C26	N1	Ru1	129.47(13)	N1	C26	C27	125.06(16)
C26	N1	C25	119.13(15)	C3	C4	C5	110.39(15)

**Table 7.6.16. Bond Angles for cs2921-[Ru] 3a.**

Atom	Atom	Atom	Angle/°	Atom	Atom	Atom	Angle/°
C6	C1	P1	112.24(12)	C7	C12	C11	111.63(15)
C6	C1	C2	109.65(14)	C29	C28	C27	119.66(17)
C2	C1	P1	112.87(12)	C4	C5	C6	112.24(16)
C12	C7	P1	112.49(12)	C28	C29	C30	120.36(18)
C12	C7	C8	110.15(15)	C24	C23	C22	120.66(18)
C8	C7	P1	116.64(12)	C20	C19	Ru1	117.42(13)
C4	C3	C2	110.91(15)	C9	C8	C7	110.61(15)
C32	C27	C26	117.28(16)	C21	C22	C23	120.16(18)
C32	C27	C28	119.58(17)	C17	C16	C15	110.57(16)
C28	C27	C26	123.14(16)	C9	C10	C11	110.89(16)
C17	C18	C13	110.03(15)	C10	C9	C8	110.79(17)
C20	C25	N1	113.30(15)	C16	C15	C14	110.66(16)
C24	C25	N1	125.91(16)				

**Table 7.6.17. Torsion Angles for cs2921-[Ru] 3a.**

A	B	C	D	Angle/°	A	B	C	D	Angle/°
Ru1	P1	C1	C6	52.64(13)	C25	C24	C23	C22	0.7(3)
Ru1	P1	C1	C2	-71.89(13)	C13	P1	C1	C6	-67.63(14)
Ru1	P1	C7	C12	-67.08(13)	C13	P1	C1	C2	167.84(13)

**Table 7.6.17. Torsion Angles for cs2921-[Ru] 3a.**

A	B	C	D	Angle/°	A	B	C	D	Angle/°
Ru1	P1	C7	C8	164.26(11)	C13	P1	C7	C12	63.63(14)
Ru1	P1	C13	C18	50.15(14)	C13	P1	C7	C8	-65.03(15)
Ru1	P1	C13	C14	-179.40(12)	C13	C18	C17	C16	-57.6(2)
Ru1	N1	C25	C20	7.09(17)	C13	C14	C15	C16	57.2(2)
Ru1	N1	C25	C24	-173.17(15)	C20	C25	C24	C23	2.1(3)
Ru1	N1	C26	C27	13.8(3)	C20	C21	C22	C23	0.5(3)
Cl1	Ru1	C19	C20	89.66(13)	C6	C1	C2	C3	57.84(19)
Cl2	Ru1	C19	C20	-83.51(13)	C24	C25	C20	C21	-3.5(3)
P1	Ru1	C19	C20	-178.06(12)	C24	C25	C20	C19	176.59(16)
P1	C1	C6	C5	178.80(13)	C24	C23	C22	C21	-2.0(3)
P1	C1	C2	C3	-176.22(12)	C2	C1	C6	C5	-54.9(2)
P1	C7	C12	C11	172.90(13)	C2	C3	C4	C5	57.5(2)
P1	C7	C8	C9	-173.15(13)	C31	C30	C29	C28	-1.5(3)
P1	C13	C14	C15	169.43(14)	C17	C18	C13	P1	-167.86(13)
N1	Ru1	C19	C20	5.04(13)	C17	C18	C13	C14	57.9(2)
N1	C25	C20	C21	176.24(15)	C17	C16	C15	C14	-55.6(2)
N1	C25	C20	C19	-3.7(2)	C30	C31	C32	C27	2.9(3)
N1	C25	C24	C23	-177.60(17)	C32	C27	C26	N1	-153.95(17)
C1	P1	C7	C12	172.27(12)	C32	C27	C28	C29	1.4(3)

**Table 7.6.17. Torsion Angles for cs2921-[Ru] 3a.**

A	B	C	D	Angle/°	A	B	C	D	Angle/°
C1	P1	C7	C8	43.61(15)	C32	C31	C30	C29	-0.4(3)
C1	P1	C13	C18	168.88(13)	C21	C20	C19	Ru1	177.58(14)
C1	P1	C13	C14	-60.67(15)	C11	C10	C9	C8	56.7(2)
C1	C6	C5	C4	53.8(2)	C26	N1	C25	C20	-160.39(16)
C7	P1	C1	C6	177.38(12)	C26	N1	C25	C24	19.3(3)
C7	P1	C1	C2	52.84(14)	C26	C27	C32	C31	176.94(16)
C7	P1	C13	C18	-82.53(14)	C26	C27	C28	C29	-178.86(17)
C7	P1	C13	C14	47.92(16)	C4	C3	C2	C1	-59.89(19)
C7	C8	C9	C10	-58.3(2)	C12	C7	C8	C9	57.1(2)
C3	C4	C5	C6	-54.4(2)	C12	C11	C10	C9	-54.8(2)
C27	C28	C29	C30	0.9(3)	C28	C27	C32	C31	-3.4(3)
C18	C13	C14	C15	-58.2(2)	C28	C27	C26	N1	26.4(3)
C18	C17	C16	C15	56.4(2)	C19	C20	C21	C22	-177.95(18)
C25	N1	C26	C27	178.50(16)	C8	C7	C12	C11	-55.1(2)
C25	C20	C21	C22	2.2(3)	C10	C11	C12	C7	54.4(2)
C25	C20	C19	Ru1	-2.5(2)					

**Table 7.6.18. Solvent masks information for cs2921-[Ru] 3a.**

<b>Number</b>	<b>X</b>	<b>Y</b>	<b>Z</b>	<b>Volume</b>	<b>Electron count</b>	<b>Content</b>
1	0.161	0.250	-0.292	400.9	90.3	2 pentane
2	-0.161	0.750	-0.625	400.9	87.6	2 pentane

This report has been created with Olex2, compiled on 2022.04.07 svn.rca3783a0 for OlexSys. Please [let us know](#) if there are any errors or if you would like to have additional features.

## Chapter 8. Summary and Future Outlook

In this dissertation, I developed a new synthetic approach to preparing hyperbranched polymers: *self-condensing ring-opening metathesis polymerization* (ROMP). Hyperbranched ROMP polymers have been prepared by using multi-functional ROMP monomers or a combination of two synthetic approaches. However, self-condensing ROMP enables the synthesis of hyperbranched polymers using any ROMP monomers in a single step. This approach introduces a new class of olefin metathesis catalysts, an inimer, having both the ROMP initiator and monomer.

Throughout this research, I have synthesized a series of olefin metathesis catalysts to study the catalyst stability and activity (Chapters 2 and 3, **Figure 8.1**). NMR spectroscopy and X-ray diffraction confirmed the synthesis of these catalysts. I used Differential Scanning Calorimetry (DSC) to determine the catalyst activation temperature. In Chapter 2, I studied the monomer and catalyst identity effects on the activation temperature using five different olefin metathesis catalysts and a series of ROMP monomers. This study confirms the activation temperature of the catalyst dependence on the catalyst and monomer identity. Olefin metathesis catalysts can be activated at a low temperature in polymerizing ROMP monomers having high strain energy and low melting temperature. The activation temperature increases as the monomer strain energy decreases. Catalyst ligands and ring-size chelation also affect the catalyst activation temperature. The results obtained from Chapter 2 will guide the selection of optimal conditions for initiating olefin metathesis catalysts. For example, in this dissertation, I designed and synthesized the ROMP inimers presented in Chapters 4 and 5 based on the results in Chapter 2.

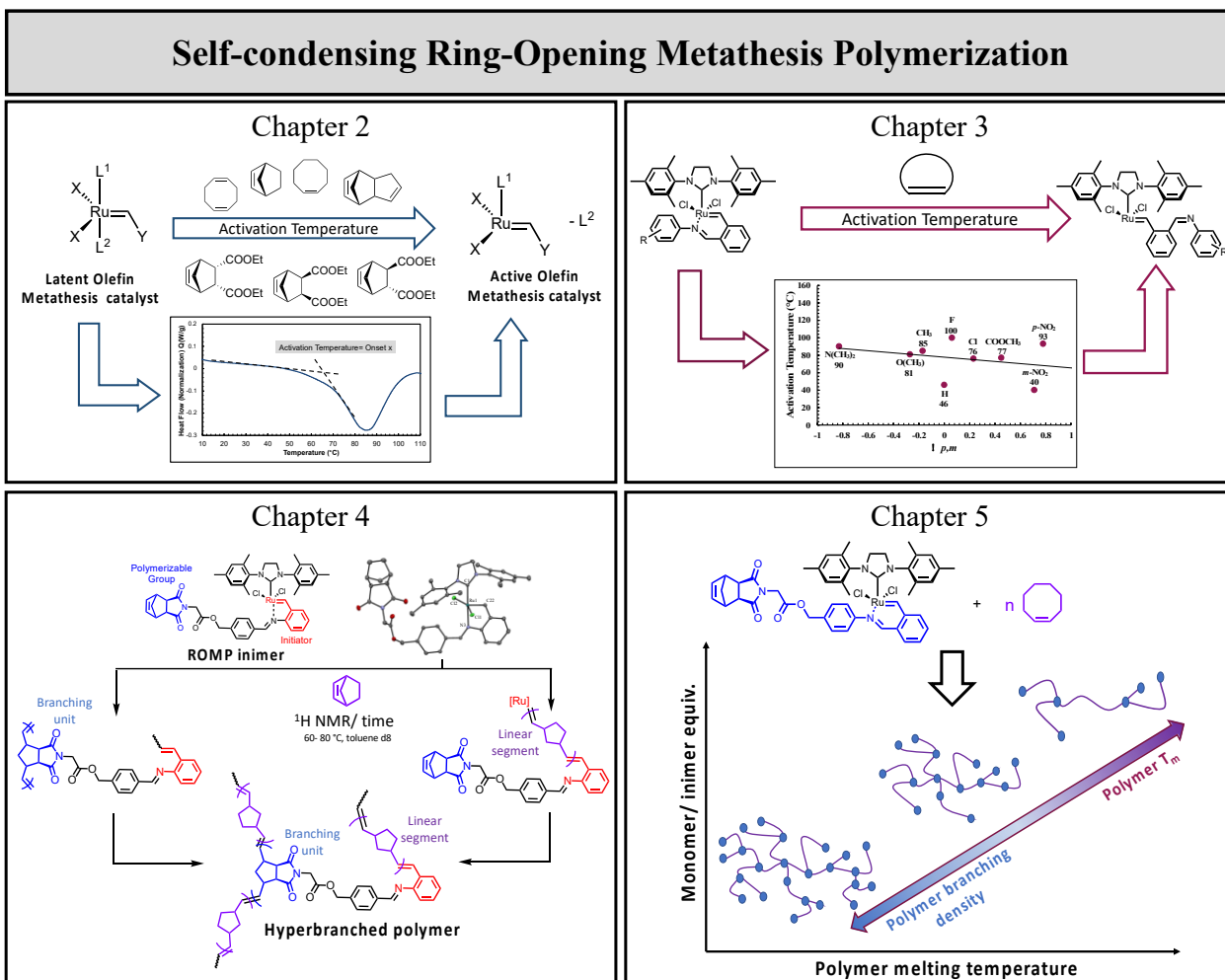


**Figure 8.1. Summary of research presented in Chapters 2-5.**

I developed a synthetic approach to synthesize a ROMP inimer by coupling a ROMP monomer to a latent olefin metathesis catalyst without initiating polymerization. Imine- and azo-chelating ruthenium olefin metathesis catalysts showed high stability at room temperature, and enabled ROMP monomer functionalization via an ester linkage. The inimers have varied activation temperatures depending on the chelation group and chelation ring size. The activation temperature of these inimers also varied in polymerizing different ROMP monomers.

In Chapter 4, I explored how monomer identity affects in both the inimer activation temperature and the initiation and propagation rate. Self-condensing ROMP of highly reactive norbornene showed a low inimer activation temperature with a high propagation and low initiation rate resulting in the formation of longer linear segments with few branching units. I investigated the possibility to slow the propagation rate to give the ROMP inimer enough time to initiate. A  $^1\text{H}$  NMR kinetic experiment showed that polymerizing a monomer having lower reactivity than norbornene lowered the propagation rate and increased the inimer initiation rate.

To further study the possibility of enhancing the inimer initiation rate, I synthesized a series of imine-chelated olefin metathesis catalysts with different electron-donating and electron-withdrawing groups on the benzyldiene ligand (Chapter 3 **Figure 8.1**). The goal was to decrease the electron density around the N–Ru chelation center to weaken the chelation and speed up the initiation. However, the DSC activation temperature measurements of the functionalized olefin metathesis catalysts showed an unclear trend and were affected by both the monomer identity and the catalyst functionality. For future work, exploring the behavior of the catalysts in solution would provide insight into the activation temperatures and rates of initiation and propagation.

To investigate the chelation effect in the olefin metathesis complexes, I synthesized a series of ROMP inimers with imine and azo chelation (Chapter 5 **Figure 8.1**). I assessed their activation temperature in bulk polymerization by DSC measurements, and in solution polymerizations by  $^1\text{H}$  NMR. The results in Chapter 5 showed the dependence of inimer activation temperature on both the ROMP monomer and inimer identity. Furthermore, the

inimer-to-monomer ratio affects the polymer melting temperature. As the inimer ratio increases, more branching forms and decreases the polymer  $T_m$ . With increasing the monomer ratio, the hyperbranched polymer had fewer branching units and a higher melting temperature.

The results of Chapters 4 and 5 provide a synthetic tool for producing hyperbranched polymers with any ROMP monomer. The hyperbranched polymer properties can be controlled by altering the monomer-to-inimer ratio, and monomer and inimer identity. As the activation temperature of the ROMP inimer is critical to initiate the self-condensing polymerization and enhance the rate of initiation, inimer modification is required. Inimer modification includes varying the atom chelation and ligands. Exploring the steric and electronic effects of the inimer ligands could affect the inimer activity and enhance the polymer initiation rate.

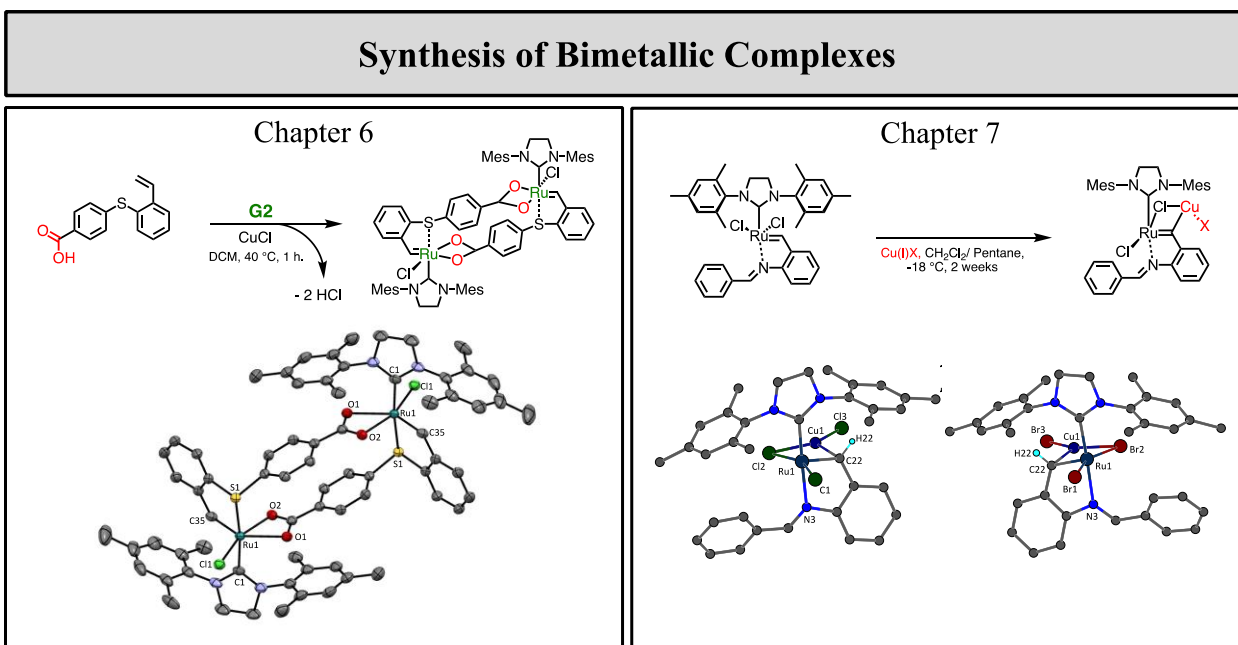


**Figure 8.2. Summary of research presented in Chapters 6 and 7.**

In this dissertation, I also developed two synthetic approaches to preparing bimetallic complexes (Chapters 6 and 7, **Figure 8.1**). Chapter 6 illustrates the possibility of synthesizing diruthenium bimetallic complexes via catalyst dimerization. A benzylidene ligand with a carboxylic acid underwent a carbene exchange reaction with Grubbs second generation catalyst to produce a dimerized catalyst. The ruthenium atom can chelate the two oxygen of the carboxylic acid. This finding can be used to prepare novel dimer complexes with different atoms and ligands chelation.

Chapter 7 introduces the possibility of copper insertion into the ruthenium complexes. The heterobimetallic complexes achieved in Chapter 7 provide a new chemistry of adding metal salts to the carbene reaction. Further metal salts can be added to test the possibility of preparing new complexes.